SANDIA REPORT
SAND2009-1278
Unlimited Release
Printed March 2009

Sensitivity of Storage Field Performance to Geologic and Cavern Design Parameters in Salt Domes

Byoung Yoon Park and Brian L. Ehgartner

Prepared by
Sandia National Laboratories
Albuquerque, New Mexico 87185 and Livermore, California 94550

Sandia is a multiprogram laboratory operated by Sandia Corporation,
a Lockheed Martin Company, for the United States Department of Energy's
National Nuclear Security Administration under Contract DE-AC04-94AL85000.

Issued by Sandia National Laboratories, operated for the United States Department of Energy by Sandia Corporation.

Available to DOE and DOE contractors from
U.S. Department of Energy
Office of Scientific and Technical Information
P.O. Box 62
Oak Ridge, TN 37831

Telephone: (865) 576-8401
Facsimile: (865) 576-5728
E-Mail: reports@adonis.osti.gov
Online ordering: http://www.osti.gov/bridge

Available to the public from
U.S. Department of Commerce
National Technical Information Service
5285 Port Royal Rd.
Springfield, VA 22161

Telephone: (800) 553-6847
Facsimile: (703) 605-6900
E-Mail: orders@ntis.fedworld.gov
Online order: http://www.ntis.gov/help/ordermethods.asp?loc=7-4-0#online

SAND2009-1278
Unlimited Release
Printed March 2009

Sensitivity of Storage Field Performance to Geologic and Cavern Design Parameters in Salt Domes

Byoung Yoon Park[1] and Brian L. Ehgartner[2]
[1]-Performance Assessment & Decision Analysis Department
Sandia National Laboratories
4100 National Parks Highway,
Carlsbad, NM 88220-MS1395
[2]-Geotechnology and Engineering Department
Sandia National Laboratories
P.O. Box 5800
Albuquerque, NM 87185-MS0706

Abstract

A sensitivity study was performed utilizing a three dimensional finite element model to assess allowable cavern field sizes for strategic petroleum reserve salt domes. A potential exists for tensile fracturing and dilatancy damage to salt that can compromise the integrity of a cavern field in situations where high extraction ratios exist. The effects of salt creep rate, depth of salt dome top, dome size, caprock thickness, elastic moduli of caprock and surrounding rock, lateral stress ratio of surrounding rock, cavern size, depth of cavern, and number of caverns are examined numerically. As a result, a correlation table between the parameters and the impact on the performance of storage field was established. In general, slower salt creep rates, deeper depth of salt dome top, larger elastic moduli of caprock and surrounding rock, and a smaller radius of cavern are better for structural performance of the salt dome.

ACKNOWLEDGMENTS

This research is funded by SPR programs administered by the Office of Fossil Energy (FE) of the U.S. Department of Energy.

Dr. Courtney G. Herrick (SNL, Dept. 6711) provided a technical review and Dr. David J. Borns (SNL, Dept. 6312) provided a management review. This report has been improved by these individuals.

CONTENTS

FIGURES

TABLES

NOMENCLATURE

3D	Three Dimensional
C	Cavern
CR	CapRock
DOE	U.S. Department of Energy
DILFAC	DILatant damage FACtor
FCS	Fast Creeping Salt
FEM	Finite Element Method
MCS	Minimum Compressive Stress
MSF	Minimum Safety Factor
MMB	Million Barrels
OB	OverBurden
RF	elastic modulus Reduction Factor
SC	Secondary Creep
SD	Salt Dome
SMF	Structural Multiplication Factor
SNL	Sandia National Laboratories
SO	StandOff Distance
SPR	Strategic Petroleum Reserve
SR	Surrounding Rock
WH	West Hackberry

1. INTRODUCTION

A sensitivity study was performed utilizing a three dimensional (3D) finite element model to assess the effect of various cavern field sizes for salt domes. A potential exists for tensile fracturing and dilatancy damage to salt that may compromise the integrity of a cavern field in situations where high extraction ratios exist. Parameters such as volumetric closure rate, which is a function of salt creep rate and cavern depth, and the depth to salt dome top are believed to be influencing factors. Situations that give rise to and/or intensify tensile fracturing or salt damage failure to occur in cavern fields can be investigated by 3D geomechanics modeling.

1.1. Background

Salt domes have served as excellent hosts for the storage of oil and gas in underground caverns. Because of the desire to expand their use, there are concerns about the integrity of the salt surrounding these storage caverns that need to be addressed. An actual example of a dome that experienced salt damage with a resulting loss of an underground oil storage capacity is the Weeks Island dome. Oil was stored in an abandoned room and pillar mine. A sinkhole developed as a result of salt cracks that formed along the top of the dome that penetrated into the mined facility. Finite element analyses predicted salt dilatant damage and tensile stresses to form as a result of subsidence over time [Hoffman, 1996]. Similar to the analyses, a large amount of subsidence and volumetric change of caverns due to salt creep closure was predicted and measured. It appears that salt domes have limits to the amount and/or rate of underground closure allowed.

Based on experience suggested from past numerical analyses [Ehgartner and Sobolik, 2002; Park et al., 2005; Park et al., 2006; Park and Ehgartner, 2008], one area of concern is the possible loss of integrity to the salt above the caverns. Dilatant damage may develop over time in a small dome with fast creeping salt where damage may initiate at the top of the dome and extend downward with time to the roof of the cavern field. Another area of possible concern is the effect of the combination of numerous large deep caverns in a single dome. Again, this is especially important in a fast creeping salt.

1.2. Approach

The cavern field studied herein will be symmetric so that readily deployed pie-slice models can be used. The base model will be the 19 cavern field model used for West Hackberry (WH) [Ehgartner and Sobolik, 2002]. The 30-degree wedge model will incorporate a dome edge appropriate for the site. Periodic workovers† will be simulated, but progressive leaches of the caverns for the drawdowns‡ will not be considered. Individual parameters will be varied from the base model to access their impact on the integrity of the salt. This will assess the sensitivity of the predicted safety factor against damage to the individual parameter variations of interest.

† "Workover" is when the wellhead pressure in the cavern is dropped to zero for the maintenance.

‡ "Drawdown" is when the crude oil is withdrawn from the cavern. Fresh water is used to withdrawal the crude oil. Because the cavern enlarges due to salt dissolving from the cavern walls, it is called a "drawdown leach".

1.3. Objectives

The goal is to establish conditions whereby cavern field integrity may be compromised. The contributing factors are to be identified and quantified relative to their impacts. The results may be generalized to defining conditions for allowable underground closure relative to dome size. If damage is predicted, then obviously certain cavern field designs in combination with certain geologic conditions are unacceptable. These will need to be quantified.

1.4. Applications

The results from this study will be used for cavern design, dome selection, monitoring, and forecasting potential problems. While we have the latitude to vary design parameters to accommodate a specific dome, many times we also have the ability to select a particular dome. Therefore, the results of this study can aid in dome selection and design of a cavern field to suit a particular dome. For existing sites, this parametric study may foresee certain conditions that could become problematic as additional caverns are added to a field or existing ones enlarged.

1.5. Report Organization

The remainder of this report describes the analyses details. Section 2 describes the parameters and their variant to examine their impacts. Section 3 presents an overview of the geomechanical models including salt dome geometry, cavern geometries and layout, model history, thermal conditions, and so forth. The constitutive model and material properties are also described. This section provides the discretized finite element meshes for examining the effect of each parameter. Section 4 provides the criteria for checking the structural stability of caverns, wells, and surface structures. Section 5 lists the computer codes used in these analyses and the file naming convention for the calculation and storing the files in a database. Section 6 describes the analyses results such as the cavern deformation due to salt creep, storage loss with time, subsidence on the surface, integrity of cavern wells, and cavern stability using criteria for dilatant damage and tensile failure, and so forth from the baseline model. The stress distributions around the caverns in the salt dome are illustrated in this section. Section 7 provides the effect of each parameter through comparing the results with variant value of each parameter to those from the baseline calculation. Section 8 provides summary of these calculations and concluding remarks. References are listed in Section 9. Every computational script such as FASTQ script for mesh generation, FORTRAN script for calculating the temperature at each node, input files for JAS3D, user-supplied subroutine to provide an internal pressure state in the caverns and to calculate the volume change of each caverns, ALGEBRA scripts for computing the subsidence, principal stresses, safety factor against dilatant damage, safety factor for shear failure are provided in the appendices. The computer analyses results from the models to examine each parameter effect are also provided in the appendices.

2. PARAMETERS

Parameters of interest are those capable of leading to salt damage around the cavern field. As mentioned in Section 1.1, the most likely place for damage to be initiated is at the top of a salt dome. This damage may become extensive enough to propagate across the salt and jeopardize the integrity of the caverns. Continued deformation and subsidence may result in crack propagation and/or dilation that extends into the storage areas. This situation appears to be associated with large volumetric closures in caverns in a small dome. Therefore, our suggested baseline model is a small dome in a relatively fast creeping salt formation. Individual parameters will be varied (one by one) from the baseline model to assess the impact on the integrity of the salt. This will establish the sensitivity of the predicted safety factor against damage to the individual parameter variations of interest. It will also constitute the initial scoping part of the study. If necessary and realistic, additional parameter sets will be selected dependent upon after review of the results. The specific modeling parameters to examine their impacts on the salt dome damage are listed in Table 1 along with the typical base values and the variants. Note that the first 7 items in the table are geologic parameters, which are characteristics of a site that cannot be changed, only measured. The final 3 parameters in the table are design related. Figure 1 shows the denotation of each parameter in Table 1 on the mesh.

Table 1: The specific modeling parameters with the typical base values and its variant.

	Check Effect	Parameter	Baseline	Variant	Comment
Geologic Parameter	Salt Creep Rate	Secondary Creep Constant, A_{SC} (s^{-1})	$A_{SC} = 11\times10^{12}$	$A_{SC} = 5\times10^{11}$ and $A_{SC} = 2\times10^{14}$	n=5 and μ=12.4 GPa, Q=10,000 cal/mol†
	Top of Salt Dome Depth ($d_{SD} = t_{OB} + t_{CR}$)	Thickness (ft) of Overburden, t_{OB}, and Caprock, t_{CR}	$t_{OB} = 1600$ $t_{CR} = 400$ $d_{SD} = 2000$	$t_{OB} = 100$ $t_{CR} = 400$ $d_{SD} = 500$	Maintain 400 ft of caprock, reduce overburden to 100 ft
	Dome Size, Standoff Distance	Dome Radius, r_{SD} (ft)	$r_{SD} = 3000$	$r_{SD} = 1700$	From center of model
	Caprock Thickness	Caprock Thickness, t_{CR} (ft)	$t_{OB} = 1600$ $t_{CR} = 400$	$t_{OB} = 400$ $t_{CR} = 1600$	Reduce overburden thickness to 400 ft and increase caprock thickness to 1600 ft
	Elastic Modulus of Caprock	Modulus of Caprock, E_{CR} (GPa)	$E_{CR} = 7$	$E_{CR} = 1$, $E_{CR} = 20$, and $E_{CR} = 100$	Based on Hoffman and Ehgartner [1992]
	Elastic Modulus of Surrounding Rock	Modulus of Rock, E_{SR} (GPa)	$E_{SR} = 70$	$E_{SR} = 4$, $E_{SR} = 10$, $E_{SR} = 20$, and $E_{SR} = 30$	High and low values are based on Richton data [Tammemagi et al., 1986]
	Lateral Stress Ratio†† of Surrounding Rock	Coefficient of Rock, $\mathcal{K}_{SR}$	$\mathcal{K}_{SR} = 0.49$	$\mathcal{K}_{SR} = 1$, and $\mathcal{K}_{SR} = 2$	Based on Lambe and Whitman [1979]; Hoek and Brown [1980]
Design Parameter	Cavern Size	Cavern Radius, r_C (ft)	$r_C = 100$	$r_C = 200$	Radius held constant with depth. Spacing of caverns is 750 ft
	Cavern Depth	Cavern Depth, d_C (ft)	$d_C = 2500$	$d_C = 1000$, $d_C = 2100$, and $d_C = 4000$	Cavern height (h_C) maintained at 2000 ft
	Number of Caverns	Number of Caverns, N_C	$N_C = 19$	$N_C = 31$	

†: variables in Eq. (2); ††: the ratio of the average horizontal to vertical stress.

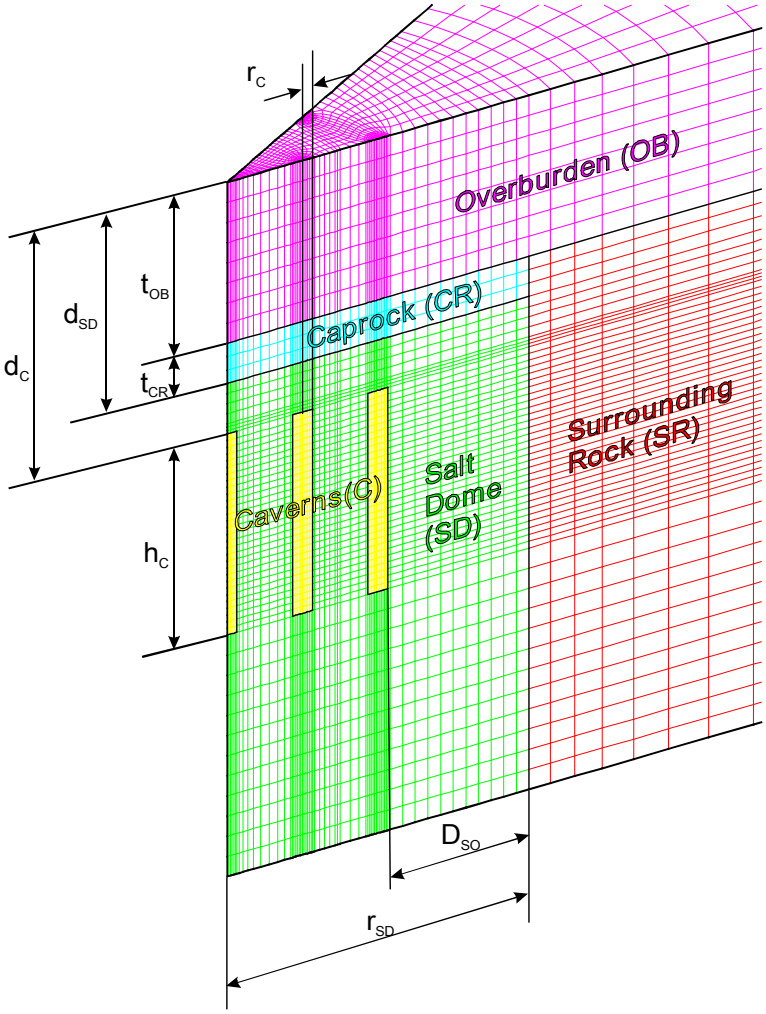

Figure 1: Denotation of each parameter in Table 1.

3. ANALYSIS MODEL

3.1. Baseline Model

3.1.1. Geomechanical model

Salt constitutive model

The scalar secondary creep strain rate is determined from the following law:

$$\dot{\varepsilon} = A_{SC}\left(\frac{\overline{\sigma}}{\mu}\right)^{n} \exp\left(-\frac{Q}{RT}\right) \tag{1}$$

where, $\dot{\varepsilon}$ = scalar secondary creep strain rate; $\overline{\sigma} = \sigma_1 - \sigma_3$ = Tresca equivalent stress; σ_1 = maximum principal stress; σ_3 = minimum principal stress; μ = elastic shear modulus = $E/2(1+\nu)$; E = elastic modulus; ν = Poisson's ratio; T = absolute temperature (K); A_{SC} = secondary creep constant (s^{-1}), n = stress exponent; Q = activation energy (cal/mole); and R = universal gas constant (cal/(mole·K)).

To make the simulations more manageable, the transient creep effects were ignored and the steady state creep response was treated using the power law creep model in JAS3D. In essence the transient creep in the early-time response was not represented in these simulations. The scalar secondary creep strain rate for the power law creep model in JAS3D is given by:

$$\dot{\varepsilon} = A\overline{\sigma}_{vm}^{n} \exp\left(-\frac{Q}{RT}\right) \tag{2}$$

where A = power law creep constant (Pa^{-n}/s) and $\overline{\sigma}_{vm} = \sqrt{3J_2}$ = von Mises equivalent stress (Pa); J_2 = second invariant of the deviatoric stress tensor.

For the case of triaxial compression ($\sigma_1 = \sigma_2 > \sigma_3$, where σ_i are the principal stresses), the Tresca equivalent stress and the von Mises equivalent stress are equal. Equating the two equations for scalar secondary creep strain rate allows the determination of the creep constant, *A*, used in the power law creep model [Munson et al., 1989].

$$A = \frac{A_{SC}}{\mu^{n}} \tag{3}$$

The values used as baseline input data in the present analyses are listed in Table 2.

Table 2: Material properties of salt for baseline analyses.

Parameter	Unit	Value	Reference
Young's modulus (*E*)	GPa	31	Krieg, 1984
Density (ρ)	kg/m^3	2300	Krieg, 1984
Poisson's ratio (ν)	-	0.25	Krieg, 1984
Elastic modulus reduction factor (*RF*)	-	1.0	
Bulk modulus (*K*)	GPa	20.7	Computed from *E* and ν
Elastic shear modulus (μ)	GPa	12.4	Computed from *E* and ν
Stress exponent (*n*)	-	5.0	
Secondary creep constant (A_{SC})	s^{-1}	1.1×10^{13}	
Power law creep constant (*A*)	Pa^{-n}/s	3.75×10^{-38}	Computed from A_{SC}
Structure multiplication factor (*SMF*)	-	1.0	
Activation energy (*Q*)	cal/mol	10,000	
Universal gas constant (*R*)	cal/(mol·K)	1.987	-
Input thermal constant (*Q/R*)	K	5033	-
Lateral stress ratio (κ)	-	1.0	σ_h / σ_v

Lithologies around the salt dome

An elastic model is assumed for the lithologies encompassing the salt dome. The surface overburden layer is assumed to exhibit elastic material behavior. The overburden layer is considered isotropic and has no assumed failure criteria. The caprock layer is also assumed to behave elastically. The rock surrounding the salt dome is assumed isotropic, homogeneous elastic rock. The mechanical properties used in the baseline analysis are listed in Table 3.

Table 3: Material properties of lithologies around salt dome used in the analyses.

	Unit	Overburden	Caprock	Surrounding Rock
Young's modulus (*E*)	GPa	0.1	7.0	70
Density (ρ)	kg/m^3	1874	2500	2500
Poisson's ratio (ν)	-	0.33	0.29	0.33
Lateral stress ratio (κ)	-	0.49	0.41	0.49

3.1.2. Cavern geometry and layout

Symmetric 19-cavern field model at West Hackberry is used for the baseline model so that readily deployed pie-slice models can be used [Ehgartner and Sobolik, 2002]. The 30-degree wedge model incorporates dome geometry appropriate for the site. Periodic workovers are simulated, but

progressive leaches of the caverns for the drawdowns are not considered. Figure 2 shows the schematic of 19-cavern field layout and cavern rings to consider the periodic workovers. Figure 3 shows the computational mesh and boundary conditions used for the baseline calculation. Four material blocks are used in the model. They are overburden, caprock, salt dome, and the lithologies surrounding the salt dome.

The diameter of the caverns is 200 ft, the distance between caverns is 750 ft, the dome radius is 3000 ft, and the far-field boundary is 15,000 ft from the center of the dome. As listed in Table 1, the overburden thickness is 1600 ft, the caprock thickness is 500 ft, the depth of salt dome top is 2000 ft, and the depth of cavern top is 2500 ft.

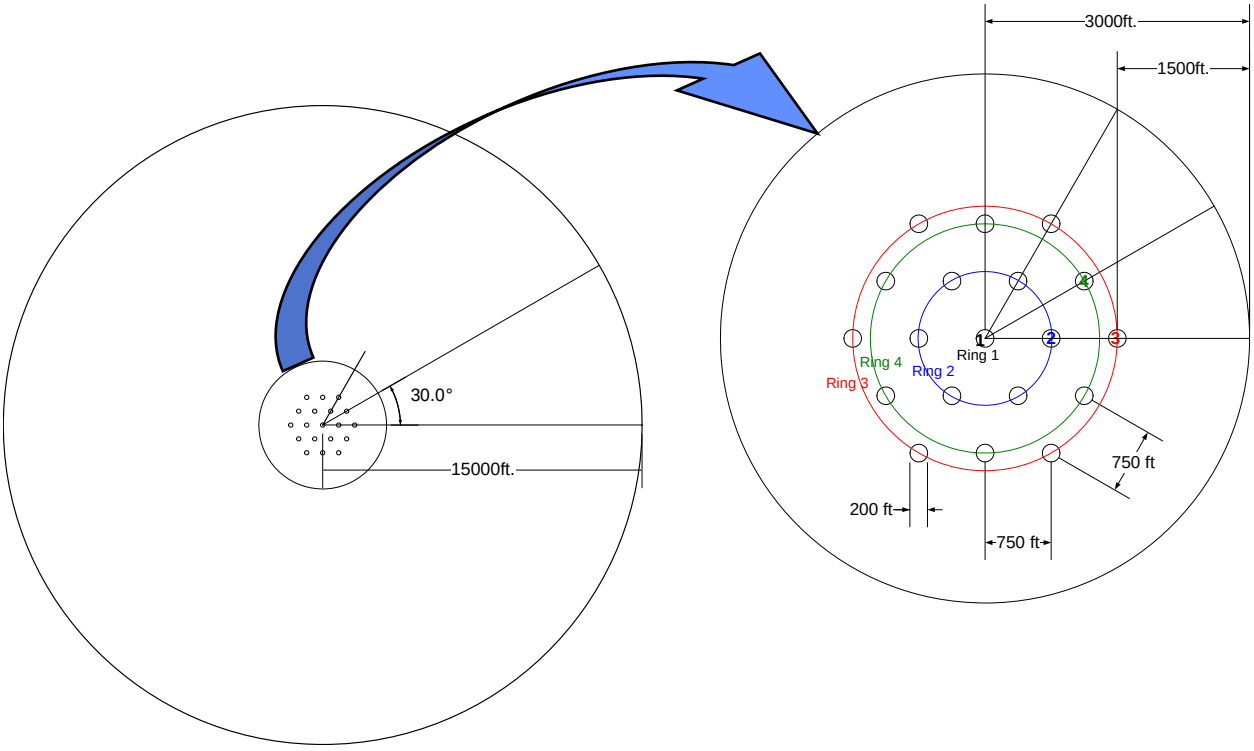

Figure 2: Schematic of 19-cavern field layout and cavern ring nomenclature.

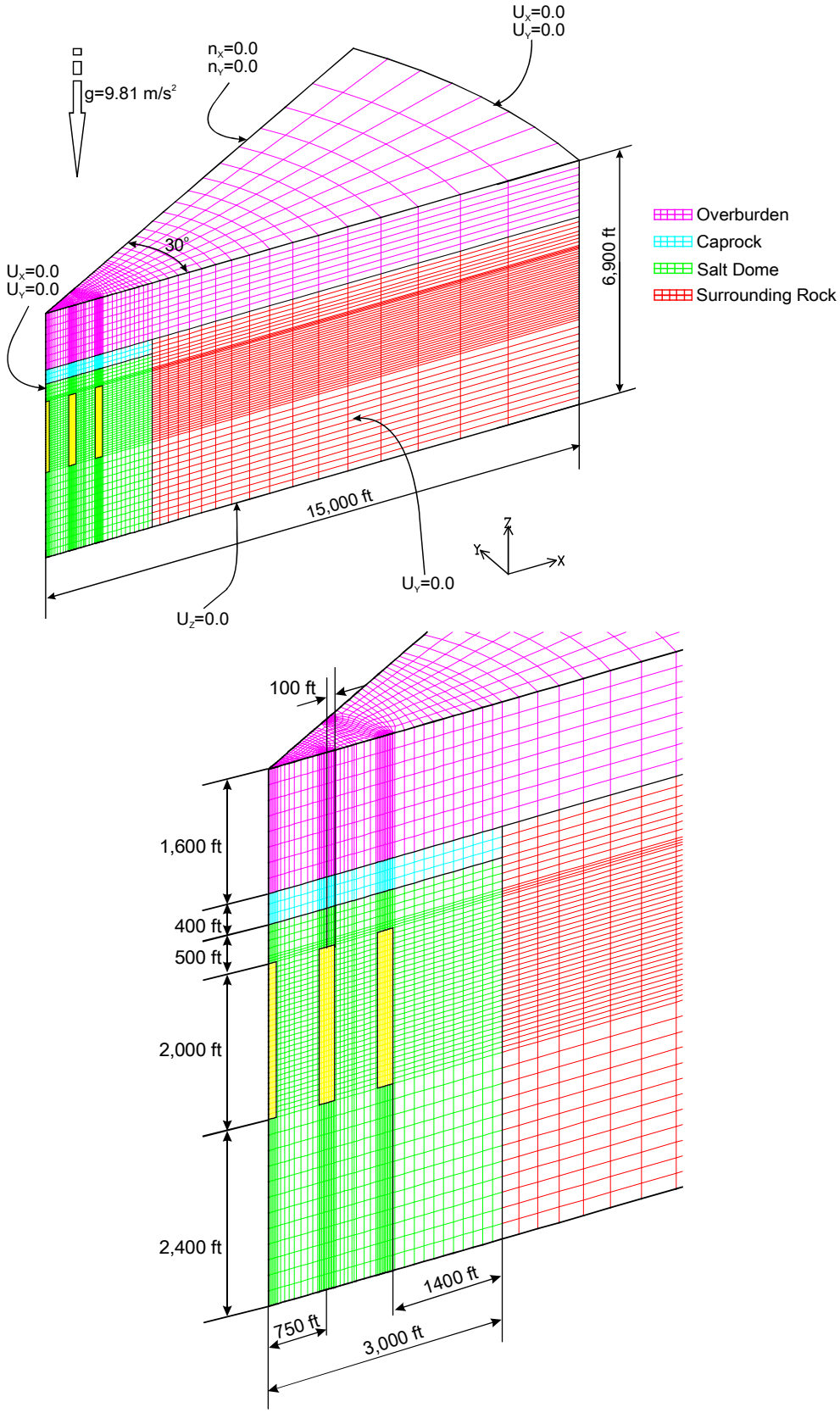

Figure 3: Computational mesh and boundary conditions for the baseline calculation.

3.1.3. Model history

The analysis simulates cavern leaching by gradually and systematically replacing the salt mesh regions of the cavern volume with fresh water regions over the one year construction period. At this point in time, the SPR caverns were assumed to be filled with crude oil and then permitted to creep for 45 years. Leaching is assumed to occur uniformly along the entire height of the cavern. However, leaching is not permitted in the floor or the roof of the caverns. The simulation was performed up to 46 years. After the initial leach, all caverns in the array were periodically and systematically subjected to cavern workovers.

Both normal cavern operating conditions and workover conditions are simulated. For normal operating conditions, the cavern pressure is based on a wellhead pressure of 925 psi because the depth of cavern roof is 2,500 ft. For workover conditions, zero wellhead pressure is used. Workover durations are three months. For both normal and workover conditions, the caverns are assumed to be full of oil having a pressure gradient of 0.37 psi/ft of depth.

The schedule for workover is based on dividing the cavern array into "cavern rings" of constant radius, where the numbered caverns shown in the 30^{o} wedge section of Figure 2 each represent the several caverns of the ring. The solution results for the representative cavern are identical for all of the caverns in a given ring. Thus, Cavern Ring 1 represents one cavern, Cavern Ring 2 represents six caverns, as does Cavern Ring 3 and Cavern Ring 4.

To better simulate actual field conditions, not all caverns are in workover mode at the same time. The central cavern (Cavern 1 in Figure 2) in the field is the first cavern in the workover sequence beginning one year after initial cavern leaching, and thereafter undergoes a workover every five years until the end of the simulations. The next closest neighboring caverns (Cavern Ring 2 in Figure 2) are due to be worked over the following year. Because of mesh symmetry, this means workover pressures are applied to the six caverns that make up this second set of caverns, containing Cavern 2, at the same time. This results in the six caverns closest to Cavern 1 at low pressure beginning workover one year after workover of the central cavern. This condition enables the web of salt between adjacent caverns in workover mode to be examined for stability. In addition, the webs of salt between caverns in workover mode and those under normal operating pressures can be studied. The workover sequence continues with the outmost cavern along the 0° symmetry plane (Cavern Ring 3 in Figure 2) being subject to workover pressures one year after the second set of caverns. The final set of caverns to undergo workover in the fifth year is that along 30° symmetry plane (Cavern Ring 4 in Figure 2). This cycle is repeated every five years until the end of the simulations. Figure 4 shows the wellhead pressure change in each cavern.

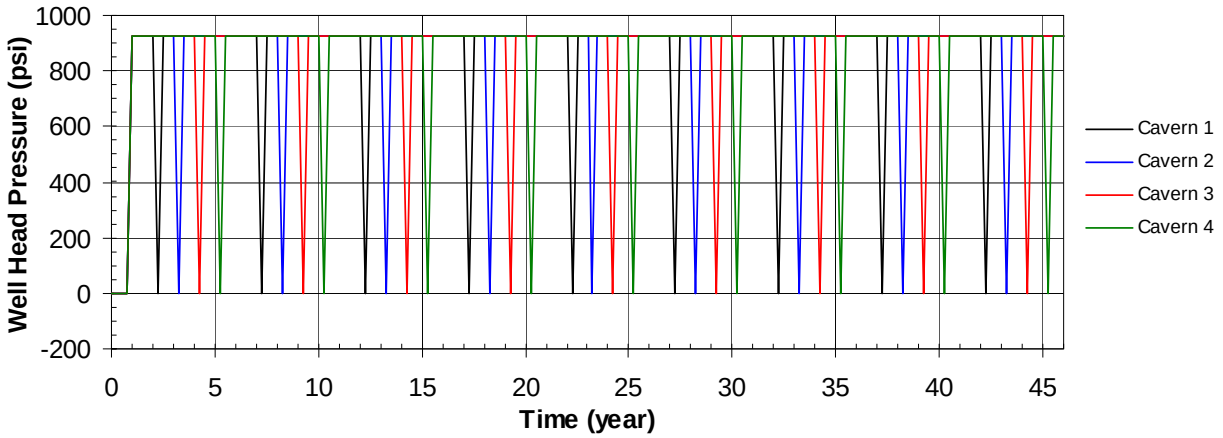

Figure 4: Wellhead pressure change in each SPR cavern.

3.1.4. Thermal conditions

The finite element model includes a depth-dependent temperature gradient, which starts at 98.6°F (37.0°C) at the surface and increases at the rate of 0.0107°F/ft (1.95°C/100 m). The temperature profile is based on the average temperature data recorded in well logs from West Hackberry prior to leaching [Ballard and Ehgartner, 2000]. The temperature distribution is important because the creep response of the salt is temperature dependent. Radial temperature gradients due to cavern cooling effects from the cavern contents are not considered in these calculations. Previous 2D cavern studies have shown the predicted cavern deformation to be insensitive to the developed radial thermal gradients [Hoffman, 1992]. The FORTRAN script for calculating the temperature at each node is provided in Appendix B.

3.2. Model Changes to Examine the Effect of Salt Creep Rate

To examine the salt creep rate effect, the analyses are conducted using secondary creep constants of 5×10^{11} (s^{-1}) and 2×10^{14} (s^{-1}) instead of 1.1×10^{13} (s^{-1}) for the baseline. Then power law creep constants for the computer input data are calculated to be 1.71×10^{-39} (Pa^{-n}/s) and 6.82×10^{-37} (Pa^{-n}/s), respectively instead of 3.75×10^{-38} (Pa^{-n}/s). The mesh, the model history, and the thermal conditions are the same as those for the baseline. All of the material properties except the creep constant for the salt dome are also the same as those for the baseline.

3.3. Model Changes to Examine the Depth of Salt Dome Top Effect

To examine the depth effect of salt dome top, the mesh was modified so that the depth of salt dome top is 500 ft (Figure 5) instead of 2000 ft for the baseline. The cavern depth is maintained at 2500 ft. The material properties for the salt dome, the overburden, the caprock, and the surrounding rock are the same as those for the baseline. The model history and the thermal conditions are also the same as those for the baseline.

To examine the depth of salt dome top effect with faster salt creep rate, a secondary creep constant of 2×10^{14} (s^{-1}) instead of 1.1×10^{13} (s^{-1}) was applied on the modified mesh. The material properties for the fast creeping salt (FCS) based on a dome in the Gulf Coast are also applied for

examining with the actual lithologies. The FCS dome, which has faster salt creep rate than other sites, is located east of Galliano, LA in Lafourche Parish. All of the material properties except the creep constant for the salt dome are the same as those for the baseline. The model history and the thermal conditions are also the same as those for the baseline. The model history and the thermal conditions are also the same as those for the baseline. Table 4 lists the parameter values used for the computer input to examine the depth of salt dome top effect. The bold fonts indicate the different values from the baseline.

Table 4: The parameter values used to examine the depth of salt dome top effect.

Parameter	Unit	Baseline d_{SD}=2000 A_{SC}=1.1×10^{13}	d_{SD}=500 A_{SC}=1.1×10^{13}	d_{SD}=500 FCS	d_{SD}=500 A_{SC}=2×10^{14}
Overburden Thickness (t_{OB})	ft	1600	**100**	**100**	**100**
Caprock Thickness (t_{CR})	ft	400	400	400	400
Depth of Salt Dome Top ($d_{SD} = t_{OB} + t_{CR}$)	ft	2000	**500**	**500**	**500**
Depth of Caverns (d_C)	ft	2500	2500	2500	2500
Secondary Creep Constant (A_{SC})	s^{-1}	1.1×10^{13}	1.1×10^{13}	**2.26×10^{13}**	**2×10^{14}**
Power Law Creep Constant (A)	Pa^{-n}/s	3.75×10^{-38}	3.75×10^{-38}	**7.72×10^{-38}**	**6.82×10^{-37}**
Bulk modulus (K)	Pa	2.07×10^{10}	2.07×10^{10}	**3.41×10^{10}**	2.07×10^{10}
Two mu (2μ)	Pa	2.48×10^{10}	2.48×10^{10}	**1.94×10^{10}**	2.48×10^{10}

3.4. Model Changes to Examine the Effect of Dome Size and Standoff Distance

To examine the effect of dome size and standoff distance, the mesh was modified so that the radius of salt dome is 1700 ft instead of 3000 ft for the baseline as shown Figure 6. The standoff distance from the edge of the outmost cavern to the edge of the dome is then 100 ft instead of 1400 ft for the baseline. The material properties for the salt dome, the overburden, the caprock, and the surrounding rock are the same as those for the baseline. The model history and the thermal conditions are also the same as those for the baseline.

3.5. Model Changes to Examine the Effect of Caprock Thickness

To examine the effect of caprock thickness, the mesh was modified so that the caprock thickness is 1600 ft instead of 400 ft for the baseline as shown Figure 7. The depth of salt dome top was maintained at 2000 ft. The overburden thickness was then 400 ft instead of 1600 ft for the baseline. The material properties for the salt dome, the overburden, the caprock, and the surrounding rock are the same as those for the baseline. The model history and the thermal conditions are also the same as those for the baseline.

3.6. Model Changes to Examine the Effect of the Elastic Modulus of the Caprock

To examine the effect of the elastic modulus of the caprock, analyses were conducted using 1 GPa, 20 GPa, 100 GPa as the elastic moduli of caprock instead of 7 GPa for the baseline . The baseline mesh shown in Figure 3 was used. The model history and the thermal conditions are the same as those for the baseline. All of the material properties except the elastic modulus of caprock are also the same as those for the baseline.

3.7. Model Changes to Examine the Effect of the Elastic Modulus of the Surrounding Rock

To examine the effect of the elastic modulus of the surrounding rock, analyses were conducted using 4 GPa, 10 GPa, 20 GPa and 30 GPa for the elastic moduli of surrounding rock instead of 70 GPa used in the baseline. The upper and lower bound values are derived from the Richton site data [Tammermagi et al., 1986]. The baseline mesh was used. The model history and the thermal conditions are the same as those for the baseline. All of the material properties except the elastic modulus of surrounding rock are also the same as those for the baseline.

3.8. Model Changes to Examine the Effect of the Lateral Stress Ratio of the Surrounding Rock

The ratio of horizontal to vertical stress in subsurface is expressed by a factor called the *coefficient of lateral stress* or *lateral stress ratio* [Lambe and Whitman, 1979], and is denoted by the symbol $\mathcal{K}$:

$$\mathcal{K} = \frac{\sigma_h}{\sigma_v} \tag{4}$$

where, σ_h = average horizontal stress; and σ_v = vertical stress [Hoek and Brown, 1980].

The lateral stress ratio of surrounding rock rather than those of caprock or overburden may have large impact on the salt dome behavior because the dome is encircled by the surrounding rock. To examine the effect of lateral stress ratio of the surrounding rock, analyses are conducted using $\mathcal{K}$ values of 1.0 and 2.0 instead of 0.49 for the baseline. The baseline mesh was used. The model history and the thermal conditions are the same as those for the baseline. All of the material properties except the lateral stress ratio of surrounding rock are the same as those for the baseline.

3.9. Model Changes to Examine the Effect of Cavern Size

To examine the effect of cavern size, the mesh was modified so that the cavern radius is 200 ft instead of 100 ft for the baseline (Figure 8). The spacing of caverns was maintained at 750 ft as the baseline. The material properties for the salt dome, the overburden, the caprock, and the surrounding rock are the same as those for the baseline. The model history and the thermal conditions are also the same as those for the baseline.

3.10. Model Changes to Examine the Effect of Cavern Depth

To examine the effect of cavern depth, the mesh was modified so that the top of the caverns are at 1000 ft, 2100 ft, and 4000 ft depth instead of 2500 ft for the baseline as shown Figures 9 through 11. The depth to the top of the salt dome is maintained at 2000 ft. However, the depth of salt dome top is decreased to 500 ft when a cavern depth of 1000 ft was modeled (Figure 9).

Table 5 lists the parameter values for the mesh used to examine the depth of cavern effect. The material properties for the salt dome, the overburden, the caprock, and the surrounding rock are the same as those for the baseline. The model history and the thermal conditions are also the same as those for the baseline except for the cavern pressure for normal operating conditions because the wellhead pressure depends on the cavern depth. The wellhead pressures for the cavern depths of 1000 ft, 2100 ft, and 4000 ft are 370 psi, 777 psi, and 1480 psi, respectively, instead of 925 psi for the baseline. The bold fonts indicate the different values from the baseline.

Table 5: The parameter values to examine the depth of cavern effect.

Parameter	Unit	d_C=1000 (Figure 9)	d_C=2100 (Figure 10)	Baseline d_C=2500 (Figure 3)	d_C=4000 (Figure 11)
Overburden Thickness (t_{OB})	ft	**100**	1600	1600	1600
Caprock Thickness (t_{CR})	ft	400	400	400	400
Depth of Salt dome top ($d_{SD} = t_{OB} + t_{CR}$)	ft	**500**	2000	2000	2000
Depth of Caverns (d_C)	ft	**1000**	**2100**	2500	**4000**
Wellhead Pressure for Normal Operating Conditions	psi	**370**	**777**	925	**1480**

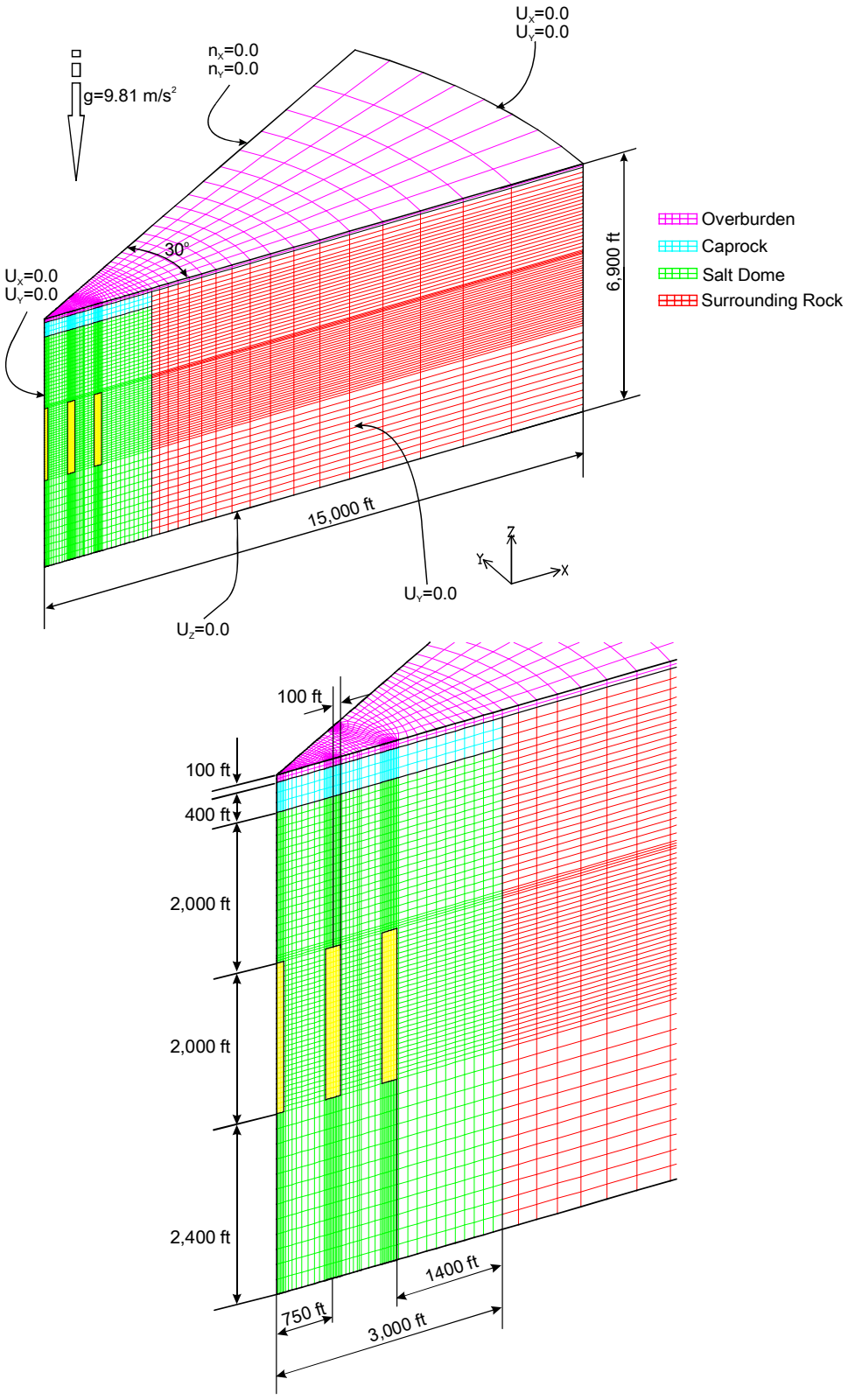

Figure 5: Computational mesh and boundary conditions to examine the depth of salt dome top effect, 500 ft instead of 2000 ft (cavern depth, 2500 ft).

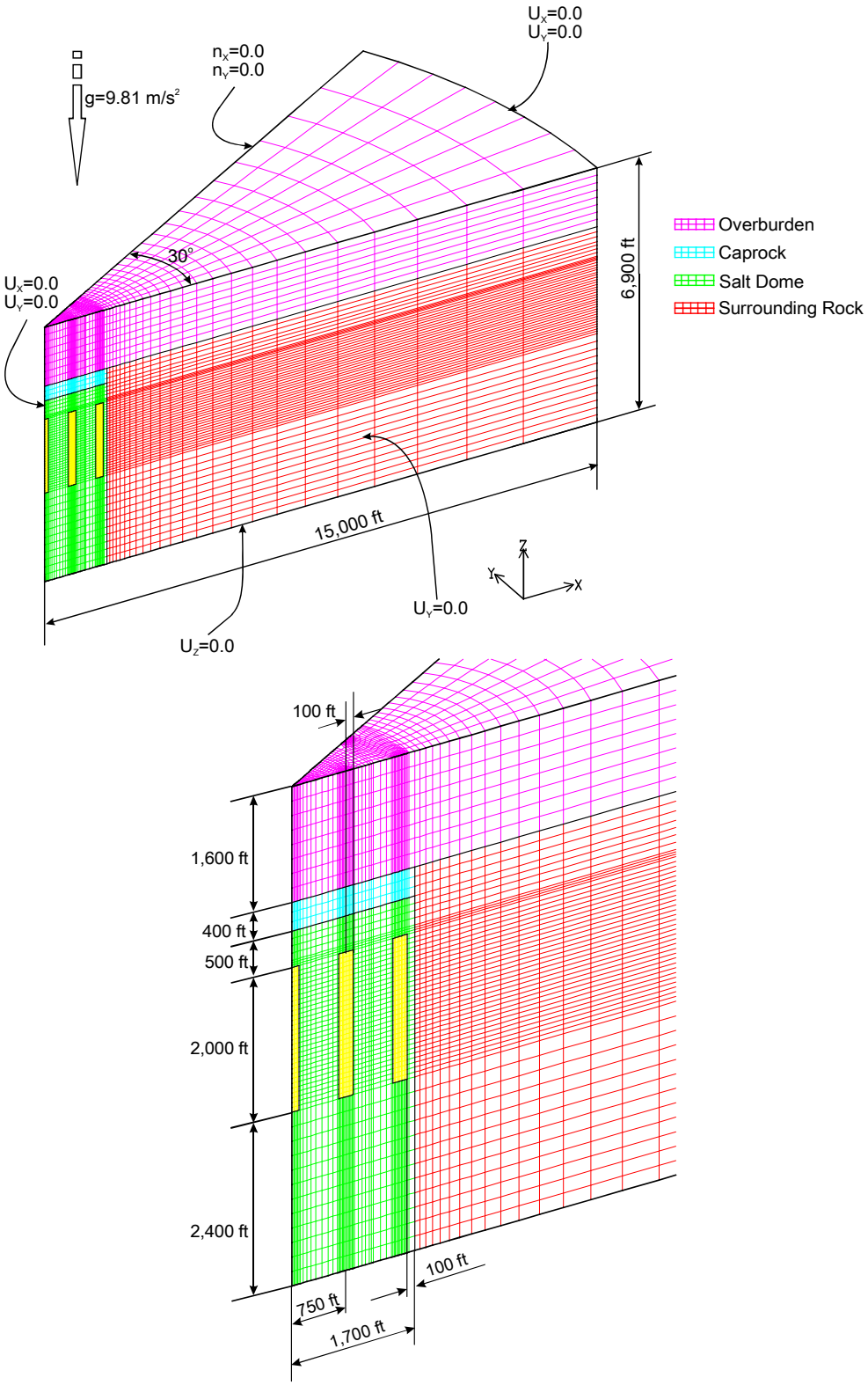

Figure 6: Computational mesh and boundary conditions used to examine the dome size and standoff distance effect. Dome radius is 1700 ft instead of 3000 ft. Standoff distance is 100 ft instead of 1400 ft.

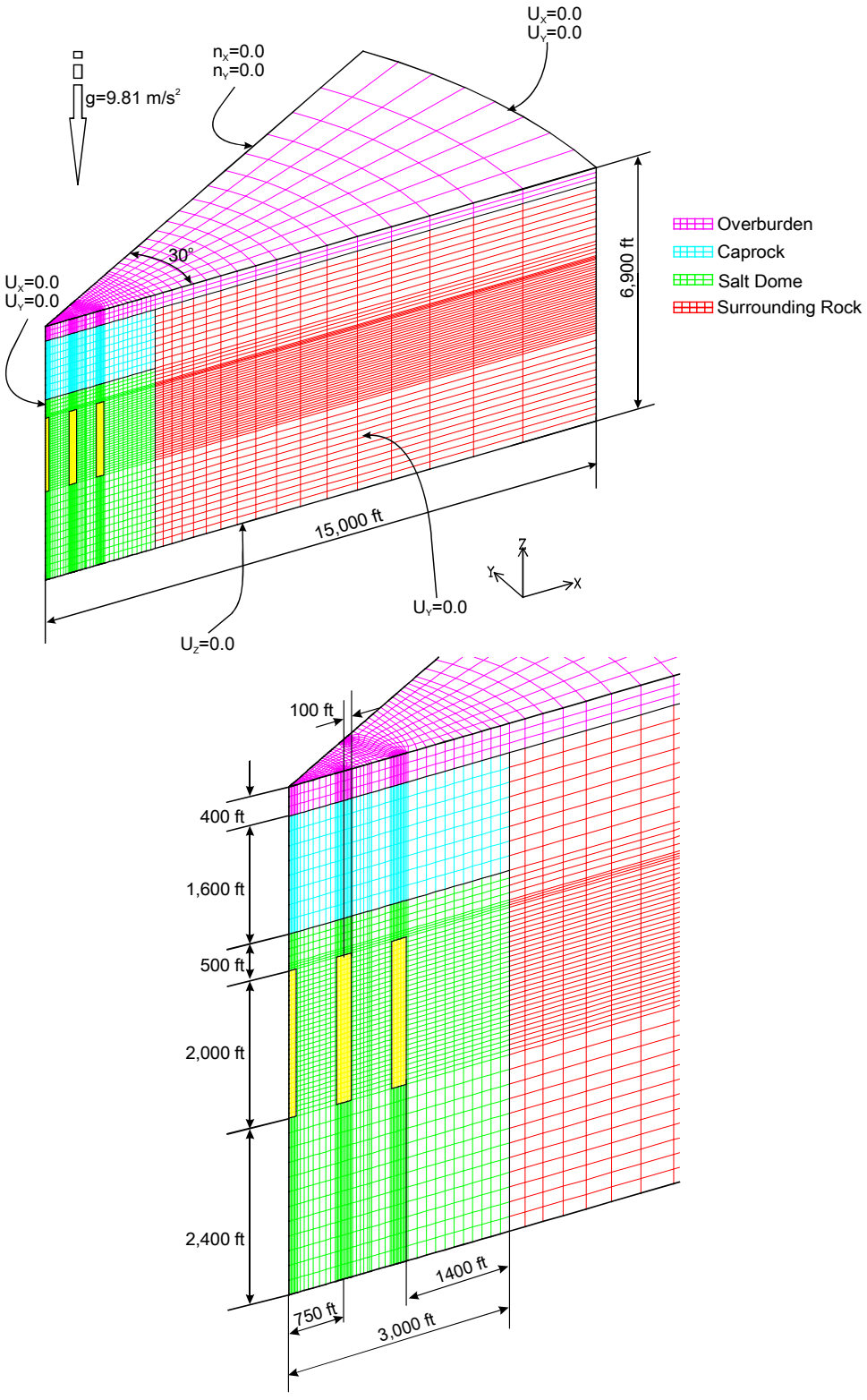

Figure 7: Computational mesh and boundary conditions used to examine the caprock thickness effect. Caprock thickness is 1600 ft instead of 400 ft. Overburden thickness is 400 ft instead of 1600 ft.

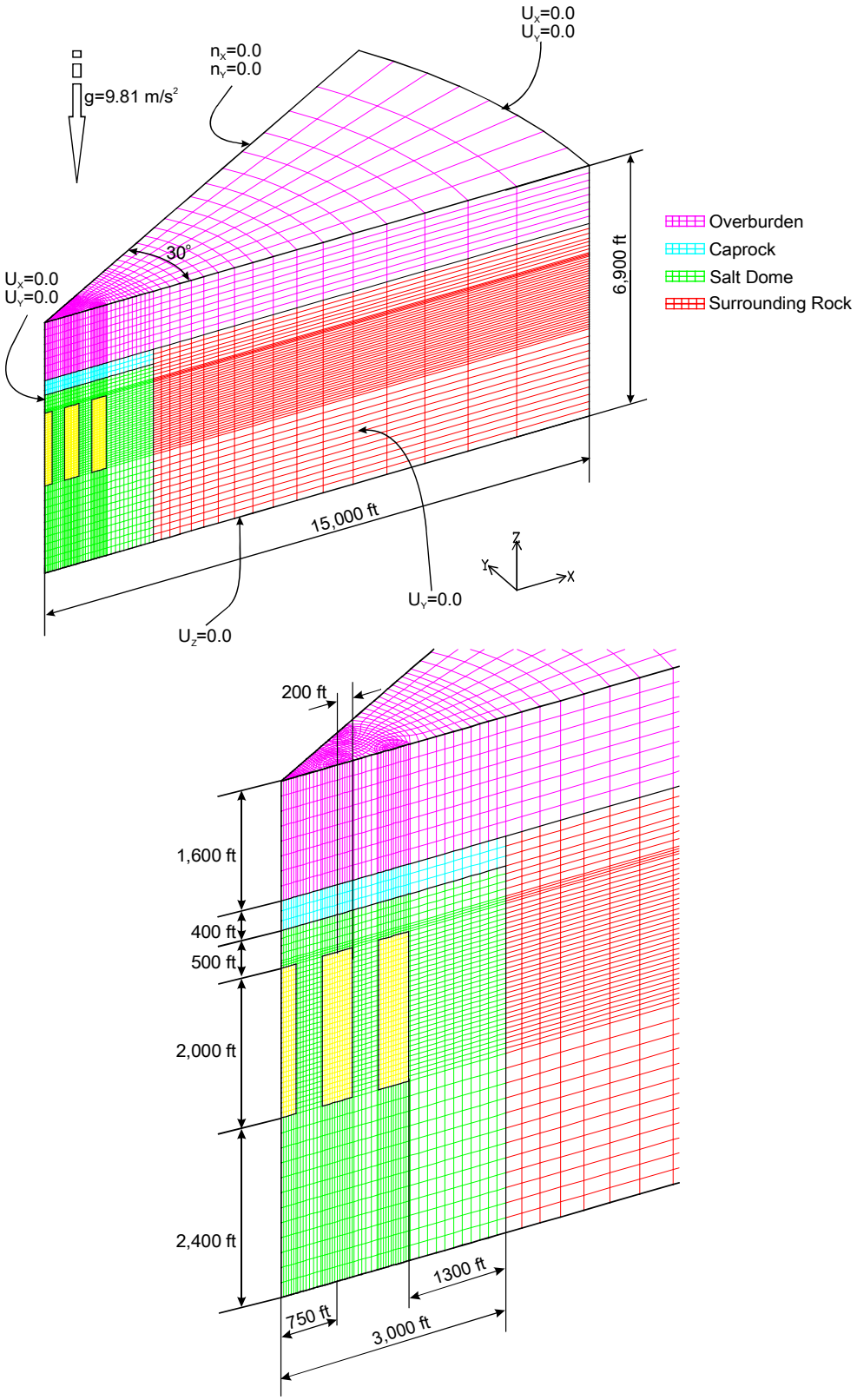

Figure 8: Computational mesh and boundary conditions used to examine the cavern size effect. Cavern radius is 200 ft instead of 100 ft.

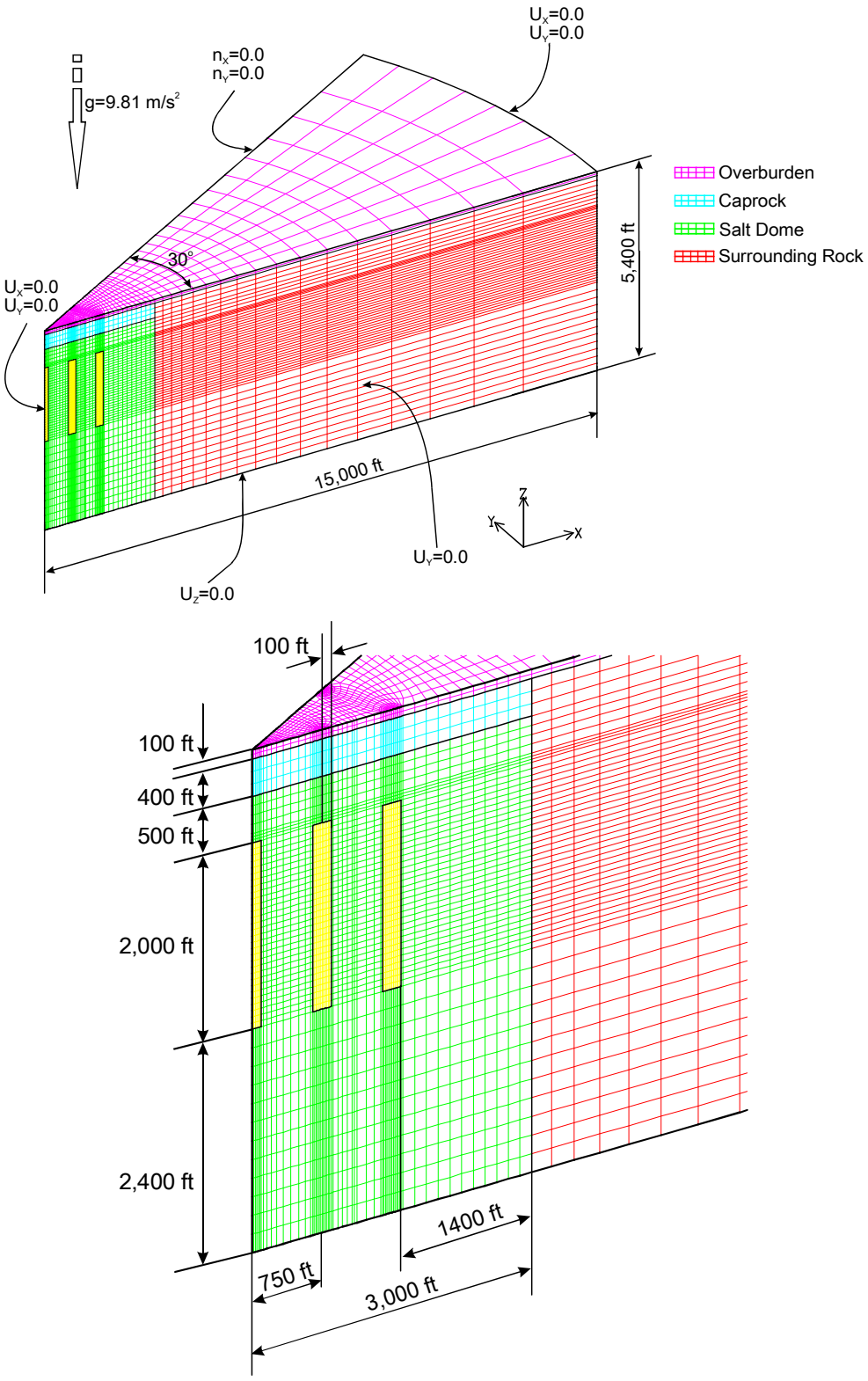

Figure 9: Computational mesh and boundary conditions used to examine the depth of cavern effect. Cavern depth is 1000 ft instead of 2500 ft. Thickness of overburden is 100 ft instead of 1600 ft.

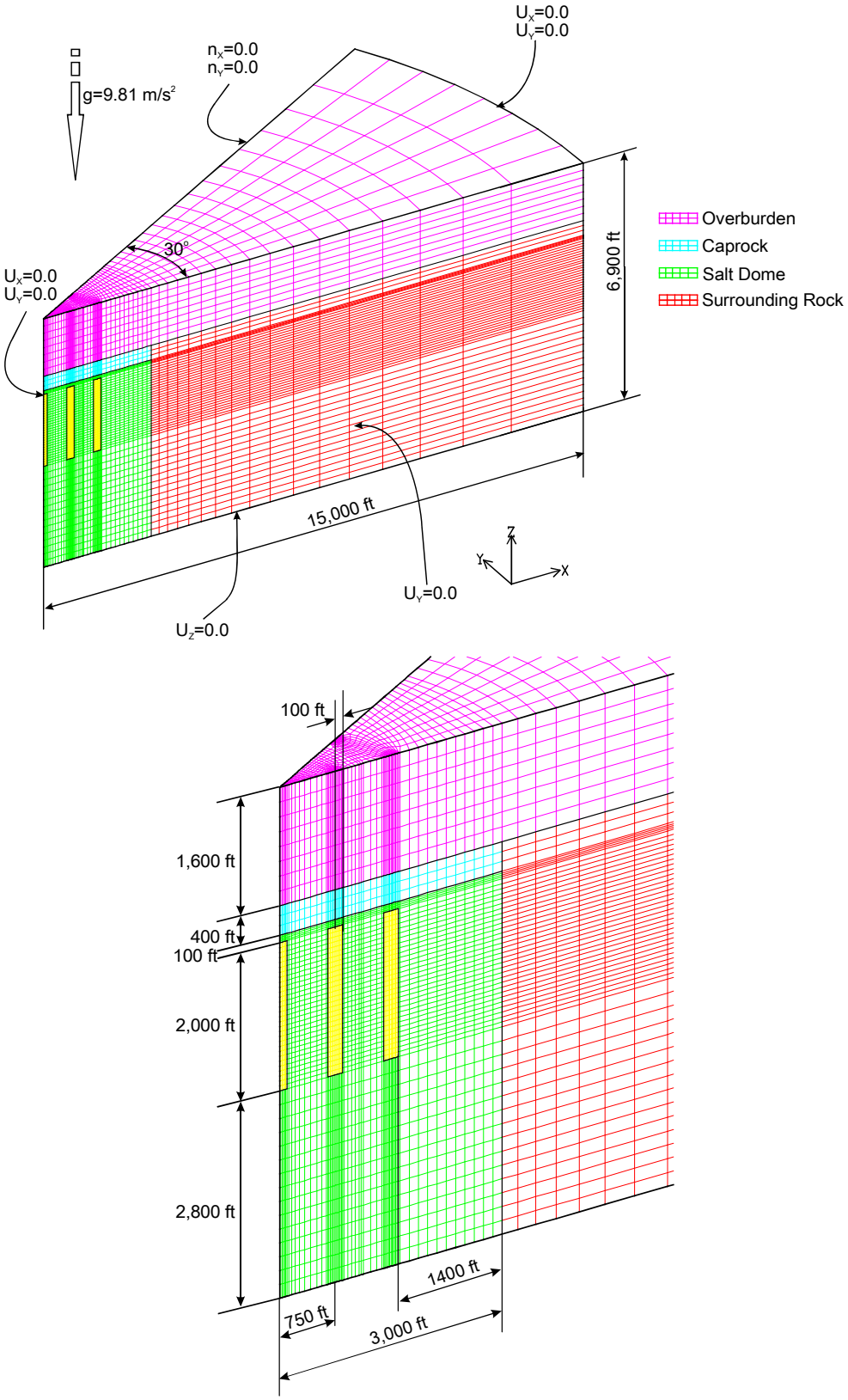

Figure 10: Computational mesh and boundary conditions used to examine the depth of cavern effect. Cavern depth is 2100 ft instead of 2500 ft.

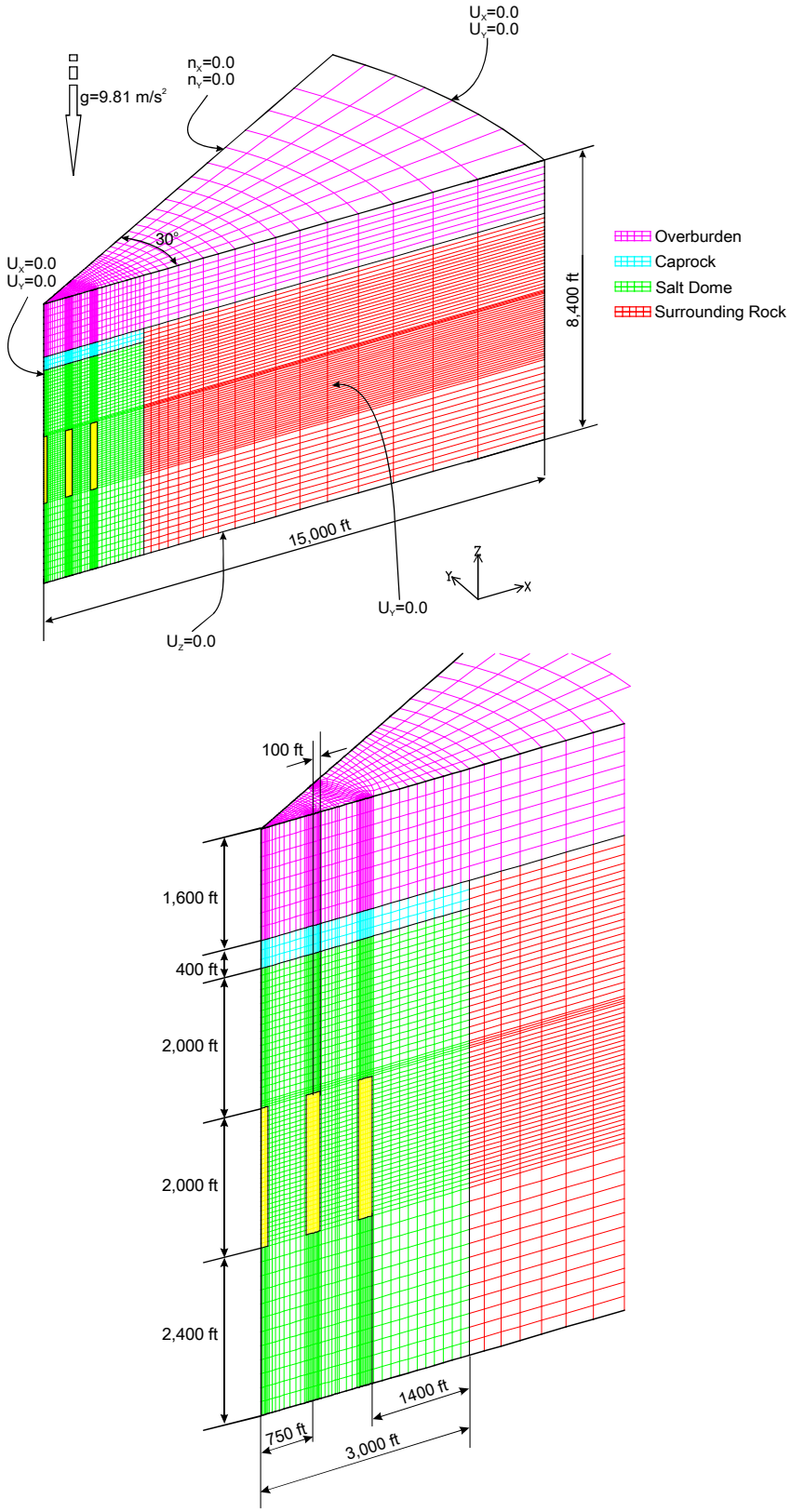

Figure 11: Computational mesh and boundary conditions used to examine the depth of cavern effect. Cavern depth is 4000 ft instead of 2500 ft.

3.11. 31-Cavern Model to Examine the Number of Caverns Effect

3.11.1. Material properties

The overburden, the caprock, and the surrounding rock material properties for the 31-cavern salt dome model are the same as those for the baseline.

3.11.2. Model cavern geometry and layout

To examine the number of caverns effect, a symmetric 31-cavern field model was established so that readily deployed pie-slice models can be used. The 30-degree wedge model incorporates dome geometry appropriate for the site. Periodic workovers are simulated, but progressive leaches of the caverns for the drawdowns are not considered. Figure 12 shows the schematic of 31-cavern field layout and cavern rings considered during the periodic workovers. Figure 19 shows the computational mesh and boundary conditions for 31-cavern model calculation. Again the same four baseline material blocks are used in the model: the overburden, caprock, salt dome, and surrounding lithologies.

The diameter of the caverns is 200 ft, the distance between the caverns is 750 ft, the dome radius is 3000 ft, and the far-field boundary is 15,000 ft from the center of the dome as for the baseline. The overburden thickness, the caprock thickness, the depth of salt dome top, and the depth of cavern top are the same as those for the baseline.

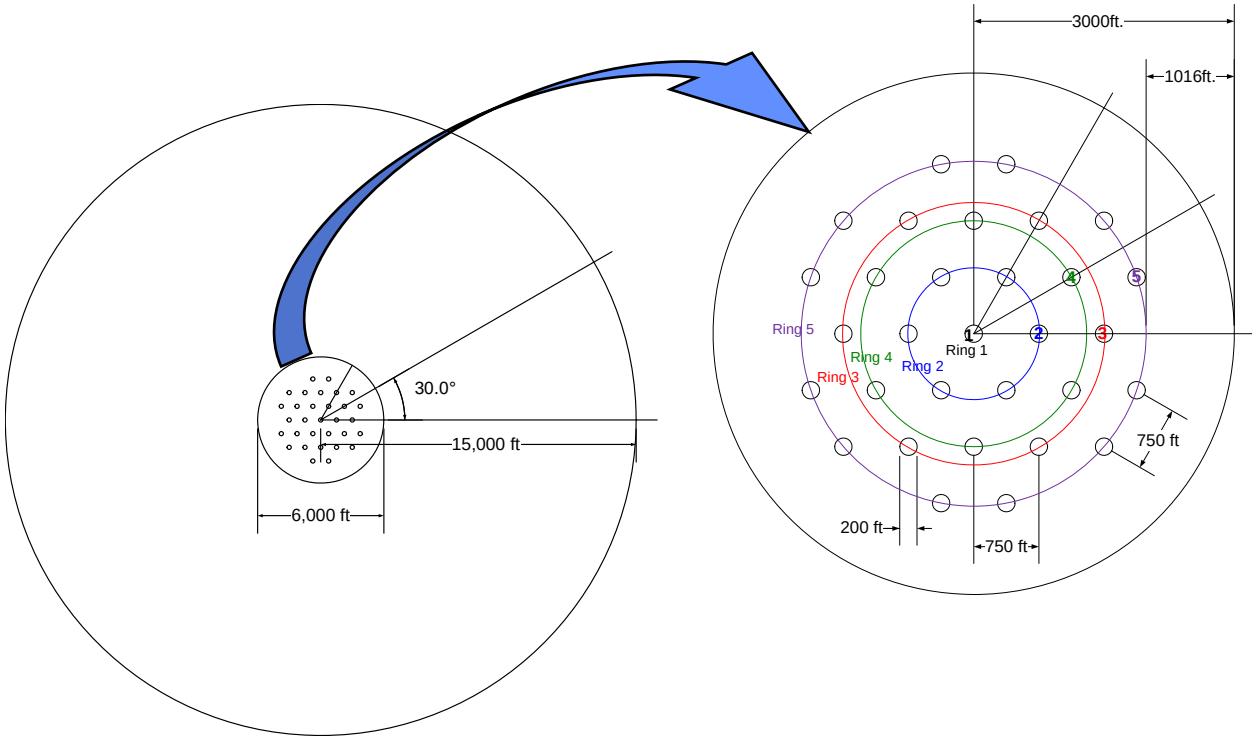

Figure 12: Schematic of 31-cavern field layout and cavern ring nomenclature.

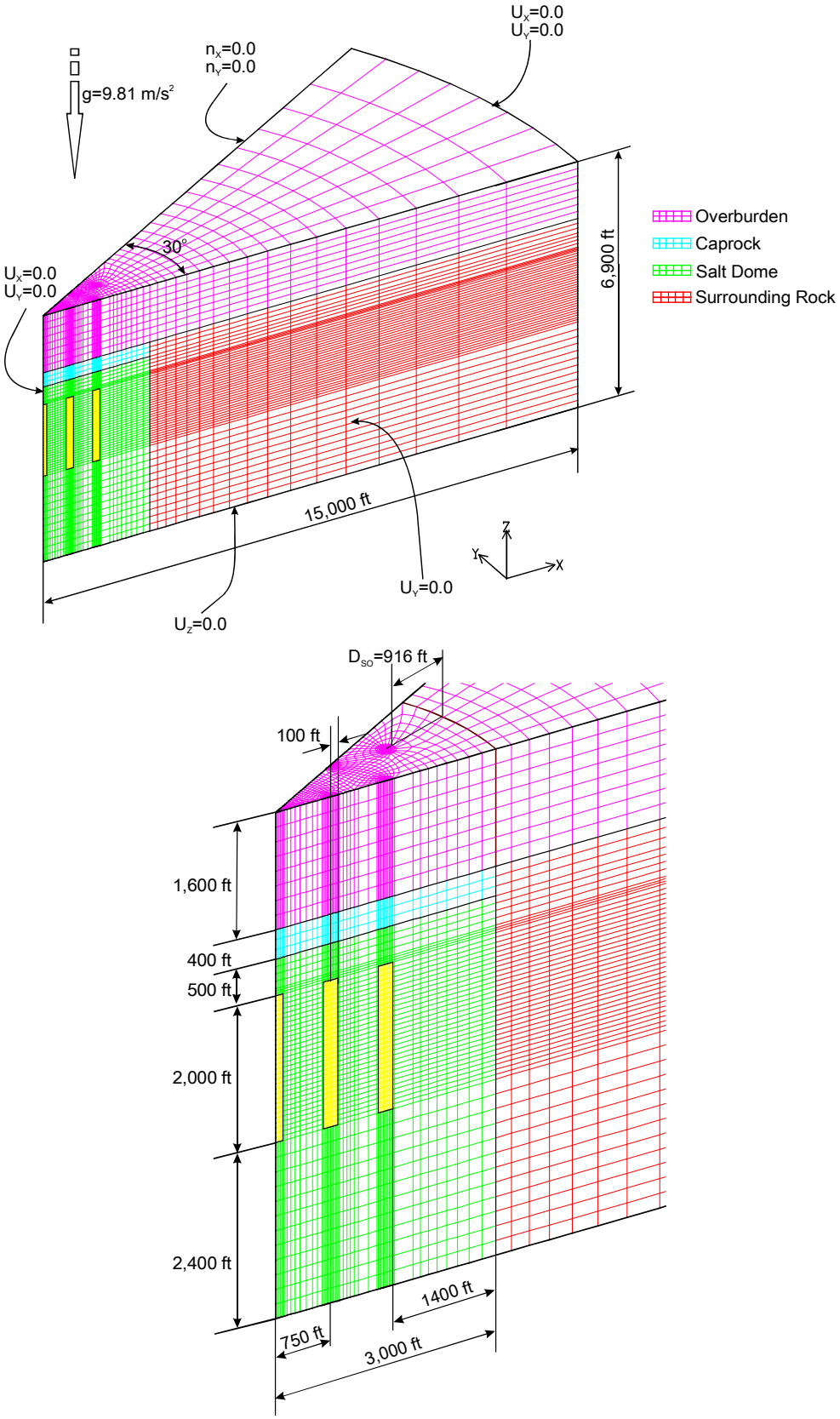

Figure 13: Computational mesh and boundary conditions for 31-cavern model. Standoff distance is 916 ft instead of 1400 ft for 19-cavern model.

3.11.3. Model history

The 31-cavern model history was the same as that for the baseline except for the workover schedule. As before, the schedule for workover was based on dividing the cavern array into "cavern rings" of constant radius where the numbered caverns, shown in the 30° wedge section of Figure 12, represent several caverns of the ring. Thus, Cavern Ring 1 represents one cavern; Cavern Ring 2 represents six caverns, as does Cavern Rings 3 and 4. Cavern Ring 5 represents 12 caverns. The solution results for the representative cavern are identical for all of the caverns in a given ring.

To better simulate actual field conditions, not all caverns are in workover mode at the same time. The central cavern (Cavern 1 in Figure 12) in the field is the first cavern in the workover sequence beginning one year after initial cavern leaching. It undergoes a workover every five years until the end of the simulations. The next closest neighboring caverns (Cavern Ring 2 in Figure 12) are due to be worked over the following year. Because of mesh symmetry, this means workover pressures are applied to the six caverns that make up this second set of caverns at the same time. This results in the six caverns closest to Cavern 1 being at low pressure beginning workover one year after workover of the central cavern. This enables the web of salt between adjacent caverns in workover mode to be examined for stability. In addition, the webs of salt between caverns in workover mode and those under normal operating pressures can be studied. The workover sequence continues with the cavern along the 0° symmetry plane (Cavern Ring 3 in Figure 12) being subject to workover pressures one year after the second set of caverns. The forth set of caverns, those along the 30° symmetry plane corresponding to Cavern Ring 4 in Figure 12, undergo workover in the third year after workover of Cavern 1. The final set of outmost caverns to undergo workover, in the fifth year of the cycle, is that set which includes Cavern 5 (Cavern Ring 5 in Figure 12). This cycle is repeated every five years until the end of the simulations. Figure 14 shows the wellhead pressure change in each cavern in the 31-cavern model.

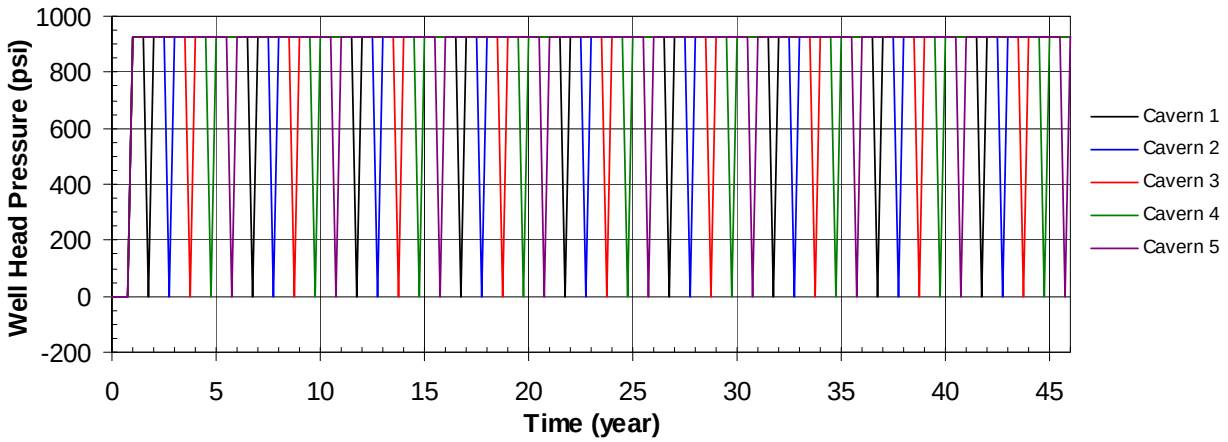

Figure 14: Wellhead pressure change in each SPR cavern in the 31-cavern model.

4. FAILURE CRITERIA

4.1. Structural Stability of Salt Dome

Potential damage to or around the SPR caverns was evaluated based on two failure criteria: dilatant damage and tensile failure. To check for dilatant damage, the following dilatancy criterion [Tavares, 1994] is used:

$$D = \frac{0.25 \cdot I_1}{\sqrt{J_2}} \tag{4}$$

where, $D =$ damage factor

$I_1 = \sigma_1 + \sigma_2 + \sigma_3 = 3\sigma_m$ is the first invariant of the stress tensor.

$\sqrt{J_2} = \sqrt{\frac{(\sigma_1 - \sigma_2)^2 + (\sigma_2 - \sigma_3)^2 + (\sigma_3 - \sigma_1)^2}{6}}$ is the square root of the second invariant of the deviatoric stress tensor

σ_1, σ_2, and σ_3 are the maximum, intermediate, and minimum principal stresses, respectively.

σ_m is the mean stress.

When $D \leq 1$, the shear stresses in the salt (J_2) are large compared to the mean stress (I_1) and dilatant damage is expected. When $D > 1$, the shear stresses are small compared to the mean stress and dilatancy is not expected [Speirs et al., 1988; Van Sambeek et al., 1993]. Based on an evaluation of the SPR rock mechanics test data in terms of the above criteria, failure occurs when the damage factor (D) is less than 0.6.

In order to check for tensile failure the tensile strength of the salt is conservatively assumed to be zero. Tensile cracking in rock salt initiates perpendicular to the largest tensile stress direction.

4.2. Allowable Strains for Well and Surface Structures

The physical presence of wells and surface structures are not included in the finite element model, but the potential for ground deformation producing damage in these structures can be conservatively estimated by assuming that they will deform according to the predicted ground deformation.

Subsidence will primarily induce elongation of the axis of the well. Under these conditions, the cemented annulus of the wells may crack, forming a horizontal tensile fracture that may extend around the wellbore. Vertical fluid migration is not expected under these conditions, however horizontal flow could occur. The allowable axial strain for purposes of this study is assumed to be 2 millistrains in compression and 0.2 millistrains in tension [Thorton and Lew, 1983]. The benefit of the steel casings in reinforcing the strength of the cement, especially under elongation, is not accounted for in this evaluation. The 2 millistrain limit is also representative of the typical yield point for steel casings in the SPR.

Structural damage on the surface is typically caused by the accumulation of large surface strains due to subsidence. These strains can cause distortion, damage, and failure of infrastructure such as buildings, pipelines, roads, and bridges. Surface strains will accumulate in structures over time, which increases the possibility of damage in older facilities. For purposes of this study, the allowable strain is taken to be 1 millistrain for either compression or tension.

5. COMPUTER CODES AND FILE NAMING CONVENTION

5.1. Computer Codes

The finite element code JAS3D [Blanford, 2001] is used in the present calculations. Two material models were chosen for use in the analyses: an elastic model for the overburden material (sand), caprock, and sandstone; and a power law creep model for the salt. Related preprocessing, mesh generation, and post processing codes were used in conjunction with JAS3D. Applicable software and version numbers used in this analysis are listed in Table 6. A number of commercial off-the-shelf software programs, including MathCAD®, Excel®, Visio®, CorelDRAW®, or Corel Paint Shop Pro X® running on MS Windows XP®-based PC workstations, were also utilized.

Table 6: Applicable software and version number

Code Name	Version	Use
APREPRO	2.05	Preprocessor
FASTQ	3.16	Mesh generation
GEN3D	1.20	Mesh generation
GJOIN	1.43	Mesh generation
EMERGE	1.50	Adds temperature to the mesh
JAS3D	2.2.A	FEM solver
ALGEBRA2	1.27	Postprocessor
BLOT II-2	1.56	Postprocessor
EX2EX1V2	2.04	Exodus II to Exodus I database translator

5.2. File Naming Convention

These calculations were performed on Sandia National Laboratories' HP PROLIANT DL360 G5 workstation (SEALS), using the operating system Redhat kernel version 2.6. The general path for any of these subdirectories is 'SEALS: //home/bypark/SPR/para/'. The files related to the mesh generation, the FEM solver, and the volume calculations reside in the subdirectories ~/para/base/mesh/, ~/para/base/solv/, and ~/para/base/volc/ for the baseline calculation, respectively. Table 7 lists the directory names for each parametric analysis. All the files that remain within each subdirectory are listed and described in Table 8. *Input Files* are files that should be obtained from SEALS in order to run the programs; *Intermediate Files* are created during the execution; *Output files* are created as a result of execution and which are stored in SEALS. *Intermediate files* are typically output files created by one program and used as input to another program. Table 8 also lists the names of the *user defined subroutines*, and the names of any *executables* needed to run the entire analysis from grid generation through post processing. FASTQ files for mesh generation; FORTRAN scripts for calculating the temperature at each node; JAS3D input files; user-supplied subroutine to provide an internal pressure state in the

caverns; user-supplied subroutines to calculate the volume change of each cavern; and ALGEBRA scripts for computing the subsidence, principal stresses, safety factor against dilatant damage are provided in Appendices A, B, C, D, E, and F, respectively.

Table 7: Directory name on SEALS and description

Directory Name	Description
/home/bypark/SPR/para/base/mesh	Mesh generation for the baseline calculation
/home/bypark/SPR/para/base/solv	FEM analysis for the baseline calculation
/home/bypark/SPR/para/base/volc	Volume calculation for the baseline calculation
/home/bypark/SPR/para/base/solv/a_2e14	FEM analysis for $A_{SC} = 2\times10^{14}$ (s^{-1})
/home/bypark/SPR/para/base/solv/a_5e11	FEM analysis for $A_{SC} = 5\times10^{11}$ (s^{-1})
/home/bypark/SPR/para/base/solv/e_cr_1p	FEM analysis for E_{SR} = 1.0 GPa
/home/bypark/SPR/para/base/solv/e_cr_20p	FEM analysis for E_{SR} = 20. GPa
/home/bypark/SPR/para/base/solv/e_cr_100p	FEM analysis for E_{SR} = 100. GPa
/home/bypark/SPR/para/base/solv/e_sr_4p0	FEM analysis for E_{SR} = 4.0 GPa
/home/bypark/SPR/para/base/solv/e_sr_10p	FEM analysis for E_{CR} = 10. GPa
/home/bypark/SPR/para/base/solv/e_sr_20p	FEM analysis for E_{CR} = 20. GPa
/home/bypark/SPR/para/base/solv/e_sr_30p	FEM analysis for E_{CR} = 30. GPa
/home/bypark/SPR/para/base/solv/K=1	FEM analysis for $\mathcal{K}_{SR}$ = 1
/home/bypark/SPR/para/base/solv/K=2	FEM analysis for $\mathcal{K}_{SR}$ = 2
/home/bypark/SPR/para/domedp/mesh	Mesh generation to examine the depth effect of salt dome top, d_{SD}=500 ft, d_C=2500 ft
/home/bypark/SPR/para/domedp/solv	FEM analysis to examine the depth effect of salt dome top, d_{SD}=500 ft, d_C=2500 ft
/home/bypark/SPR/para/domedp/solv/a_2e14	FEM analysis to examine the depth effect of salt dome top, d_{SD}=500 ft, d_C=2500 ft, $A_{SC} = 2\times10^{14}$ (s^{-1})
/home/bypark/SPR/para/domedp/solv/fcs	FEM analysis to examine the depth effect of salt dome top, d_{SD}=500 ft, d_C=2500 ft, FCS material properties
/home/bypark/SPR/para/domedp/volc	Volume calculation to examine the depth effect of salt dome top, d_{SD}=500 ft, d_C=2500 ft
/home/bypark/SPR/para/domesz/mesh	Mesh generation to examine the dome size effect
/home/bypark/SPR/para/domesz/solv	FEM analysis to examine the dome size effect
/home/bypark/SPR/para/domesz/volc	Volume calculation to examine the dome size effect
/home/bypark/SPR/para/caproc/mesh	Mesh generation to examine the caprock thickness effect
/home/bypark/SPR/para/caproc/solv	FEM analysis to examine the caprock thickness effect
/home/bypark/SPR/para/caproc/volc	Volume calculation to examine the caprock thickness effect
/home/bypark/SPR/para/cavsz/mesh	Mesh generation to examine the cavern size effect
/home/bypark/SPR/para/cavsz/solv	FEM analysis to examine the cavern size effect
/home/bypark/SPR/para/cavsz/volc	Volume calculation to examine the cavern size effect
/home/bypark/SPR/para/cavdp/1000/mesh	Mesh generation to examine the cavern depth effect, d_{SD}=500 ft, d_C=1000 ft
/home/bypark/SPR/para/cavdp/1000/solv	FEM analysis to examine the cavern depth effect, d_{SD}=500 ft, d_C=1000 ft
/home/bypark/SPR/para/cavdp/1000/volc	Volume calculation to examine the cavern depth effect, d_{SD}=500 ft, d_C=1000 ft
/home/bypark/SPR/para/cavdp/2100/mesh	Mesh generation to examine the cavern depth effect, d_C=2100 ft

Directory Name	Description
/home/bypark/SPR/para/cavdp/2100/solv	FEM analysis to examine the cavern depth effect, d_C=2100 ft
/home/bypark/SPR/para/cavdp/2100/volc	Volume calculation to examine the cavern depth effect, d_C=2100 ft
/home/bypark/SPR/para/cavdp/4000/mesh	Mesh generation to examine the cavern depth effect, d_C=4000 ft
/home/bypark/SPR/para/cavdp/4000/solv	FEM analysis to examine the cavern depth effect, d_C=4000 ft
/home/bypark/SPR/para/cavdp/4000/volc	Volume calculation to examine the cavern depth effect, d_C=4000 ft
/home/bypark/SPR/para/31cav/mesh	Mesh generation to examine the number of caverns effect
/home/bypark/SPR/para/31cav/solv	FEM analysis to examine the number of caverns effect
/home/bypark/SPR/para/31cav/volc	Volume calculation to examine the number of caverns effect

Table 8: File naming convention for the analyses (* means wild card)

File Name	Description	Appendix provided in
Input Files		
*.fsq	FASTQ file for 2D mesh generation	Appendix A
*cav0d.pts	Define the mesh coordinates	Appendix A
*.gen3d	A GENESIS database 2D to 3D transformation file	Appendix A
*.gjn	Files for merging two or more GENESIS databases	Appendix A
thickness.txt	Input data for the thickness of each layer	Appendix A
units.txt	Unit conversion file	Appendix A
units_fortran.txt	Unit conversion file for FORTRAN script	Appendix A
*cav0d_2d.g	2D GENESIS mesh generated using FASTQ	
*cav0d.g0	3D GENESIS mesh generated using GEN3D	
*cav0d.g	3D GENESIS mesh contains the temperature data at each node and used for the execution of JAS3D	
wh_*cav0d.nod	ASCII node data of coordinates	
emerge.inp	Emerge input file for merging the temperature data onto the mesh	
spr_wh_US.alg	ALGEBRA script for computing the subsidence, principal stresses, safety factor against dilatant damage	Appendix F
wh_*cav0d.i	JAS3D input files	Appendix C
Intermediate Files		
wh_*cav0d.th	Binary temperature data of each node	
tempz_wh_*cav0d.f	FORTRAN file for calculating the temperature at each node	Appendix B
*.blk	BLK file for compiling FORTRAN files	
usrpbc_wh_*cav0d.o	Objective file from compiling FORTRAN file	
User Defined Subroutines		
usrpbc_wh_*cav0d.f	User-supplied subroutine to provide an internal pressure state in the caverns	Appendix D
volcav.f	User-supplied subroutine to calculate the volume change of each cavern as a function of time	Appendix E
Output files		
temp_check.dat	ASCII data for checking the temperature at each node	

File Name	Description	Appendix provided in
*.ps	Post script file from the post-process	
wh_*cav0d_smax_mindil_minshr.dat	ASCII data of the principal stresses, safety factor against dilatant damage	
cntr_to_bound_11_21_46.dat	ASCII data of the subsidence with distance from the center to the edge of the model	
dz_on_roof_surface_at_centers.dat	ASCII data of the subsidence with time at the cavern centers	
wh_*cav0d.e	EXODUS output files	
wh_*cav0d.ea	EXODUS output files manipulated using ALGEBRA script	
volcav.csv	Excel output from the volume calculation of caverns with time	
wh_*cav0d.o	ASCII output file	
wh_*cav0d.s	ASCII output summary file	
*.log	Log file during execution	
Executables		
a.out	Calculates the temperature at each node	
3dmesh_seal.run	Command scripts for mesh generation	Appendix A
addtemp_seal.run	Command script for adding the temperature data to the mesh	
jas3d	FEM solver	
Makefile	Commands to compile volcav.f	
volcav	Calculates the volume change of each cavern with time	
volcav.run	Commands to run volcav	

6. ANALYSES RESULTS

6.1. Baseline

6.1.1. Cavern deformation

Creep closure decreases cavern volume over time and is more pronounced near the bottom of the caverns. The flow of salt can be illustrated by displacements vectors at each node. Figure 15 show the deformed cavern shapes and displacement vectors at 46 years. The salt flows are primarily downward near the roofs of the caverns, upward near the floors, and lateral in the pillar. The largest displacements occur at the roof of Cavern 1. Lateral salt deformation causes the cavern walls to move inward over time.

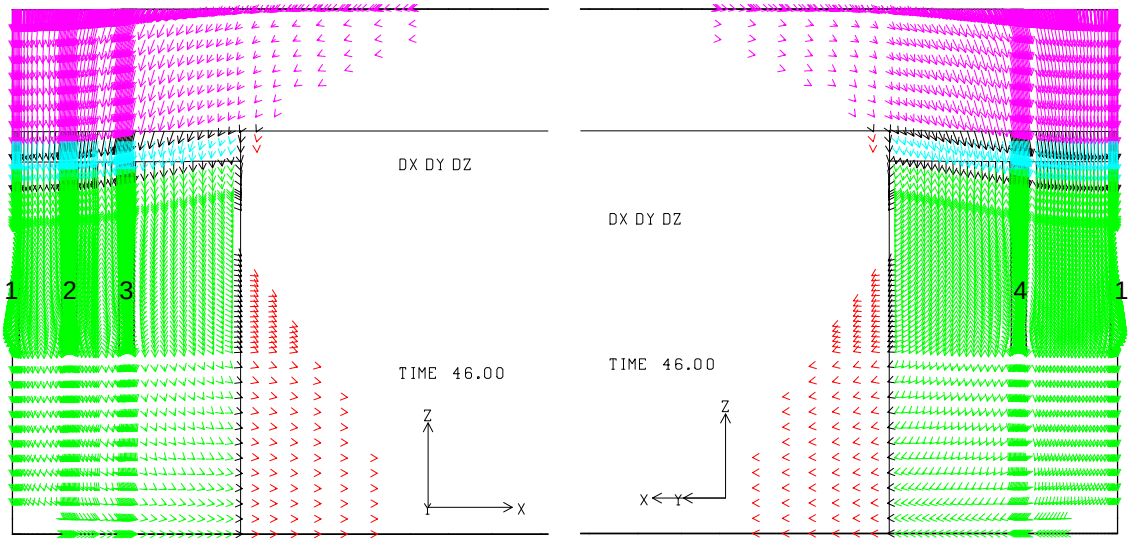

Figure 15: Displacement vectors around the caverns at 46 years.

Figure 16 shows the quantified vertical displacements contours around the SPR caverns at 21 and 46 years. Negative displacements are directed downward. As anticipated, the vertical displacements increase with time. The maximum downward vertical displacement occurs in the roof of Cavern 1 (central cavern).

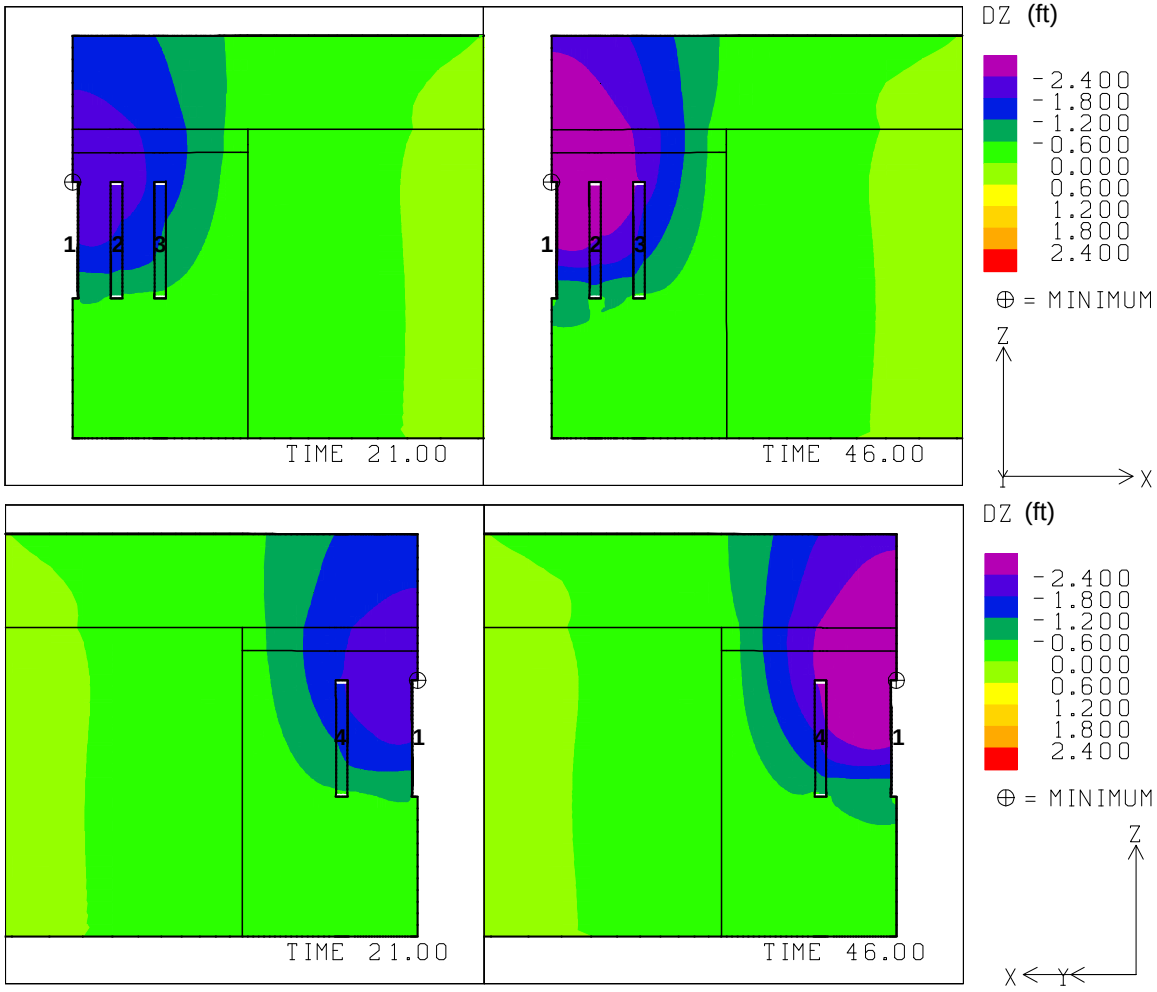

Figure 16: Vertical displacement contours around the caverns at 21 and 46 years.

6.1.2. Storage loss

Figure 17 shows the predicted total volumetric closure normalized to initial total storage volume for the 19 SPR caverns. The total storage volume decreases by about 1.9% during 45 years. The peaks in the graphs for each cavern at every 5 years appear when the well head pressures drop down to zero psi during the workovers.

Figure 18 shows the predicted volumetric closure normalized to each initial cavern volume. The impact of workover pressure is evident in the figure by the abrupt increase in normalized volumetric closures for each cavern at every five years. The closure rate of Cavern 2 is largest and the rates decrease in order of Cavern 1, Cavern 4, and Cavern 3, respectively. Figure 19 shows the volume change of each cavern due to salt creep closure over time. The initial volume of each cavern, 11.19 MMB, decrease down to about 10.96 MMB for 45 years.

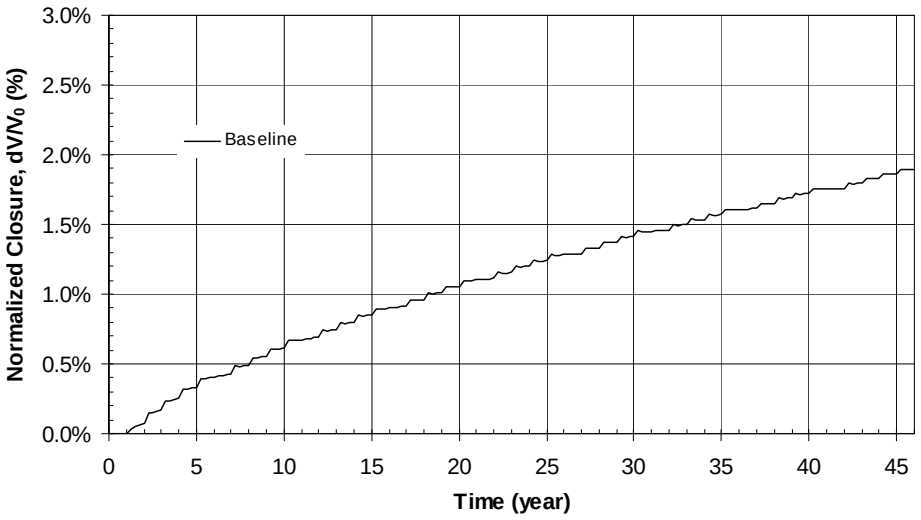

Figure 17: Predicted total volumetric closure normalized to initial total storage volume for the 19 SPR caverns.

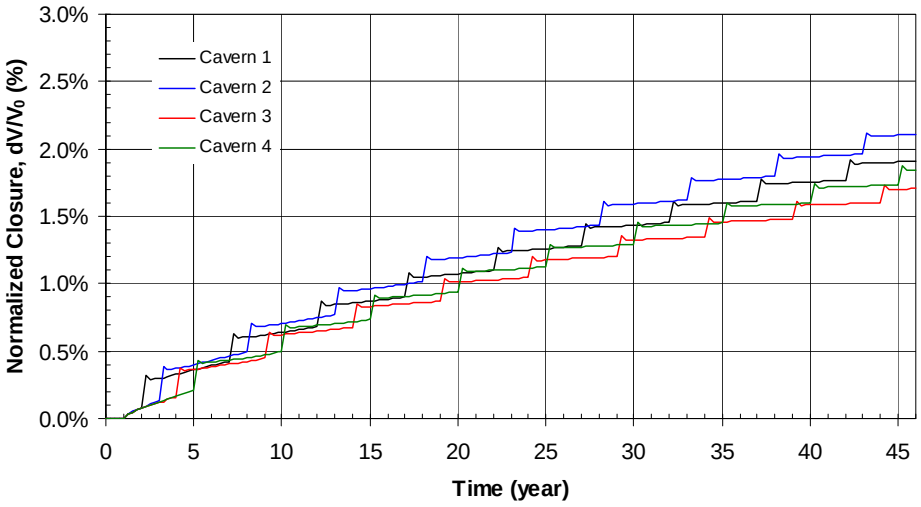

Figure 18: Predicted volumetric closure normalized to each initial cavern volume.

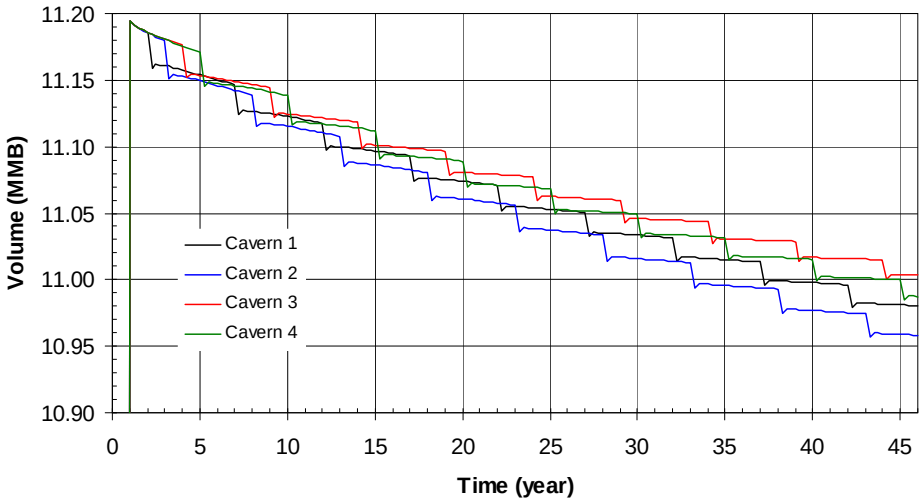

Figure 19: Predicted volume change of each cavern due to salt creep closure over time.

6.1.3. Subsidence

The subsidence above the center of each SPR cavern is plotted as a function of time in Figure 20. The magnitude of subsidence slowly increases with time as a result of salt creep closure. The subsidence above Cavern 1 is larger than that above the other caverns. The location of Cavern 1 is the center of the dome. This suggests that the amount of subsidence depends on the location at which the subsidence is calculated, and subsidence contributed by other caverns has a compounding effect.

Figure 21 shows the predicted displacement between the top of the central cavern (Cavern 1) and the surface above the cavern as a function of time. The subsidence rate of the top of the cavern is faster than that of the surface. Figure 22 shows the predicted surface subsidence troughs as a function of distance from the center to the edge of the model at 11 years, 21 years, and 46 years. The influence of subsidence is predicted to extend beyond the edge of the salt dome, to about 6000 ft.

Figure 23 shows the calculated surface strains at 21 years and 46 years. The accumulated strain is below the limiting value of one millistrain and thus structural damage should not occur.

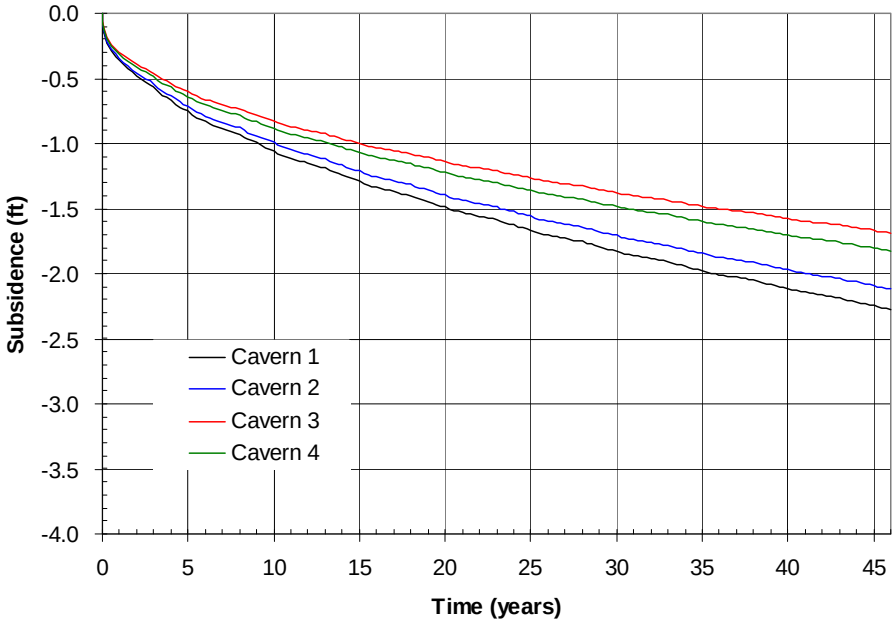

Figure 20: Predicted subsidence on the surface above the center of each SPR cavern.

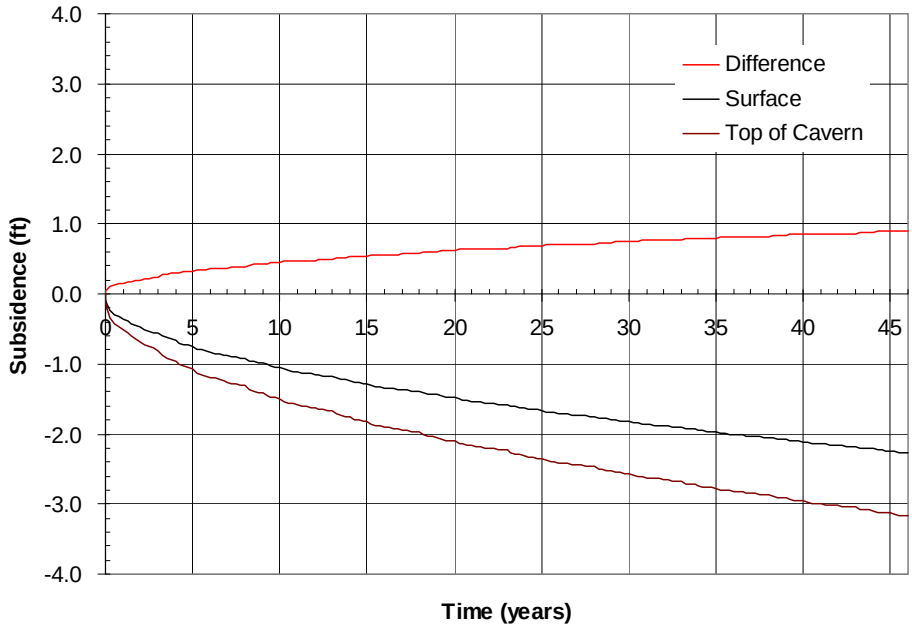

.

Figure 21: Predicted difference between vertical displacement of the top of the central cavern (Cavern 1) and the surface above the cavern as a function of time.

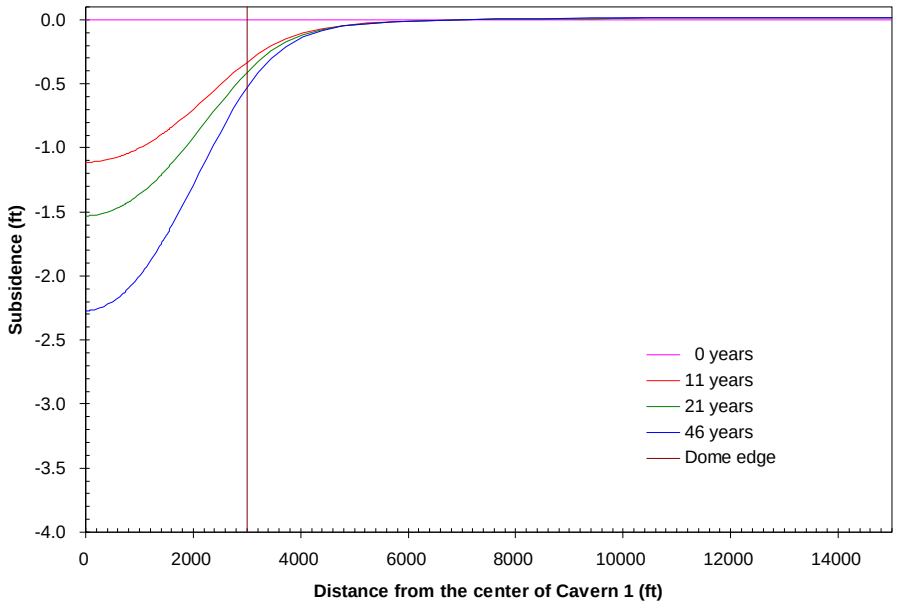

Figure 22: Predicted subsidence on the surface from model center to edge with time.

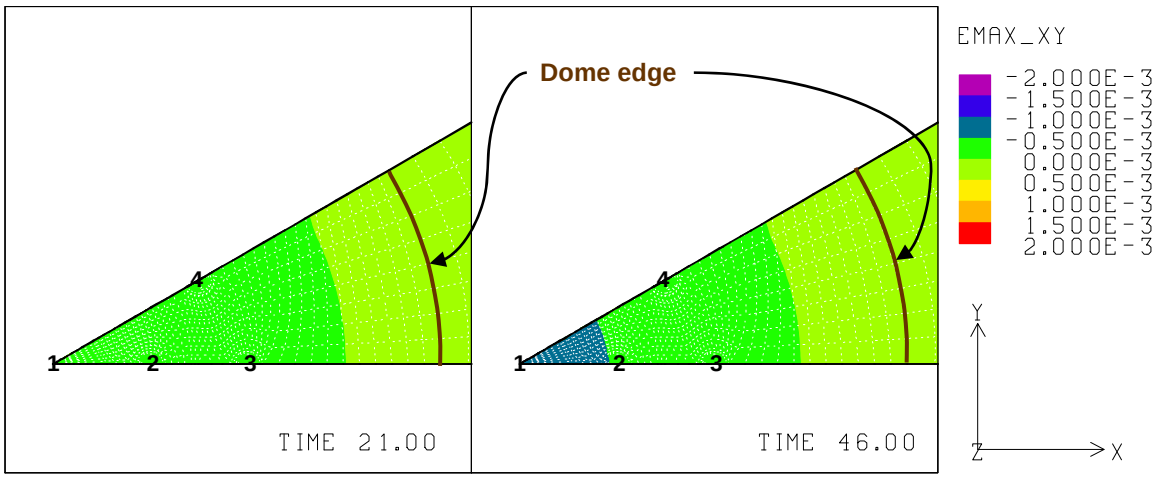

Figure 23: Predicted radial surface strains at 21 years and 46 years.

6.1.4. Cavern wells

The calculated vertical ground strains around the roof of caverns are shown in Figure 24 at 21 years and 46 years. Of interest are the magnitudes in the proximity of the cavern wells from the surface to the cavern roofs. Well casings typically extend from the surface to about 100 ft above the cavern roof (cavern diameter is 200 ft). The collapse strength of the steel component of a well is reduced as the casing stretches. In general, steel casing will not yield until about 2 millistrains. Also, fracturing in the grout surrounding the steel is thought to occur for tensile strains greater than 0.2 millistrains. Therefore, predicted strains near the cavern wells larger than 0.2 millistrains in tension are predicted to cause failure in the grout.

The predicted strains over 100 ft above the cavern roofs of caverns at 21 and 46 years are less than 2 millistrains, thus the steel casing should not yield.

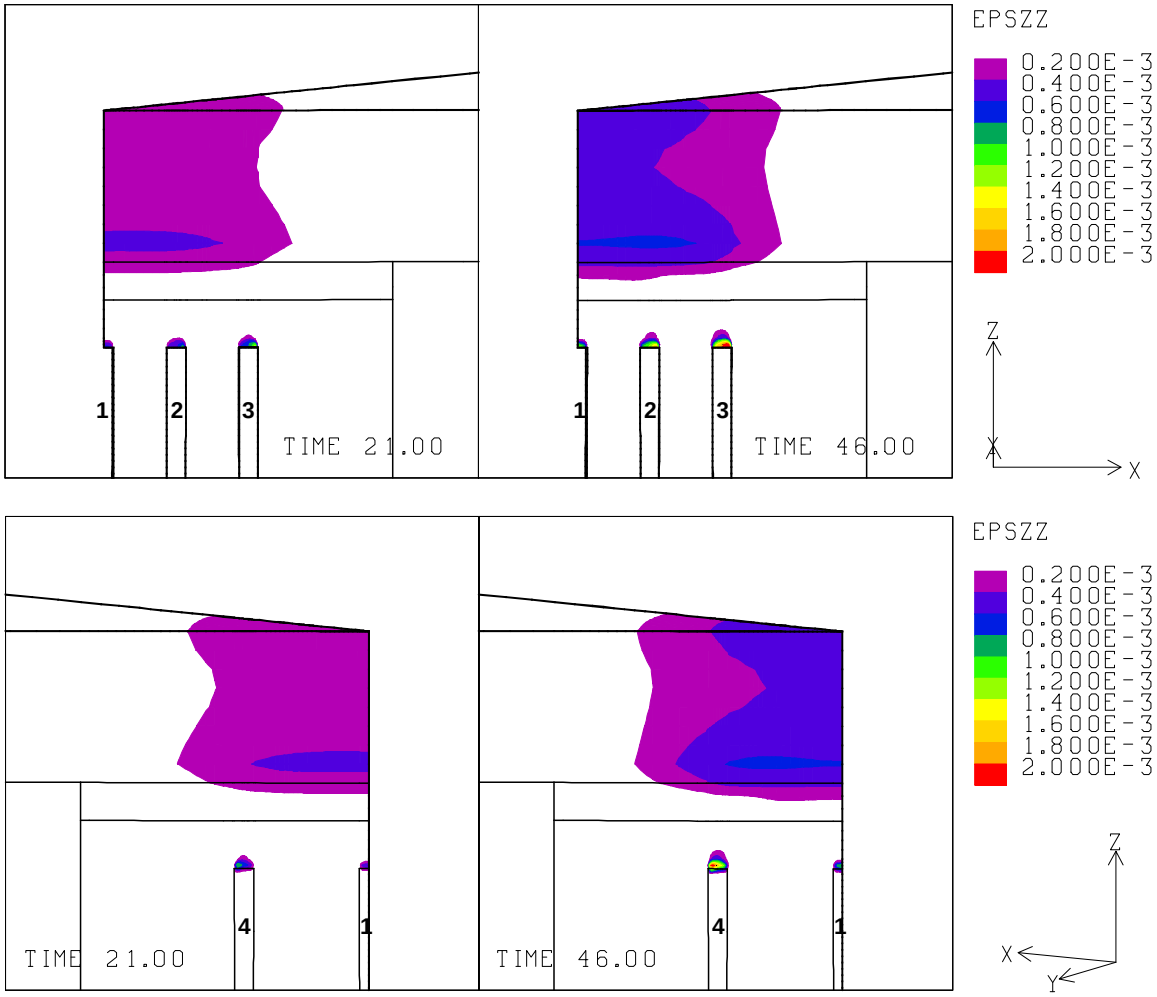

Figure 24: Vertical strains around the roof of caverns at 21 years and 46 years.

6.1.5. Cavern stability against tensile failure

As mentioned in Section 4.1, the stability of the caverns is evaluated by examination for any tensile stresses and by calculation of the safety factors against dilatant damage. Figure 25 shows the minimum compressive stress[§] (MCS) histories from the baseline model. The MCS in the entire salt dome was calculated to be -904 psi at 44.25 year during Cavern 3 workover. The negative sign (-) indicates a compressive stress. The most critical location is found to be in the roof of the caverns as shown in Figure 26. The MCS around the caverns appear to be low enough to be structurally safe.

All stresses were found to be compressive. Thus, all caverns predicted to be structurally stable against tensile failure throughout the entire simulation time. From a compressive stress stability

§ The compressive stresses are calculated in every element in the salt dome at each time step. The minimum compressive stress means the minimum value among the stresses in every element at a specific time.

viewpoint, based on this analysis, the roofs of the caverns appear to be areas of greater concern than the webs between the caverns.

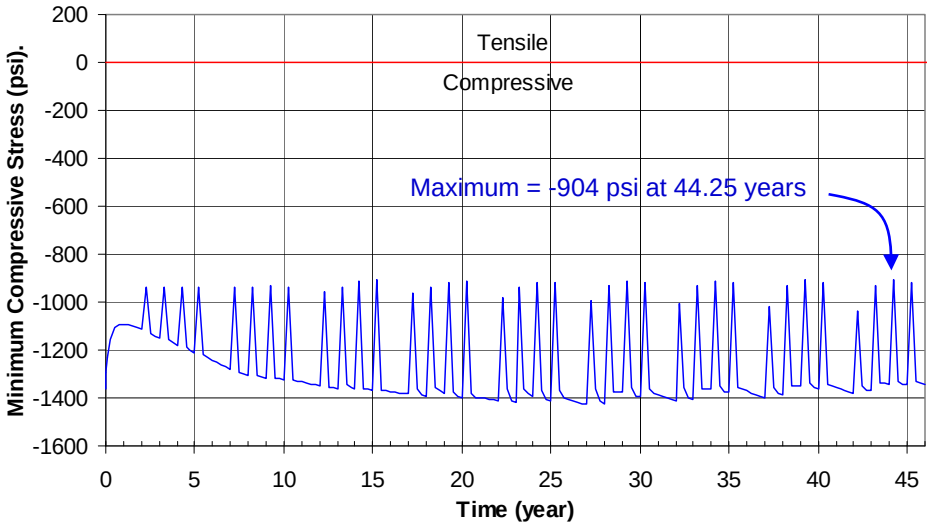

Figure 25: Minimum compressive stress history from the baseline model.

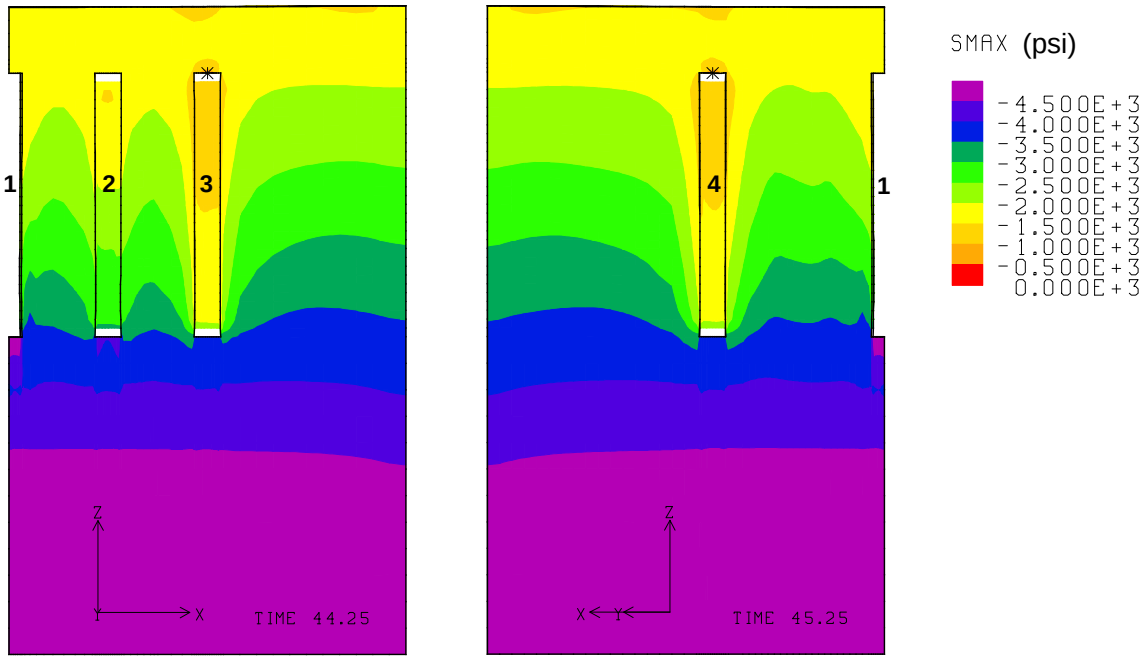

Figure 26: Compressive stress contours around the caverns during workover of Cavern 3 and Cavern 4 at 44.25 years and 45.25 years, respectively.

Figure 27 shows the predicted minimum compressive stress contours in the overburden, caprock, salt dome, and surrounding rock during workover of Cavern 3 at 44.25 years. The areas in white indicate tensile stress, hence a tensile failure zone. Tensile failure is predicted to occur at the top of the caprock and the surrounding rock around the dome edge. Even though the salt dome is

safe against tensile failure, tensile cracks can be propagating in the caprock and surrounding rock (tensile zone). Also any fluid that enters a crack will pressurize the crack and tend to separate it.

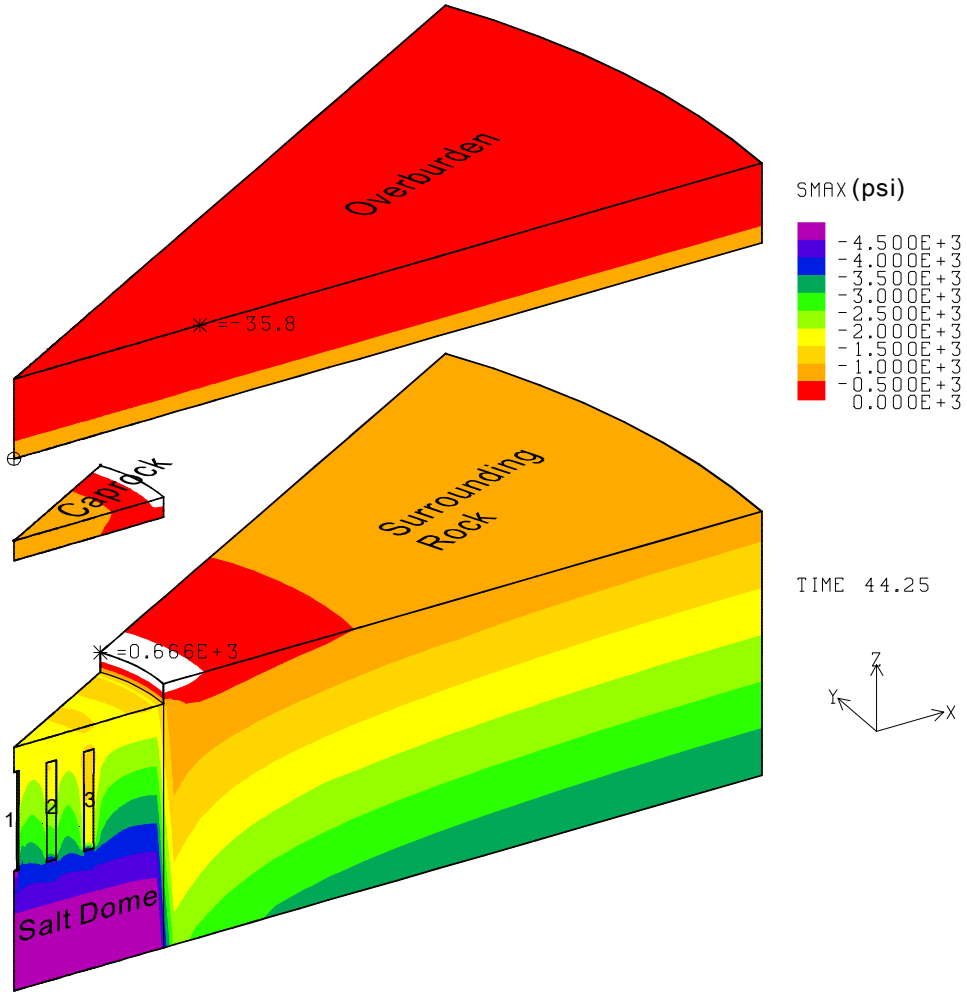

Figure 27: Compressive stress contours in the four blocks at 44.25 years.

The stress changes with time are checked at the several elements expected to experience tensile failure as shown in Figure 28. Figure 29 through Figure 31 show the change of stress over time at the considered elements. The horizontal Y-directional (Figure 30) and vertical Z-directional (Figure 31) stresses at all examined elements are negative, which means the elements are in a compressive stress state. However, the X-directional stresses at the elements 6105 (caprock) and 38709 (surrounding rock) change from negative to positive at 3.75 years and 8.25 years, respectively after the simulation starts. This means the stress state at the elements 6150 and 38709 changed from compressive to tensile in the X-direction. Therefore, tensile cracks can be propagating parallel to the interface between caprock and surrounding rock in the tensile zone in Figure 27.

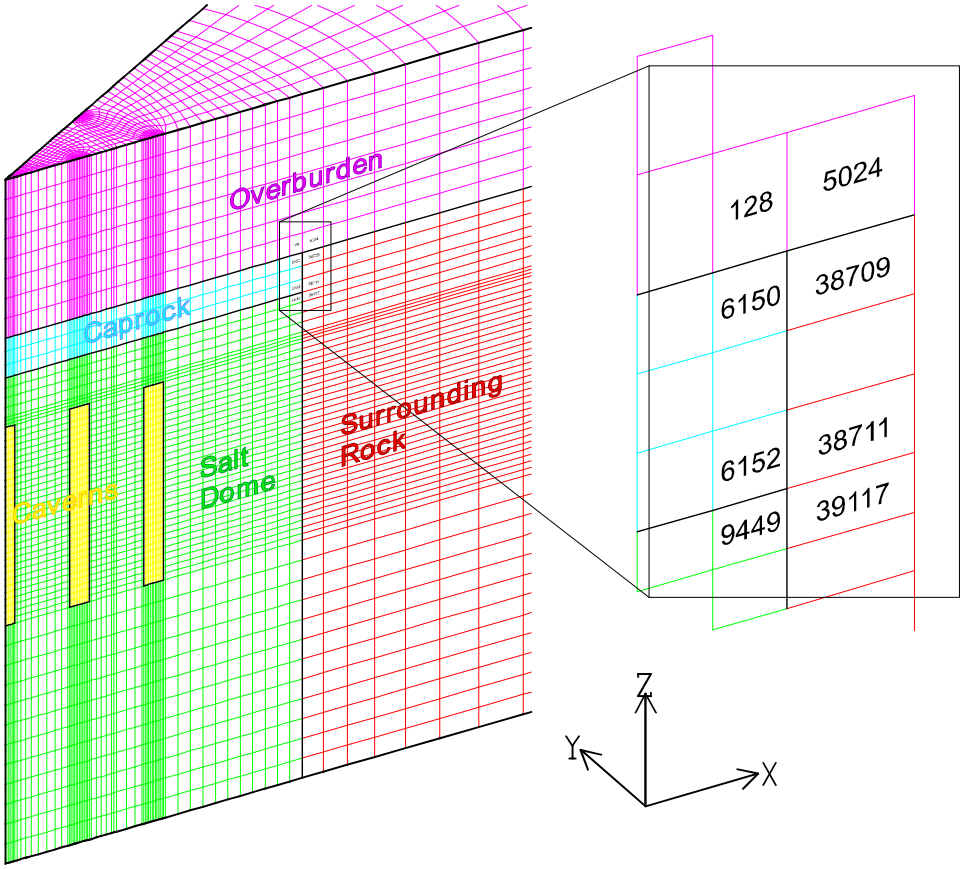

Figure 28: Number of elements expected to experience tensile cracks.

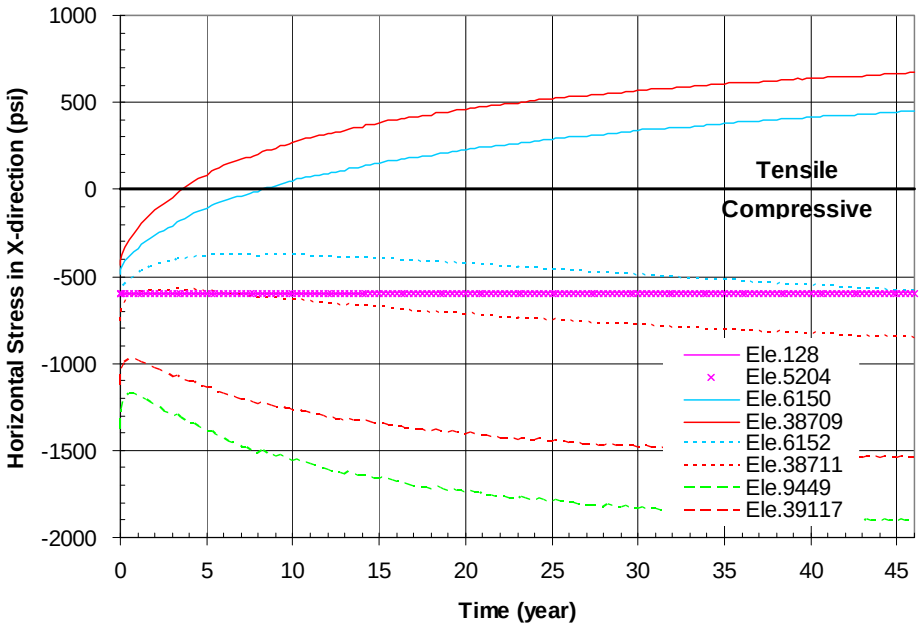

Figure 29: Predicted X-directional stress history in elements 128, 5204, 6150, 38709, 6152, 38711, 9449, and 39117 shown in Figure 28.

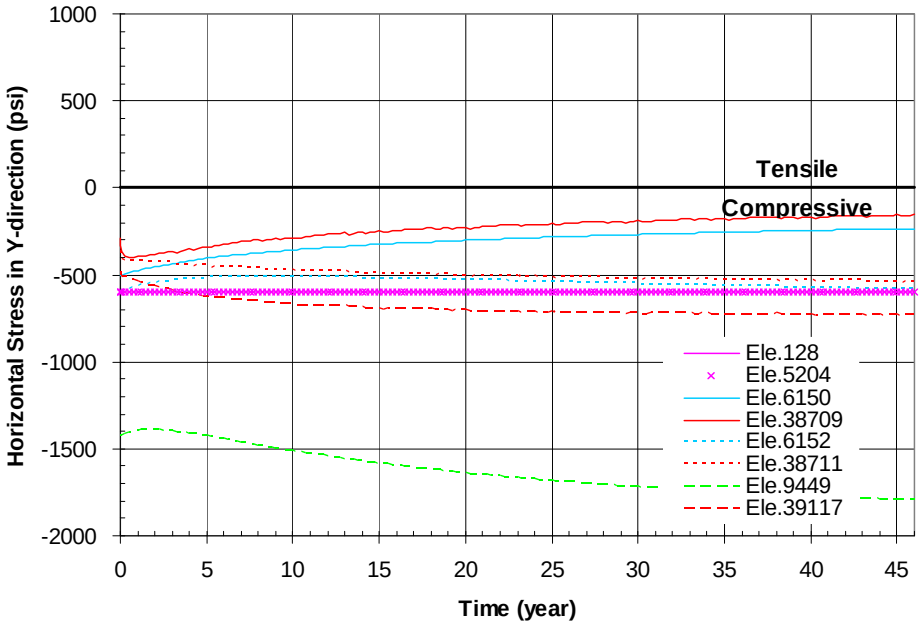

Figure 30: Predicted Y-directional stress history in elements 128, 5204, 6150, 38709, 6152, 38711, 9449, and 39117 shown in Figure 28.

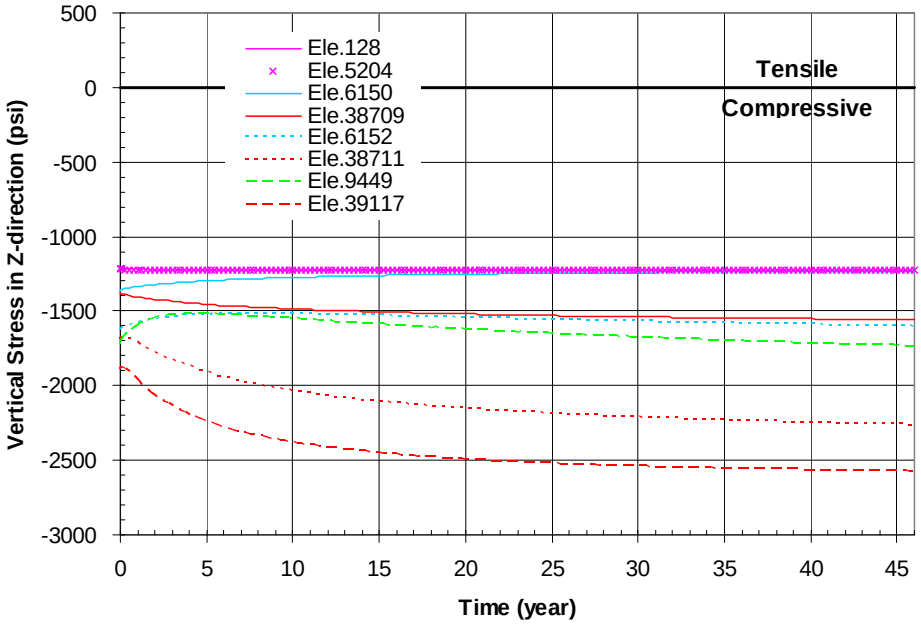

Figure 31: Predicted Z-directional stress history in elements 128, 5204, 6150, 38709, 6152, 38711, 9449, and 39117 shown in Figure 28.

6.1.6. Cavern stability against dilatant damage

The minimum safety factor** histories against dilatancy damage (DILFAC) for the baseline model are plotted in Figure 32. The minimum DILFAC is predicted to be 2.23 at 5.25 years when Cavern 4 undergoes workover. The potential dilatant damage does not occur since the DILFAC is larger than 1.0 as discussed in Section 4.1, thus all caverns are structurally stable against dilatant damage through 46 years.

Examinations of a typical safety factor distribution for dilatant damage over the cavern surface are provided in Figure 33 at 5.25 years in the caverns along the two symmetry planes at 0° and 30°. These figures show effects of workover. Areas where DILFAC is less than 1.0 do not exist, thus the dilatant damage is not expected to occur. The lowest safety factor is predicted at the upper wall near the roof of the caverns.

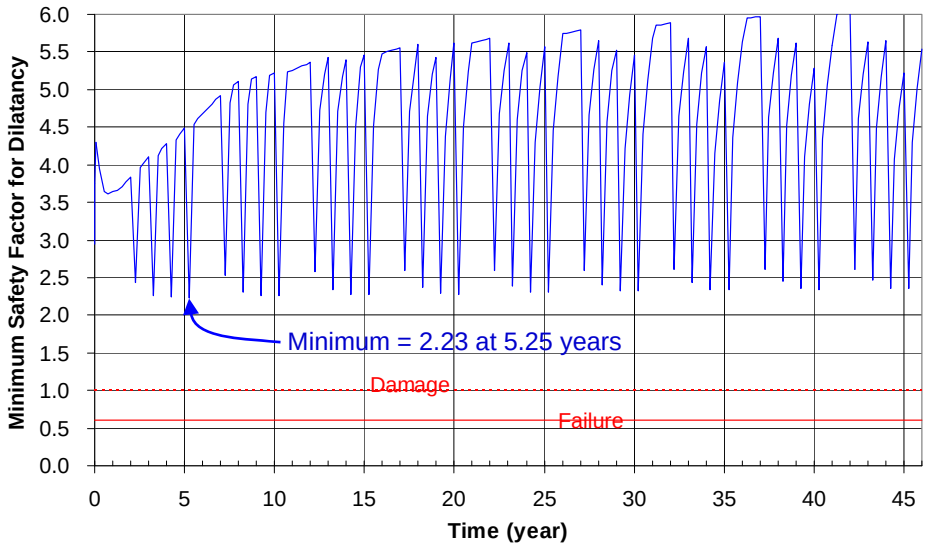

Figure 32: Minimum safety factor history against dilatant damage from the baseline model.

** The safety factors are calculated in every element in the salt dome at each time step. The minimum safety factor means the minimum value among the safety factors in every element at a specific time.

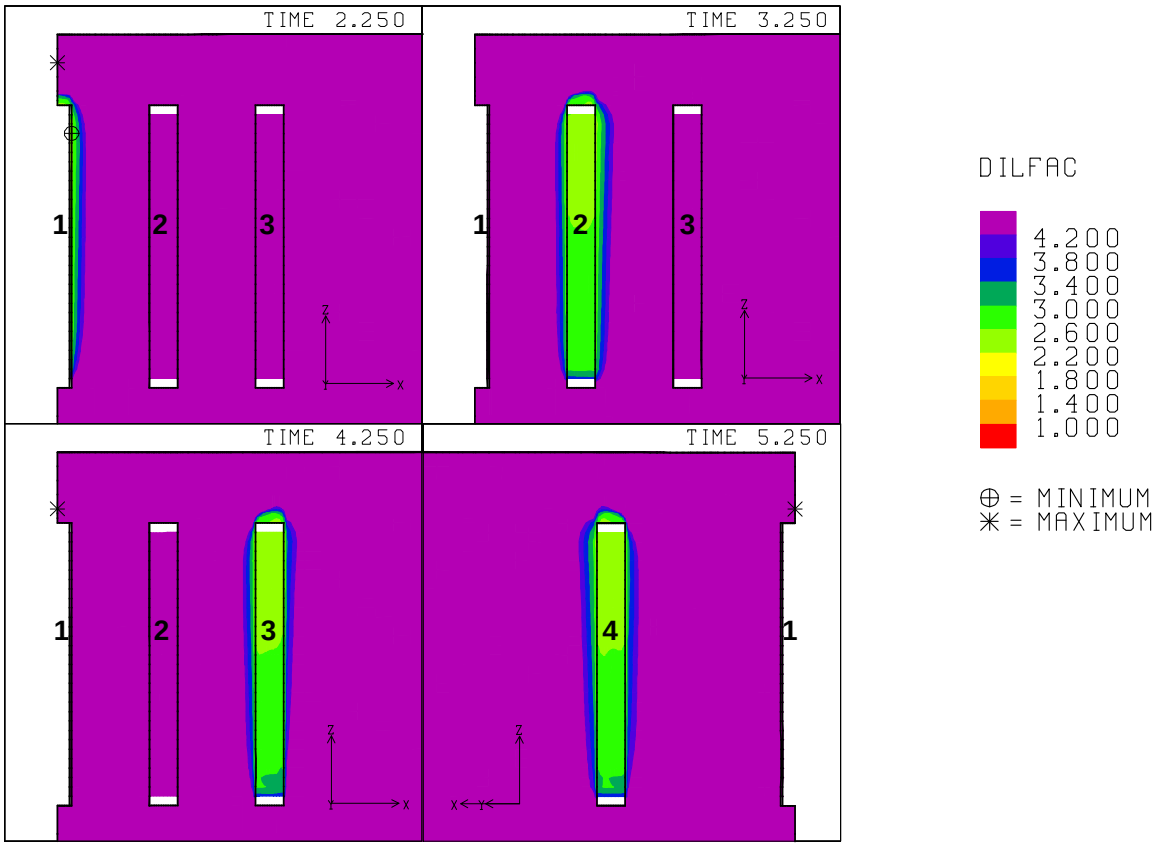

Figure 33: Safety factor contours against dilatant damage around the caverns during workover of Caverns 1, 2, 3 and 4 at 2.25 years, 3.25 years, 4.25 years and 5.25 years, respectively.

6.2. Analyses Results from Changed Models

The analyses results from the models to examine the salt creep rate effect, the depth of salt dome top effect, the dome size and standoff distance effect, the elastic modulus effect of caprock, the caprock thickness effect, the elastic modulus effect of surrounding rock, the lateral stress coefficient effect of surrounding rock, the cavern size effect, the cavern depth effect, and the number of caverns effect are provided as the same subsections as those in Section 6.1 in Appendix G.

7. EFFECT OF EACH PARAMETER

7.1. Effect of Salt Creep Rate

To examine the effect of salt creep rate, analyses are conducted with the secondary creep constants listed in Table 9.

Table 9: The secondary creep constant values to examine the effect of salt creep rate.

Parameter	Unit	Lower	Baseline	Upper
Secondary creep constant (A_{SC})	s^{-1}	5.0×10^{11}	1.1×10^{13}	2.0×10^{14}
Power law creep constant (A)	Pa^{-n}/s	1.71×10^{-39}	3.75×10^{-38}	6.82×10^{-37}

Figure 34 shows the vertical displacement contours for the different secondary creep constants at 46 years. The vertical displacement increases with increasing the value of the secondary creep constant.

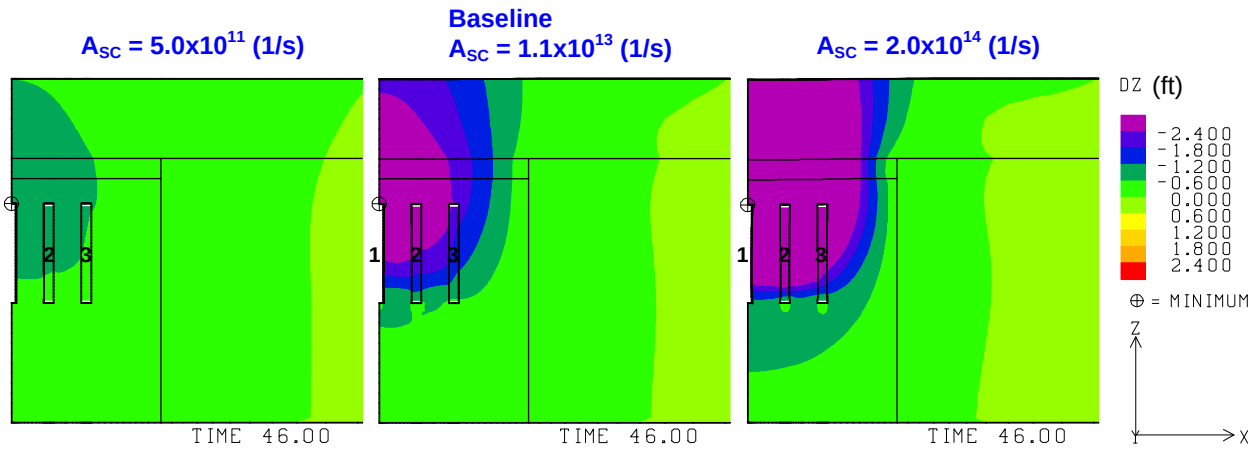

Figure 34: Vertical displacement contours at 46 years.

Figure 35 shows the predicted total volumetric closure normalized to initial total storage volume for the 19-cavern model. The cavern volume loss rate due to salt creep closure increases with increasing the value of the secondary creep constant. Smaller value of the creep constant is better from a storage loss viewpoint.

Figure 36 shows the predicted subsidence on the surface above Cavern 1 with time for the different values of secondary creep constants. Figure 37 shows the predicted subsidence on the surface from the center to the edge of the model at 46 years for the three constant values. The subsidence on the surface above the center of Cavern 1 increases with increasing the value of the secondary creep constant. A smaller value of the creep constant is better from a subsidence viewpoint.

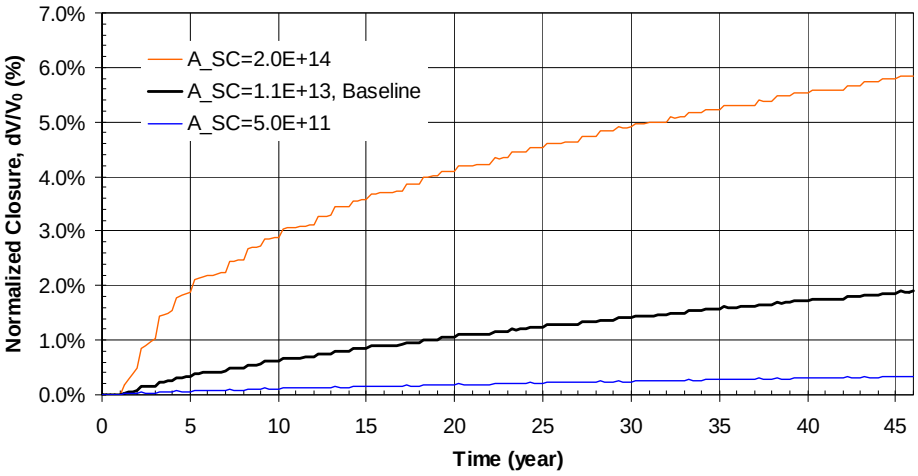

Figure 35: Comparison of predicted total volumetric closure normalized to initial total storage volume for the 19 SPR caverns with differing secondary creep constants.

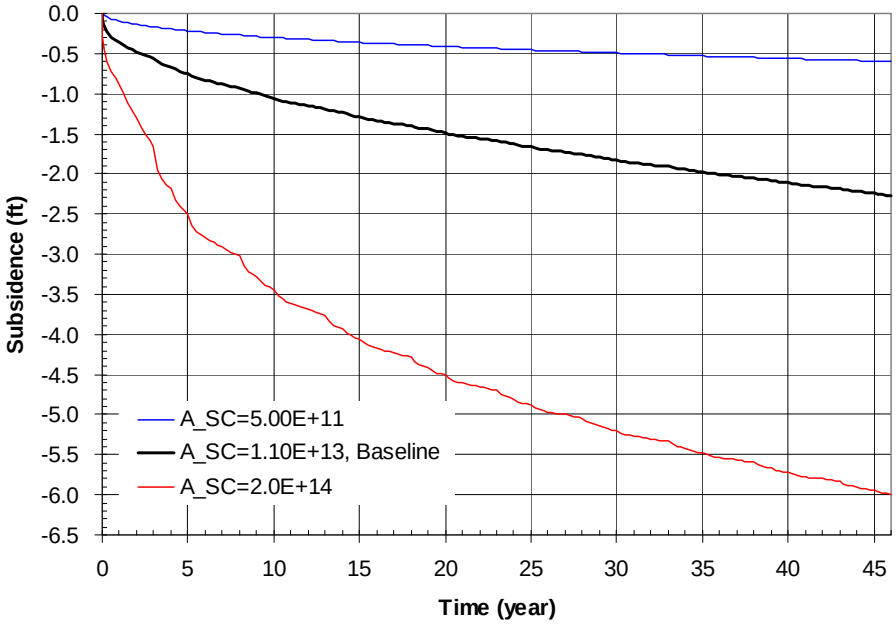

Figure 36: Comparison of predicted subsidence on the surface above Cavern 1 with time for three different secondary creep constant values.

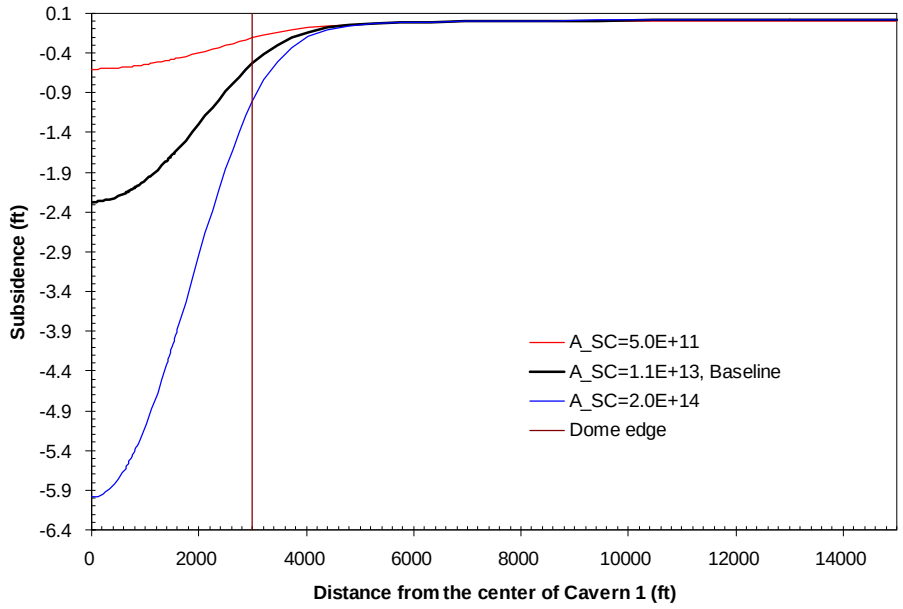

Figure 37: Comparison of predicted subsidence on the surface from model center to edge at 46 years for the different secondary creep constants.

Figure 38 shows the predicted radial surface strains at 46 years with secondary creep constant values. The radial surface strain increases with increasing the value of the secondary creep constant. A smaller value of the creep constant is better from a radial surface strain. The strain for $A_{SC} = 2.0\times10^{14}$ (s^{-1}) is beyond the allowable strain for surface structures (one millistrain in either compression or tension).

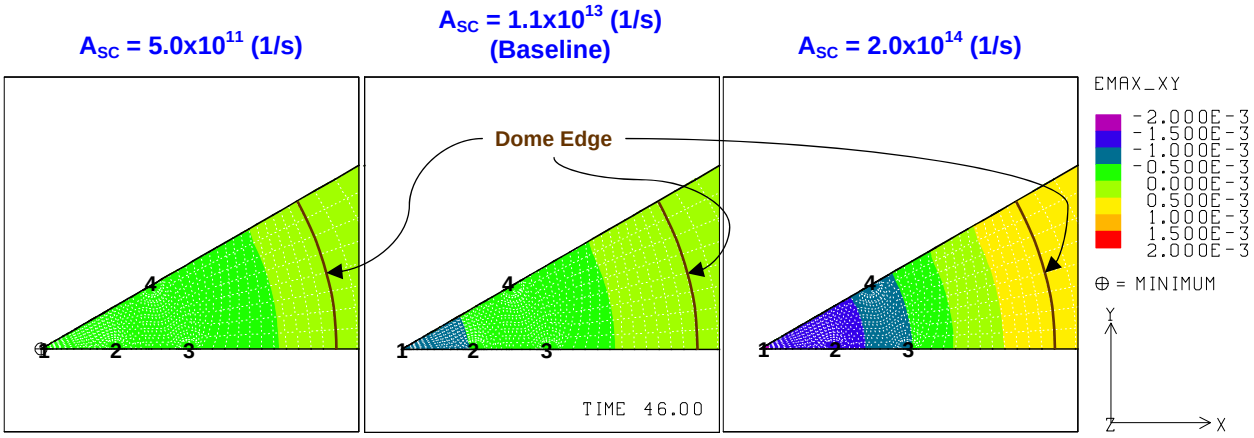

Figure 38: Predicted radial surface strains at 46 years for three different secondary creep constants.

Figure 39 shows the predicted vertical strains around the roof of the caverns at 46 years with the different secondary creep constants. The vertical strain increases with increasing the value of the secondary creep constant. Smaller value of the constant is better from a vertical strain viewpoint. Well casings typically extend from the surface to about 100 ft above the cavern roof (Cavern diameter is 200 ft). The strain for $A_{SC} = 2.0\times10^{14}$ (s^{-1}) at 100 ft above the cavern roof is beyond

the allowable strain for cemented annulus of the well (0.2 and 2 millistrains in tension for cement and steel casing, respectively).

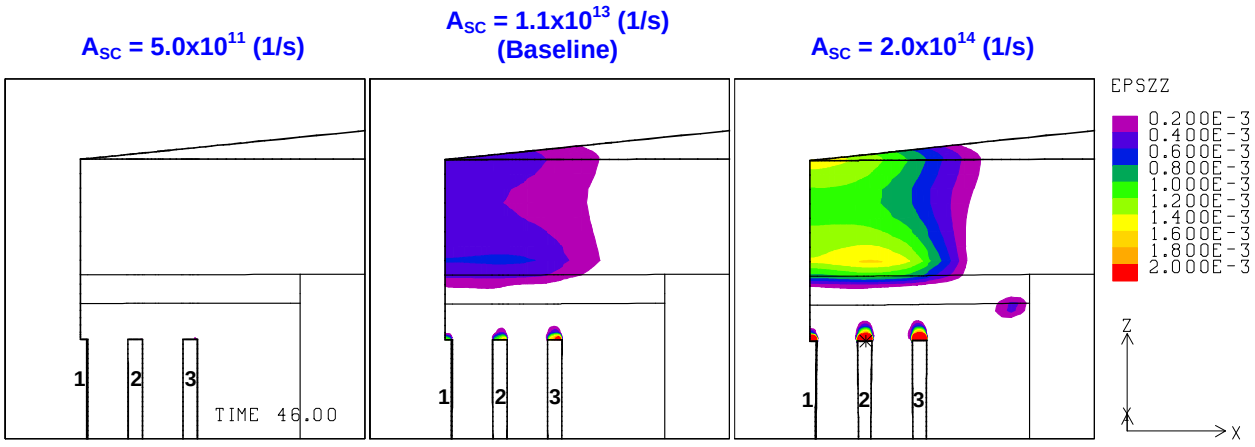

Figure 39: Predicted vertical strains around the roof of caverns at 46 years for three different secondary creep constants.

Figure 40 shows the predicted minimum compressive stress history in the salt dome with the various secondary creep constants. The negative sign (-) indicates a compressive stress. The peaks appear during the workover of the caverns. To see the tendency of the minimum compressive stress at the peaks, the peaks are connected using the dash-doted lines for each secondary creep constant.

The structural stability against tensile failure decreases with increasing the value of the secondary creep constant after about 17 years. However, this tendency disappears until about 17 years since the initial leach. Tensile failure is predicted to occur for $A_{SC} = 2.0\times10^{14}$ (s^{-1}) after about 40 years.

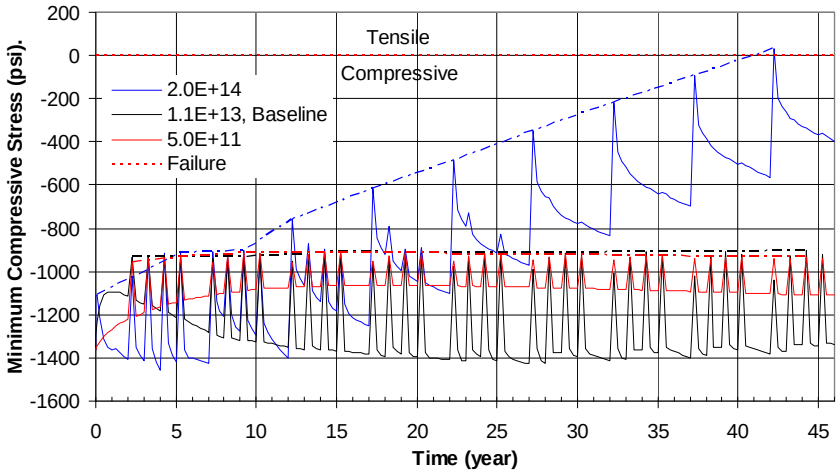

Figure 40: Comparison of predicted minimum compressive stress history in the salt dome for three different values of the secondary creep constants.

Figure 41 shows the predicted minimum safety factor (MSF) history against dilatant damage in the salt dome with the secondary creep constants. The peaks appear during the workover of the caverns. To see the tendency of the minimum safety factor at the peaks, the peaks are connected using dash-doted lines for each secondary creep constant.

The safety factor against dilatancy is greater for increasing values of the secondary creep constant until about 12 years. After 12 years the MSF for $A_{SC} = 2\times10^{14}$ (s^{-1}) begins to decrease, while the others remain at constant levels. After 17 years, the baseline value appears to be the safest. Therefore, the optimum value of the secondary creep constant against dilatancy damage exists between upper and lower values. Dilatant damage is predicted to occur at 42.25 years when $A_{SC} = 2.0\times10^{14}$ (s^{-1}).

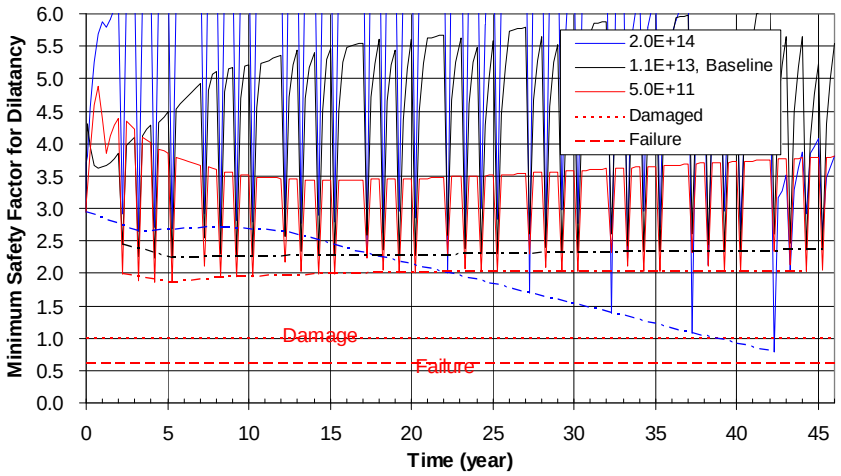

Figure 41: Comparison of predicted minimum safety factor history against dilatant damage in salt dome for three different secondary creep constant values.

In conclusion, smaller values of the secondary creep constant are more advantageous from a storage loss, subsidence, integrity of surface structure, and cemented well annulus viewpoints. A smaller value of the creep constant does not always appear better from a tensile failure viewpoint. Until about 17 years, a larger value of the secondary creep constant is better from a dilatancy damage viewpoint. The optimum value of the constant against tensile failure and dilatancy exists between upper (2.0×10^{14} (s^{-1})) and lower bounding values (5.0×10^{11} (s^{-1})).

7.2. Depth of Salt Dome Top Effect with Salt Creep Rate

To examine the depth of salt dome top effect with salt creep rate, analyses were conducted with the parameter values as listed in Table 4.

Figure 42 shows the vertical displacement contours for the baseline and a salt dome top depth of 500 ft with various secondary creep constants at 46 years. The vertical displacement increases with decreasing the depth of salt dome top and increasing the value of the secondary creep constant.

Note that not only the value of secondary creep constant, 2.26×10^{13} (s^{-1}), but also the values of bulk modulus and elastic shear modulus for FCS site are different from those for the baseline as listed in Table 4. Thus, "FCS" rather than A_{SC} is used for the legend in Figure 42 through Figure 52.

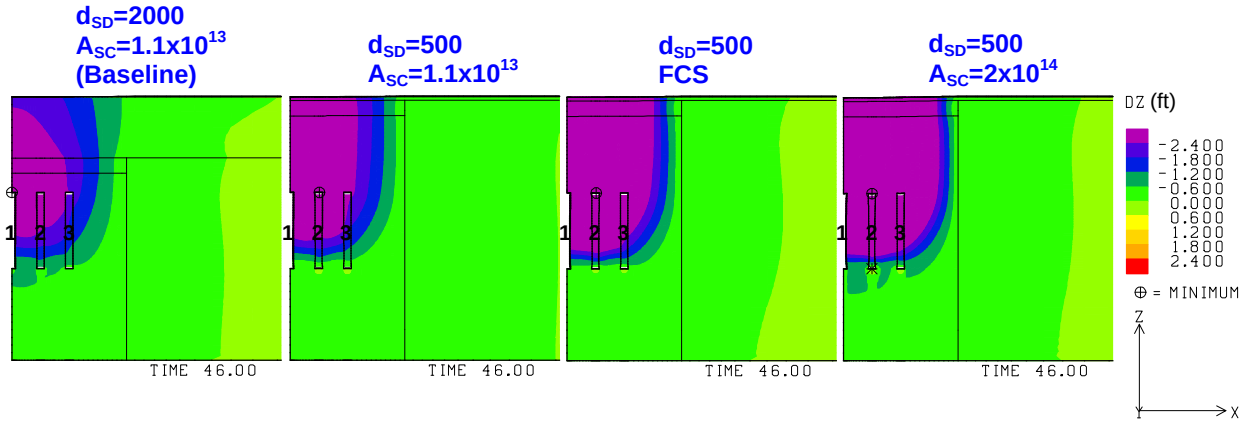

Figure 42: Predicted vertical displacement contours at 46 years for different values of the depth of the salt dome top and secondary creep constant.

Figure 43 shows the predicted total volumetric closure normalized to initial total storage volume for the 19 SPR caverns. The cavern volume loss rate due to salt creep closure increases with decreasing depth of the salt dome top and increasing value of the secondary creep constant. Deeper depth of the salt dome top and smaller value of the creep constant are better from a storage loss viewpoint.

Figure 44 shows the predicted subsidence on the surface above Cavern 1 with time for different depth of salt dome top and secondary creep constant values. Figure 45 shows the predicted subsidence on the surface from the center to the edge of the model at 46 years for the depth and creep constant values. The subsidence on the surface above the center of Cavern 1 increases with decreasing depth of the salt dome top and increasing the value of the secondary creep constant. Deeper depth of the salt dome top and smaller value of the creep constant are better from a subsidence viewpoint.

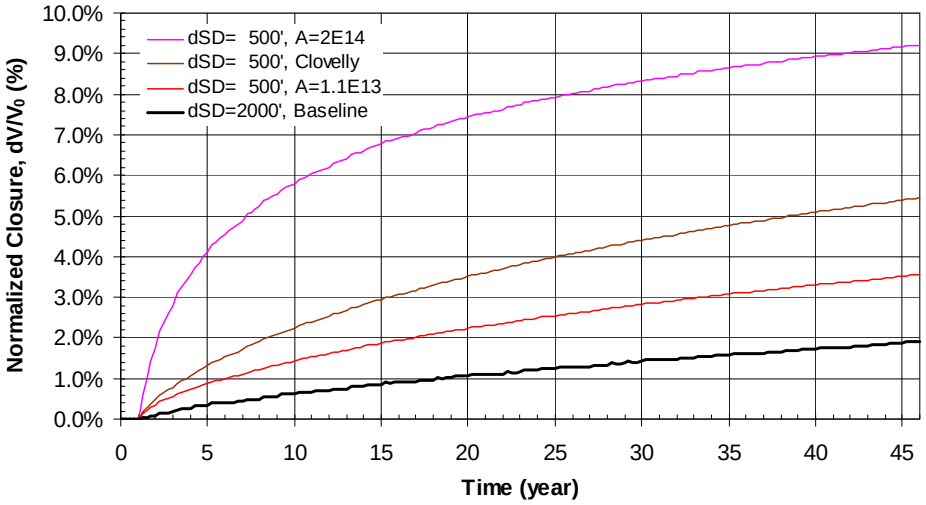

Figure 43: Comparison of predicted total volumetric closure normalized to initial total storage volume for the 19 SPR caverns for different depths of salt dome top and secondary creep constant values.

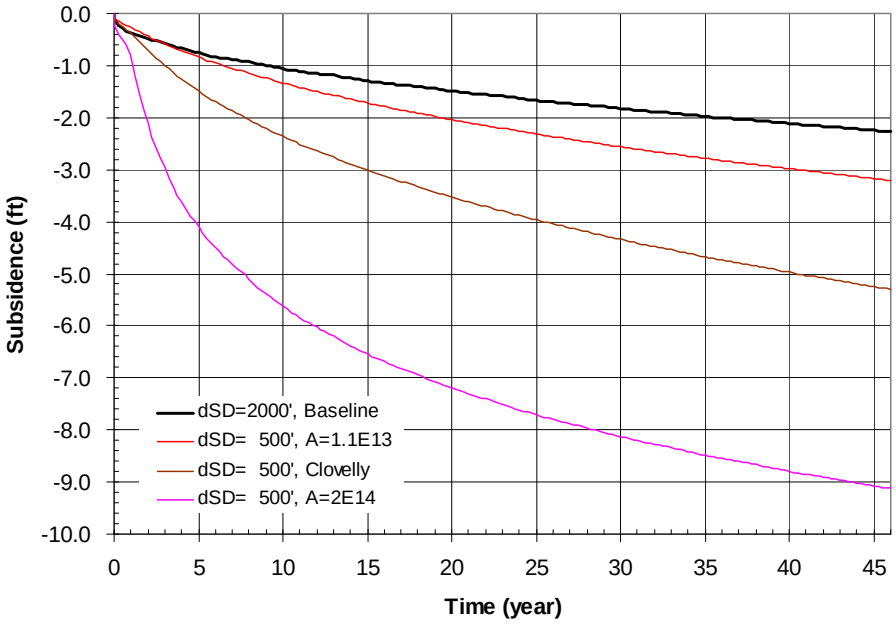

Figure 44: Comparison of predicted subsidence on the surface above Cavern 1 with time for different depths of salt dome top and secondary creep constant values.

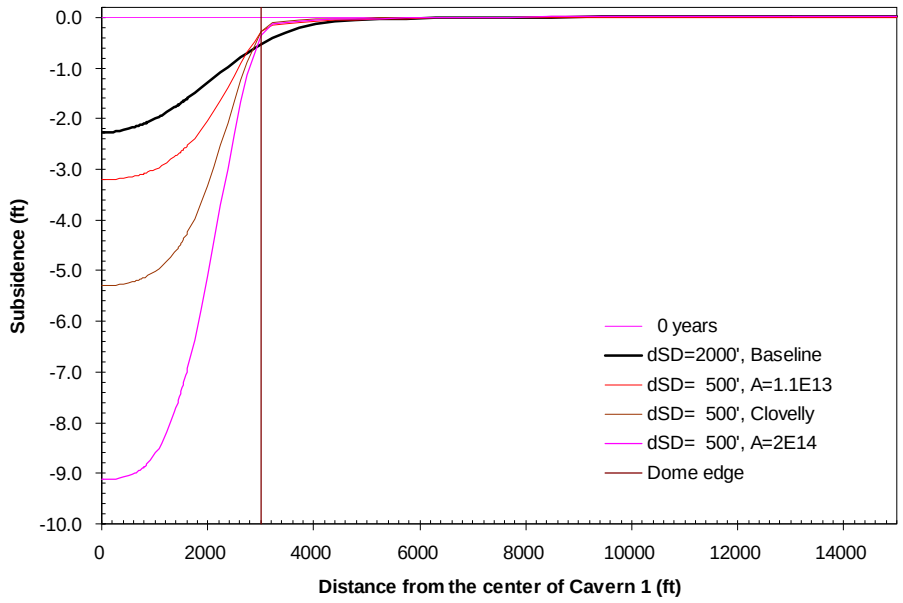

Figure 45: Comparison of predicted subsidence on the surface from model center to edge at 46 years for different depths of salt dome top and secondary creep constant values.

Figure 46 shows the predicted radial surface strains at 46 years with the depth of the salt dome top and the secondary creep constant values. The radial surface strain increases with decreasing the depth of the salt dome top and increasing the value of the secondary creep constant. Deeper depth of the salt dome top and smaller value of the creep constant are better for radial surface strain. The strain on the surface above the edge of salt dome, when the value of secondary creep constant is more than 1.1×10^{13} (s^{-1}) and depth of salt dome top is 500 ft, is beyond the allowable strain for surface structure (1 millistrain in either compression or tension).

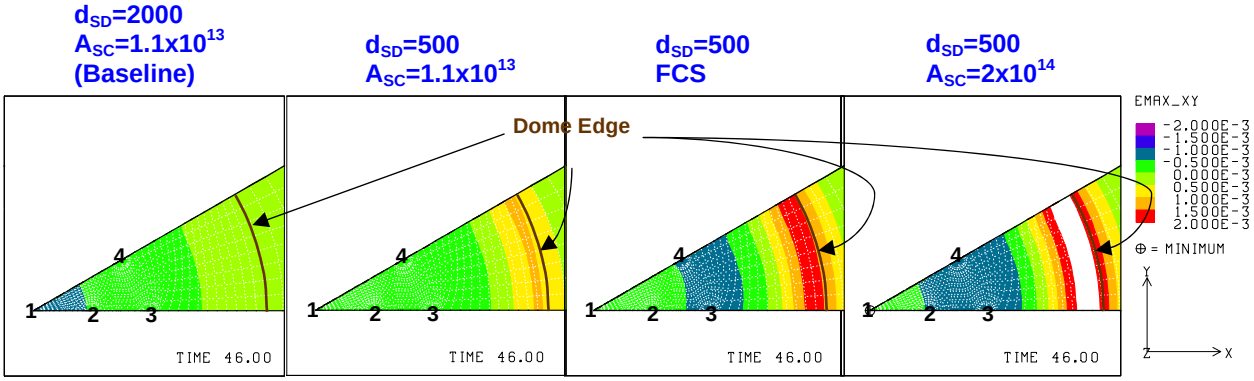

Figure 46: Predicted radial surface strains at 46 years for different depths of salt dome top and secondary creep constant values.

Figure 47 shows the predicted vertical strains around the roof of the caverns at 46 years with the depth of the salt dome top and the secondary creep constants. The vertical strain increases with decreasing the depth of the salt dome top and increasing the value of the secondary creep constant. A deeper depth of the salt dome top and smaller value of the creep constant are better

from a vertical strain viewpoint. Well casings typically extend from the surface to about 100 ft above the cavern roof (compare with 200 ft of the cavern diameter). The strain for d_{SD} = 500 ft and A_{SC} = 2.0×10^{14} (s^{-1}) at 100 ft above the cavern roof is beyond the allowable strain for cemented annulus of the well (0.2 and 2 millistrain in tension for cement and steel casing, respectively).

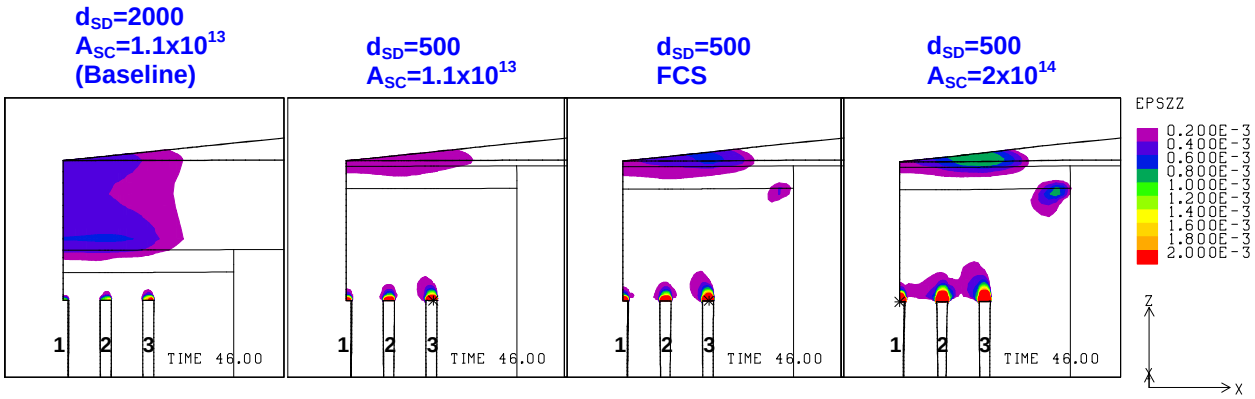

Figure 47: Predicted vertical strains around the roof of caverns at 46 years for different depths of salt dome top and secondary creep constant values

Figure 48 shows the predicted minimum compressive stress history in the salt dome with the depth of the salt dome top and the secondary creep constants. The negative sign (-) indicates a compressive stress. The peaks appear during the workover of the caverns.

Structural stability against tensile failure decreases with decreasing the depths of the salt dome top. Larger thicknesses of the overburden and the caprock are better from a tensile failure perspective. Tensile failure is predicted to occur around the top of the salt dome edge as shown Figure 49 when the value of secondary creep constant is more than 1.1×10^{13} (s^{-1}) and depth of salt dome top is 500 m. The stability of the salt dome top against tensile failure is increased with the smaller value of the secondary creep constant.

Figure 50 shows the predicted minimum compressive stress contours in the overburden, caprock, salt dome, and surrounding rock for different depths of salt dome top and secondary creep constant values. The areas in white indicate the predicted tensile failure zone. Tensile failure is predicted to occur in the caprock and rock surrounding the dome edge for all cases. When the salt dome top depth is 500 ft, the failure zone appears in a larger area. This implies that a shallower depth of the salt dome top yields a greater tensile failure zone in the caprock and surrounding rock. When the salt dome top depth is 500 ft and the secondary creep constant is 2×10^{14} (s^{-1}), the tensile failure occurs even on the surface (overburden) at 12.25 years.

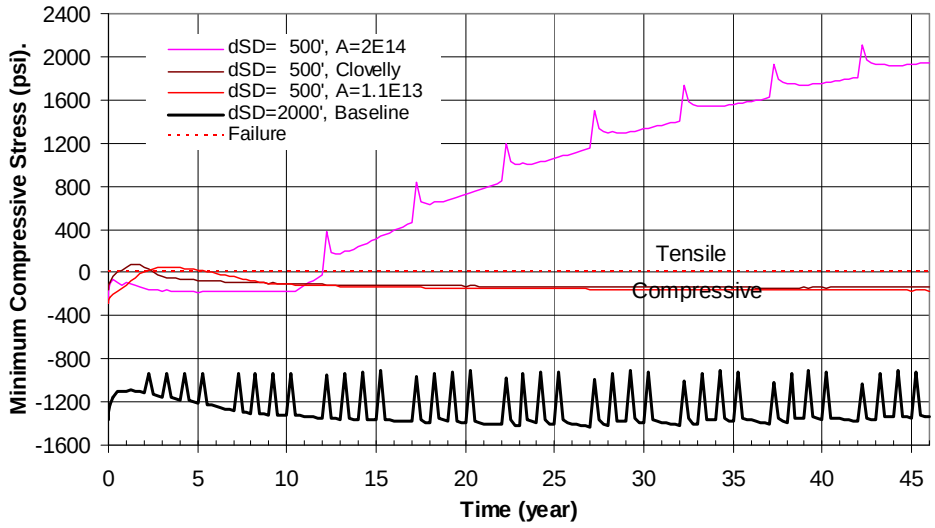

Figure 48: Comparison of predicted minimum compressive stress history in the salt dome for different depths of salt dome top and secondary creep constant values.

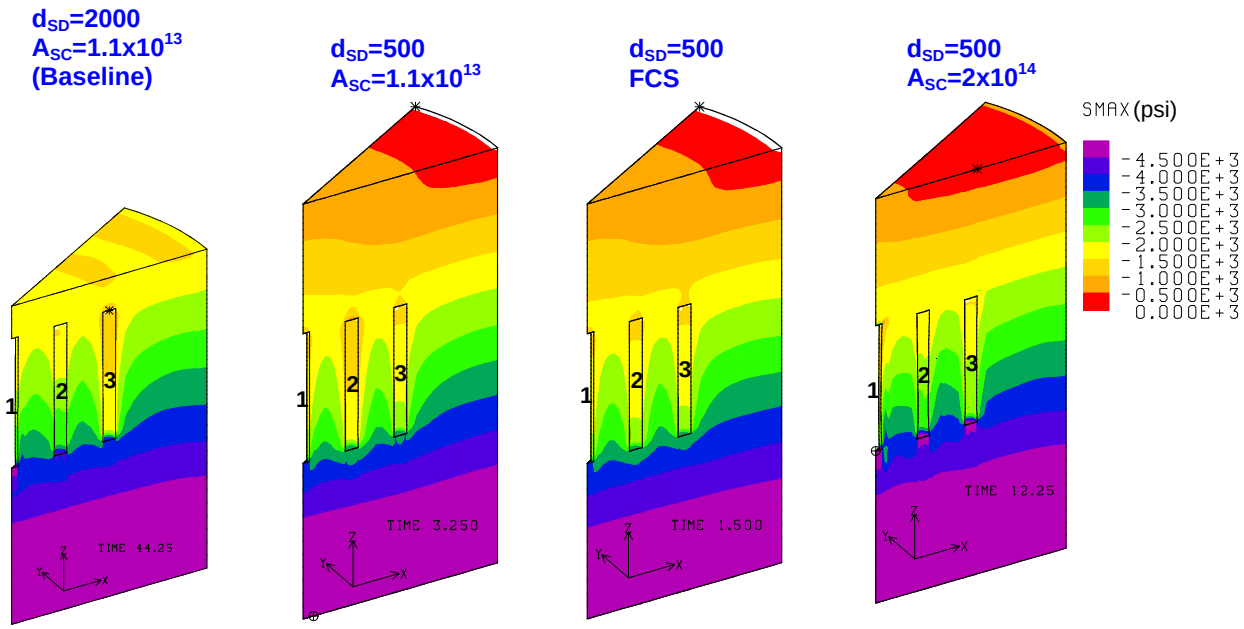

Figure 49: Compressive stress contours in the dome for different depths of salt dome top and secondary creep constant values. Tensile failure occurs around the top of the dome edge when the depth of salt dome top is 500 ft.

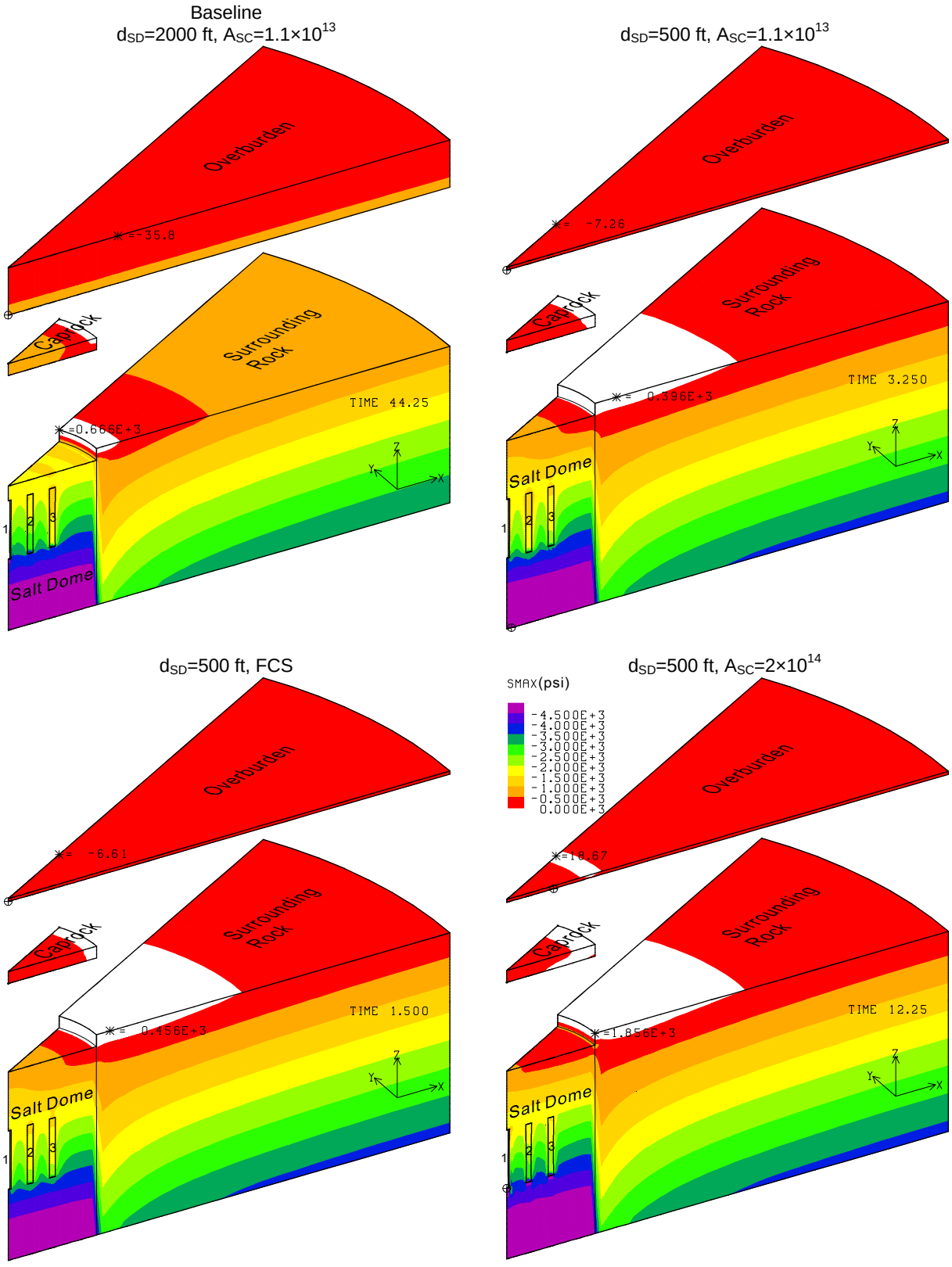

Figure 50: Compressive stress contours in the four blocks for different depths of salt dome top and secondary creep constant values.

Figure 51 shows the predicted minimum safety factor history against dilatant damage in the salt dome with differences in the depth of the salt dome top and secondary creep constants. The peaks appear during the workover of the caverns. Safety factor against dilatancy decreases with decreasing the depth of the salt dome top. Dilatant damage is predicted to occur when the value of secondary creep constant is more than 1.1×10^{13} (s^{-1}) and depth of salt dome top is 500 m. A smaller value of secondary creep constant is better from a dilatant damage viewpoint. Dilatant damage is predicted to occur around the salt dome top edge when the depth of the salt dome top is 500 ft and A_{SC} values are those for the baseline and FCS. Dilatant damage is predicted to occur at the roof of Cavern 1 at 12.25 years when $A_{SC} = 2\times10^{14}$ (s^{-1}) as shown Figure 52.

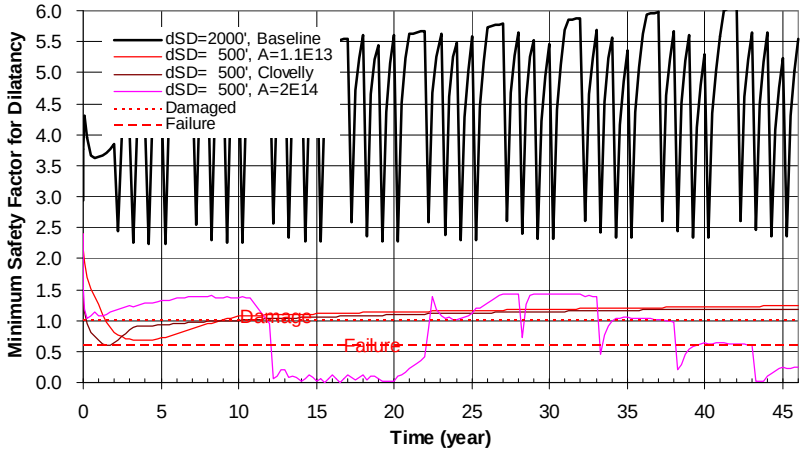

Figure 51: Comparison of predicted minimum safety factor history against dilatant damage in salt dome for different depths of salt dome top and secondary creep constant values.

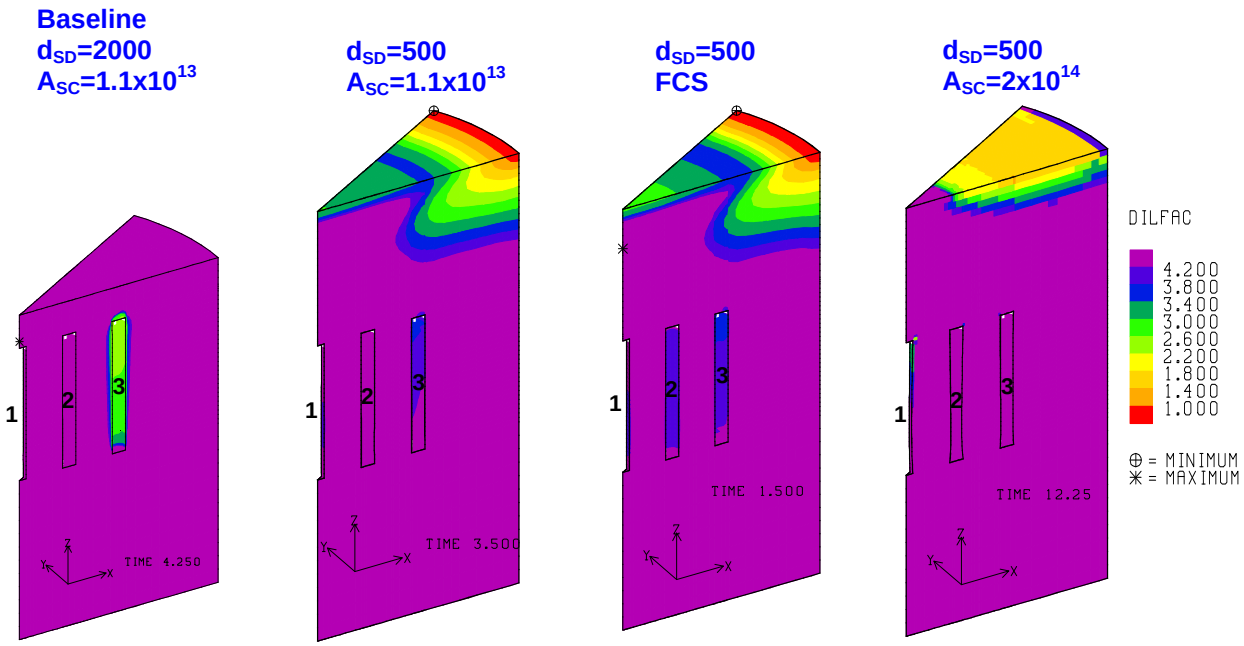

Figure 52: Safety factor contours against dilatant damage in the dome for different depths of salt dome top and secondary creep constant values.

In conclusion, a deeper depth of the salt dome top is more advantageous from a storage loss, subsidence, integrity of surface structure, cemented annulus well and structural stability viewpoints.

Smaller value of secondary creep constant (slower creep rate) is more advantageous from a storage loss, subsidence, integrity of surface structure, cemented annulus well and structural stability viewpoint like the result in Section 7.1 even though the depth of the salt dome top is shallow.

7.3. Effect of Dome Size and Standoff Distance

To examine the effect of the salt dome size and the standoff distance between the edge of the outmost cavern and the salt dome, the analyses were conducted with the model given in Section 3.4.

Figure 53 shows the vertical displacement contours at 46 years for the baseline case and a salt dome having a radius of 1700 ft, respectively. The vertical displacement decreases with decreasing the radius of the salt dome.

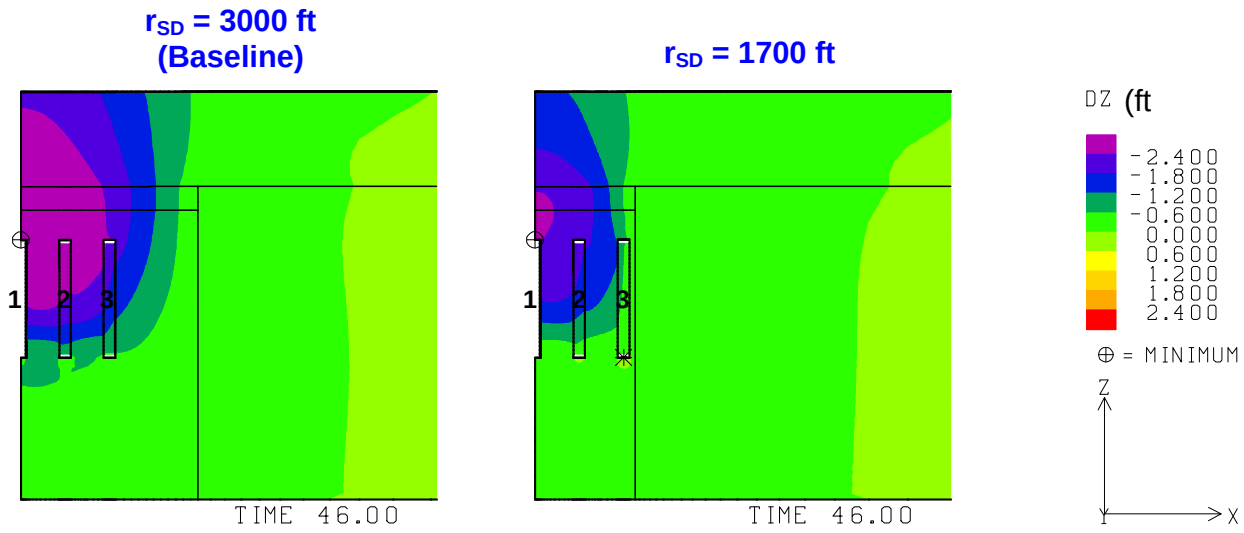

Figure 53: Vertical displacement contours at 46 years for salt domes of radii r_{SD} = 3000 (baseline) and 1700 ft.

Figure 54 shows the predicted total volumetric closure normalized to initial total storage volume for the two salt dome models with different radii. The cavern volume loss rate due to salt creep closure decreases with decreasing the dome radius. A smaller dome radius is better from a storage loss viewpoint.

Figure 55 shows the predicted subsidence on the surface above Cavern 1 with time for the baseline model and the model having a dome radius of 1700 ft. Figure 56 shows the predicted subsidence on the surface from the centers to the edges of the models at 46 years for the baseline and the dome radius of 1700 ft. The subsidence on the surface above the center of Cavern 1

decreases with decreasing the dome radius. Smaller radius of the dome is better from a subsidence viewpoint.

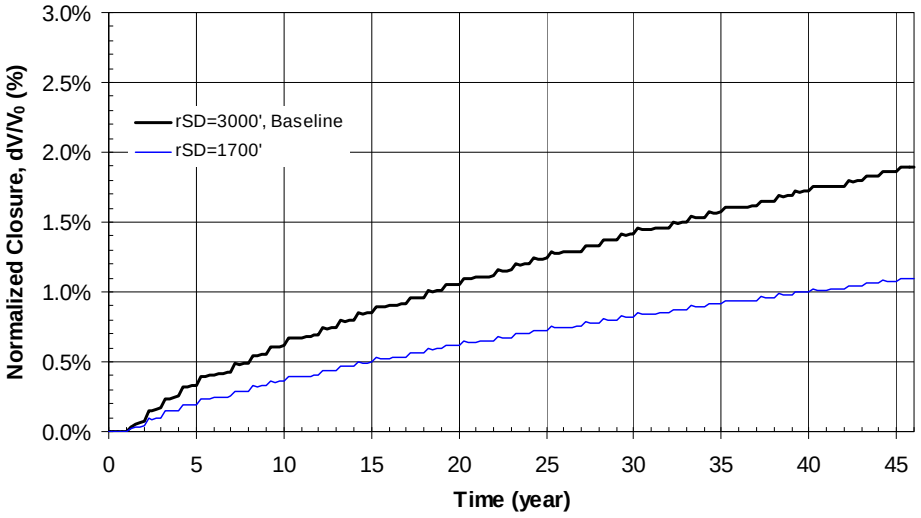

Figure 54: Comparison of predicted total volumetric closure normalized to initial total storage volume for the 19 SPR caverns for salt domes of radii r_{SD} = 3000 (baseline) and 1700 ft.

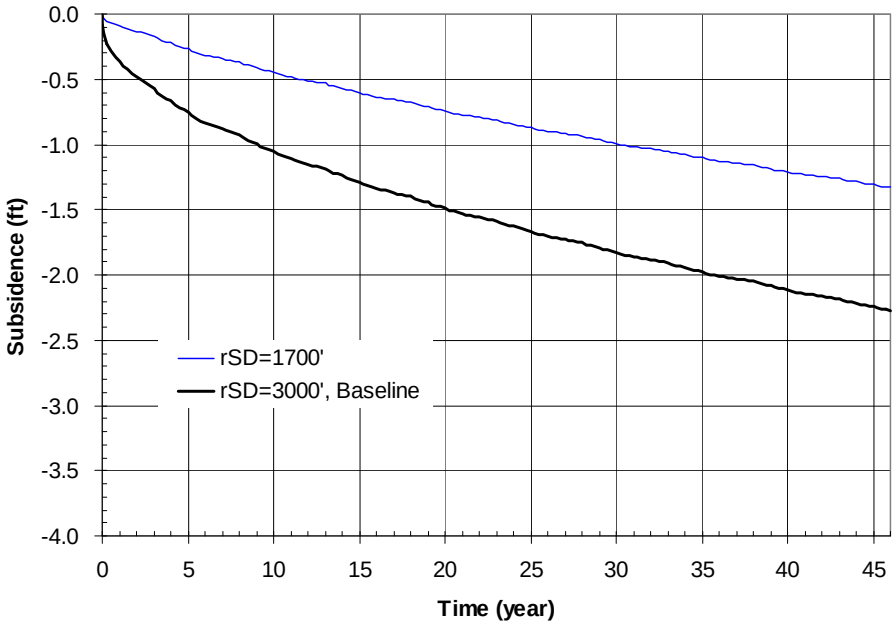

Figure 55: Comparison of predicted subsidence on the surface above Cavern 1 with time for salt domes of radii r_{SD} = 3000 (baseline) and 1700 ft.

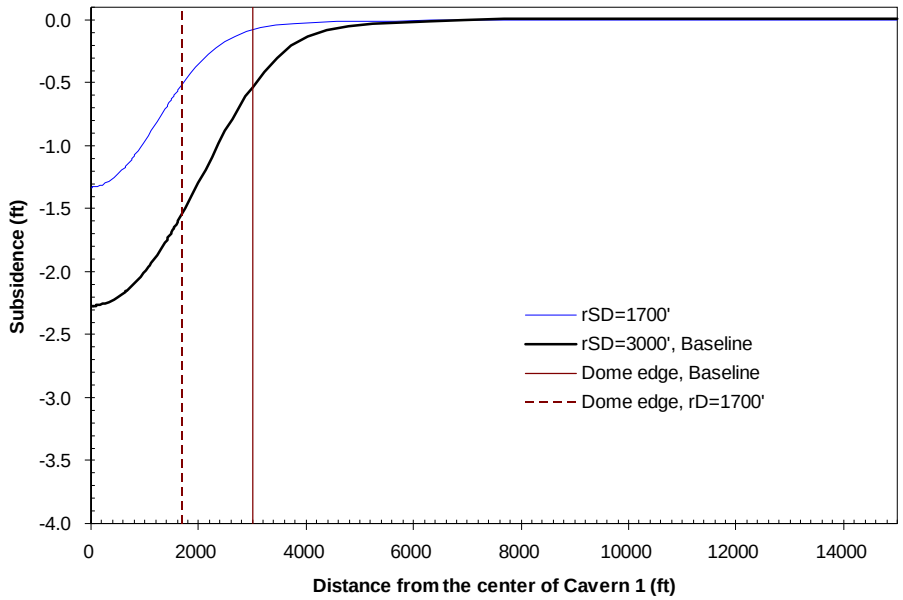

Figure 56: Comparison of predicted subsidence on the surface from model center to edge at 46 years for salt domes of radii r_{SD} = 3000 (baseline) and 1700 ft.

Figure 57 shows the predicted radial surface strains at 46 years for the baseline model and the model with a dome radius of 1700 ft. The radial surface strain decreases with decreasing the radius of the salt dome. A smaller dome radius is better in terms of the radial surface strain. The strain on the surface above the salt dome, when the radius of the salt dome is either 3000 ft or 1700 ft, is within the allowable strain for surface structure (1 millistrain in either compression or tension).

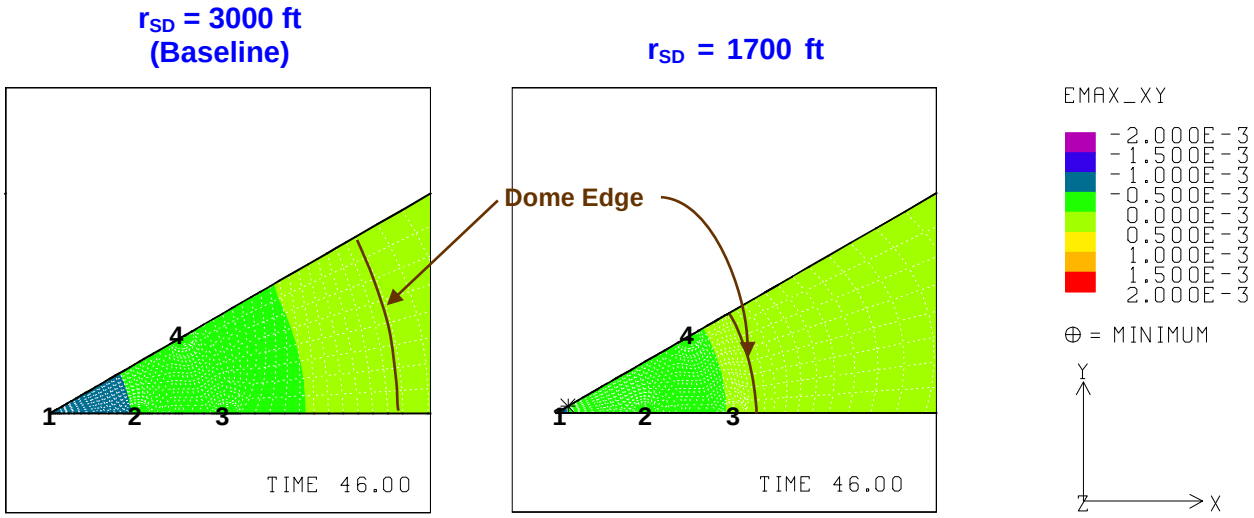

Figure 57: Predicted radial surface strains at 46 years for salt domes of radii r_{SD} = 3000 (baseline) and 1700 ft.

Figure 58 shows the predicted vertical strains around the roof of the caverns at 46 years for the baseline model and the model with a dome radius of 1700 ft. The vertical strain at the roof of the outmost cavern (Cavern 3) increases with decreasing the radius of the salt dome. A smaller

standoff distance, from the outmost cavern to the dome edge, increases the vertical strain in the roof of the outmost cavern. A larger standoff distance is better in terms of accumulated vertical strain.

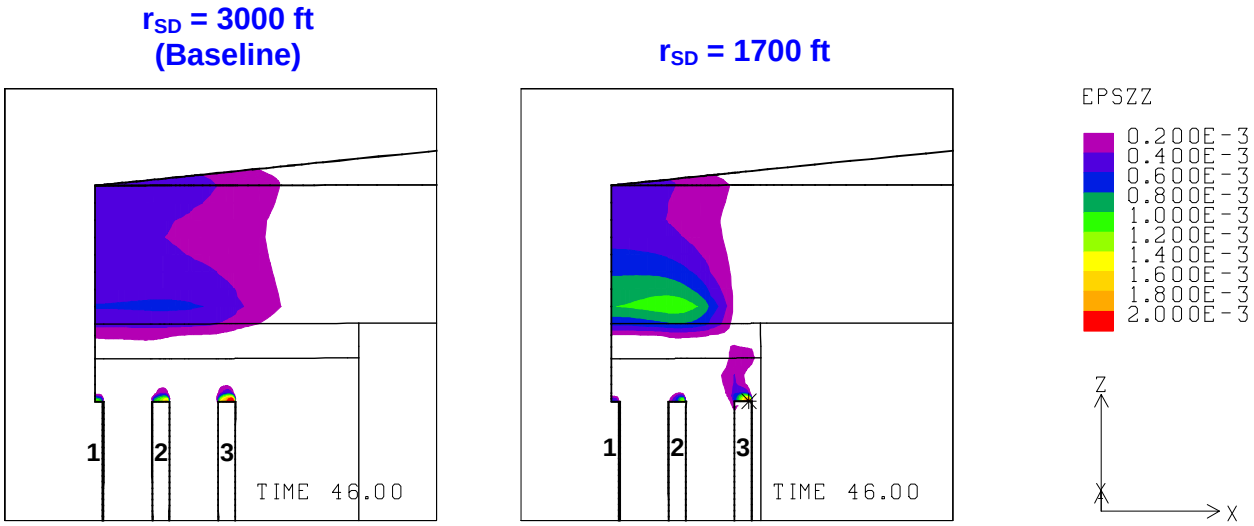

Figure 58: Predicted vertical strains around the roof of caverns at 46 years for salt domes of radii r_{SD} = 3000 (baseline) and 1700 ft.

Figure 59 shows the predicted minimum compressive stress history in the salt dome for the baseline model and the model with a dome radius of 1700 ft. The negative sign (-) indicates a compressive stress. The peaks appear during the workover of the caverns. The radius of the salt dome has little effect on the structural stability of the dome against tensile failure.

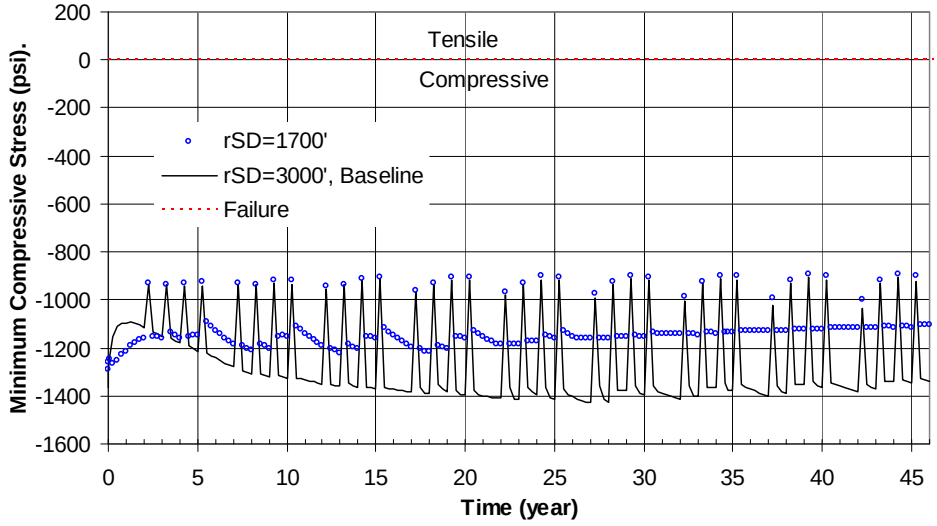

Figure 59: Comparison of predicted minimum compressive stress history in the salt dome for salt domes of radii r_{SD} = 3000 (baseline) and 1700 ft.

Figure 60 shows the predicted minimum safety factor history against dilatant damage in the salt dome for the baseline model and the model with a dome radius of 1700 ft. The peaks appear during the workover of the caverns. A salt dome with a smaller yields a slightly larger safety factor against dilatancy during workovers. All caverns in the salt dome are structurally stable against tensile failure and dilatant damage for either the baseline model or a 1700 ft radius dome.

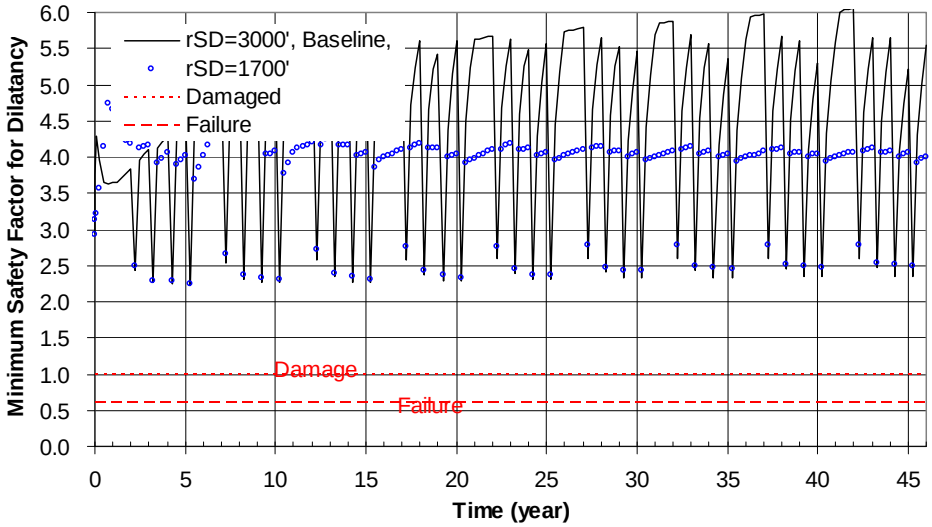

Figure 60: Comparison of predicted minimum safety factor history against dilatant damage in salt dome for salt domes of radii r_{SD} = 3000 (baseline) and 1700 ft.

In conclusion, a smaller radius of salt dome is more advantageous from a storage loss, subsidence, integrity of surface structure, and dilatant damage viewpoints. The radius of the salt dome has little effect on the structural stability against tensile failure. Smaller standoff distance from the edge of the outmost cavern to the dome edge is not better from a vertical strain above the roof of the outmost cavern viewpoint.

7.4. Effect of Caprock Thickness

To examine the caprock thickness effect, the analyses were conducted with the model in Section 3.5. In this comparison the depth to salt dome top is kept constant, and the caprock and overburden thicknesses were reversed.

Figure 61 shows the vertical displacement contours at 46 years for the baseline model and a model with a caprock thickness of 1600 ft, respectively. The vertical displacement decreases with increasing the thickness of the caprock.

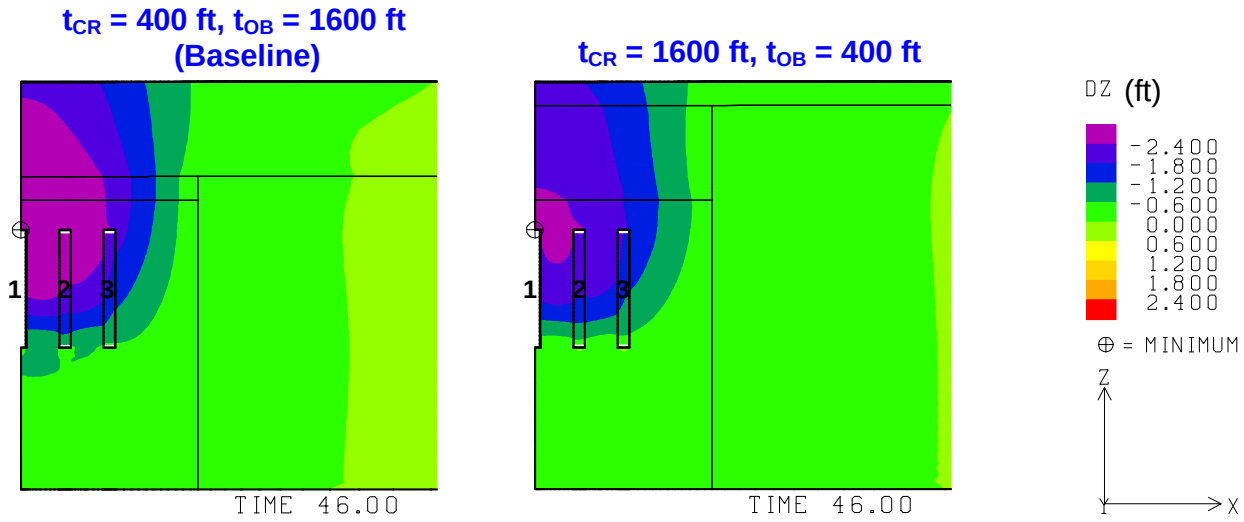

Figure 61: Vertical displacement contours at 46 years using two different thicknesses for the caprock.

Figure 62 shows the predicted total volumetric closure normalized to initial total storage volume for the two models. The cavern volume loss rate due to salt creep closure increases with increasing the caprock thickness. A smaller caprock thickness is better from a storage loss perspective.

Figure 63 shows the predicted subsidence on the surface above Cavern 1 with time for the baseline model and model with a caprock thickness of 1600 ft. Figure 64 shows the predicted subsidence on the surface from the center to the edge at 46 years for the two models. The subsidence on the surface above the center of Cavern 1 decreases with increasing caprock thickness. A larger thickness of the caprock is better for subsidence.

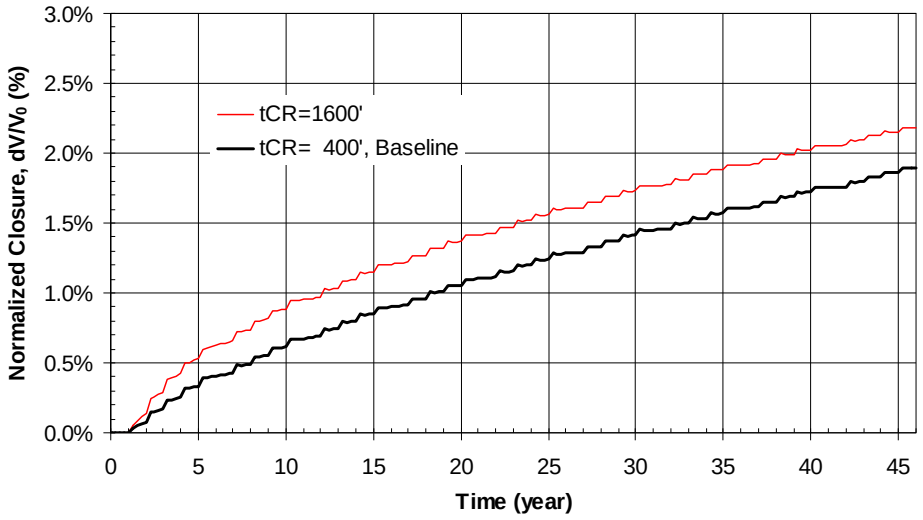

Figure 62: Comparison of predicted total volumetric closure normalized to initial total storage volume for the 19 SPR cavern model using two different thicknesses for the caprock.

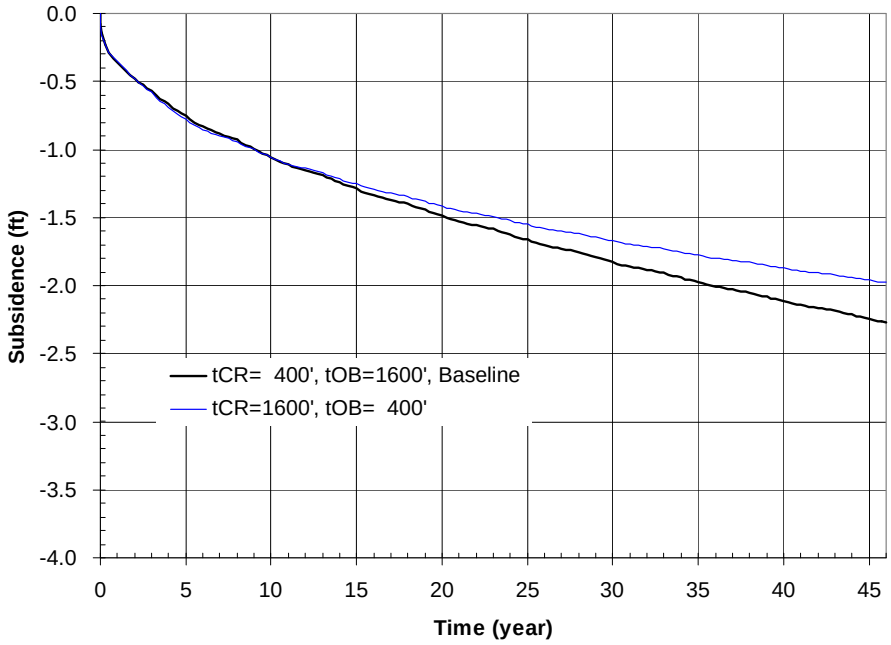

Figure 63: Comparison of predicted subsidence on the surface above Cavern 1 with time using two different thicknesses for the caprock.

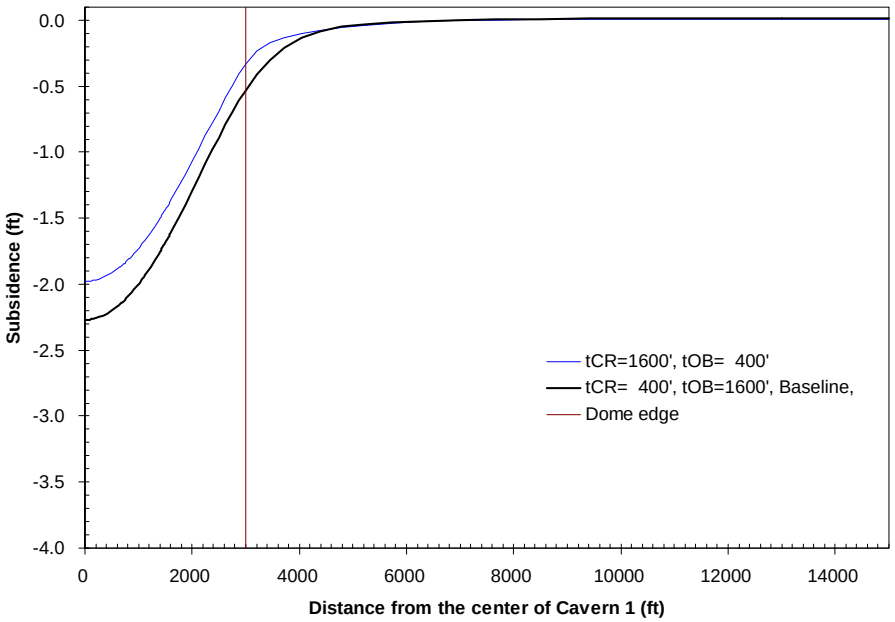

Figure 64: Comparison of predicted subsidence on the surface from model center to edge at 46 years using two different thicknesses for the caprock.

Figure 65 shows the predicted radial surface strains at 46 years for the baseline model and the model with a caprock thickness of 1600 ft. Radial surface strain slightly decreases with increasing the thickness of the caprock. Caprock thickness has little effect on the radial surface

strain. The strains on the surface above the salt dome for both cases are within the allowable strain for a surface structure (1 millistrain in either compression or tension).

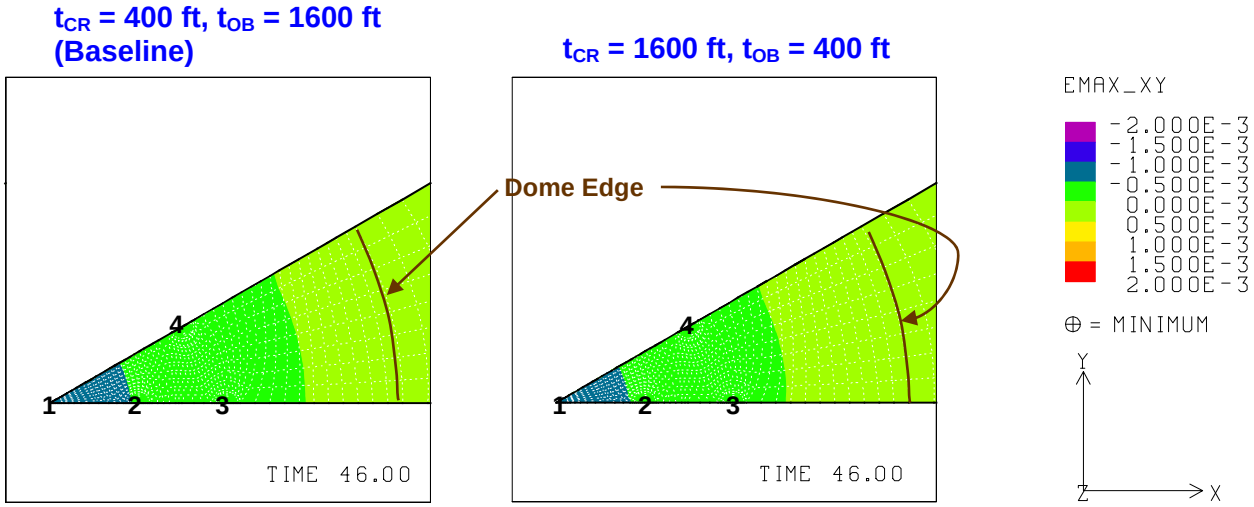

Figure 65: Predicted radial surface strains at 46 years using two different thicknesses for the caprock.

Figure 66 shows the predicted vertical strains around the roof of the caverns at 46 years for the baseline model and a model with a caprock thickness of 1600 ft. Vertical strain at the roof of caverns increases slightly with increasing the thickness of the caprock. A larger caprock thickness slightly increases the vertical strain at the roof of the caverns. Therefore, a smaller caprock thickness is better in terms of a vertical strain.

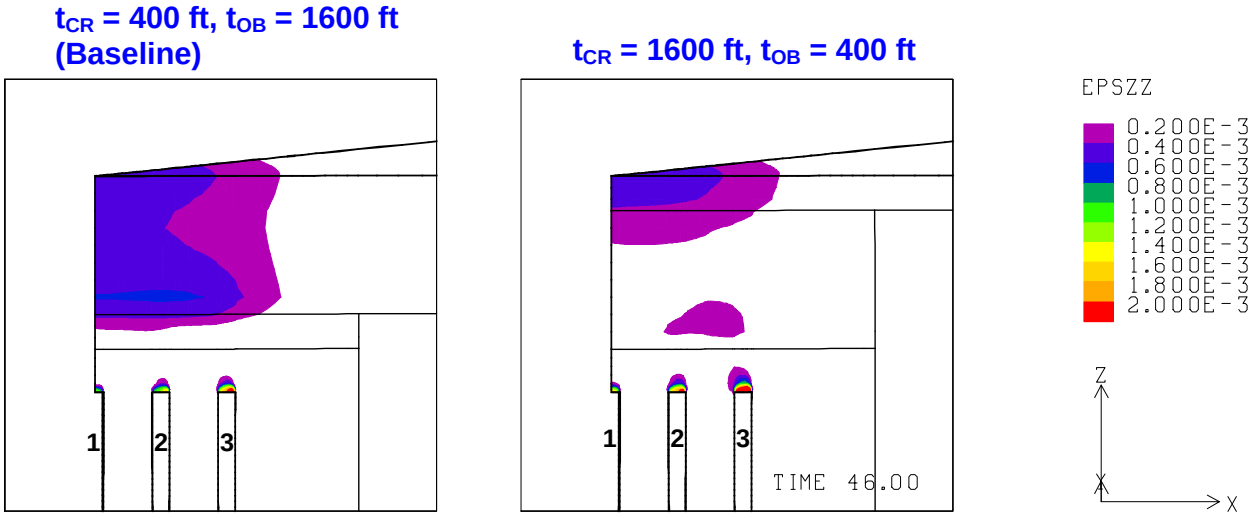

Figure 66: Predicted vertical strains around the roof of caverns at 46 years for two different thicknesses for the caprock

Figure 67 shows the predicted minimum compressive stress history in the salt dome for the baseline model and a model with a caprock thickness of 1600 ft. The negative sign (-) indicates a

compressive stress. The peaks appear during the workover of the caverns. Figure 67 suggests that the thickness of the caprock has little effect on the structural stability against tensile failure.

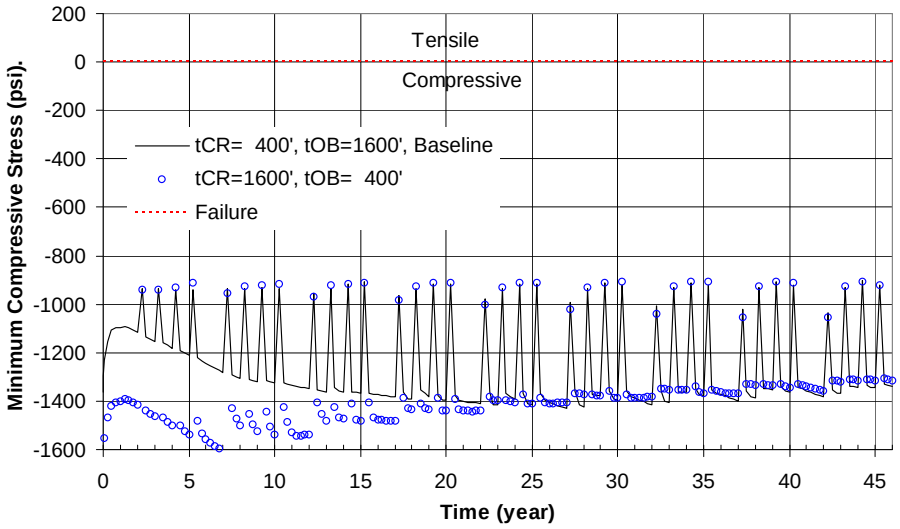

Figure 67: Comparison of predicted minimum compressive stress history in the salt dome using two different thicknesses for the caprock.

Figure 68 shows the predicted minimum safety factor history against dilatant damage in the salt dome for the baseline model and a model with a caprock thickness of 1600 ft. The peaks appear during the workover of the caverns. The thickness of the caprock does not affect the dome's structural stability against dilatant damage much. All caverns and the salt dome are structurally stable against tensile failure and dilatant damage for either the baseline model or the model with a caprock thickness of 1600 ft.

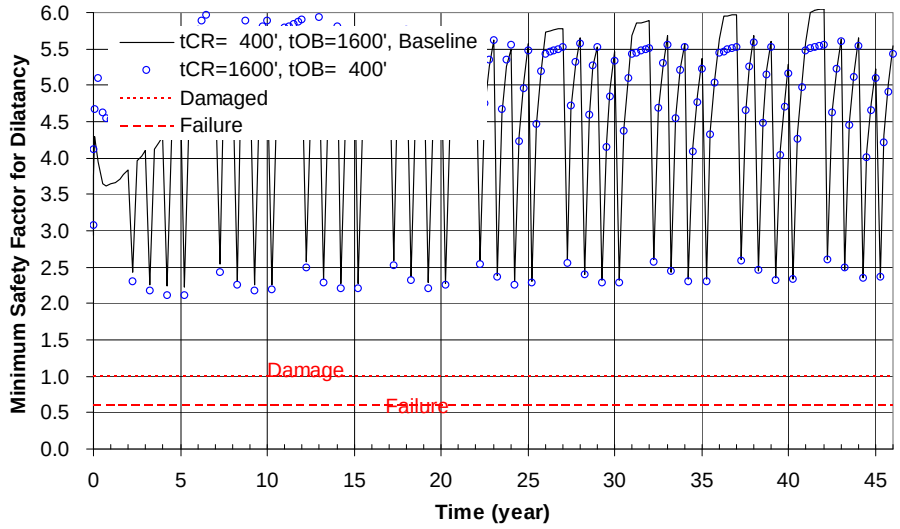

Figure 68: Comparison of predicted minimum safety factor history against dilatant damage in salt dome using two different thicknesses for the caprock.

In conclusion, a larger thickness of caprock is more advantageous from a subsidence viewpoint. However, it is not better from a storage loss and vertical strain above the roof of the caverns viewpoint. But, those impacts are not much in terms of the overall stability of the salt in the dome. The thickness of the caprock has a little effect on the radial surface strain and the structural stability against tensile failure and dilatant damage.

7.5. Elastic Modulus Effect of Caprock Rock

To examine the effect of the elastic modulus of the caprock, analyses were conducted with the baseline model given in Section 3.6.

Figure 69 shows the vertical displacement contours for the baseline model with various elastic moduli of caprock at 46 years. The vertical displacement slightly decreases with increasing the value of elastic modulus of the caprock.

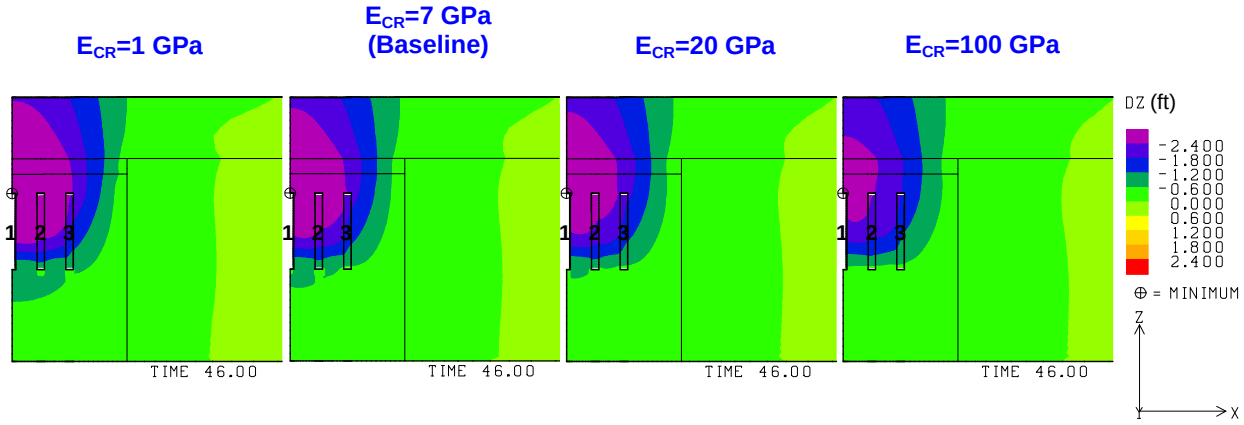

Figure 69: Vertical displacement contours using various elastic moduli of caprock at 46 years.

Figure 70 shows the predicted total volumetric closure normalized to initial total storage volume for the different models. Cavern volume loss rate due to salt creep closure decreases with increasing the value of elastic modulus of the caprock. A larger value of the elastic modulus of the caprock is better from a storage loss perspective.

Figure 71 shows the predicted subsidence on the surface above Cavern 1 with time for the models with various elastic moduli of caprock. Figure 72 shows the predicted subsidence on the surface from the center to the edge of the model at 46 years. Subsidence on the surface above the center of Cavern 1 slightly decreases with increasing the value of elastic modulus of the caprock. Therefore, a larger value of elastic modulus of the caprock is slightly better from a subsidence viewpoint.

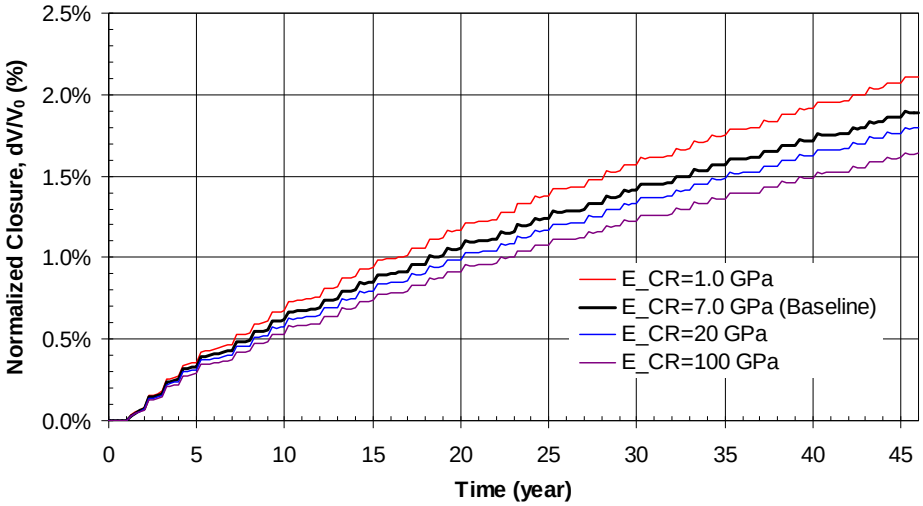

Figure 70: Comparison of predicted total volumetric closure normalized to initial total storage volume for the 19 SPR caverns for the four different elastic moduli of caprock.

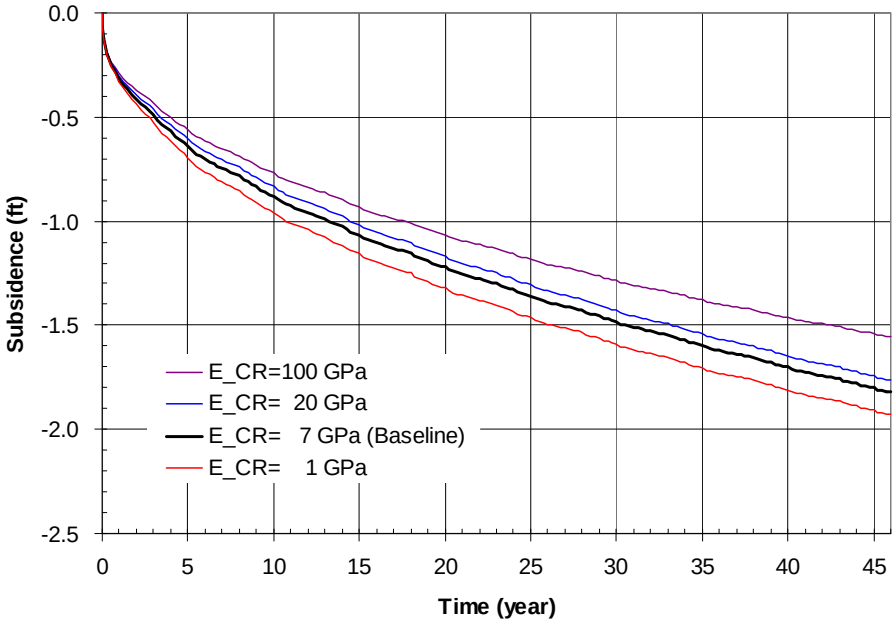

Figure 71: Comparison of predicted subsidence on the surface above Cavern 1 with time for the four different elastic moduli of caprock.

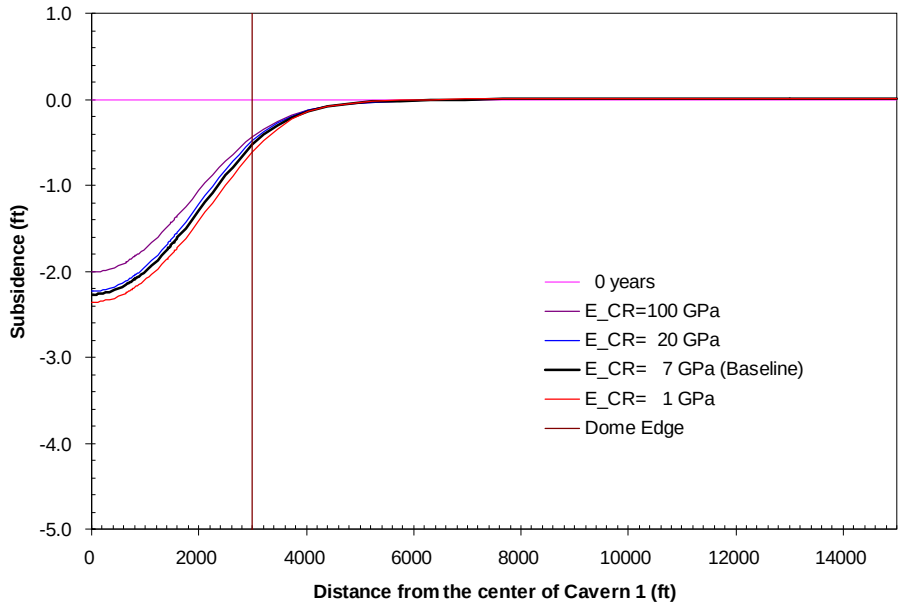

Figure 72: Comparison of predicted subsidence on the surface from model center to edge at 46 years for the four different elastic moduli of caprock.

Figure 73 shows the predicted radial surface strains at 46 years for the models with various elastic moduli of caprock. Radial surface strain slightly decreases with increasing the value of elastic modulus. A larger value of elastic modulus of the caprock is better for a radial surface strain.

The strain on the surface in the middle of salt dome is within the allowable strain for surface structures when the elastic modulus of caprock is larger than 1 GPa (1 millistrain in either compression or tension).

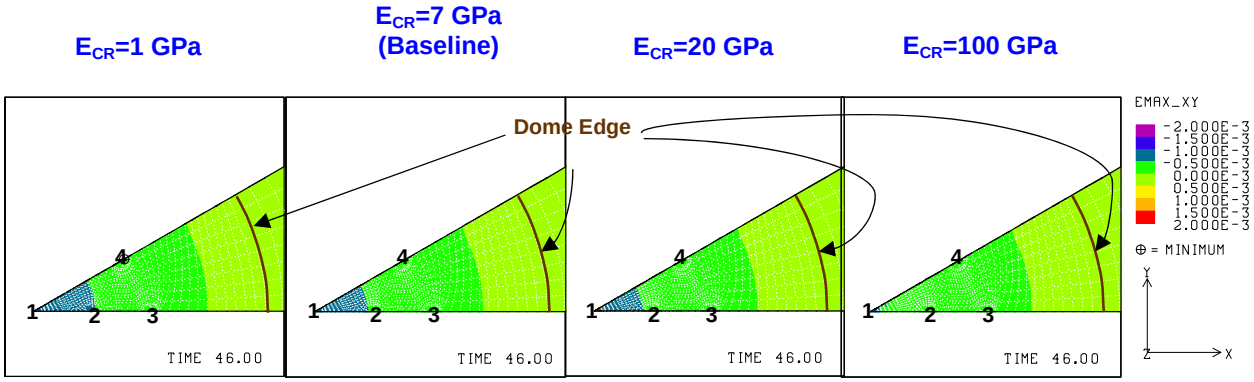

Figure 73: Predicted radial surface strains at 46 years for the four different elastic moduli of caprock.

Figure 74 shows the predicted vertical strains around the roof of the caverns at 46 years for the models with various elastic moduli of caprock. Vertical strain at the roof of the caverns slightly decreases with increasing the value of elastic modulus of the caprock. The elastic modulus of caprock has a little effect on the vertical strains near the cavern wells. The strain for all elastic

moduli above the cavern roof is within the allowable strain for the cemented annulus of the well (0.2 and 2 millistrains in tension for cement and steel casing, respectively).

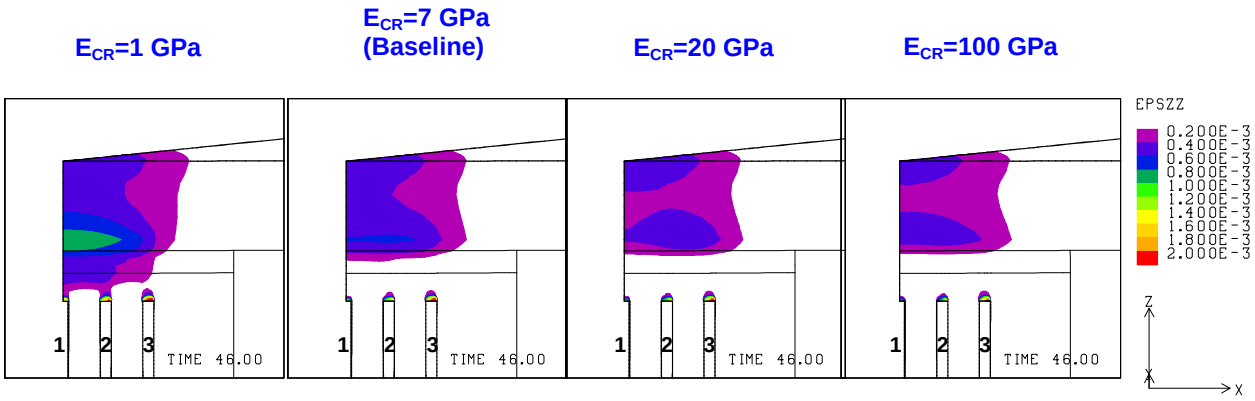

Figure 74: Predicted vertical strains around the roof of caverns at 46 years for the four different elastic moduli of caprock

Figure 75 shows the predicted minimum compressive stress history in the salt dome for the models with different elastic moduli of caprock. The negative sign (-) indicates a compressive stress. The peaks appear during the workover of the caverns. The value of elastic modulus of the caprock does not have an effect on the structural stability against tensile failure when the value is larger than 7 GPa.

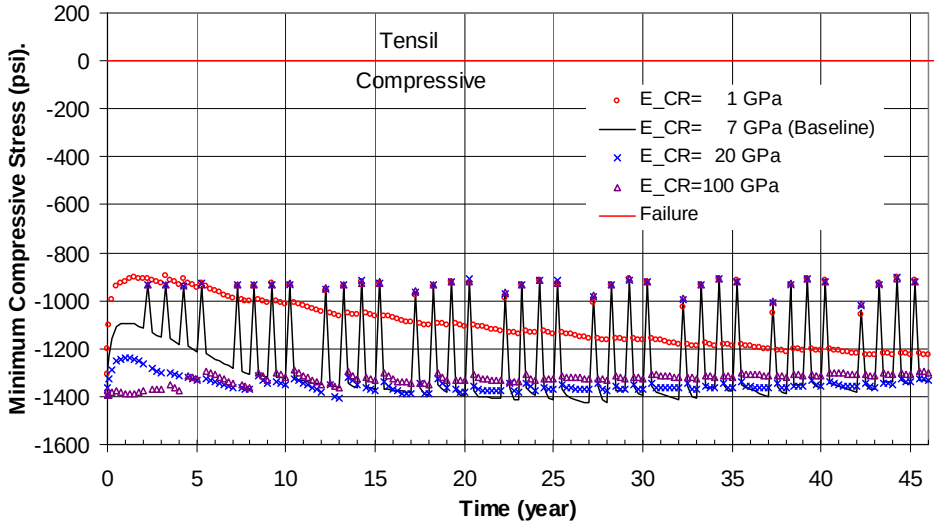

Figure 75: Comparison of predicted minimum compressive stress history in the salt dome for the four different elastic moduli of caprock.

Figure 76 shows the predicted minimum safety factor history against dilatant damage in the salt dome for the models with various elastic moduli of caprock. The peaks appear during the workover of the caverns. The value of elastic modulus of the caprock has only a small effect on the structural stability against dilatant damage, it particular when its value is 1 GPa.

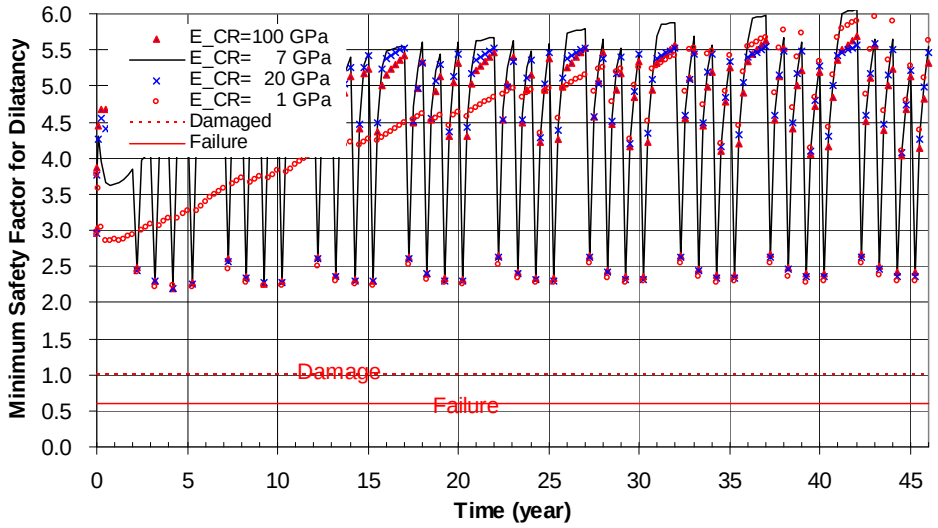

Figure 76: Comparison of predicted minimum safety factor history against dilatant damage in salt dome for the four different elastic moduli of caprock.

In conclusion, a larger value for the elastic modulus of the caprock is slightly more advantageous from a storage loss, subsidence, integrity of surface structure and cemented annulus well perspective. The value of elastic modulus of the caprock does not affect the structural stability of the caverns when the value is larger than 7 GPa.

7.6. Elastic Modulus Effect of Surrounding Rock

To examine the elastic modulus effect of surrounding rock, the analyses are conducted with the baseline model given in Section 3.7.

Figure 77 shows the vertical displacement contours for the baseline model with various elastic moduli of surrounding rock at 46 years. The vertical displacement rapidly increases with decreasing the value of elastic modulus of the surrounding rock.

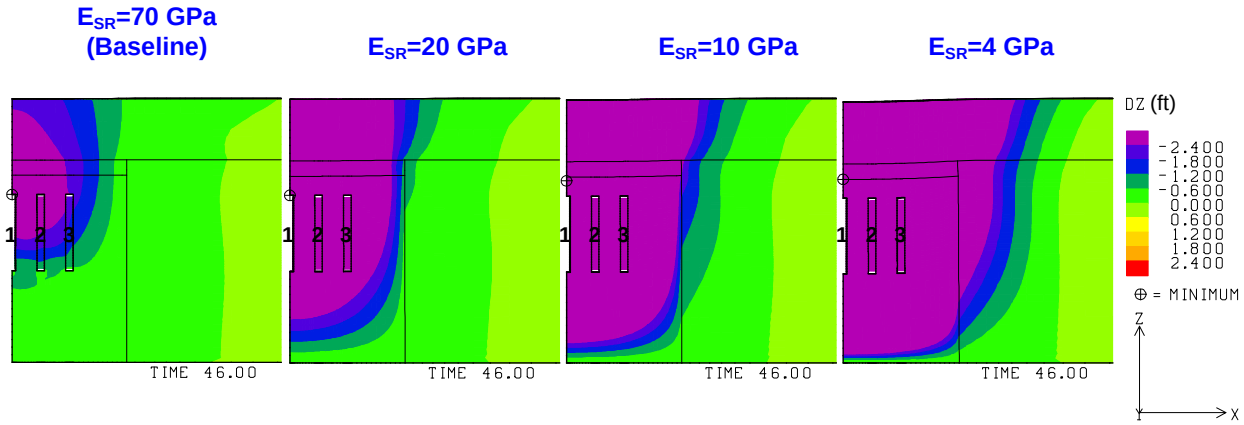

Figure 77: Vertical displacement contours using various elastic moduli of surrounding rock at 46 years.

Figure 78 shows the predicted total volumetric closure normalized to initial total storage volume for the 19 SPR cavern models with differing elastic moduli of the surrounding rock. Cavern volume loss rate due to salt creep closure increases with increasing the value of elastic modulus of the surrounding rock. A smaller value of elastic modulus of the surrounding rock is better from a storage loss perspective.

Figure 79 shows the predicted subsidence on the surface above Cavern 1 with time for the models with various elastic moduli of surrounding rock. Figure 80 shows the predicted subsidence on the surface from the center to the edge of the model at 46 years. Subsidence on the surface above the center of Cavern 1 increases with decreasing value of elastic modulus of the surrounding rock. A larger value of elastic modulus of the surrounding rock is better from a subsidence viewpoint. The subsidence rate rapidly increases when the value of elastic modulus of the surrounding rock is less than 10 GPa.

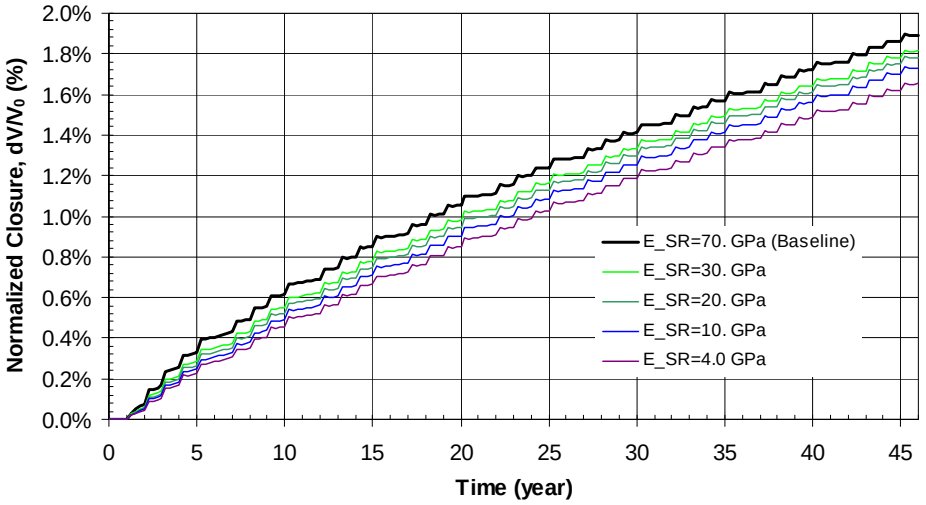

Figure 78: Comparison of predicted total volumetric closure normalized to initial total storage volume for the 19 SPR caverns for four different elastic moduli of surrounding rock.

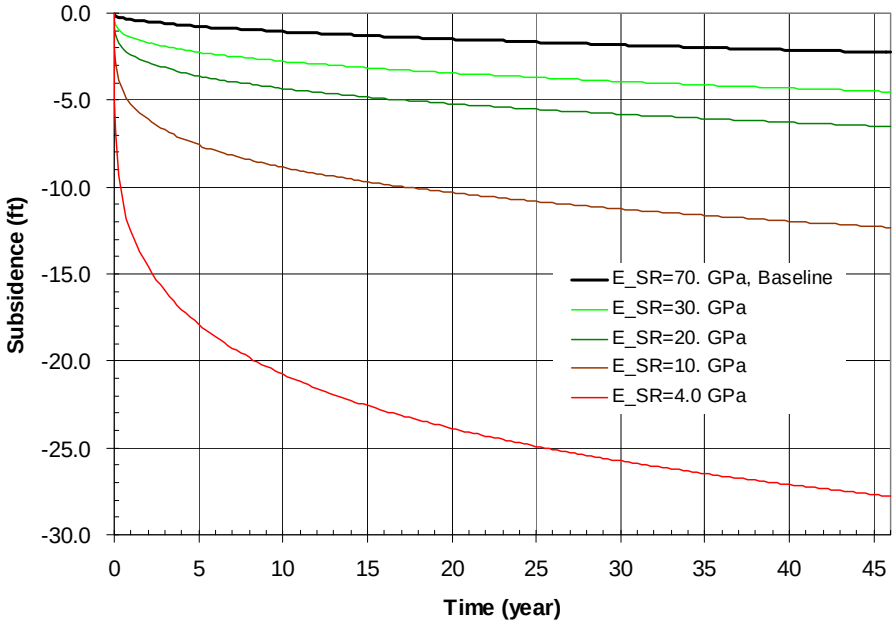

Figure 79: Comparison of predicted subsidence on the surface above Cavern 1 with time for four different elastic moduli of surrounding rock.

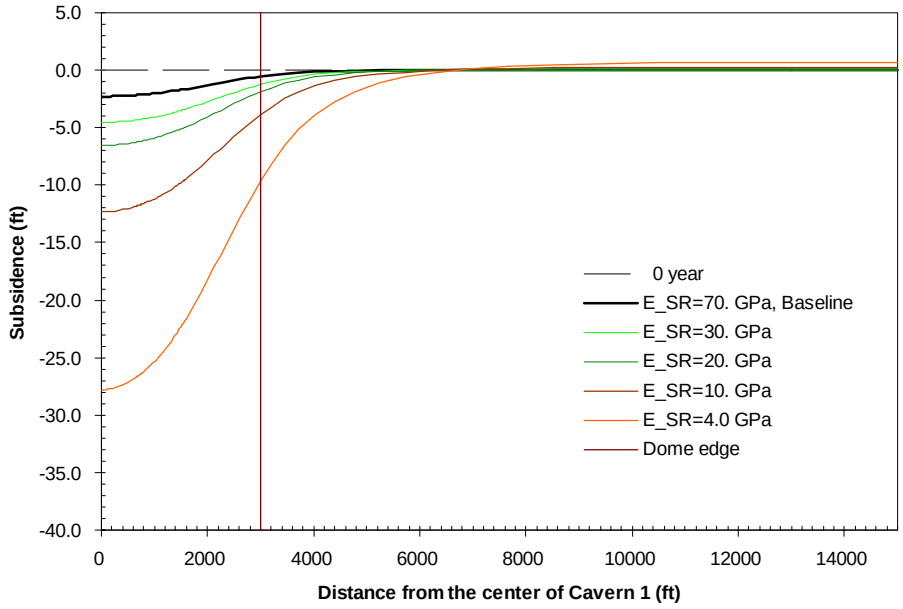

Figure 80: Comparison of predicted subsidence on the surface from model center to edge at 46 years for four different elastic moduli of surrounding rock.

Figure 81 shows the predicted radial surface strains at 46 years for the baseline model with various elastic moduli of surrounding rock. Radial surface strain increases with decreasing the value of elastic modulus of the surrounding rock. A larger value of elastic modulus of the surrounding rock is better in terms of radial surface strain.

When the value of elastic modulus of the surrounding rock is less than 20 GPa, the strain on the surface in the middle of salt dome is beyond the allowable strain for surface structures (1 millistrain in either compression or tension). This suggests that a limiting value of elastic modulus for the surrounding rock exists between 20 GPa and 30 GPa when the values of other parameters are the same as those for the baseline case from a radial surface strain viewpoint.

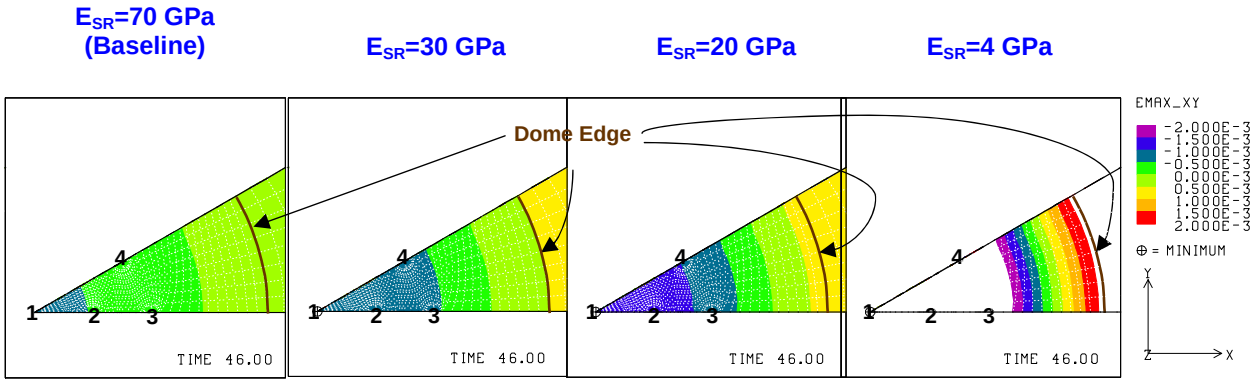

Figure 81: Predicted radial surface strains at 46 years for the four different elastic moduli of surrounding rock.

Figure 82 shows the predicted vertical strains around the roof of the caverns at 46 years for the models with differing elastic moduli of surrounding rock. Vertical strain at the roof of the caverns slightly decreases with decreasing the value of elastic modulus of the surrounding rock. However, vertical strain in the layers above the salt dome rapidly increases with decreasing value of elastic modulus of the surrounding rock. The strain for all elastic moduli above the cavern roof is within the allowable strain for a cemented well annulus (0.2 and 2 millistrains in tension for cement and steel casing, respectively). However, the cemented annulus of the well in the overburden and caprock layers can be damaged severely when the elastic modulus of the surrounding rock is less than 10 GPa.

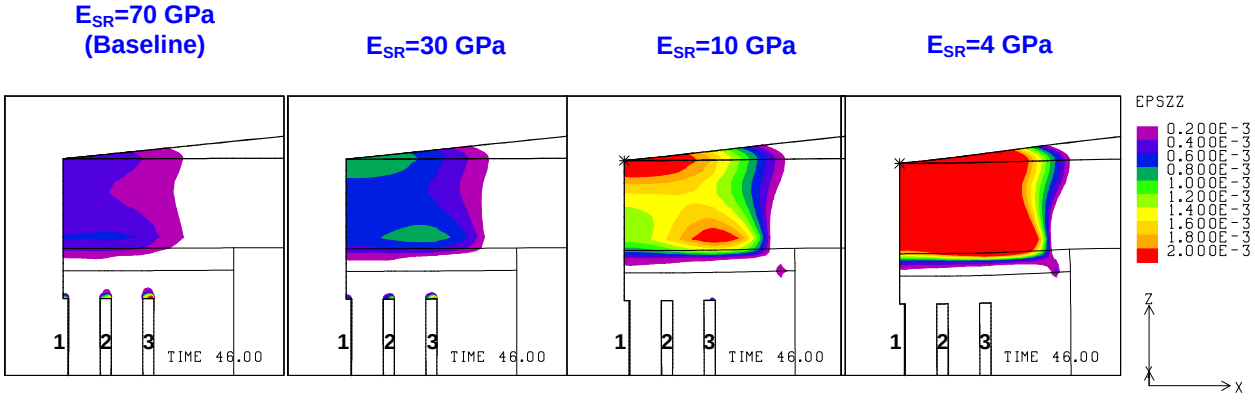

Figure 82: Predicted vertical strains around the roof of caverns at 46 years for the four different elastic moduli of surrounding rock

Figure 83 shows the predicted minimum compressive stress history in the salt dome for the models with various elastic moduli of surrounding rock. The negative sign (-) indicates a compressive stress. The peaks appear during the workover of the caverns.

The value of elastic modulus of the surrounding rock does not have an effect on the structural stability against tensile failure when the value is larger than 20 GPa. Structural stability against tensile failure rapidly decreases with decreasing the value of elastic modulus of the surrounding rock when the value is less than 10 GPa.

Minimum compressive stress occurs in the roof of the caverns during workover as shown Figure 84. We can see the value of elastic modulus of the surrounding rock does not affect the structural stability against tensile failure much when the value is larger than 10 GPa.

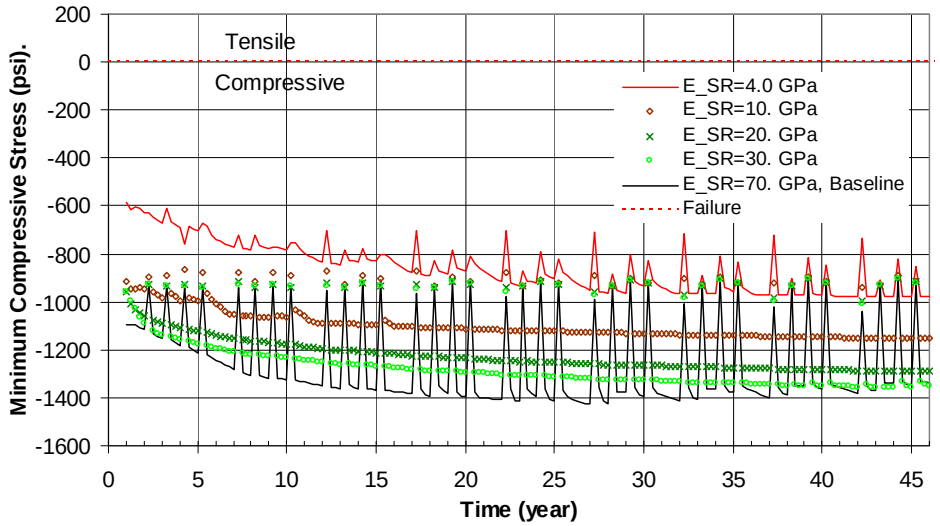

Figure 83: Comparison of predicted minimum compressive stress history in the salt dome for the four cases of different elastic moduli of surrounding rock.

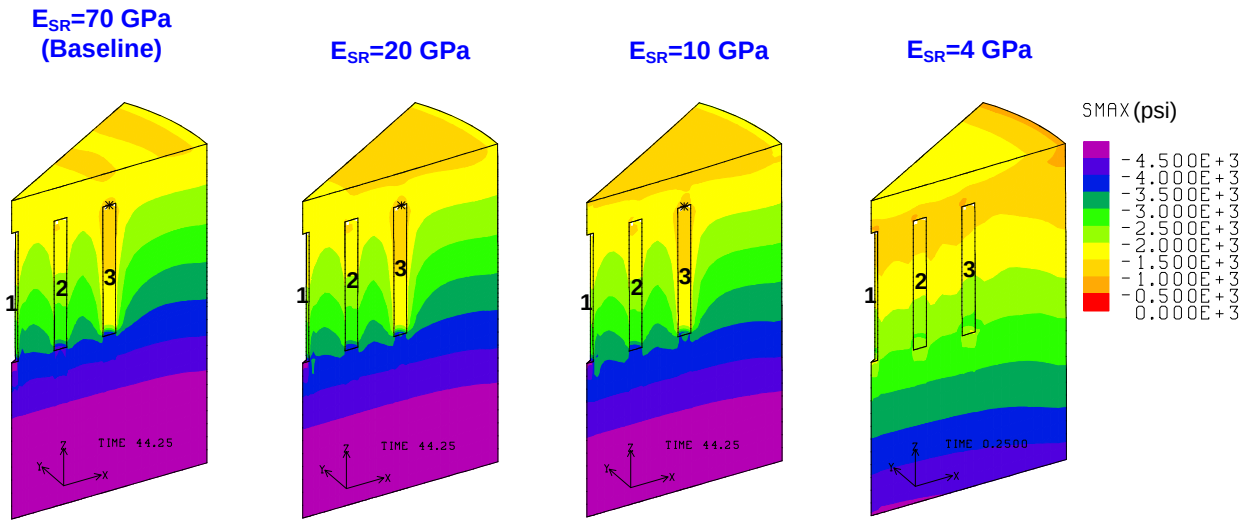

Figure 84: Compressive stress contours in the salt dome for the four models with different elastic moduli of surrounding rock.

Figure 85 shows the predicted minimum safety factor history against dilatant damage in the salt dome for the four models with various elastic moduli of surrounding rock. The peaks appear

during the workover of the caverns. The value of elastic modulus of the surrounding rock has only a small effect on the structural stability against dilatant damage when its value is larger than 10 GPa.

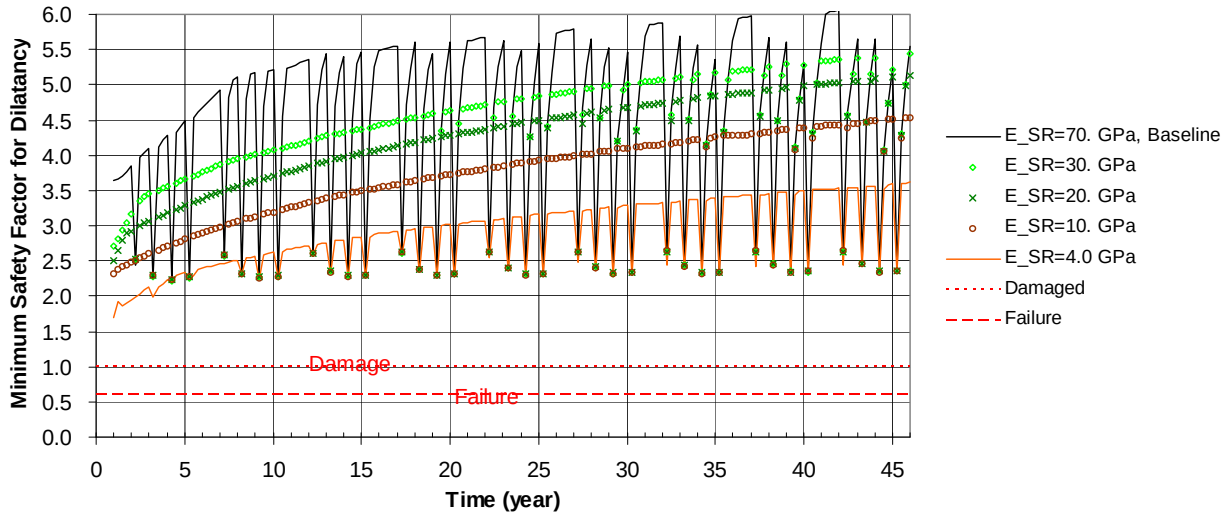

Figure 85: Comparison of predicted minimum safety factor history against dilatant damage in salt dome for the four different elastic moduli of surrounding rock.

In conclusion, a smaller value for the elastic modulus of the surrounding rock is slightly more advantageous from a storage loss and stability of a cemented well annulus perspective. However, larger value is more advantageous for the integrity of surface structures. The value of elastic modulus of the surrounding rock does not affect the structural stability of the caverns much when the value is larger than 10 GPa.

7.7. Lateral Stress Ratio Effect of Surrounding Rock

To examine the lateral stress ratio effect of surrounding rock, analyses were conducted with the model changes described in Section 3.8.

Figure 86 shows the vertical displacement contours at 46 years for three models with various lateral stress coefficients of surrounding rock. Vertical displacement increases upward with increasing the coefficient of the lateral stress of the surrounding rock. The direction of the vertical displacement changes from downward to upward when $\mathcal{K}$ changes from less than one to more than one.

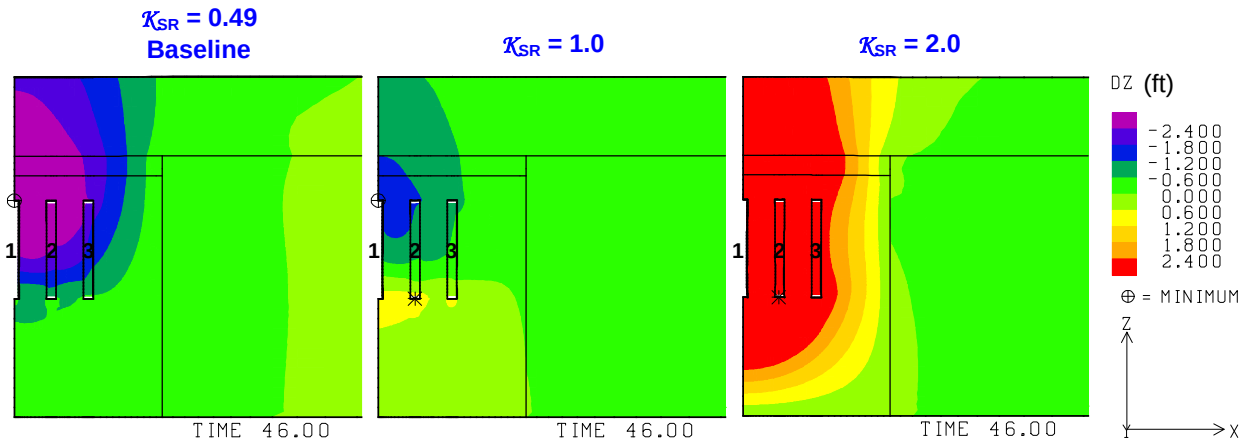

Figure 86: Vertical displacement contours at 46 years for the three models with different lateral stress coefficients of surrounding rock.

Figure 87 shows the predicted total volumetric closure normalized to initial total storage volume for the three models. Cavern volume loss rate due to salt creep closure increases with increasing lateral stress coefficient of surrounding rock. A smaller coefficient is better from a storage loss viewpoint.

Figure 88 shows the predicted subsidence on the surface above Cavern 1 with time for the three models with differing lateral stress coefficients of surrounding rock. Figure 89 shows the predicted subsidence on the surface from the center to the edge of the model at 46 years. Uplift on the surface above the center of Cavern 1 increases with increasing the lateral stress coefficient of surrounding rock when K is more than about 1.0. Subsidence on the surface above the center of Cavern 1 increases with decreasing the lateral stress coefficient of surrounding rock when K is less than about 1.0. The closer the value of the coefficient to one is the better from a subsidence viewpoint.

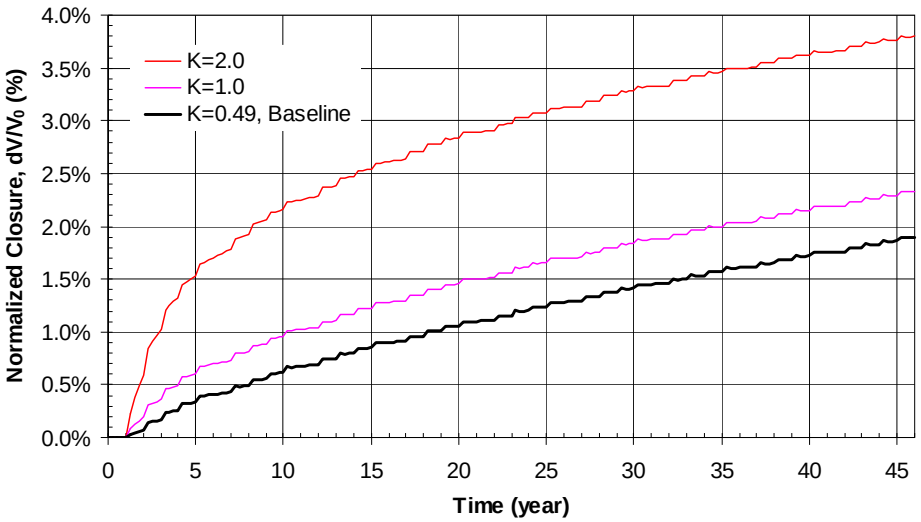

Figure 87: Comparison of predicted total volumetric closure normalized to initial total storage volume for the 19 SPR caverns for three different lateral stress coefficients of surrounding rock.

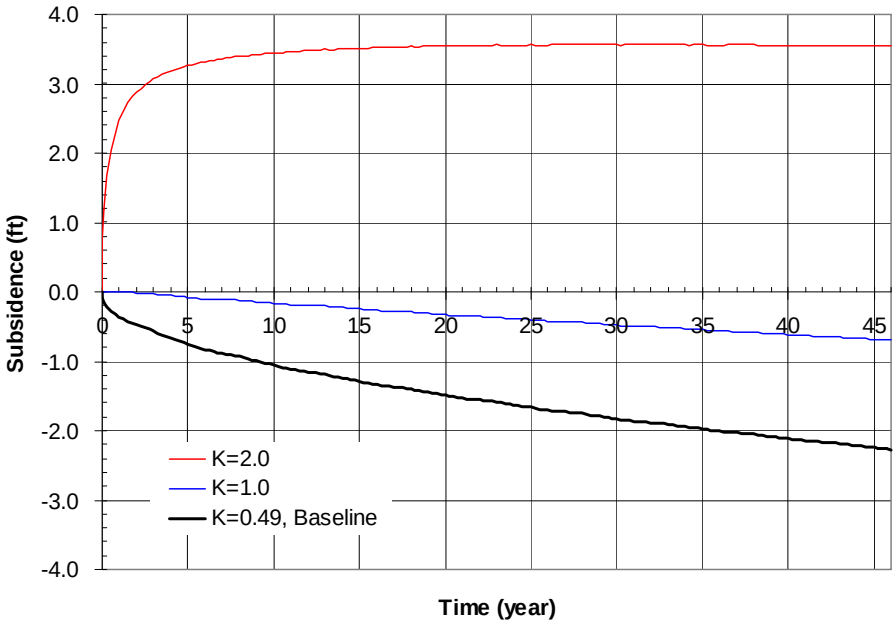

Figure 88: Comparison of predicted subsidence on the surface above Cavern 1 with time for three different lateral stress coefficients of surrounding rock.

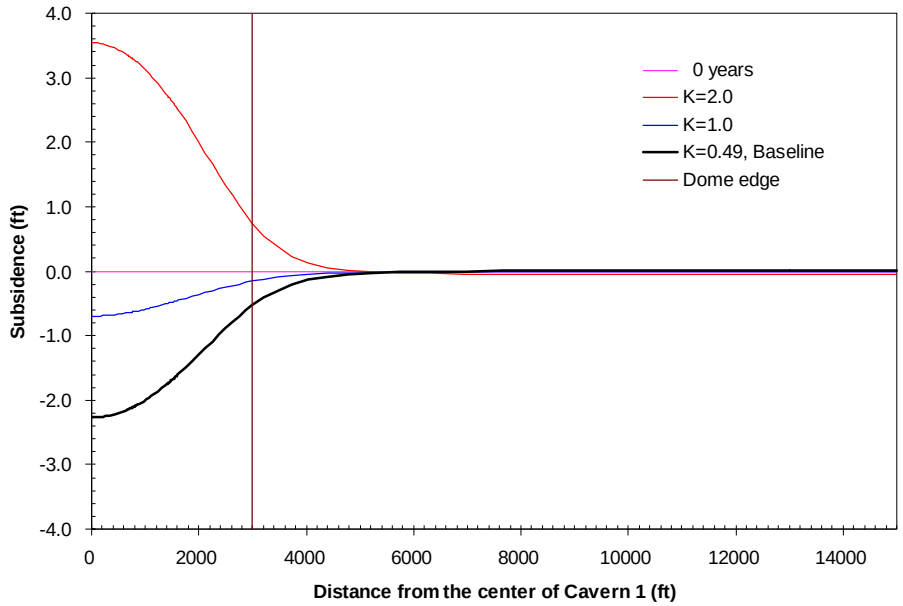

Figure 89: Comparison of predicted subsidence on the surface from model center to edge at 46 years for three different lateral stress coefficients of surrounding rock.

Figure 90 shows the predicted radial surface strains at 46 years for the models with various lateral stress coefficients of surrounding rock. Radial surface strain decreases as the coefficient of lateral stress approaches one. A coefficient closer to one is better in terms of radial surface strain. The surface strain for $0.49 < \mathcal{K}_{SR} < 2$ is within the allowable strain for surface structures (1 millistrain in either compression or tension).

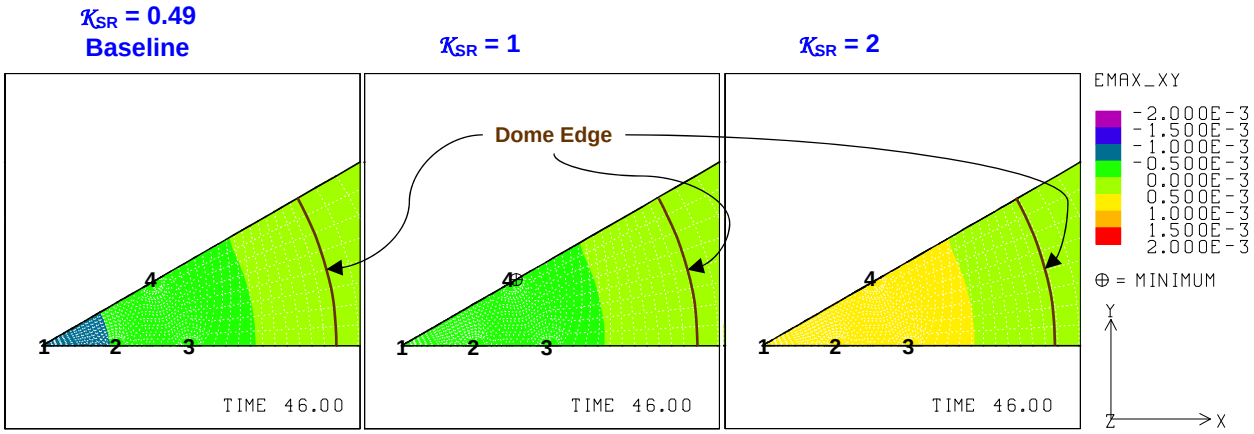

Figure 90: Predicted radial surface strains at 46 years for three different lateral stress coefficients of surrounding rock.

Figure 91 shows the predicted vertical strains around the roof of the caverns at 46 years for the model with various lateral stress coefficients of surrounding rock. Vertical strain increases with increasing lateral stress coefficient of surrounding rock. A smaller value of the coefficient is better from a vertical strain viewpoint. The strain for $\mathcal{K}_{SR}$ = 2.0 at 100 ft above the cavern roof is

beyond the allowable strain for a cemented well annulus (0.2 and 2 millistrain in tension for cement and steel casing, respectively).

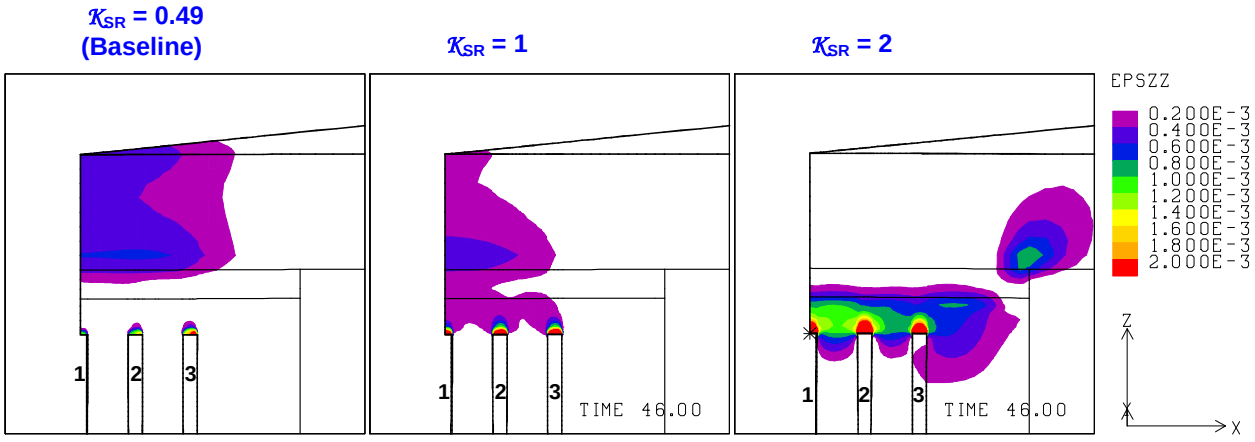

Figure 91: Predicted vertical strains around the roof of caverns at 46 years for three different lateral stress coefficients of surrounding rock.

Figure 92 shows the predicted minimum compressive stress history in the salt dome for the three models with various lateral stress coefficients of surrounding rock. The negative sign (-) indicates a compressive stress. The peaks appear during the workover of the caverns. Structural stability against tensile failure decreases with increasing the lateral stress coefficient of surrounding rock when K is more than about 1.0. However, the K value does not have effect on structural stability against tensile failure when K is less than about 1.0.

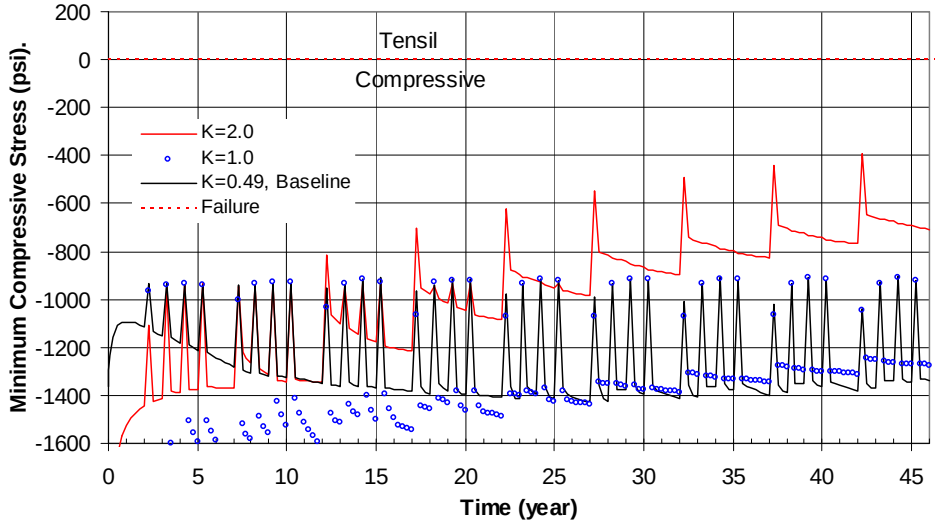

Figure 92: Comparison of predicted minimum compressive stress history in the salt dome for three different lateral stress coefficients of surrounding rock.

Figure 93 shows the predicted minimum safety factor history against dilatant damage in the salt dome for the three models with differing lateral stress coefficients of surrounding rock. The

peaks appear during the workover of the caverns. When $\mathcal{K}$ is more than about 1.0, the safety factor against dilatancy decreases with increasing the lateral stress coefficient of surrounding rock. When $\mathcal{K}$ is less than about 1.0, the lateral stresses coefficient has little effect on safety factor against dilatancy.

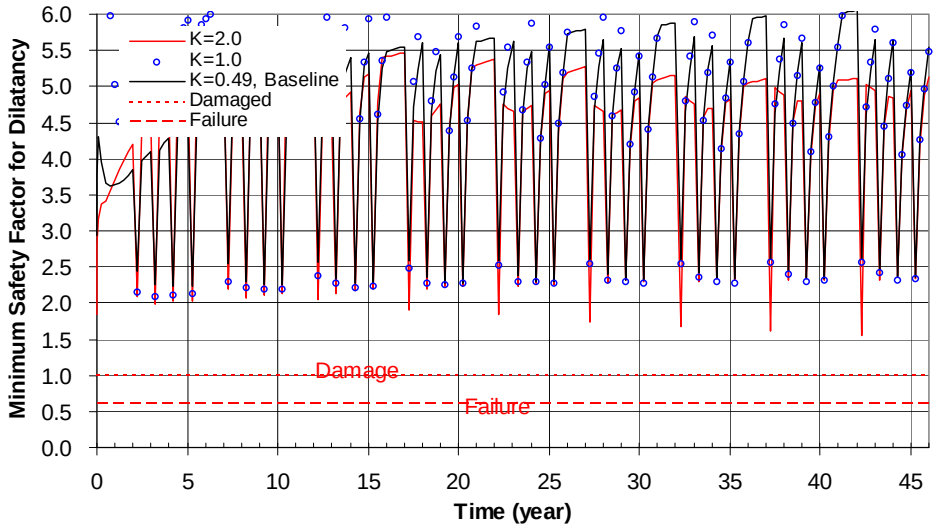

Figure 93: Comparison of predicted minimum safety factor history against dilatant damage in salt dome for three different lateral stress coefficients of surrounding rock.

In conclusion, when the lateral stress coefficient of surrounding rock ($\mathcal{K}$) is closer to about 1.0, it is more advantageous from a vertical displacement, subsidence, and integrity of surface structure viewpoints. A smaller value of $\mathcal{K}$ appears more advantageous from a storage loss and cemented well annulus perspective. The surface above the salt dome can move upward with time when $\mathcal{K}$ is more than about 1.0. When $\mathcal{K}$ is more than about 1.0, a larger value of $\mathcal{K}$ is not better for the structural stability of caverns. When $\mathcal{K}$ is less than about 1.0, $\mathcal{K}$ does not have effect on the structural stability of caverns. $\mathcal{K}$ is one of important parameters for the site selection and the design of SPR caverns. Therefore, data of in-suit stresses with depth in the surrounding rock should be acquired from the field if possible.

7.8. Effect of Cavern Size

To examine the cavern size effect, analyses were conducted using the model changes given in Section 3.9.

Figure 94 shows the vertical displacement contours at 46 years for the baseline case and a model having an initial cavern radius of 200 ft, respectively. The vertical displacement increases with increasing the radius of the caverns.

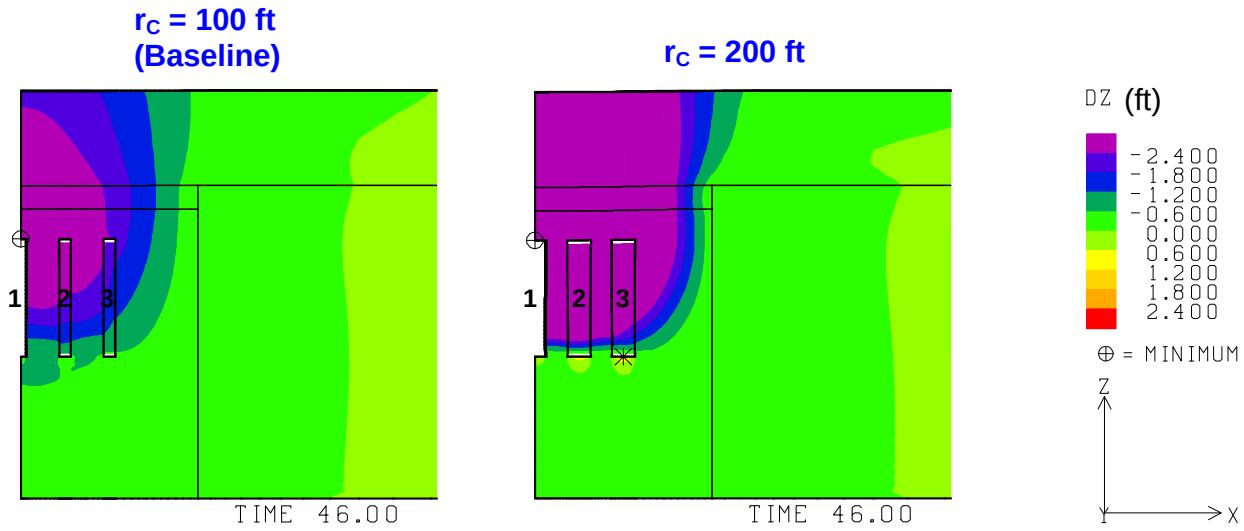

Figure 94: Vertical displacement contours using two different radii of cavern at 46 years.

Figure 95 shows the predicted total volumetric closure normalized to initial total storage volume for the 19 SPR caverns. The cavern volume loss rate due to salt creep closure increases with increasing cavern radius. This suggests that a dome design with smaller cavern radii is better from a storage loss viewpoint.

Figure 96 shows the predicted subsidence on the surface above Cavern 1 with time for the baseline case and a model using cavern radii of 200 ft. Figure 97 shows the predicted subsidence at 46 years on the surface from the center to the edge of the model. The subsidence on the surface above the center of Cavern 1 increases with increasing the cavern radius. Therefore, a dome design with smaller cavern radii is better from a subsidence viewpoint.

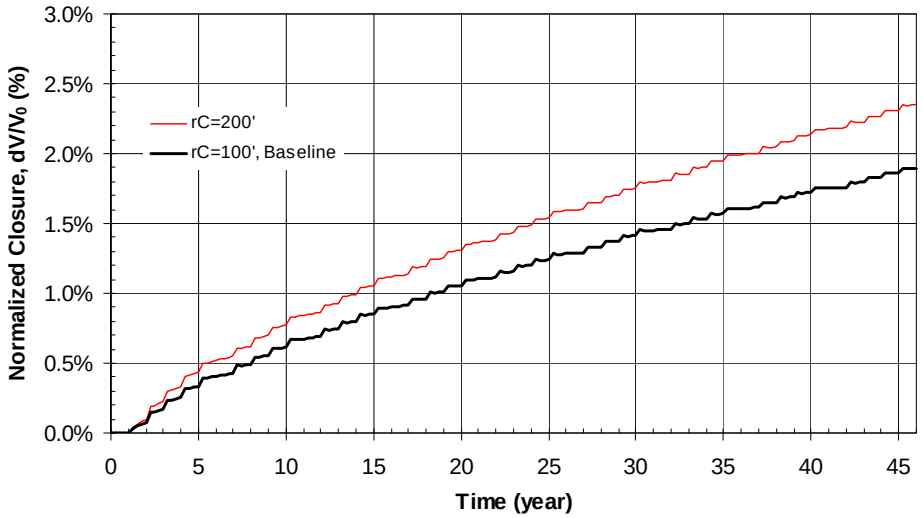

Figure 95: Comparison of predicted total volumetric closure normalized to initial total storage volume for the 19 SPR caverns with differing radii of cavern.

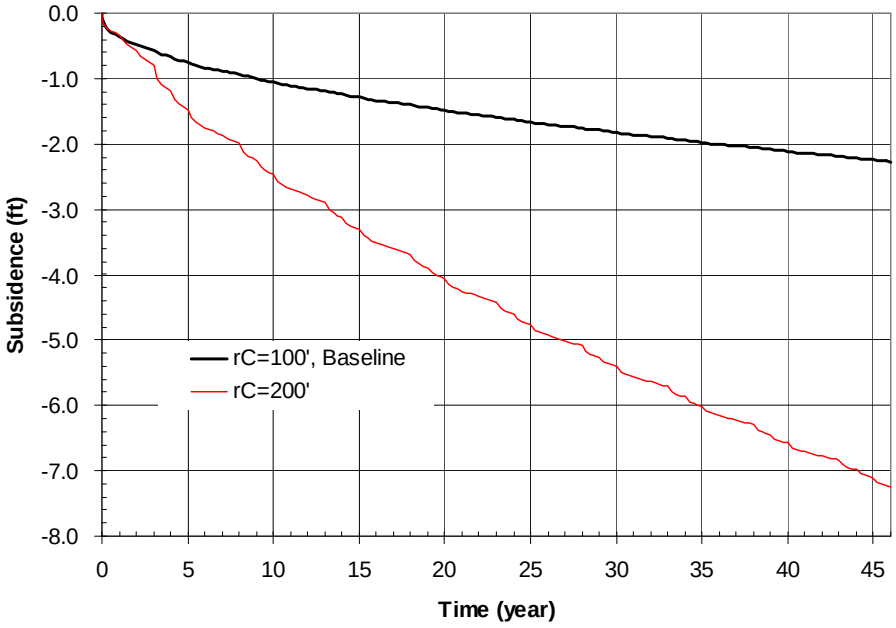

Figure 96: Comparison of predicted subsidence on the surface above Cavern 1 with time for the two different radii of caverns.

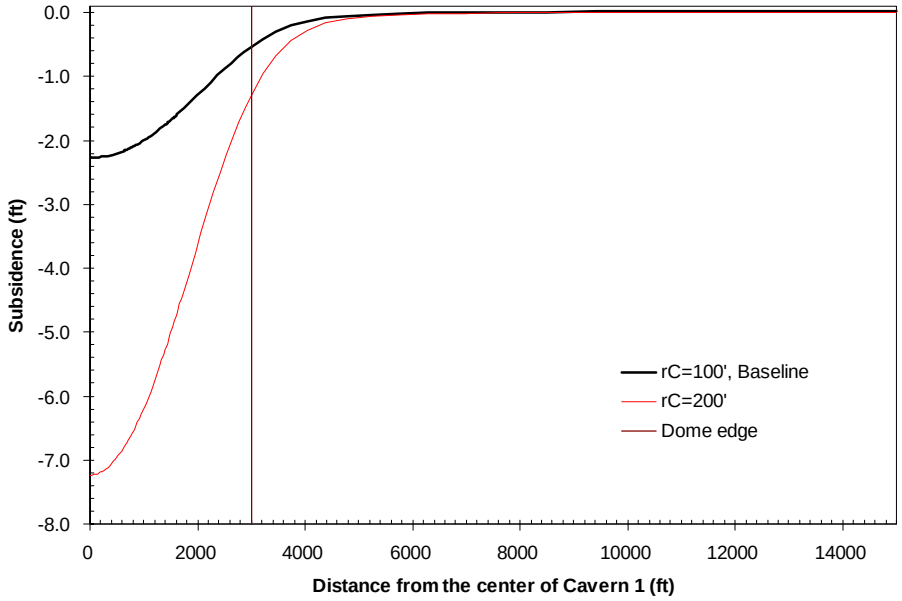

Figure 97: Comparison of predicted subsidence on the surface from model center to edge at 46 years for two different radii of caverns.

Figure 98 shows the predicted radial surface strains at 46 years for the baseline case and a case where the cavern radii are 200 ft. Radial surface strain increases with increasing radius of cavern. When the radii of caverns are 200 ft, the radial surface strain is beyond the allowable strain for a surface structure at 46 years (1 millistrain in either compression or tension).

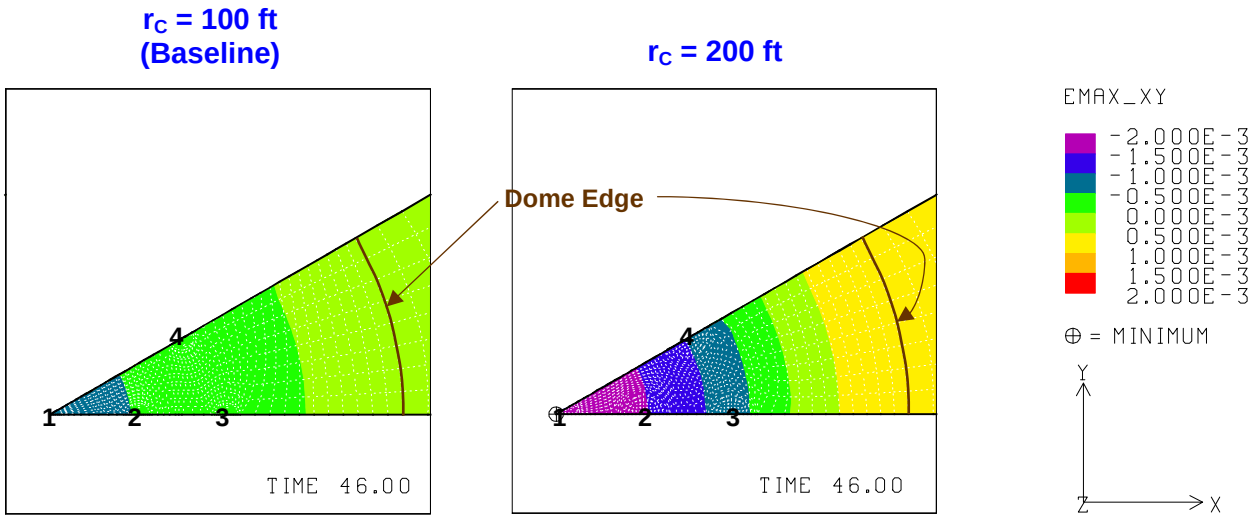

Figure 98: Predicted radial surface strains at 46 years using two different radii of cavern.

Figure 99 shows the predicted vertical strains around the roof of the caverns at 46 years for domes with the baseline and 200 ft cavern radii. Vertical strain in the roofs of the caverns increases with increasing the radii of the caverns. A smaller radius of the cavern is better from a vertical strain viewpoint.

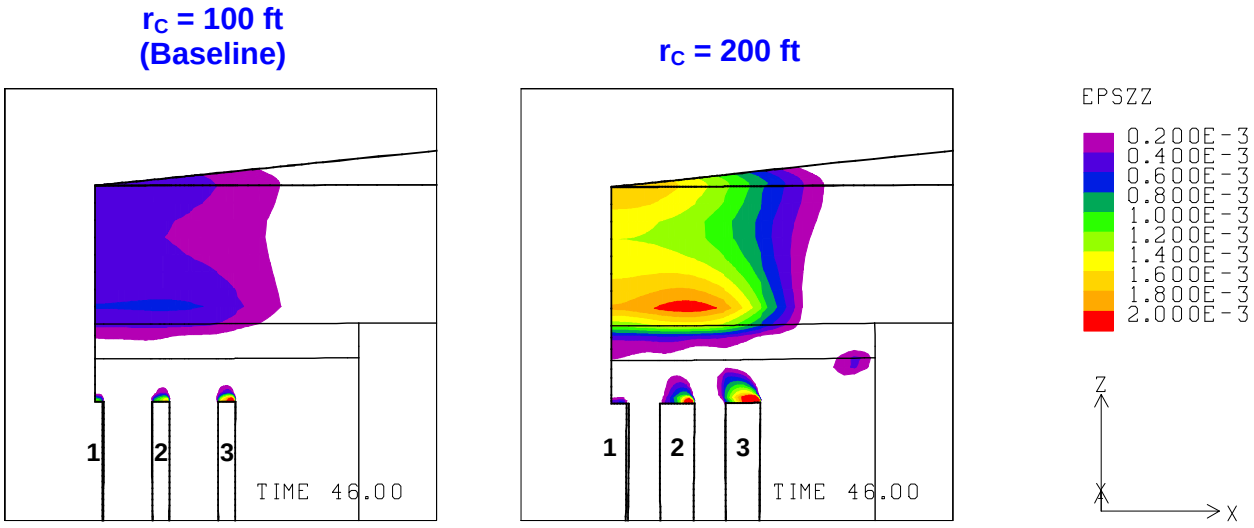

Figure 99: Predicted vertical strains around the roof of caverns using two different radii of cavern at 46 years

Figure 100 shows the predicted minimum compressive stress history in a salt dome for the baseline and cavern radius of 200 ft cases. The negative sign (-) indicates a compressive stress. The peaks appear during the workover of the caverns. The structural stability against tensile failure decreases with increasing the radius of caverns. A smaller cavern size is better from a structural stability against tensile failure viewpoint. The caverns are structurally stable against tensile failure when the radii of caverns are as large as 200 ft. The weakest spot against tensile failure is located in the roof of workovered cavern when the radius of cavern is either 100 ft or 200 ft as shown Figure 101.

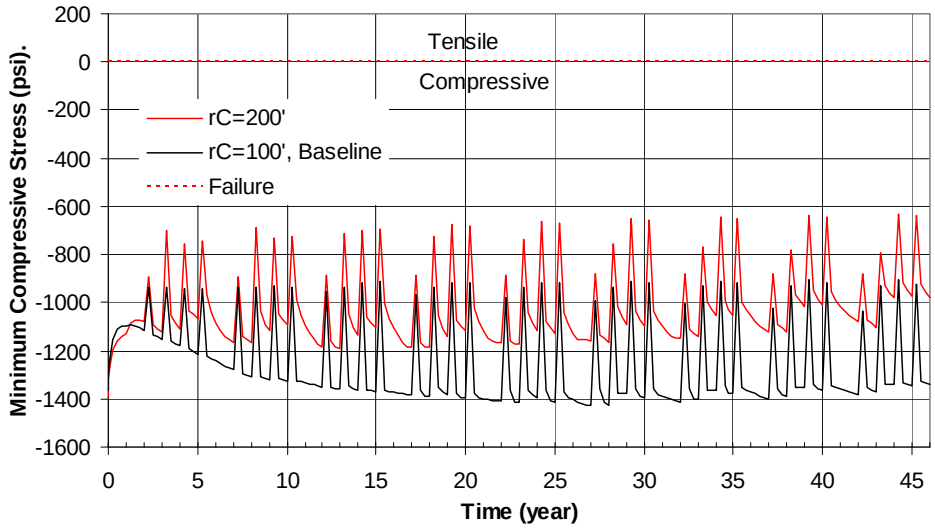

Figure 100: Comparison of predicted minimum compressive stress history in the salt dome for two different radii of cavern.

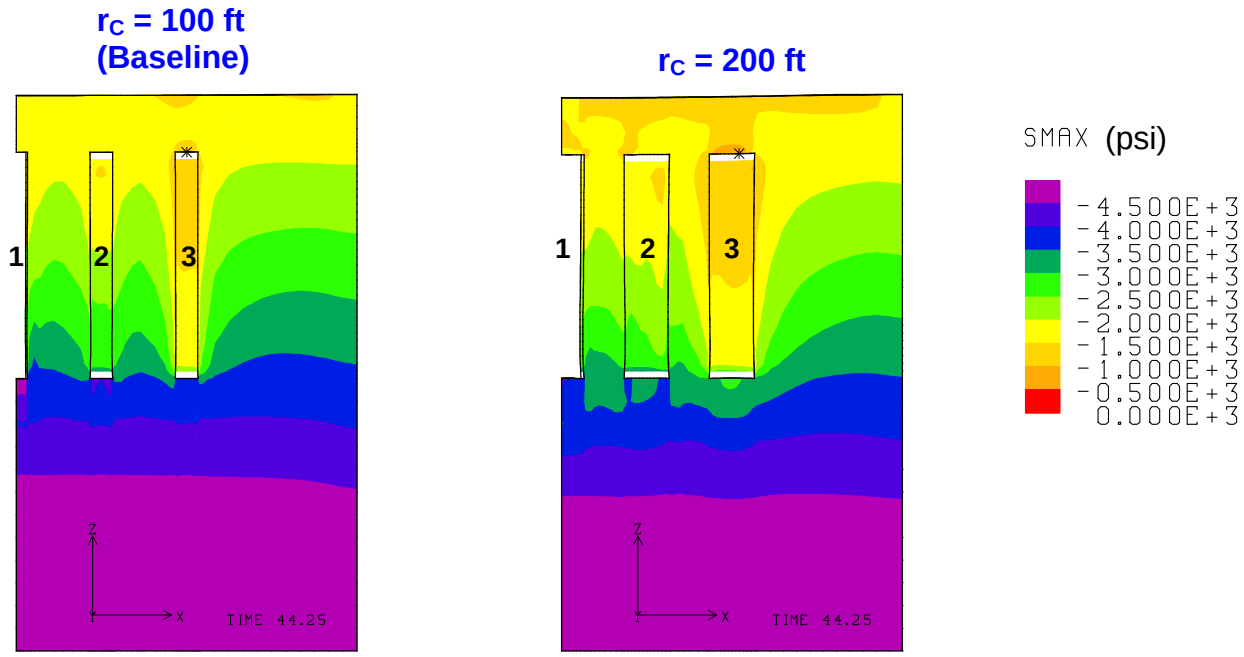

Figure 101: Compressive stress contours using two different radii of cavern in the salt dome.

Figure 102 shows the predicted minimum safety factor history against dilatant damage in a salt dome for the two differing cases of cavern radii. The peaks appear during the workover of the caverns. The safety factor against dilatant damage decreases with increasing the radius of caverns. A smaller size of cavern is better from a dilatant damage viewpoint. The caverns remain structurally stable against dilatant damage when the radii of caverns are increased to 200 ft. The

weakest area against dilatant damage is located in the roof of workovered cavern for both cavern radii as shown Figure 103.

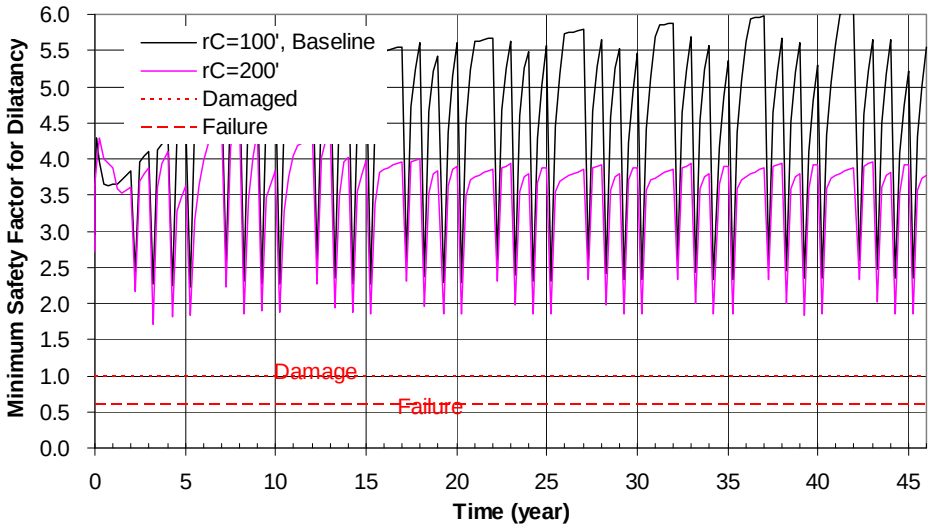

Figure 102: Comparison of predicted minimum safety factor history against dilatant damage in a salt dome for two different radii of cavern.

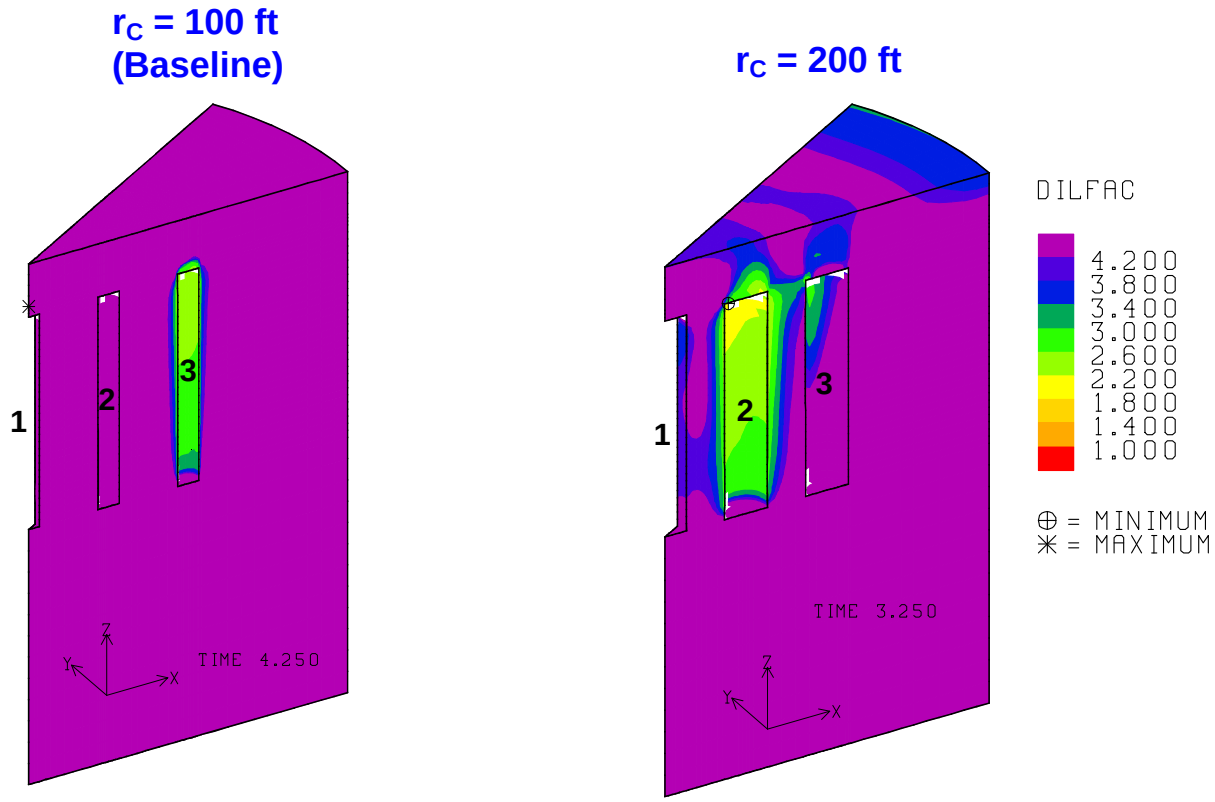

Figure 103: Safety factor contours against dilatant damage using two different radii of cavern.

In conclusion, a smaller cavern radius is more advantageous from storage loss, subsidence, integrity of surface structures, vertical strain above the roof of the cavern, and structural stability viewpoints. However, it is not better from a storage capacity per dome viewpoint. The optimum radius of cavern for each site should be analyzed on a case by case basis.

7.9. Depth Effect of Cavern

To examine the effect of cavern depth, analyses were conducted with the models described in Section 3.10.

Figure 104 shows vertical displacement contours at 46 years in domes with various depths of caverns. The vertical displacement increases with increasing the depth of the caverns.

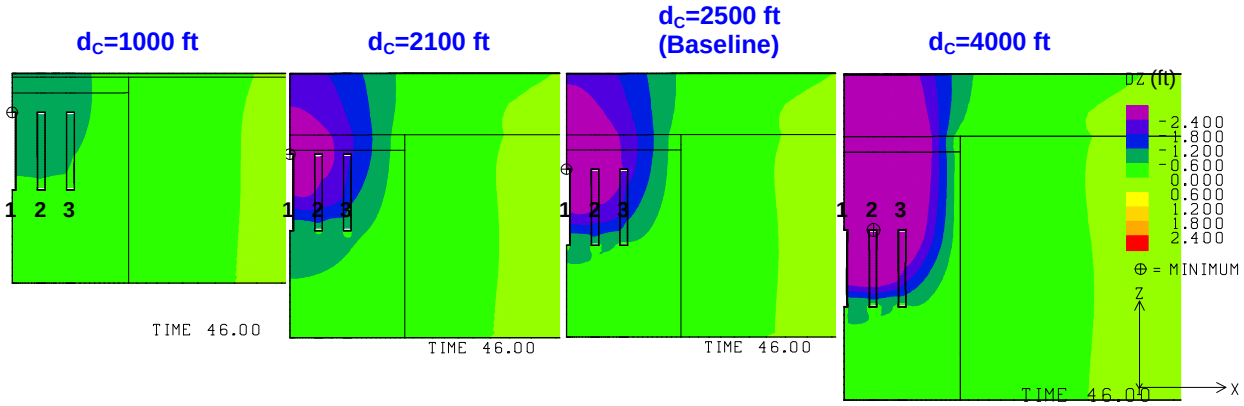

Figure 104: Vertical displacement contours in feet using four different depths of cavern at 46 years.

Figure 105 shows the predicted total volumetric closure normalized to initial total storage volume for the 19 SPR caverns modeled with different cavern depths. Cavern volume loss rate due to salt creep closure increases with increasing cavern depth. A shallower depth of the caverns is better from a storage loss viewpoint.

Figure 106 shows the predicted subsidence on the surface above Cavern 1 with time the various depths of the caverns. Figure 107 shows the predicted subsidence on the surface from the center to the edge of the model at 46 years. Subsidence on the surface increases with increasing the depth of the caverns. A shallower depth of the caverns is better from a subsidence viewpoint.

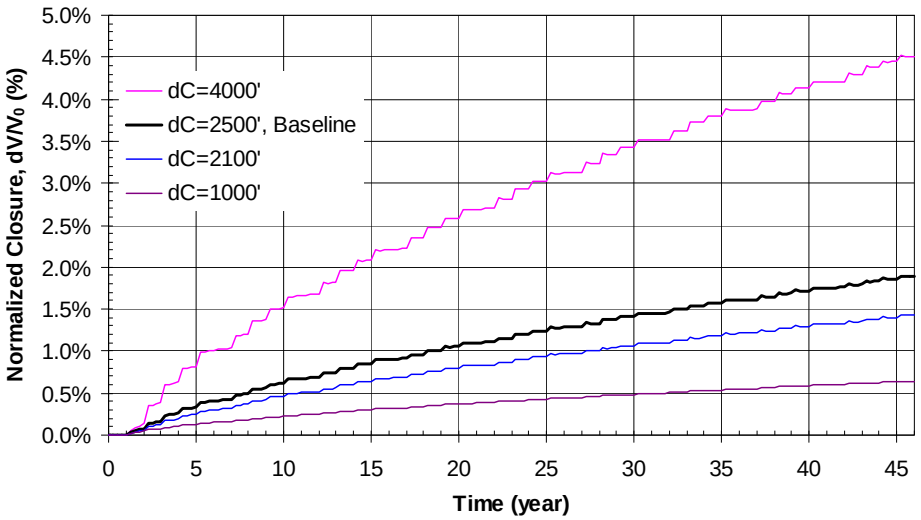

Figure 105: Comparison of predicted total volumetric closure normalized to initial total storage volume for the 19 SPR caverns for the four different depths of caverns.

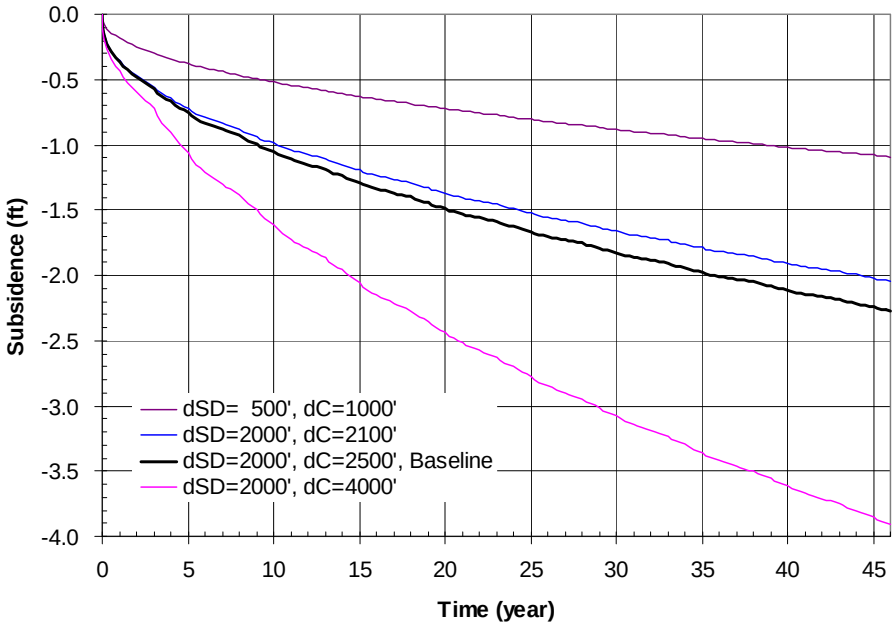

Figure 106: Comparison of predicted subsidence on the surface above Cavern 1 with time for the four different depths of caverns.

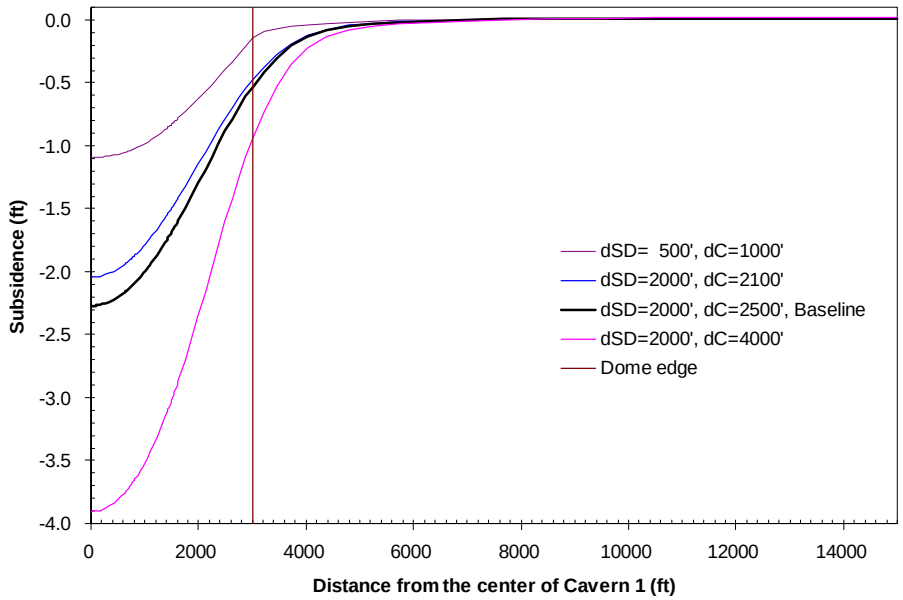

Figure 107: Comparison of predicted subsidence on the surface from model center to edge at 46 years for the four different depths of caverns.

Figure 108 shows the predicted radial surface strains at 46 years for the various depths of caverns. Radial surface strain increases with increasing the depth of the caverns. A shallower depth for the caverns is better from a radial surface strain viewpoint. In all cases, the strain on the surface above the edge of salt dome is within the allowable strain for surface structures when the cavern depth is to 4000 ft (1 millistrain in either compression or tension).

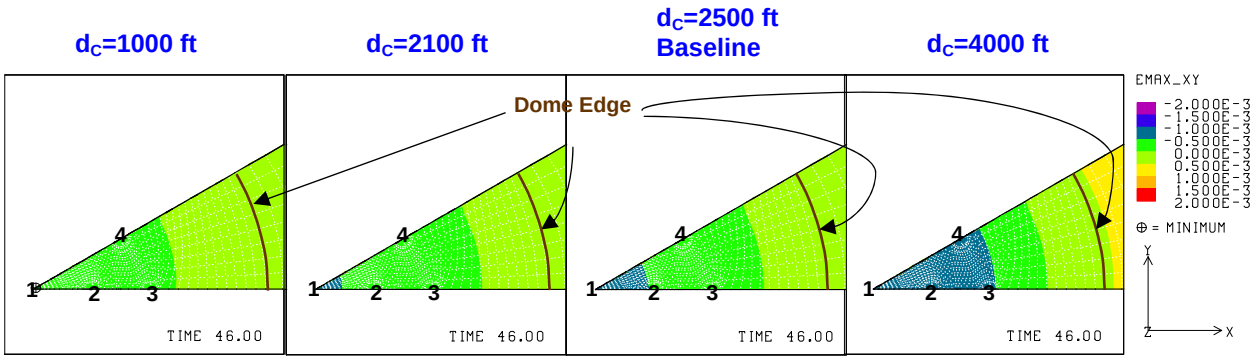

Figure 108: Predicted radial surface strains using four different depths of cavern at 46 years.

Figure 109 shows the predicted vertical strains around the roofs of the caverns at 46 years for the various depths of caverns. Vertical strain at the roofs of the caverns increases with increasing the depth of the caverns. A shallower depth for the cavern is better from a vertical strain viewpoint.

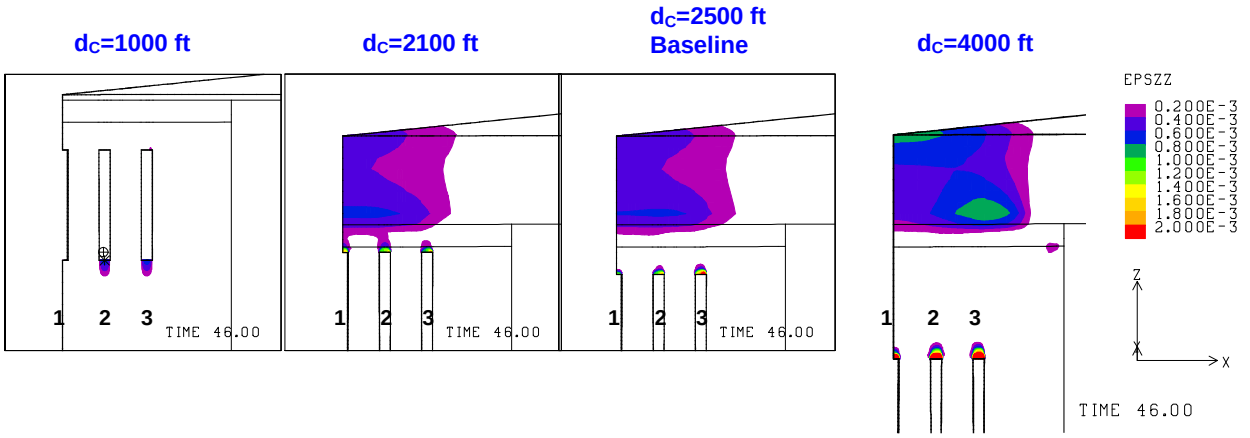

Figure 109: Predicted vertical strains around the roof of caverns using four different depths of cavern at 46 years.

Figure 110 shows the predicted minimum compressive stress history in a salt dome with caverns at various depths. The negative sign (-) indicates a compressive stress. The peaks appear during workover of the caverns. Structural stability against tensile failure increases with increasing depth of the caverns. A deeper depth for the caverns is better from a tensile failure viewpoint. When the depth of the caverns is 1000 ft, the salt dome is close to possible tensile failure. The high possibility of tensile failure occurs in the area of salt dome top rather than in the salt around the caverns, thus the peaks during workovers does not appear.

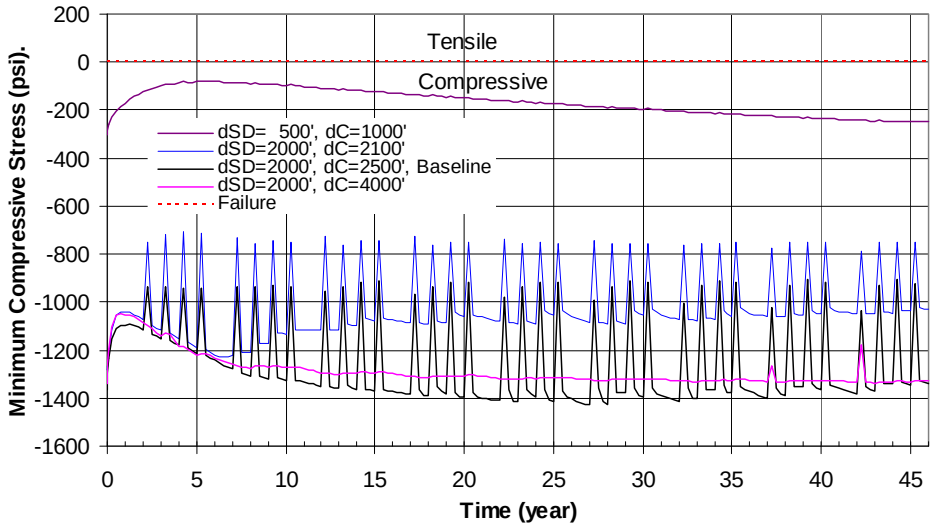

Figure 110: Predicted minimum compressive stress history in the salt dome for the four different depths of cavern.

Figure 111 shows the predicted minimum safety factor history against dilatant damage in a salt dome for the various depths of caverns. The peaks appear during workover of the caverns. The safety factor against dilatant damage increases with increasing the depth of caverns. A deeper

depth for the caverns is better from a dilatant damage viewpoint. The salt dome is close to undergoing dilatant damage when the cavern depth is 1000 ft.

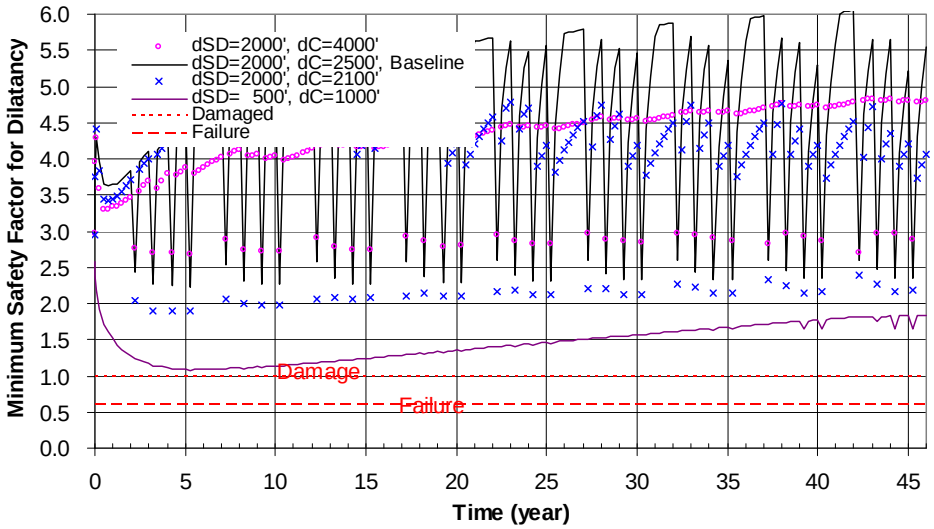

Figure 111: Predicted minimum safety factor history against dilatant damage in salt dome for the four different depths of cavern.

In conclusion, a shallower depth for SPR caverns is more advantageous from a storage loss, amount of subsidence, integrity of surface structures, and cemented well annulus viewpoints. On the other hand, a deeper depth for the caverns is more advantageous from a structural stability against tensile failure and dilatant damage viewpoint. However, operational efficiency decreases with increasing the depth of cavern. Therefore, the optimum depth should be sought for each site.

7.10. Effect of Number of Caverns

To examine the effect of the number of caverns, analyses were conducted with the model described in Section 3.11.

Figure 112 shows the vertical displacement contours at 46 years for the 19-Cavern model and the 31-Cavern model, respectively. The vertical displacement increases with increasing number of caverns.

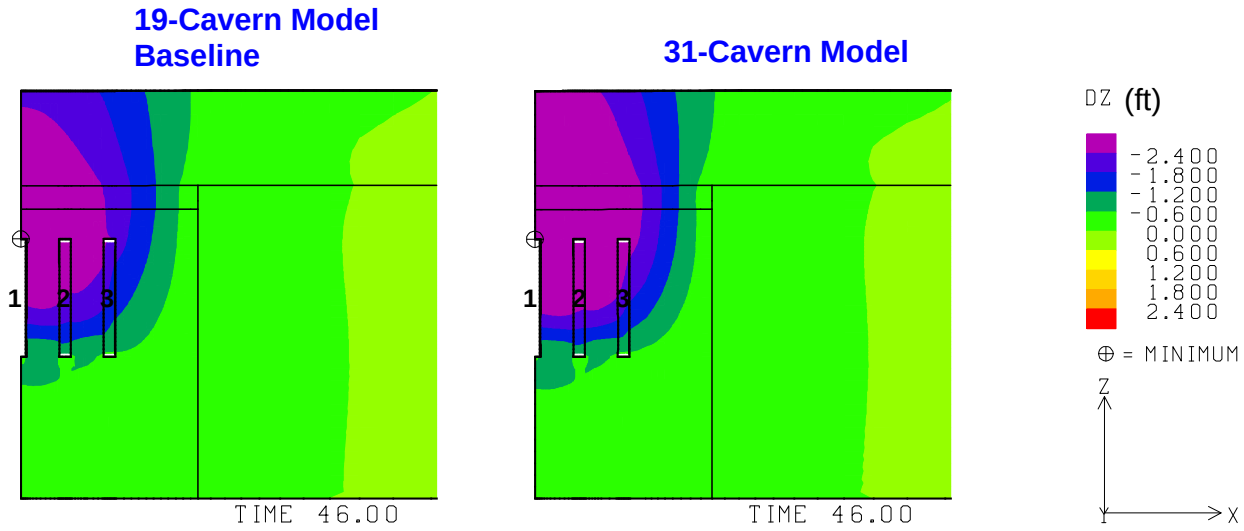

Figure 112: Vertical displacement contours at 46 years using two models with a different number of caverns.

Figure 113 shows the predicted total volumetric closure normalized to initial total storage volume for the 19 SPR caverns and 31 SPR cavern models. The number of caverns does not affect the normalized cavern volume loss rate due to salt creep closure.

Figure 114 shows the predicted subsidence on the surface above Cavern 1 with time for the baseline and the 31-Cavern models. Figure 115 shows the predicted subsidence on the surface from the center to the edge of the model at 46 years for the baseline and 31-Cavern models. The subsidence on the surface increases with increasing number of caverns. Therefore, a smaller number of caverns is better in terms of the predicted subsidence.

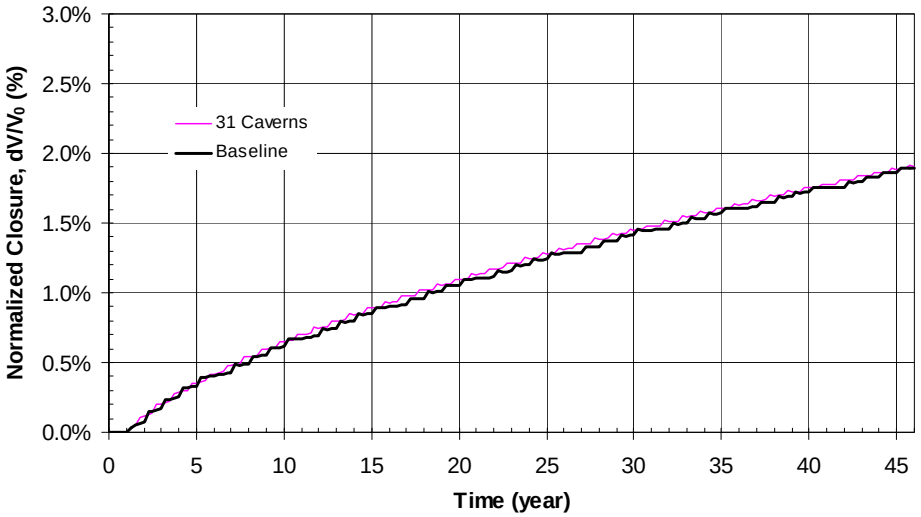

Figure 113: Comparison of predicted total volumetric closure normalized to initial total storage volume for the 19 SPR cavern and 31 SPR cavern models.

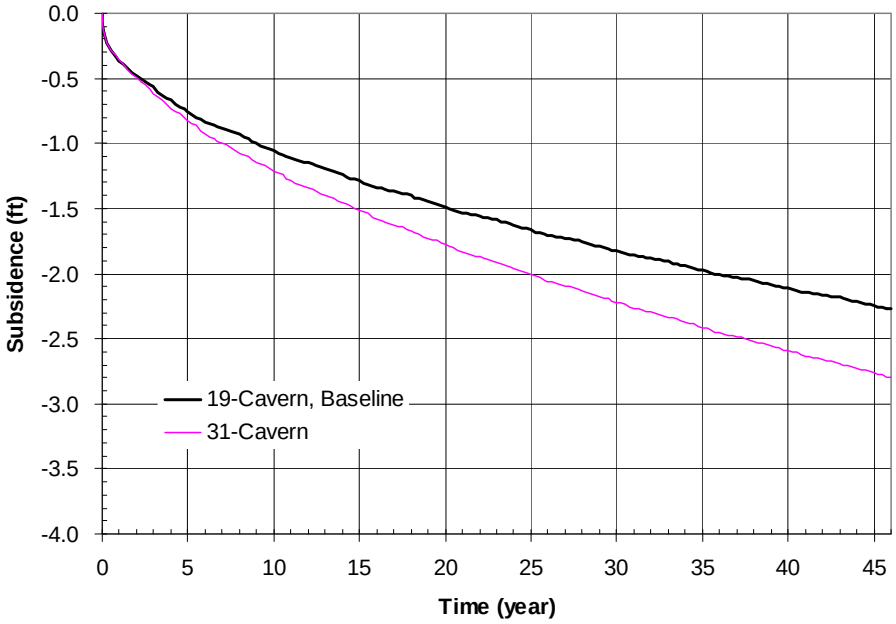

Figure 114: Predicted subsidence on the surface above Cavern 1 with time for the two different models.

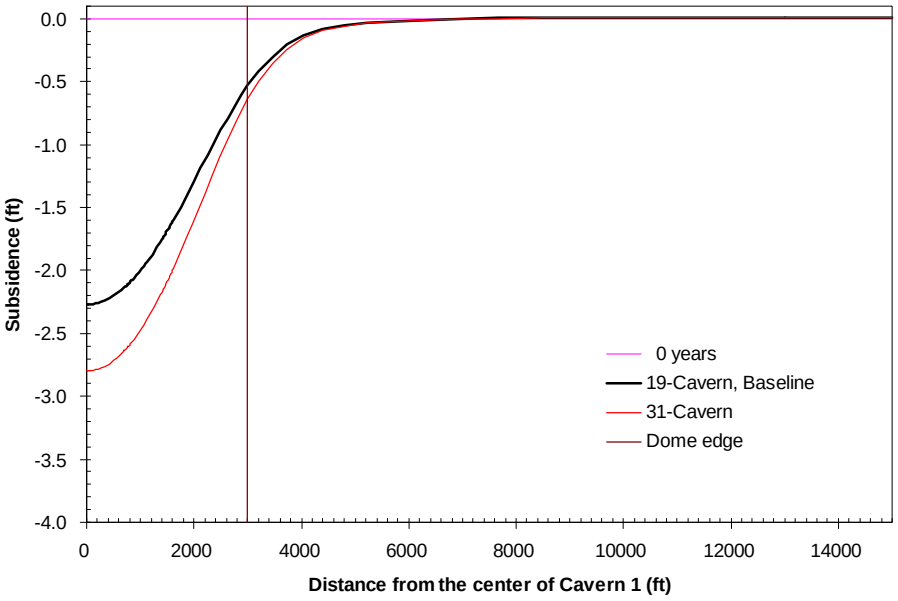

Figure 115: Predicted subsidence on the surface from model center to edge at 46 years for the two different models.

Figure 116 shows the predicted radial surface strains at 46 years for the baseline and the 31-Cavern models. Radial surface strain increases slightly with increasing number of caverns. The strain on the surface above the salt dome for both models is within the allowable strain for a surface structure at 46 years (1 millistrain in either compression or tension).

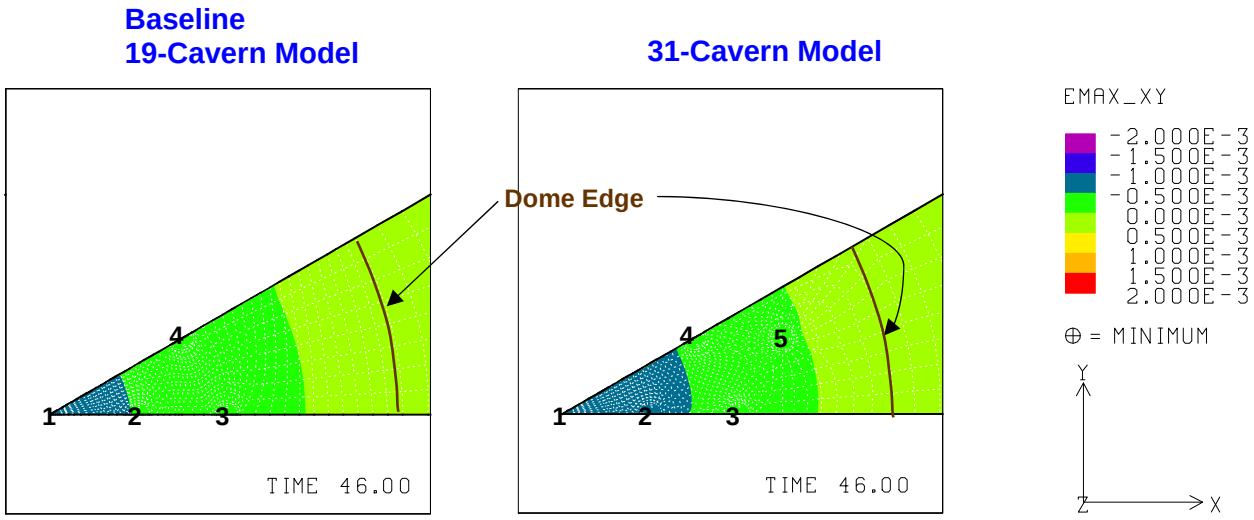

Figure 116: Predicted radial surface strains using two different models at 46 years.

Figure 117 shows the predicted vertical strains around the roof of the caverns at 46 years for the baseline and 31-Cavern models. Number of caverns does not have much of an effect on the vertical strain in the roofs of caverns.

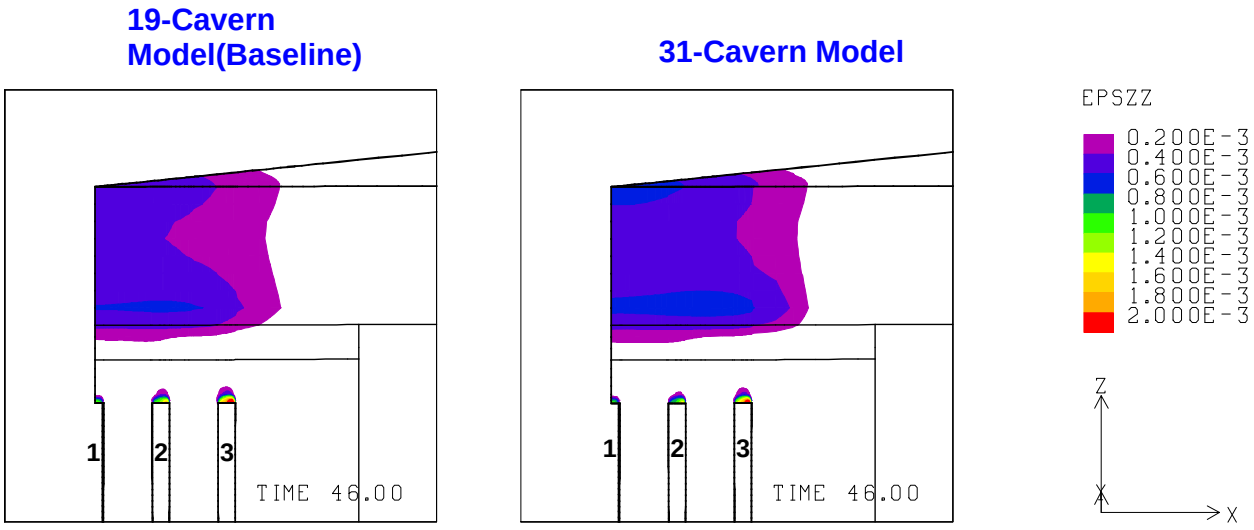

Figure 117: Predicted vertical strains around the roof of caverns at 46 years using two different models

Figure 118 compares the predicted minimum compressive stress histories in a salt dome for the baseline and the 31-Cavern models. The negative sign (-) indicates a compressive stress. The peaks appear during the workover of the caverns. Caverns in 19-Cavern model are slightly more stable against tensile failure. A smaller number of caverns is slightly better from a structural stability against tensile failure viewpoint. The caverns are structurally stable against tensile failure for both 19-Cavern model and 31-Cavern model.

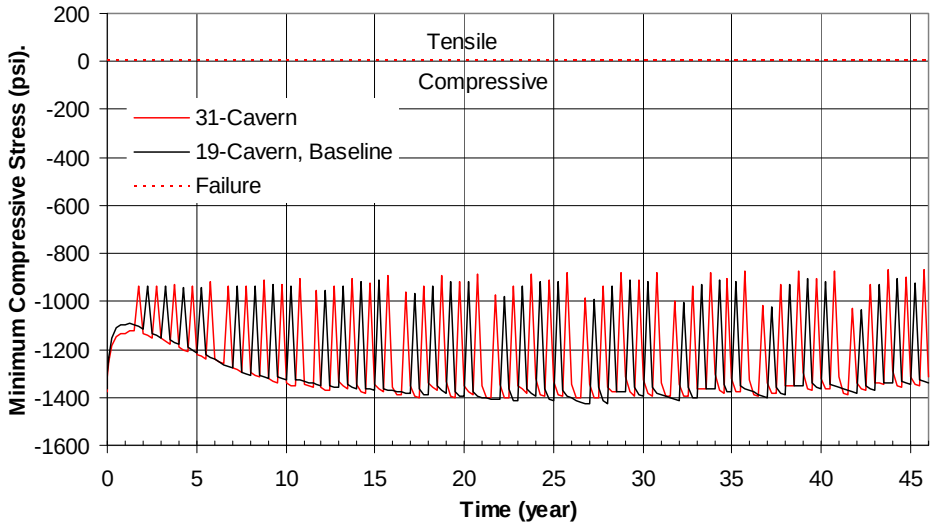

Figure 118: Comparison of predicted minimum compressive stress history in the salt dome for the two different models.

Figure 119 shows the predicted minimum safety factor history against dilatant damage in the salt dome for the baseline and the 31-Cavern models. The peaks appear during the workover of the caverns. Caverns in 19-Cavern model are slightly more stable against dilatant damage. A smaller number of caverns is slightly better from a safety factor against dilatant damage viewpoint. The caverns are structurally stable against dilatant damage for both the 19-Cavern and 31-Cavern models.

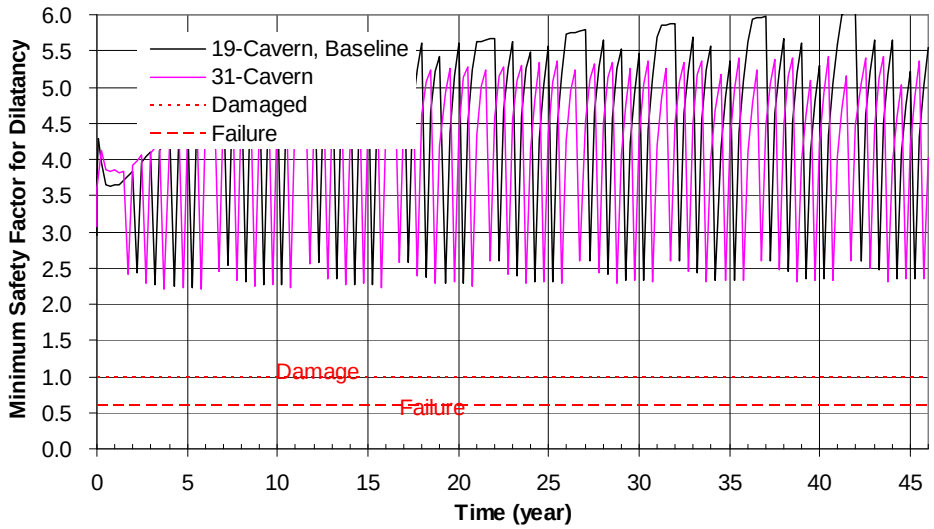

Figure 119: Comparison of predicted minimum safety factor history against dilatant damage in salt dome for the two different models.

In conclusion, a smaller number of caverns is more advantageous from a subsidence viewpoint. The number of caverns has little effect on the normalized storage loss and vertical strain above

the roof of the cavern. The 31-Cavern model shows a slight increase in radial surface strain. Caverns in 19-Cavern model are slightly more stable against tensile failure and dilatant damage than those in 31-Cavern model. The 31-Cavern model has a larger storage capacity per dome and the impacts on SPR cavern integrity are small.

8. SUMMARY AND CONCLUDING REMARKS

A sensitivity study was performed utilizing a three-dimensional finite element model to define allowable cavern field-sizes for a SPR salt dome. The effects of the parameters for creep rate, depth of salt dome top, dome size, caprock thickness, elastic modulus of caprock, elastic modulus of surrounding rock, lateral stress ratio of surrounding rock, cavern size, depth of cavern, and number of caverns were examined.

Table 10 lists the correlation between the parameters and their impact on the performance of the storage field. An upward pointing arrow (⬆) indicates a direct relationship between a parameter and an impact. For instance, the salt creep rate has a direct relationship on storage loss, i.e. a faster salt creep rate yields more storage loss of caverns with time. On the other hand, a downward pointing arrow (⬇) indicates inverse relationship. If the symbol is red, it indicates a disadvantageous relationship for cavern field performance. For example, a faster salt creep rate yields greater storage loss which is not good for the storage performance. A large symbol indicates a strong relationship. For example, the cavern depth has strong relationships with normalized storage loss, subsidence, possibility of tensile failure, possibility of dilatant damage, and operational efficiency. The cavern depth has relatively weak relationship with radial surface strain and vertical strains near wellhead. The cavern depth has no relationship with storage capacity per dome. A leftward pointing arrow to 1 **(➡1)** indicates the lateral stress coefficient is close to one.

We can obtain useful clues from this table for selecting a site and designing storage caverns by anticipating the degree in which the parameters impact the performance of the storage field. If we focus on the caprock thickness for example, a larger caprock thickness yields more storage loss and larger vertical strains near wellhead, smaller subsidence, and an ignorable smaller radial surface strain. The caprock thickness has no relationship with the possibility of tensile failure, dilatant damage, and storage capacity of the dome.

This table can be utilized from the perspective of choosing a site based on design criteria. For instance, if the important issue in the design is the subsidence on the surface, the designer needs to consider a site with smaller salt creep rate, deeper depth of salt dome top, smaller radius of salt dome, larger thickness of caprock, larger elastic modulus of caprock and surrounding rock, a lateral stress coefficient of surrounding rock closer to one; and a cavern field design with smaller cavern radii, shallower depth of caverns, and smaller number of caverns. The more important factors for reducing the subsidence appear to be salt creep rate, elastic modulus of surrounding rock, lateral stress ratio of surrounding rock, cavern radius, and cavern depth. For another example, if a designer wants to develop a larger storage capacity per dome, he should consider more caverns in the dome rather than a larger cavern size. The table shows a larger radius of caverns yields more disadvantage than more caverns.

In general, a smaller salt creep rate, deeper depth of salt dome top, larger elastic modulus of the caprock and surrounding rock, and smaller cavern radius are better for the performance of SPR cavern field.

⬆: Direct relationship
▪ : No relationship
⬇: Inverse relationship
Red: Disadvantageous
Blue: Advantageous

Table 10: Correlation Table

Parameter \ Impact on		Storage Loss	Subsidence	Radial Surface Strain	Vertical Strains near Wellhead	Possibility of Tensile Failure	Possibility of Dilatant Damage	Storage Capacity per Dome
Geologic parameters	Salt Creep Rate (⬆)	⬆	⬆	⬆	⬆	▪ ⬆ ††	⬇ ⬆ ‡‡	▪
	Depth of Salt Dome Top (⬆)	⬇	⬇	⬇	⬇	⬇	⬆	▪
	Dome Radius(⬆) Standoff Distance (⬆)	⬆	⬆	⬆	⬇	⬇	⬆	▪
	Caprock Thickness (⬆)	⬆	⬇	⬇	⬆	▪	▪	▪
	Elastic Modulus of Caprock (⬆)	⬇	⬇	⬇	⬇	▪	▪	▪
	Elastic Modulus of the Surrounding Rock (⬆)	⬆	⬇	⬇	⬆	⬇ ▪ §§	⬇ ▪ ***	▪
	Lateral Stress Ratio of Surrounding Rock (➡1 †††)		⬇	⬇				▪
	Lateral Stress Ratio of Surrounding Rock (⬆)	⬆			⬆	⬆	⬆	▪
Design parameters	Cavern Radius (⬆)	⬆	⬆	⬆	⬆	⬆	⬆	⬆
	Cavern Depth (⬆)	⬆	⬆	⬆	⬆	⬇	⬇	▪
	Number of Caverns (⬆)	▪	⬆	⬆	▪	⬆	⬆	⬆

††: increases after 17 years, ‡‡: increases after 12 years, §§: no relationship when E_{SR} > 20 GPa, ***: no relationship when E_{SR} > 10 GPa,
†††: closer to 1

9. REFERENCES

Ballard, S. and Ehgartner, B.L., 2000, *CAVEMAN Version 3.0: System for SPR Cavern Pressure Analysis*, SAND2000-1751, Sandia National Laboratories, Albuquerque, NM 87185-0750.

Blanford, M.L., 2001. *JAS3D – A Multi-Strategy Iterative Code for Solid Mechanics Analysis: User's Instructions*, Release 2.0, Sandia National Laboratories, Albuquerque, New Mexico.

Ehgartner, B.L. and Sobolik, S.R., 2002. *3-D Cavern Enlargement Analyses*, SAND2002-0526, Sandia National Laboratories, Albuquerque, NM 87185-0706.

Hoek E. and E.T. Brown, 1980. *Underground Excavations in Rock*, published by The Institution of Mining and Metallurgy, London.

Hoffman, E.L., 1992, *Investigation of Analysis Assumptions for SPR Calculations*, memo to J. K. Linn, Sandia National Laboratories, Albuquerque, New Mexico, February 7, 1992.

Hoffman, E.L. and B.L. Ehgartner, 1993. *Evaluating the Effects of the Number of Caverns on the Performance of Underground Oil Storage Facilities*. Int. J. Mech. Min. Sci. & Geomechanics, Vol. 30, No. 7, 1993.

Hoffman, E.L. and B.L. Ehgartner, 1996. *Three Dimensional Finite Element Simulations of Room and Pillar Mines in Rock Salt*, SAND96-0988C, Presented at Second North American Rock Mechanics Symposium, Montreal, Quebec, June 9-12, 1996.

Lambe, T.W and R.V. Whitman, 1979. *Soil Mechanics, SI Version*, published by John Wiley & Sons.

Munson, D.E., A.F. Fossum, and P.E. Senseny, 1989. *Advances in Resolution of Discrepancies between Predicted and Measured in Situ WIPP Room Closures*, SAND88-2948, Sandia National Laboratories, Albuquerque, New Mexico.

Park, B.Y., B.L. Ehgartner, M.Y. Lee, and S.R. Sobolik, 2005. *Three Dimensional Simulation for Big Hill Strategic Petroleum Reserve (SPR)*, SAND2005-3216, Sandia National Laboratories, Albuquerque, NM.

Park, B.Y., B.L. Ehgartner, and M.Y. Lee, 2006. *Three Dimensional Simulation for Bayou Choctaw Strategic Petroleum Reserve (SPR)*, SAND2006-7589, Sandia National Laboratories, Albuquerque, NM.

Park, B.Y. and B.L. Ehgartner, 2008. *Expansion Analyses of Strategic Petroleum Reserve in Bayou Choctaw Salt Dome*, SAND2008-6408, Sandia National Laboratories, Albuquerque, NM.

Speirs, C.J., C. J. Peach, R.H. Brzesowsky, P.M.T.M. Schutjens, J. L. Liezenberg, and H.J. Zwart, 1988. *Long Term Rheological and Transport Properties of Dry and Wet Rocks*, EUR 11848, prepared for Commission of the European Communities, by University of Utrecht, Utrecht, The Netherlands.

Tammemagi, H.Y., M.C. Loken, J.D. Osnes, and R.A. Wagner, 1986. *A Compilation of Data for Thermomechanical Analyses of Four Potential Salt Repositories*, Technical Report, prepared for Office of Nuclear Waste Isolation Battelle Memorial Institute, 505 King Avenue Columbus, OH 43201-2693.

Thorton, C.H. and I.P. Lew, 1983. *Concrete and Design Construction*, Standard Handbook for Civil Engineers, Chapter 8, 3rd ed., F.S. Merritt, editor, McGraw-Hill, NY.

Van Sambeek, L., J. Ratigan, and F. Hansen, 1993. *Dilatancy of Rock Salt in Laboratory Tests*, Proc. 34th U.S. Symposium on Rock Mechanics, p.245-248.

APPENDIX A: MESH GENERATION INPUT FOR BASELINE

A-1. FASTQ INPUT

```
TITLE
Dome sizing study - 19 caverns facility (Radius of dome=3000 ft)

{include("19cav0d.pts")}

$ nodebc 1 - X-axis boundary of mesh - zero disp. B.C.
nodebc 1 500 4 16 18 19 25 26 27 33 34 36 37 43 44 45 51 52
$ nodebc 2 - angled boundary of mesh - zero displ. B.C.
nodebc 2 501 5 17 35 55 61 62 63 69 70
$ Far field boundary of mesh - zero displ. B.C.
nodebc 3   100
$ Node point BC along well 1 axis
poinbc 5   1
$
elembc 10  104                $ Side set BC inside well 1 (center)
elembc 20  127                $ Side set BC inside well 2 (7-cav sim.)
elembc 30  145                $ Side set BC inside well 3 (19-cav sim.)
elembc 40  163                $ Side set BC inside well 4 (19-cav sim.)

$ Well 1 - well material is mat. 10
region  11 10 -1 -500 -104 -501 -3
$ In situ rock near Well 1 (Salt is mat. 1; caprock mat. 2; overburden mat. 3)
region  17 1  -4 -116 -5   -104
$ Well 2
region  21 10 -127 -25 -26
$ In situ rock near Well 2 (Salt is mat. 1; caprock mat. 2; overburden mat. 3)
region  27 1  -19 -127 -27 -133
$ Well 3
region  31 10 -145 -43 -44
$ In situ rock near Well 3 (Salt is mat. 1; caprock mat. 2; overburden mat. 3)
region  37 1  -37 -145 -45 -151
$ Well 4
region  41 10 -163 -61 -62
$ In situ rock near Well 4 (Salt is mat. 1; caprock mat. 2; overburden mat. 3)
region  47 1 -55 -163 -63 -169
$rock out to far field boundary
region  1  4 -70 -503 -100 -502 -52 -152  $ Rock surrounding Salt Dome mat. 4
region  2  1 -34 -36 -151 -51 -152 -69 -169 -35 -134
region  3  1 -16 -18 -133 -33 -134 -17 -116

scheme 1 m
scheme 2 u6s $u6s
scheme 3 u6s $u6s
scheme 11 t6s
scheme 17 m
scheme 21 c6s
scheme 27 m
scheme 31 c6s
scheme 37 m
scheme 41 c6s
scheme 47 m

body 2 3 11 17 21 27 31 37 41 47
$body 2

Exit
```

A-2. PTS for defining the mesh coordinates

```
$ Unit conversion:
$ 1(ft)={ft_m=0.3048}(m), 1(m)={m_ft=1/0.3048}(ft)

$ Dimensions of mesh
$
$ Salt Dome Boundary, domebc={domebc=3000*ft_m}(m)
$ Wedge angle in degress = {wedge=30.}(deg.) {th=30*RAD}(rad)
$ Far field boundary, rmax={rmax=15000*ft_m}(m)
$ Initial cavern radious,r0={r0=100*ft_m}(m)
$ Initial well spacing, center-to-center,dcen={dcen=750*ft_m}(m)
$ dr={dr=20*ft_m}(m), outside circles of the caverns
$ rout={rout=13000*ft_m}(m), to avoid "INCONSISTENT KINEMATIC
$ CONTRAINTS ON NODEs in far field boundary and x-axis (or wedge) boundary"
```

```
$ Primary boundaries of mesh
point    1    {0.}     {0.}
point    2    {rmax}   {0.}
point    3    {rmax*cos(th)}    {rmax*sin(th)}
point  502    {rout}   {0.}
point  503    {rout*cos(th)}    {rout*sin(th)}
$ Points for initial center cavern
point  500    {r0/6.}  {0.}
point  501    {r0*cos(th)/6.}    {r0*sin(th)/6.}
point    4    {r0}   {0.}
point    5    {r0*cos(th)}    {r0*sin(th)}
point   16    {r0+dr}   {0.}
point   17    {(r0+dr)*cos(th)}    {(r0+dr)*sin(th)}
$ Point halfway between well 1 and well 2 (7-cavern well)
point   18    {5.*dcen/9.}     {0.}
$ Points surrounding well 2
point   19    {dcen-r0-dr}   {0.}
point   25    {dcen-r0}     {0.}
point   26    {dcen}        {0.}
point   27    {dcen+r0}     {0.}
point   33    {dcen+r0+dr}  {0.}
point   34    {rr2=dcen+r0+11*dr} {0.}
point   35    {rr2*cos(th)} {rr2*sin(th)}
$ Point halfway between well 2 and well 3 (19-cavern well)
point   36    {3.*dcen/2.}     {0.}
$ Points surrounding well 3
point   37    {2.*dcen-r0-dr}   {0.}
point   43    {2.*dcen-r0}     {0.}
point   44    {2.*dcen}        {0.}
point   45    {2.*dcen+r0}     {0.}
point   51    {2.*dcen+r0+dr}  {0.}
point   52    {domebc}               {0.}

$ {d19=2.*dcen*cos(th)}
$ Point halfway between well 1 and well 4 (19-cavern well)
point   54    {d19/2.*cos(th)}     {d19/2.*sin(th)}
$ Points surrounding well 4
point   55    {(d19-r0-dr)*cos(th)}  {(d19-r0-dr)*sin(th)}
point   61    {(d19-r0)*cos(th)}     {(d19-r0)*sin(th)}
point   62    {(d19)*cos(th)}        {(d19)*sin(th)}
point   63    {(d19+r0)*cos(th)}     {(d19+r0)*sin(th)}
point   69    {(d19+r0+dr)*cos(th)}  {(d19+r0+dr)*sin(th)}
point   70    {domebc*cos(th)}       {domebc*sin(th)}


$ Mesh boundaries - x-axis symmetry plane
line   1 str   1 500   0  1 1.0
line 500 str 500   4   0  5 1.0
line   4 str   4  16   0  1 1.0
line  16 str  16  18   0  4 1.2
line  18 str  18  19   0  3 {1./1.2} $ 2 to 3
line  19 str  19  25   0  1 1.0
line  25 str  25  26   0  6 1.0
line  26 str  26  27   0  6 1.0
line  27 str  27  33   0  1 1.0
line  33 str  33  34   0  4 1.0 $ 4 to 4
line  34 str  34  36   0  2 1.0 $ 3 to 2, 1.2 to 1.0
line  36 str  36  37   0  3 {1/1.2} $ {1/1.2} to {1/1.2}
line  37 str  37  43   0  1 1.0
line  43 str  43  44   0  6 1.0
line  44 str  44  45   0  6 1.0
line  45 str  45  51   0  1 1.0
line  51 str  51  52   0 11 1.0 $ 13 to 11
line  52 str  52 502   0 16 1.13
line 502 str 502   2   0  1 1.0
$ Mesh boundaries - angled symmetry plane
line   3 str   1 501   0  1 1.0
line 501 str 501   5   0  5 1.0
line   5 str   5  17   0  1 1.0
line  17 str  17  35   0 20 1.0 $ 0.85 to 0.9
line  35 str  35  55   0  1 1.0 $ 3 to 3
line  55 str  55  61   0  1 1.0
line  61 str  61  62   0  6 1.0
line  62 str  62  63   0  6 1.0
line  63 str  63  69   0  1 1.0
line  69 str  69  70   0 17 1.0
line  70 str  70 503   0 16 1.13
line 503 str 503   3   0  1 1.0
$ Mesh boundaries - far field
```

```
$ nth = {nth = 8}   dth = {dth = 1.0}
line  100 circ   2   3  1 {nth} {dth}
line  134 circ  34  35  1 {nth} {dth} $ dth to dth
line  152 circ  52  70  1 {nth} {dth}
$Arcs connecting symmetry planes - well 1 region
line  104 circ   4   5  1 {nth} {dth}
line  116 circ  16  17  1 {nth} {dth}

$Arcs for the well 2 region
line  133 circ  33  19 26 {1.5*nth} {dth}
line  127 circ  27  25 26 {1.5*nth} {dth}

$Arcs for the well 3 region
line  151 circ  51  37 44 {1.5*nth} {dth}
line  145 circ  45  43 44 {1.5*nth} {dth}

$Arcs for the well 4 region
line  169 circ  55  69 62 {1.5*nth} {dth}
line  163 circ  61  63 62 {1.5*nth} {dth}
```

A-3. GEN3D for 2D to 3D as an Example (19cav_saltbot.gen3d)

```
{include("thickness.txt")}

translate 12 {sboth} 1.
nsets back 4
offset 0., 0., {-(ovrth+capth+st1th+st2th+cavht)}
change sideset 10 910
change sideset 20 920
change sideset 30 930
change sideset 40 940
```

A-4. GJN for Merging GENESIS Databases as an Example (19cav0d.gjn)

```
19cav_over.g1
19cav_cap1.g1
COMB
NO
10.0000E-3

BLOCKS
COMBINE 3 310
COMBINE 2 210
UP

ADD
19cav_salttop.g1
COMB
NO
10.0000E-3

ADD
19cav_cavern.g1
COMB
NO
10.0000E-3

ADD
19cav_saltbot.g1
COMB
NO
10.0000E-3

BLOCKS
COMBINE 1 110
UP
SSETS
DELETE 910
DELETE 920
DELETE 930
DELETE 940
UP

ADD
19cav_rock.g1
```

```
COMB
NO
10.0000E-3

FINISH
19cav0d.g0
```

A-5. Input Data for defining the thickness of each layer

```
$ Unit conversion:
$ 1(ft)={ft_m=0.3048}(m), 1(m)={m_ft=1/0.3048}(ft)

$ Thicknesses of each layer
$
$ overburden thickness: ovrth={ovrth=1600*ft_m}(m)
$ caprock thickness:    capth={capth=400*ft_m}(m)
$ salt dome top 1 thickness: st1th={st1th=400*ft_m}(m)
$ salt dome top 2 thickness: st2th={st2th=100*ft_m}(m)
$ salt cavern height:   cavht={cavht=2000*ft_m}(m)
$ salt bottom thickness:sboth={sboth=2400*ft_m}(m)
```

A-6. Unit Conversion File

```
$Unit conversion:
$
$Length:
$ ft   = {ft_m=0.3048} m
$ m    = {m_ft=1/ft_m} ft
$
$Pressure:
$ MPa  = {MPa_Pa  = 1E6} Pa
$ Pa   = {Pa_MPa  = 1/MPa_Pa} MPa
$
$Time:
$ min  = {min_s   = 60           } s
$ h    = {h_min   = 60           } min
$ d    = {d_h     = 24           } h
$ mon  = {mon_d   = 30.4166666667} d
$ yr   = {yr_d    = 365          } d
$ dec  = {dec_yr  = 10           } yr
$ cen  = {cen_dec = 10           } dec
$ mil  = {mil_cen = 10           } cen
$ h    = {h_s     = h_min*min_s  } s
$ d    = {d_s     = d_h*h_s      } s
$ mon  = {mon_s   = mon_d*d_s    } s
$ yr   = {yr_s    = yr_d*d_s     } s
$ dec  = {dec_s   = dec_yr*yr_s  } s
$ cen  = {cen_s   = cen_dec*dec_s} s
$ mil  = {mil_s   = mil_cen*cen_s} s
$
```

A-7. Unit Conversion File for FORTRAN

```
!--- Unit conversion:
!
!--- Length:
      ft_m=0.3048
      m_ft=1/ft_m
!
!--- Pressure:
      MPa_Pa  = 1E6
      Pa_MPa  = 1/MPa_Pa
!
!--- Time:
      min_s   = 60
      h_min   = 60
      d_h     = 24
      mon_d   = 30.4166666667
      yr_d    = 365
      dec_yr  = 10
      cen_dec = 10
      mil_cen = 10
      h_s     = h_min*min_s
      d_s     = d_h*h_s
```

```
      mon_s   = mon_d*d_s
      yr_s    = yr_d*d_s
      dec_s   = dec_yr*yr_s
      cen_s   = cen_dec*dec_s
      mil_s   = mil_cen*cen_s
!
```

A-8. Command Scripts for Mesh Generation

```
# For caverns (holes) in the salt dome
/opt/ACCESS/etc/fastq -aprepro -m hole1.g1 19cav_hole1.fsq
/opt/ACCESS/etc/fastq -aprepro -m hole2.g1 19cav_hole2.fsq
/opt/ACCESS/etc/fastq -aprepro -m hole3.g1 19cav_hole3.fsq
/opt/ACCESS/etc/fastq -aprepro -m hole4.g1 19cav_hole4.fsq
/opt/ACCESS/etc/fastq -aprepro -m salt.g1 19cav0d_salt.fsq

# For salt layer over the caverns
/opt/ACCESS/etc/gen3d -aprepro salt.g1 salttop.g1 < 19cav_salttop.gen3d
/opt/ACCESS/etc/gen3d -aprepro hole1.g1 hole1top.g1 < hole1top.gen3d
/opt/ACCESS/etc/gen3d -aprepro hole2.g1 hole2top.g1 < hole2top.gen3d
/opt/ACCESS/etc/gen3d -aprepro hole3.g1 hole3top.g1 < hole3top.gen3d
/opt/ACCESS/etc/gen3d -aprepro hole4.g1 hole4top.g1 < hole4top.gen3d
/opt/ACCESS/bin/gjoin < 19cav_salttop.gjn

# For salt layer below the caverns
/opt/ACCESS/etc/gen3d -aprepro salt.g1 saltbot.g1 < 19cav_saltbot.gen3d
/opt/ACCESS/etc/gen3d -aprepro hole1.g1 hole1bot.g1 < hole1bot.gen3d
/opt/ACCESS/etc/gen3d -aprepro hole2.g1 hole2bot.g1 < hole2bot.gen3d
/opt/ACCESS/etc/gen3d -aprepro hole3.g1 hole3bot.g1 < hole3bot.gen3d
/opt/ACCESS/etc/gen3d -aprepro hole4.g1 hole4bot.g1 < hole4bot.gen3d
/opt/ACCESS/bin/gjoin < 19cav_saltbot.gjn


# For slat layer containing caverns
/opt/ACCESS/etc/gen3d -aprepro hole1.g1 19cav_hole1.g1 < 19cav_cavern.gen3d
/opt/ACCESS/etc/gen3d -aprepro hole2.g1 19cav_hole2.g1 < 19cav_cavern.gen3d
/opt/ACCESS/etc/gen3d -aprepro hole3.g1 19cav_hole3.g1 < 19cav_cavern.gen3d
/opt/ACCESS/etc/gen3d -aprepro hole4.g1 19cav_hole4.g1 < 19cav_cavern.gen3d
/opt/ACCESS/etc/gen3d -aprepro salt.g1 19cav_salt.g1 < 19cav_cavern.gen3d
/opt/ACCESS/bin/gjoin < 19cav_cavern.gjn

# For surrounding rock (far field)
/opt/ACCESS/etc/fastq -aprepro -m rock.g1 19cav0d_rock.fsq
/opt/ACCESS/etc/gen3d -aprepro rock.g1 rock_over.g1 < 19cav_rockover.gen3d
/opt/ACCESS/etc/gen3d -aprepro rock.g1 rock_cap1.g1 < 19cav_rockcap1.gen3d
/opt/ACCESS/etc/gen3d -aprepro rock.g1 rock_top.g1 < 19cav_rocktop.gen3d
/opt/ACCESS/etc/gen3d -aprepro rock.g1 rock_cavern.g1 < 19cav_cavern.gen3d
/opt/ACCESS/etc/gen3d -aprepro rock.g1 rock_bot.g1 < 19cav_rockbot.gen3d
/opt/ACCESS/bin/gjoin < 19cav_rock.gjn

# For entire mesh
/opt/ACCESS/etc/fastq -aprepro -m 19cavwedge.g1 19cav0d.fsq
/opt/ACCESS/etc/gen3d -aprepro 19cavwedge.g1 19cav_over.g1 < 19cav_over.gen3d
/opt/ACCESS/etc/gen3d -aprepro 19cavwedge.g1 19cav_cap1.g1 < 19cav_cap1.gen3d
/opt/ACCESS/bin/gjoin < 19cav0d.gjn
```

APPENDIX B: FORTRAN FILE FOR THE TEMPERATURE

```
program load
      parameter (ntimes=2,numnod=51606)
      dimension temp(numnod),tdays(ntimes),
     1          z(numnod)
      character*5 stuff
      open(unit=7,file="wh_19cav0d.th",form="UNFORMATTED")
      open(unit=9,file="temp_check.dat")
      open(8,file="wh_19cav0d.nod",status="OLD")
C --- from 0 day to 2000 years
      data (tdays(i),i=1,ntimes) /0.,730000./
C
      numen=numnod
      do 10 i=1,numnod
      read(8,*,err=500) stuff,j,x,y,z(i)
      if (j.ne.i.or.j.gt.numnod) go to 500
C --- West Hackberry temperature profile (SAND2002-0526)
C --- Temp. at Top of Surface=36.98 dC, Absolute Temp=273.15 dK= 0 dC,
C --- Temp Slope with Depth=0.0107 dF/ft=0.0195 dC/m
C-----(C:\Sandia.dat\SPR\Big_Hill\Calculation\rv1\Temperature slope.xls)
      temp(j)=273.15+36.98-z(j)*0.0195
      write(9,901) i, j, numnod, z(j), temp(j)
  901 format(i6,2x,i6,2x,i6,2x,f10.3,2x,f10.3)
   10 continue
         i=0
 3       continue
C --- make .th file at t=0 and 2000 years
         i=i+1
         time=tdays(i)*86400.
         write(*,*) time
         write(7) time, (temp(j), j=1,numen)
         if (i.ge.ntimes) go to 1
         go to 3
 1    continue
C
      close(8)
      stop
 500  write(*,900) j,numnod
 900  format("*** Number of nodes in nodes file does not match ",
     1 "numnod in source code!! ***",i6,1x,i6)
      stop 1
      end
```

APPENDIX C: JAS3D INPUT FILES FOR BASELINE

```
{include("units.txt")}
{include("thickness.txt")}

title
Dome sizing study - 19 caverns facility, Baseline, no drawdown

$Material Properties
$
$Salt (Material 1):
$ Young's Modulus={E1=31.0E9} (Krieg, 1984)
$ Density={rho1=2300.},Poisson's Ratio={nu1=0.25} (Krieg, 1984)
$ Bulk Modulus={K1=E1/(3.*(1.-2.*nu1))},Shear Modulus={mu1=E1/(2.*(1.+nu1))}
$ Creep Constant={A=3.752e-38},Stress Exponent={n=5} (Ehgartner, 2008)
$ Thermal Constant={Q=10.0E3}(Ehgartner, 2008), Universal gas constant={R=1.987}
$ Salt Reduction Factor={RF=1.0} (Baseline)
$ Structure Factor Multiplication Factor={SMF=1.0} (Baseline)
$
$Caprock (Material 2):
$ Young's Modulus={E2=7.0E9}(Hoffman and Ehgartner, 1992)
$ Density={rho2=2500.},Poisson's Ratio={nu2=0.29}(Hoffman and Ehgartner, 1992)
$
$Overburden (Material 3):
$ Young's Modulus={E3=0.1E9}(Hoffman and Ehgartner, 1992)
$ Density={rho3=1874.},Poisson's Ratio={nu3=0.33}(Hoffman and Ehgartner, 1992)
$
$Surrounding Rock (Material 4):
$ Young's Modulus={E4=70E9}(Ehgartner, 2008)
$ Density={rho4=2500.},Poisson's Ratio={nu4=0.33}(Lama and Vutukuri, 1978)

$Time at the initial leaches begin
$ bgn_s  = {bgn_s=0.} s
$Time at the simulaton completes
$ end_s = {end_s=46.*yr_s} s $ {end_s/yr_s} years

$ number of nodes = {nnod = 48312.}

start time 0.0
  ITERATION PRINT, 20
  MAXIMUM ITERATIONS, {nnod}  $ number of nodes
  TARGET TOLERANCE, 5.e-5  $ was 5.e-5
  ACCEPTABLE TOLERANCE .00001
  predictor scale factor, 0.0,0.0
  time steps, 1   $1 step={d_s/1/d_s} day
  PLOT every, 1
  print every, 1
  write restart frequency, 0
next time {1.*d_s}  $ 1 days
  time steps, 9   $1 step={(10.*d_s-1.*d_s)/9/d_s} day
  PLOT every, 9
  print every, 9
  write restart frequency, 0
next time {10.*d_s}  $ 10 days
  time steps, 4   $1 step={(mon_s-10.*d_s)/4/d_s} days
  PLOT every, 4
  print every, 1
  write restart frequency, 0
next time {mon_s}    $ 1 month
  time steps, {ITS=12}  $1 step={(3.*mon_s-mon_s)/ITS/d_s} days
  PLOT every, {ITS}
  print every, {ITS}
  write restart frequency, 0
next time {3.*mon_s} $ 3 months
  time steps, 9      $1 step={(bgn_s+yr_s-3.*mon_s)/9/d_s} days
  PLOT every, 3
  print every, 9
next time {bgn_s+yr_s} $ Change to oil/brine in caverns: {(bgn_s+yr_s)/yr_s} years
  time steps, {45*ITS}    $ 1 step={(end_s-(bgn_s+yr_s))/(45*ITS)/mon_s} months
  write restart every, 0
  PLOT every, 3
  print every, {ITS}
end time  {end_s} $ {(end_s-bgn_s)/yr_s} years since initial leach

$ Output
thermal stress external, tmpnod
plot state, EqCS, temp
```

```
plot nodal, displacement, tmpnod
plot element, sig, vonmis, eps, pressure

$ Node boundary
no displacement Z 4 $ bottom of mesh
no displacement x 3 $ far-field boundary
no displacement y 3 $ far-field boundary
no displacement x 5 $ vertical axis at origin (cavern 1)
no displacement y 5 $ vertical axis at origin (cavern 1)
no displacement y 1 $ x-axis boundary of mesh
prescribed displacement normal, 2, 3, 0.0, 0,0,0, {-sin(30*RAD)},{cos(30*RAD)},0 $ wedge boundary
of mesh

$ Pressures on side set are the initial cavern pressure
pressure 10 user 1. $ pressure in cavern 1
pressure 20 user 1. $ pressure in cavern 2
pressure 30 user 1. $ pressure in cavern 3
pressure 40 user 1. $ pressure in cavern 4

gravity
  gravitational constant = 9.81
  direction 0. 0. -1.
  magnitude 1.0
  use function 3
end gravity

material 1, power law creep, {rho1}   $ Salt, Baseline
 bulk modulus = {K1/RF}
 two mu = {2*mu1/RF}
 creep constant = {SMF*A}
 stress exponent = {n}
 thermal constant = {Q/R}
END
$ Salt thickness, thick1={thick1=st1th+st2th+cavht+sboth} m

active limits, 10, 0.0,0.01   $ Initial leach of caverns
material 10, power law creep, {rho1} $ Salt, Baseline (Caverns 1-4, original leach)
 bulk modulus = {K1/RF}
 two mu = {2*mu1/RF}
 creep constant = {SMF*A}
 stress exponent = {n}
 thermal constant = {Q/R}
END

material 2, elastic, {rho2}    $ Caprock, Baseline
 youngs modulus = {E2}
 poissons ratio = {nu2}
end
$ Caprock thickness, thick2={thick2=capth} m

material 3, elastic, {rho3}    $ Overburden, Baseline
 youngs modulus = {E3}
 poissons ratio = {nu3}
end
$ Overburden thickness, thick3={thick3=ovrth} m

material 4, elastic, {rho4}    $ Farfield, Baseline
 youngs modulus = {E4}
 poissons ratio = {nu4}
end
$ Surrounding rock thickness, thick4={thick4= thick1+thick2} m

initial value USIGZZ=Function Z 1, 1., material 3
initial value USIGXX=Function Z 1, {nu3/(1.-nu3)}, material 3
initial value USIGYY=Function Z 1, {nu3/(1.-nu3)}, material 3
initial value USIGZZ=Function Z 1, 1., material 2
initial value USIGXX=Function Z 1, {nu2/(1.-nu2)}, material 2
initial value USIGYY=Function Z 1, {nu2/(1.-nu2)}, material 2
initial value USIGZZ=Function Z 2, 1., material 4
initial value USIGXX=Function Z 2, {nu4/(1.-nu4)}, material 4
initial value USIGYY=Function Z 2, {nu4/(1.-nu4)}, material 4
initial value USIGZZ=Function Z 1, 1., material 1
initial value USIGXX=Function Z 1, 1., material 1
initial value USIGYY=Function Z 1, 1., material 1
initial value USIGZZ=Function Z 1, 1., material 10
initial value USIGXX=Function Z 1, 1., material 10
initial value USIGYY=Function Z 1, 1., material 10

$ {sigover = -rho3*9.81*thick3}           $ Vertical stress at botttom of overburden or top of
caprock
$ {sigcr   = sigover - rho2*9.81*thick2} $ Vertical stress at botttom of caprock or top of salt
```

```
$ {sigbot  = sigcr - rho1*9.81*thick1}   $ Vertical stress at bottom of salt

function 1 linear  $ initial stress function for overburden (mat.3), caprock (mat.2), and salt
(mat.1)
  {-thick1 - thick2 - thick3} {sigbot}   $ Bottom of salt
  {-thick2 - thick3}          {sigcr}    $ Bottom of caprock or top of salt
  {-thick3}                   {sigover}  $ Botttom of overburden or top of caprock
  0.0                         0.0        $ Top of overburden
end function 1

function 2 linear     $ initial stress function for surrounding rock (mat. 4)
  {-thick1 - thick2 - thick3} {sigover - rho4*9.81*thick4} $ Bottom of salt
  {-thick3}                     {sigover}                      $ Bottom of Overburden or top of
surrounding rock
end function 2

function 3  $ Gravity and normal displacement function
     0.            1.0
 {end_s}                1.0
end function 3

exit
```

APPENDIX D: USER-SUPPLIED SUBROUTINE TO PROVIDE AN INTERNAL PRESSURE STATE IN THE CAVERNS

```
C $Id: usrpbc.f,v 5.0 1998/08/07 21:42:02 mlblanf Exp $
C
C Modified for Baseline Calculation by B.Y.Park, 4/24/2008
C The stabilizing process of lithologies does not conduct.
C It does not include progressive leaches (drawdowns) of the caverns
C after the field is initially developed.
C
      SUBROUTINE USRPBC( FAC,CORDES,KSFLG,SCALE,NE,TIME,NESNS,NEBLK,
     *  NSPC )
C
C ***********************************************************************
C
C   DESCRIPTION:
C     This routine provides pressure boundary conditions to JAS3D
C
C   FORMAL PARAMETERS:
C     FAC      REAL        Array which must be returned
C                          with the required face pressure
C     CORDES   REAL        Nodal coordinate array
C     KSFLG    INTEGER     Side set ID for this pressure BC
C     SCALE    REAL        Pressure scale factor from input record
C     NE       INTEGER     Number of faces having this pressure BC
C     TIME     REAL        Problem time
C     NESNS    INTEGER     Number of Element Side Nodes
C     NEBLK    INTEGER     Number of Elements per Vector Block
C     NSPC     INTEGER     Number of Spatial Coordinate Components
C
C   CALLED BY: EXLOAD, called once per iteration for each user-defined
C                      pressure BC
C
C ***********************************************************************
C23456789012345678901234567890123456789012345678901234567890123456789012345678901234567890
C
      INCLUDE 'precision.blk'
      INCLUDE 'rcdata.blk'
      INCLUDE 'numbers.blk'
C
C declare logical variables for drawdown flags
C
      LOGICAL FINIT
C declare real variables in units_fortran.txt
      Real min_s,h_min,d_h,mon_d,yr_d,dec_yr,cen_dec,mil_cen
     *     h_s,d_s,mon_s,yr_s,dec_s,cen_s,mil_s
C
      DIMENSION FAC(NEBLK),CORDES(NESNS,NEBLK,NSPC)
C
C --- After stabilizing process of lithologies for this simulation,
C --- the caverns is formed from 0 to 1 year using freshwater,
C --- translating linearly in time from lithostatic pressure with salt to
C --- hydrostatic pressure with water.
C --- The oil/brine setup is held in place using the corresponding
C --- hydrostatic pressure
C
      INCLUDE 'units_fortran.txt'
C
C  Define times at each event - BYP 7/30/2007
C  Time at the initial leaches start
      bgn_s=0.
C  Skip for stabilizing process of lithologies BYP 9.20.2006
      IF (TIME.LT.bgn_s) GO TO 1001
C  Truncates Time
      TIMEYR=(TIME-bgn_s)/yr_s
      A1=AINT(TIMEYR)
      A2=AINT(A1/5.)
      A3=A2*5.+1.
      A4=TIMEYR-A3
      if (A1.GE.5.and.A4.LE.0.) A4=A4+5.
C
C  initialize the drawdown flags
C
      FINIT = .FALSE.
C
C  rho-g factors for oil, fresh water, brine in Pa/m
C  in psi/ft, brine=0.52, oil=0.37, fresh water=0.43
C  convert with 1psi=6894.757 Pa, 1 ft=.3048 m
```

```
C
      GRAVITY=9.81
      OVRNU=0.33
C
      RGOVR=1874.*GRAVITY
      RGCAP=2500.*GRAVITY
      RGSALT=2300.*GRAVITY
C
      RGH2O=9726.86
      RGOIL=8369.62
      RGBRINE=11762.7
C
C  overburden thickness=1600 ft, caprock thickness=400 ft
C  z-locations for layer interfaces, m
C
      ZSURF=0.
      ZOVR=-487.68
      ZCAP=-609.6
C
C  The depth of cavern head = 2500 ft
C  Well head pressure = 2500 ft * 0.37 psi/ft = 925 psi
C  Use a well head pressure of 925 psi for all caverns.
C
      IF ((KSFLG.EQ.  10) .OR. (KSFLG.EQ.  20) .OR. (KSFLG.EQ.  30)
     *.OR.(KSFLG.EQ.  40)) THEN
        PHEAD=925.0*6894.757
      ELSE
        PHEAD=0.
      ENDIF
C Dead Load
      DEADLOAD=RGOVR*(ZSURF-ZOVR)+RGCAP*(ZOVR-ZCAP)
C
C Set zero on the face
      DO 10 I = 1,NE
        FAC(I)=0.0
   10 CONTINUE
C
      S1 = SCALE
C
      DO 1000 I = 1,NE
C
C Coordinates of the center of the face
C
        XFAC = PFORTH*(CORDES(1,I,1) + CORDES(2,I,1) +
     *                 CORDES(3,I,1) + CORDES(4,I,1))
        YFAC = PFORTH*(CORDES(1,I,2) + CORDES(2,I,2) +
     *                 CORDES(3,I,2) + CORDES(4,I,2))
        ZFAC = PFORTH*(CORDES(1,I,3) + CORDES(2,I,3) +
     *                 CORDES(3,I,3) + CORDES(4,I,3))
C
        PLITHO = DEADLOAD + RGSALT*(ZCAP-ZFAC)
        PH2O =   RGH2O*(ZSURF-ZFAC)
        POIL  =  RGOIL*(ZSURF-ZFAC)
        PBRI = RGBRINE*(ZSURF-ZFAC)
C
        PHH2O =  PH2O +PHEAD
        PHOIL =  POIL +PHEAD
        PHBRI =  PBRI +PHEAD
C
C --- Revised pressure calculation of changing to other liquid 1 year
C --- after the stabilization.
C
   52 IF (TIME.LE.(bgn_s+yr_s+d_s)) THEN
         PWELL=(PHH2O-PLITHO)*(TIME-bgn_s)/yr_s + PLITHO
        ELSE
          PWELL=PHOIL
      ENDIF
C23456789112345678921234567893123456789412345678951234567896123456789712
C
C --- Determine which drawdown the simulation is at
C
      IF ((KSFLG.EQ.  10) .OR. (KSFLG.EQ.  20) .OR. (KSFLG.EQ.  30)
     *.OR.(KSFLG.EQ.  40)) FINIT = .TRUE.
C
C --- Determine if well is down for workover (zero pressure for 3 months)
C
   54 IF (TIME.GT.(bgn_s+yr_s+d_s)) THEN
      IF ((A4.GE.1.0001.AND.A4.LE.1.2501).AND.
     *    (KSFLG.EQ.10))  PWELL=PWELL-PHEAD
      IF ((A4.GE.2.0001.AND.A4.LE.2.2501).AND.
     *    (KSFLG.EQ.20))  PWELL=PWELL-PHEAD
```

```
      IF ((A4.GE.3.0001.AND.A4.LE.3.2501).AND.
     *    (KSFLG.EQ.30))  PWELL=PWELL-PHEAD
      IF ((A4.GE.4.0001.AND.A4.LE.4.2501).AND.
     *    (KSFLG.EQ.40))  PWELL=PWELL-PHEAD
      ENDIF
c
      IF (FINIT) THEN
        FAC(I) = S1 * PWELL
      ELSE
        FAC(I) = 0.0
      ENDIF
C
 1000 CONTINUE
C
C For checking
C234567891123456789212345678931234567894123456789512345678961234567897 12
 1001 CONTINUE
      if ((time.ge.(bgn_s- 900.*yr_s).and.time.le.(bgn_s+ 2.0*d_s))
     *.or.(time.ge.(bgn_s+ 0.44*yr_s).and.time.le.(bgn_s+ 0.54*yr_s))
     *.or.(time.ge.(bgn_s+ 0.99*yr_s).and.time.le.(bgn_s+ 2.99*yr_s))
     *.or.(time.ge.(bgn_s+ 5.99*yr_s).and.time.le.(bgn_s+10.99*yr_s))
     *.or.(time.ge.(bgn_s+30.99*yr_s).and.time.le.(bgn_s+35.99*yr_s))
     *.or.(time.ge.(bgn_s+43.99*yr_s))) then
C
        if ((NE.LT.32).and.(KSFLG.eq.10))
     *    write(*,"(' Years ',1x,'  A4  ',1x,'NE',1x,
     *   '  ZFAC ',1x,'KSFLG',1x,' FAC(NE)  '1x,
     *   '  PLITHO  ',1x,'  PHH20   ',1x,'   PHBRI  ',1x,
     *   '   POIL   ',1x,'  PHEAD   ')")
        if (NE.LT.32)
     *    write(*,"(F7.4,1x,F6.3,1x,I2,1X,F7.1,1X,I5,1X,
     *      6(E10.4,1X))") TIMEYR,A4,NE,ZFAC,KSFLG,
     *      FAC(NE),PLITHO,PHH2O,PHBRI,POIL,PHEAD
      endif
      RETURN
      END
```

APPENDIX E: USER-SUPPLIED SUBROUTINE TO CALCULATE THE VOLUME CHANGE OF EACH CAVERN

```
PROGRAM VOLCAV2
c234567890123456789012345678901234567890123456789012345678901234567890123456789012
C========================================================================

C   --*** EX2EX1V2 *** EXODUS II to EXODUS I translator
C   --   Written by Lynn Clements (RE/SPEC) - 01/15/92
C   --   Updated to ExodusII V2.0 Specs by V.R. Yarberry 11/2/93
C   --   Parametric Study based on West Hackberry Site
C   --   Baseline calculation
C   --   Modified by Byoung-Yoon Park (SNL) - 04/28/2008
C   --
C   --EX2EX1V2 reads the EXODUS II V2.02 and V2.03
C   --regular and history files and writes an EXODUS I database file.
C   --
C   --Expects the output database on unit 11.

      include 'exodusII.inc'
c
c  ----- user input parameters:
c  -----   nx0   = number of nodes
c  -----   nx1   = number of elements
c  -----   nx2   = number of side sets (or larger) = numess
c  -----   nx3   = length of node list in the side sets = lessnl
c  -----   nx4   = number of time steps (or larger)
c  ---bh19cav0d, dome radius  = 3000 ft, far field radius = 15000 ft
      parameter (nx0=51606, nx1=45780, nx2=5, nx3=9884, nx4=1000)

      CHARACTER*8 QAINFO(6)
      PARAMETER (MAXQA = 100, MAXINF = 100)
c      CHARACTER*32 QAREC(4,MAXQA)
c      CHARACTER*80 INFO(MAXINF)

C ... Names read in are 32-characters long
      CHARACTER*(mxstln) MAMECO(6)
      CHARACTER*(mxstln) MAMES(256)
C ... Names written out are 8-characters long, truncate with no warning
      CHARACTER*8 NAMECO(6)
      CHARACTER*8 NAMELB(256)
      CHARACTER*8 NAMES(256)

      CHARACTER*80 TITLE

      DIMENSION A(1), ia(1)
C      --A - the dynamic memory base array
      equivalence (a(1), ia(1))
      CHARACTER*1 c(1)
c
c ------- arrays added by SRS
c ------- data from exodus file
      dimension x(nx0),y(nx0),z(nx0)
      integer ssid(nx2,3),ssnodes(nx3)
      real r0(nx2),h0(nx2),th0(nx2),xc(nx2),yc(nx2),zc(nx2),
     1 vol0(nx2),chvol(nx2)
      real volcav(nx2,nx4),time(nx4)
      common /nodec/ hx(8),hy(8),hz(8)
      character*1 comma(nx2)
      character*6 displx,disply,displz
c

      CHARACTER*5 STRA, STRB
      CHARACTER*8 STR8
      character*256 netfil, ndbfil, errmsg
      character*(mxstln) name, cdummy
      LOGICAL WHOTIM
      real wtime, htime
      integer hisid, cpuws, iows
      LOGICAL MDEBUG

      DATA (QAINFO(I), I=1,3) / 'EX2EX1V2', '09/29/98', 'V 2.04  ' /
      data iin,iout /5,6/
      data cpuws, iows /0,0/
      data displx,disply,displz /'DISPLX','DISPLY','DISPLZ'/
      data (comma(i),i=1,nx2) /nx2*','/
C
```

```
c234567890123456789012345678901234567890123456789012345678901234567890123456789012
C================================================================================
c ------ See 3dmesh_seal.log & wh_19cav0d.o
      data (ssid(i,1),i=1,nx2) /7,10,20,30,40/
      data (r0(i),i=1,nx2) /4572.,4*30.48/
      data (h0(i),i=1,nx2) /487.68,4*609.6/
      data (th0(i),i=1,nx2) /30.,30.,3*180./
c ------ xc and yc are center coordinates of wells - get from aprepros
c ------ version of .pts file (Points 1, 1, 26, 44, 62)
      data (xc(i),i=1,nx2) /0.,0.,228.6,457.2,342.9/
      data (yc(i),i=1,nx2) /0.,0.,  0. ,  0. ,197.9734073/
c ------ zc is vertical center of cavern - get cavern.gen3d file,
c ------ add 1/2*translate distance + offset distance
c ------ ovrth/2+0=487.68m/2=243.84m,
c ------(cavht/2=609.6m/2)+(ovrth+capth+st1th+st2th=762m)=1066.8m
      data (zc(i),i=1,nx2) /-243.84,4*-1066.8/
c ------
      open(15,file='volcav.out')
      open(16,file='volcav.csv')

      CALL STRTUP (QAINFO)

      CALL BANNER (0, QAINFO,
     &   'EXODUS II V2.03 TO EXODUS I DATABASE'//
     &   ' TRANSLATOR',' ', ' ')
      call exinq (netid, EXLBVR, idummy, exlibversion, name, nerr)
      write(*,'(A,F6.3)')'ExodusII Library version ',
     1         exlibversion

      CALL MDINIT (A)
      CALL MCINIT (C)
      CALL MDSTAT (NERR, MEM)
      IF (NERR .GT. 0) GOTO 130

      MDEBUG = .false.
      if (MDEBUG) then
         call mlist()
      end if
c
c       make netCDF and exodus errors not show up
c
c      call ncpopt (0)
      call exopts (0,ierr)
c
c       open the netcdf file
c

      net = 11
      call exname (net, netfil, lnam)
c
c -- SRS - changed netfil(1:lnam) to interactive input of file name
c
      write(*,'(a)') 'Name of EXODUS input file:',netfil(1:lnam)
c      read(*,*) netfil
      netid = EXOPEN(netfil(1:lnam), EXREAD, cpuws, iows, vers, nerr)
      if (nerr .lt. 0) then
        write(errmsg,'("could not open input file, error=",i3)')nerr
        call exopts (EXVRBS,ierr)
        call exerr('volcav', errmsg, nerr)
         goto 140
      endif

      write(15,*) 'Input file name: ',netfil(1:lnam)
      call exinq (netid, EXVERS, idummy, exversion, name, nerr)
      write(*,'(A,F6.3)')
     & 'This database was created by ExodusII version ', exversion

c - SRS - removed history section here
C       open the output database and write the initial variables

      NDB = 20

      call exname (ndb, ndbfil, lnam)

      CALL OPNFIL (NDB, 'U', 'U', 0, IERR)
      if (ierr .gt. 0) then
        write(errmsg,'("error opening output file ", a)')ndbfil(1:lnam)
        call exopts (EXVRBS,ierr)
        call exerr('volcav', errmsg, ierr)
        goto 140
      endif
```

```
      write(*,*) 'Output file name: ',ndbfil(1:lnam)
c
c       get initialization parameters from regular netcdf file
c
      CALL EXGINI (netid, title, ndim, numnp, numel,
     &       nelblk, numnps, numess, nerr)
      if (nerr .lt. 0) then
        call exopts (EXVRBS,ierr)
        call exerr('volcav', 'Error from exgini', ierr)
        goto 140
      endif
      if (numnp.ne.nx0) then
           call exerr('volcav', 'Error: nx0 .ne. numnp', -1)
         write(*,'(A)') 'Error: nx0 .ne. numnp'
         write(*,*) nx0,numnp
           goto 140
         endif
      if (numel.ne.nx1) then
           call exerr('volcav', 'Error: nx1 .ne. numel', -1)
         write(*,'(A)') 'Error: nx1 .ne. numel'
         write(*,*) nx1,numel
           goto 140
         endif
      if (numess.gt.nx2) then
           call exerr('volcav', 'Error: nx2 .lt. numess', -1)
         write(*,'(A)') 'Error: nx2 .lt. numnps'
         write(*,*) nx2,numess
           goto 140
         endif
c
c       get the length of the node sets node list
c
      if (numnps .gt. 0) then
         CALL EXINQ (netid, EXNSNL, lnpsnl, dummy, cdummy, nerr)
         if (nerr .lt. 0) then
           call exopts (EXVRBS,ierr)
           call exerr('volcav', 'Error from exqini', ierr)
           goto 140
         endif
      else
         lnpsnl = 0
      endif
c
      if (numess .gt. 0) then
c
c       get the length of the side sets node list
c
        CALL EXINQ (netid, EXSSNL, lessnl, dummy, cdummy, nerr)
        if (nerr .lt. 0) then
           call exopts (EXVRBS,ierr)
           call exerr('volcav', 'Error from exqini', ierr)
           goto 140
        endif
c
c       get the length of the side sets distribution factor list
c
         CALL EXINQ (netid, EXSSDF, lessdl, dummy, cdummy, nerr)
         if (nerr .lt. 0) then
           call exopts (EXVRBS,ierr)
           call exerr('volcav', 'Error from exqini', ierr)
           goto 140
         endif
c
c       get the length of the side sets element list
c
         CALL EXINQ (netid, EXSSEL, lessel, dummy, cdummy, nerr)
         if (nerr .lt. 0) then
           call exopts (EXVRBS,ierr)
           call exerr('volcav', 'Error from exqini', ierr)
           goto 140
         endif
      else
         lessnl = 0
         lessel = 0
         lessdl = 0
      endif
c
c       write the initialization information to the EXODUS 1.0 database
c --- commented by SRS
c      CALL DBOINI (NDB, TITLE, NDIM, NUMNP, NUMEL, NELBLK,
```

```
c     &   NUMNPS, LNPSNL, NUMESS, LESSEL, LESSNL)
c
      CALL DBPINI ('TIS', NDB, TITLE, NDIM, NUMNP, NUMEL, NELBLK,
     &   NUMNPS, LNPSNL, NUMESS, LESSEL, LESSNL,
     &   IDUM, IDUM, IDUM, IDUM)

C   --Read the coordinates
      write(*,'(A)') 'Reading coordinates'
      CALL MDRSRV ('XN', KXN, NUMNP)
      CALL MDRSRV ('YN', KYN, NUMNP)
      IF (NDIM .GE. 3) THEN
        CALL MDRSRV ('ZN', KZN, NUMNP)
        CALL MDSTAT (NERR, MEM)
        IF (NERR .GT. 0) GOTO 130
c        write(*,*)' ************************ NDIM: ',ndim
        CALL EXGCOR(netid, a(kxn), a(kyn), a(kzn), nerr)
         if (nerr .lt. 0) then
           call exopts (EXVRBS,ierr)
           call exerr('volcav', 'Error from exgcor', ierr)
           goto 140
         endif

c-SRS         CALL DBOXYZ (NDB, NDIM, NUMNP, A(KXN), A(KYN), A(KZN))

c-JEB         CALL MDDEL ('XN')
c-JEB         CALL MDDEL ('YN')
c-JEB         CALL MDDEL ('ZN')
      ELSE
        CALL EXGCOR(netid, a(kxn), a(kyn), dummy, nerr)
         if (nerr .lt. 0) then
           call exopts (EXVRBS,ierr)
           call exerr('volcav', 'Error from exgcor', ierr)
           goto 140
         endif

c-SRS         CALL DBOXYZ (NDB, NDIM, NUMNP, A(KXN), A(KYN), dummy)

c-JEB         CALL MDDEL ('XN')
c-JEB         CALL MDDEL ('YN')
      ENDIF

      do 10 i=1,numnp
 10   x(i)=a(kxn+i-1)
      do 11 i=1,numnp
 11   y(i)=a(kyn+i-1)
      if (ndim.gt.2) then
        do 12 i=1,numnp
 12     z(i)=a(kzn+i-1)
      endif
      write(*,*) kxn,kyn,kzn
      write(*,*) x(1),y(1),z(1)
      write(*,*) x(numnp),y(numnp),z(numnp)

C   --Read the element order map
      write(*,'(A)') 'Reading element order map'
      CALL MDRSRV ('MAPEL', KMAPEL, NUMEL)
      CALL MDSTAT (NERR, MEM)
      IF (NERR .GT. 0) GOTO 130

      CALL EXGMAP (netid, a(KMAPEL), nerr)
c      write(*,*) nerr
      do 29 i=2,numel
      do 29 j=1,i-1
      if (ia(kmapel+i-1).eq.ia(kmapel+j-1)) then
      write(*,'(A)') '****************************'
      write(*,'(A)') 'Element order map contains duplicate element IDs'
      write(*,'(A)') '**** Setting nerr to 17 ****'
      nerr=17
      go to 28
      endif
   29 continue
   28 if (nerr .ne. 0) then
         if (nerr .eq. 17) then

C   -- no element order map in the EXODUS II file; create a dummy one
            do 30 i=1,numel
               ia(KMAPEL+i-1) = i
30          continue
         else
            goto 140
         endif
```

```
      endif

c      CALL DBOMAP (NDB, NUMEL, A(KMAPEL))
c      write(*,*) a(kmapel+3),ia(kmapel+3),kmapel
c      write(*,*) kmapel
c-delete this line when ready      call getar1d (ia(KMAPEL),mapeo,numel)
      CALL MDDEL ('MAPEL')
c
c       Read in the element block ID array
c
      write(*,'(A)') 'Reading element block ID array'
      call MDRSRV ('IDELB', kidelb, nelblk)
      call exgebi (netid, a(kidelb), ierr)
      if (nerr .lt. 0) then
         call exopts (EXVRBS,ierr)
         call exerr('volcav', 'Error from exgebi', ierr)
         goto 140
      endif

C   --Read the element block

      write(*,'(A)') 'Reading element blocks'
      CALL MDRSRV ('NUMELB', KNELB, NELBLK)
      CALL MDRSRV ('LINK', KLINK, 0)
      CALL MDRSRV ('ATRIB', KATRIB, 0)
      CALL MDSTAT (NERR, MEM)
c      write(*,*) knelb,klink,katrib
      IF (NERR .GT. 0) GOTO 130

      nel = 0
      DO 50 IELB = 1, NELBLK

         CALL EXGELB (netid, a(kidelb+ielb-1), name,
     &        a(knelb+ielb-1), numlnk, numatr, nerr)
         if (nerr .lt. 0) then
            call exopts (EXVRBS,ierr)
            call exerr('volcav', 'Error from exgelb', ierr)
            goto 140
         endif
         namelb(ielb) = name(:8)
         call getin (a(knelb+ielb-1),num)
         if (numlnk .gt. 0) then
           CALL MDLONG ('LINK', KLINK, num*numlnk)
           CALL EXGELC (netid, a(kidelb+ielb-1),
     &         a(klink), nerr)
           if (nerr .lt. 0) then
              call exopts (EXVRBS,ierr)
              call exerr('volcav', 'Error from exgelc', ierr)
              goto 140
           endif
         end if

         if (numatr .gt. 0) then
           CALL MDLONG ('ATRIB', KATRIB, num*numatr)
           CALL EXGEAT (netid, a(kidelb+ielb-1), a(katrib), nerr)
           if (nerr .lt. 0) then
              call exopts (EXVRBS,ierr)
              call exerr('volcav', 'Error from exgeat', ierr)
              goto 140
           endif
         end if

         CALL MDSTAT (NERR, MEM)
         IF (NERR .GT. 0) GOTO 130

c-SRS         CALL DBOELB (NDB, IELB, IELB,
c-SRS     &      a(kidelb+ielb-1), A(KNELB+IELB-1), NUMLNK, NUMATR,
c-SRS     &      A(KLINK), A(KATRIB))

         nel=nel+num
         CALL MDLONG ('LINK', klink, 0)
         CALL MDLONG ('ATRIB', katrib, 0)

50    CONTINUE

      CALL MDDEL ('LINK')
      CALL MDDEL ('ATRIB')

      IF (NEL .NE. NUMEL) THEN
         CALL INTSTR (1, 0, NEL, STRA, LSTRA)
         CALL INTSTR (1, 0, NUMEL, STRB, LSTRB)
```

```
         CALL PRTERR ('WARNING',
     &      'NUMBER OF ELEMENTS IN BLOCK = ' // STRA(:LSTRA)
     &      // ' does not match TOTAL = ' // STRB(:LSTRB))
      END IF

C   --Read the node sets
      write(*,'(A)') 'Reading node sets'
      write(15,'(A)') 'Reading node sets'

      CALL MDRSRV ('IDNPS',  KIDNS, NUMNPS)  ! Node set ids array
      CALL MDRSRV ('NNNPS', KNNNS, NUMNPS)   ! Node set node count array
      CALL MDRSRV ('NDNPS', KNDNS, NUMNPS)   ! Node set df count array
      CALL MDRSRV ('IXNNPS', KIXNNS, NUMNPS) ! Node set nodes index array
      CALL MDRSRV ('IXDNPS', KIXDNS, NUMNPS) ! Node set df index array
      CALL MDRSRV ('LSTNPS', KLSTNS, LNPSNL) ! Node set node list array
      CALL MDRSRV ('FACNPS', KFACNS, LNPSNL) ! Node set df list array
      CALL MDRSRV ('XFACNP', KXFACN, LNPSNL) ! Expanded df list array
      CALL MDSTAT (NERR, MEM)

c      write(*,*) kidns,knnns,kndns,kixnns,kixdns,klstns,kfacns,kxfacn

      if (numnps .gt. 0) then
         call exgcns (netid, a(kidns), a(knnns), a(kndns), a(kixnns),
     &               a(kixdns), a(klstns), a(kfacns), nerr)
         if (nerr .lt. 0) then
            call exopts (EXVRBS,ierr)
            call exerr('volcav', 'Error from exgcns', ierr)
            goto 140
         endif
      endif
C
C     Massage node sets distribution factors to include '1' for node sets
C       without Dfs by walking KNDNS array, checking for 0, and filling where
C       necessary.
C
      do 64 i=0, numnps-1
        if (ia(kndns+i) .eq. 0) then
          do 60 ii=0, ia(knnns+i)-1
            a(kxfacn+ia(kixnns+i)-1+ii) = 1.0! Force unity distribution factor
60        continue
        else
          do 62 ii=0, ia(kndns+i)-1
            a(kxfacn+ia(kixnns+i)-1+ii) = a(kfacns+ia(kixdns+i)-1+ii)
62        continue
        endif
64      continue

c-SRS       CALL DBONPS (NDB, NUMNPS, LNPSNL,
c-SRS     &   A(KIDNS), A(KNNNS), A(KIXNNS), A(KLSTNS), A(KXFACN))

      CALL MDDEL ('IDNPS')
      CALL MDDEL ('NNNPS')
      CALL MDDEL ('NDNPS')
      CALL MDDEL ('IXNNPS')
      CALL MDDEL ('IXDNPS')
      CALL MDDEL ('LSTNPS')
      CALL MDDEL ('FACNPS')
      CALL MDDEL ('XFACNP')
      CALL MDSTAT (NERR, MEM)
      write(15,'(A)') '   Node sets processing complete'
      IF (NERR .GT. 0) GOTO 130

C   --Read the side sets
      write(*,'(A)') 'Reading side sets'

      CALL MDRSRV ('IDESS', KIDSS, NUMESS)   ! side set id array
c     write(*,*)'side set id array size: ',numess
      CALL MDRSRV ('NEESS', KNESS, NUMESS)   ! number of ss elems array
c     write(*,*)'number of side set elements  array size: ',numess
      CALL MDRSRV ('NDESS', KNDSS, NUMESS)   ! number of dist factors array
c     write(*,*)'number of dist factors array size: ',numess
      CALL MDRSRV ('NNESS', KNNSS, NUMESS)   ! number of nodes array
c     write(*,*)'number of side set nodes array size: ',numess
      CALL MDRSRV ('IXEESS', KIXESS, NUMESS) ! index into elements array
c     write(*,*)'index into side set elements array size: ',numess
      CALL MDRSRV ('IXDESS', KIXDSS, NUMESS) ! index into dist factors array
c     write(*,*)'index into side set dist factors  array size: ',numess
      CALL MDRSRV ('IXNESS', KIXNSS, NUMESS) ! index into nodes array
c     write(*,*)'index into side set nodes array size: ',numess
      CALL MDRSRV ('LTEESS', KLTESS, LESSEL) ! element list
c     write(*,*)'side set element list array size: ',lessel
```

```
      CALL MDRSRV ('LTNESS', KLTNSS, LESSNL) ! node list (21 is max possible)
c     write(*,*)'side set node list array size: ',lessnl
      CALL MDRSRV ('LTNNSS', KLTNNS, LESSEL) ! node count array
c     write(*,*)'side set node count array size: ',lessel
      CALL MDRSRV ('LTSESS', KLTSSS, LESSEL) ! side list
c     write(*,*)'side set side list array size: ',lessel
      CALL MDRSRV ('FACESS', KFACSS, LESSDL) ! dist factors list
c     write(*,*)'side set dist factors list array size: ',lessdl
      CALL MDRSRV ('XFACES', KXFACS, LESSNL) ! dist factors list(w/all DF)
      CALL MDSTAT (NERR, MEM)
      IF (NERR .GT. 0) GOTO 130

      if (numess .gt. 0) then
        call exgcss (netid, a(kidss), a(kness), a(kndss),
     &               a(kixess), a(kixdss),
     &               a(kltess), a(kltsss), a(kfacss), nerr)
        if (nerr .lt. 0) then
           call exopts (EXVRBS,ierr)
           call exerr('volcav', 'Error from exgcss', ierr)
           goto 140
        endif

C Convert sides to nodes

        isoff = 0            ! offset into element list for current side set
        nodcnt = 0           ! node count for current side set
        do 104 i=0,numess-1  ! loop thru ss elem blks

          ia(kixnss+i)=nodcnt+1                          ! update index array

          call exgsp(netid,ia(kidss+i),nsess,ndess,nerr)! get num of sides & df
          if (nerr .lt. 0) then
             call exopts (EXVRBS,ierr)
             call exerr('volcav', 'Error from exgsp', ierr)
             goto 140
          endif
         write(*,*)'SS ID: ',ia(kidss+i)
         write(15,*)'SS ID: ',ia(kidss+i)
         write(*,*)' # of sides: ',nsess
         write(15,*)' # of sides: ',nsess
         i1=0
         do 86 i0=1,nx2
         if (ssid(i0,1).eq.ia(kidss+i)) then
            i1=i0
            ssid(i0,2)=nsess
            ssid(i0,3)=nodcnt+1
            go to 87
         endif
   86    continue
   87    if(i1.eq.0) then
           write(*,*) '*** mismatched side set IDs, loop 86'
           stop 1
         endif

c         write(*,*)' # of dist factors: ',ndess

          call exgssn(netid,ia(kidss+i),a(kltnns+isoff),
     &               a(kltnss+nodcnt),nerr)         ! get side set nodes
          if (nerr .lt. 0) then
             call exopts (EXVRBS,ierr)
             call exerr('volcav', 'Error from exgssn', ierr)
             goto 140
          endif
          nness = 0
          do 102 ii=0,nsess-1                       ! sum node counts to
            nness=nness+ia(kltnns+isoff+ii)         ! calculate next index
102       continue
c         write(*,*)' # of nodes: ',nness
          write(*,*) nodcnt,nness
          write(15,*) nodcnt,nness
          do 234 j=1,nness
          ssnodes(nodcnt+j)=ia(kltnss+nodcnt+j-1)
 234      continue
          do 235 j=1,nness,12
 235      write(15,*) (ssnodes(nodcnt+j0),j0=j,j+11)
          ia(knnss+i)=nness
          nodcnt=nodcnt+nness
          isoff=isoff+nsess
104     continue
      endif
C
```

```
C     Massage side sets distribution factors to include '1' for side sets
C       without Dfs by walking KNDSS array, checking for 0, and filling where
C       necessary.
C
      do 110 i=0, numess-1
        if (ia(kndss+i) .eq. 0) then
          do 106 ii=0, ia(knnss+i)-1
            a(kxfacs+ia(kixnss+i)-1+ii) = 1.0! Force unity distribution factor
106       continue
        else
          do 108 ii=0, ia(knnss+i)-1
            a(kxfacs+ia(kixnss+i)-1+ii) = a(kfacss+ia(kixdss+i)-1+ii)
108       continue
        endif
110     continue

c-SRS       CALL DBOESS (NDB, NUMESS, LESSEL, LESSNL,
c-SRS      &   A(KIDSS), A(KNESS), A(KNNSS), A(KIXESS), A(KIXNSS),
c-SRS      &   A(KLTESS), A(KLTNSS), A(KXFACS))

      CALL MDDEL ('IDESS')
      CALL MDDEL ('NEESS')
      CALL MDDEL ('NDESS')
      CALL MDDEL ('NNESS')
      CALL MDDEL ('IXEESS')
      CALL MDDEL ('IXDESS')
      CALL MDDEL ('IXNESS')
      CALL MDDEL ('LTEESS')
      CALL MDDEL ('LTNESS')
      CALL MDDEL ('LTNNSS')
      CALL MDDEL ('LTSESS')
      CALL MDDEL ('FACESS')
      CALL MDDEL ('XFACES')

C   --Read the QA records
      write(*,'(A)') 'Reading QA records'

      nqarec = 0
      call exinq (netid, EXQA, nqarec, r, name, nerr)
      if (nerr .lt. 0) then
         call exopts (EXVRBS,ierr)
         call exerr('volcav', 'Error from exinq', ierr)
         goto 140
      endif

      if (nqarec .gt. 0 .and. nqarec .le. MAXQA) then
        call mcrsrv('QARECS', kqarec, 4*nqarec*8)
        call mcrsrv('QATMP', kqatmp, 4*nqarec*mxstln)
        call mcstat(nerr, mem)
        if (nerr .ne. 0) goto 130
      else
        kqarec = 1
      end if
      if (nqarec .gt. MAXQA) nqarec = 0

      ninfo = 0
      call exinq (netid, EXINFO, ninfo, r, name, nerr)
      if (nerr .lt. 0) then
         call exopts (EXVRBS,ierr)
         call exerr('volcav', 'Error from exinq', ierr)
         goto 140
      endif

      if (ninfo .gt. 0 .and. ninfo .le. MAXINF) then
        call mcrsrv('INFO', kinfo, ninfo*mxlnln)
        call mcstat(nerr, mem)
        if (nerr .ne. 0) goto 130
      else
        kinfo = 1
      end if
      if (ninfo .gt. MAXINF) ninfo = 0

      call rdqain (netid, nqarec, c(kqatmp), ninfo, c(kinfo))

      if (nqarec .gt. 0)
     &    call resize (nqarec, c(kqarec), c(kqatmp))

c-SRS       IF (NQAREC .GE. 0) THEN
c-SRS          CALL DBOQA (NDB, NQAREC, c(kqarec), NINFO, c(kinfo))
c-SRS       END IF
```

```
C   --Read in the number of element variable names
      write(*,'(A)') 'Reading number of element variable names'

      call exgvp (netid, 'e', nvarel, nerr)
      if (nerr .lt. 0) then
         call exopts (EXVRBS,ierr)
         call exerr('volcav', 'Error from exgvp', ierr)
         goto 140
      endif
C
C   --Read in the number of global variable names
C
      write(*,'(A)') 'Reading number of global variable names'
      call exgvp (netid, 'g', nvargl, nerr)
      if (nerr .lt. 0) then
         call exopts (EXVRBS,ierr)
         call exerr('volcav', 'Error from exgvp', ierr)
         goto 140
      endif
C
C   --Read in the number of nodal variable names
C
      write(*,'(A)') 'Reading number of nodal variable names'
      call exgvp (netid, 'n', nvarnp, nerr)
      if (nerr .lt. 0) then
         call exopts (EXVRBS,ierr)
         call exerr('volcav', 'Error from exgvp', ierr)
         goto 140
      endif
      nvarhi=0

      call mdrsrv ('ISEVOK', kievok, nvarel*nelblk)
      CALL MDSTAT (NERR, MEM)
      IF (NERR .GT. 0) GOTO 130
C
C       read in the element variable truth table
C
      write(*,'(A)') 'Reading element variable truth table'
      call exgvtt (netid, nelblk, nvarel, a(kievok), nerr)
      if (nerr .gt. 0) then
        if (nvarel .gt. 0) then
          write (*,'(4x,"must have element variable truth table")')
          goto 140
        endif
      endif
      if (nerr .lt. 0) then
         call exopts (EXVRBS,ierr)
         call exerr('volcav', 'Error from exgvtt', ierr)
         goto 140
      endif
C
C       read in the element variable names
C
      ixev = 1
      if (nvarel .gt. 0) then
        call exgvan (netid, 'e', nvarel,mames(ixev), nerr)
        if (nerr .lt. 0) then
           call exopts (EXVRBS,ierr)
           call exerr('volcav', 'Error from exgvan', ierr)
           goto 140
        endif
      end if
C
C       read in the global variable names
C
      ixgv = ixev + nvarel
      if (nvargl .gt. 0) then
        call exgvan (netid, 'g', nvargl,mames(ixgv), nerr)
        if (nerr .lt. 0) then
           call exopts (EXVRBS,ierr)
           call exerr('volcav', 'Error from exgvan', ierr)
           goto 140
        endif
      end if
C
C       read in the nodal variable names
C
      ixnv = ixgv + nvargl
      if (nvarnp .gt. 0) then
        call exgvan (netid, 'n', nvarnp, mames(ixnv), nerr)
```

```
        if (nerr .lt. 0) then
           call exopts (EXVRBS,ierr)
           call exerr('volcav', 'Error from exgvan', ierr)
           goto 140
        endif
      end if
c
c       read coordinate names
c
      call exgcon (netid, mameco, nerr)
      if (nerr .lt. 0) then
         call exopts (EXVRBS,ierr)
         call exerr('volcav', 'Error from exgcon', ierr)
         goto 140
      endif


      CALL DBPINI ('V', NTXT, TITLE, NDIM, NUMNP, NUMEL, NELBLK,
     &      NUMNPS, LNPSNL, NUMESS, LESSEL, LESSNL,
     &      NVARHI, NVARGL, NVARNP, NVAREL)

      do 111 i=1, ndim
        nameco(i) = mameco(i)(:8)
 111  continue
      idx=0
      idy=0
      idz=0
      do 112 i=1, (nvarhi+nvargl+nvarnp+nvarel)
        names(i) = mames(i)(:8)
        write(*,*) names(i)
        if (displx.eq.names(i)(:6)) idx=i-nvarel-nvargl
        if (disply.eq.names(i)(:6)) idy=i-nvarel-nvargl
        if (displz.eq.names(i)(:6)) idz=i-nvarel-nvargl
 112  continue
      write(*,*) idx,idy,idz
c
c --- calculate original volumes
c
      degrad=3.141592653/180.
      do 113 i=1,nx2
        vol0(i)=0.5*degrad*th0(i)*h0(i)*r0(i)**2
  113 continue

c      CALL DBONAM (NDB, NDIM, NELBLK, NVARHI, NVARGL, NVARNP, NVAREL,
c     &   nameco, namelb,
c     &   names(ixhv), names(ixgv), names(ixnv), names(ixev),
c     &   A(KIEVOK))



      CALL MDRSRV ('VARHI', KVARHI, NVARHI)
      CALL MDRSRV ('VARGL', KVARGL, NVARGL)
      CALL MDRSRV ('VARNP', KVARNP, NVARNP * NUMNP)
      CALL MDRSRV ('VAREL', KVAREL, NVAREL * NUMEL)
      CALL MDSTAT (NERR, MEM)
      IF (NERR .GT. 0) GOTO 130

c
c       read in the number of history time steps and the number of
C       whole time steps
c
      call exinq (netid, EXTIMS, ntime, s, name, nerr)
      if (nerr .lt. 0) then
         call exopts (EXVRBS,ierr)
         call exerr('volcav', 'Error from exqini', ierr)
         goto 140
      endif
      if (ntime .eq. 0) then
        write(errmsg,'("GENESIS file - no time steps written")')
        call exerr('volcav', errmsg, EXPMSG)
        goto 140
      endif
      numstp = ntime

      if (numstp.gt.nx4) then
          call exerr('volcav', 'Error: nx4 .lt. numstp', -1)
        write(*,'(A)') 'Error: nx4 .lt. numstp'
        write(*,*) nx4,numstp
          goto 140
        endif
```

```
      if (nvarhi .gt. 0) then
        call exinq (hisid, EXTIMS, nhtime, s, name, nerr)
        numstp = nhtime
        if (nerr .gt. 0) goto 140
      endif

c
c       read the time step information
c
      write(*,'(A)') 'Reading time step information'

      istep = 0
      call exgtim(netid, istep+1, wtime, nerr)
      if (nerr .lt. 0) then
         call exopts (EXVRBS,ierr)
         call exerr('volcav', 'Error from exgtim', ierr)
         goto 140
      endif
c      write(*,*) istep,wtime
c      write(*,'(A)') 'Inside 300 loop'
      write(16,902) (comma(n),ssid(n,1),n=1,numess)
  902 format('Time(s)',',','Time(y)',26(a1,i4))
      do 300 ihstep=1,numstp
      oldtim=wtime

        write (*,'(4x,"processing time step ", i4)') ihstep
        write (15,'(4x,"processing time step ", i4)') ihstep
c
c         get history information
c
        if (nvarhi .gt. 0) then
          whotim = .false.
          call exgtim(hisid, ihstep, htime, nerr)
          if (nerr .lt. 0) then
             call exopts (EXVRBS,ierr)
             call exerr('volcav', 'Error from exgtim', ierr)
             goto 140
          endif

          call exggv (hisid, ihstep, nvarhi, a(kvarhi), nerr)
          if (nerr .lt. 0) then
             call exopts (EXVRBS,ierr)
             call exerr('volcav', 'Error from exggv', ierr)
             goto 140
          endif
        else
          whotim = .true.
          call exgtim(netid, ihstep, wtime, nerr)
          if (nerr .lt. 0) then
             call exopts (EXVRBS,ierr)
             call exerr('volcav', 'Error from exgtim', ierr)
             goto 140
          endif
          htime = wtime
        end if
c
c          If a whole time step, do global, nodal, and element
c          variables for the time step.
c
        if ((whotim) .or. (wtime .eq. htime)) then

          whotim =.true.
          istep = istep + 1
c          write(*,*) ihstep,istep,htime,wtime,oldtim

c
c           get the global variable values
c
          if( nvargl .gt. 0) then
            call exggv (netid, istep, nvargl, a(kvargl), nerr)
            if (nerr .lt. 0) then
               call exopts (EXVRBS,ierr)
               call exerr('volcav', 'Error from exggv', ierr)
               goto 140
            endif
          end if
c
c           get the nodal variable values
c
          do 210 j=1, nvarnp
            call exgnv (netid, istep, j, numnp,
```

```
     &         a(kvarnp+(j-1)*numnp), nerr)
               if (nerr .lt. 0) then
                  call exopts (EXVRBS,ierr)
                  call exerr('volcav', 'Error from exgnv', ierr)
                  goto 140
               endif
210         continue

c
c            get element variable values
c
            if (nvarel .gt. 0) then
              ielo=0
              j0=0
              do 250 k = 1,nelblk
                l=(k-1)*nvarel
                do 240 j=1, nvarel
c
c                  If truth table indicates element values are available
c                  for the element variable, get the values for the
c                  element variable.
c
                  if(a(kievok+l +j-1) .ne. 0) then
                    call exgev (netid, istep, j, a(kidelb+k-1),
     &                   a(knelb+k-1), a(kvarel+ielo), nerr)
                    if (nerr .lt. 0) then
                       call exopts (EXVRBS,ierr)
                       call exerr('volcav', 'Error from exgev', ierr)
                       goto 140
                    endif
                    call getin (a(knelb+k-1),num)
                    ielo = ielo+num
                  end if
240               continue
250             continue
              end if
            else
              whotim=.false.
            end if

c
c ------ calculate new element variable IMPULSE for all elements
c
            time(ihstep)=wtime
            write (15,'(4x,"time ", e11.5)') wtime
            jvx=kvarnp+(idx-1)*numnp
            jvy=kvarnp+(idy-1)*numnp
            jvz=kvarnp+(idz-1)*numnp
            do 90 i=1,numess
            chvol(i)=0.0
            nsides=ssid(i,2)
            nnodes=nsides*4
            write(15,900) ssid(i,1),nsides,nnodes
  900 format('Side set number ',i3,', number of sides = ',i6,
     1       ', number of nodes = ',i6)
               j0=ssid(i,3)
               j1=j0+nnodes-1
               do 91 j=j0,j1,4
                 jm1=j-1
                 do 92 jj=1,4
                 n0=ssnodes(jm1+jj)
c                 if (ihstep.eq.69) write(15,*) jm1+jj,n0,x(n0),y(n0),z(n0),
c     1             a(jvx+n0-1),a(jvy+n0-1),a(jvz+n0-1)
                 hx(jj)=x(n0)
                 hy(jj)=y(n0)
                 hz(jj)=z(n0)
                 hx(jj+4)=x(n0)+a(jvx+n0-1)
                 hy(jj+4)=y(n0)+a(jvy+n0-1)
                 hz(jj+4)=z(n0)+a(jvz+n0-1)
                 dx=dx+a(jvx+n0-1)
                 dy=dy+a(jvy+n0-1)
                 dz=dz+a(jvz+n0-1)
   92            continue
c ---- calculate volume of hexahedron from displacements
                 call hexvol(hvol)
c ---- make sure volume vector is calculated correctly
                 fac=1.0
                 a0=xc(i)-hx(1)
                 b0=yc(i)-hy(1)
                 c0=zc(i)-hz(1)
                 a1=hx(2)-hx(1)
```

```
          b1=hy(2)-hy(1)
          c1=hz(2)-hz(1)
          a2=hx(4)-hx(1)
          b2=hy(4)-hy(1)
          c2=hz(4)-hz(1)
          dot=a0*(b1*c2-b2*c1)+b0*(c1*a2-c2*a1)+c0*(a1*b2-a2*b1)
          if (dot.lt.0.) fac=-1.
          if (fac.lt.0.) write(15,*) '** Problem!! **',
     1         ihstep,i,n0,x(n0),y(n0),z(n0),fac,hvol
          chvol(i)=chvol(i)+fac*hvol
   91   continue
c -- if i=1, then side set is top surface
        if (i.eq.1) then
          volcav(i,ihstep)=chvol(i)
        else
          volcav(i,ihstep)=vol0(i)-chvol(i)
        endif
        write(15,*) ihstep,i,vol0(i),chvol(i),volcav(i,ihstep)
   90   continue
        wyear=wtime/3600/24/365
        write(16,901) wtime,wyear,(comma(n),volcav(n,ihstep),n=1,numess)
  901   format(e12.5,',',F9.4,26(a1,f10.1))

c        CALL DBOSTE (NDB, ihstep, NVARHI, NVARGL, NVARNP, NUMNP,
c     &      NVAREL, NELBLK, a(knelb), a(kievok),
c     &      HTIME, WHOTIM, A(KVARHI), A(KVARGL), A(KVARNP),
c     &      A(KVAREL))


300   continue

      call MDDEL ('IDELB')
      CALL MDDEL ('VARHI')
      CALL MDDEL ('VARGL')
      CALL MDDEL ('VARNP')
      CALL MDDEL ('VAREL')
      CALL MDDEL ('NUMELB')

120   CONTINUE
      CALL INTSTR (1, 0, IHSTEP-1, STR8, LSTR)
      WRITE (*, 10010) STR8(:LSTR)
10010  FORMAT (/, 4X, A,
     &   ' time steps have been written to the database')

      GOTO 140

  130 CONTINUE
      CALL MEMERR
      GOTO 140

  140 CONTINUE
c
c       close all files
c
      CLOSE (NDB, IOSTAT=IDUM)
      close(15)
      close(16)
      if (nvarhi .gt. 0) then
        if (hisid .ge. 0) call exclos (hisid, ierr)
      endif

999   if (netid .ge. 0 ) call exclos (netid, ierr)


      CALL WRAPUP (QAINFO(1))

      END

      subroutine hexvol (hvol)
c
      common /nodec/ hx(8),hy(8),hz(8)
      data o64th /0.0156250/
c
c  Jacobian matrix
c
      x17=hx(7)-hx(1)
      x28=hx(8)-hx(2)
      x35=hx(5)-hx(3)
      x46=hx(6)-hx(4)
      y17=hy(7)-hy(1)
      y28=hy(8)-hy(2)
```

```
      y35=hy(5)-hy(3)
      y46=hy(6)-hy(4)
      z17=hz(7)-hz(1)
      z28=hz(8)-hz(2)
      z35=hz(5)-hz(3)
      z46=hz(6)-hz(4)
c
      aj1=x17+x28-x35-x46
      aj2=y17+y28-y35-y46
      aj3=z17+z28-z35-z46
      a17=x17+x46
      a28=x28+x35
      b17=y17+y46
      b28=y28+y35
      c17=z17+z46
      c28=z28+z35
c
      aj4=a17+a28
      aj5=b17+b28
      aj6=c17+c28
      aj7=a17-a28
      aj8=b17-b28
      aj9=c17-c28
c
c   Jacobian
c
      aj5968=aj5*aj9-aj6*aj8
      aj6749=aj6*aj7-aj4*aj9
      aj4857=aj4*aj8-aj5*aj7
c
      hvol=o64th*(aj1*aj5968+aj2*aj6749+aj3*aj4857)
c
      return
      end
c

      subroutine mlist()
      call mdlist(6)
      return
      end


      subroutine rdqain (ndb, nqarec, qarec, ninfo, info)
      include 'exodusII.inc'
      integer ndb
      character*(32) qarec(4,nqarec)
      character*(80) info(ninfo)

      if (nqarec .gt. 0) then
         call exgqa (ndb, qarec, nerr)
         if (nerr .lt. 0) then
            call exopts (EXVRBS,ierr)
            call exerr('volcav', 'Error from exgqa', ierr)
         endif
      endif
      if (ninfo .gt. 0) then
         call exginf (ndb, info, nerr)
         if (nerr .lt. 0) then
            call exopts (EXVRBS,ierr)
            call exerr('volcav', 'Error from exginf', ierr)
         endif
      endif

      return
      end

C=======================================================================
      SUBROUTINE RESIZE (NQAREC, QAREC, QATMP)
C=======================================================================
C   --
C   --RESIZE - resizes the qa records from length 32 to 8
C   --
C   --Parameters:
C   --   NQAREC - IN - the number of QA records
C   --   QAREC  - IN - the QA records containing size = 8
C   --   QATMP  - IN - the QA records containing size = 32

      INTEGER NQAREC
      CHARACTER*8 QAREC(4,NQAREC)
      CHARACTER*32 QATMP(4,NQAREC)
```

```
      IF (NQAREC .GT. 0) THEN
         DO 50 I = 1, NQAREC
            DO 75 J = 1, 4
               QAREC(J,I) = QATMP(J,I)
75          CONTINUE
50       CONTINUE
      END IF

      RETURN
      END
```

APPENDIX F: ALGEBRA SCRIPT FOR POST-PROCESS

```
'
' Subsidence, Principal Stress/Strain and Failure Criteria
' Journalized by B.Y.Park on June 27, 2008
'
ALLTIMES
tmin 86400
save epsxx epsyy epszz
'
' Unit conversion
'
ft_m=0.3048
m_ft=1/ft_m
psi_Pa=6894.745
Pa_psi=1/psi_Pa
'
' Difference from displacement at 1st time step (ft)
'
dx=(displx-displx:1)*m_ft
dy=(disply-disply:1)*m_ft
dz=(displz-displz:1)*m_ft
'
' Compute Maximum Principal Strain
'
emax=pmax(epsxx,epsyy,epszz,epsxy,epsyz,epszx)
emaxmx=smax(emax)
'
' Compute Maximum Radial Strain on the surface
'
emax_xy=pmax2(epsxx,epsyy,epsxy)
emaxmx_xy=smax(emax_xy)
'
' Select Salt Dome
'
blocks 1 10
'
' Compute Maximum Principal Stresses (psi)
'
smax=pmax(sigxx,sigyy,sigzz,sigxy,sigyz,sigzx)*Pa_psi
smaxmx=smax(smax)
'
' Compute Sqrt(J2) and I1 (Pa)
'
PRE=-(SIGXX+SIGYY+SIGZZ)/3.0
PRE1=ABS(PRE)-1.0e-6        'Screen out when ABS(PRE)<1.0e-6
PRE2=IFGZ(PRE1,PRE1,1.0e-6) 'If PRE1>0 then PRE1, if PRE1<0 then 1.0e-6
I1=3.*ABS(PRE2)             'I1
SJ2=VONMISES/SQRT(3.0)      'Sqrt(J2)
'
' Compute Minimum Safety Factor for Dilatancy
' Based on dilatant damage criteria for West Hackberry simulation
' [Ehgartner and Sobolik, 2002]
'
FX=0.25*I1                  'D=I1/(4*Sqrt(J2))
DPOT=SJ2/FX                 'Dilatant damage potential (DPOT=1/D)
CUT=0.01                    'Screen out when DPOT<0.01 i.e. DILFAC>100
DIL=IFLZ(DPOT-CUT,CUT,DPOT) 'If DPOT<CUT then DIL=CUT, if DPOT>CUT then DIL=DPOT
DILFAC=1/DIL                'Dilatant damage factor (DILFAC=D)
mindil=smin(DILFAC)         'Minimum safety factor against dilatant damage
'
' Compute Minimum Safety Factor for Shear Failure
' Shear Failure Criterion (Mises-Schleicher yield criterion)
'
m1=7.0E6                    'Intercept of the criterion (Pa)
m2=0.35                     'Slope of the criterion
GX=m1+m2*(I1/3.)            'Shear failure criterion (Pa)
DPOTS=SJ2/GX                'Shear failure potential
DILS=IFLZ(DPOTS-CUT,CUT,DPOTS) 'If DPOTS<CUT then DILS=CUT, if DPOTS>CUT then DILS=DPOTS
SHRFAC=1/DILS               'Shear failure safety factor
minshr=smin(SHRFAC)         'Minimum safety factor against shear failure
'
' Define time in term of year
'
TIME=TIME/3.1536e7
'
' Delete unnecessary variables
'
delete FT_M M_FT PSI_PA PA_PSI
```

```
delete PRE PRE1 PRE2 SJ2 I1 DIL DILS FX GX CUT m1 m2 SHRFAC
'
end
```

APPENDIX G: ANALYSES RESULTS FROM VARIOUS MODELS

G-1. Salt Creep Rate, $A_{SC} = 5\times10^{11}$ /s

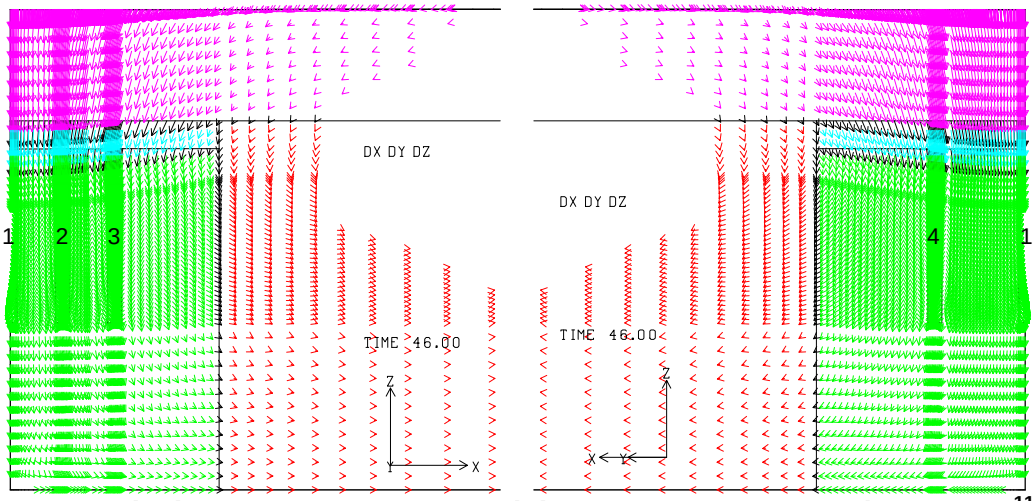

Fig. G-1. 1: Displacement vectors around the caverns at 46 years ($A_{SC} = 5\times10^{11}$ /s).

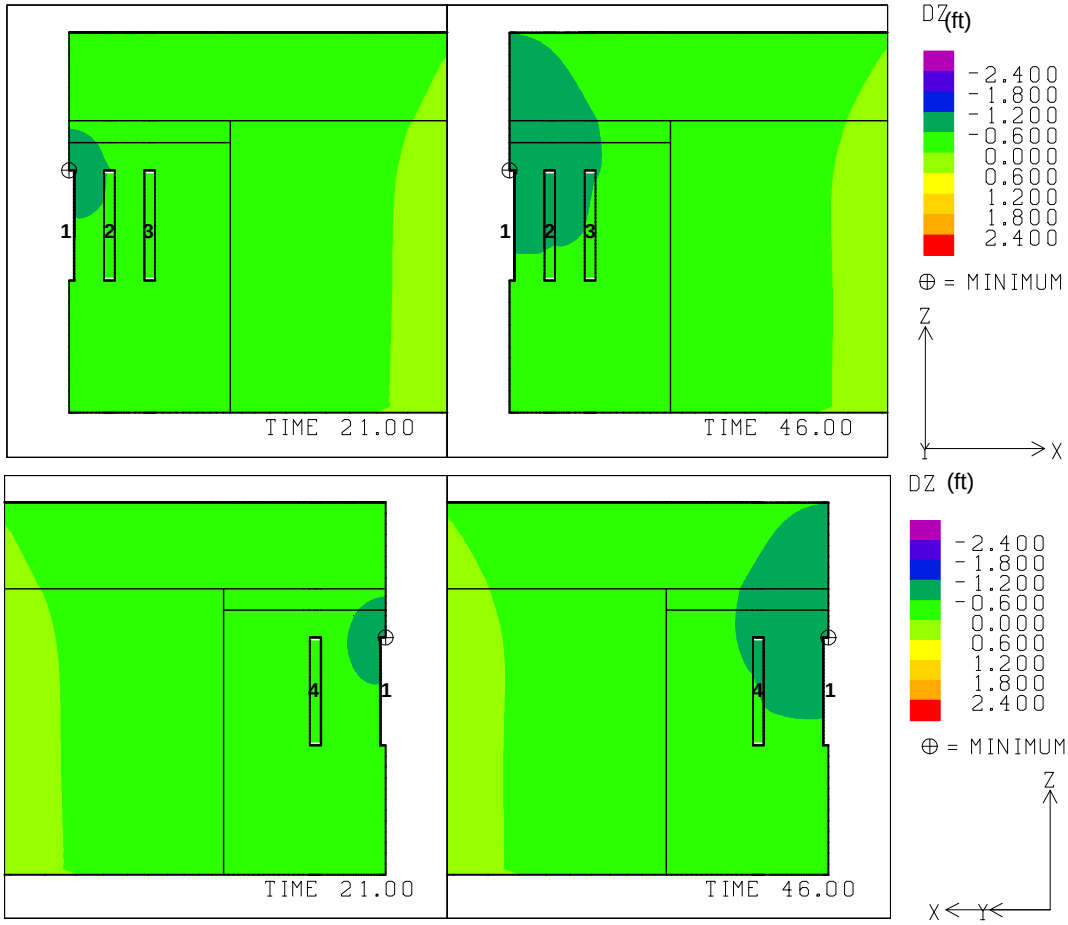

Fig. G-1. 2: Vertical displacement contours around the caverns at 21 and 46 years ($A_{SC} = 5\times10^{11}$ /s).

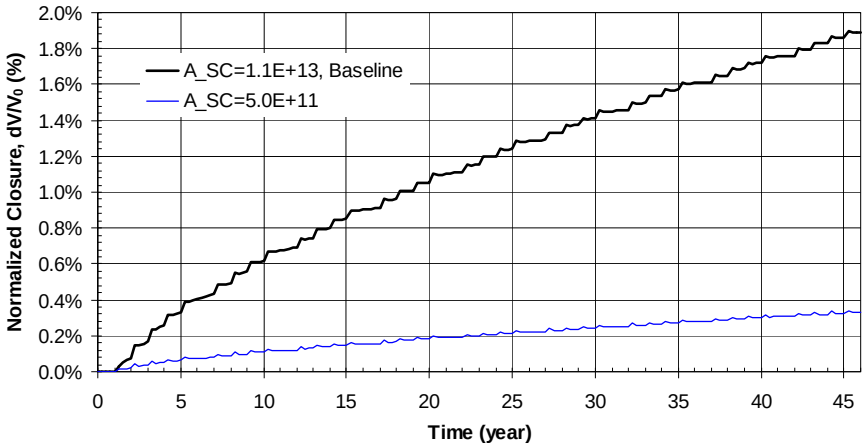

Fig. G-1. 3: Predicted total volumetric closure normalized to initial overall storage volume for the 19 SPR caverns (A_{SC} = 5×10^{11} /s).

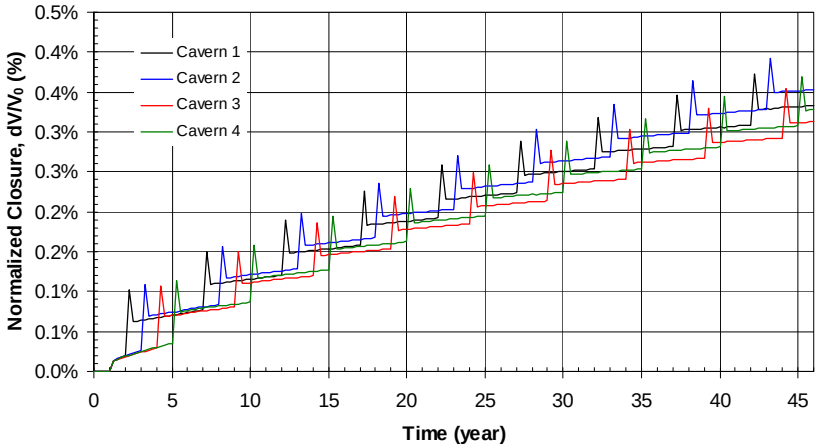

Fig. G-1. 4: Predicted volumetric closure normalized to each initial SPR cavern volume (A_{SC} = 5×10^{11} /s).

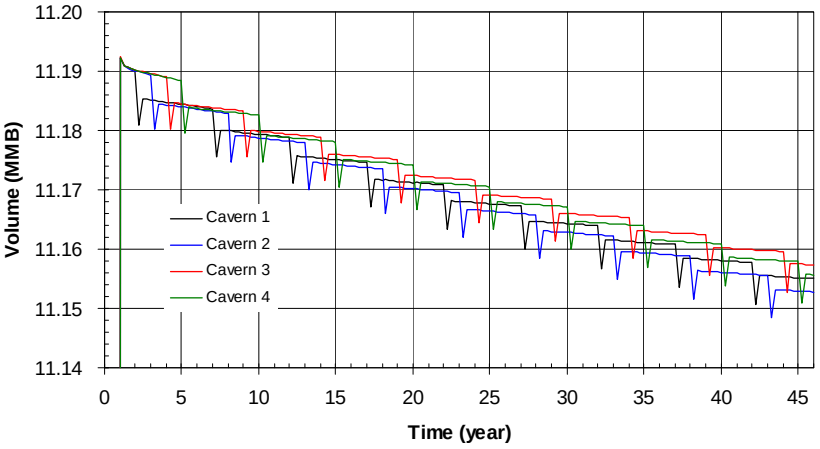

Fig. G-1. 5: Predicted volume change of each SPR cavern due to salt creep closure over time (A_{SC} = 5×10^{11} /s).

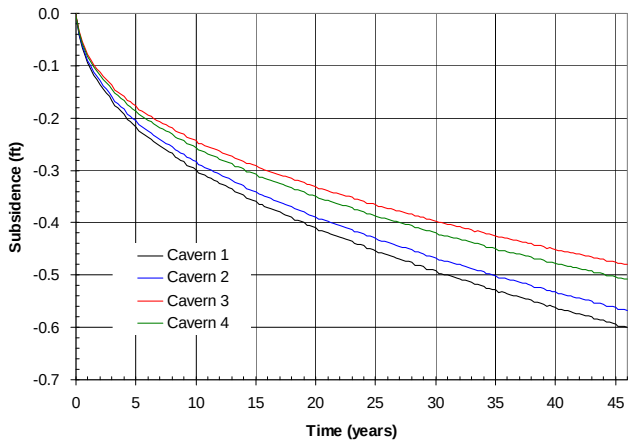

Fig. G-1. 6: Predicted subsidence on the surface above the center of SPR caverns (A_{SC} = 5×10^{11} /s).

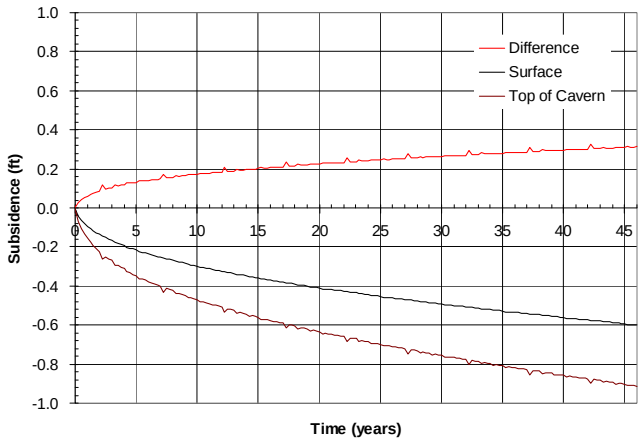

Fig. G-1. 7: Predicted difference between vertical displacement of the top of the central cavern (Cavern 1) and the surface above the cavern as a function of time (A_{SC} = 5×10^{11} /s).

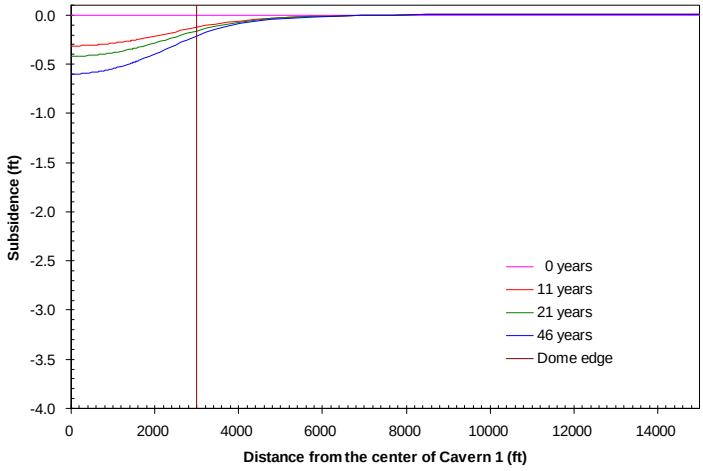

Fig. G-1. 8: Predicted subsidence on the surface from model center to edge with time (A_{SC} = 5×10^{11} /s).

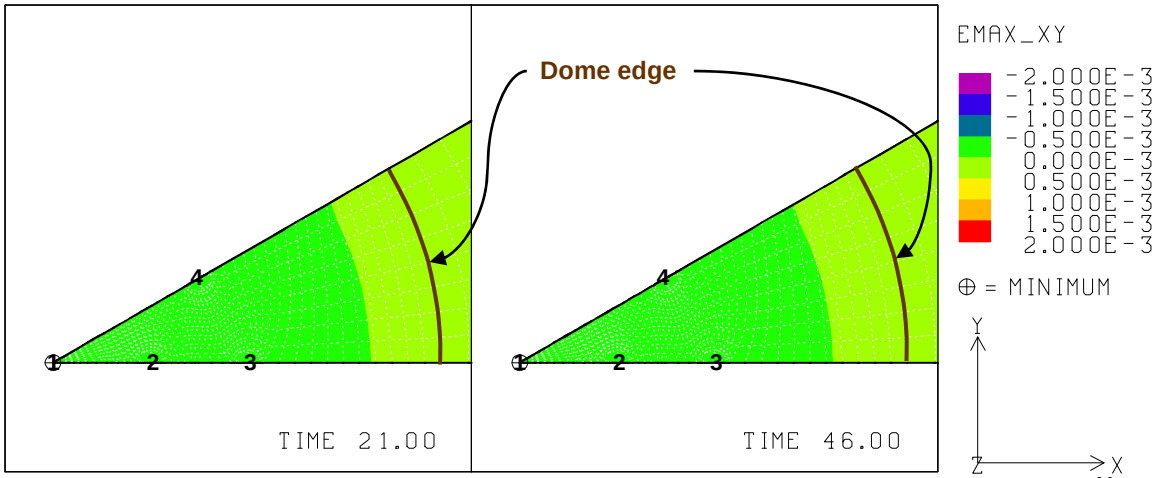

Fig. G-1. 9: Predicted radial surface strains at 21 years and 46 years ($A_{SC} = 5\times10^{11}$ /s).

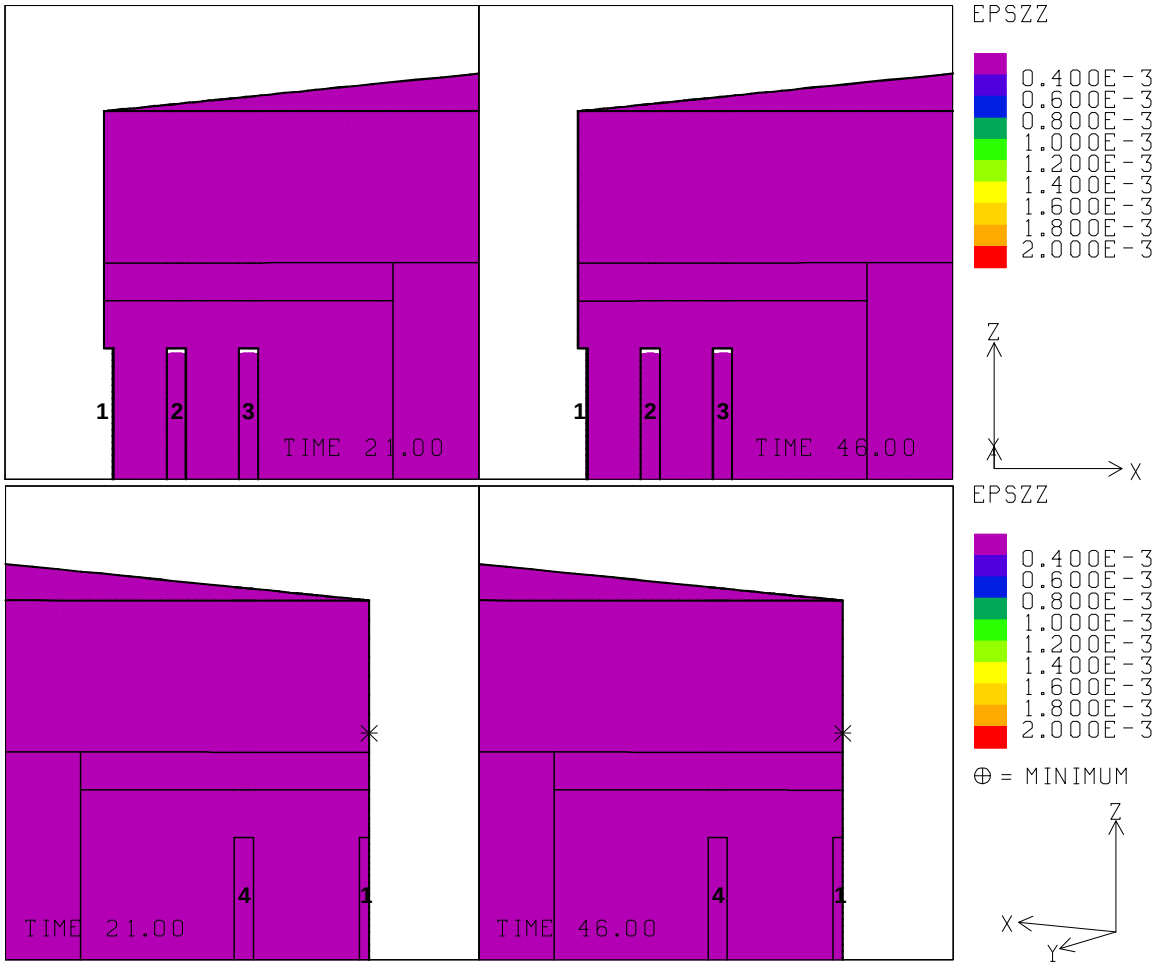

Fig. G-1. 10: Vertical strains around the roof of caverns at 21 years and 46 years ($A_{SC} = 5\times10^{11}$ /s).

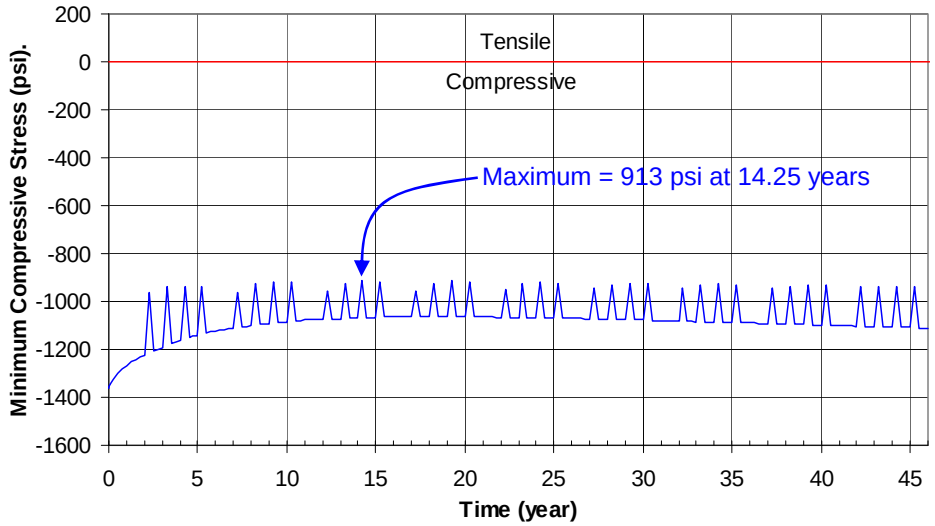

Fig. G-1. 11: Predicted minimum compressive stress history in the salt dome (A_{SC} = 5×10^{11} /s).

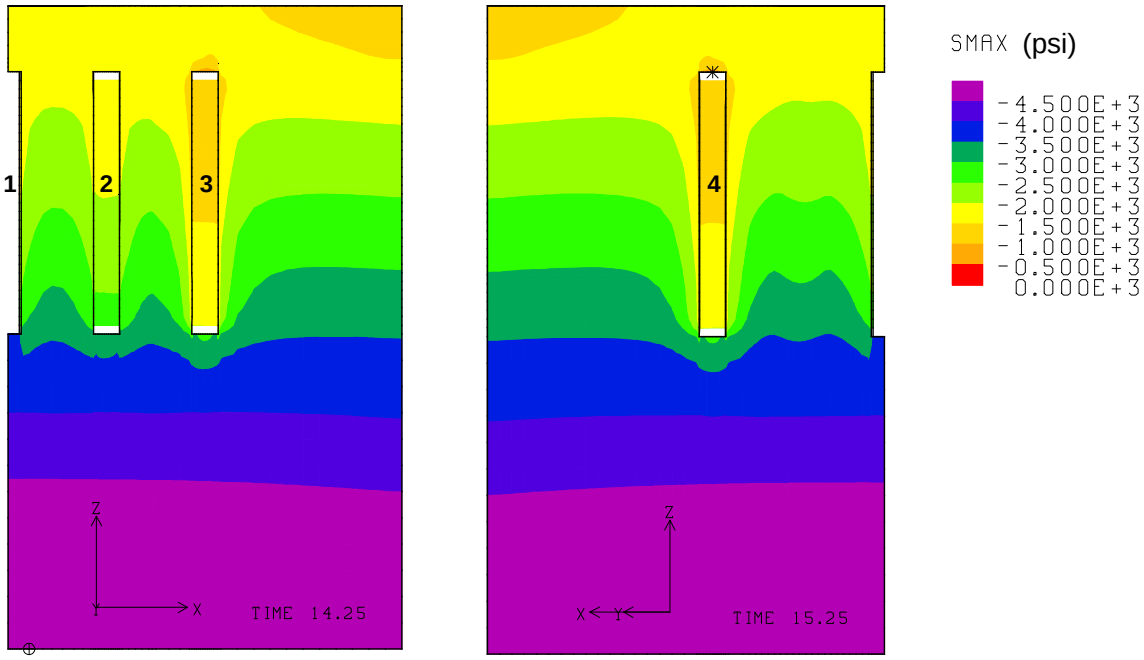

Fig. G-1. 12: Compressive stress contours around the caverns during workover of Cavern 3 and Cavern 4 at 14.25 years and 15.25 years, respectively (A_{SC} = 5×10^{11} /s).

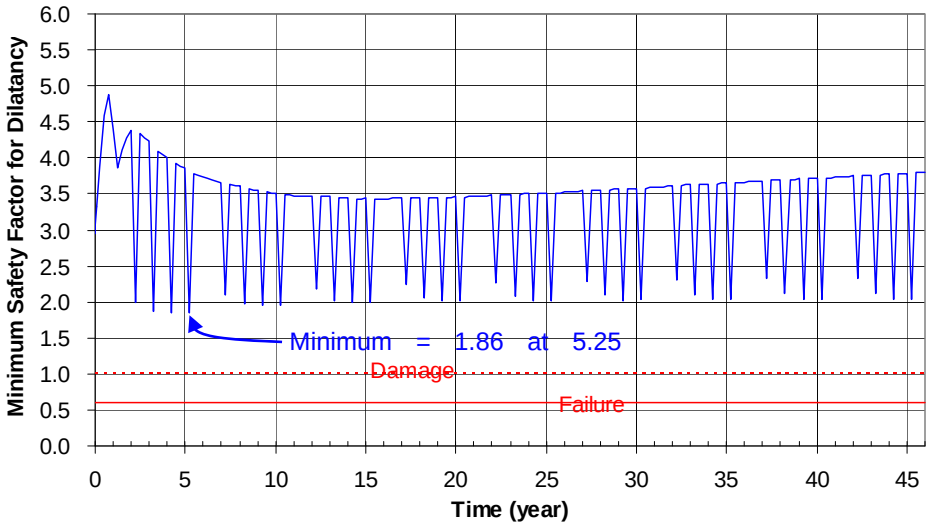

Fig. G-1. 13: Predicted minimum safety factor history against dilatant damage (A_{SC} = 5×10^{11} /s).

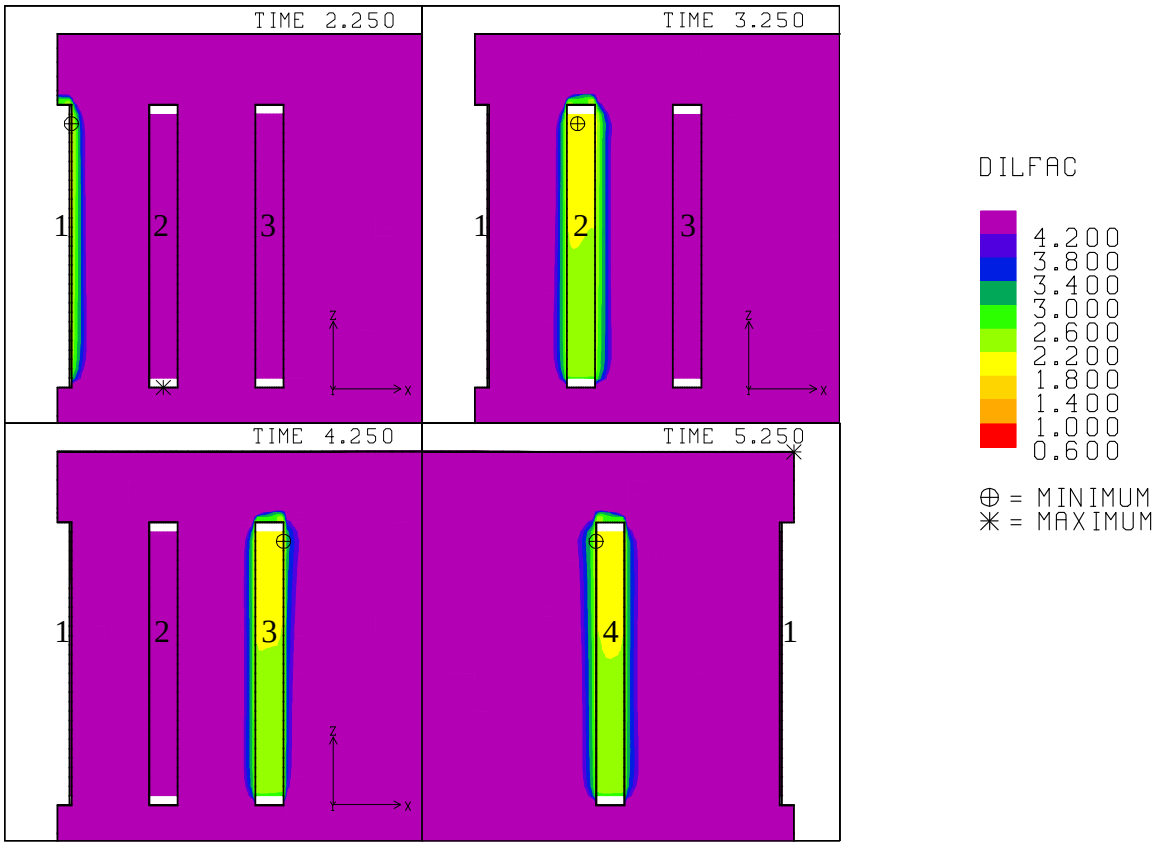

Fig. G-1. 14: Safety factor contours against dilatant damage around the caverns during workover of Caverns 1, 2, 3 and 4 at 2.25 years, 3.25 years, 4.25 years and 5.25 years, respectively (A_{SC} = 5×10^{11} /s).

G-2. Salt Creep Rate, $A_{SC} = 2\times10^{14}$ /s

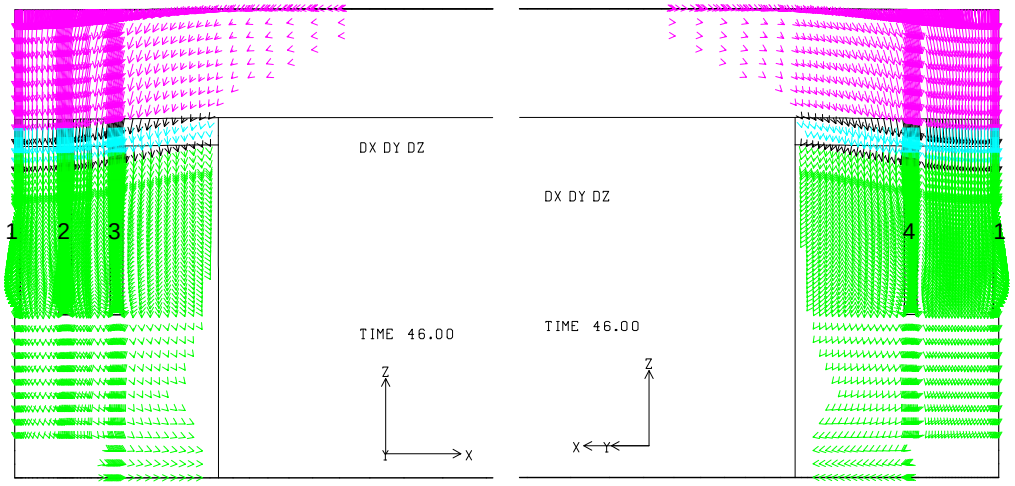

Fig. G-2. 1: Displacement vectors around the caverns at 46 years ($A_{SC} = 2\times10^{14}$ /s).

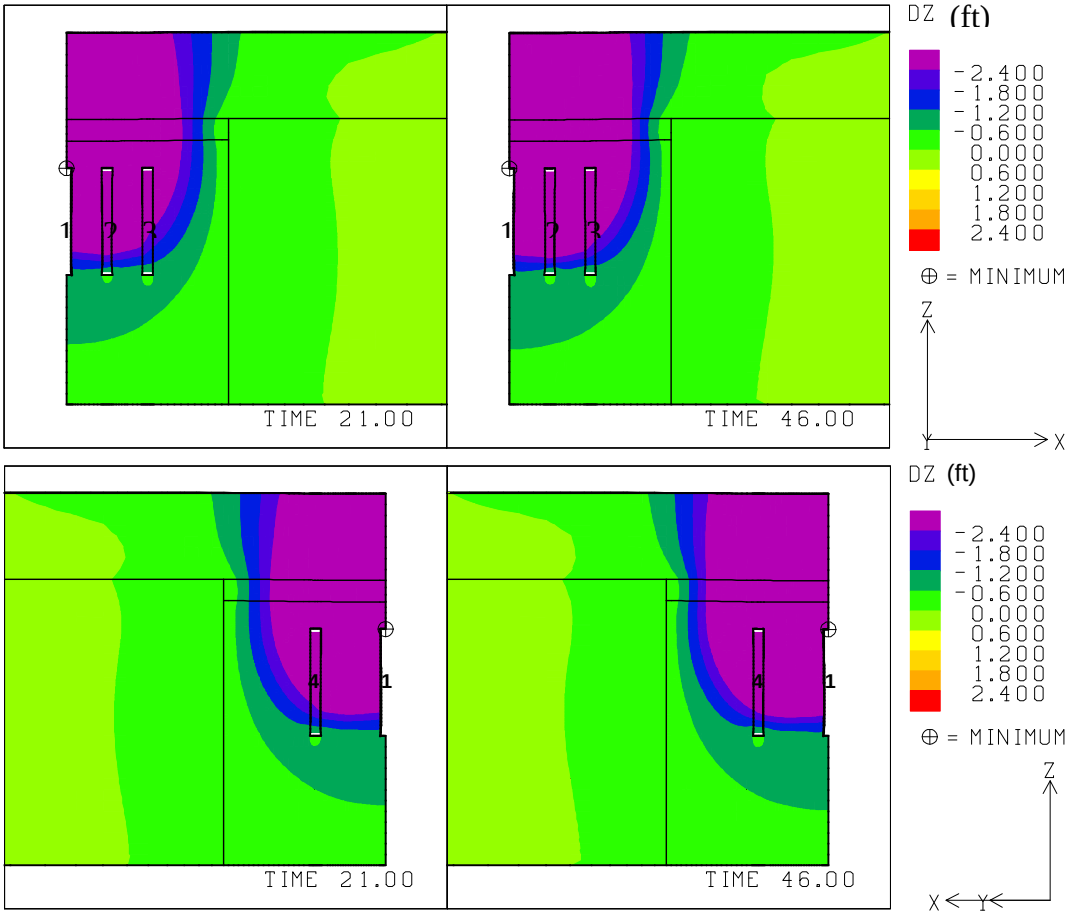

Fig. G-2. 2: Vertical displacement contours around the caverns at 21 and 46 years ($A_{SC} = 2\times10^{14}$ /s).

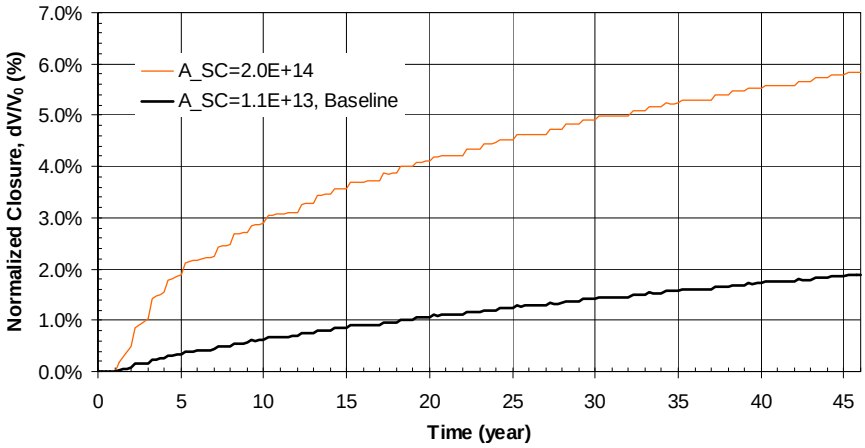

Fig. G-2. 3: Predicted total volumetric closure normalized to initial overall storage volume for the 19 SPR caverns (A_{SC} = 2×10^{14} /s).

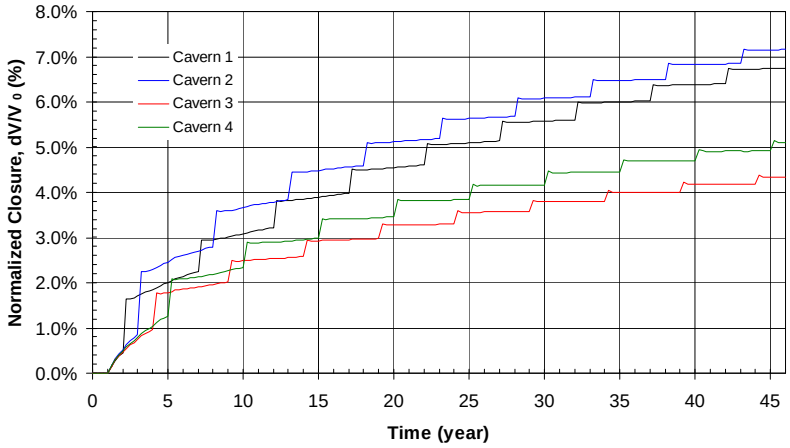

Fig. G-2. 4: Predicted volumetric closure normalized to each initial SPR cavern volume (A_{SC} = 2×10^{14} /s).

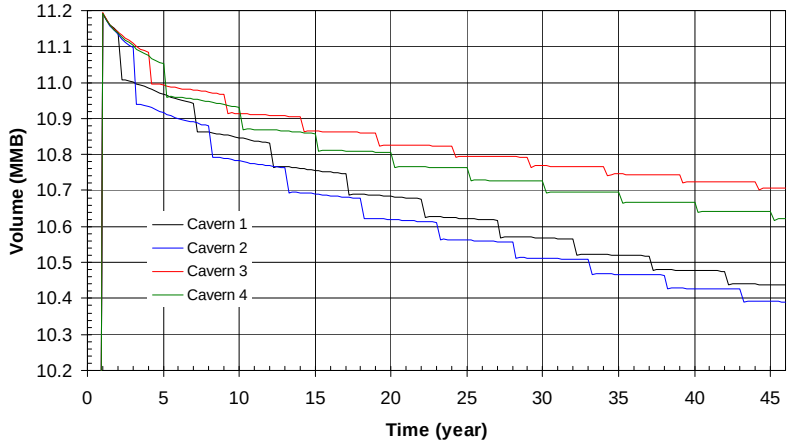

Fig. G-2. 5: Predicted volume change of each SPR cavern due to salt creep closure over time (A_{SC} = 2×10^{14} /s).

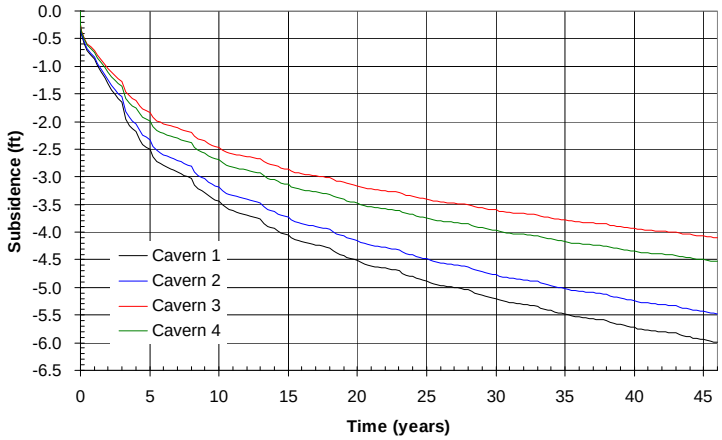

Fig. G-2. 6: Predicted subsidence on the surface above the center of SPR caverns (A_{SC} = 2×10^{14} /s).

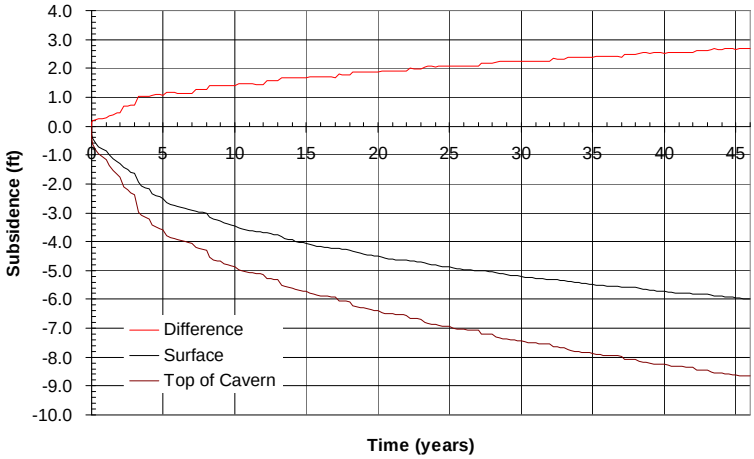

Fig. G-2. 7: Predicted difference between vertical displacement of the top of the central cavern (Cavern 1) and the surface above the cavern as a function of time.

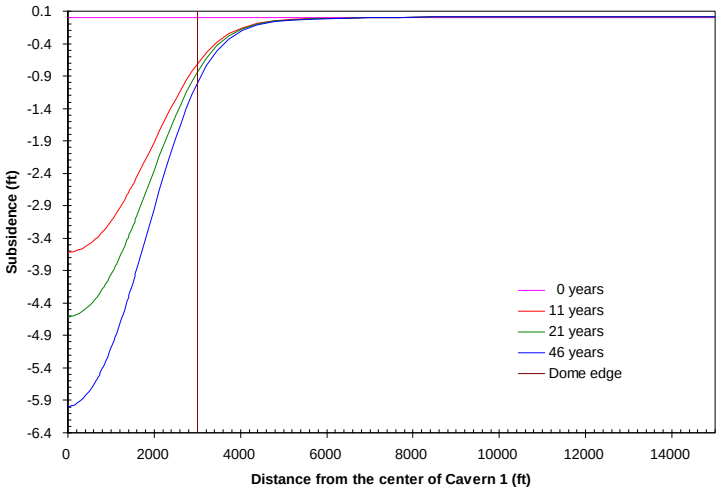

Fig. G-2. 8: Predicted subsidence on the surface from model center to edge with time.

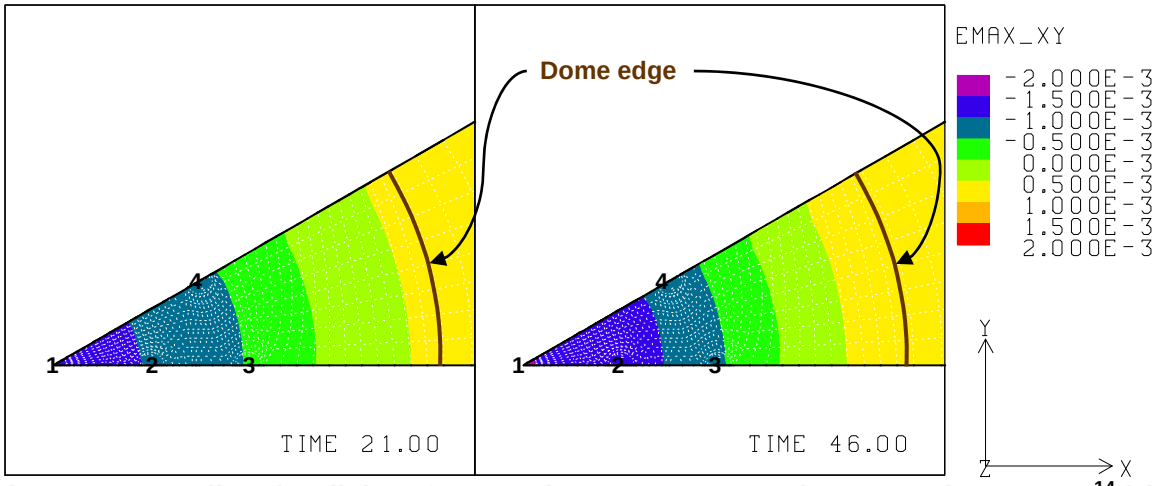

Fig. G-2. 9: Predicted radial surface strains at 21 years and 46 years (A_{SC} = 2×10^{14} /s).

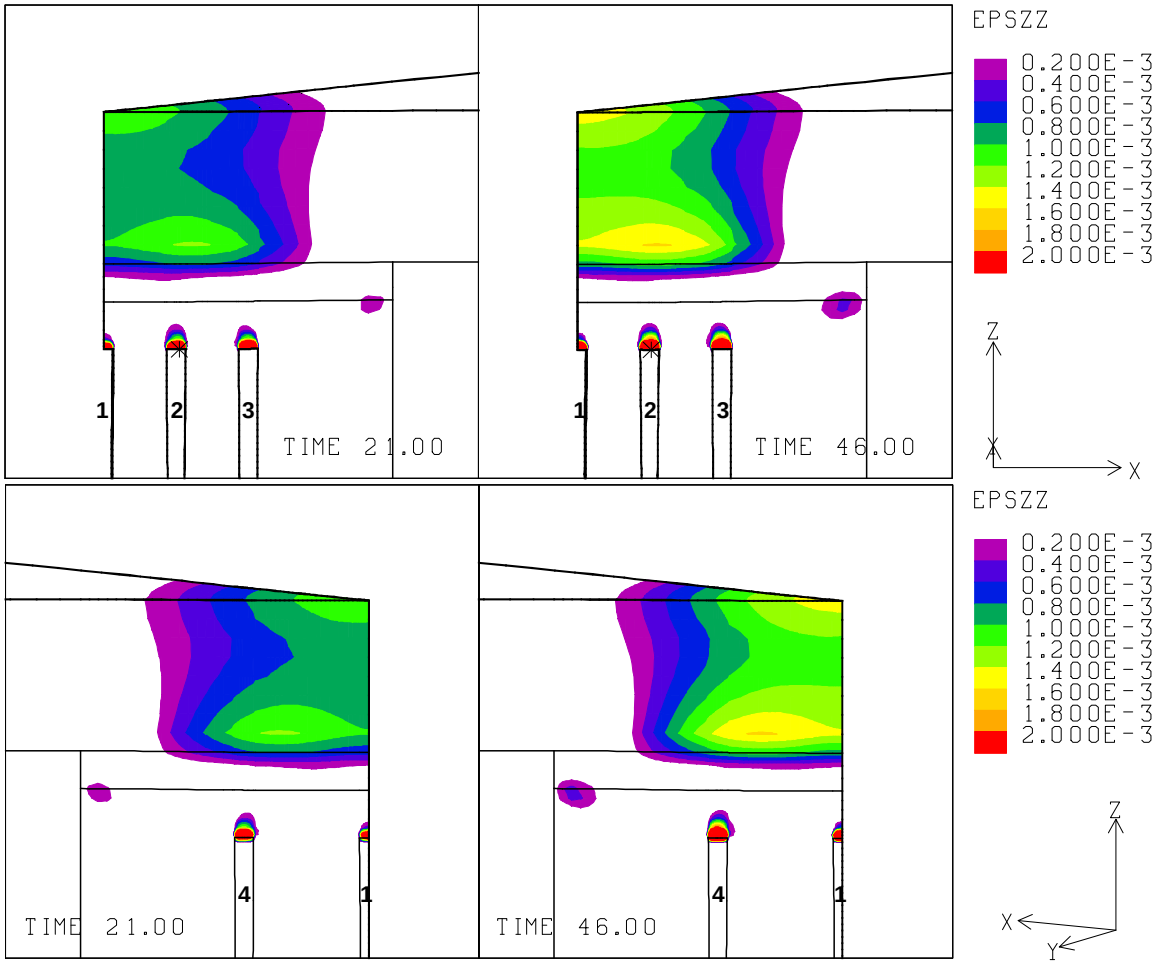

Fig. G-2. 10: Vertical strains around the roof of caverns at 21 years and 46 years (A_{SC} = 2×10^{14} /s).

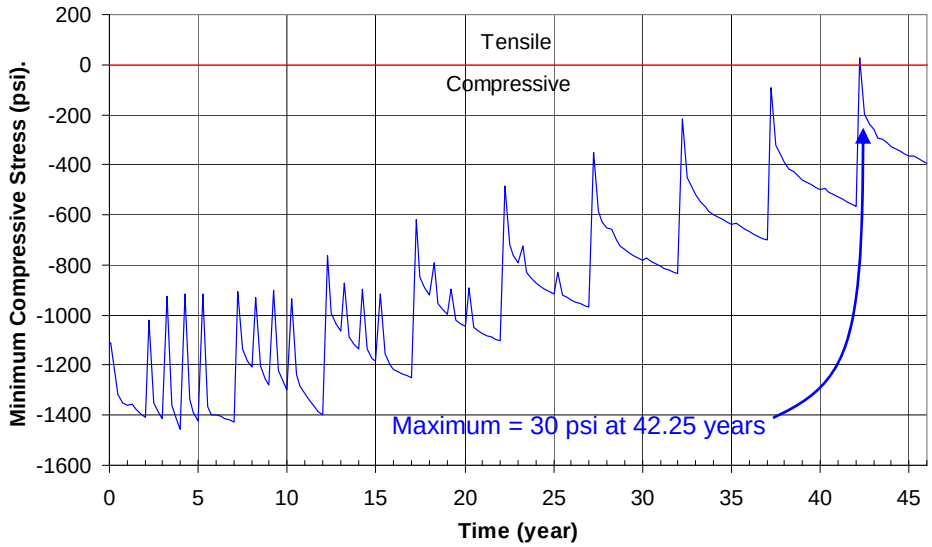

Fig. G-2. 11: Predicted minimum compressive stress history in the salt dome (A_{SC} = 2×10^{14} /s).

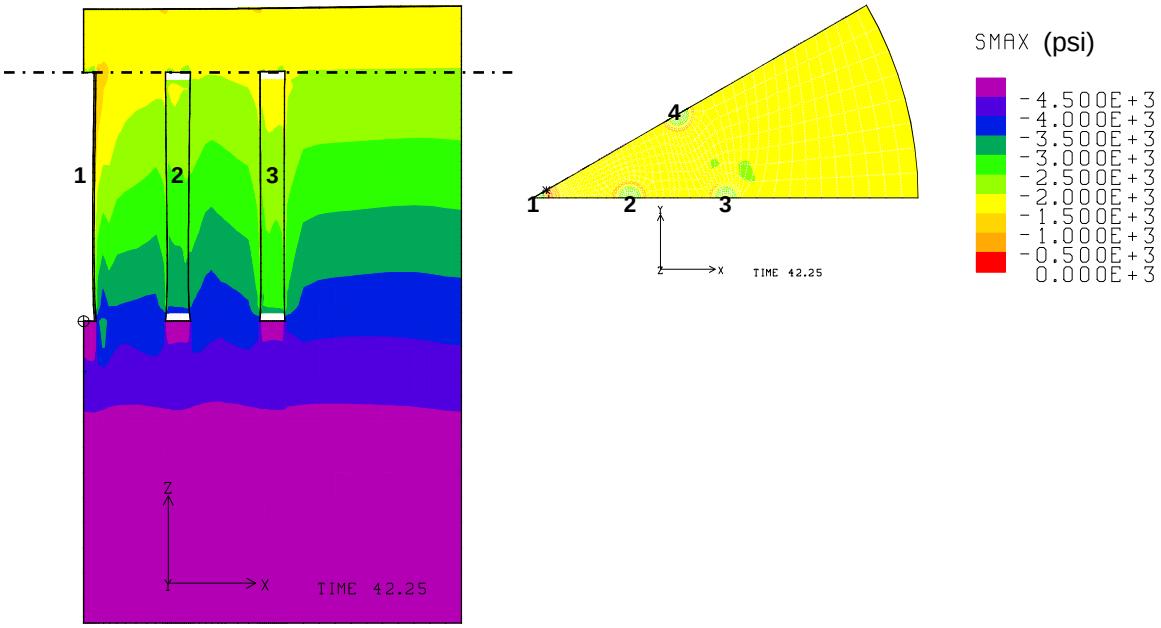

Fig. G-2. 12: Compressive stress contours around the caverns during workover of Cavern 1 at 42.25 years (Left) and horizontal cross-section at the elevation where the minimum compressive stress occurs (Right) (A_{SC} = 2×10^{14} /s).

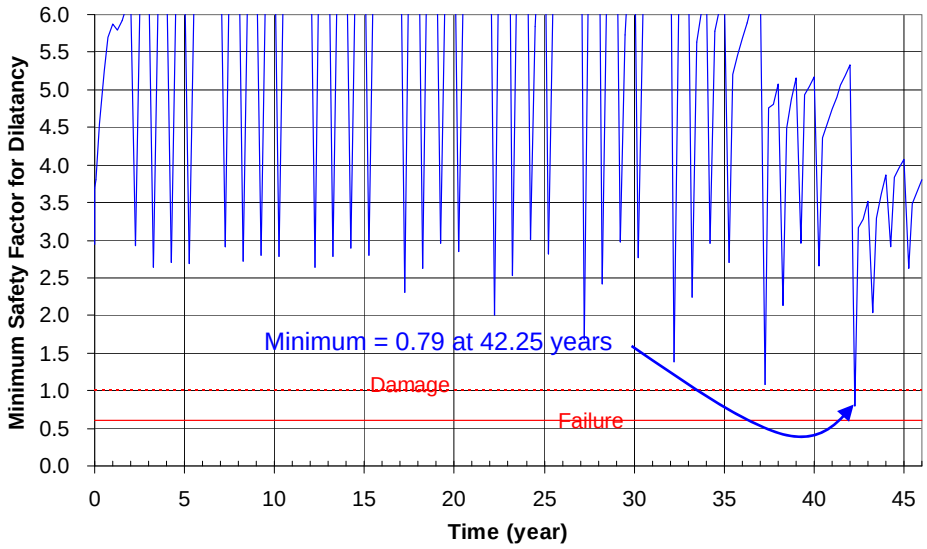

Fig. G-2. 13: Predicted minimum safety factor history against dilatant damage (A_{SC} = 2×10^{14} /s).

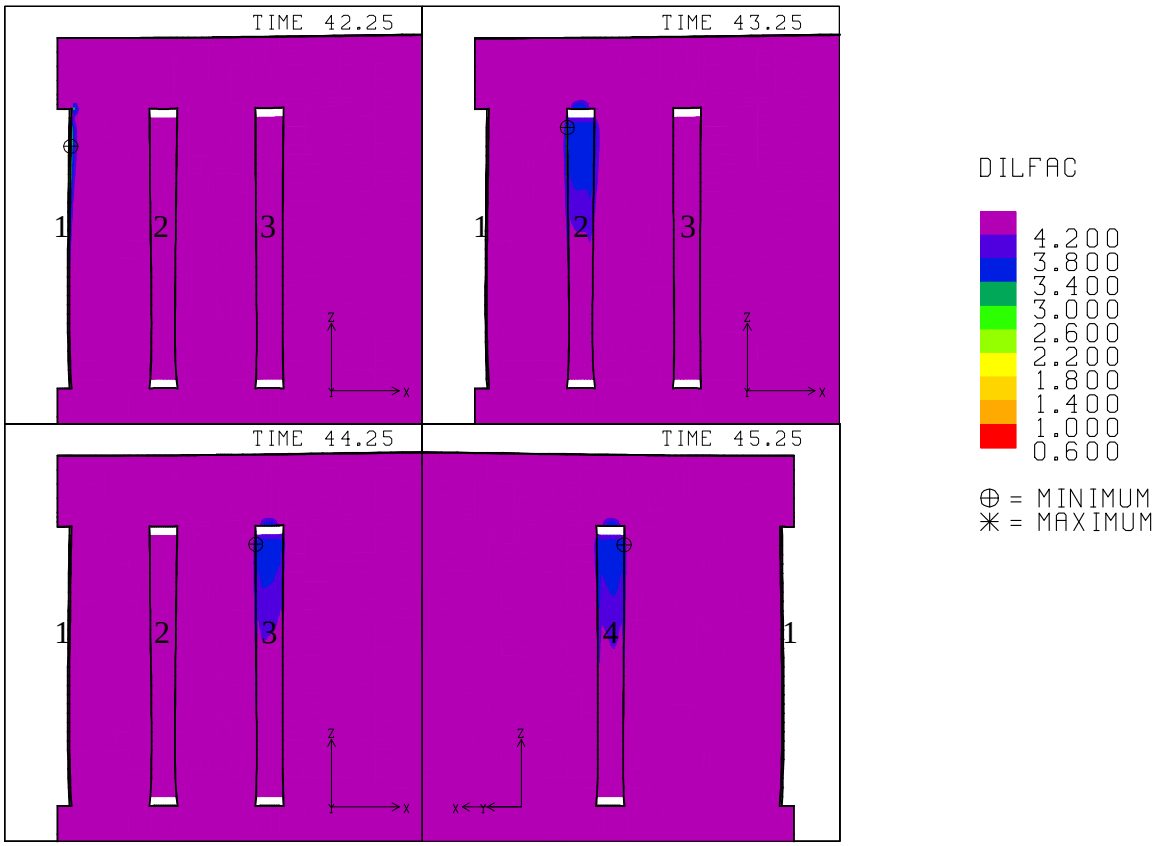

Fig. G-2. 14: Safety factor contours against dilatant damage around the caverns during workover of Caverns 1, 2, 3 and 4 at 42.25 years, 43.25 years, 44.25 years and 45.25 years, respectively (A_{SC} = 2×10^{14} /s).

G-3. Depth of Salt Dome Top, d_{SD} = 500 ft, A_{SC} = 1.1×10^{13} /s

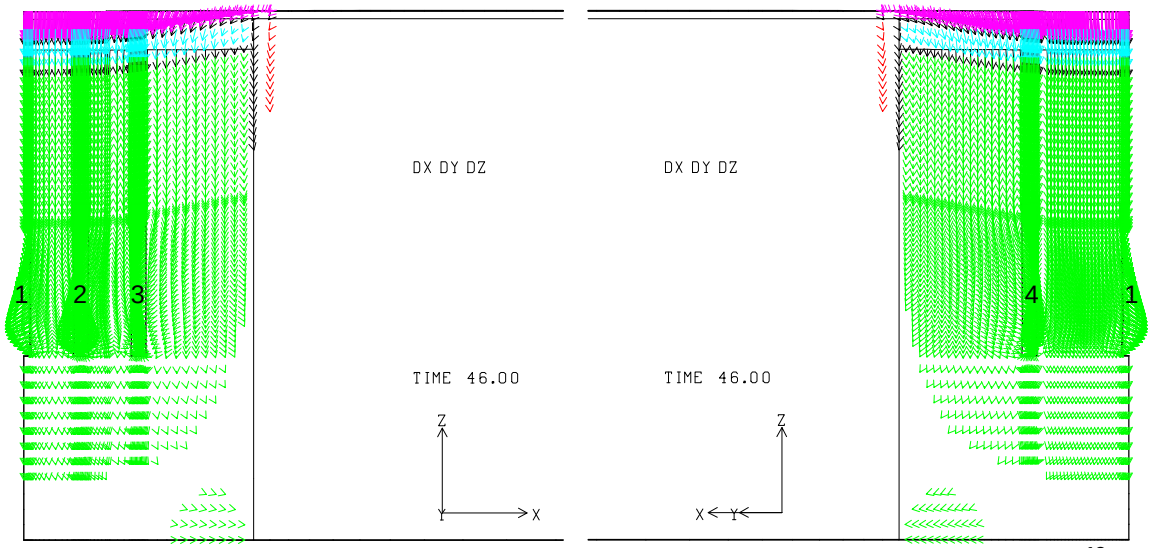

Fig. G-3. 1: Displacement vectors around the caverns at 46 years (A_{SC} = 1.1×10^{13} /s).

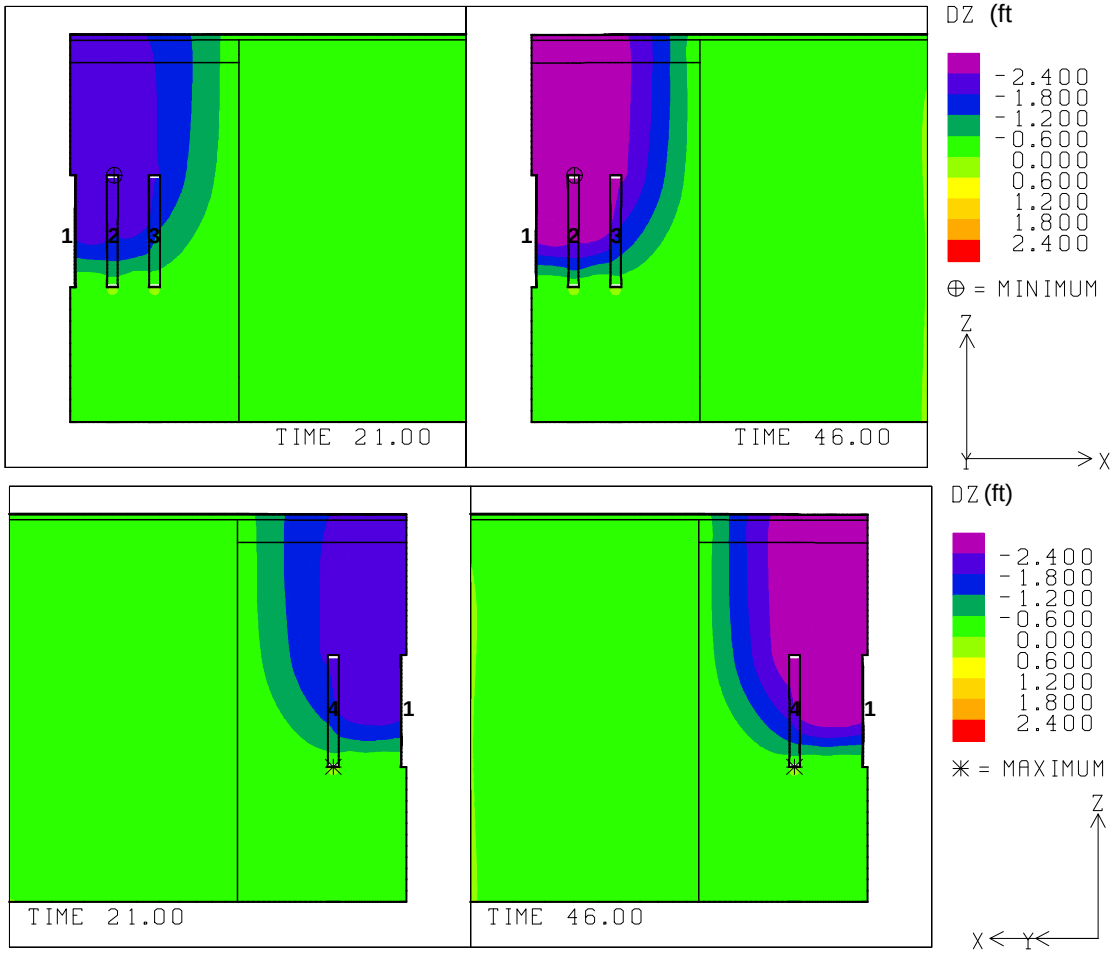

Fig. G-3. 2: Vertical displacement contours around the caverns at 21 and 46 years (A_{SC} = 1.1×10^{13} /s).

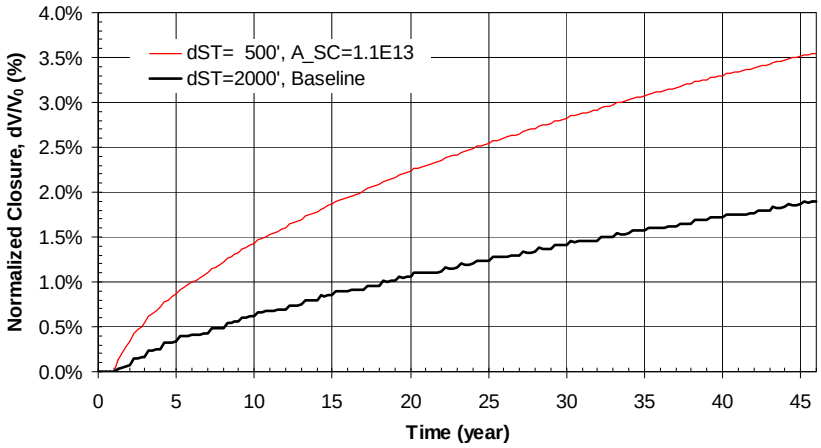

Fig. G-3. 3: Predicted total volumetric closure normalized to initial overall storage volume for the 19 SPR caverns (A_{SC} = 1.1×10^{13} /s).

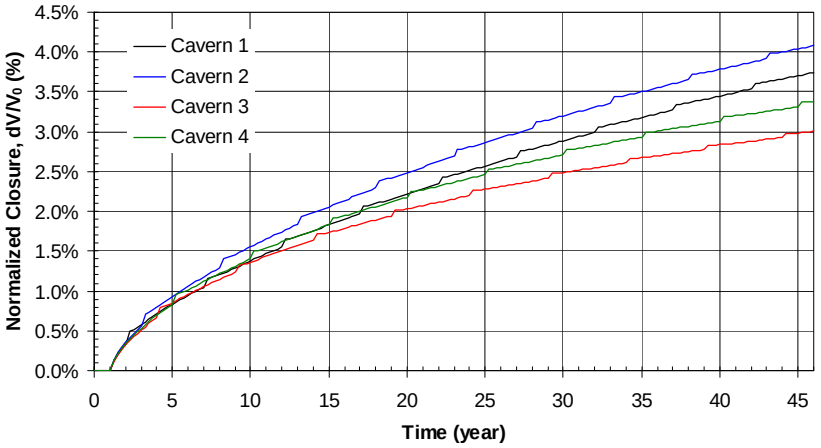

Fig. G-3. 4: Predicted volumetric closure normalized to each initial SPR cavern volume(A_{SC} = 1.1×10^{13} /s).

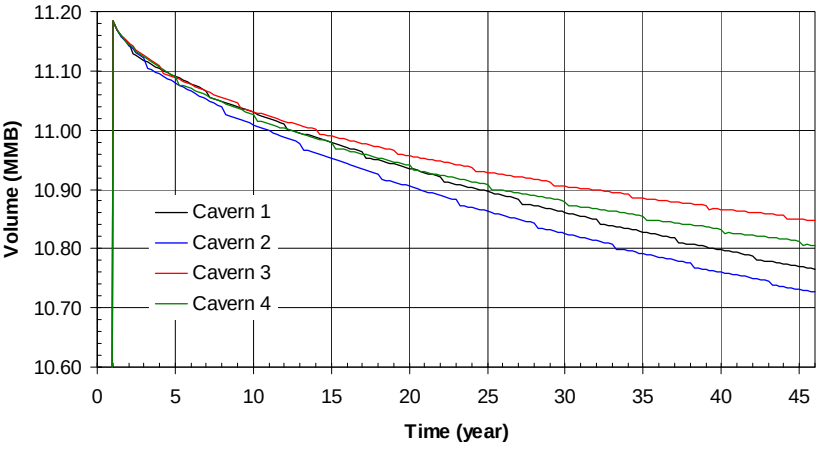

Fig. G-3. 5: Predicted volume change of each SPR cavern due to salt creep closure over time (A_{SC} = 1.1×10^{13} /s).

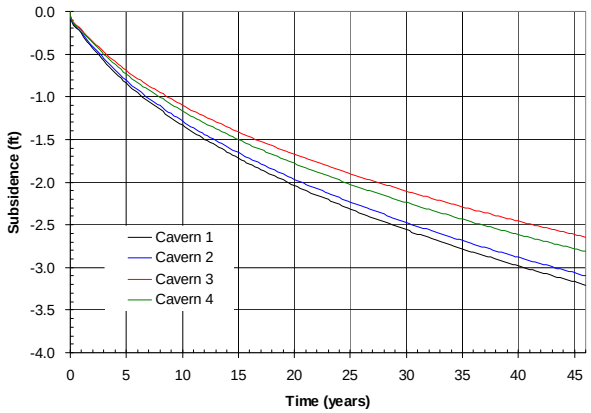

Fig. G-3. 6: Predicted subsidence on the surface above the center of SPR caverns (A_{SC} = 1.1×10^{13} /s).

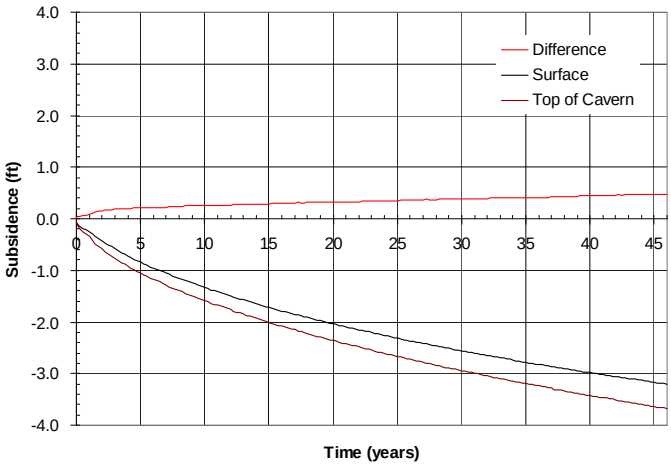

Fig. G-3. 7: Predicted difference between vertical displacement of the top of the central cavern (Cavern 1) and the surface above the cavern as a function of time.

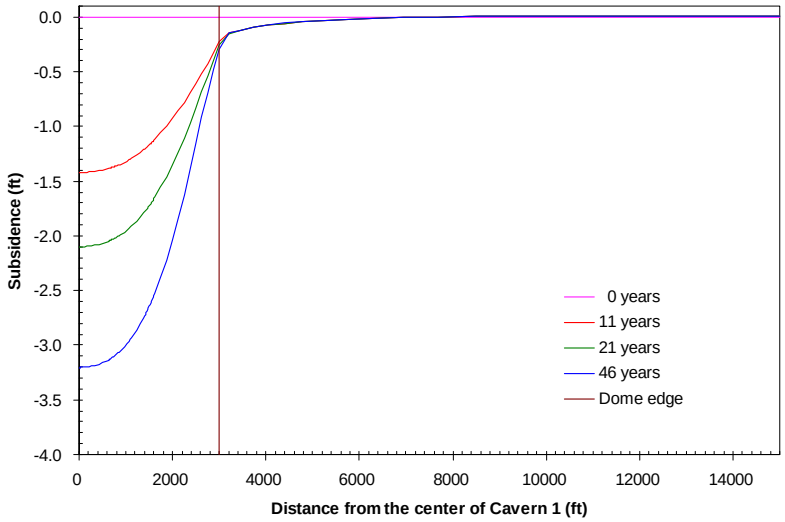

Fig. G-3. 8: Predicted subsidence on the surface from model center to edge with time.

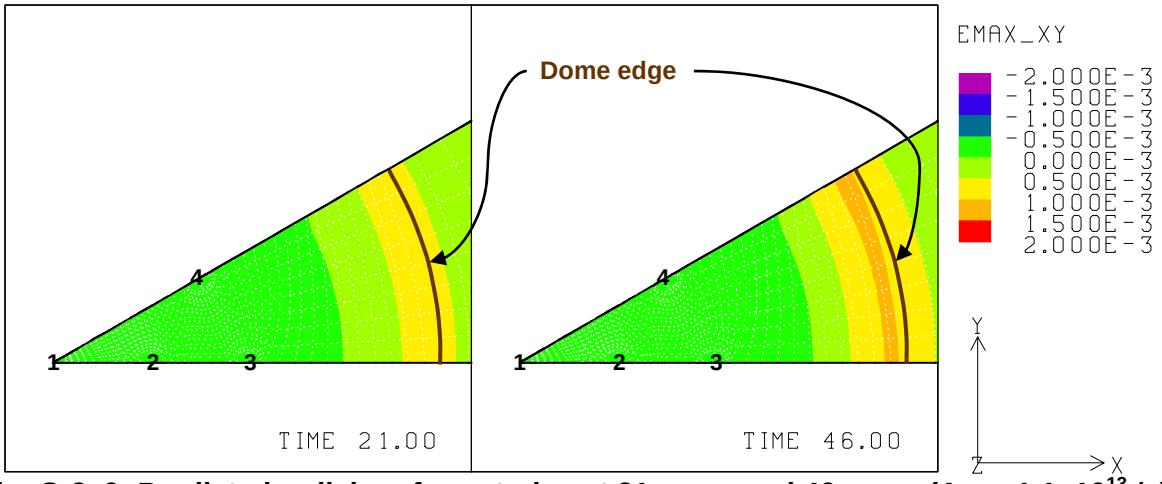

Fig. G-3. 9: Predicted radial surface strains at 21 years and 46 years (A_{SC} = 1.1×10^{13} /s).

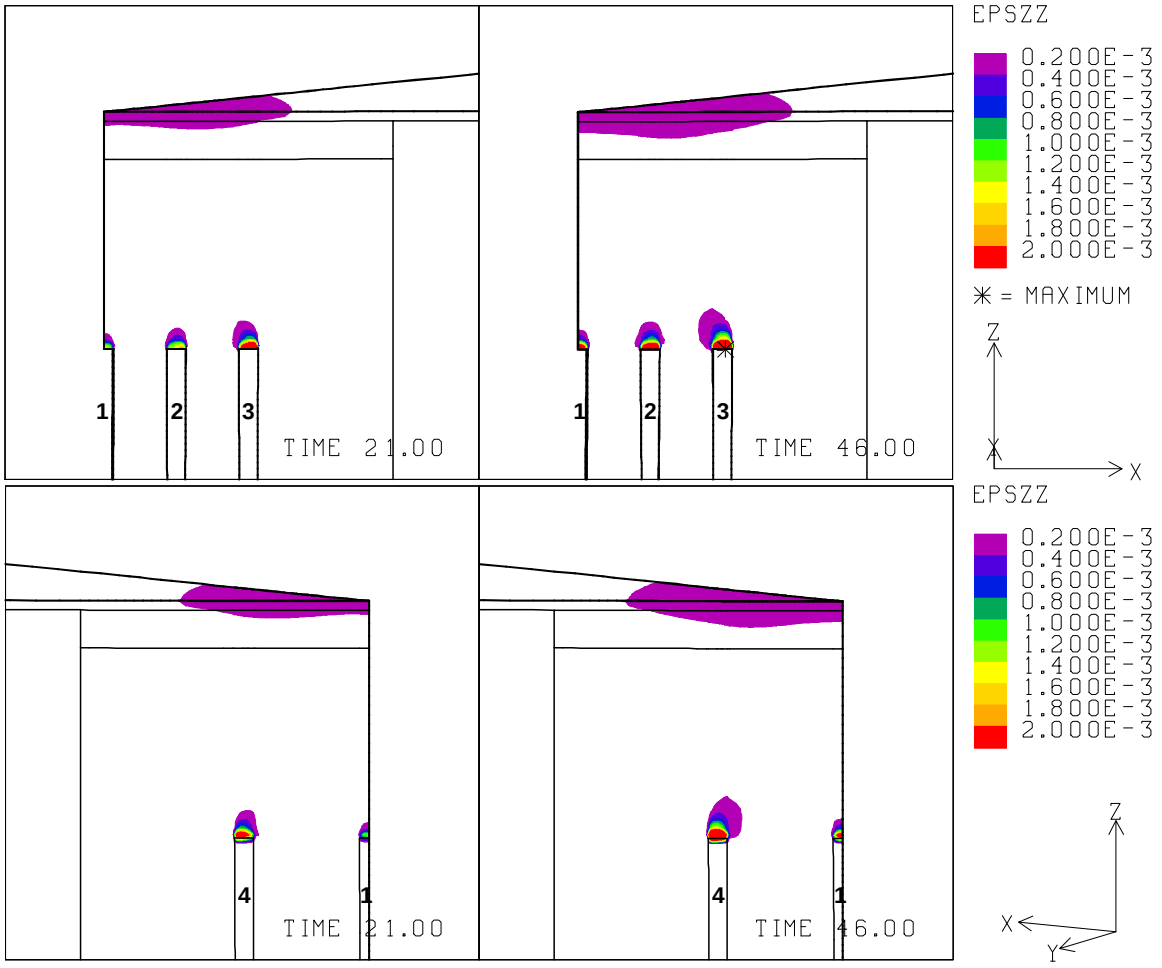

Fig. G-3. 10: Vertical strains around the roof of caverns at 21 years and 46 years (A_{SC} = 1.1×10^{13} /s).

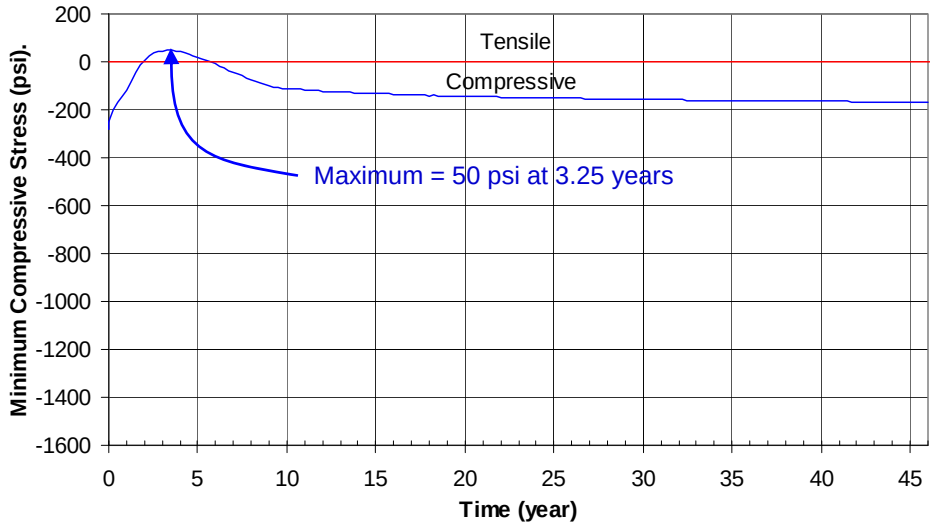

Fig. G-3. 11: Predicted minimum compressive stress history in the salt dome (A_{SC} = 1.1×10^{13} /s).

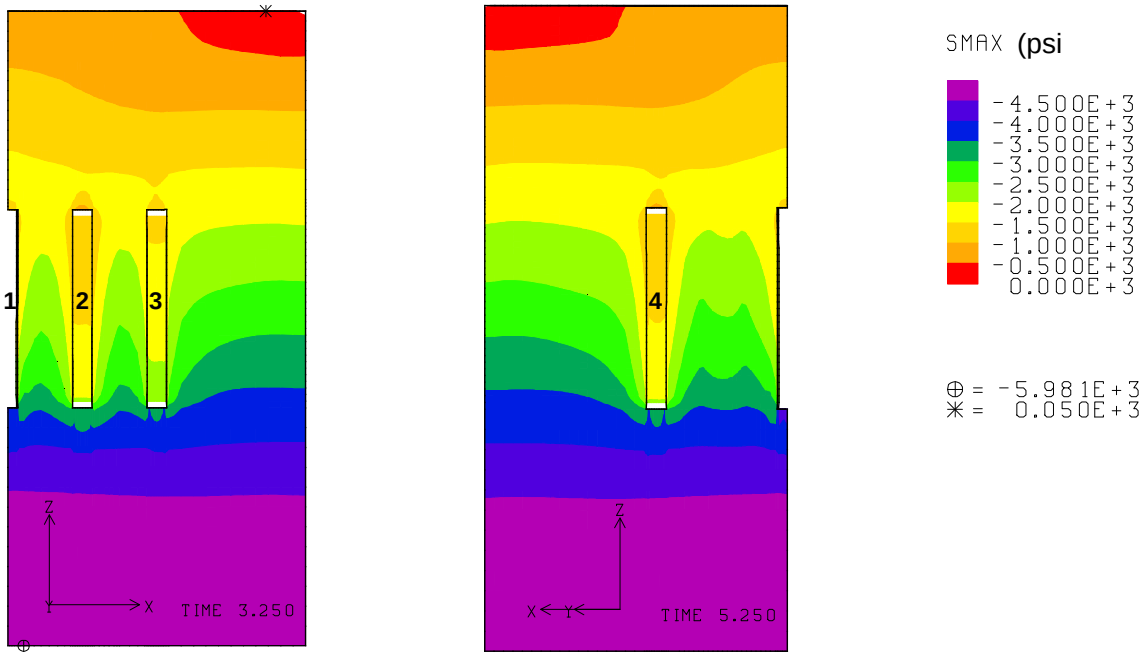

Fig. G-3. 12: Compressive stress contours around the caverns during workover of Cavern 2 and Cavern 4 at 3.25 years and 5.25 years, respectively. Tensile failure occurs around the top of the dome edge (A_{SC} = 1.1×10^{13} /s).

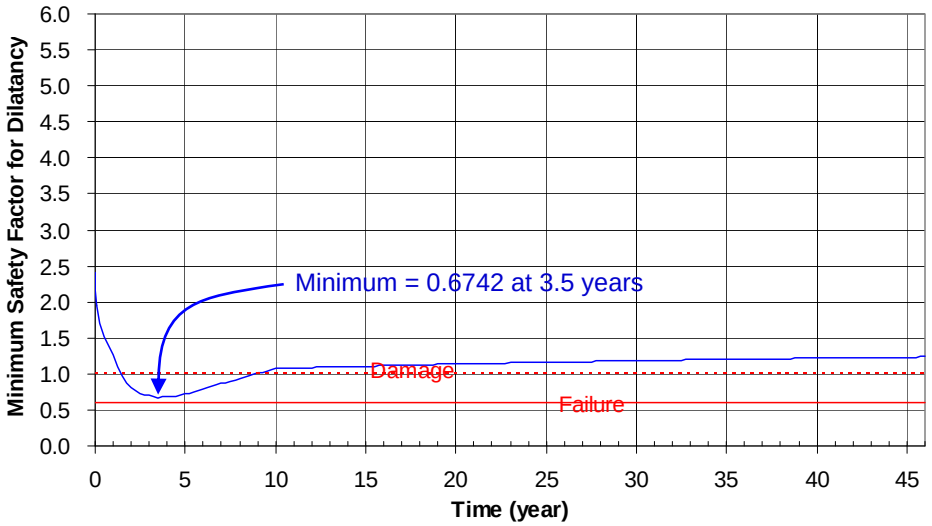

Fig. G-3. 13: Predicted minimum safety factor history against dilatant damage (A_{SC} = 1.1×10^{13} /s).

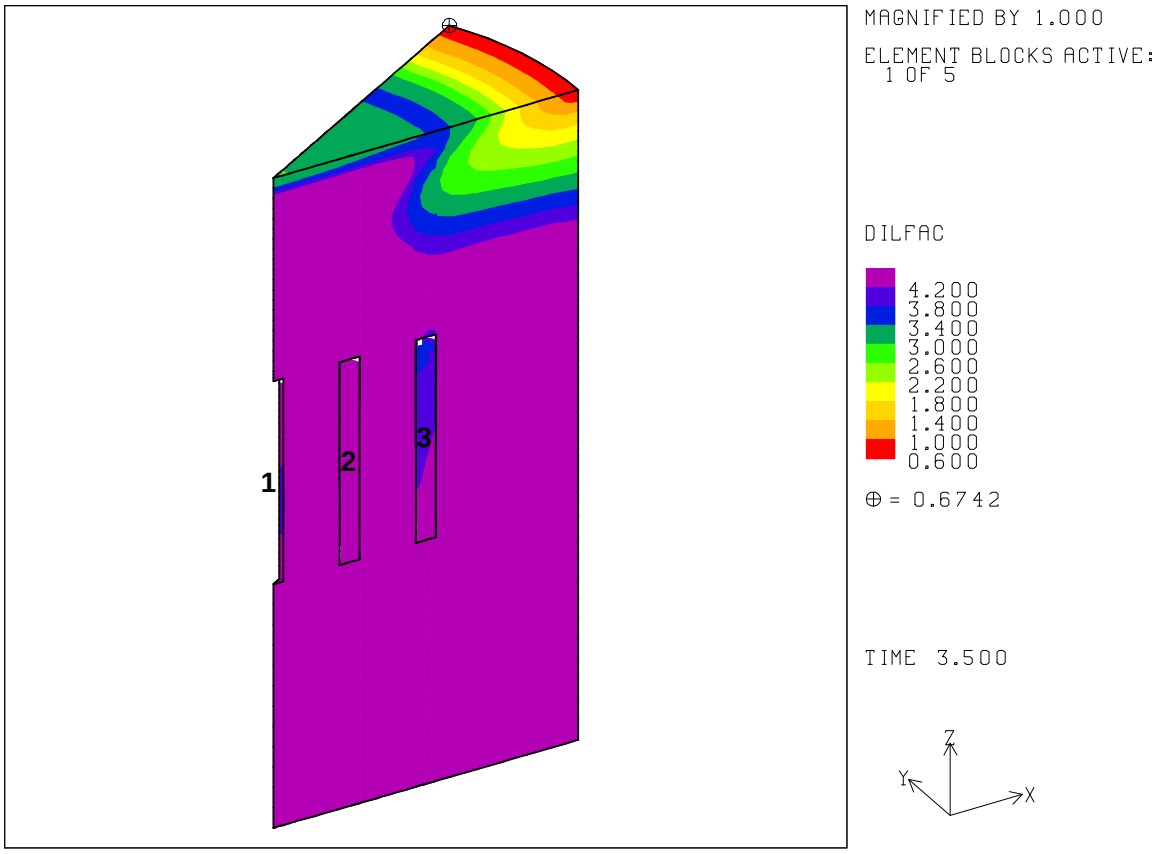

Fig. G-3. 14: Safety factor contours against dilatant damage in the dome at 3.5 years. Dilatant damage occurs around the top of the dome edge (A_{SC} = 1.1×10^{13} /s).

G-4. Depth of Salt Dome Top, d_{SD} = 500 ft, FCS

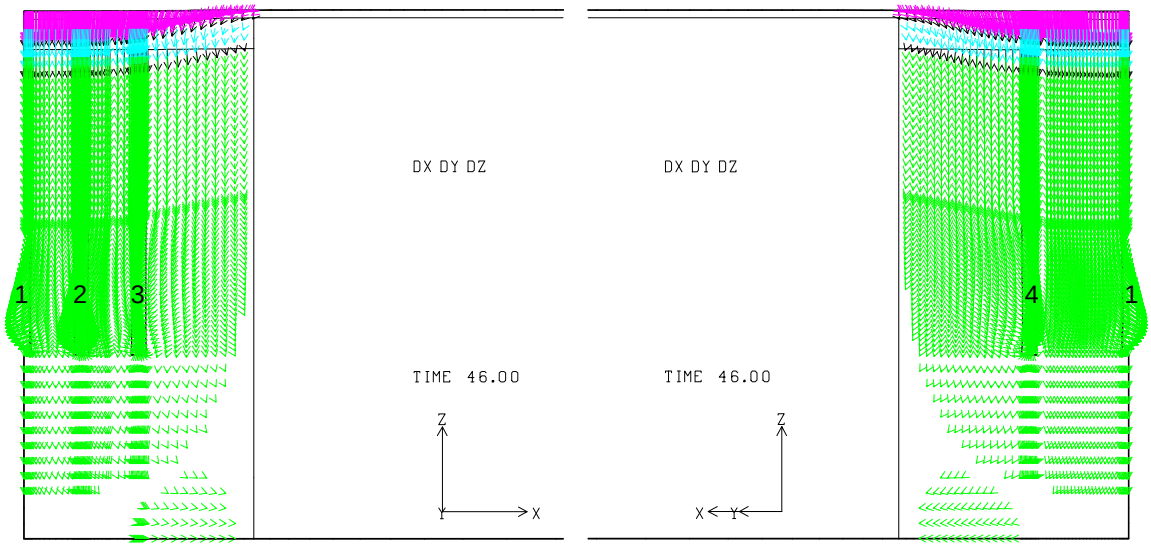

Fig. G-4. 1: Displacement vectors around the caverns at 46 years (d_{SD} = 500 ft, FCS).

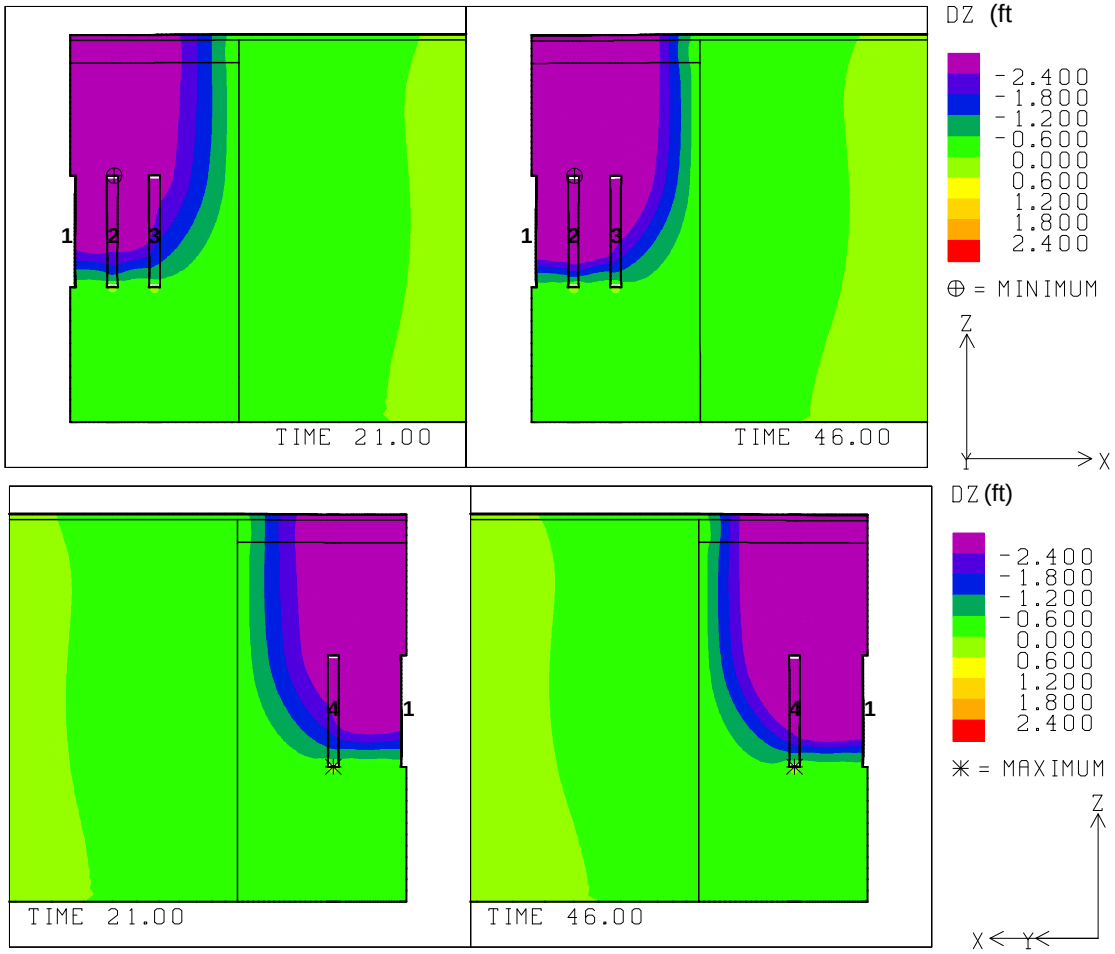

Fig. G-4. 2: Vertical displacement contours around the caverns at 21 and 46 years (d_{SD} = 500 ft, FCS).

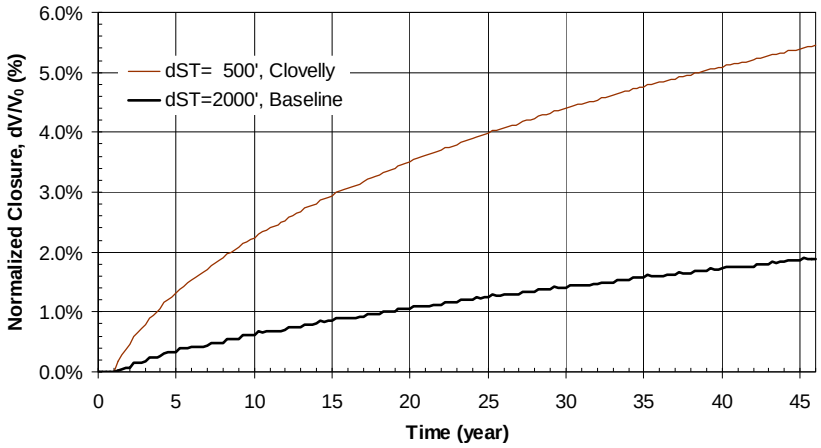

Fig. G-4. 3: Predicted total volumetric closure normalized to initial overall storage volume for the 19 SPR caverns (d_{SD} = 500 ft, FCS).

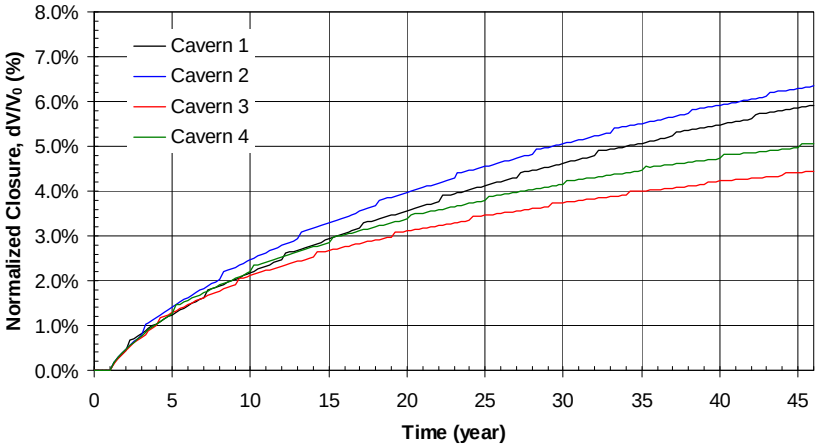

Fig. G-4. 4: Predicted volumetric closure normalized to each initial SPR cavern volume (d_{SD} = 500 ft, FCS).

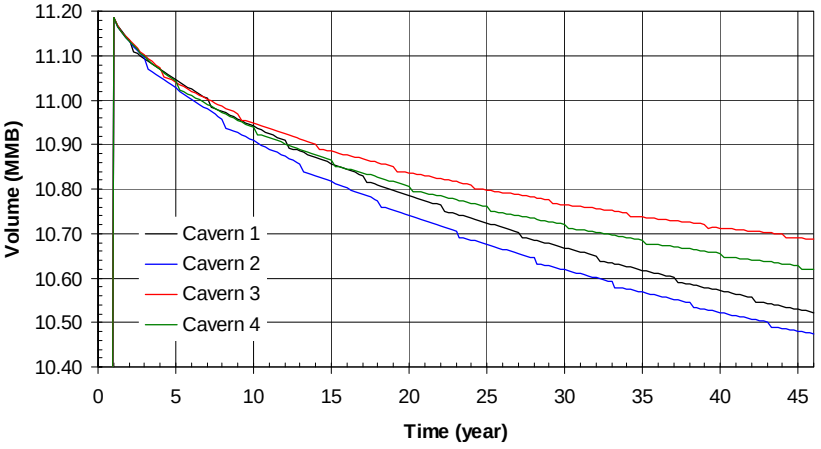

Fig. G-4. 5: Predicted volume change of each SPR cavern due to salt creep closure over time (d_{SD} = 500 ft, FCS).

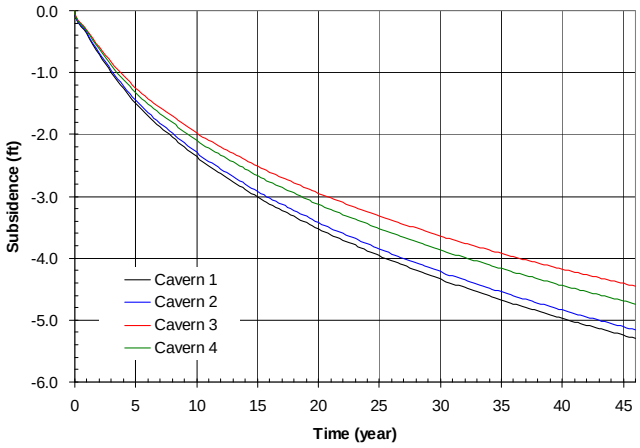

Fig. G-4. 6: Predicted subsidence on the surface above the center of SPR caverns (d_{SD} = 500 ft, FCS).

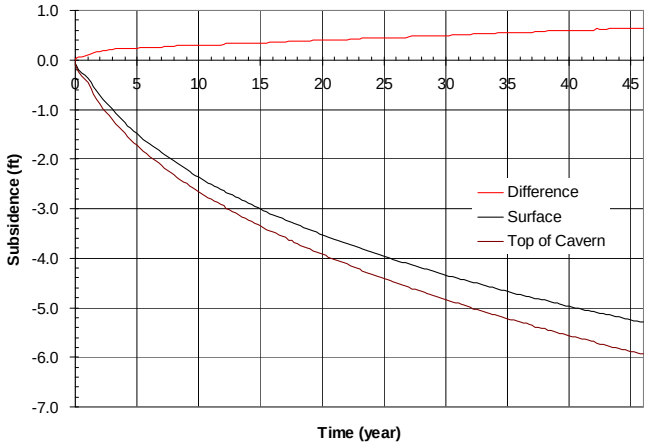

Fig. G-4. 7: Predicted difference between vertical displacement of the top of the central cavern (Cavern 1) and the surface above the cavern as a function of time.

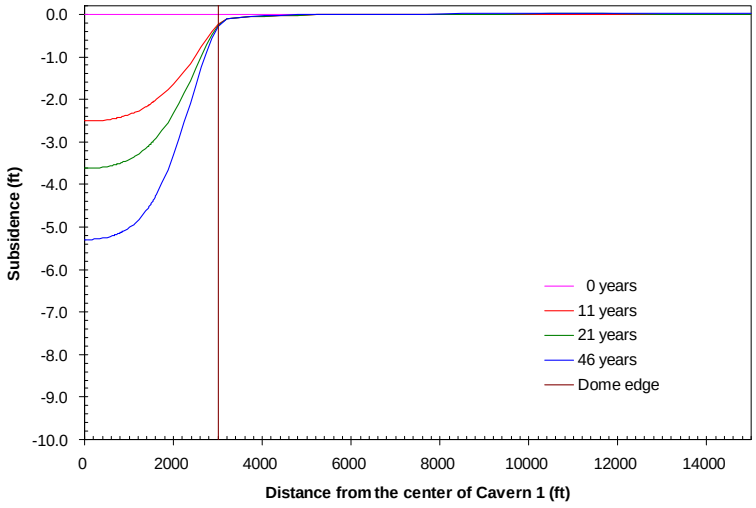

Fig. G-4. 8: Predicted subsidence on the surface from model center to edge with time.

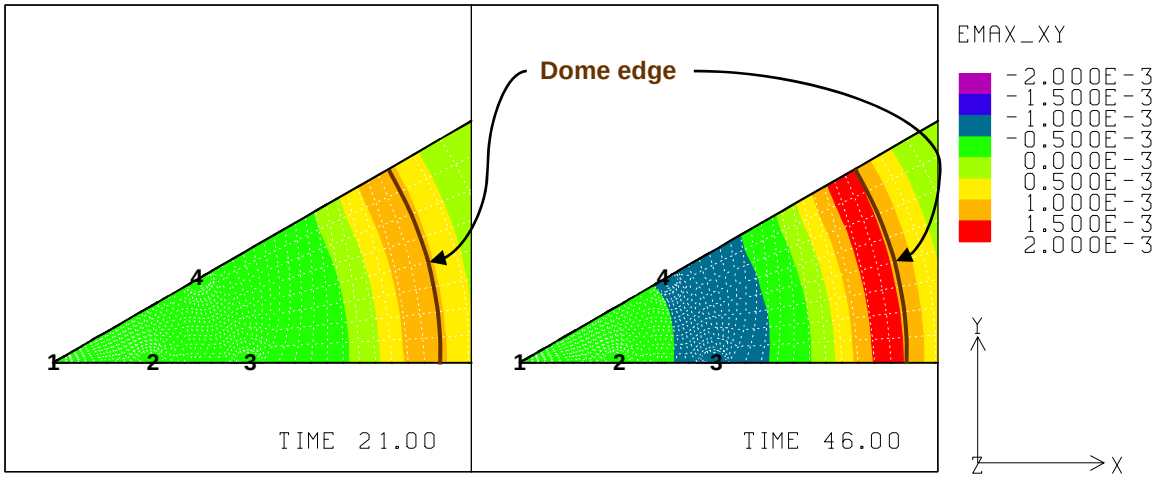

Fig. G-4. 9: Predicted radial surface strains at 21 years and 46 years (d_{SD} = 500 ft, FCS).

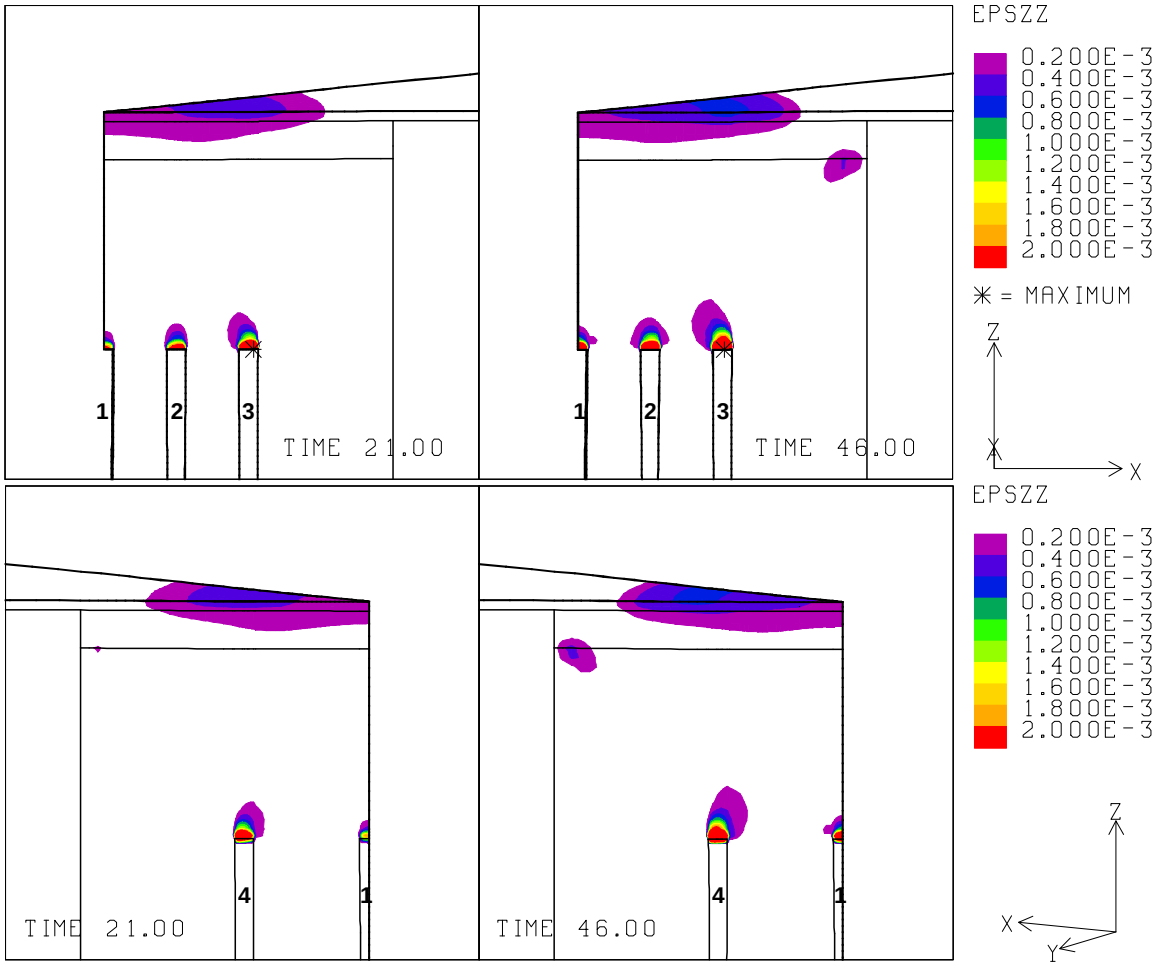

Fig. G-4. 10: Vertical strains around the roof of caverns at 21 years and 46 years (d_{SD} = 500 ft, FCS).

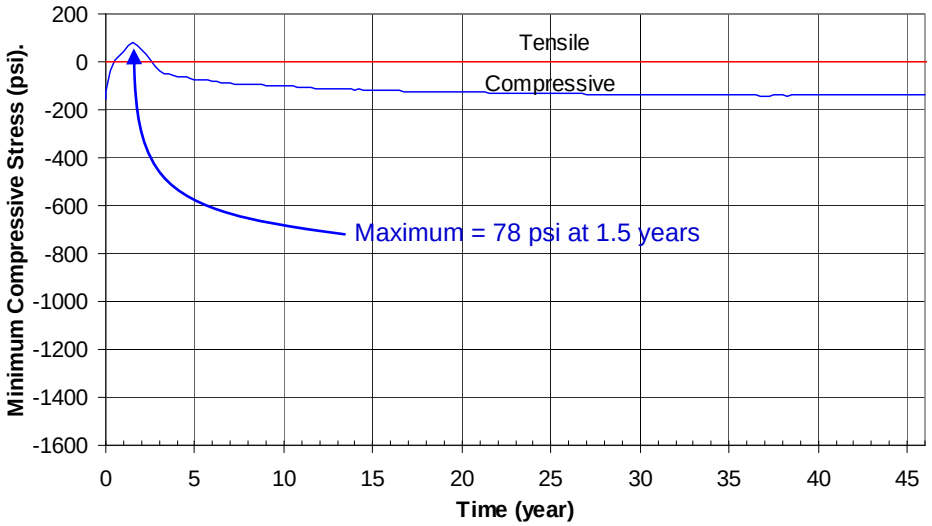

Fig. G-4. 11: Predicted minimum compressive stress history in the salt dome (d_{SD} = 500 ft, FCS).

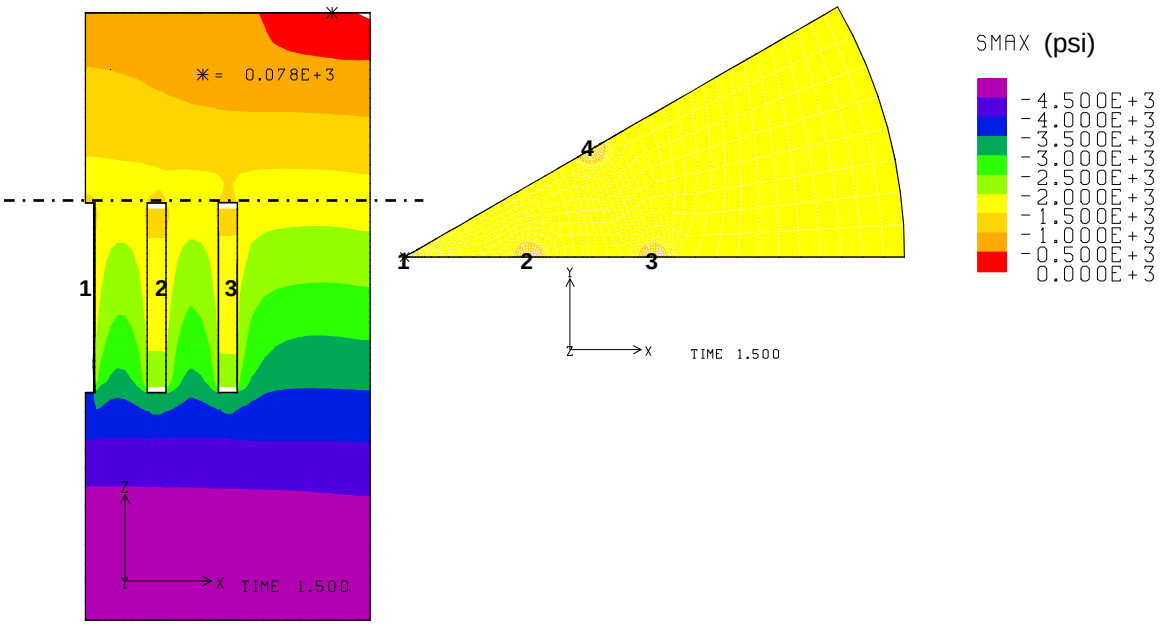

Fig. G-4. 12: Compressive stress contours around the caverns at 1.5 years (Left) and horizontal cross-section at the elevation where the minimum compressive stress occurs (Right). Tensile failure occurs around the top of the dome edge (d_{SD} = 500 ft, FCS).

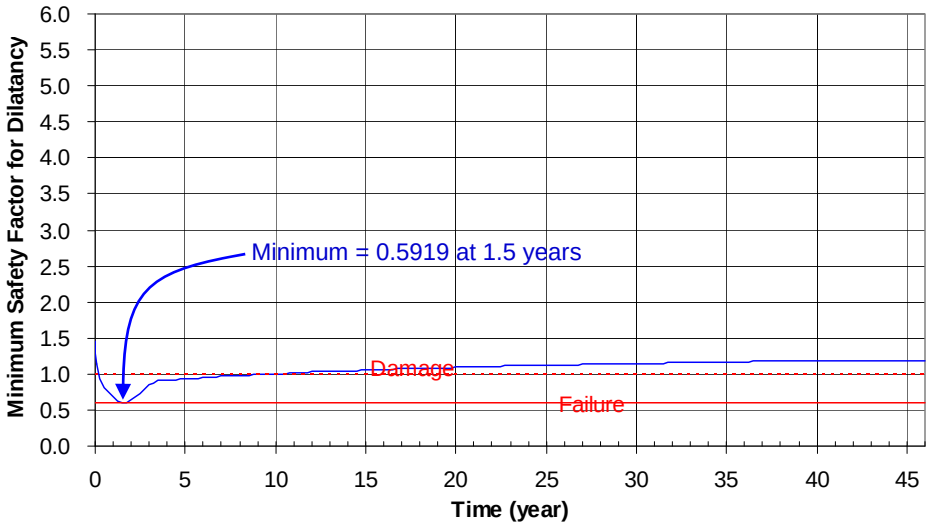

Fig. G-4. 13: Predicted minimum safety factor history against dilatant damage (d_{SD} = 500 ft, FCS).

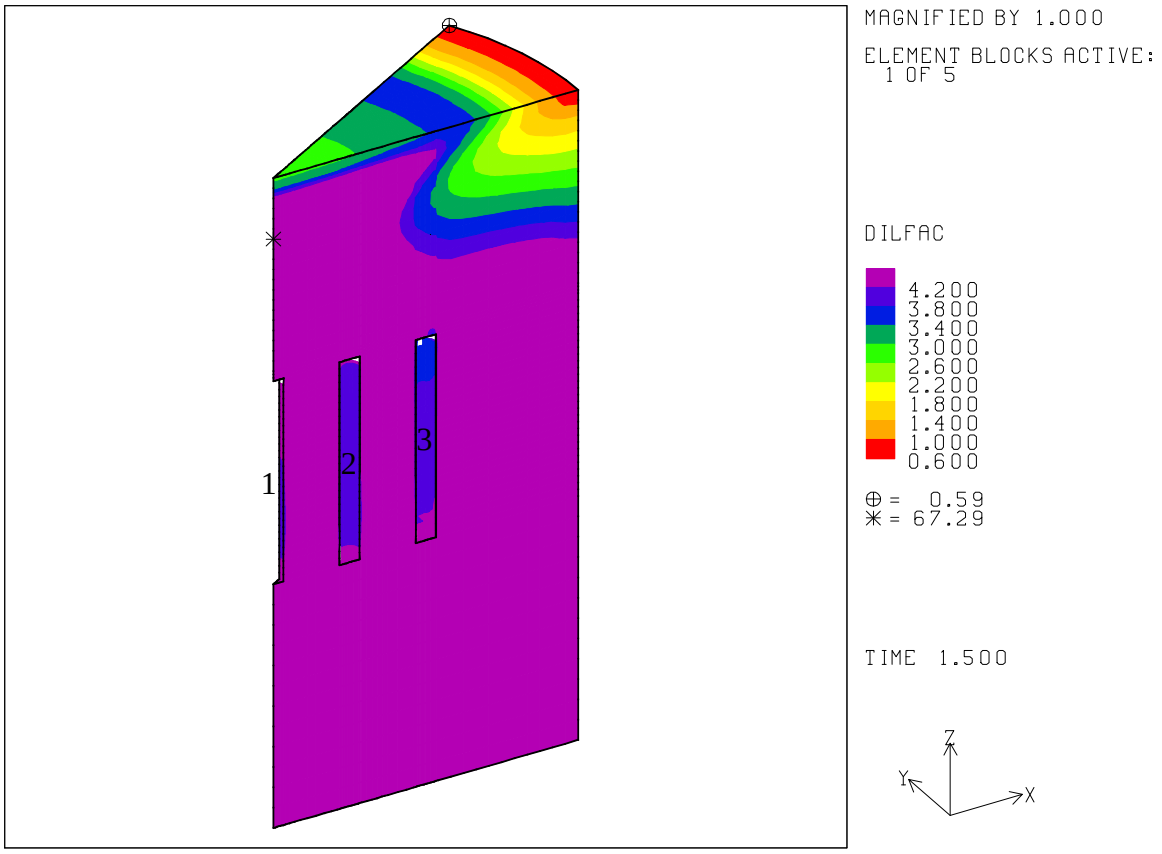

Fig. G-4. 14: Safety factor contours against dilatant damage in the dome at 1.5 years. Dilatant damage occurs around the top of the dome edge (d_{SD} = 500 ft, FCS).

G-5. Depth of Salt Dome Top, d_{SD} = 500 ft, $A_{SC}=2\times10^{14}$

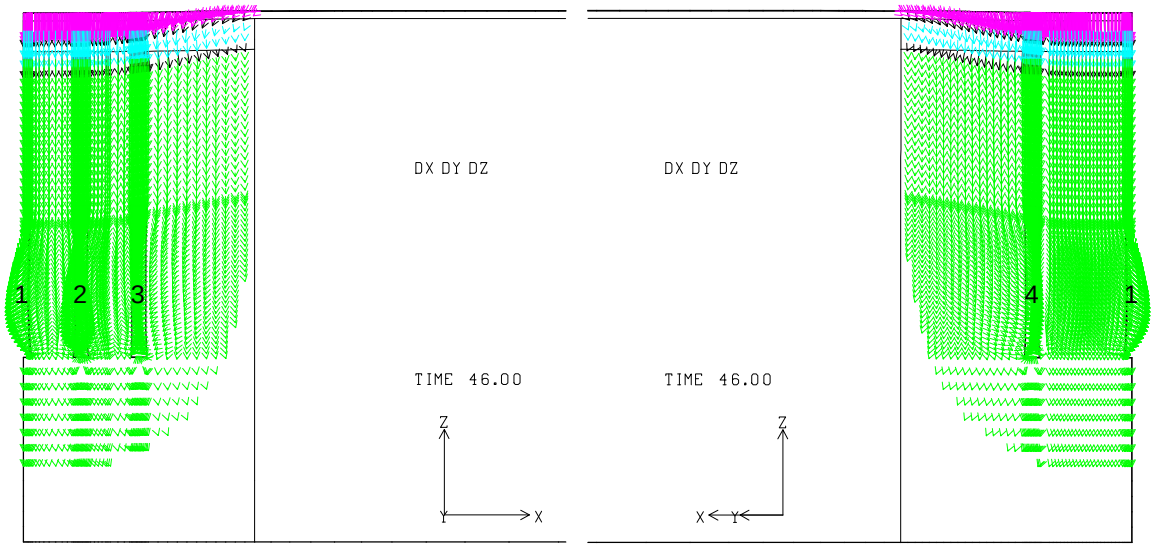

Fig. G-5. 1: Displacement vectors around the caverns at 46 years (d_{SD}=500ft, $A_{SC}=2\times10^{14}$).

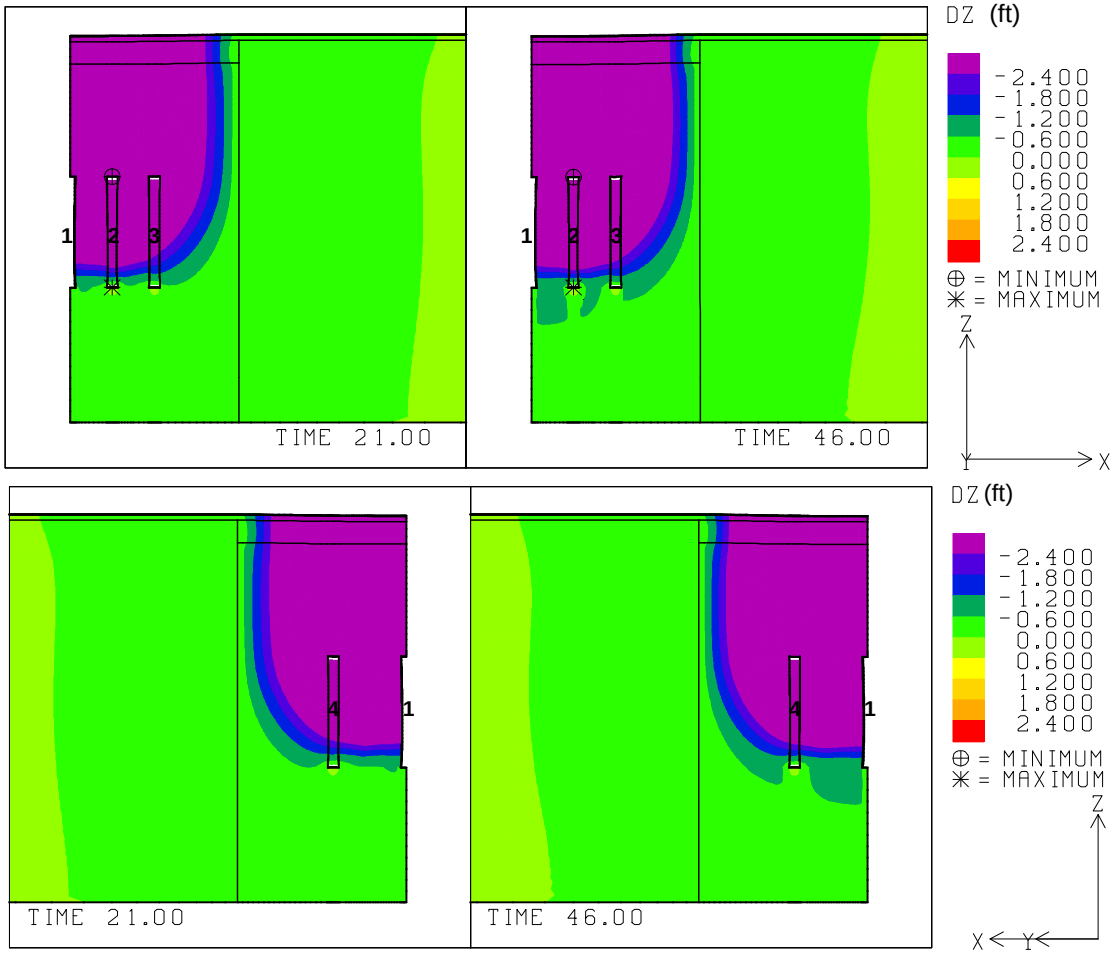

Fig. G-5. 2: Vertical displacement contours around the caverns at 21 and 46 years (d_{SD}=500ft, $A_{SC}=2\times10^{14}$).

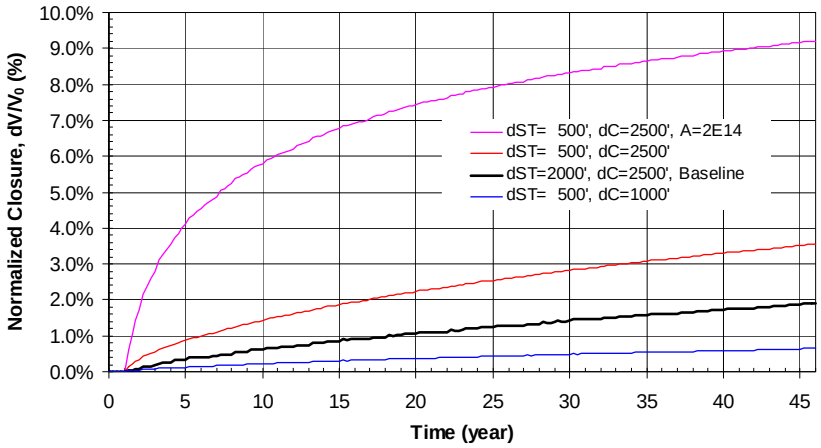

Fig. G-5. 3: Predicted total volumetric closure normalized to initial overall storage volume for the 19 SPR caverns (d_{SD}=500ft, A_{SC}=2×10^{14}).

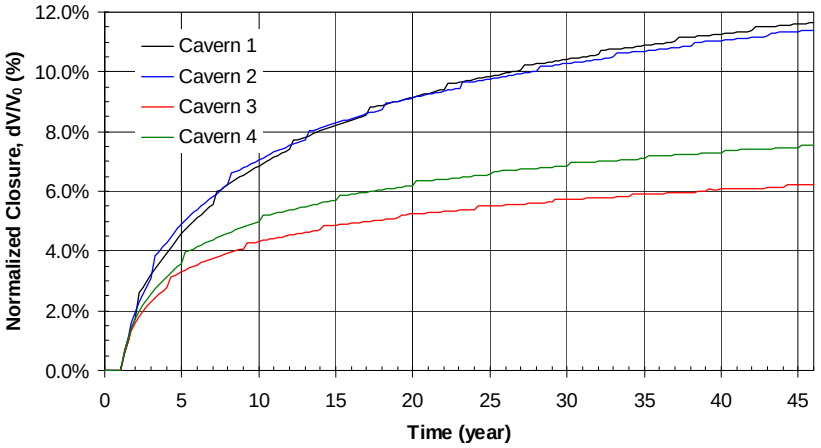

Fig. G-5. 4: Predicted volumetric closure normalized to each initial SPR cavern volume (d_{SD}=500ft, A_{SC}=2×10^{14}).

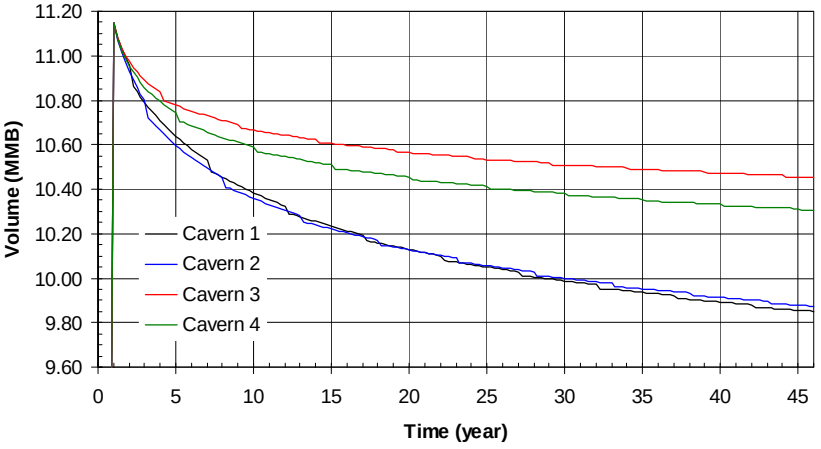

Fig. G-5. 5: Predicted volume change of each SPR cavern due to salt creep closure over time (d_{SD}=500ft, A_{SC}=2×10^{14}).

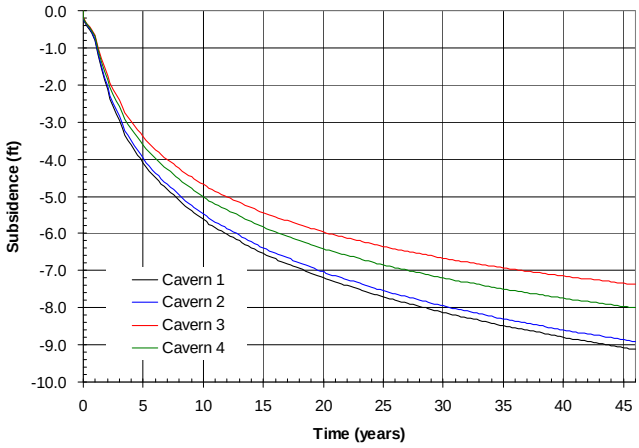

Fig. G-5. 6: Predicted subsidence on the surface above the center of SPR caverns (d_{SD}=500ft, $A_{SC}=2\times10^{14}$).

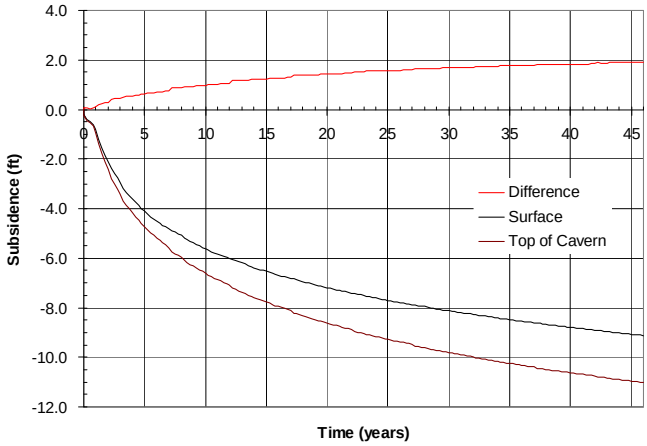

Fig. G-5. 7: Predicted difference between vertical displacement of the top of the central cavern (Cavern 1) and the surface above the cavern as a function of time.

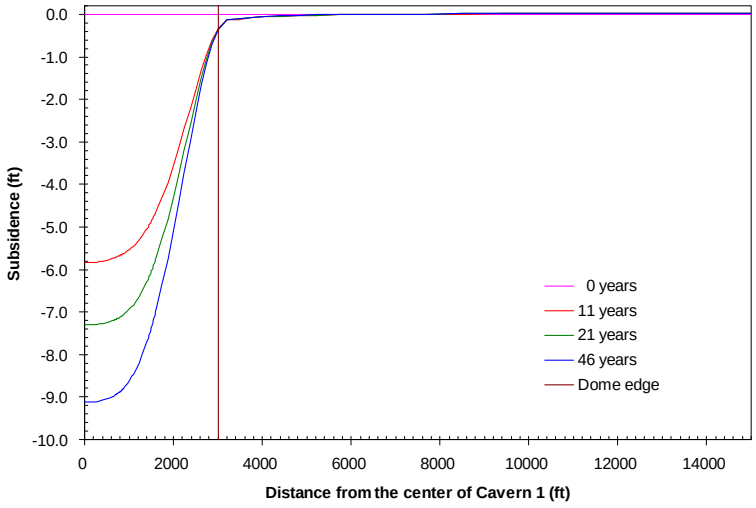

Fig. G-5. 8: Predicted subsidence on the surface from model center to edge with time.

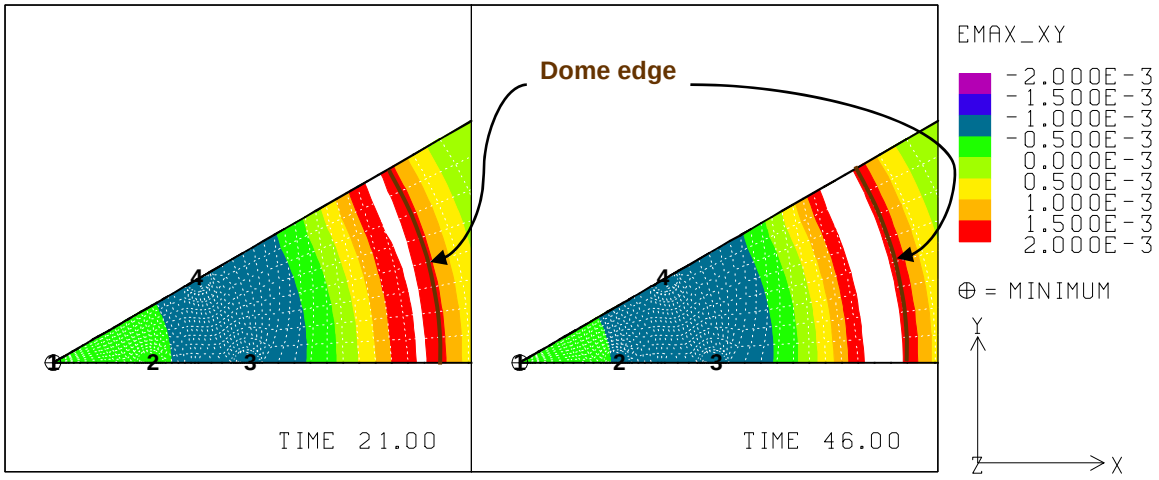

Fig. G-5. 9: Predicted radial surface strains at 21 years and 46 years (d_{SD}=500ft, A_{SC}=2×10^{14}).

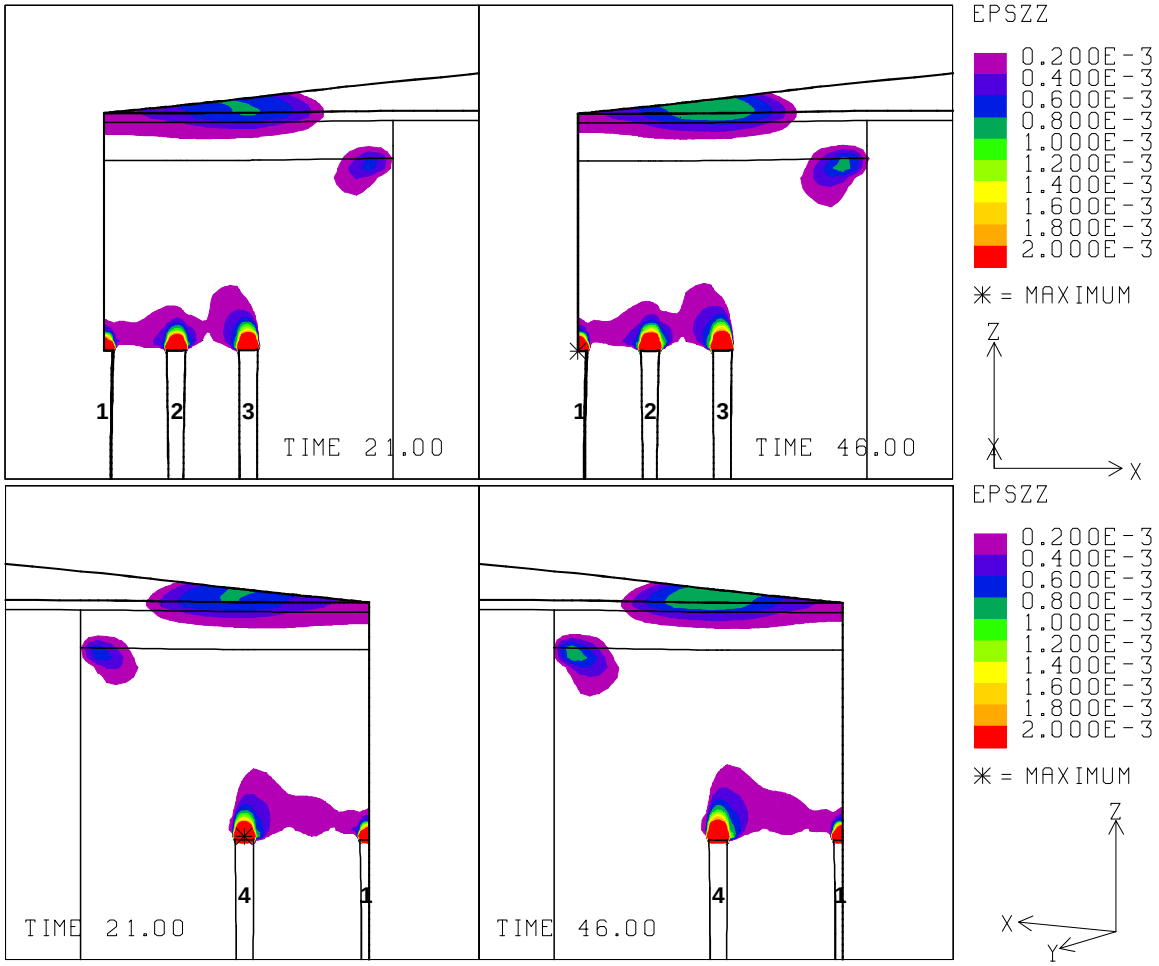

Fig. G-5. 10: Vertical strains around the roof of caverns at 21 years and 46 years (d_{SD}=500ft, A_{SC}=2×10^{14}).

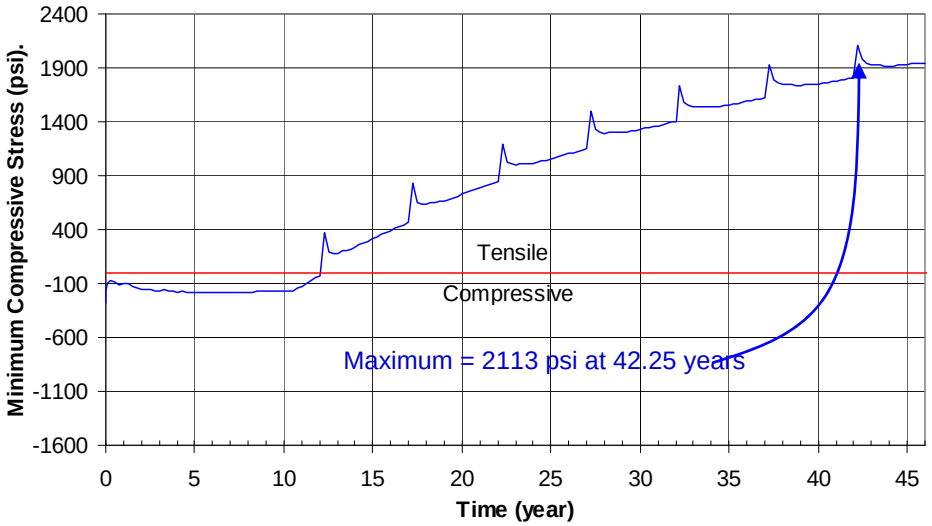

Fig. G-5. 11: Predicted minimum compressive stress history in the salt dome (d_{SD}=500ft, $A_{SC}=2\times10^{14}$).

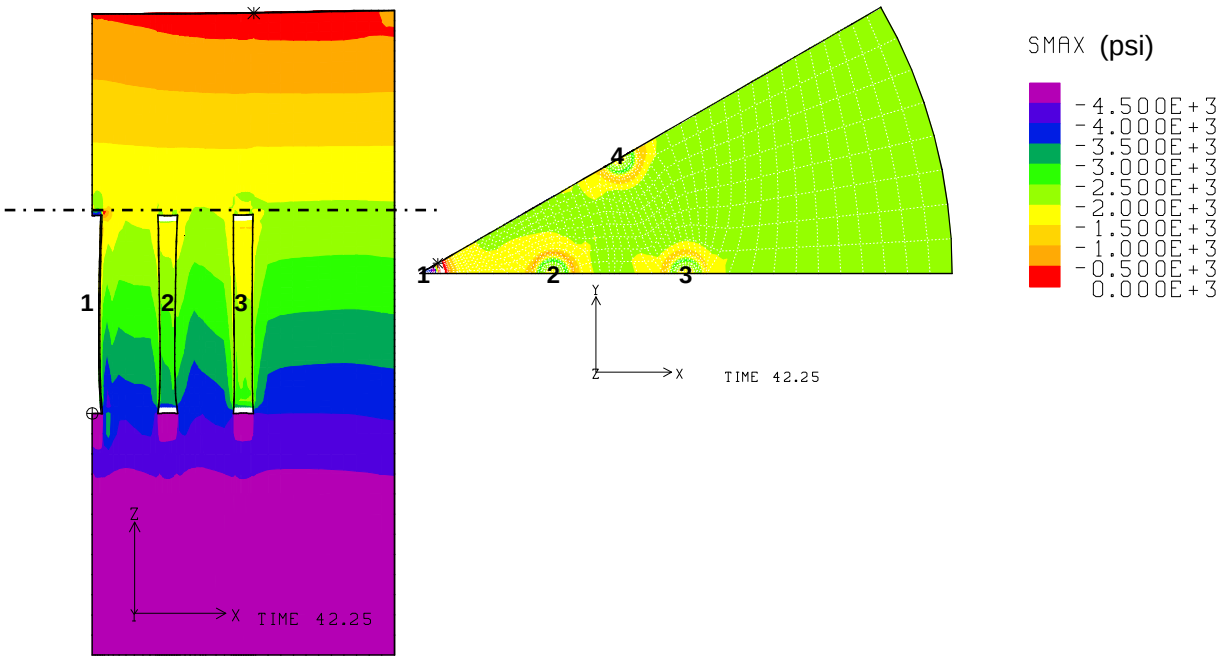

Fig. G-5. 12: Compressive stress contours around the caverns at 42.25 years (Left) and horizontal cross-section at the elevation where the minimum compressive stress occurs (Right). Tensile failure occurs at the roof of Cavern 1 and the salt dome top (d_{SD}=500ft, $A_{SC}=2\times10^{14}$).

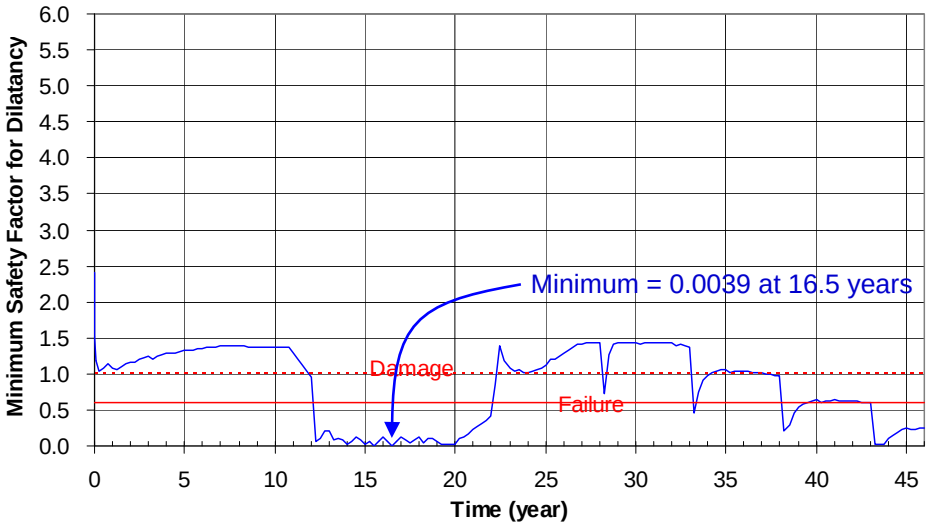

Fig. G-5. 13: Predicted minimum safety factor history against dilatant damage (d_{SD}=500ft, $A_{SC}=2\times10^{14}$).

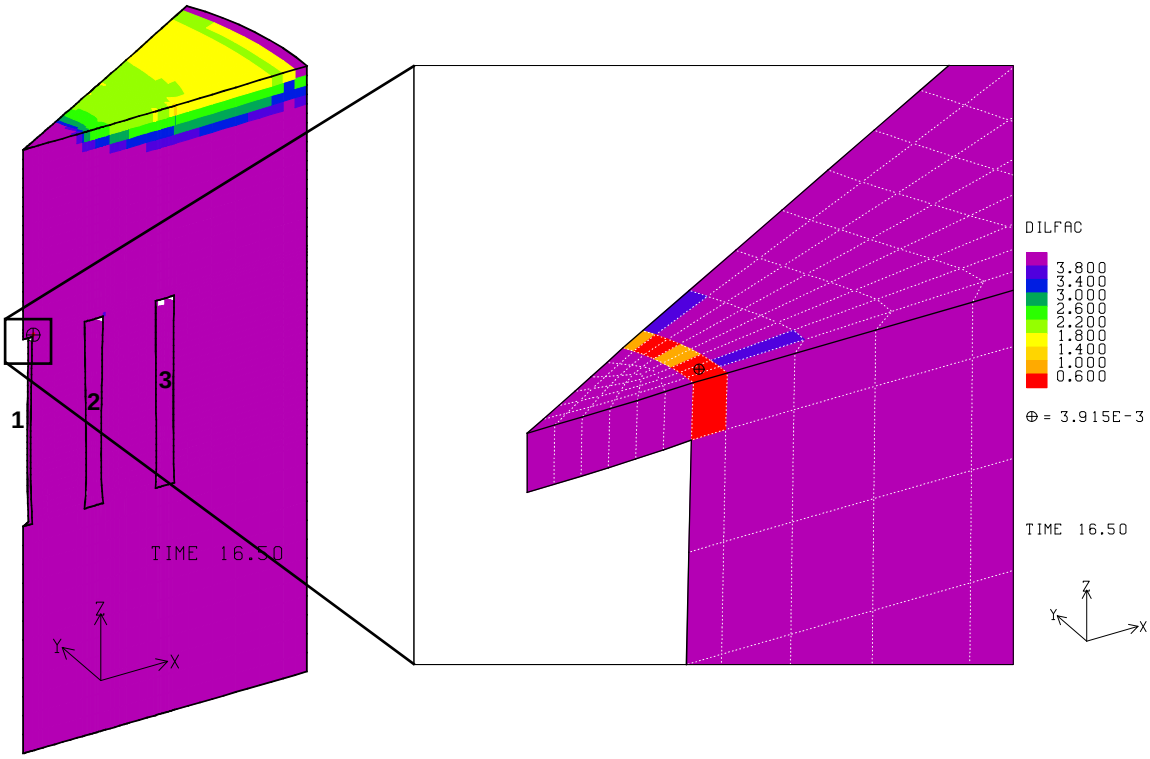

Fig. G-5. 14: Safety factor contours against dilatant damage in the dome at 16.5 years. Dilatant damage occurs at the roof of Cavern 1 (d_{SD}=500ft, $A_{SC}=2\times10^{14}$).

G-6. Dome Size, r_{SD} = 1700 ft; Standoff Distance, D_{SO} = 100 ft

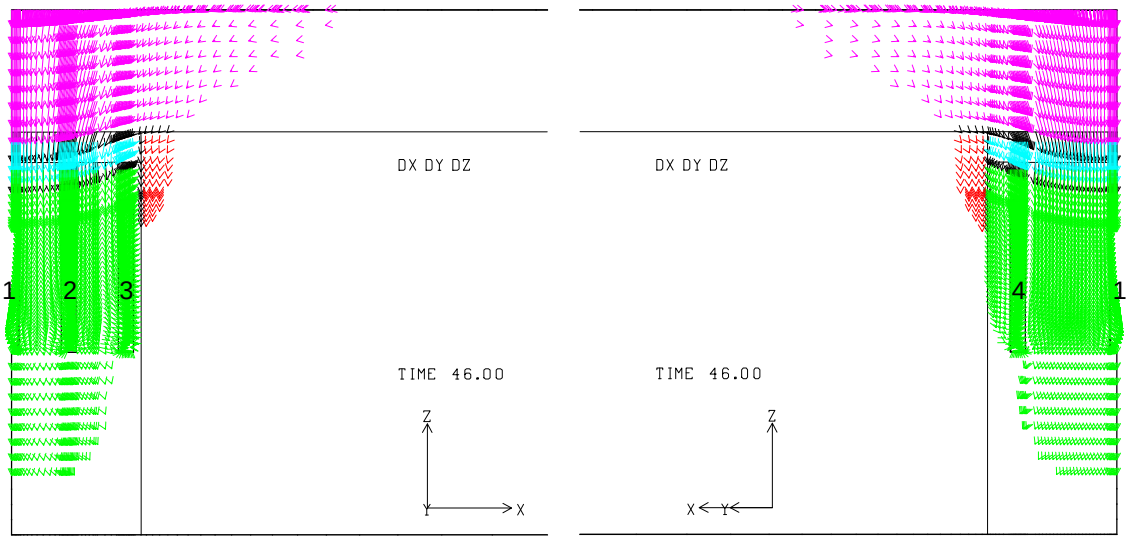

Fig. G-6. 1: Displacement vectors around the caverns at 46 years (r_{SD} = 1700 ft).

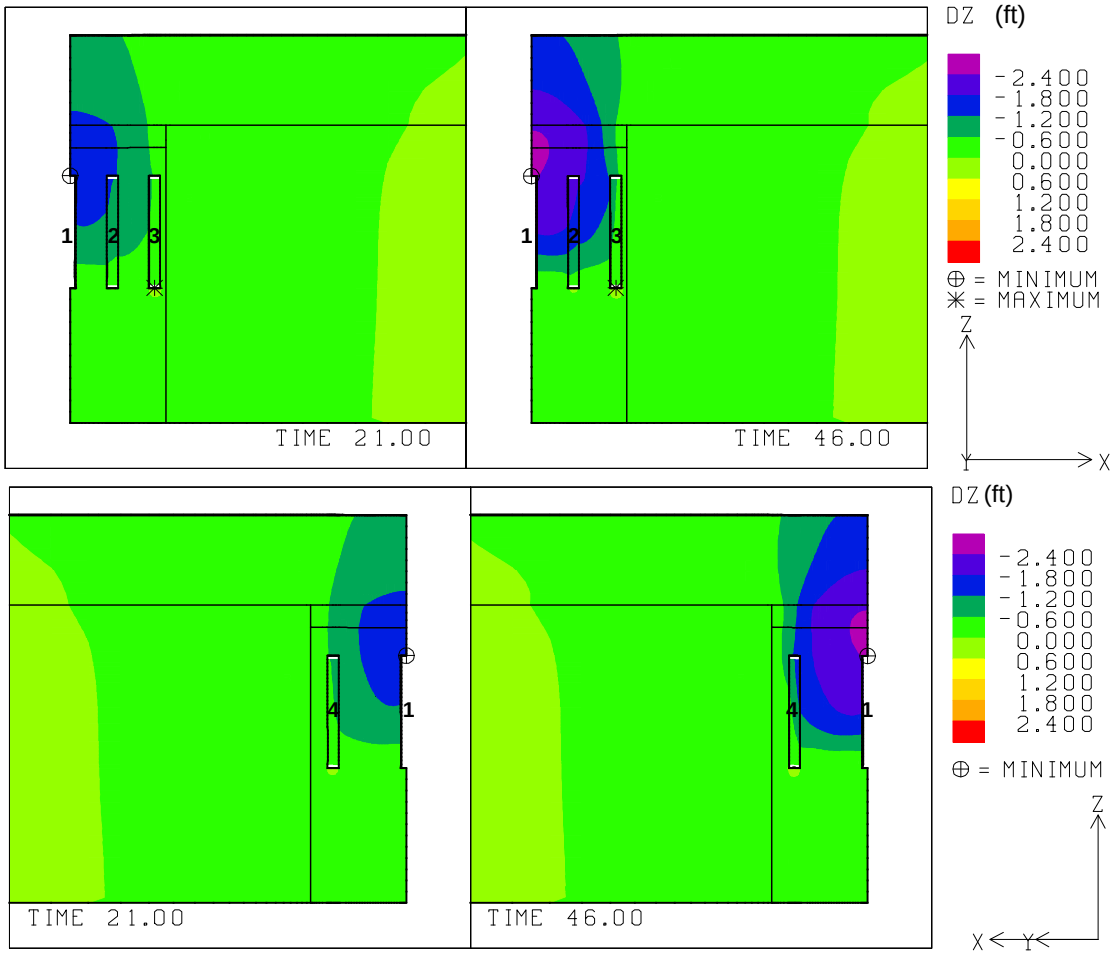

Fig. G-6. 2: Vertical displacement contours around the caverns at 21 and 46 years (r_{SD} = 1700 ft).

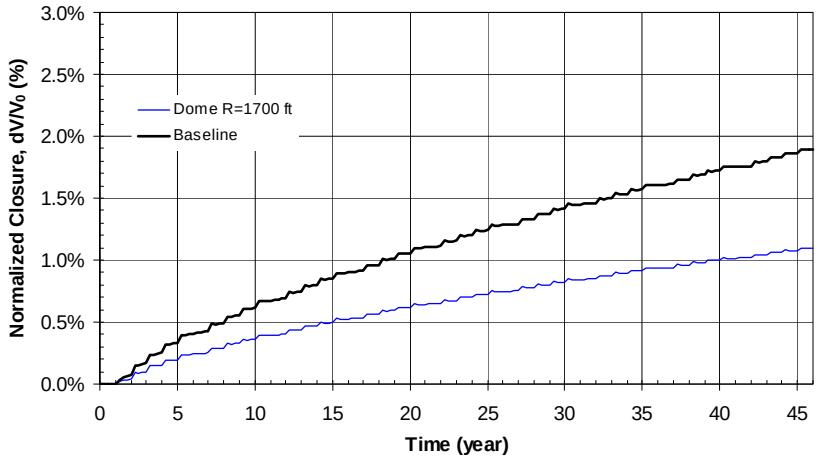

Fig. G-6. 3: Predicted total volumetric closure normalized to initial overall storage volume for the 19 SPR caverns (r_{SD} = 1700 ft).

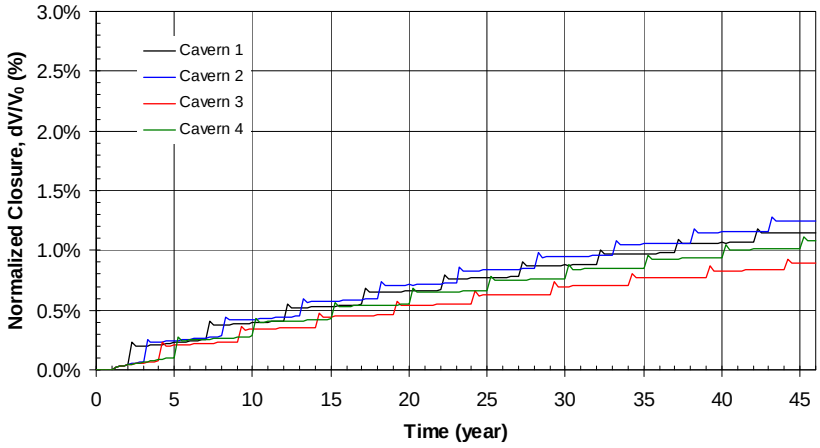

Fig. G-6. 4: Predicted volumetric closure normalized to each initial SPR cavern volume (r_{SD} = 1700 ft).

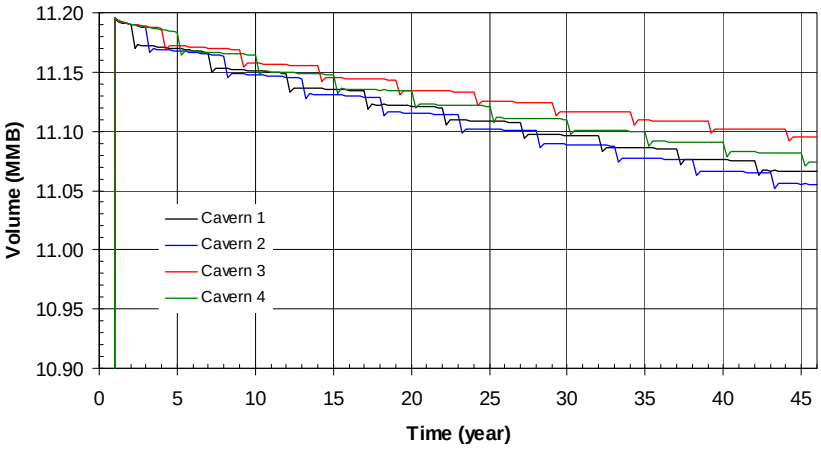

Fig. G-6. 5: Predicted volume change of each SPR cavern due to salt creep closure over time (r_{SD} = 1700 ft).

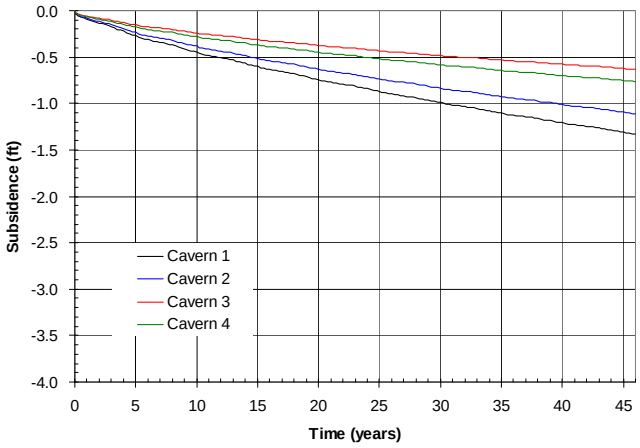

Fig. G-6. 6: Predicted subsidence on the surface above the center of SPR caverns (r_{SD} = 1700 ft).

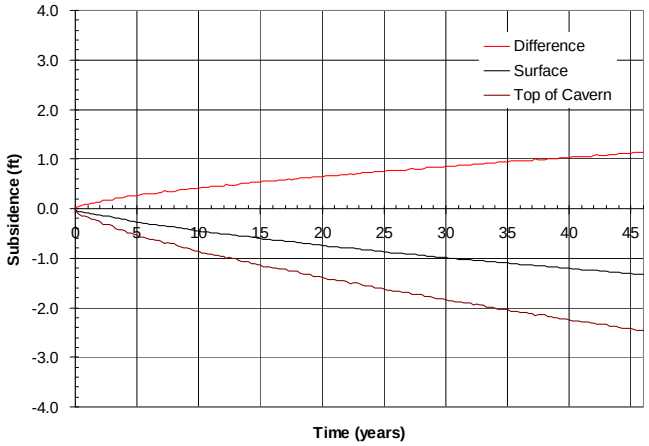

Fig. G-6. 7: Predicted difference between vertical displacement of the top of the central cavern (Cavern 1) and the surface above the cavern as a function of time.

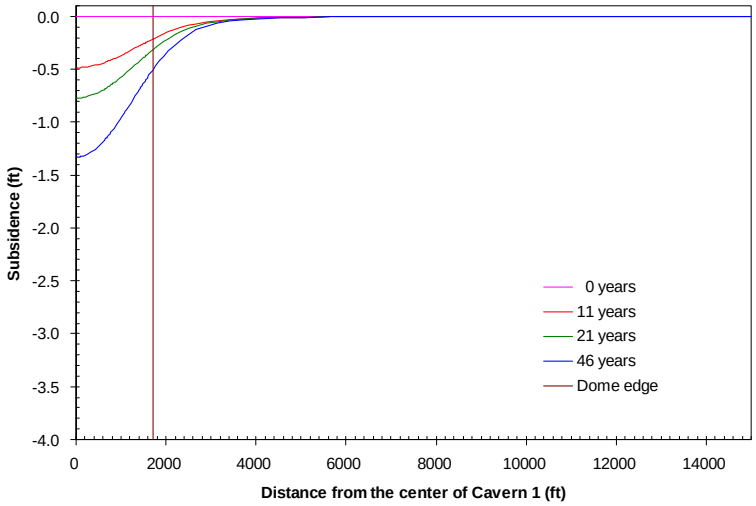

Fig. G-6. 8: Predicted subsidence on the surface from model center to edge with time.

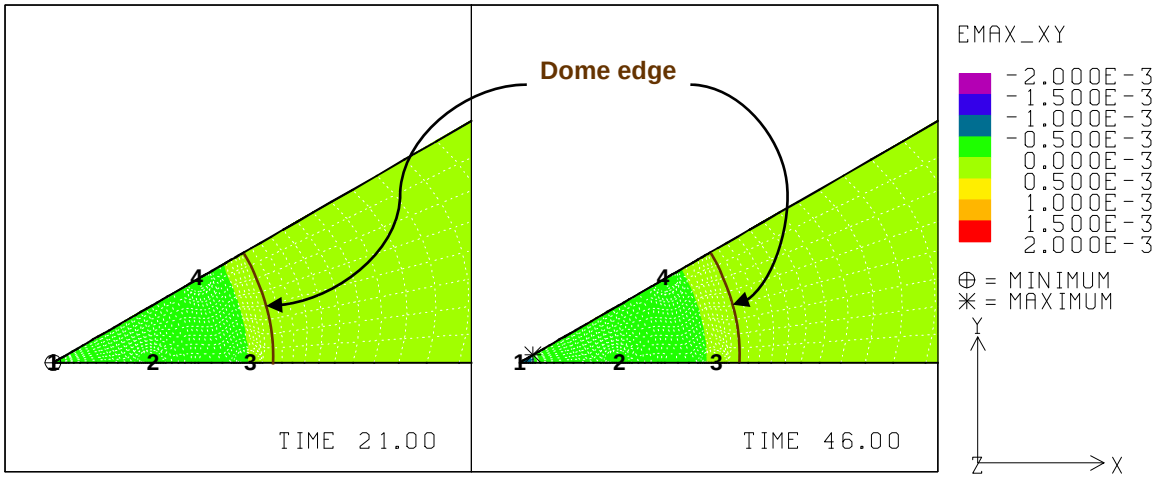

Fig. G-6. 9: Predicted radial surface strains at 21 years and 46 years (r_{SD} = 1700 ft).

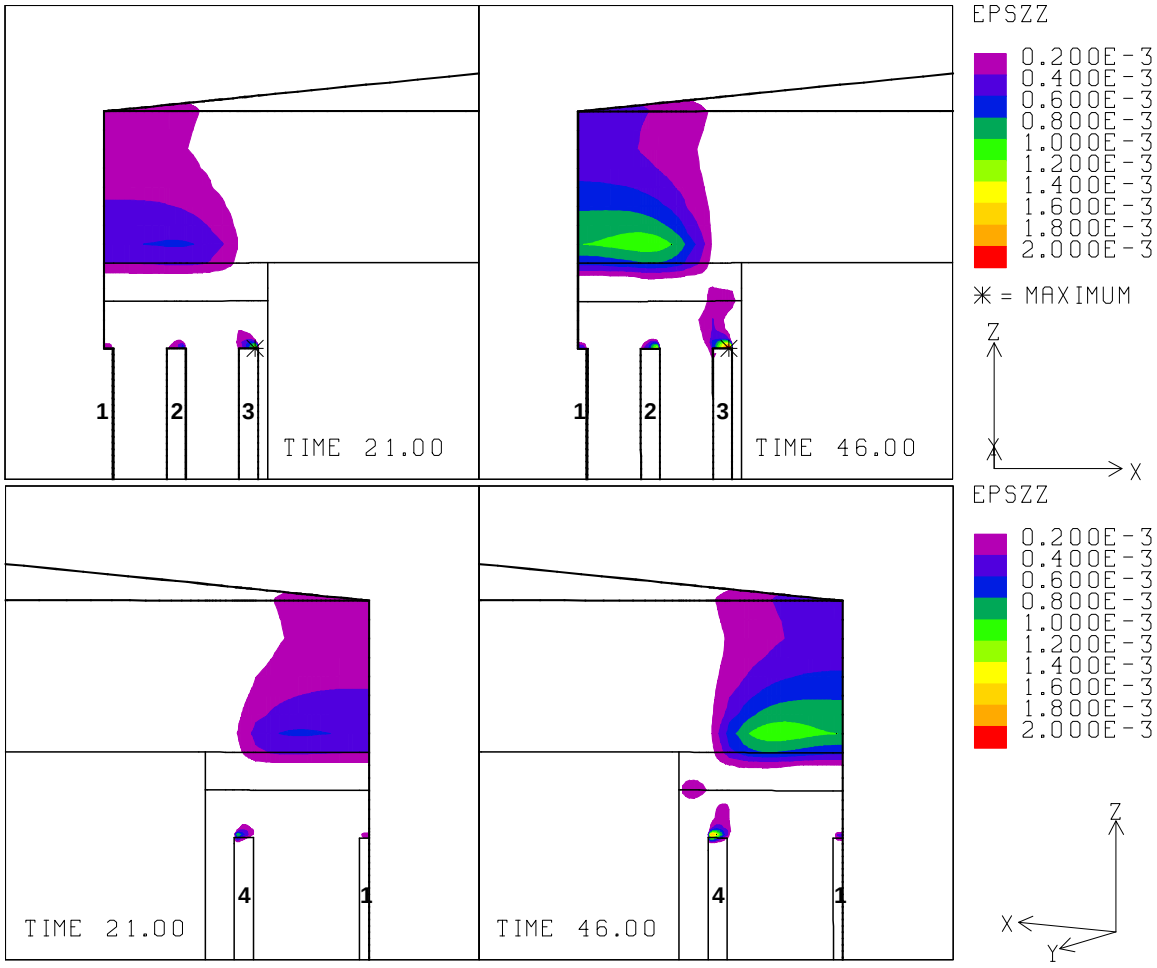

Fig. G-6. 10: Vertical strains around the roof of caverns at 21 years and 46 years (r_{SD} = 1700 ft).

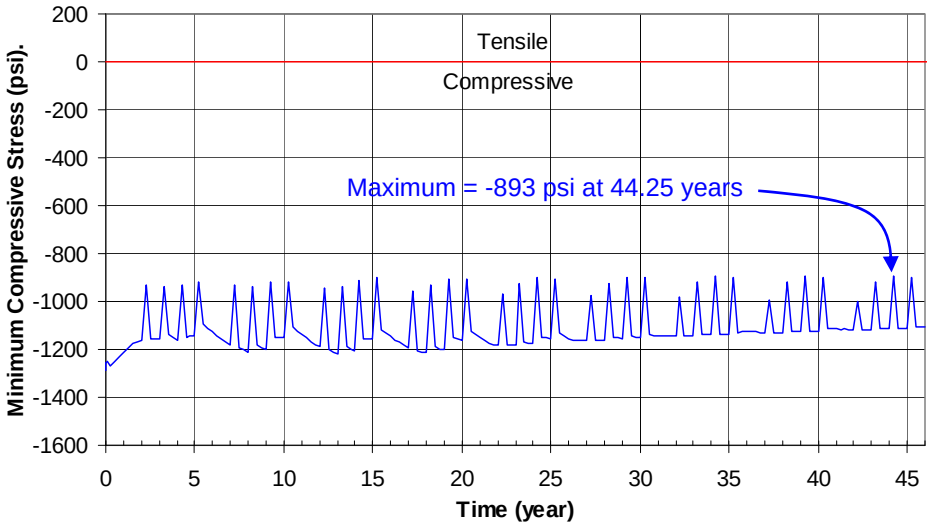

Fig. G-6. 11: Predicted minimum compressive stress history in the salt dome (r_{SD} = 1700 ft).

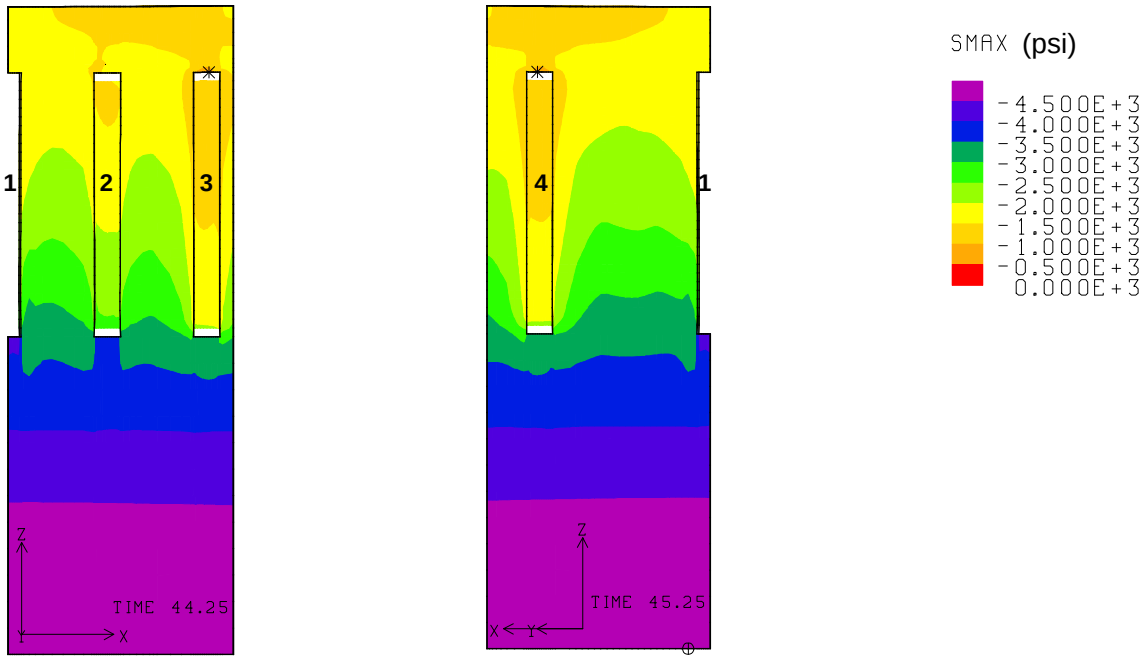

Fig. G-6. 12: Compressive stress contours around the caverns during workover of Cavern 3 and Cavern 4 at 44.25 years and 45.25 years, respectively (r_{SD} = 1700 ft).

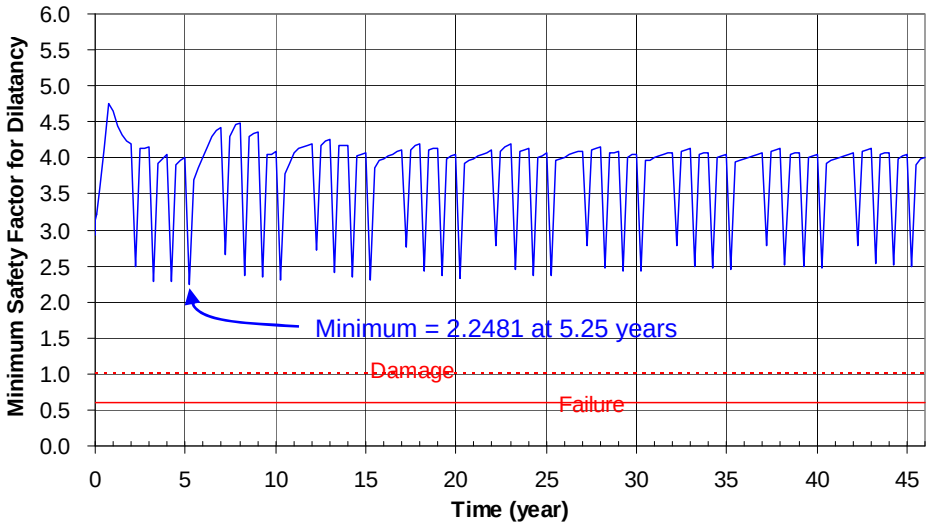

Fig. G-6. 13: Predicted minimum safety factor history against dilatant damage (r_{SD} = 1700 ft).

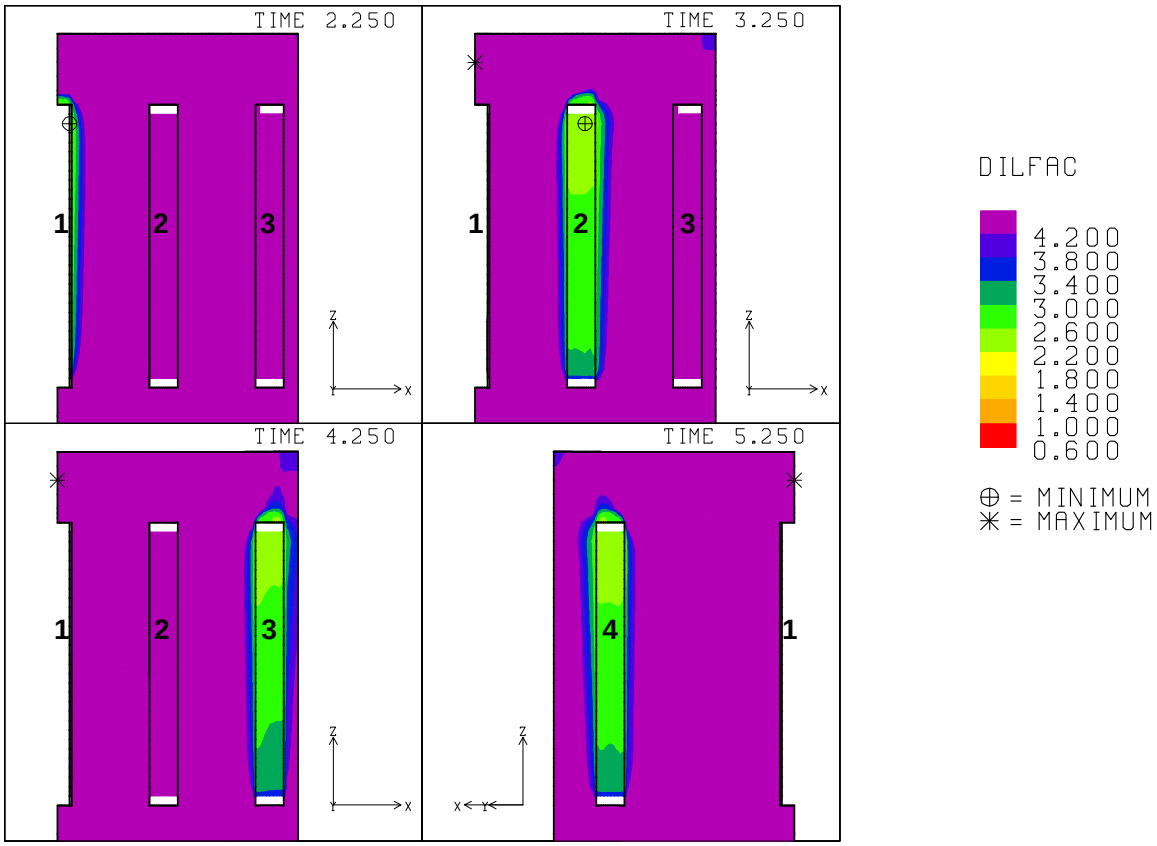

Fig. G-6. 14: Safety factor contours against dilatant damage around the caverns during workover of Caverns 1, 2, 3 and 4 at 2.25 years, 3.25 years, 4.25 years and 5.25 years, respectively (r_{SD} = 1700 ft).

G-7. Caprock Thickness, t_{CR} = 1600 ft

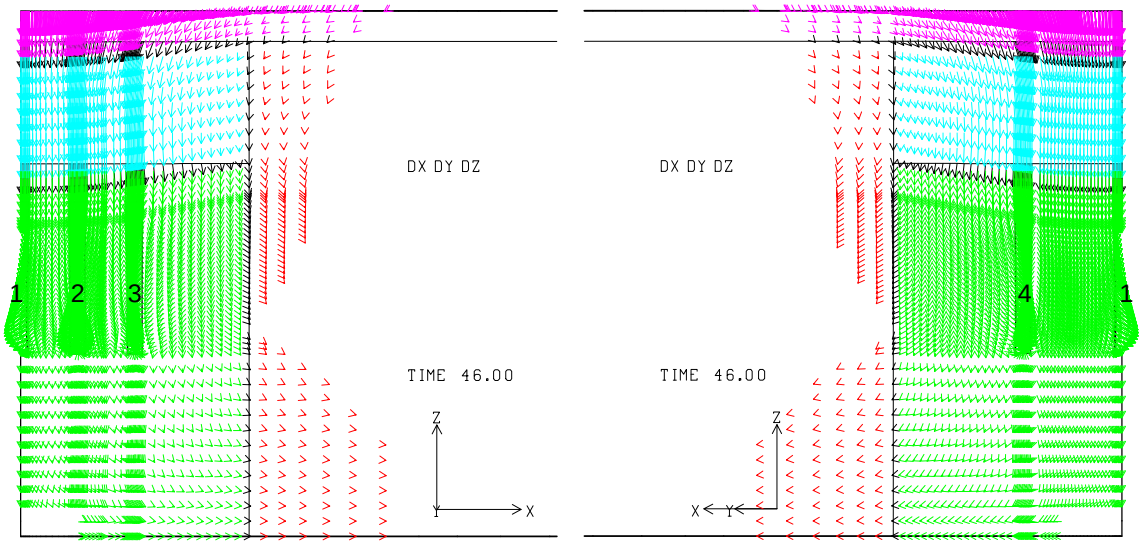

Fig. G-7. 1: Displacement vectors around the caverns at 46 years (t_{CR} = 1600 ft).

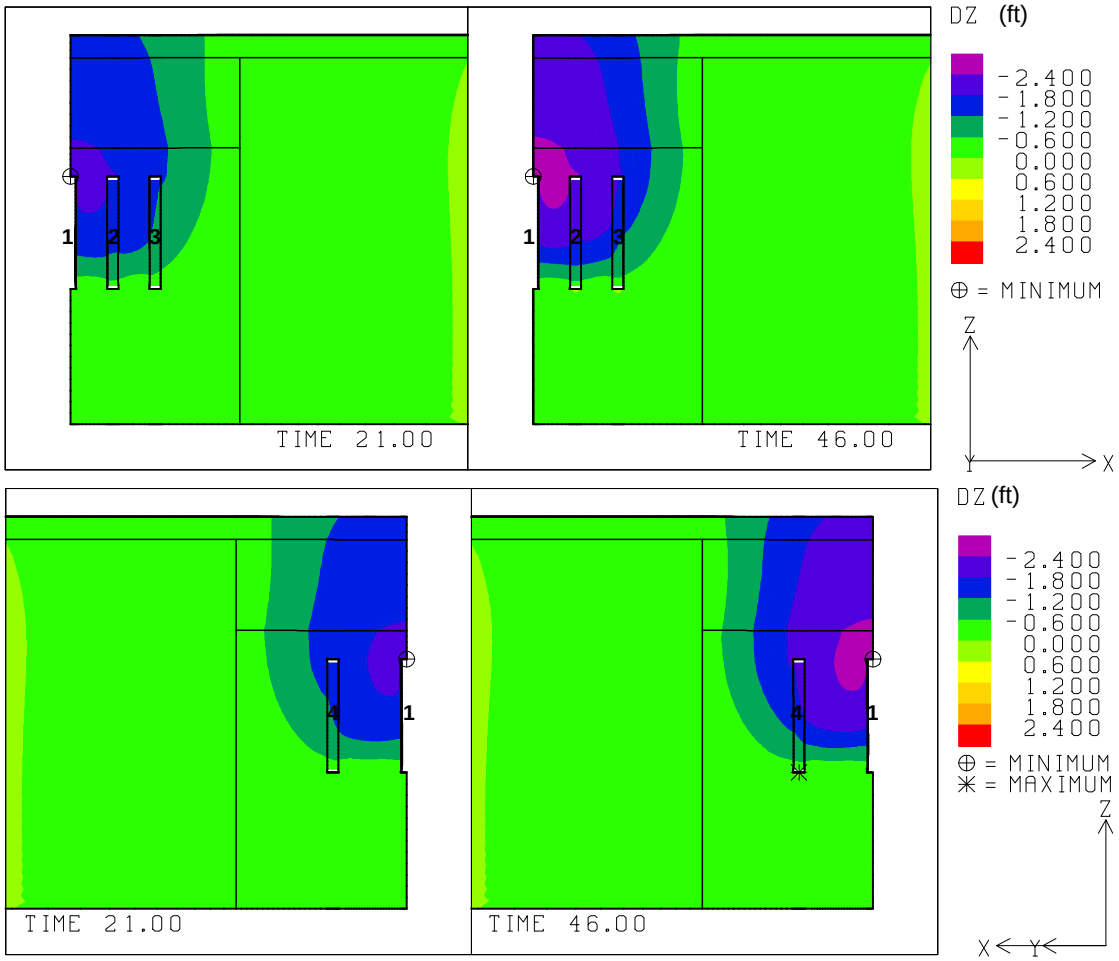

Fig. G-7. 2: Vertical displacement contours around the caverns at 21 and 46 years (t_{CR} = 1600 ft).

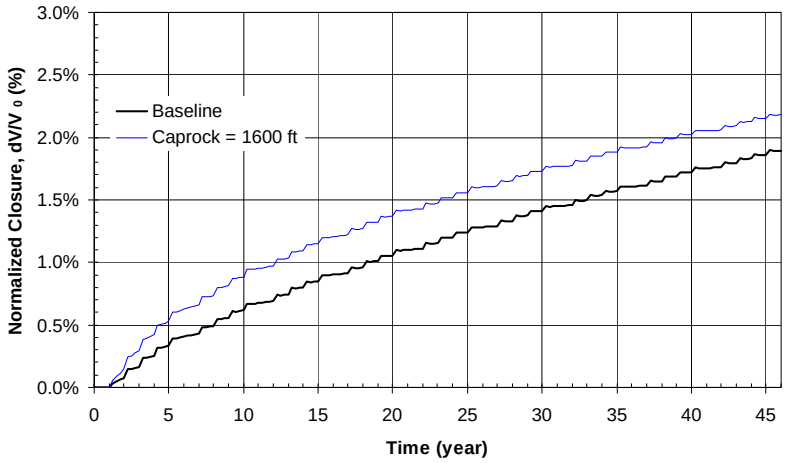

Fig. G-7. 3: Predicted total volumetric closure normalized to initial overall storage volume for the 19 SPR caverns (t_{CR} = 1600 ft).

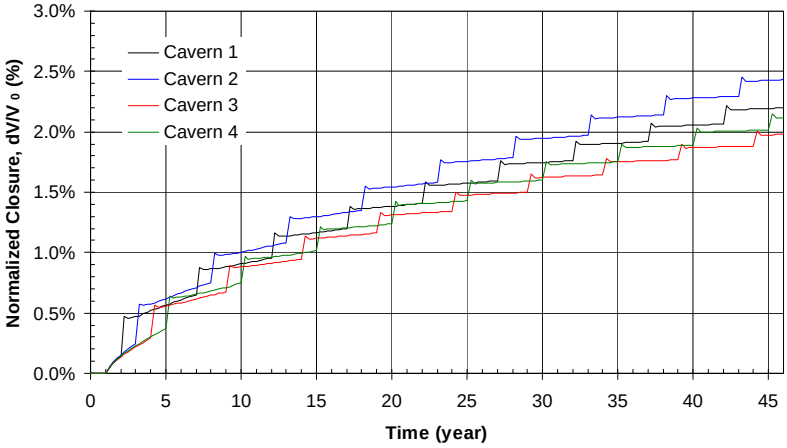

Fig. G-7. 4: Predicted volumetric closure normalized to each initial SPR cavern volume (t_{CR} = 1600 ft).

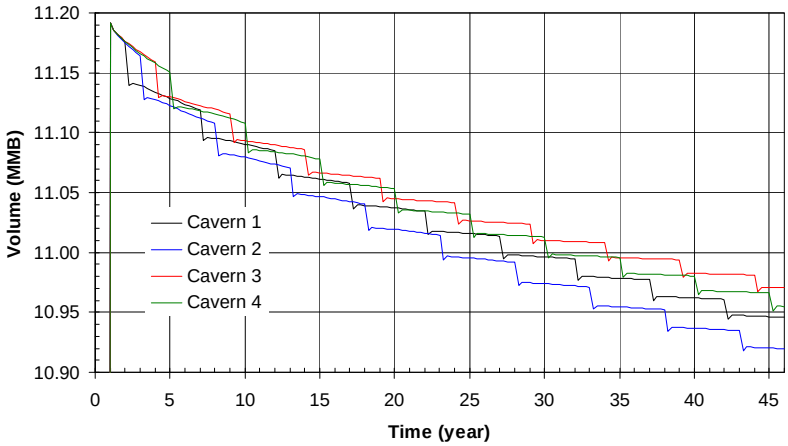

Fig. G-7. 5: Predicted volume change of each SPR cavern due to salt creep closure over time (t_{CR} = 1600 ft).

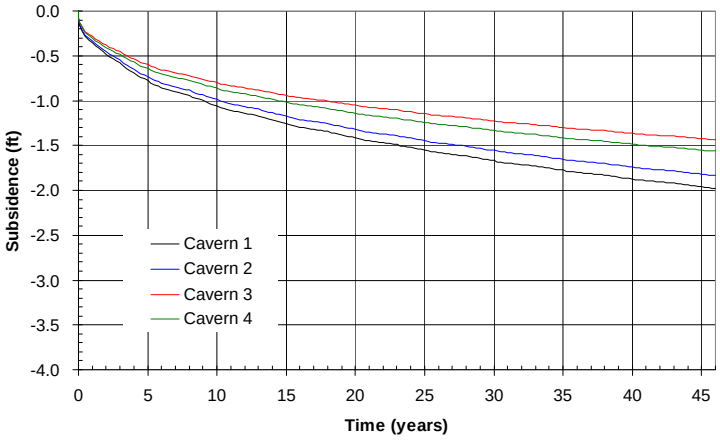

Fig. G-7. 6: Predicted subsidence on the surface above the center of SPR caverns (t_{CR} = 1600 ft).

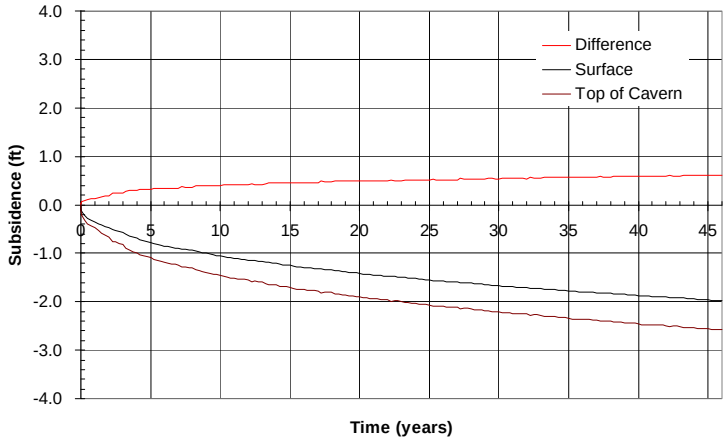

Fig. G-7. 7: Predicted difference between vertical displacement of the top of the central cavern (Cavern 1) and the surface above the cavern as a function of time.

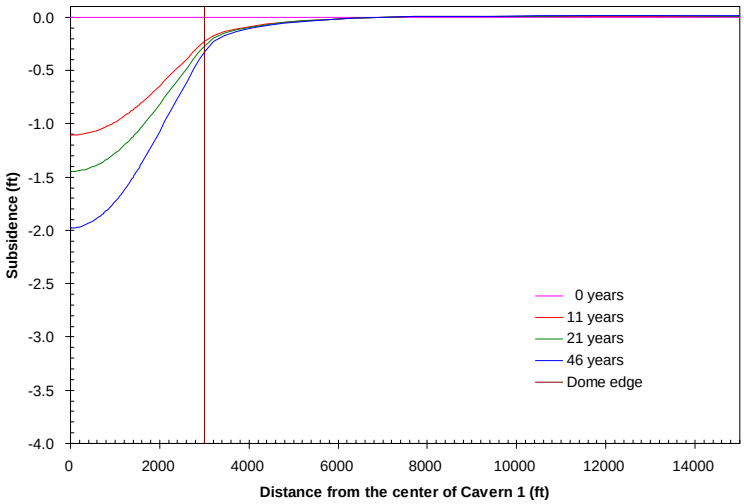

Fig. G-7. 8: Predicted subsidence on the surface from model center to edge with time.

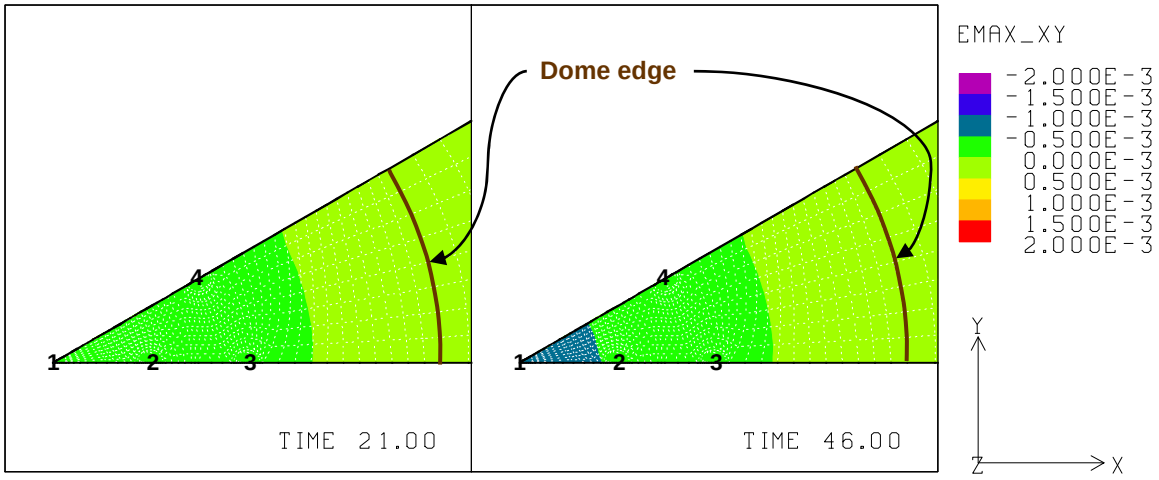

Fig. G-7. 9: Predicted radial surface strains at 21 years and 46 years (t_{CR} = 1600 ft).

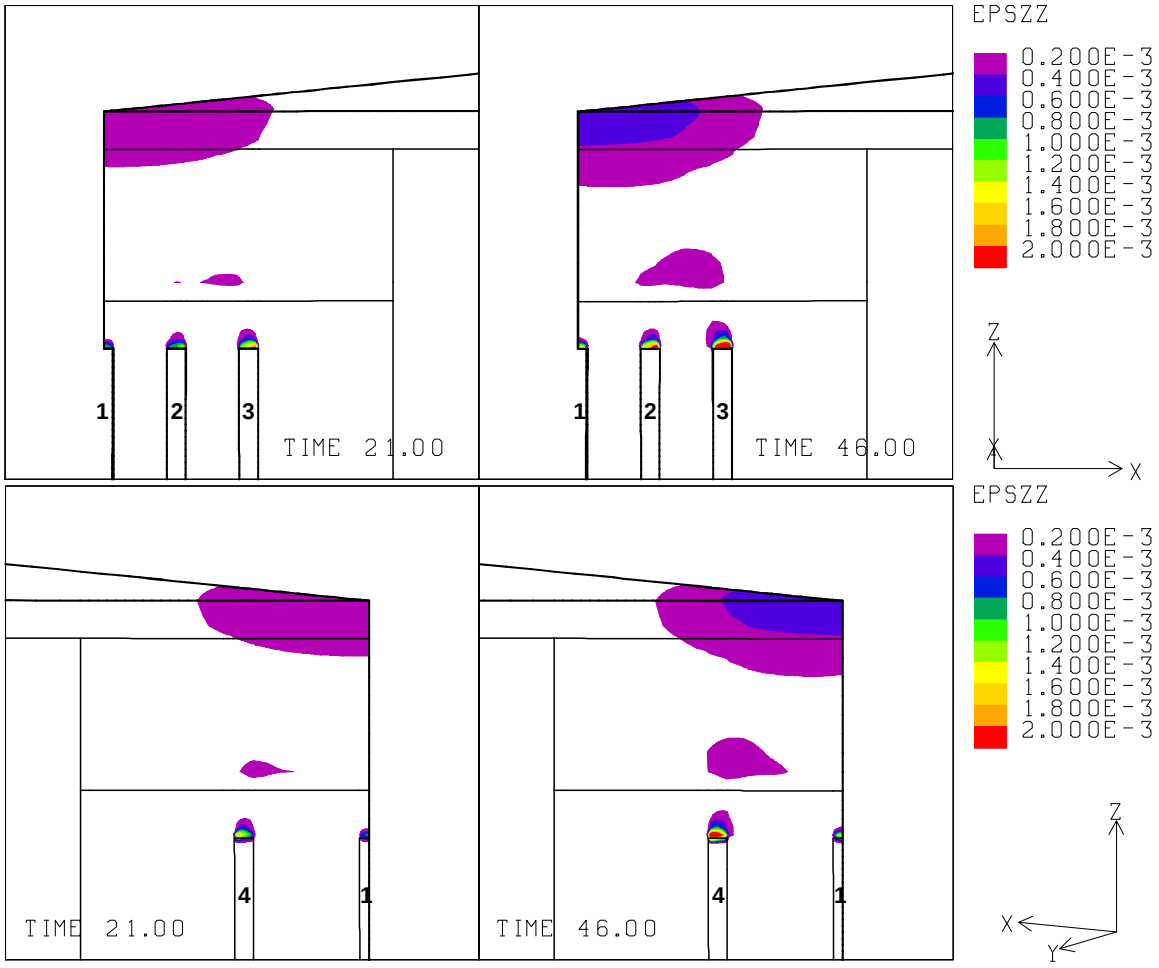

Fig. G-7. 10: Vertical strains around the roof of caverns at 21 years and 46 years (t_{CR} = 1600 ft).

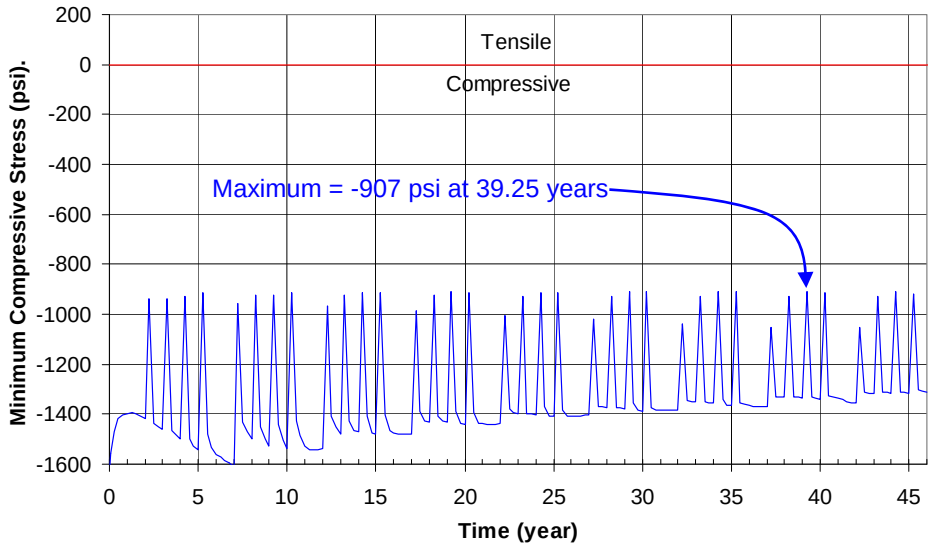

Fig. G-7. 11: Predicted minimum compressive stress history in the salt dome (t_{CR} = 1600 ft).

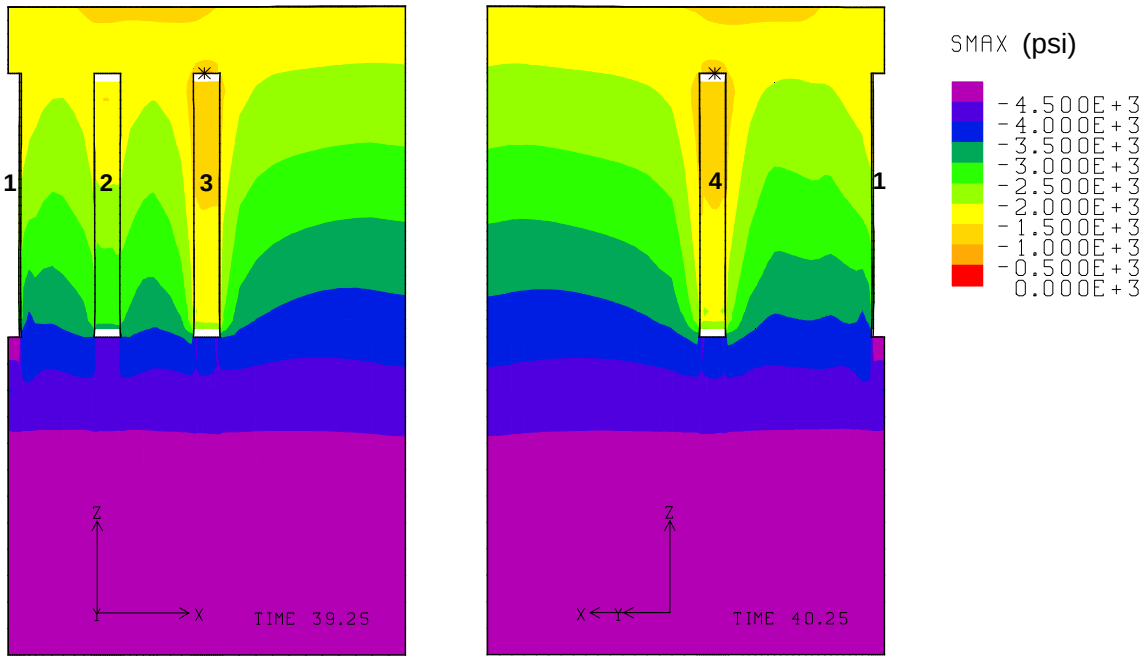

Fig. G-7. 12: Compressive stress contours around the caverns during workover of Cavern 3 and Cavern 4 at 39.25 years and 40.25 years, respectively (t_{CR} = 1600 ft).

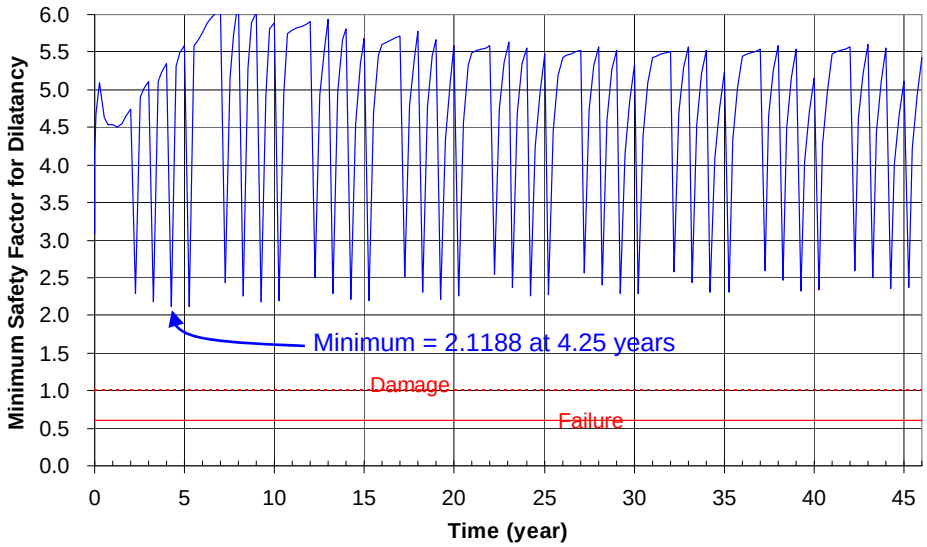

Fig. G-7. 13: Predicted minimum safety factor history against dilatant damage (t_{CR} = 1600 ft).

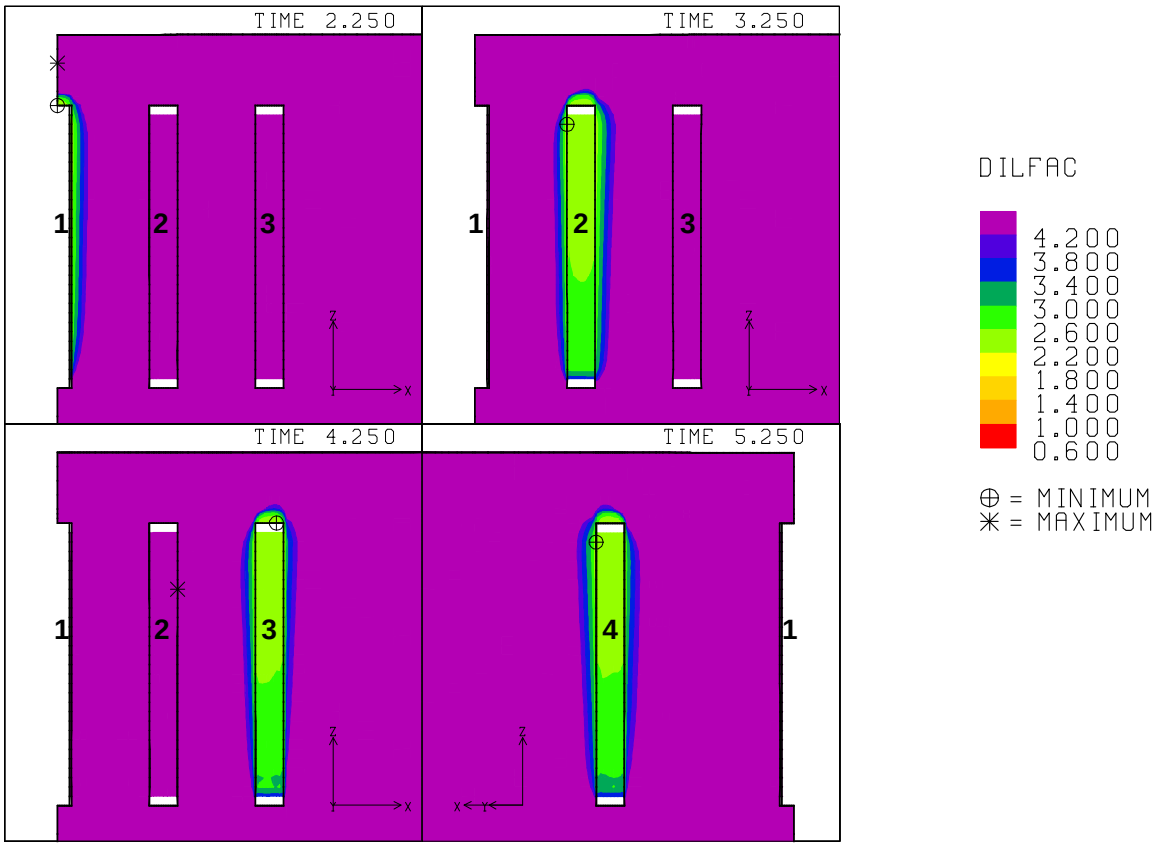

Fig. G-7. 14: Safety factor contours against dilatant damage around the caverns during workover of Caverns 1, 2, 3 and 4 at 2.25 years, 3.25 years, 4.25 years and 5.25 years, respectively (t_{CR} = 1600 ft).

G-8. Elastic Modulus of Caprock, E_{CR} = 1.0 GPa

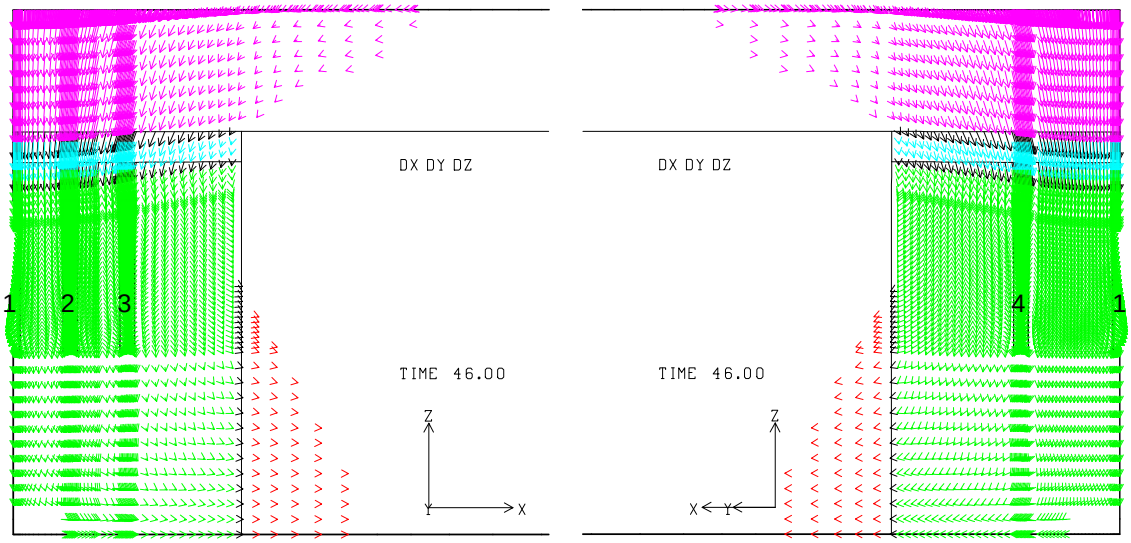

Fig. G-8. 1: Displacement vectors around the caverns at 46 years (E_{CR}=1.0 GPa).

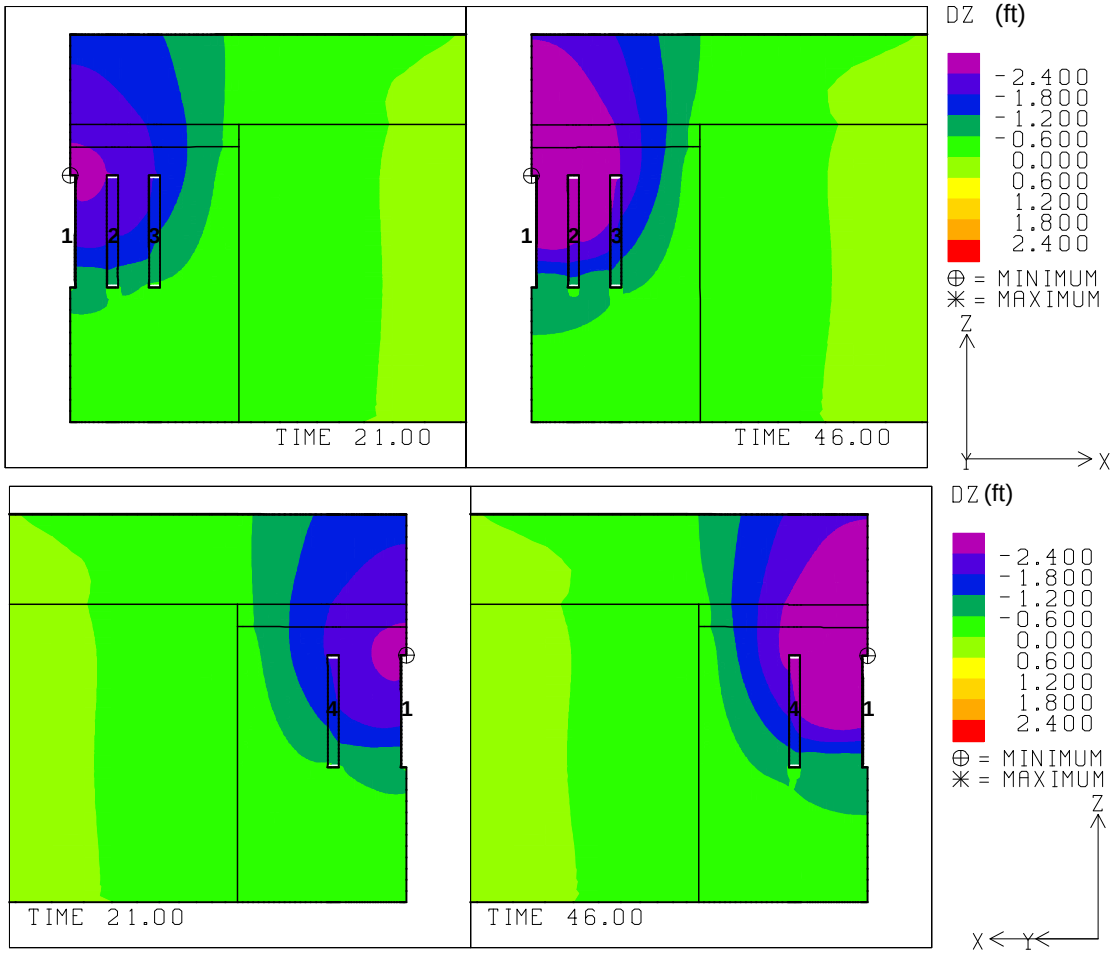

Fig. G-8. 2: Vertical displacement contours around the caverns at 21 and 46 years (E_{CR}=1.0 GPa).

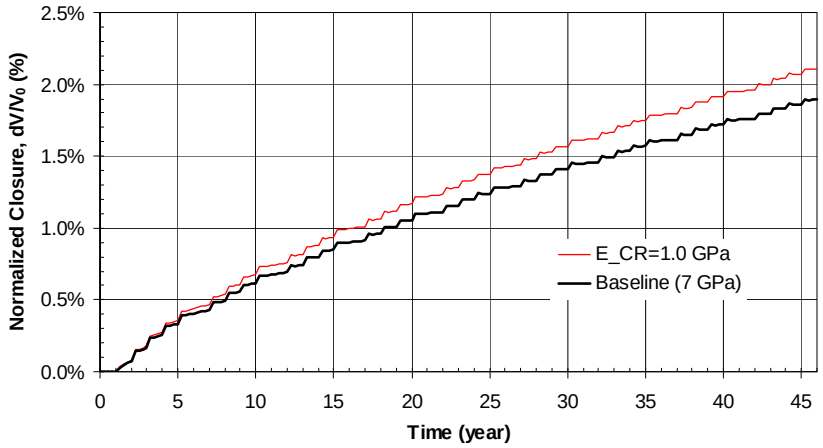

Fig. G-8. 3: Predicted total volumetric closure normalized to initial overall storage volume for the 19 SPR caverns (E_{CR}=1.0 GPa).

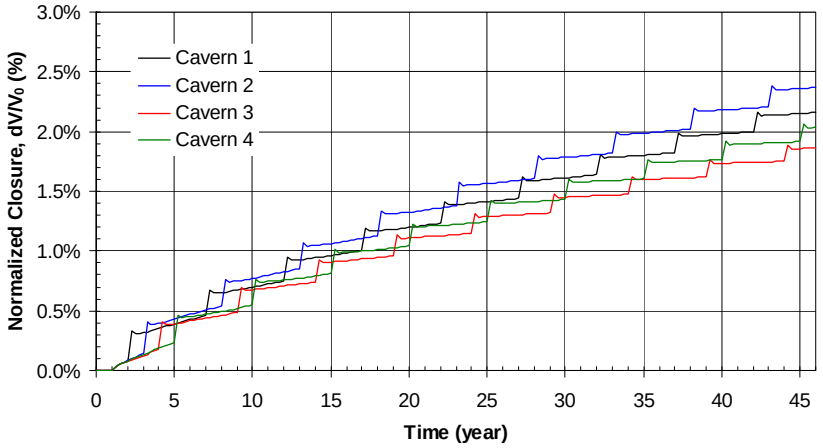

Fig. G-8. 4: Predicted volumetric closure normalized to each initial SPR cavern volume (E_{CR}=1.0 GPa).

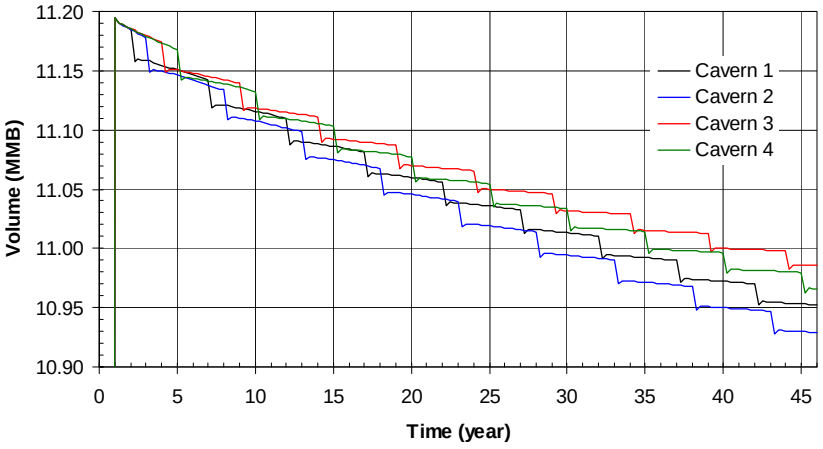

Fig. G-8. 5: Predicted volume change of each SPR cavern due to salt creep closure over time (E_{CR}=1.0 GPa).

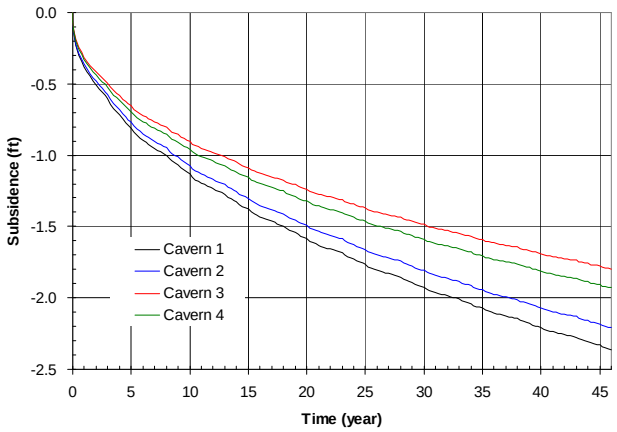

Fig. G-8. 6: Predicted subsidence on the surface above the center of SPR caverns (E_{CR}=1.0 GPa).

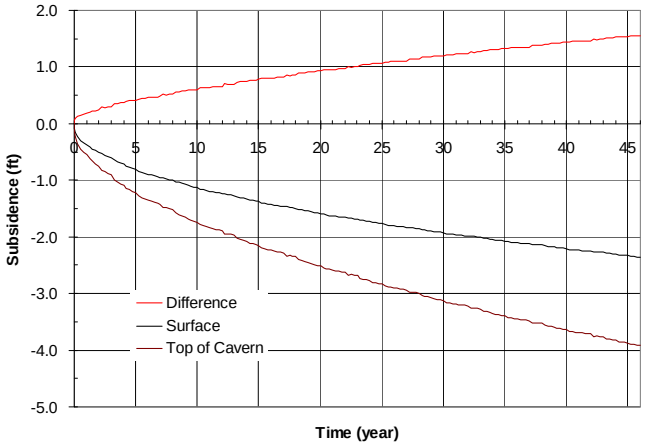

Fig. G-8. 7: Predicted difference between vertical displacement of the top of the central cavern (Cavern 1) and the surface above the cavern as a function of time.

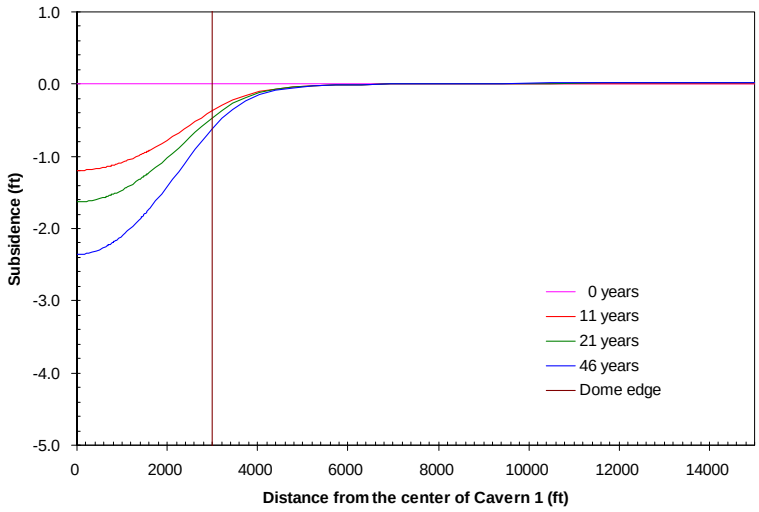

Fig. G-8. 8: Predicted subsidence on the surface from model center to edge with time.

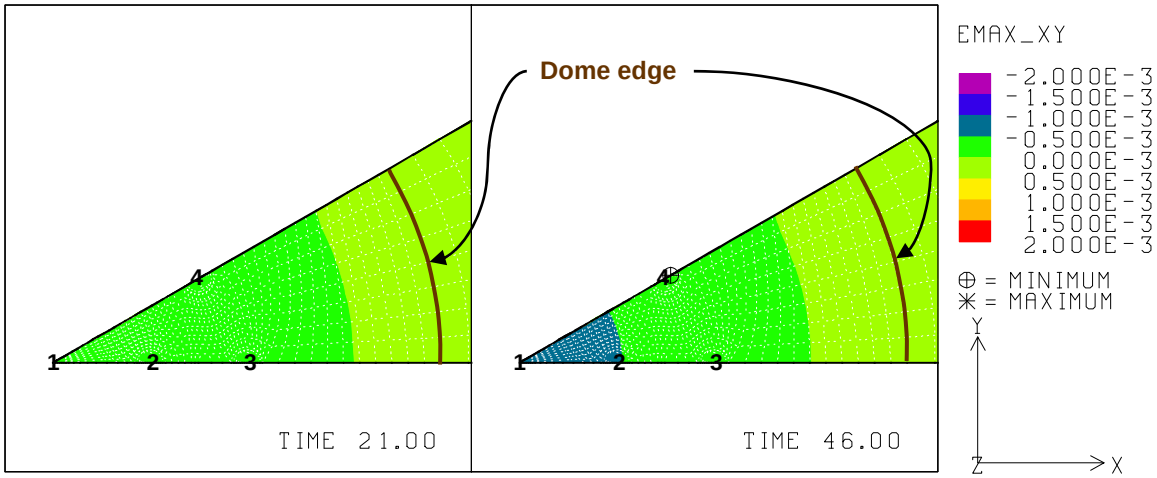

Fig. G-8. 9: Predicted radial surface strains at 21 years and 46 years (E_{CR}=1.0 GPa).

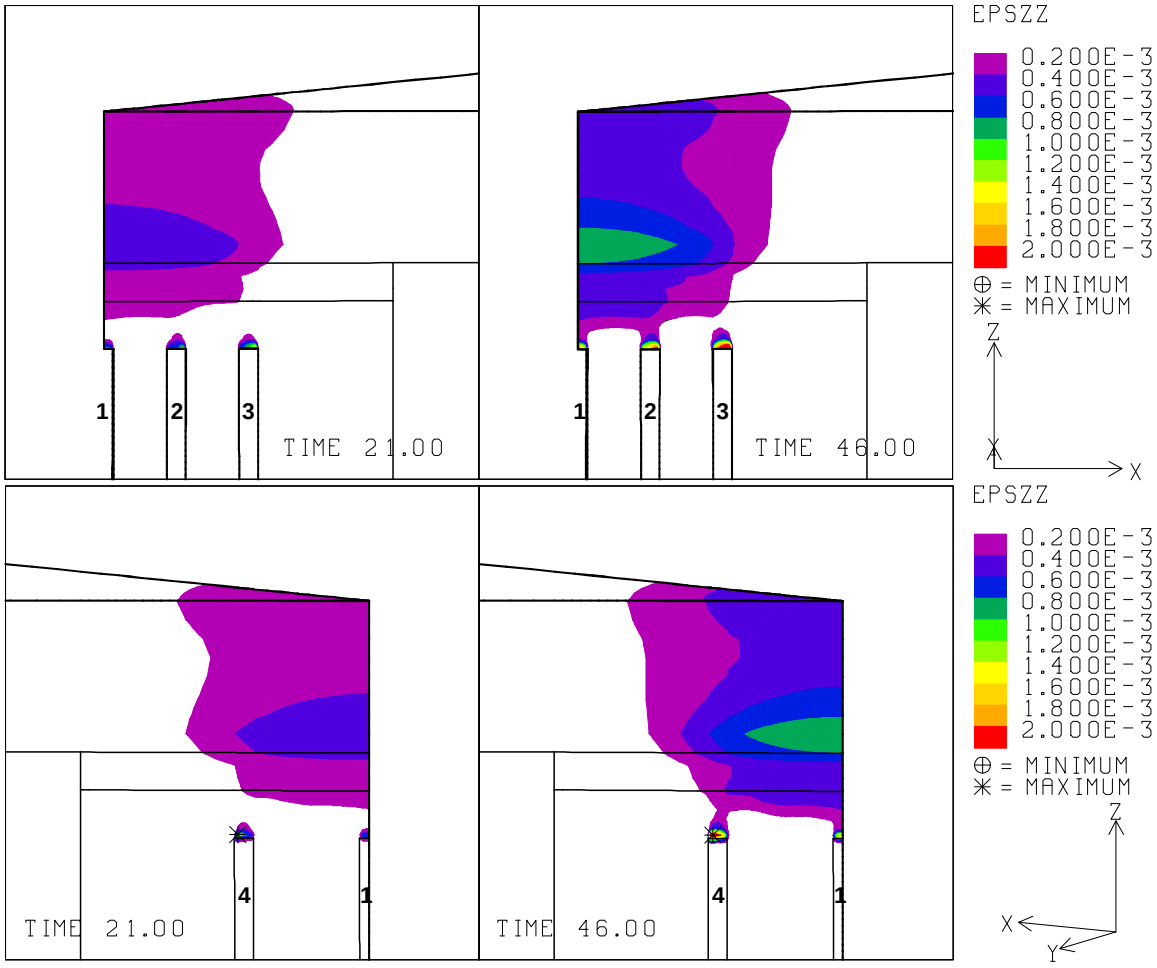

Fig. G-8. 10: Vertical strains around the roof of caverns at 21 years and 46 years (E_{CR}=1.0 GPa).

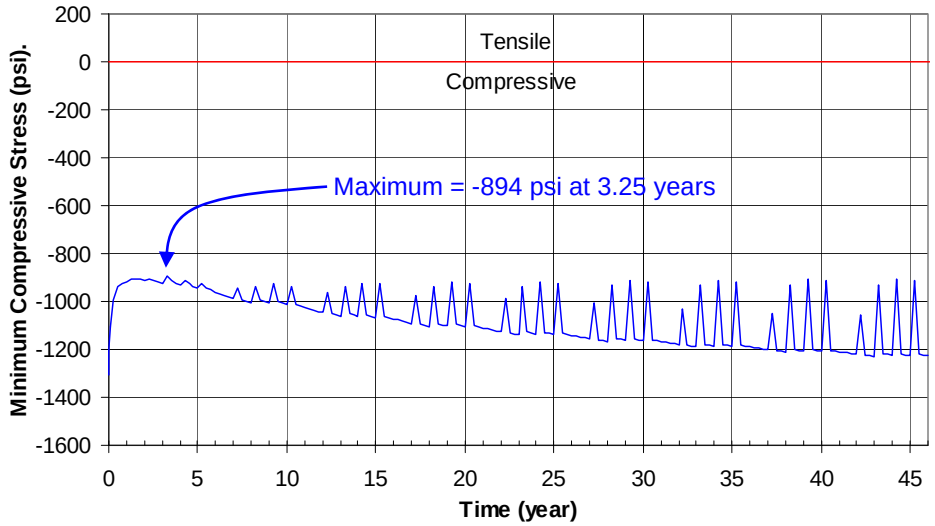

Fig. G-8. 11: Predicted minimum compressive stress history in the salt dome (E_{CR}=1.0 GPa).

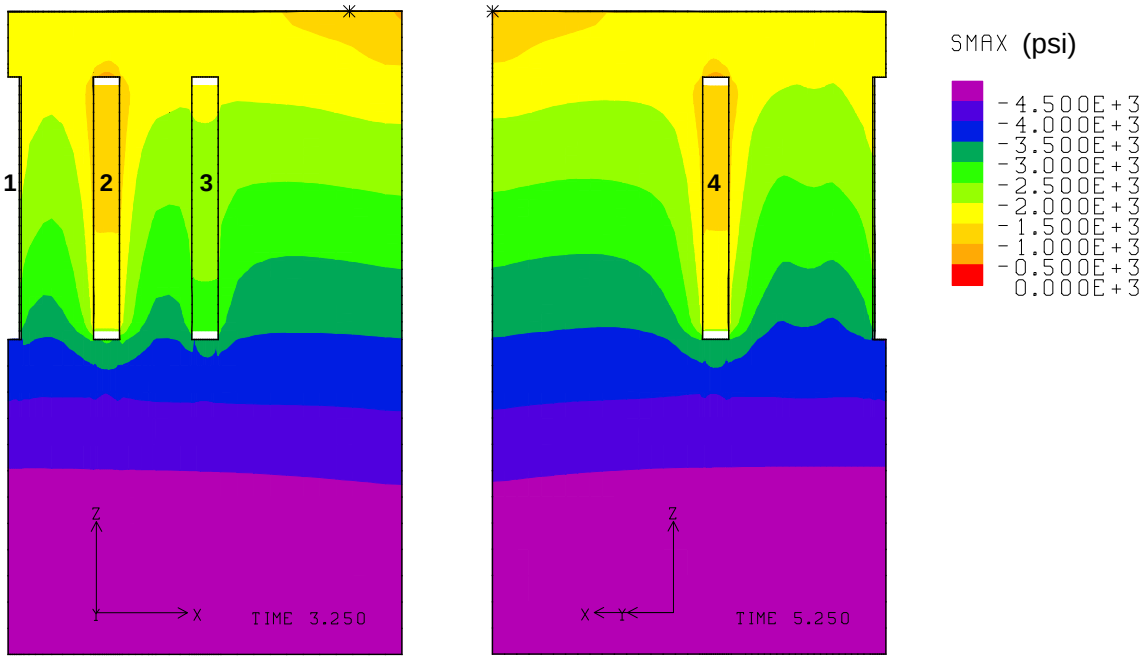

Fig. G-8. 12: Compressive stress contours around the caverns during workover of Cavern 3 and Cavern 4 at 3.25 years and 5.25 years, respectively (E_{CR}=1.0 GPa).

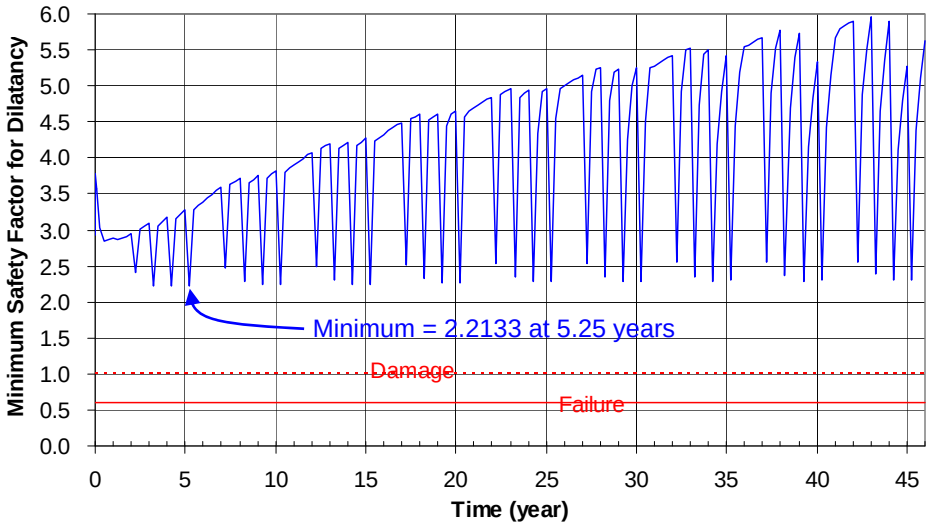

Fig. G-8. 13: Predicted minimum safety factor history against dilatant damage (E_{CR}=1.0 GPa).

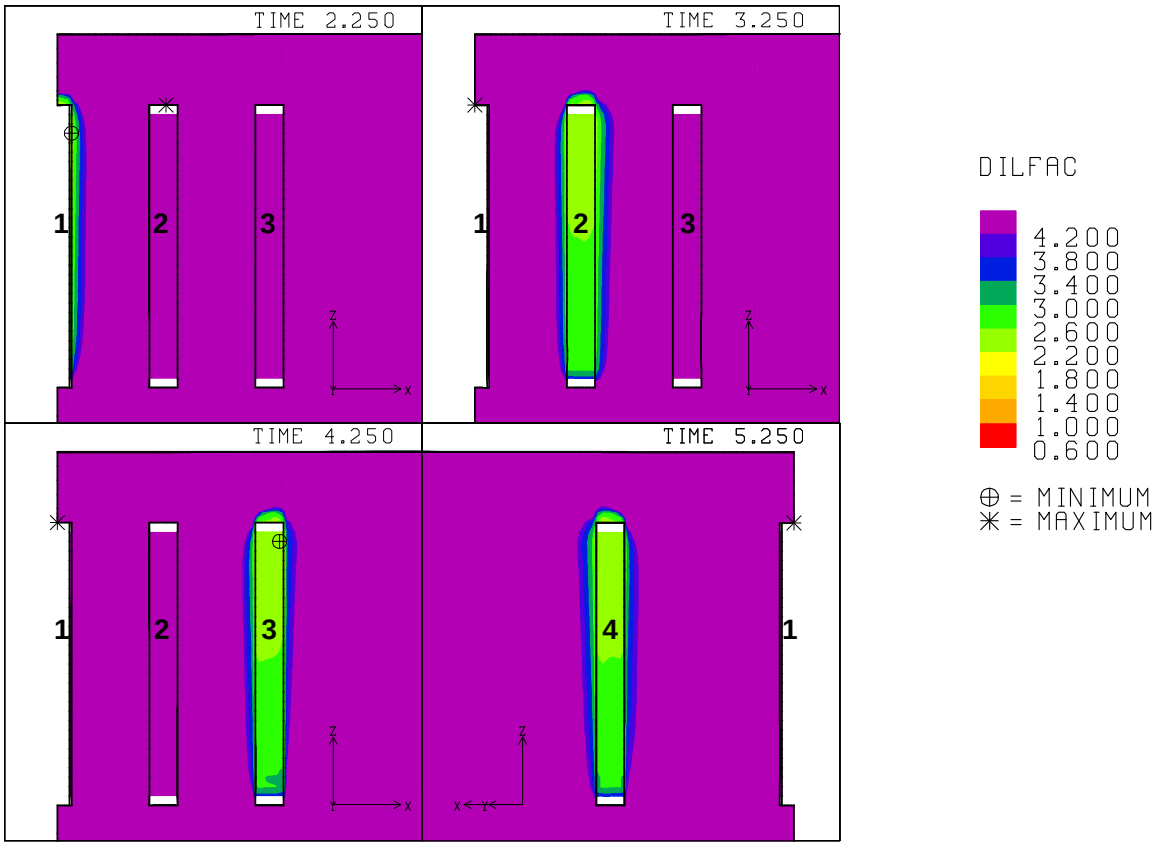

Fig. G-8. 14: Safety factor contours against dilatant damage around the caverns during workover of Caverns 1, 2, 3 and 4 at 2.25 years, 3.25 years, 4.25 years and 5.25 years, respectively (E_{CR}=1.0 GPa).

G-9. Elastic Modulus of Caprock, E_{CR} = 20 GPa

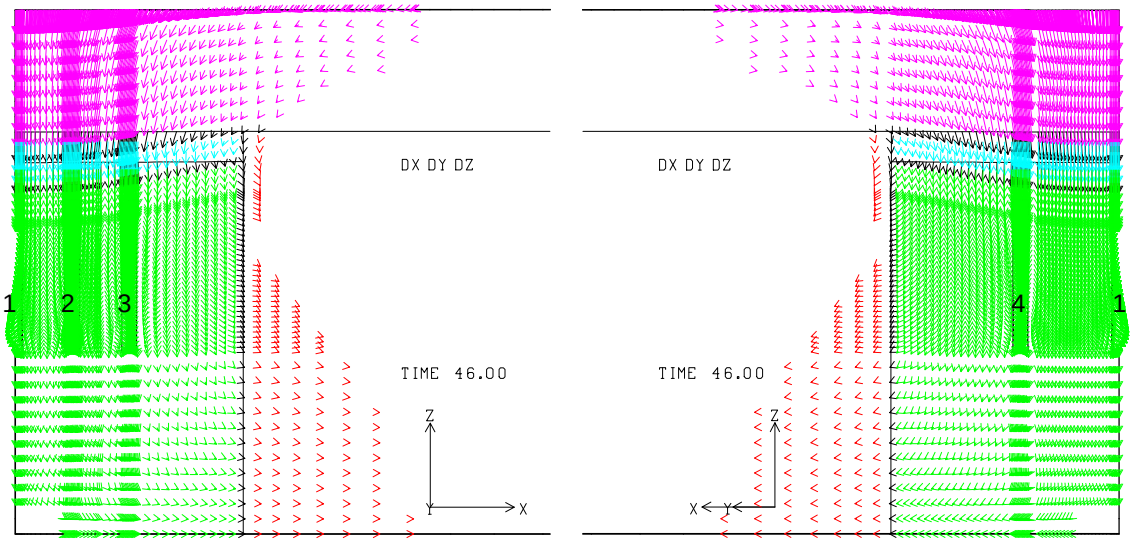

Fig. G-9. 1: Displacement vectors around the caverns at 46 years (E_{CR}=20 GPa).

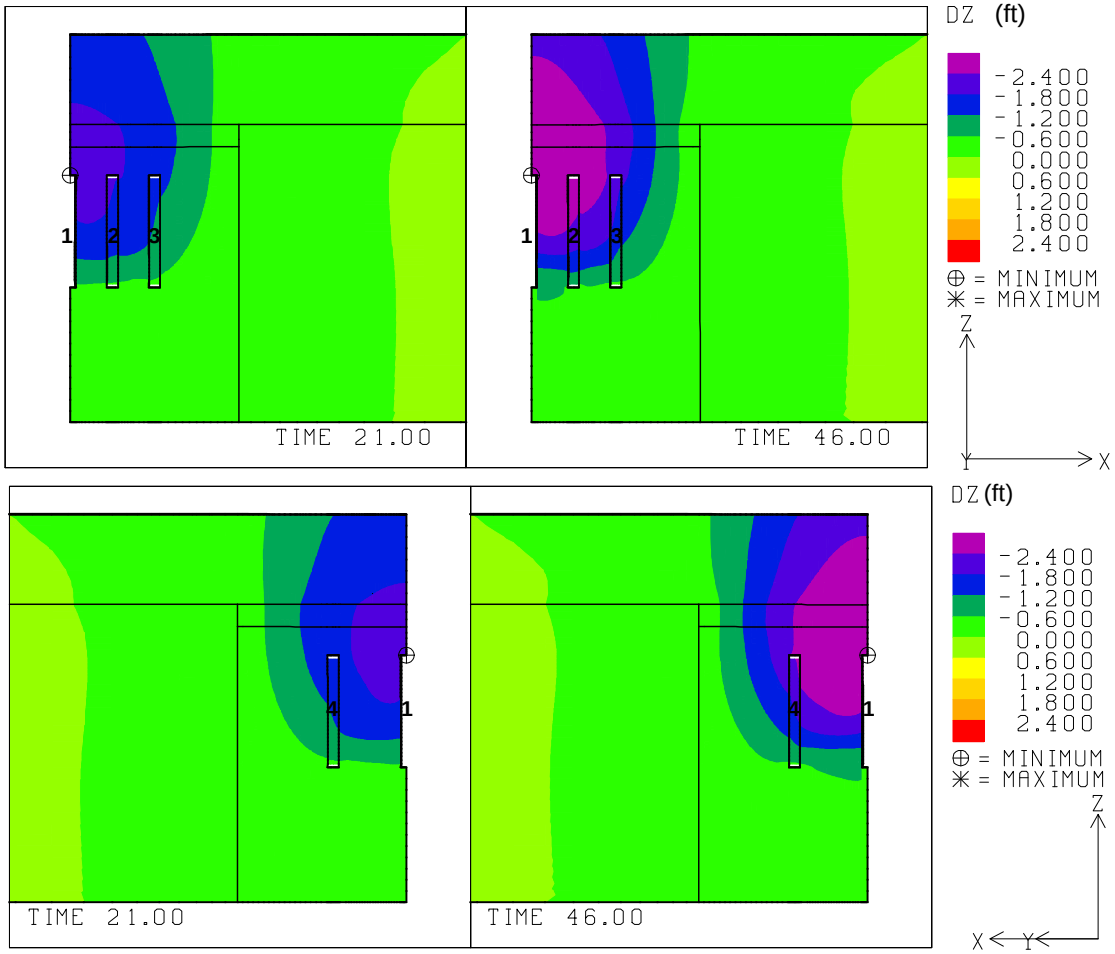

Fig. G-9. 2: Vertical displacement contours around the caverns at 21 and 46 years (E_{CR}=20 GPa).

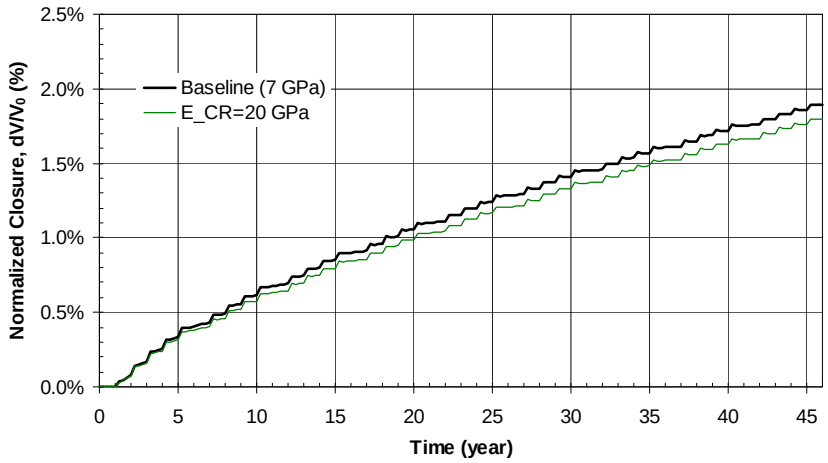

Fig. G-9. 3: Predicted total volumetric closure normalized to initial overall storage volume for the 19 SPR caverns (E_{CR}=20 GPa).

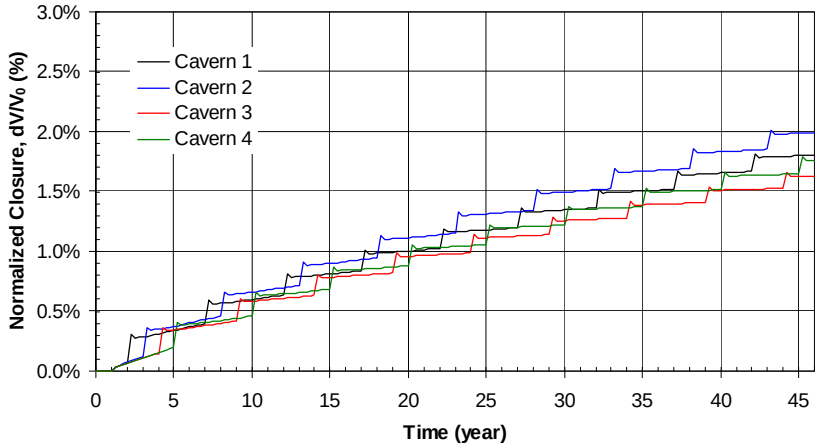

Fig. G-9. 4: Predicted volumetric closure normalized to each initial SPR cavern volume (E_{CR}=20 GPa).

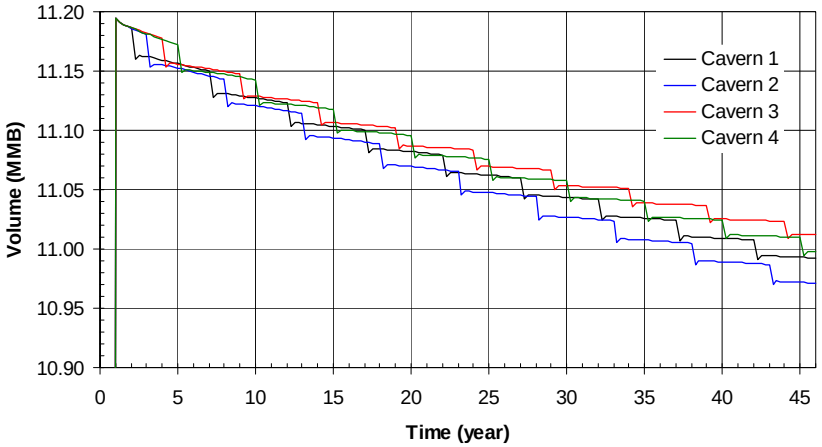

Fig. G-9. 5: Predicted volume change of each SPR cavern due to salt creep closure over time (E_{CR}=20 GPa).

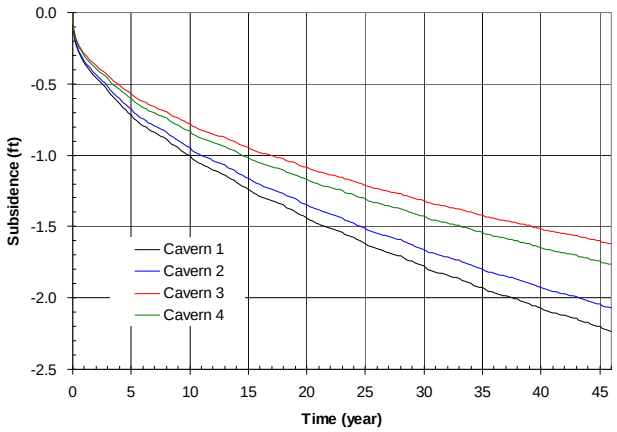

Fig. G-9. 6: Predicted subsidence on the surface above the center of SPR caverns (E_{CR}=20 GPa).

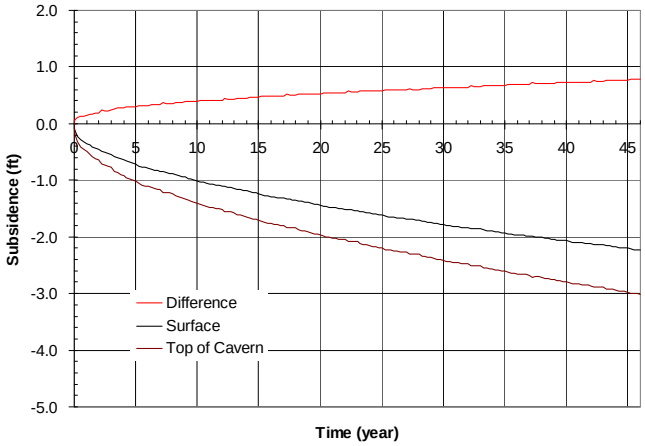

Fig. G-9. 7: Predicted difference between vertical displacement of the top of the central cavern (Cavern 1) and the surface above the cavern as a function of time.

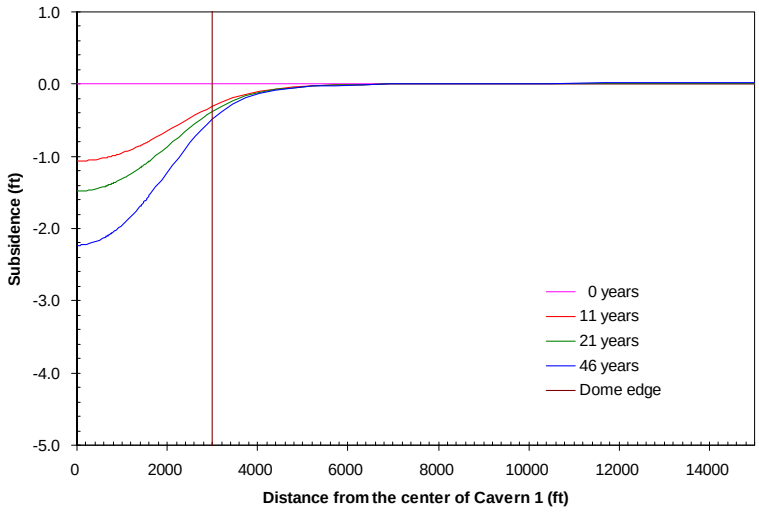

Fig. G-9. 8: Predicted subsidence on the surface from model center to edge with time.

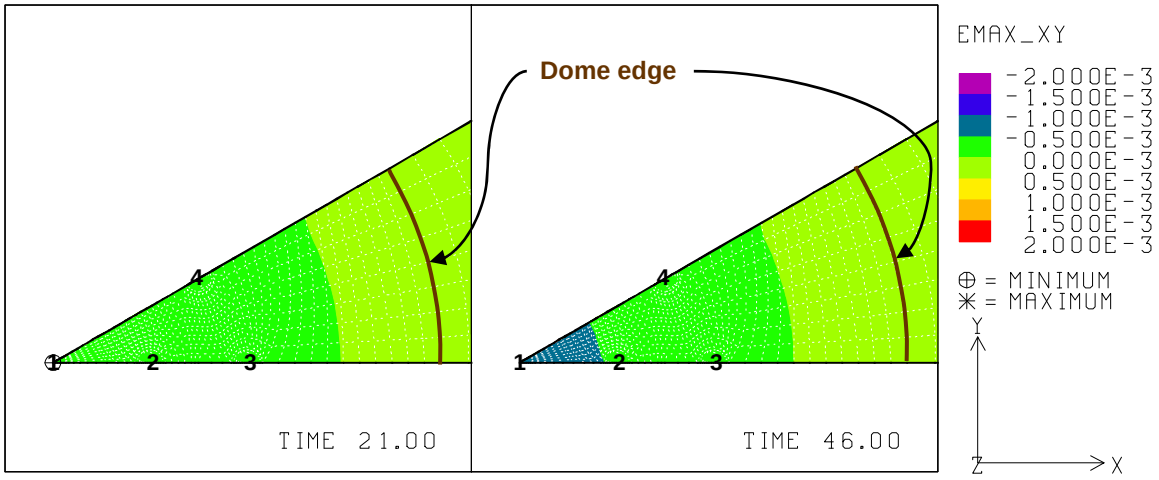

Fig. G-9. 9: Predicted radial surface strains at 21 years and 46 years (E_{CR}=20 GPa).

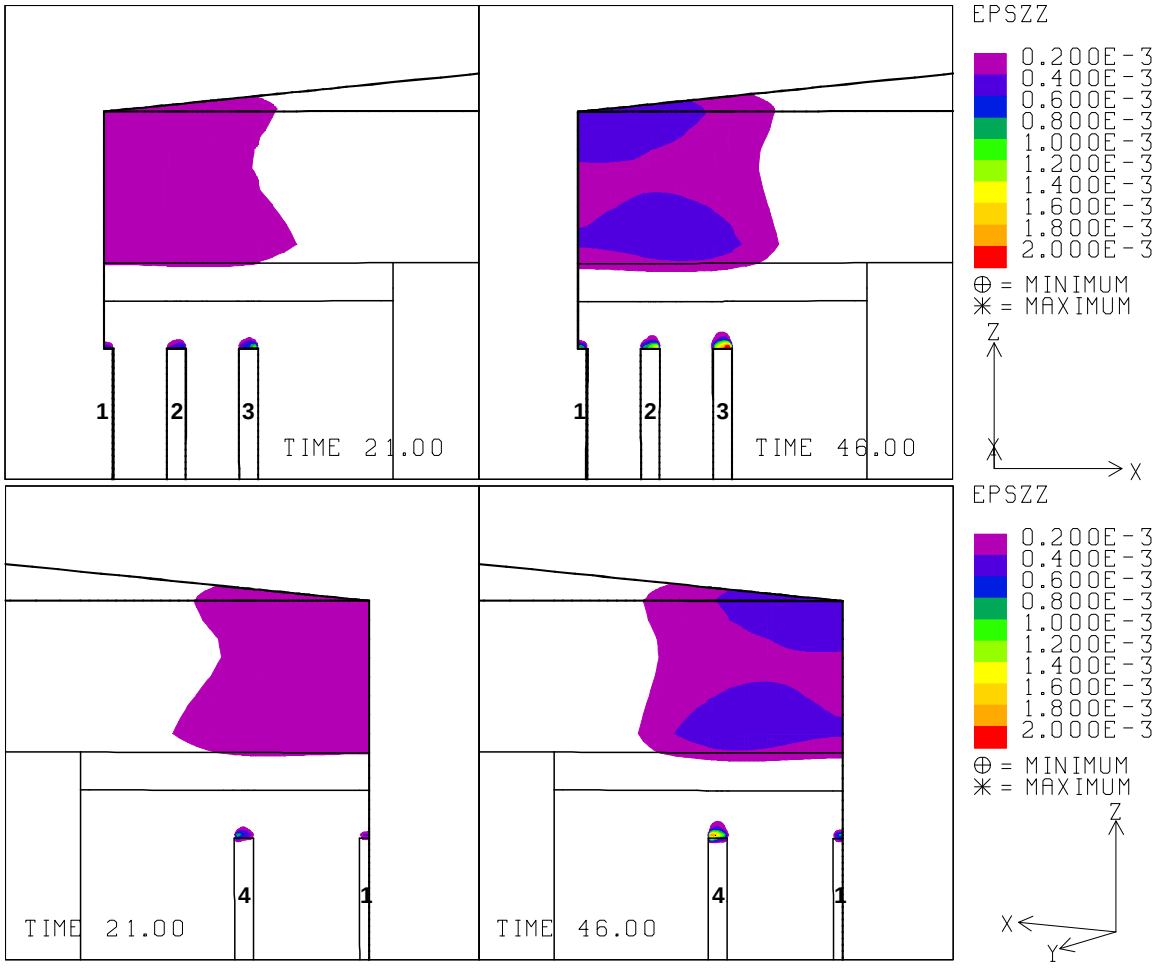

Fig. G-9. 10: Vertical strains around the roof of caverns at 21 years and 46 years (E_{CR}=20 GPa).

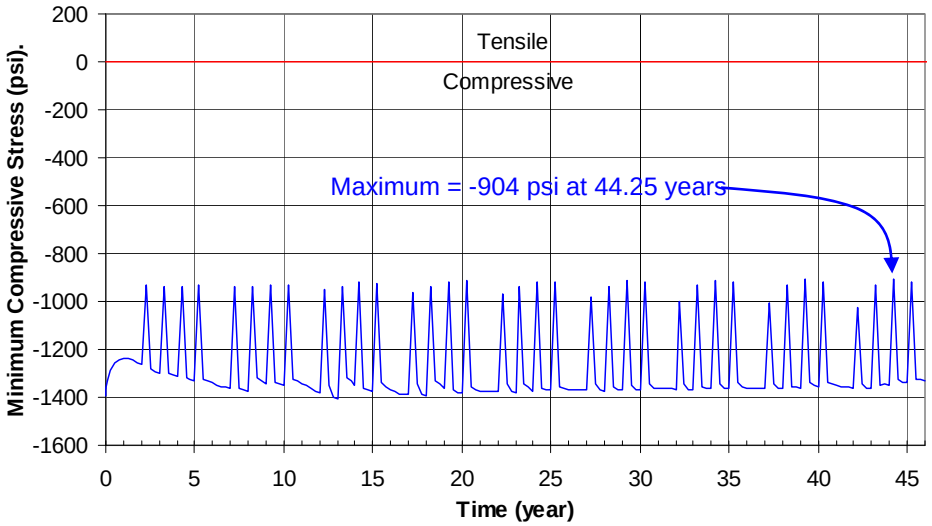

Fig. G-9. 11: Predicted minimum compressive stress history in the salt dome (E_{CR}=20 GPa).

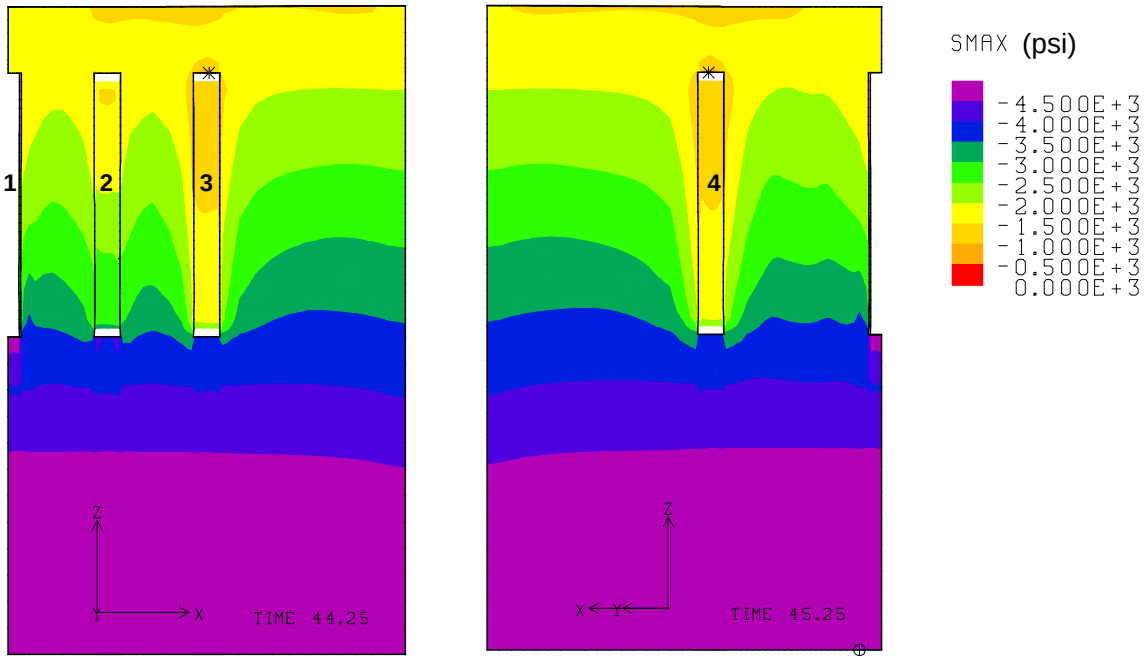

Fig. G-9. 12: Compressive stress contours around the caverns during workover of Cavern 3 and Cavern 4 at 44.25 years and 45.25 years, respectively (E_{CR}=20 GPa).

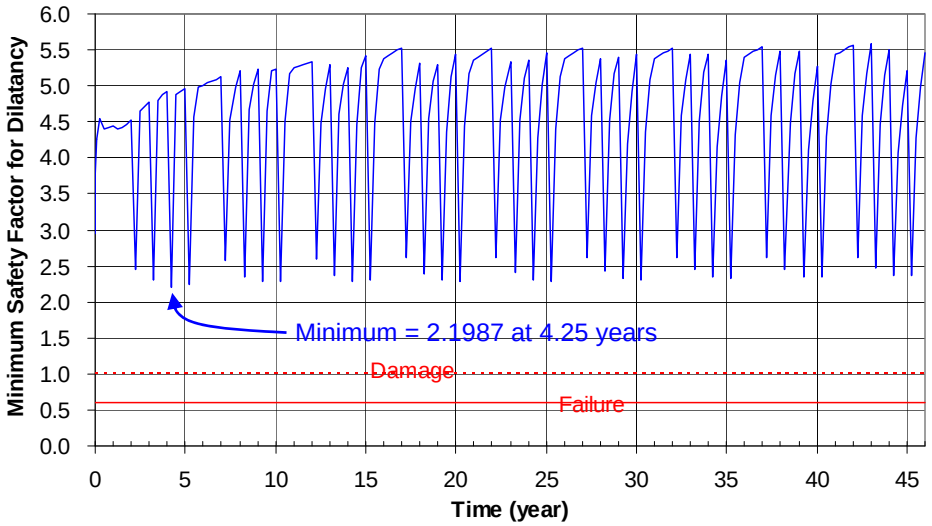

Fig. G-9. 13: Predicted minimum safety factor history against dilatant damage (E_{CR}=20 GPa).

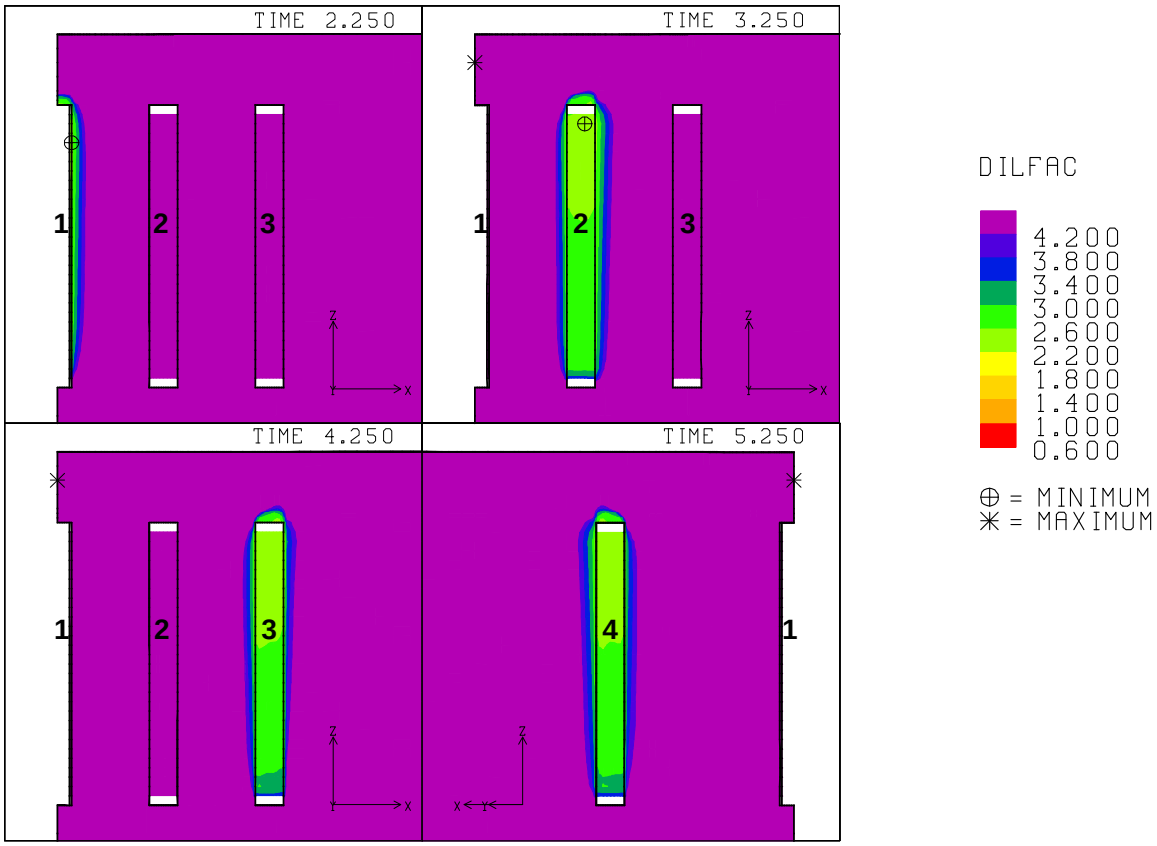

Fig. G-9. 14: Safety factor contours against dilatant damage around the caverns during workover of Caverns 1, 2, 3 and 4 at 2.25 years, 3.25 years, 4.25 years and 5.25 years, respectively (E_{CR}=20 GPa).

G-10. Elastic Modulus of Caprock, E_{CR} = 100 GPa

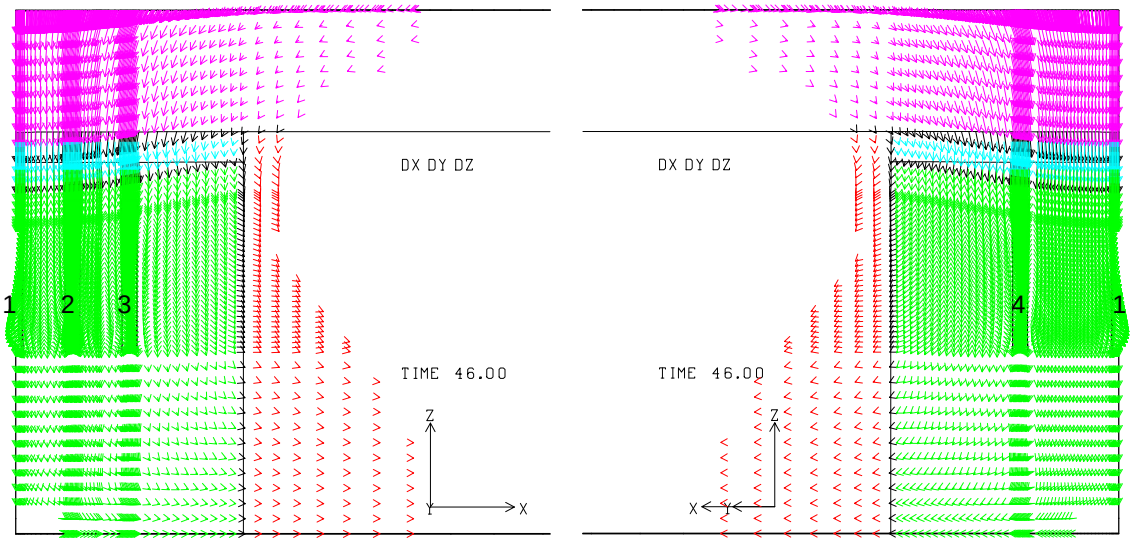

Fig. G-10. 1: Displacement vectors around the caverns at 46 years (E_{CR}=100 GPa).

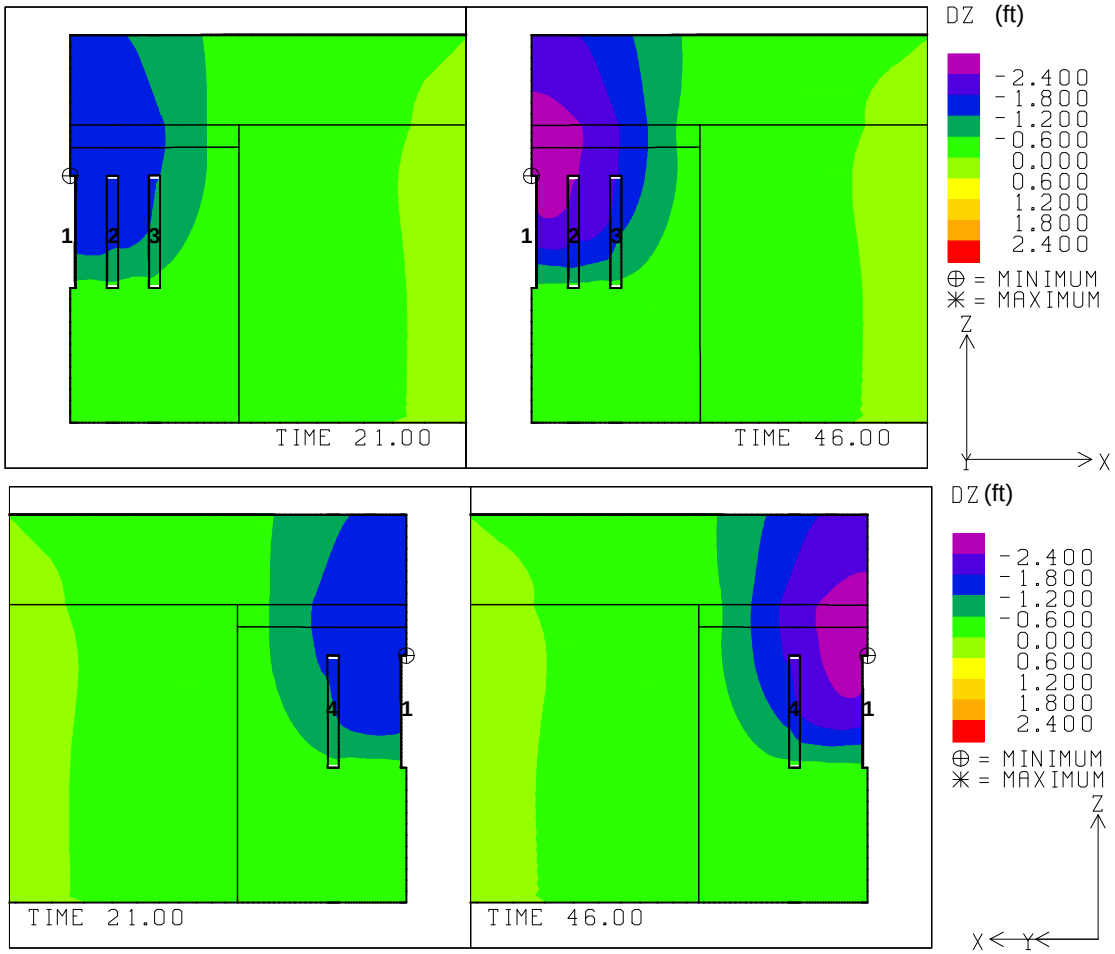

Fig. G-10. 2: Vertical displacement contours around the caverns at 21 and 46 years (E_{CR}=100 GPa).

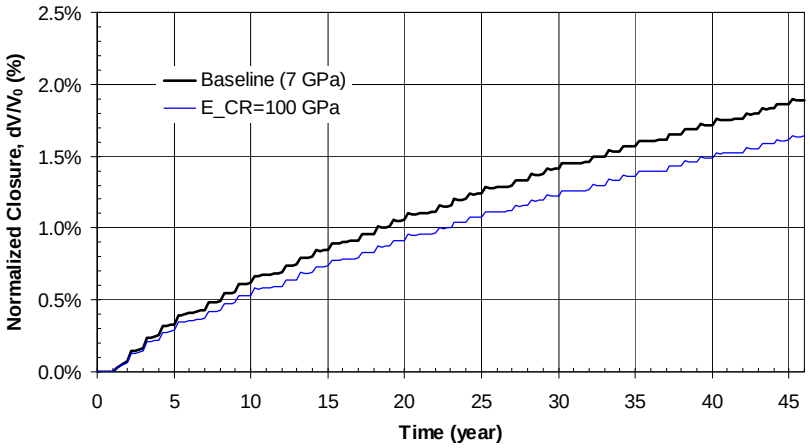

Fig. G-10. 3: Predicted total volumetric closure normalized to initial overall storage volume for the 19 SPR caverns (E_{CR}=100 GPa).

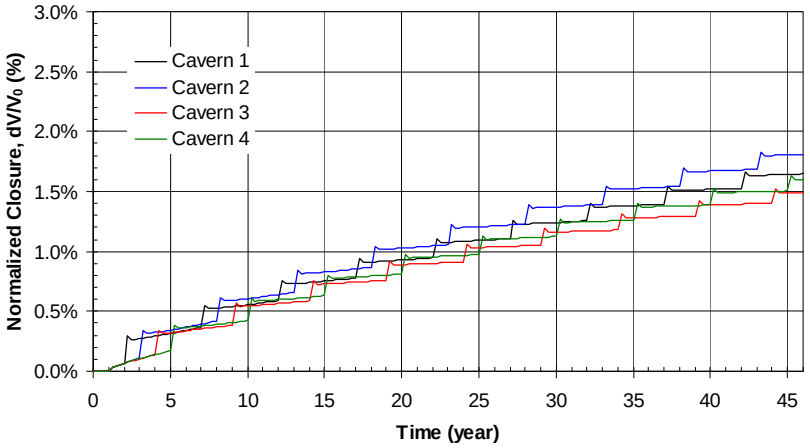

Fig. G-10. 4: Predicted volumetric closure normalized to each initial SPR cavern volume (E_{CR}=100 GPa).

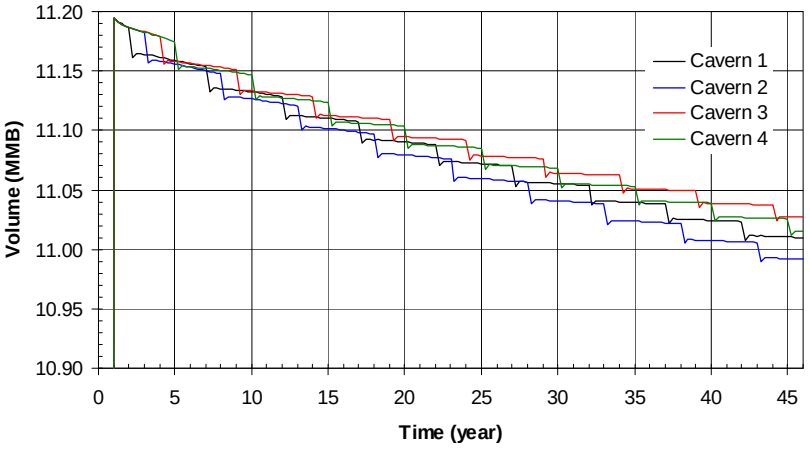

Fig. G-10. 5: Predicted volume change of each SPR cavern due to salt creep closure over time (E_{CR}=100 GPa).

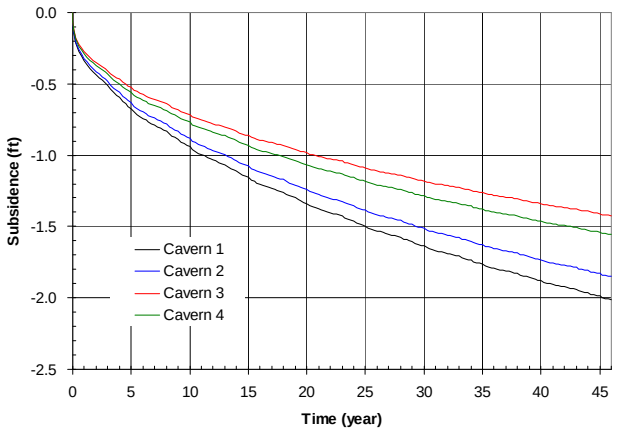

Fig. G-10. 6: Predicted subsidence on the surface above the center of SPR caverns (E_{CR}=100 GPa).

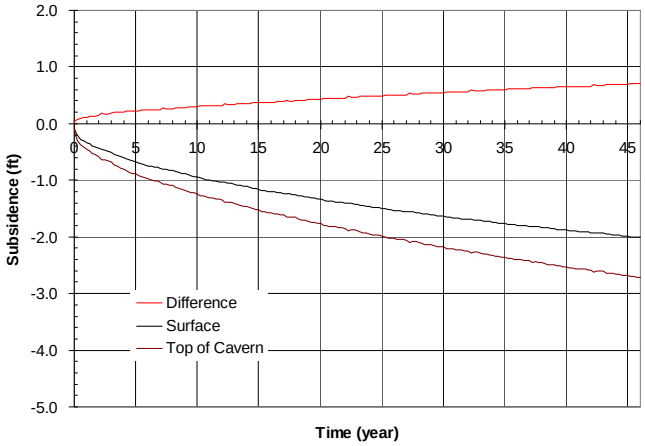

Fig. G-10. 7: Predicted difference between vertical displacement of the top of the central cavern (Cavern 1) and the surface above the cavern as a function of time.

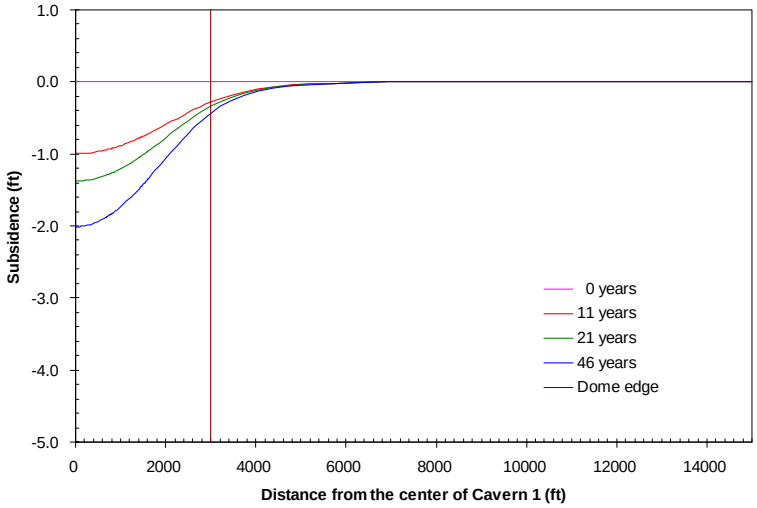

Fig. G-10. 8: Predicted subsidence on the surface from model center to edge with time.

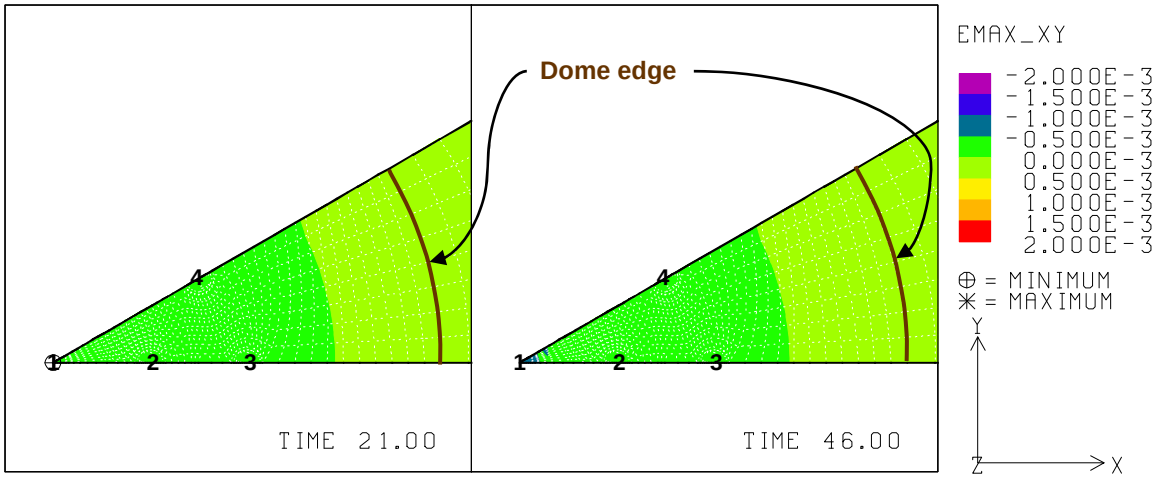

Fig. G-10. 9: Predicted radial surface strains at 21 years and 46 years (E_{CR}=100 GPa).

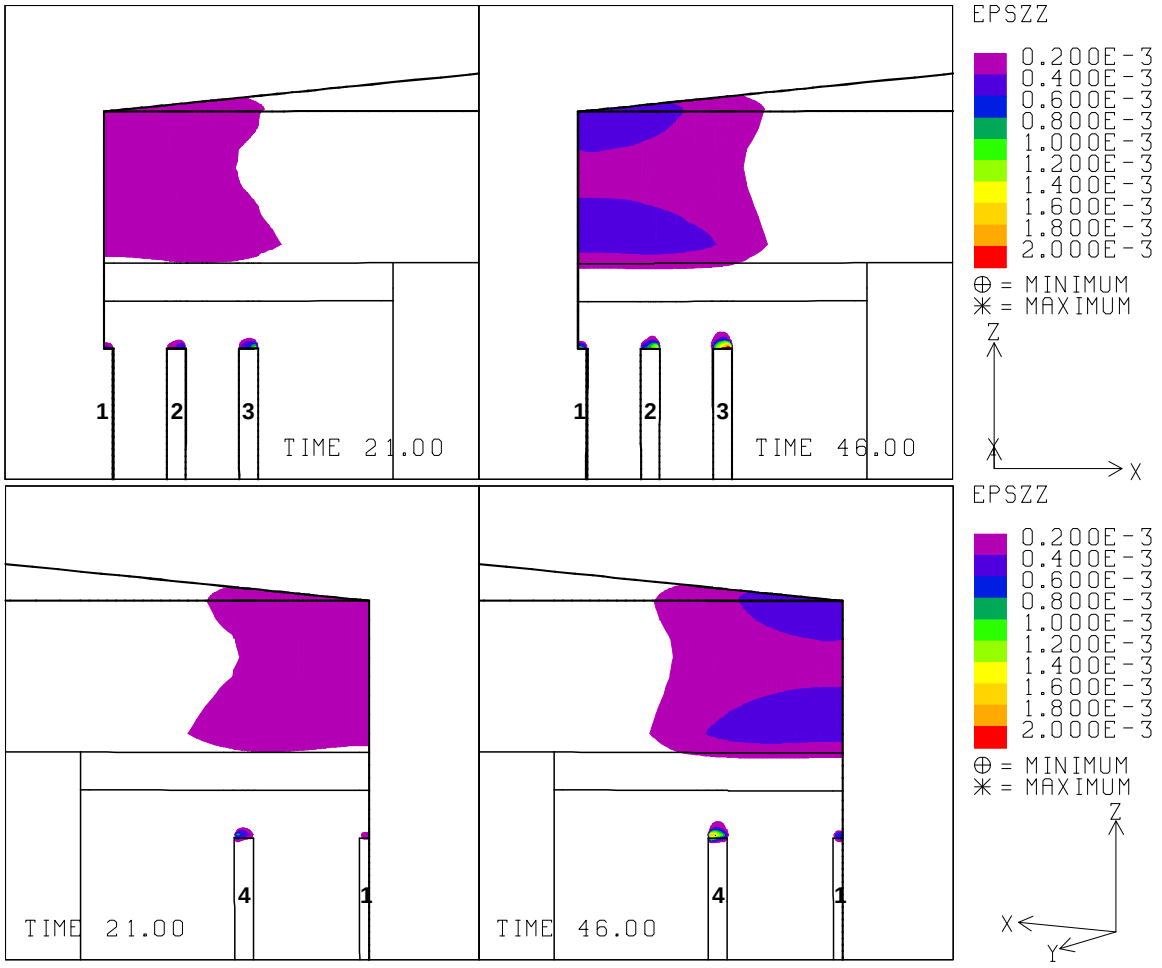

Fig. G-10. 10: Vertical strains around the roof of caverns at 21 years and 46 years (E_{CR}=100 GPa).

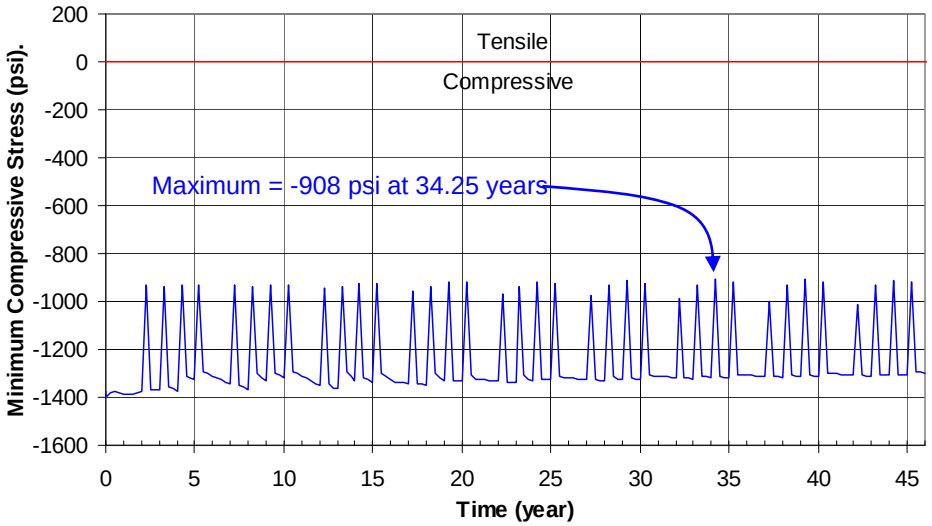

Fig. G-10. 11: Predicted minimum compressive stress history in the salt dome (E_{CR}=100 GPa).

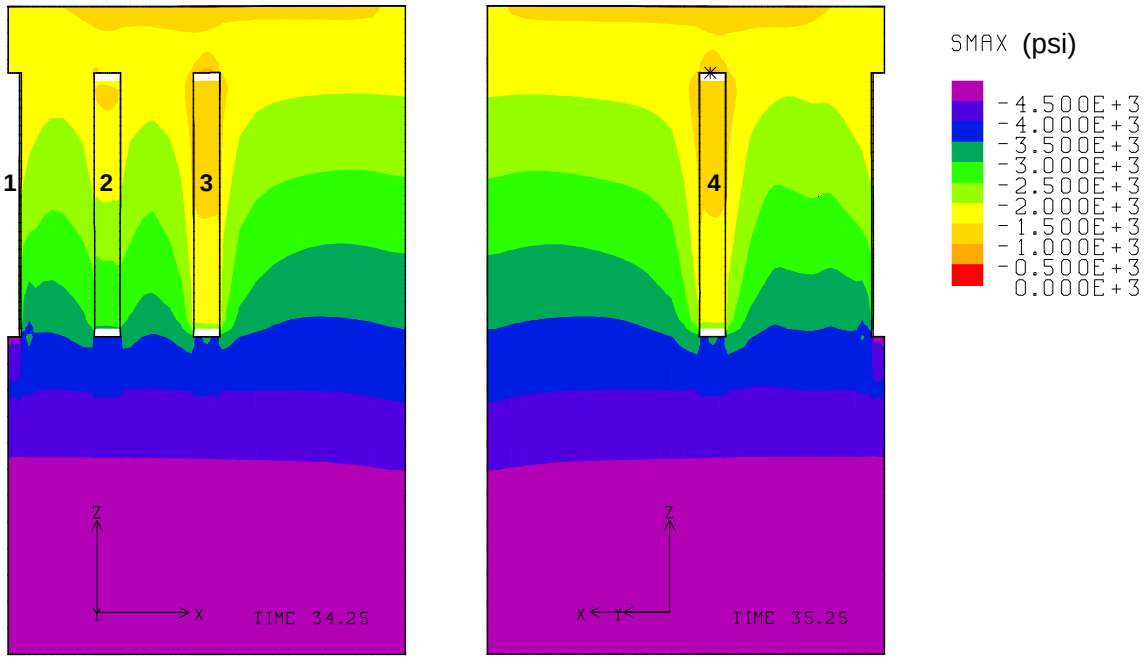

Fig. G-10. 12: Compressive stress contours around the caverns during workover of Cavern 3 and Cavern 4 at 34.25 years and 35.25 years, respectively (E_{CR}=100 GPa).

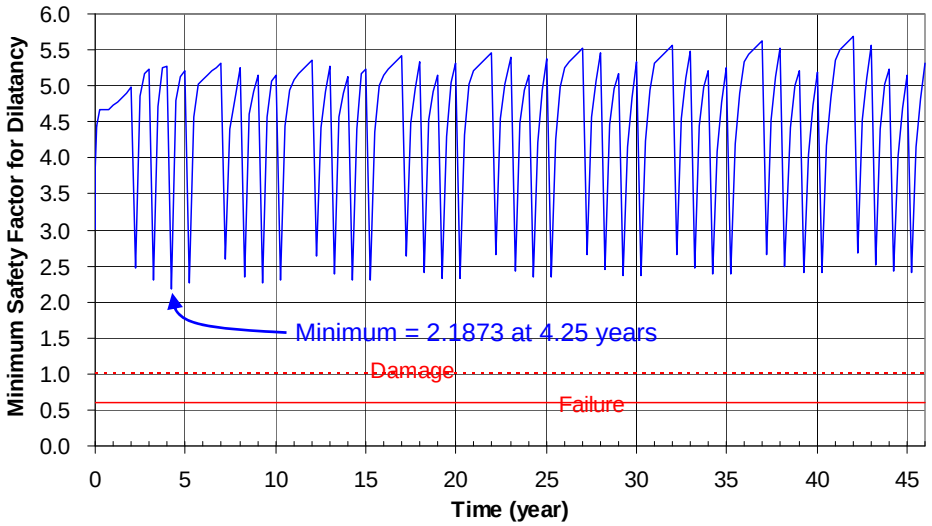

Fig. G-10. 13: Predicted minimum safety factor history against dilatant damage (E_{CR}=100 GPa).

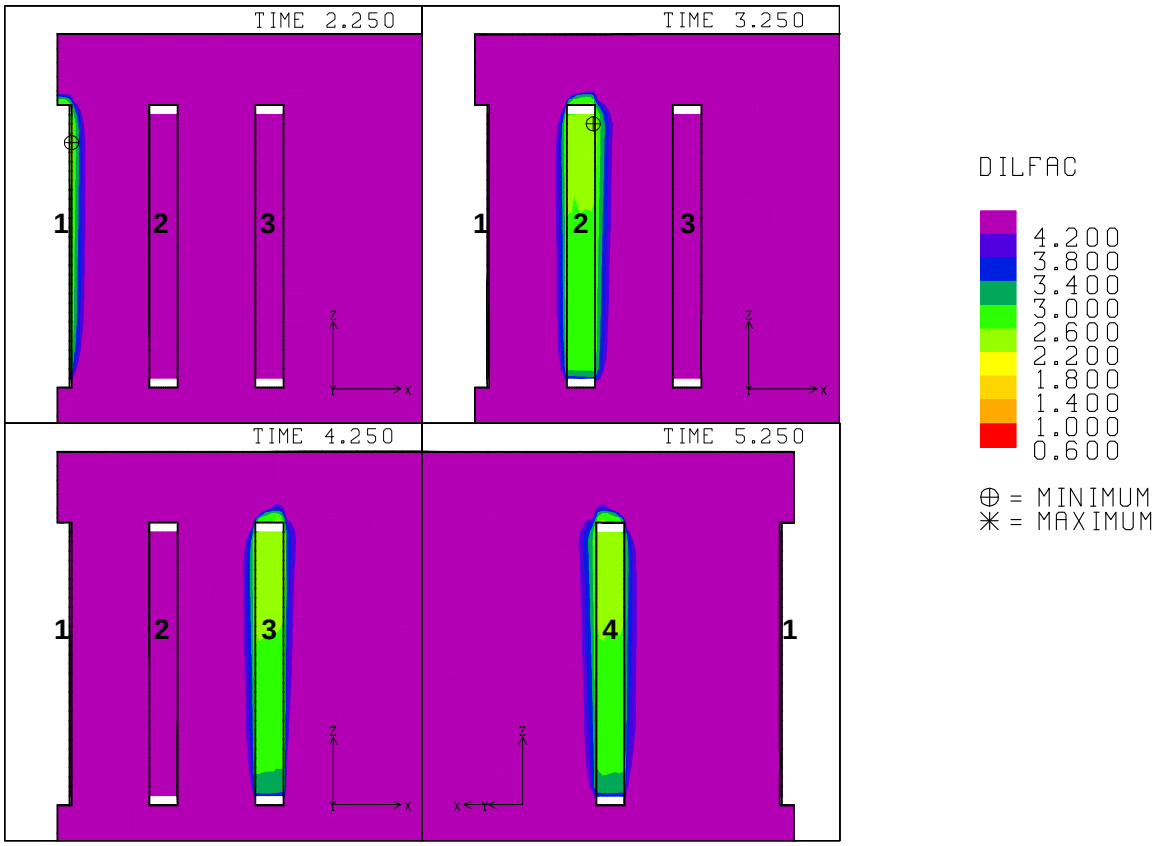

Fig. G-10. 14: Safety factor contours against dilatant damage around the caverns during workover of Caverns 1, 2, 3 and 4 at 2.25 years, 3.25 years, 4.25 years and 5.25 years, respectively (E_{CR}=100 GPa).

G-11. Elastic Modulus of Surrounding Rock, E_{SR} = 4.0 GPa

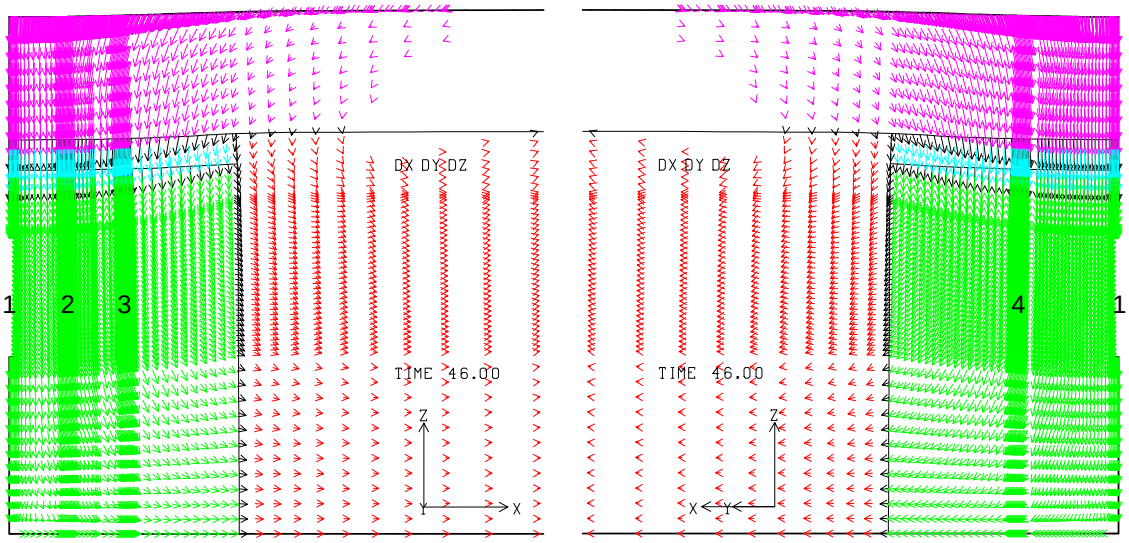

Fig. G-11. 1: Displacement vectors around the caverns at 46 years (E_{SR}=4.0 GPa).

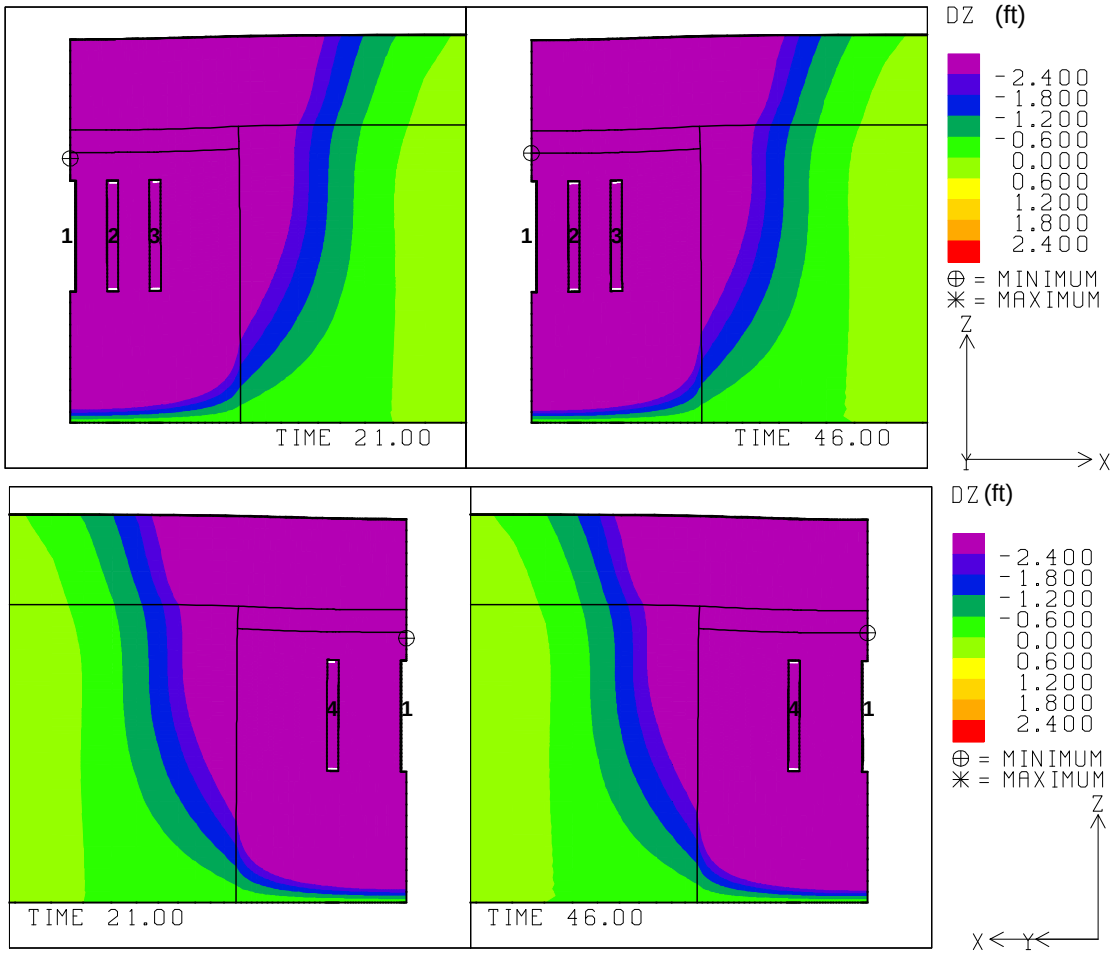

Fig. G-11. 2: Vertical displacement contours around the caverns at 21 and 46 years (E_{SR}=4.0 GPa).

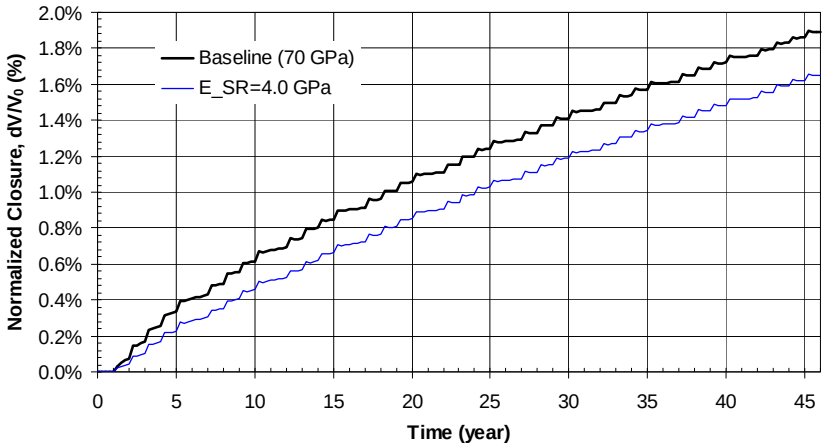

Fig. G-11. 3: Predicted total volumetric closure normalized to initial overall storage volume for the 19 SPR caverns (E_{SR}=4.0 GPa).

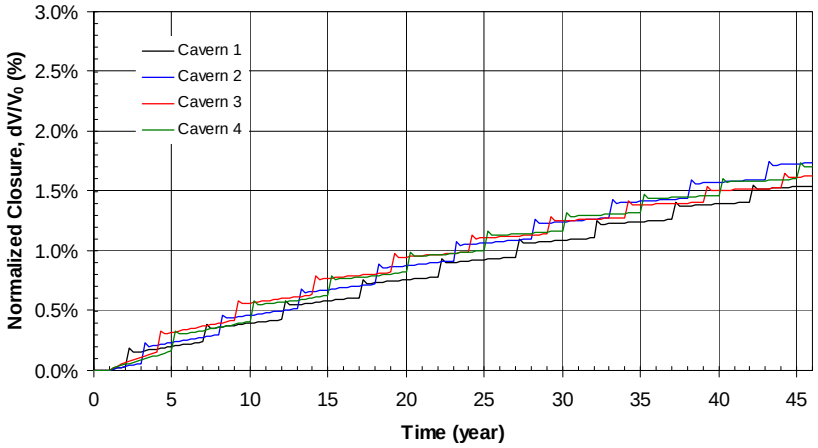

Fig. G-11. 4: Predicted volumetric closure normalized to each initial SPR cavern volume (E_{SR}=4.0 GPa).

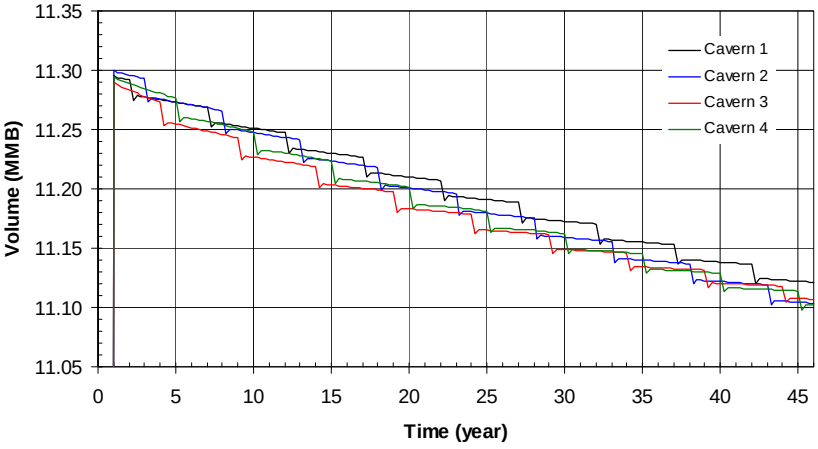

Fig. G-11. 5: Predicted volume change of each SPR cavern due to salt creep closure over time (E_{SR}=4.0 GPa).

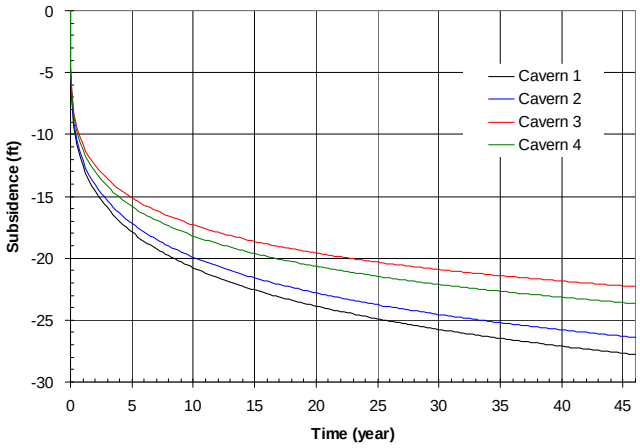

Fig. G-11. 6: Predicted subsidence on the surface above the center of SPR caverns (E_{SR}=4.0 GPa).

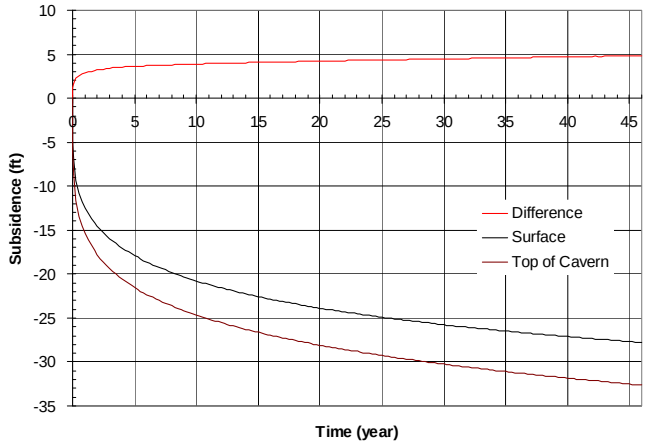

Fig. G-11. 7: Predicted difference between vertical displacement of the top of the central cavern (Cavern 1) and the surface above the cavern as a function of time.

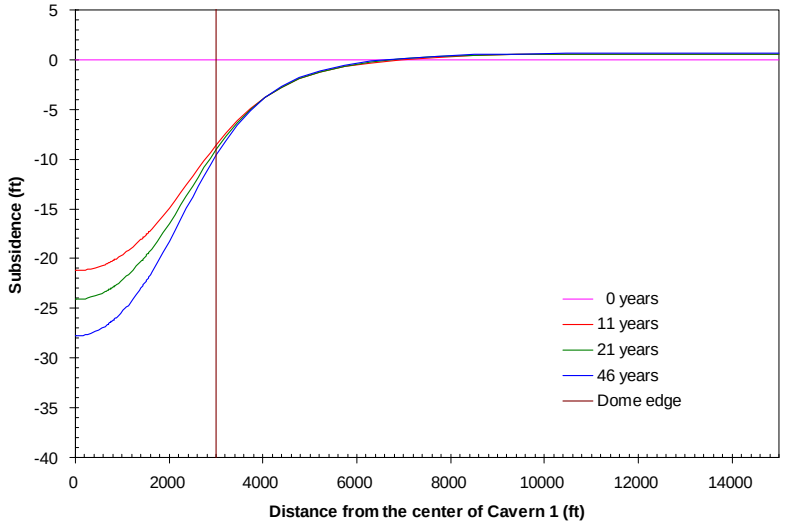

Fig. G-11. 8: Predicted subsidence on the surface from model center to edge with time.

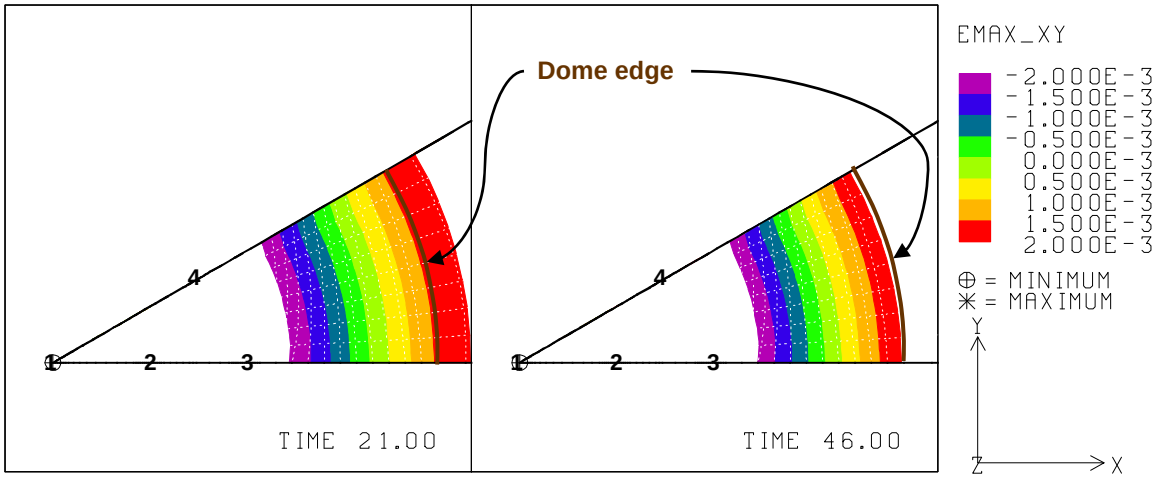

Fig. G-11. 9: Predicted radial surface strains at 21 years and 46 years (E_{SR}=4.0 GPa).

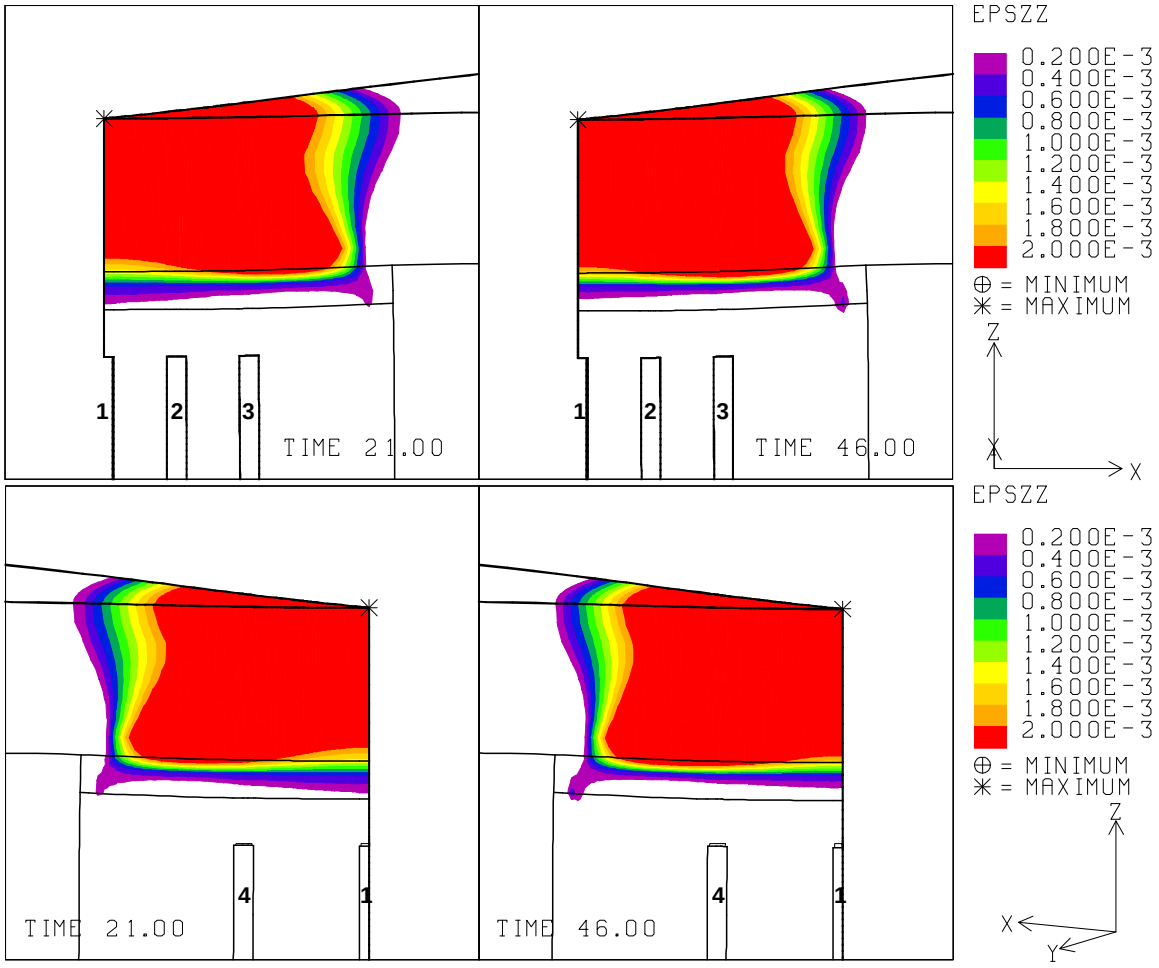

Fig. G-11. 10: Vertical strains around the roof of caverns at 21 years and 46 years (E_{SR}=4.0 GPa).

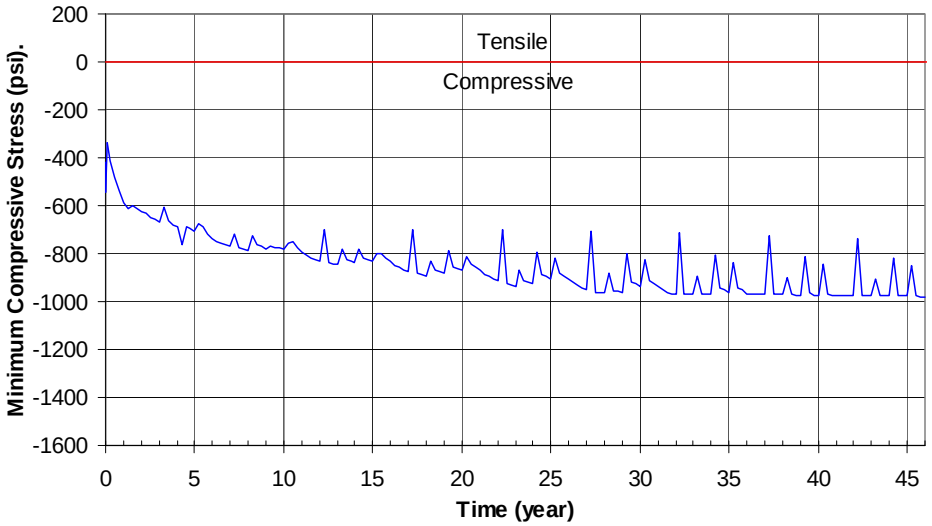

Fig. G-11. 11: Predicted minimum compressive stress history in the salt dome (E_{SR}=4.0 GPa).

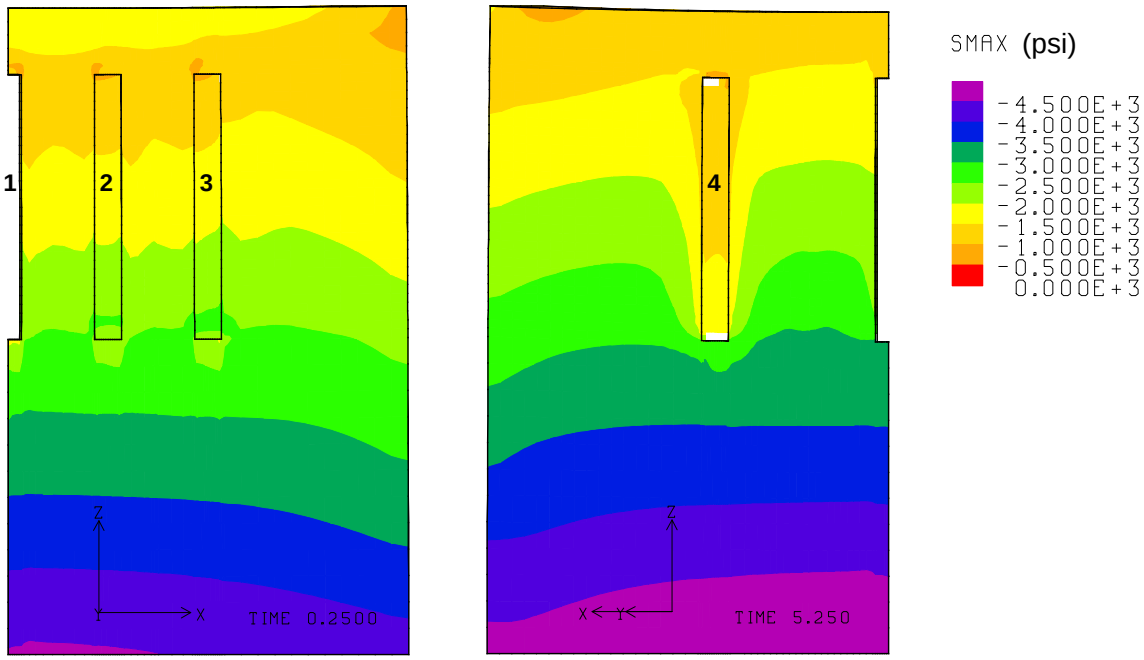

Fig. G-11. 12: Compressive stress contours around the caverns during workover of Cavern 3 and Cavern 4 at 0.25 years and 5.25 years, respectively (E_{SR}=4.0 GPa).

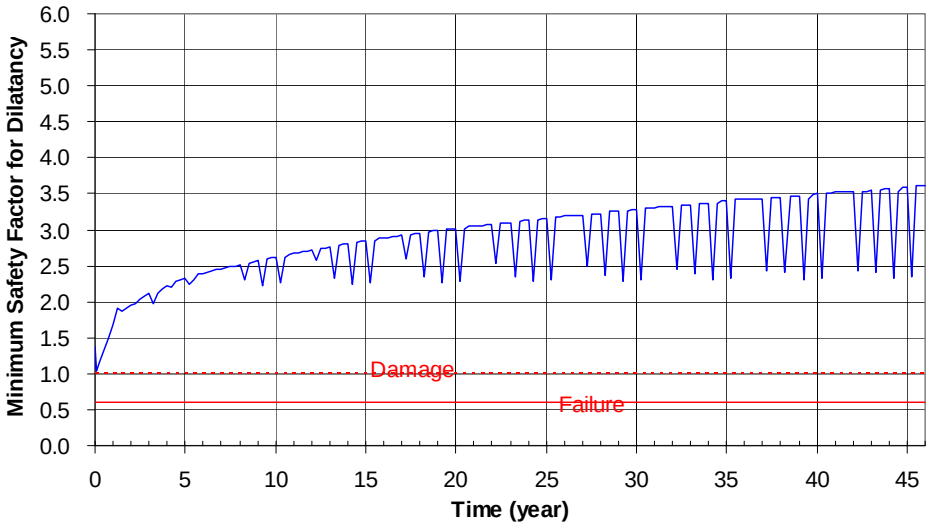

Fig. G-11. 13: Predicted minimum safety factor history against dilatant damage (E_{SR}=4.0 GPa).

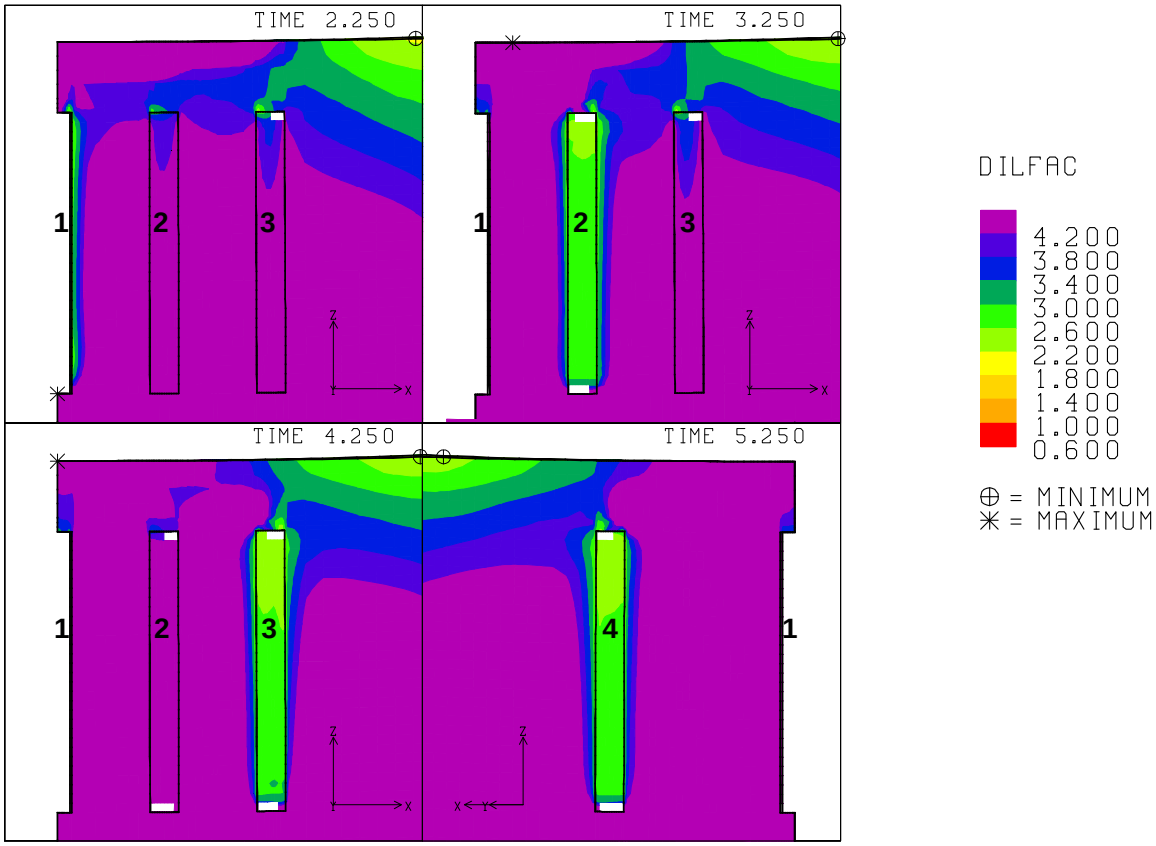

Fig. G-11. 14: Safety factor contours against dilatant damage around the caverns during workover of Caverns 1, 2, 3 and 4 at 2.25 years, 3.25 years, 4.25 years and 5.25 years, respectively (E_{SR}=4.0 GPa).

G-12. Elastic Modulus of Surrounding Rock, E_{SR} = 10.0 GPa

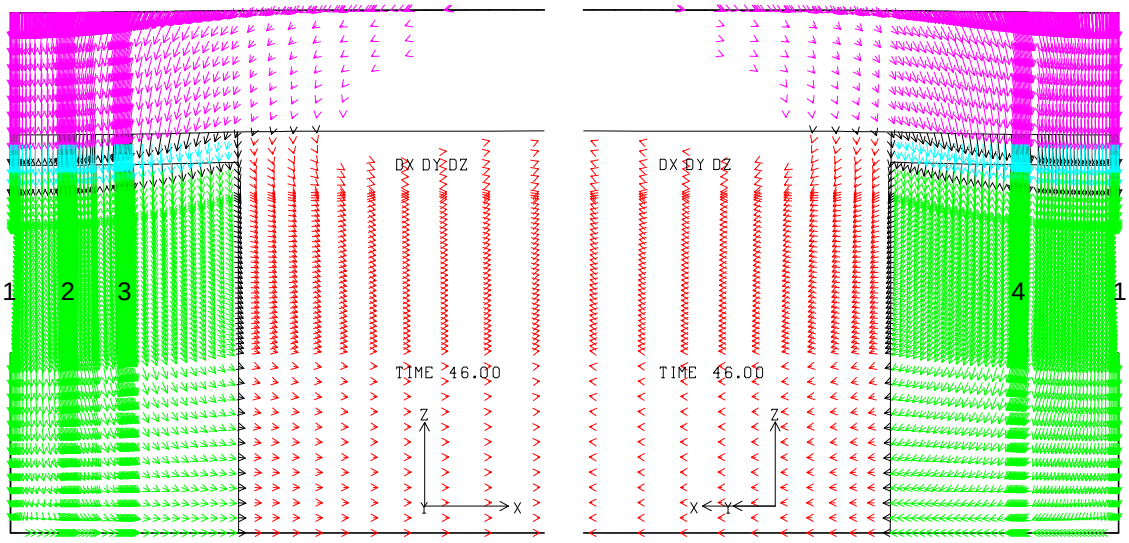

Fig. G-12. 1: Displacement vectors around the caverns at 46 years (E_{SR}=10.0 GPa).

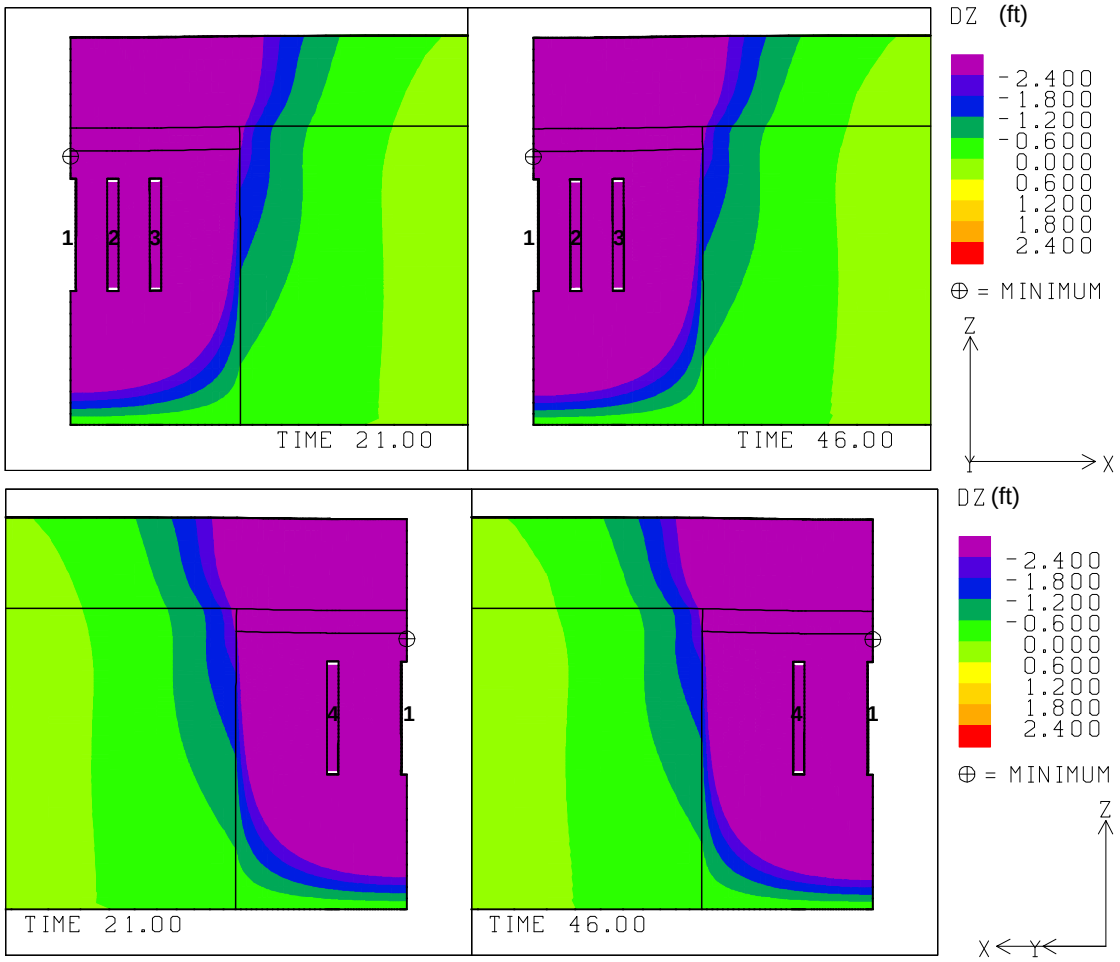

Fig. G-12. 2: Vertical displacement contours around the caverns at 21 and 46 years (E_{SR}=10.0 GPa).

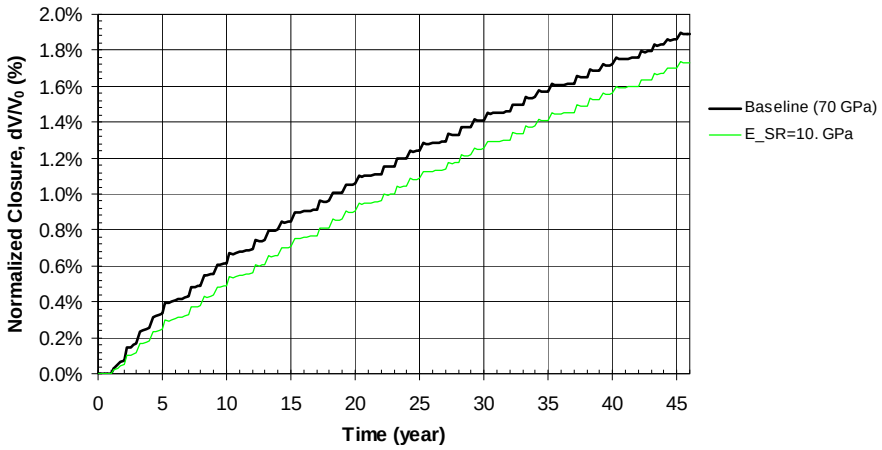

Fig. G-12. 3: Predicted total volumetric closure normalized to initial overall storage volume for the 19 SPR caverns (E_{SR}=10.0 GPa).

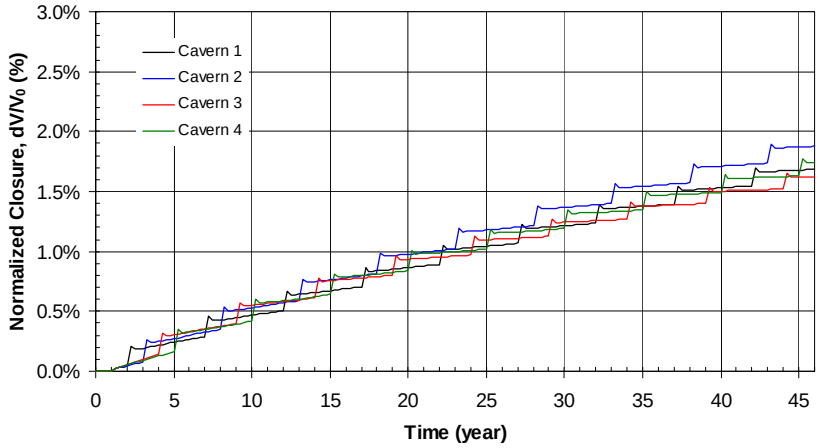

Fig. G-12. 4: Predicted volumetric closure normalized to each initial SPR cavern volume (E_{SR}=10.0 GPa).

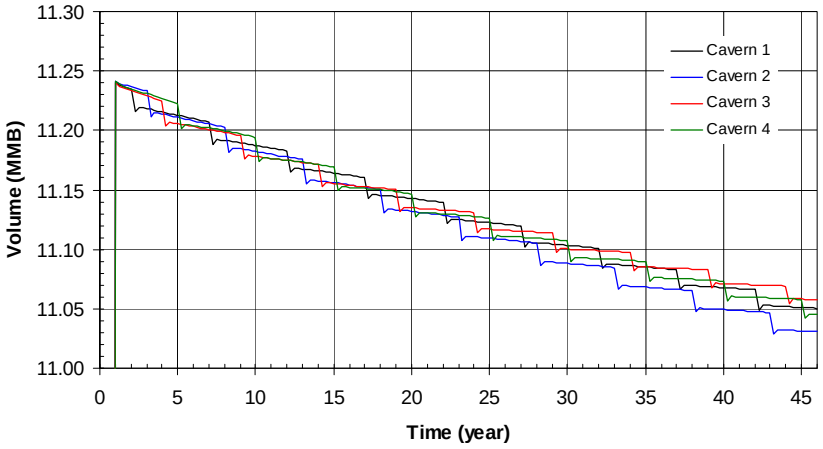

Fig. G-12. 5: Predicted volume change of each SPR cavern due to salt creep closure over time (E_{SR}=10.0 GPa).

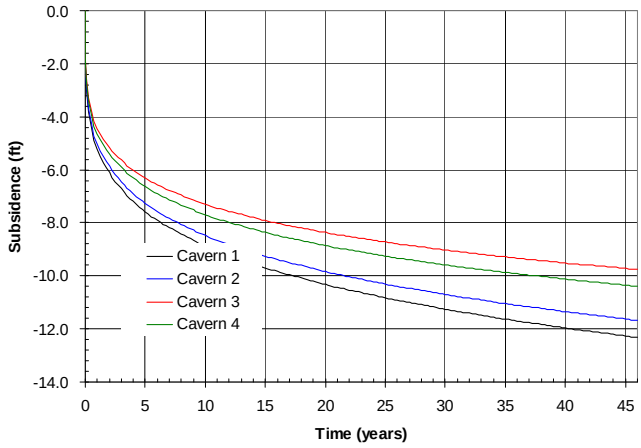

Fig. G-12. 6: Predicted subsidence on the surface above the center of SPR caverns (E_{SR}=10.0 GPa).

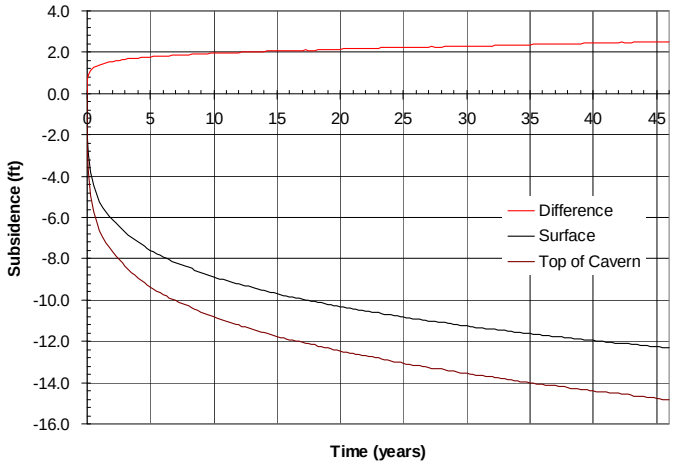

Fig. G-12. 7: Predicted difference between vertical displacement of the top of the central cavern (Cavern 1) and the surface above the cavern as a function of time.

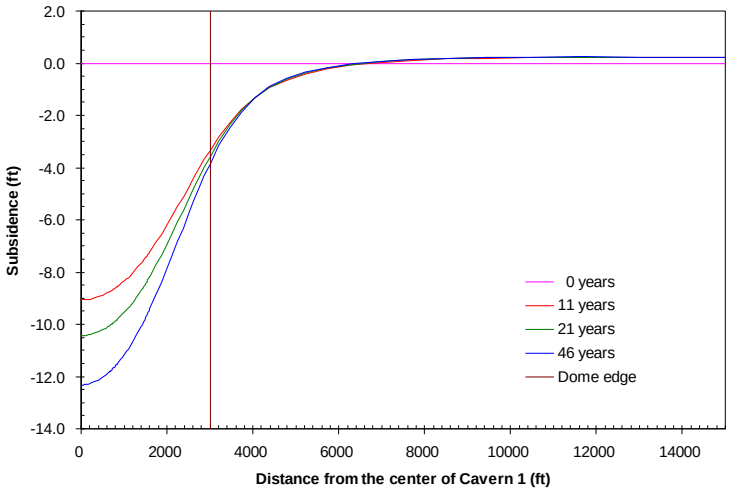

Fig. G-12. 8: Predicted subsidence on the surface from model center to edge with time.

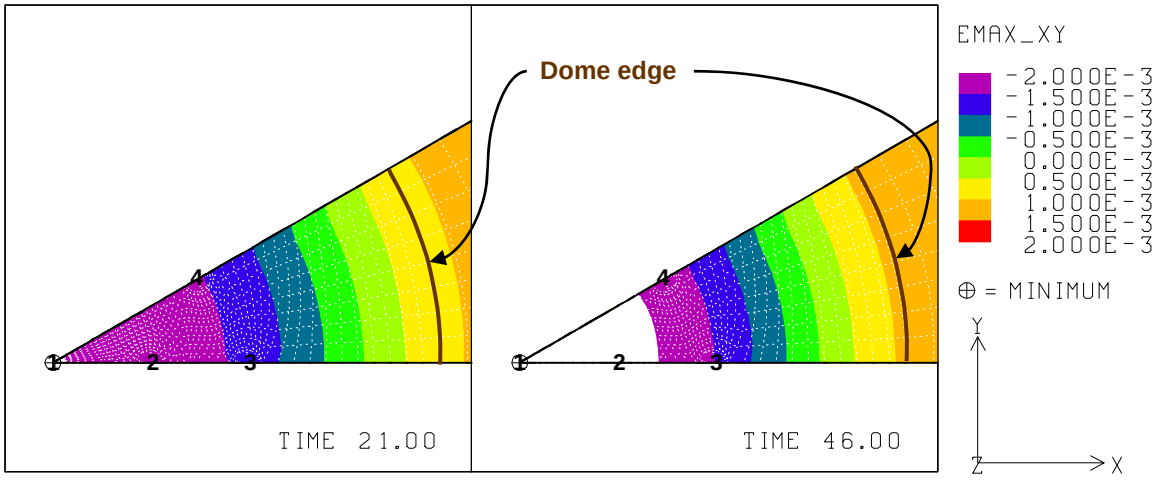

Fig. G-12. 9: Predicted radial surface strains at 21 years and 46 years (E_{SR}=10.0 GPa).

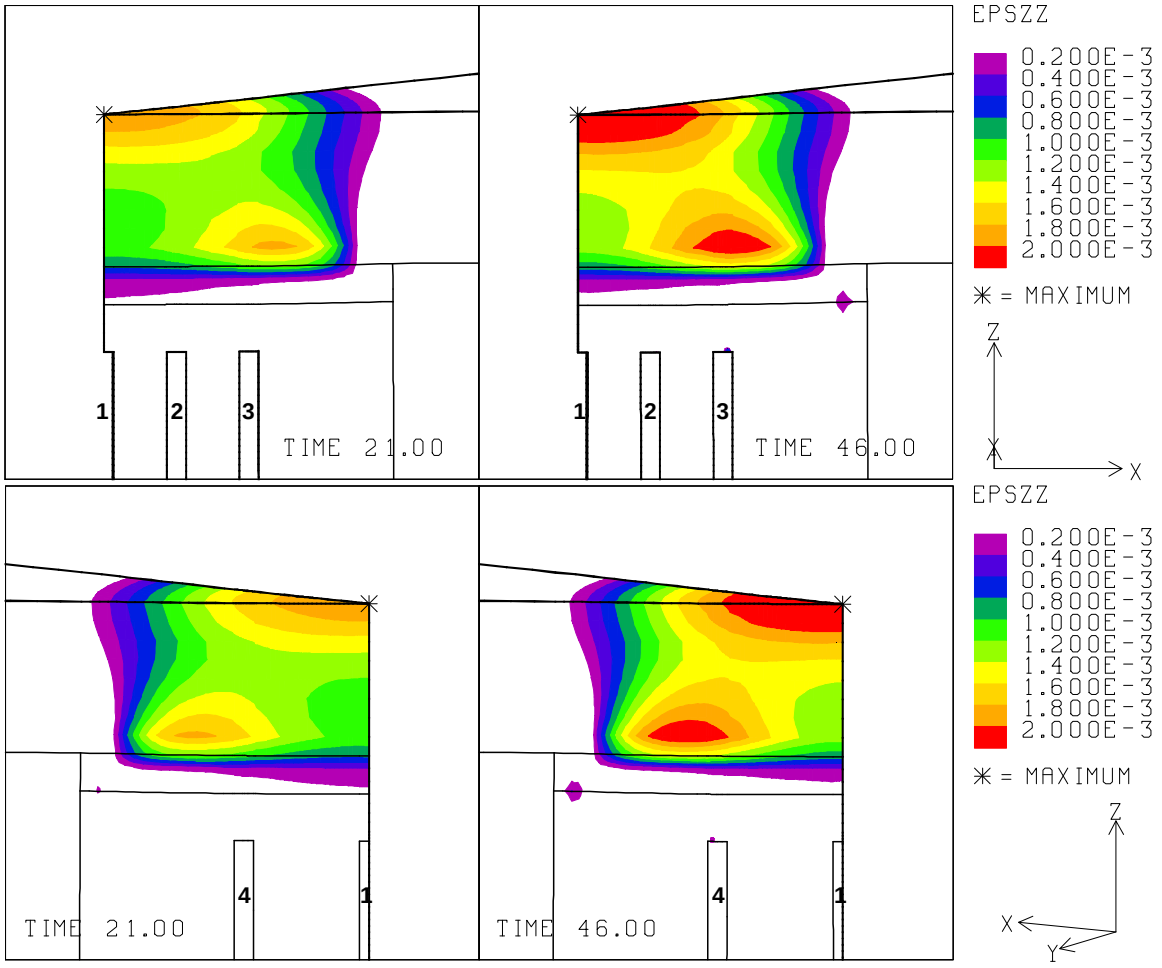

Fig. G-12. 10: Vertical strains around the roof of caverns at 21 years and 46 years (E_{SR}=10.0 GPa).

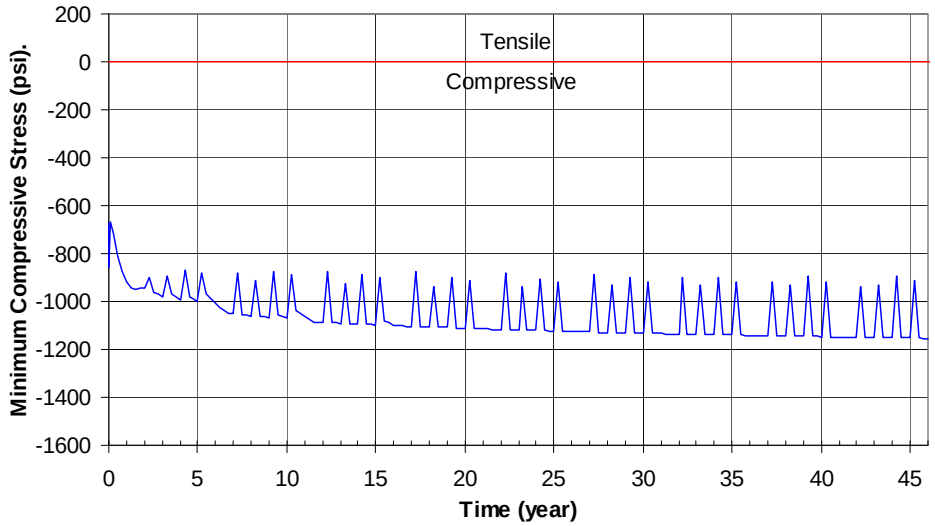

Fig. G-12. 11: Predicted minimum compressive stress history in the salt dome (E_{SR}=10.0 GPa).

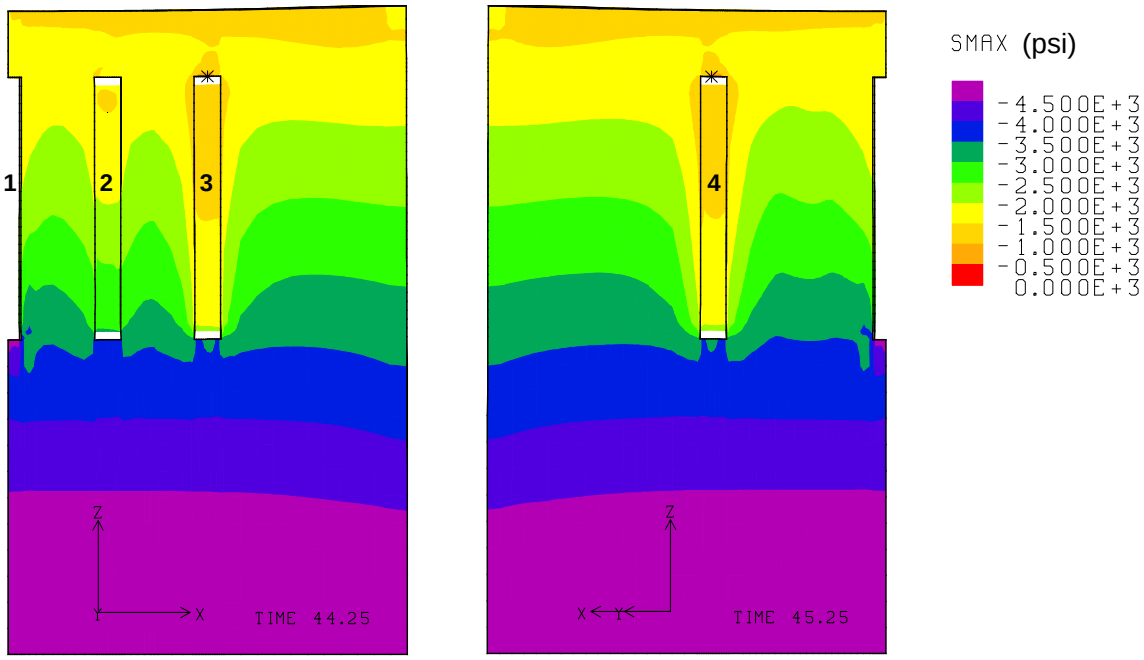

Fig. G-12. 12: Compressive stress contours around the caverns during workover of Cavern 3 and Cavern 4 at 44.25 years and 45.25 years, respectively (E_{SR}=10.0 GPa).

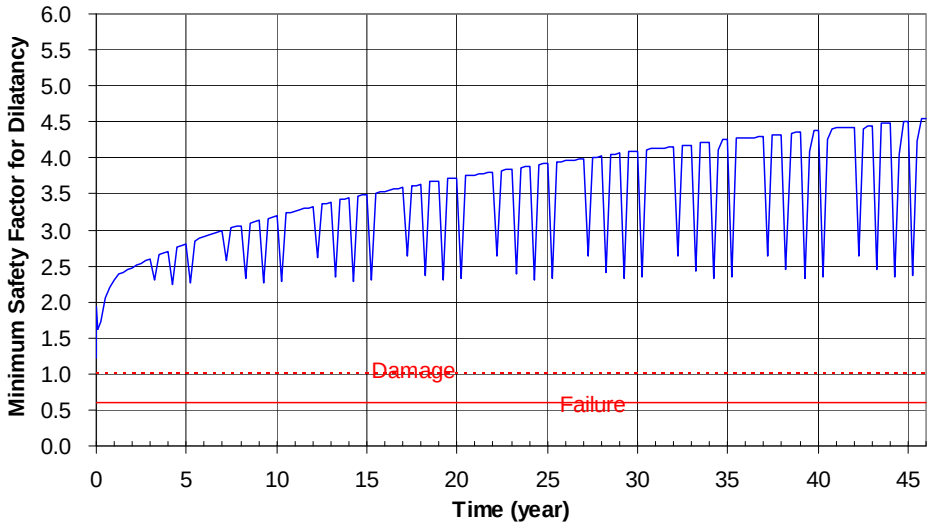

Fig. G-12. 13: Predicted minimum safety factor history against dilatant damage (E_{SR}=10.0 GPa).

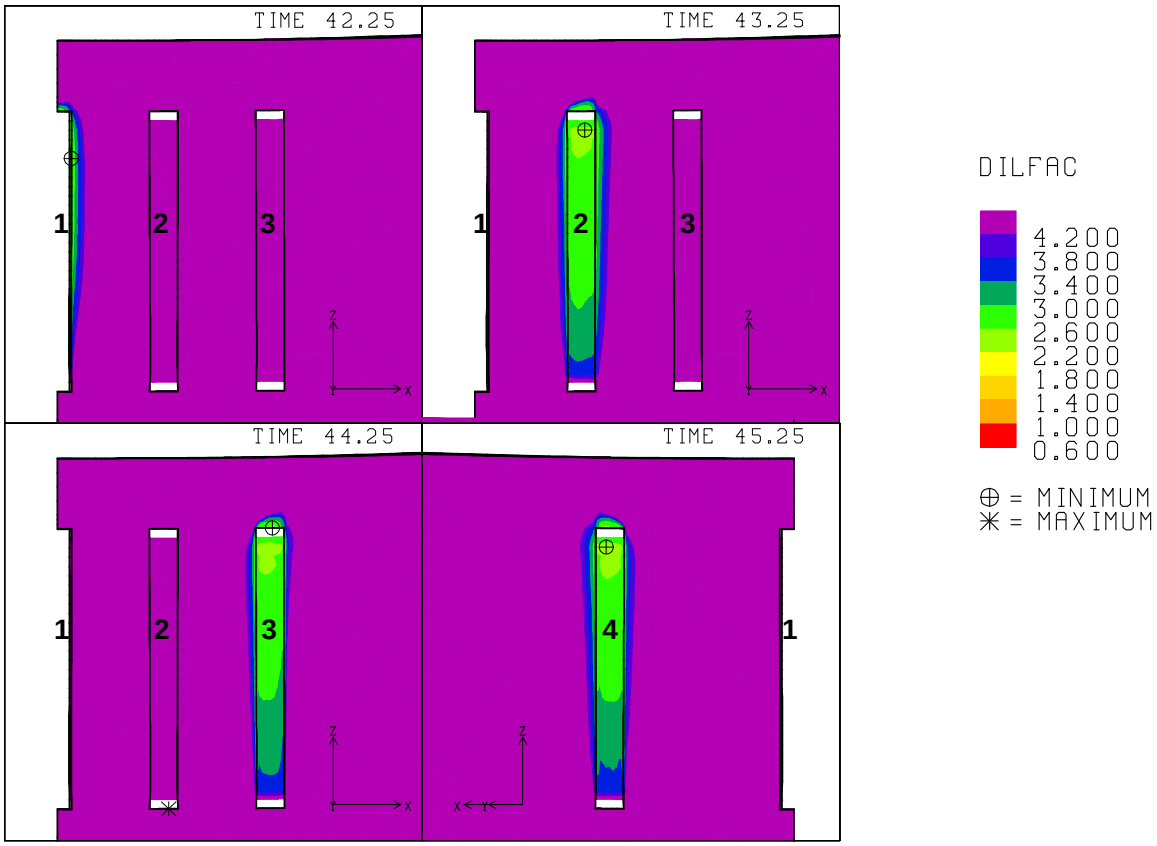

Fig. G-12. 14: Safety factor contours against dilatant damage around the caverns during workover of Caverns 1, 2, 3 and 4 at 42.25 years, 43.25 years, 44.25 years and 45.25 years, respectively (E_{SR}=10.0 GPa).

G-13. Elastic Modulus of Surrounding Rock, E_{SR} = 20.0 GPa

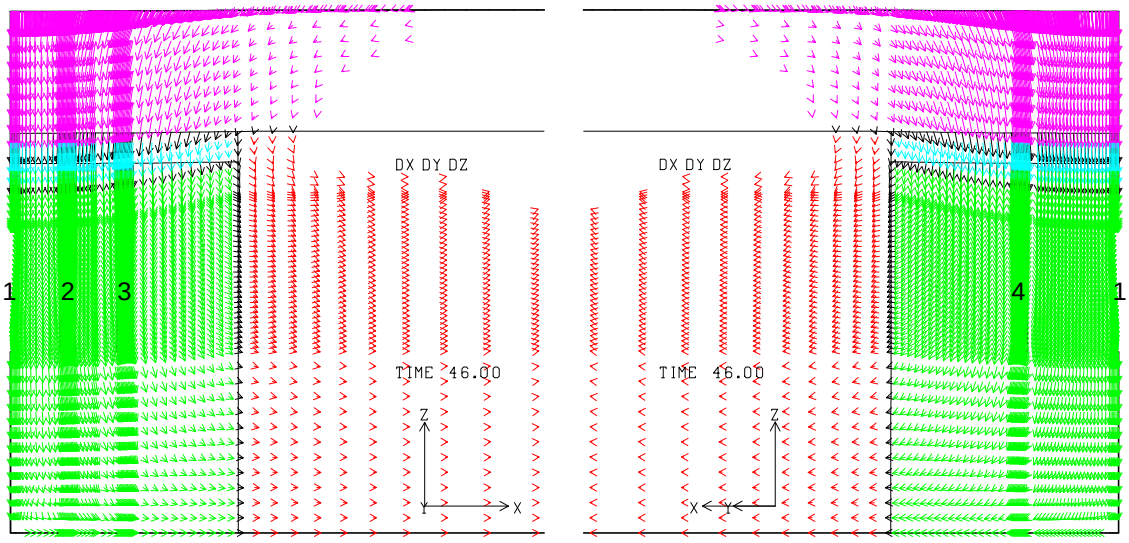

Fig. G-13. 1: Displacement vectors around the caverns at 46 years (E_{SR}=20.0 GPa).

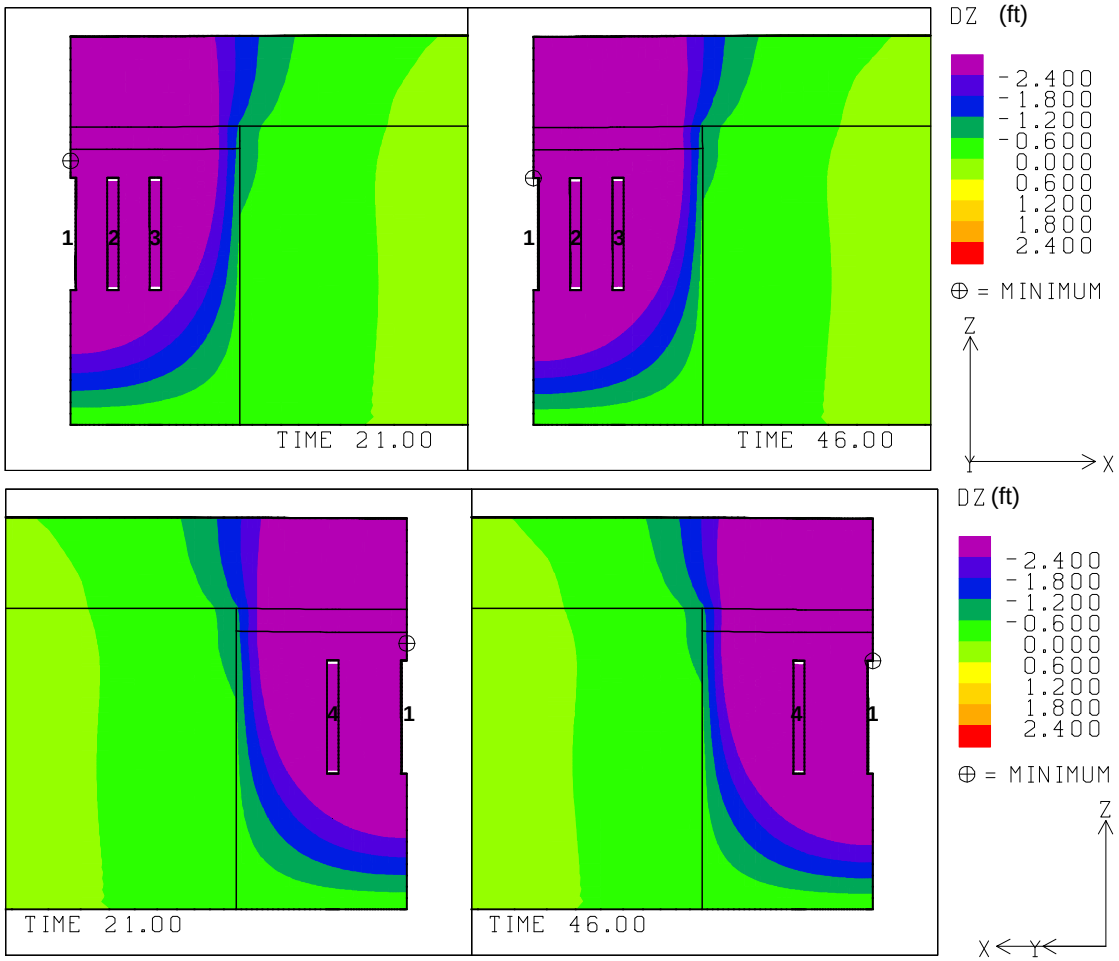

Fig. G-13. 2: Vertical displacement contours around the caverns at 21 and 46 years (E_{SR}=20.0 GPa).

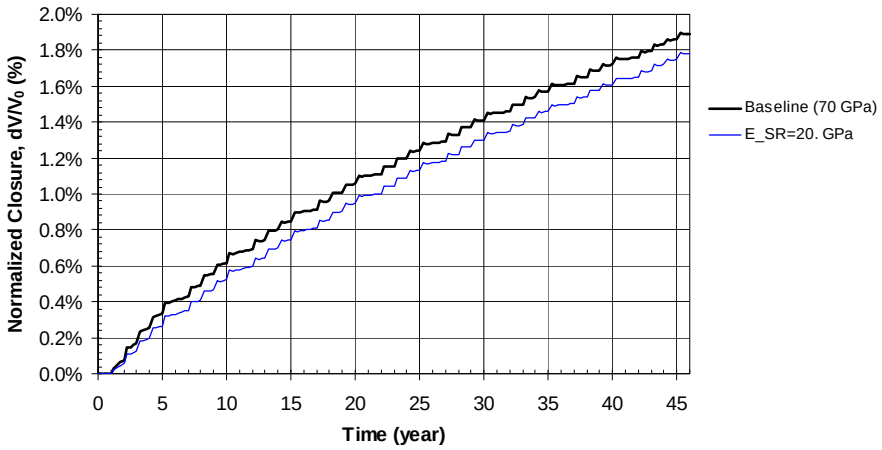

Fig. G-13. 3: Predicted total volumetric closure normalized to initial overall storage volume for the 19 SPR caverns (E_{SR}=20.0 GPa).

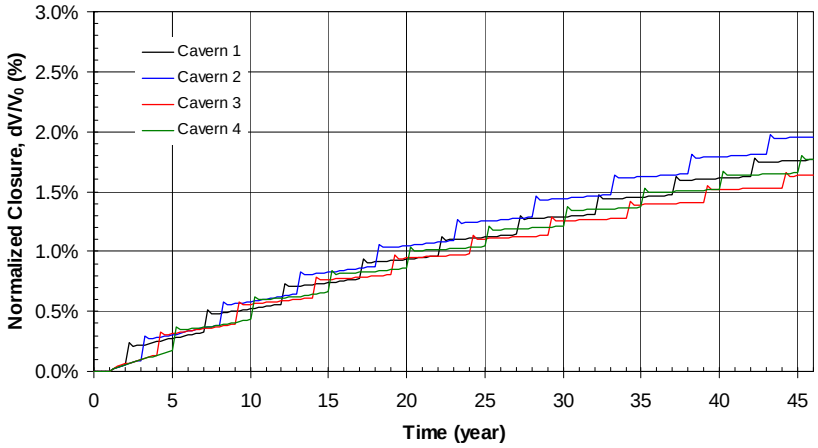

Fig. G-13. 4: Predicted volumetric closure normalized to each initial SPR cavern volume (E_{SR}=20.0 GPa).

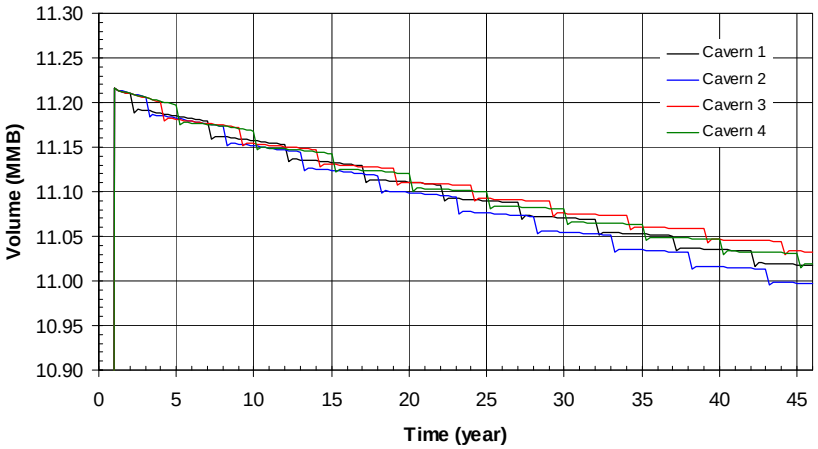

Fig. G-13. 5: Predicted volume change of each SPR cavern due to salt creep closure over time (E_{SR}=20.0 GPa).

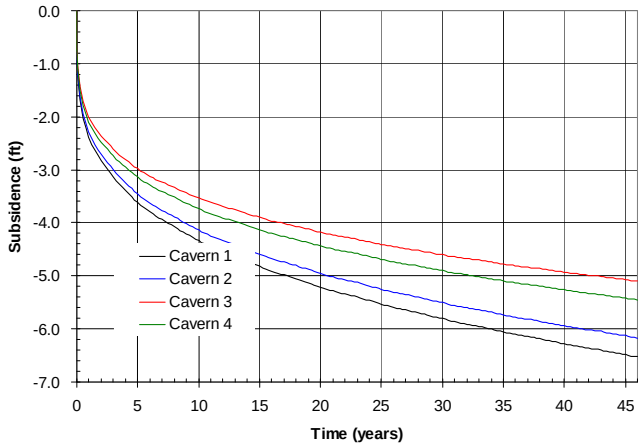

Fig. G-13. 6: Predicted subsidence on the surface above the center of SPR caverns (E_{SR}=20.0 GPa).

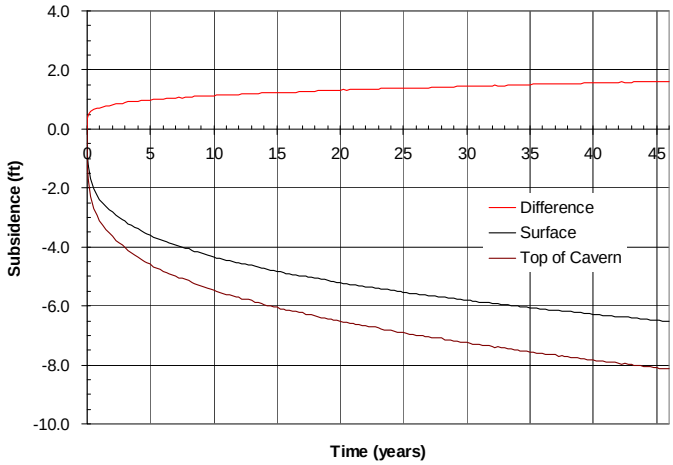

Fig. G-13. 7: Predicted difference between vertical displacement of the top of the central cavern (Cavern 1) and the surface above the cavern as a function of time.

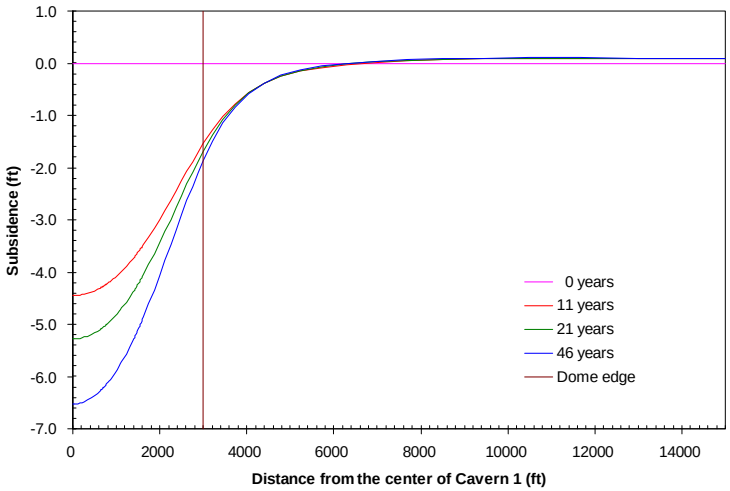

Fig. G-13. 8: Predicted subsidence on the surface from model center to edge with time.

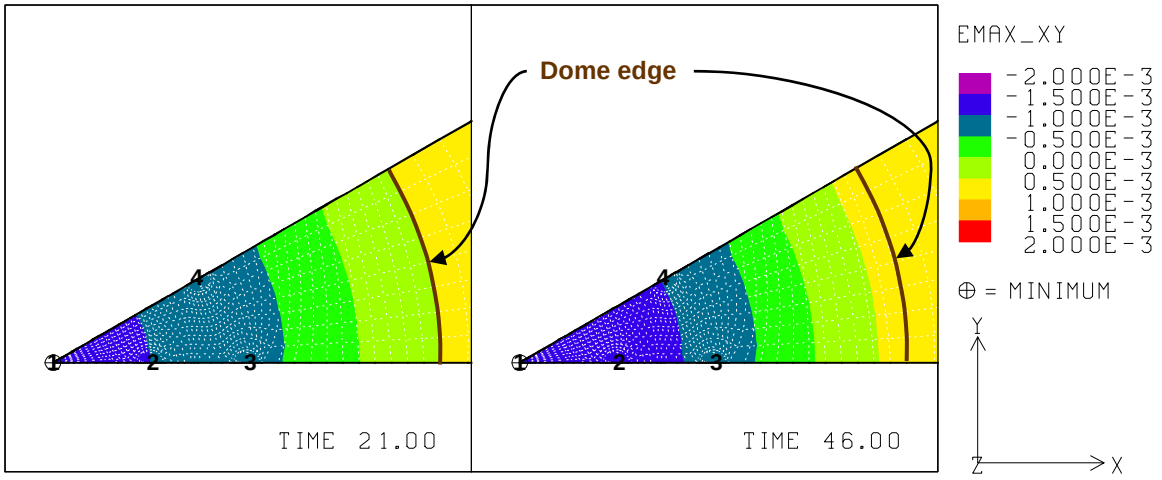

Fig. G-13. 9: Predicted radial surface strains at 21 years and 46 years (E_{SR}=20.0 GPa).

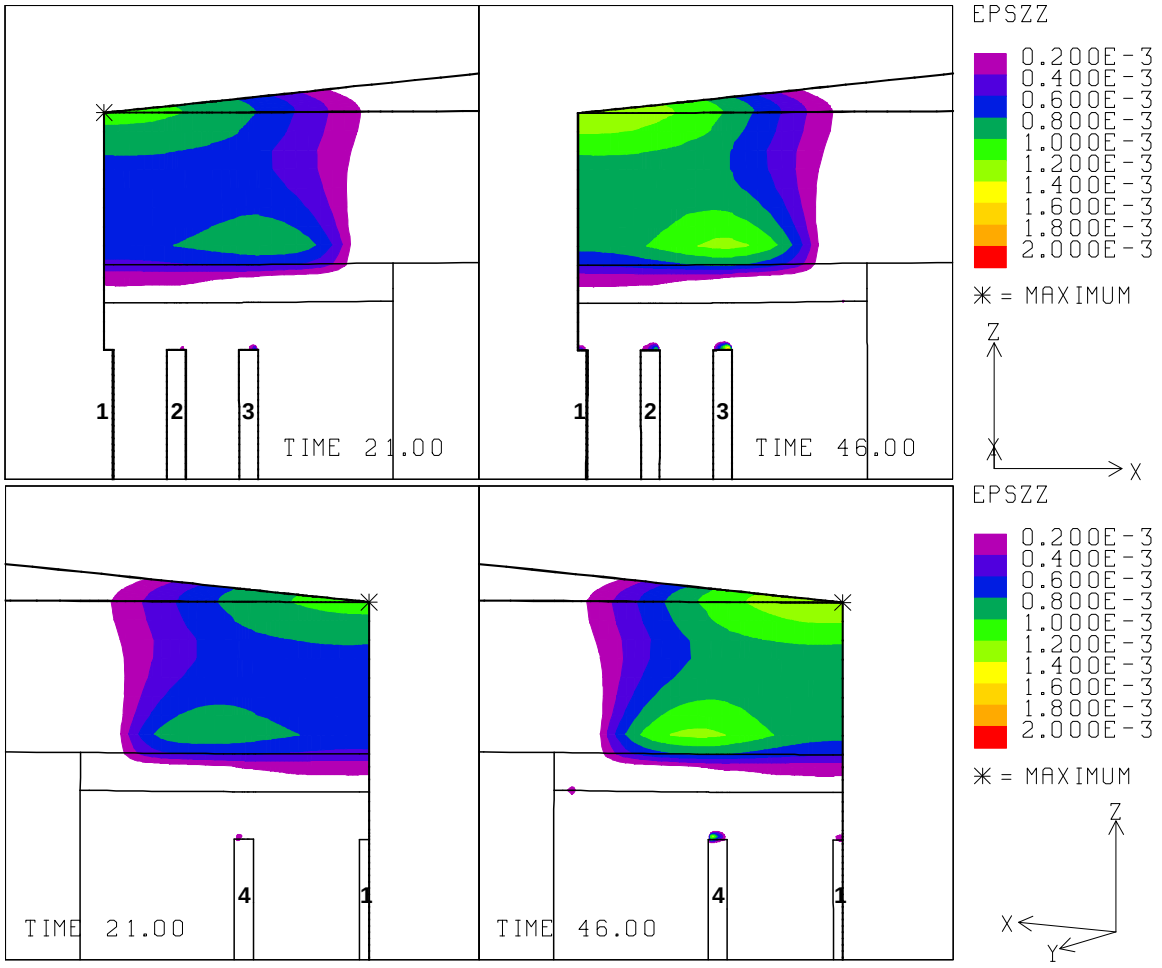

Fig. G-13. 10: Vertical strains around the roof of caverns at 21 years and 46 years (E_{SR}=20.0 GPa).

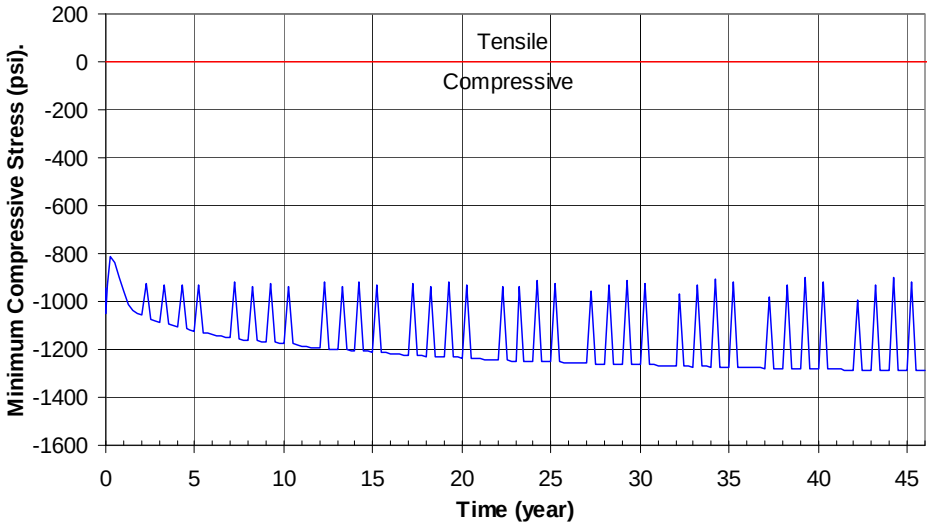

Fig. G-13. 11: Predicted minimum compressive stress history in the salt dome (E_{SR}=20.0 GPa).

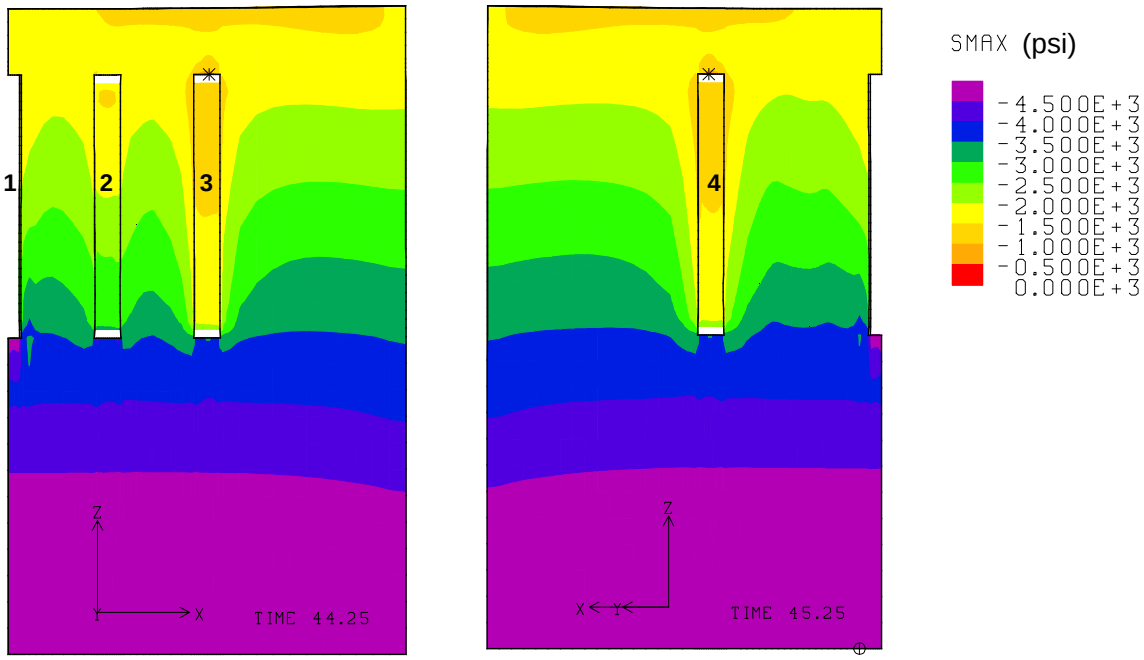

Fig. G-13. 12: Compressive stress contours around the caverns during workover of Cavern 3 and Cavern 4 at 44.25 years and 45.25 years, respectively (E_{SR}=20.0 GPa).

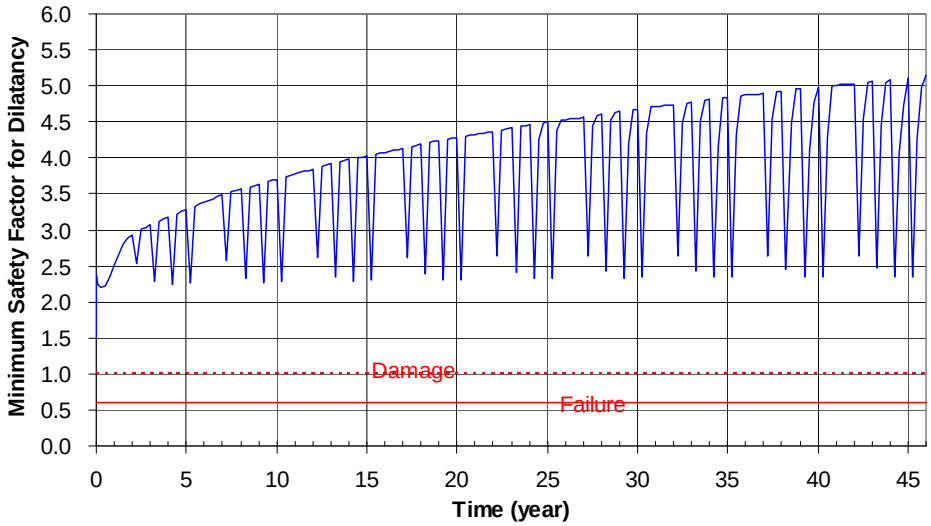

Fig. G-13. 13: Predicted minimum safety factor history against dilatant damage (E_{SR}=20.0 GPa).

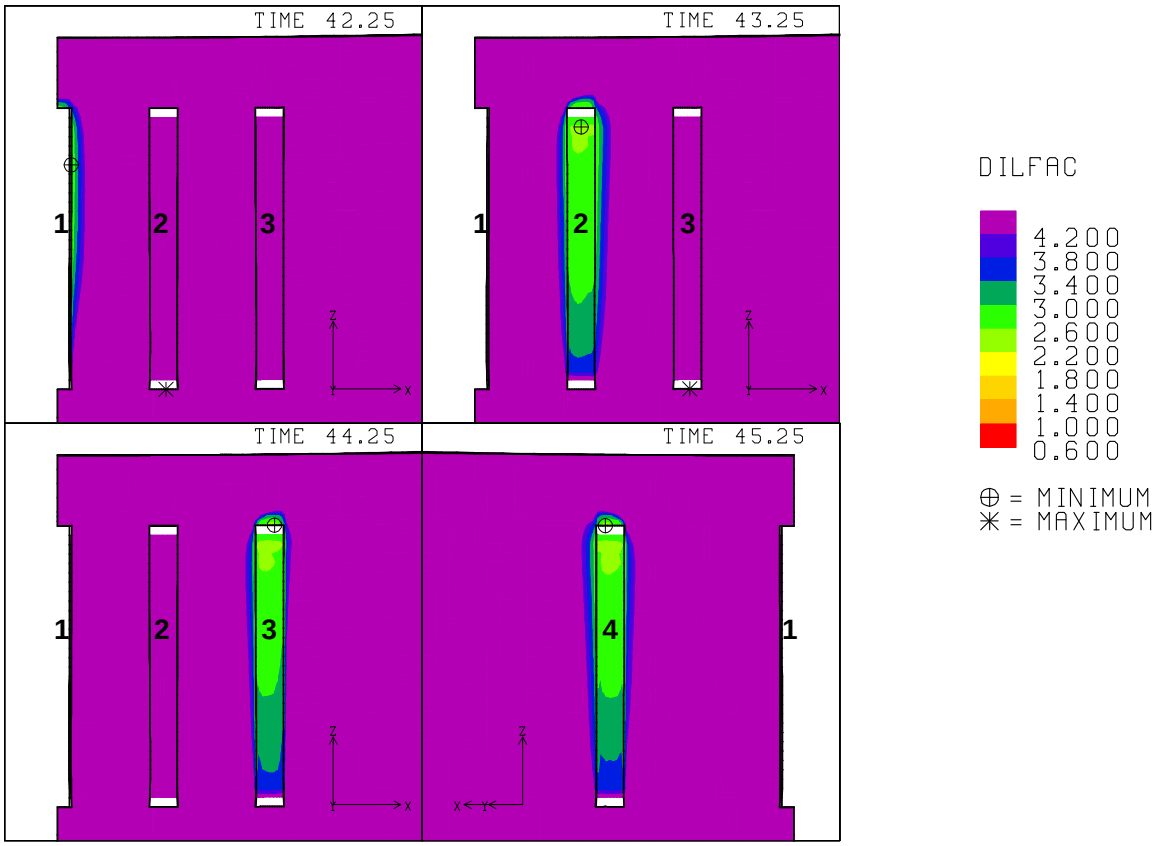

Fig. G-13. 14: Safety factor contours against dilatant damage around the caverns during workover of Caverns 1, 2, 3 and 4 at 42.25 years, 43.25 years, 44.25 years and 45.25 years, respectively (E_{SR}=20.0 GPa).

G-14. Lateral Stress Ratio of Surrounding Rock, K_{SR} = 1.0

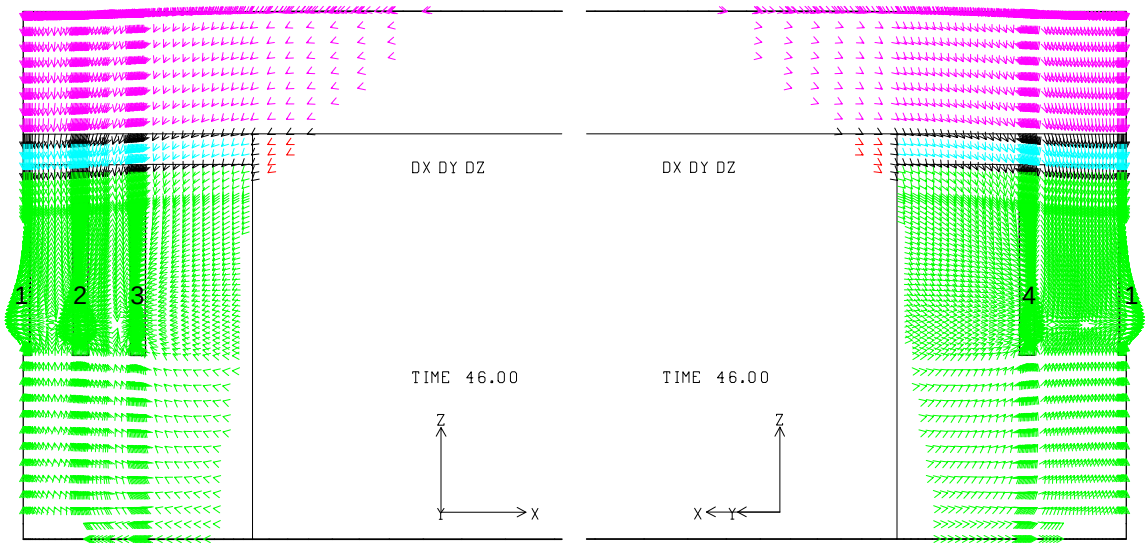

Fig. G-14. 1: Displacement vectors around the caverns at 46 years (K_{SR}=1.0).

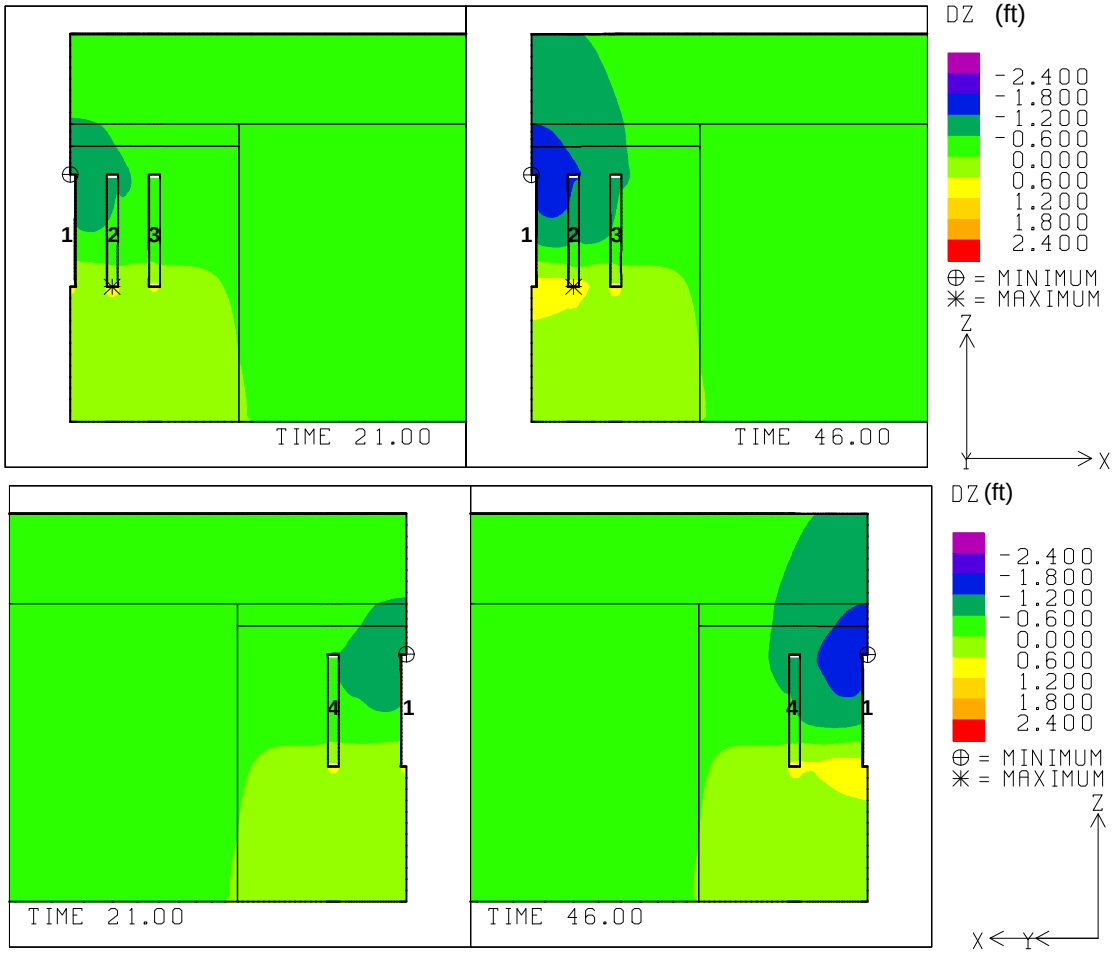

Fig. G-14. 2: Vertical displacement contours around the caverns at 21 and 46 years (K_{SR}=1.0).

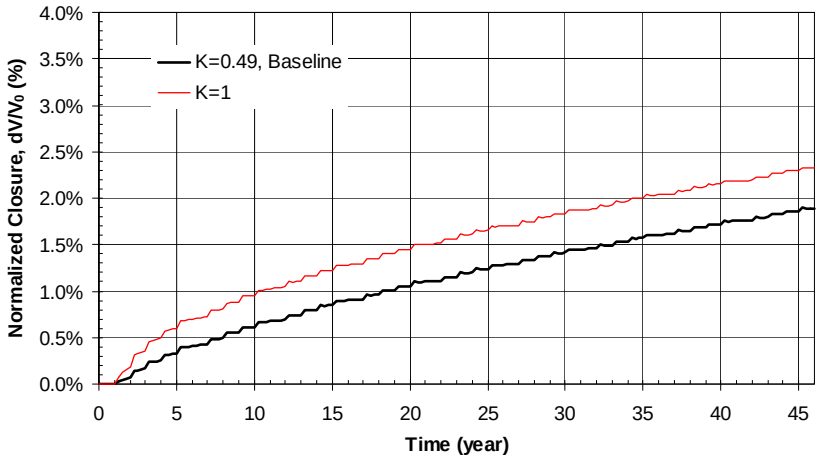

Fig. G-14. 3: Predicted total volumetric closure normalized to initial overall storage volume for the 19 SPR caverns ($\mathcal{K}_{SR}$=1.0).

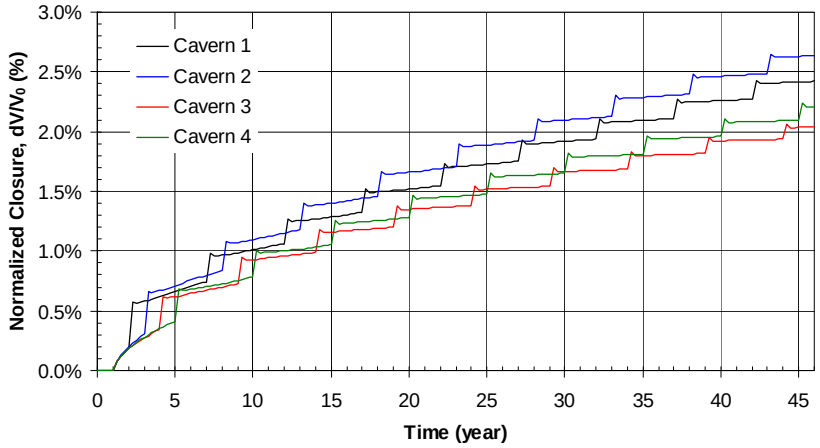

Fig. G-14. 4: Predicted volumetric closure normalized to each initial SPR cavern volume ($\mathcal{K}_{SR}$=1.0).

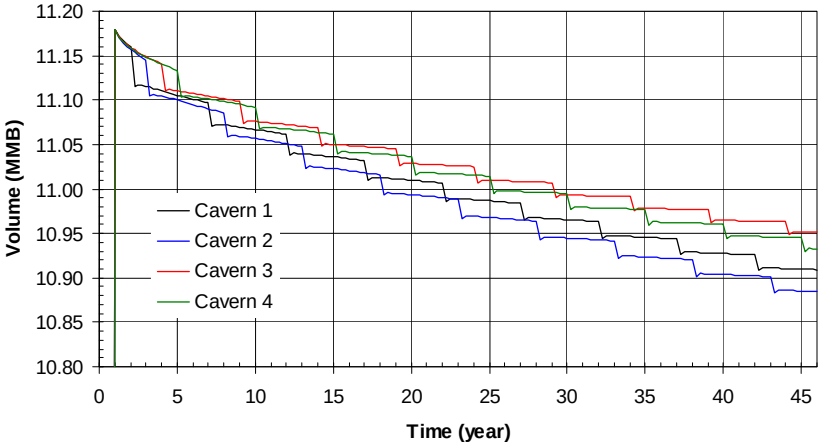

Fig. G-14. 5: Predicted volume change of each SPR cavern due to salt creep closure over time ($\mathcal{K}_{SR}$=1.0).

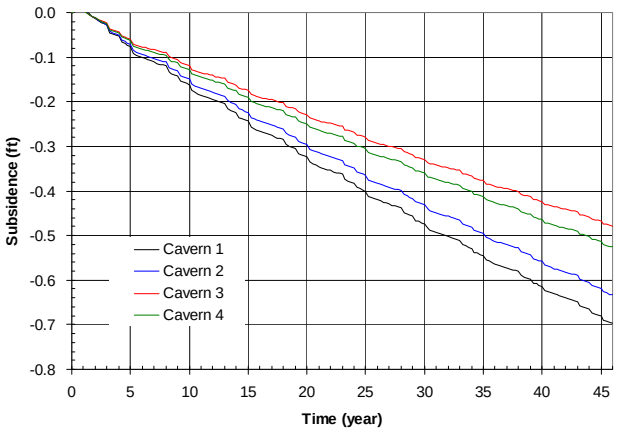

Fig. G-14. 6: Predicted subsidence on the surface above the center of SPR caverns ($\mathcal{K}_{SR}$=1.0).

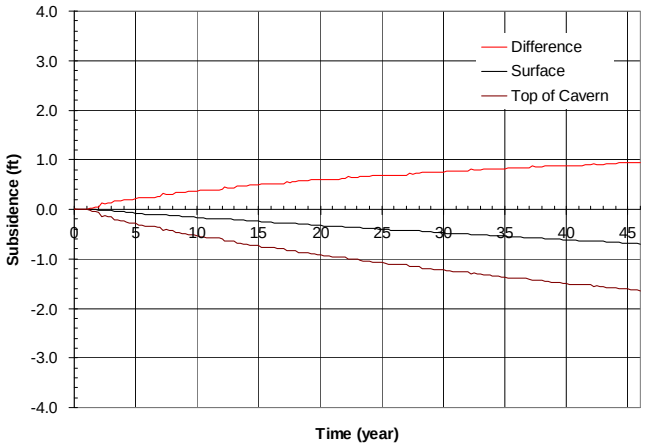

Fig. G-14. 7: Predicted difference between vertical displacement of the top of the central cavern (Cavern 1) and the surface above the cavern as a function of time.

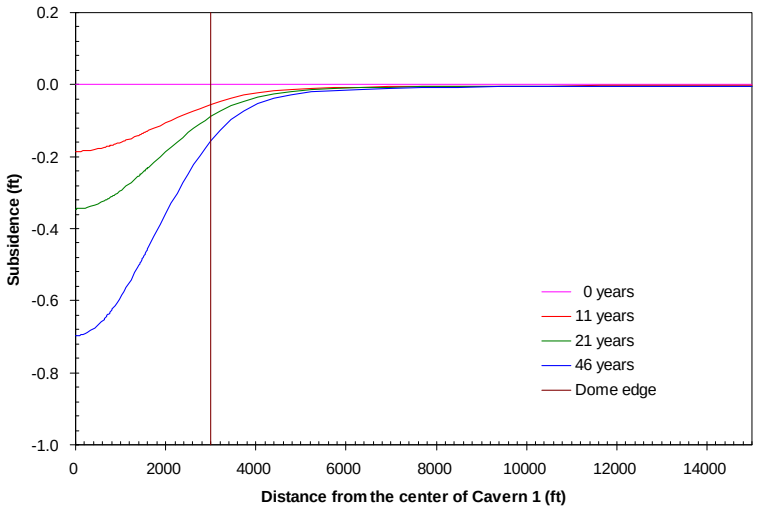

Fig. G-14. 8: Predicted subsidence on the surface from model center to edge with time.

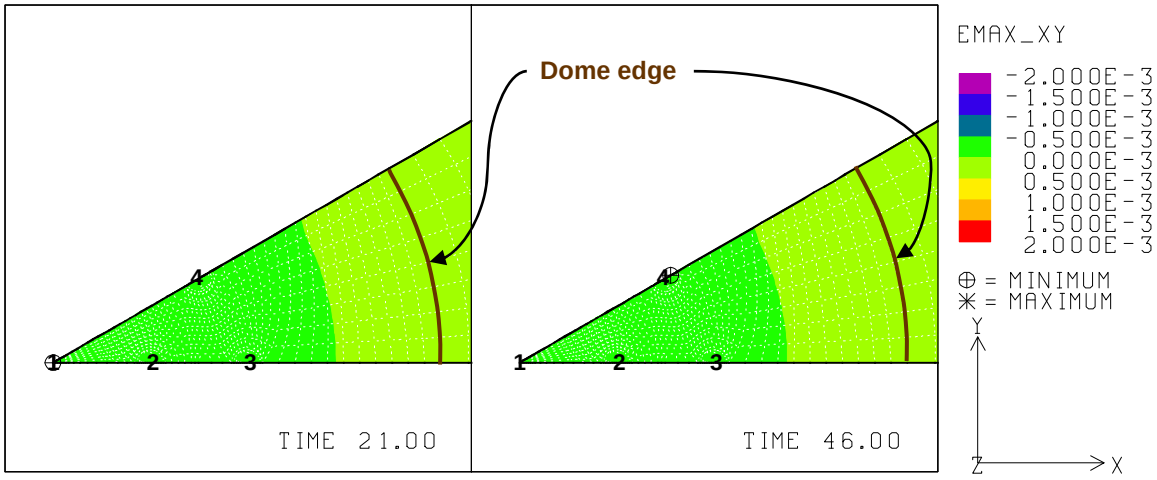

Fig. G-14. 9: Predicted radial surface strains at 21 years and 46 years ($\mathcal{K}_{SR}$=1.0).

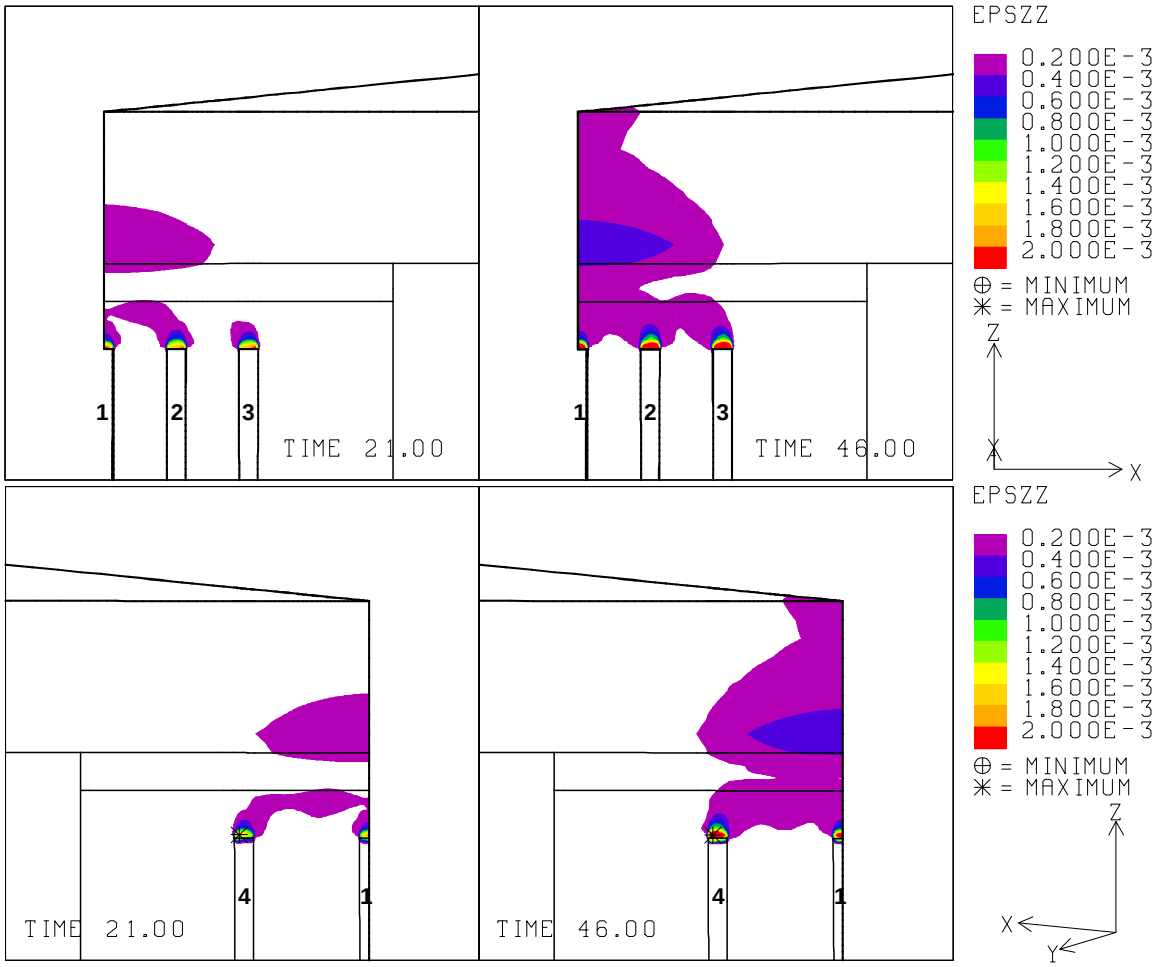

Fig. G-14. 10: Vertical strains around the roof of caverns at 21 years and 46 years ($\mathcal{K}_{SR}$=1.0).

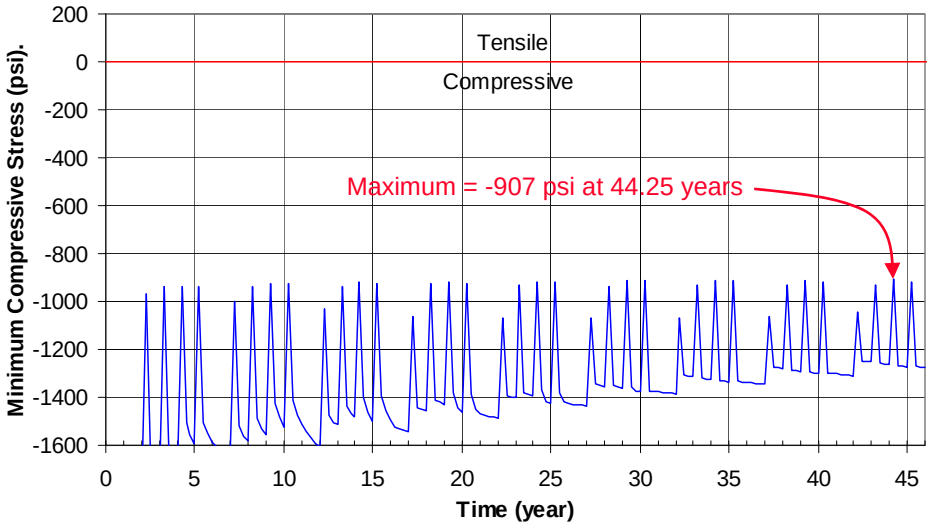

Fig. G-14. 11: Predicted minimum compressive stress history in the salt dome ($\mathcal{K}_{SR}$=1.0).

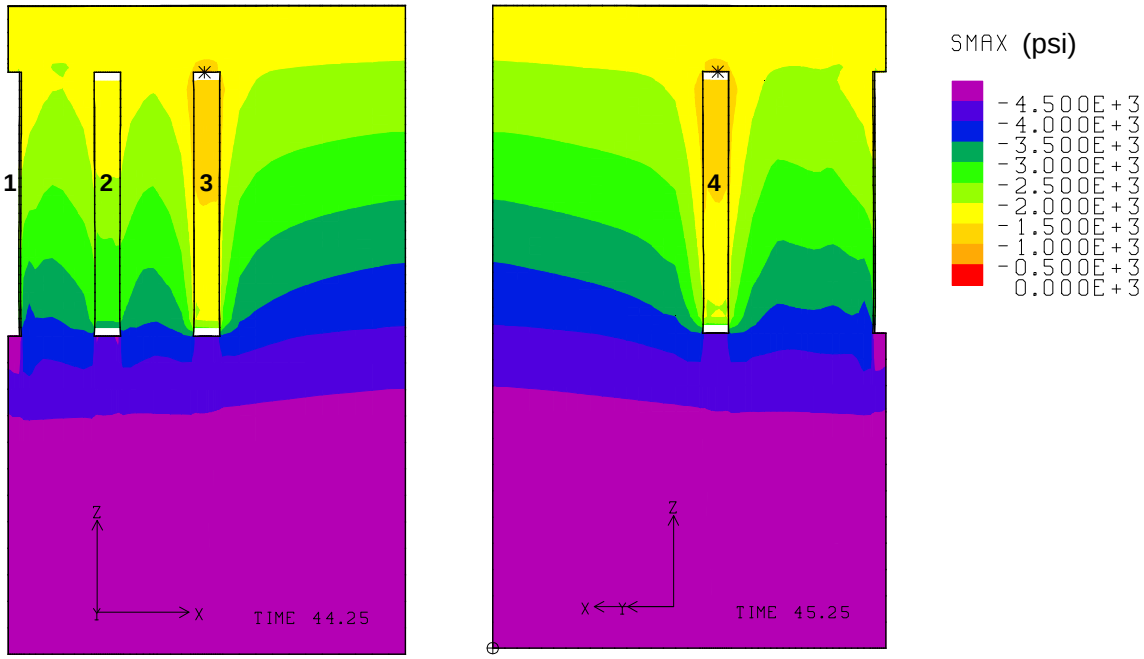

Fig. G-14. 12: Compressive stress contours around the caverns during workover of Cavern 3 and Cavern 4 at 44.25 years and 45.25 years, respectively ($\mathcal{K}_{SR}$=1.0).

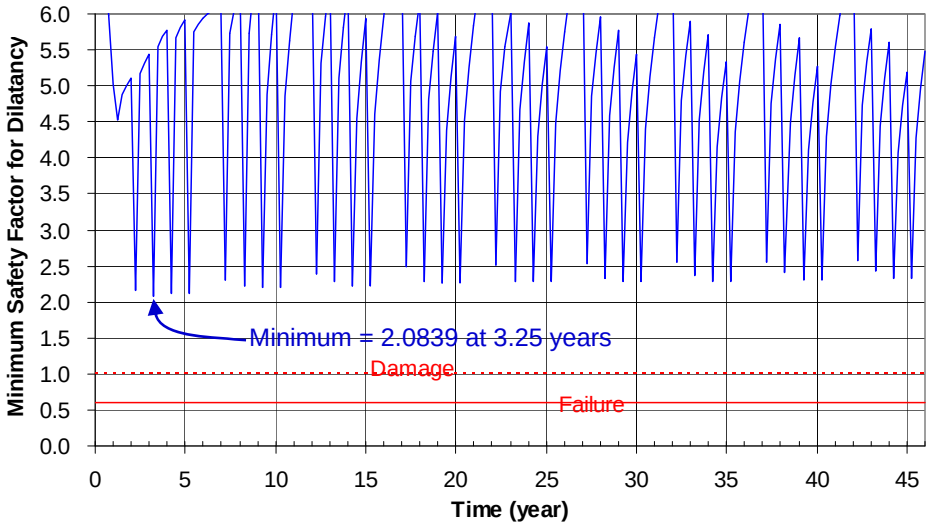

Fig. G-14. 13: Predicted minimum safety factor history against dilatant damage ($\mathcal{K}_{SR}$=1.0).

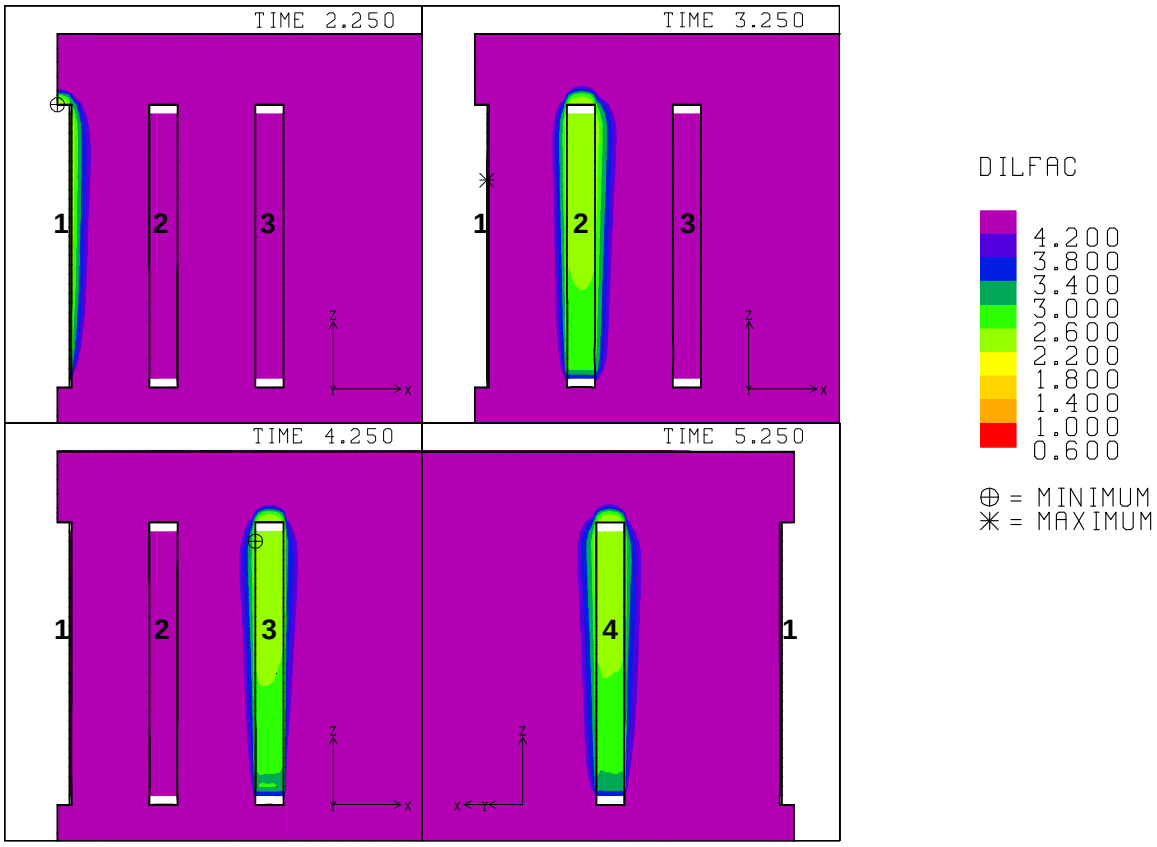

Fig. G-14. 14: Safety factor contours against dilatant damage around the caverns during workover of Caverns 1, 2, 3 and 4 at 2.25 years, 3.25 years, 4.25 years and 5.25 years, respectively ($\mathcal{K}_{SR}$=1.0).

G-15. Lateral Stress Ratio of Surrounding Rock, K_{SR} = 2.0

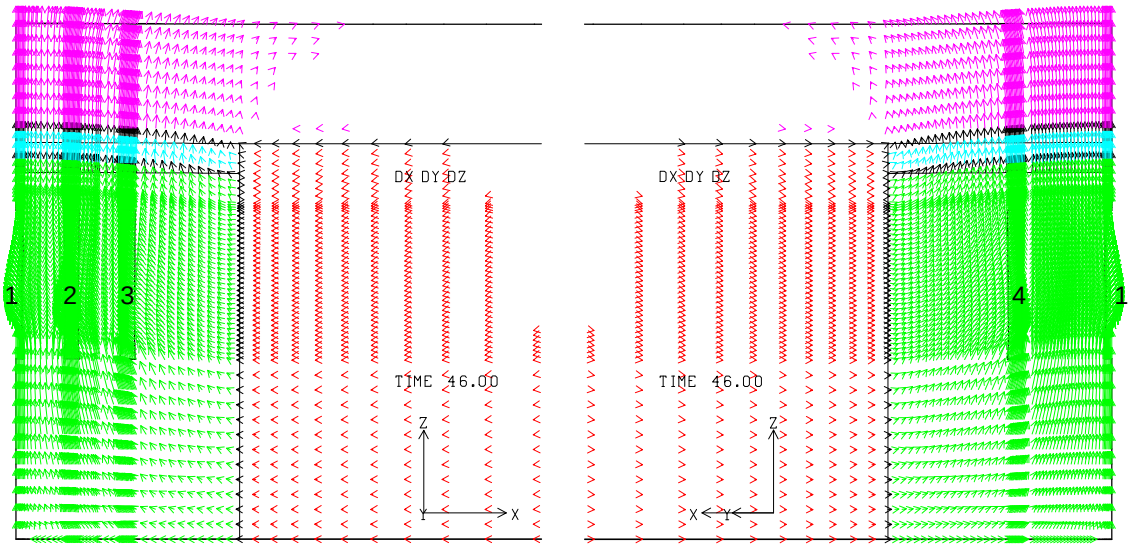

Fig. G-15. 1: Displacement vectors around the caverns at 46 years (K_{SR}=2.0).

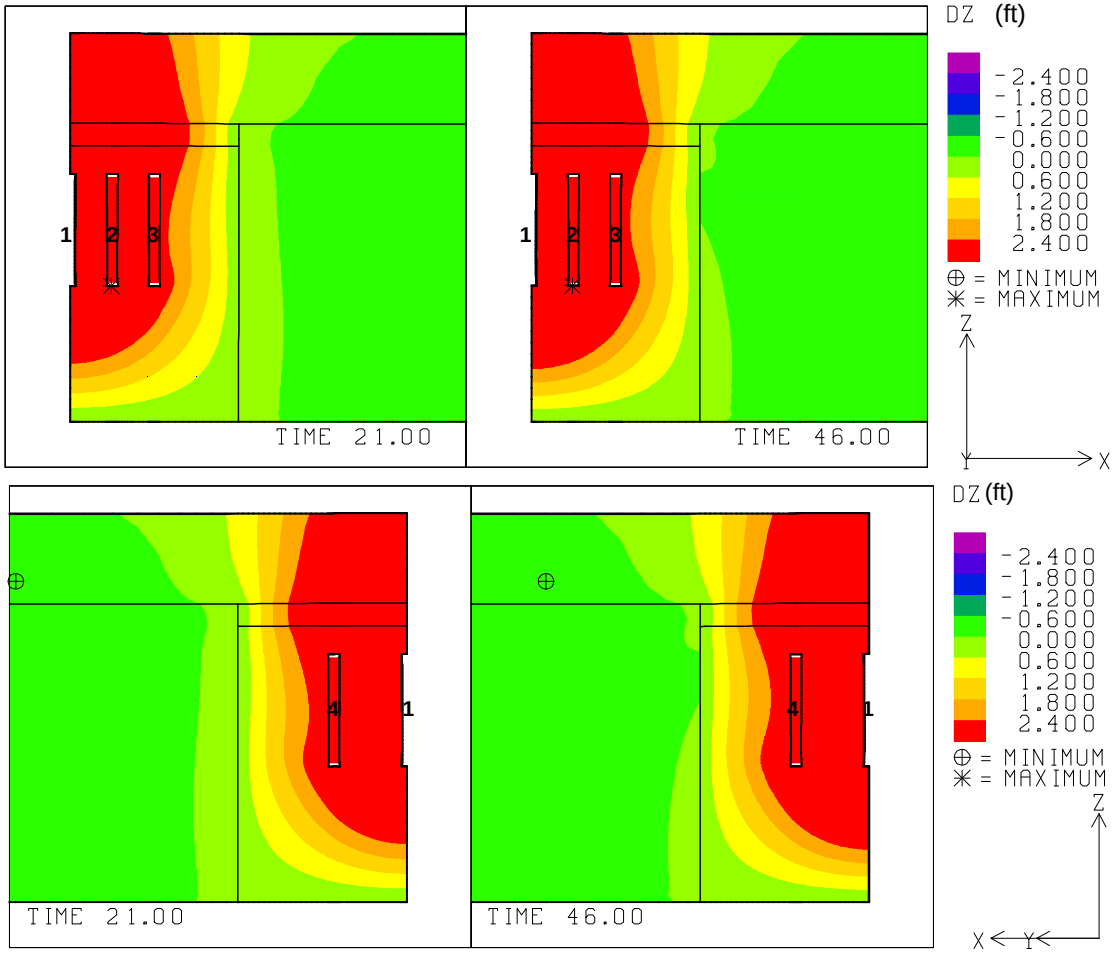

Fig. G-15. 2: Vertical displacement contours around the caverns at 21 and 46 years (K_{SR}=2.0).

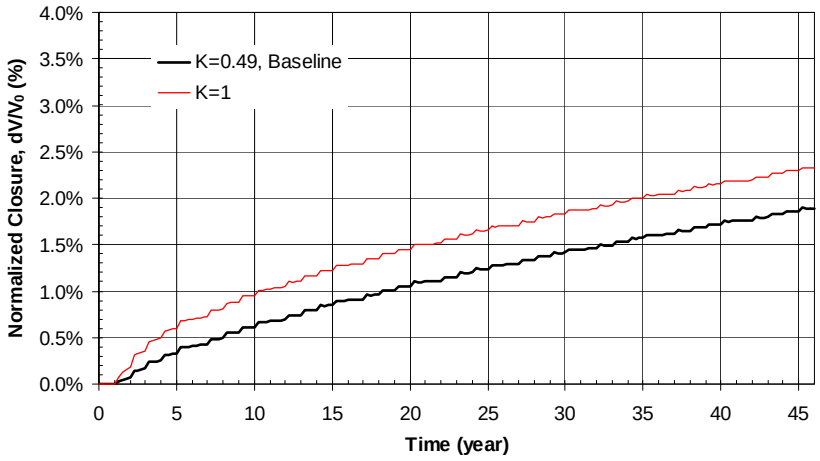

Fig. G-15. 3: Predicted total volumetric closure normalized to initial overall storage volume for the 19 SPR caverns ($\mathcal{K}_{SR}$=2.0).

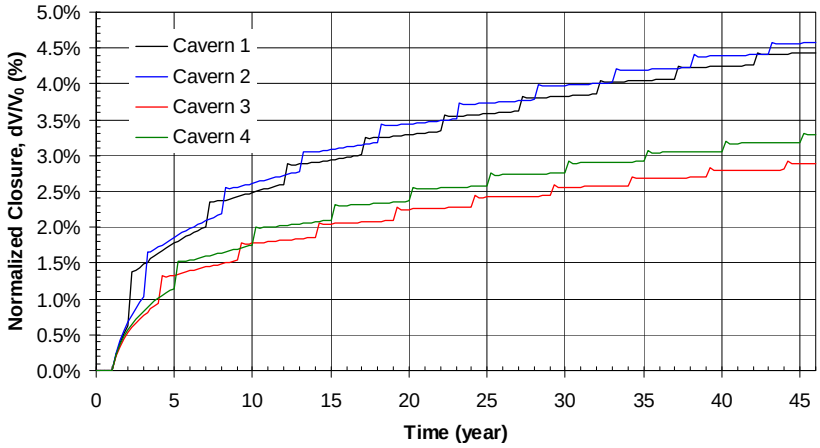

Fig. G-15. 4: Predicted volumetric closure normalized to each initial SPR cavern volume ($\mathcal{K}_{SR}$=2.0).

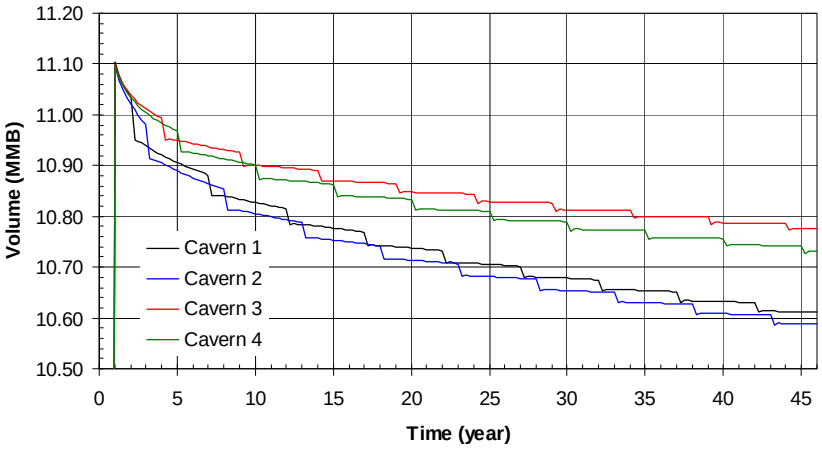

Fig. G-15. 5: Predicted volume change of each SPR cavern due to salt creep closure over time ($\mathcal{K}_{SR}$=2.0).

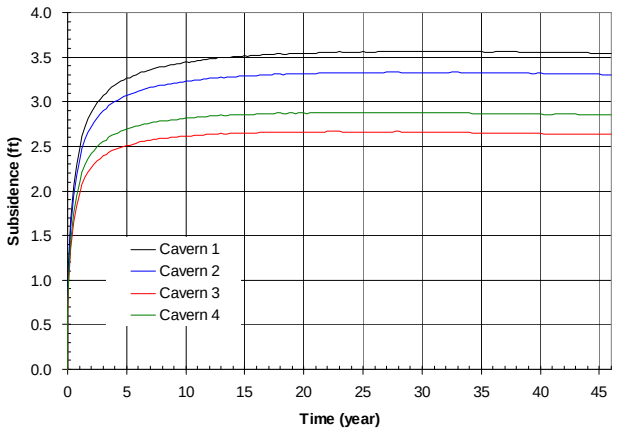

Fig. G-15. 6: Predicted subsidence on the surface above the center of SPR caverns ($\mathcal{K}_{SR}$=2.0).

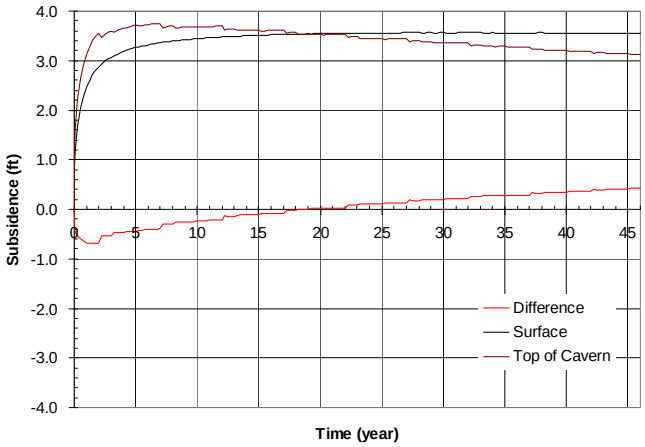

Fig. G-15. 7: Predicted difference between vertical displacement of the top of the central cavern (Cavern 1) and the surface above the cavern as a function of time.

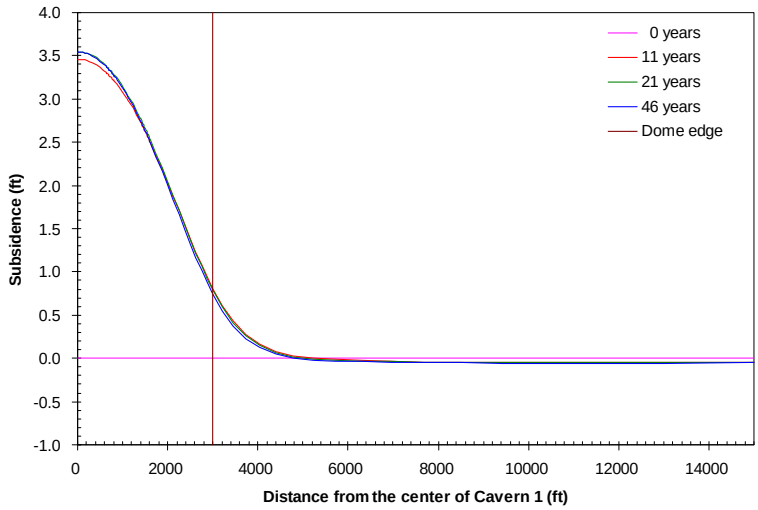

Fig. G-15. 8: Predicted subsidence on the surface from model center to edge with time.

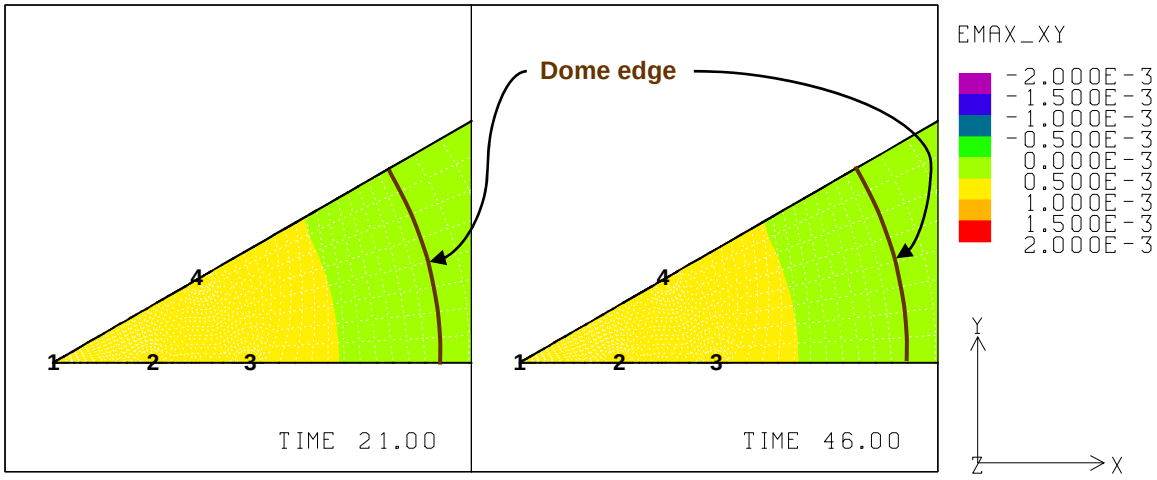

Fig. G-15. 9: Predicted radial surface strains at 21 years and 46 years (κ_{SR}=2.0).

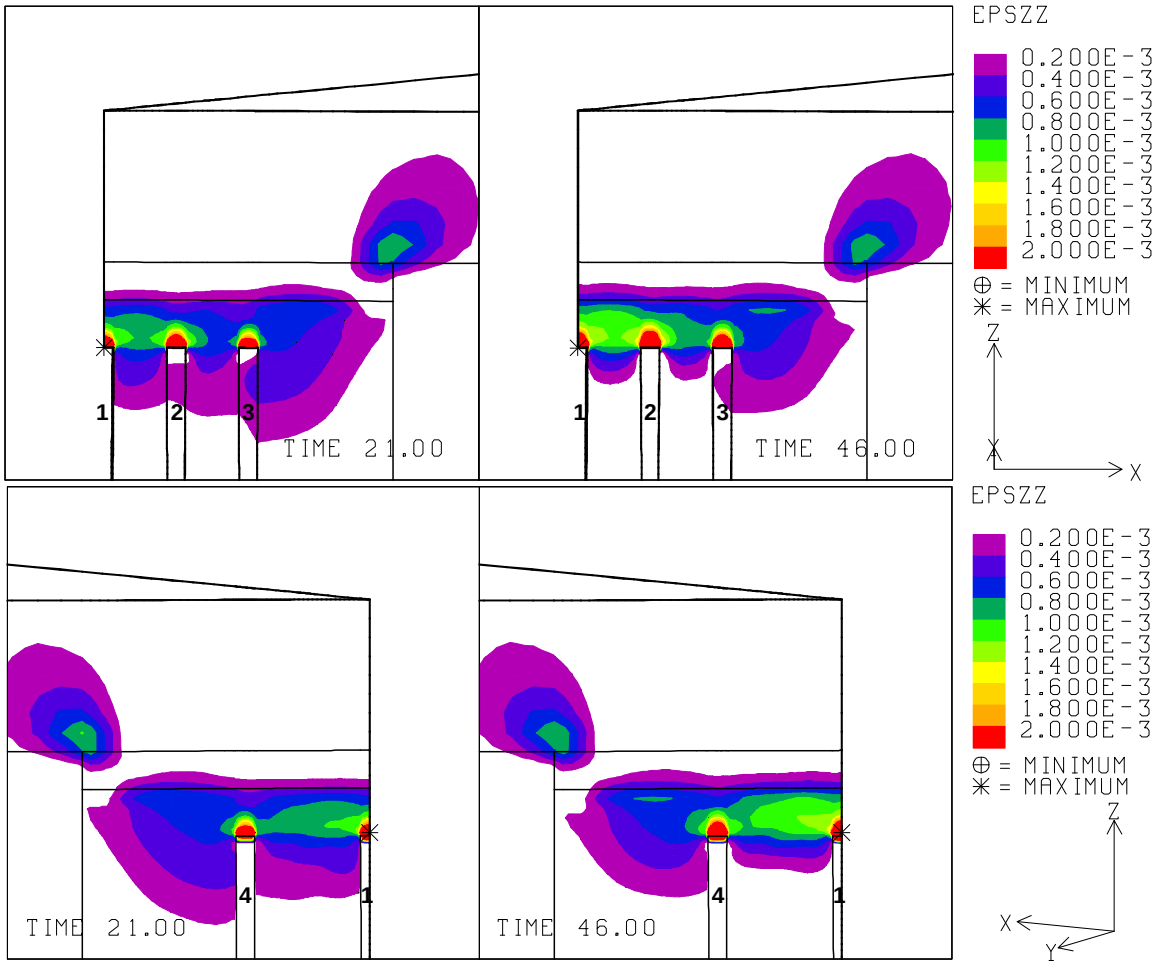

Fig. G-15. 10: Vertical strains around the roof of caverns at 21 years and 46 years (κ_{SR}=2.0).

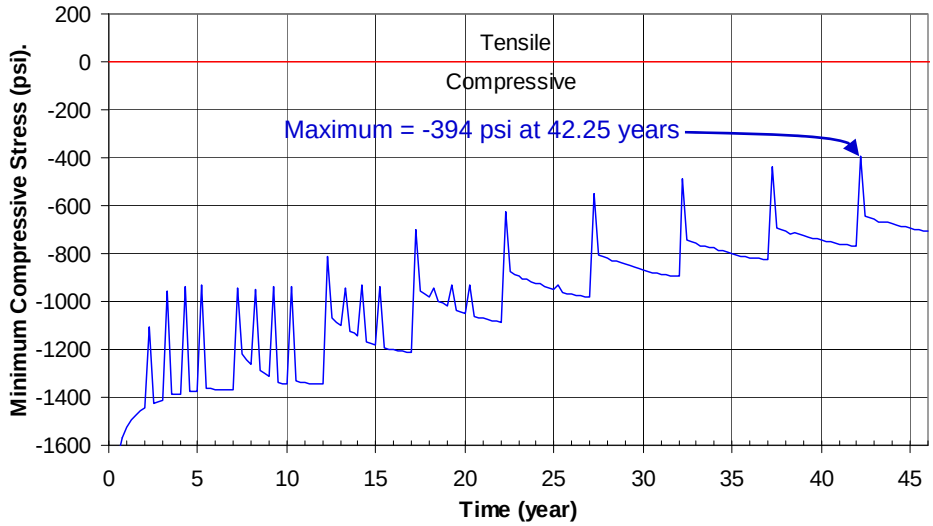

Fig. G-15. 11: Predicted minimum compressive stress history in the salt dome ($\mathcal{K}_{SR}$=2.0).

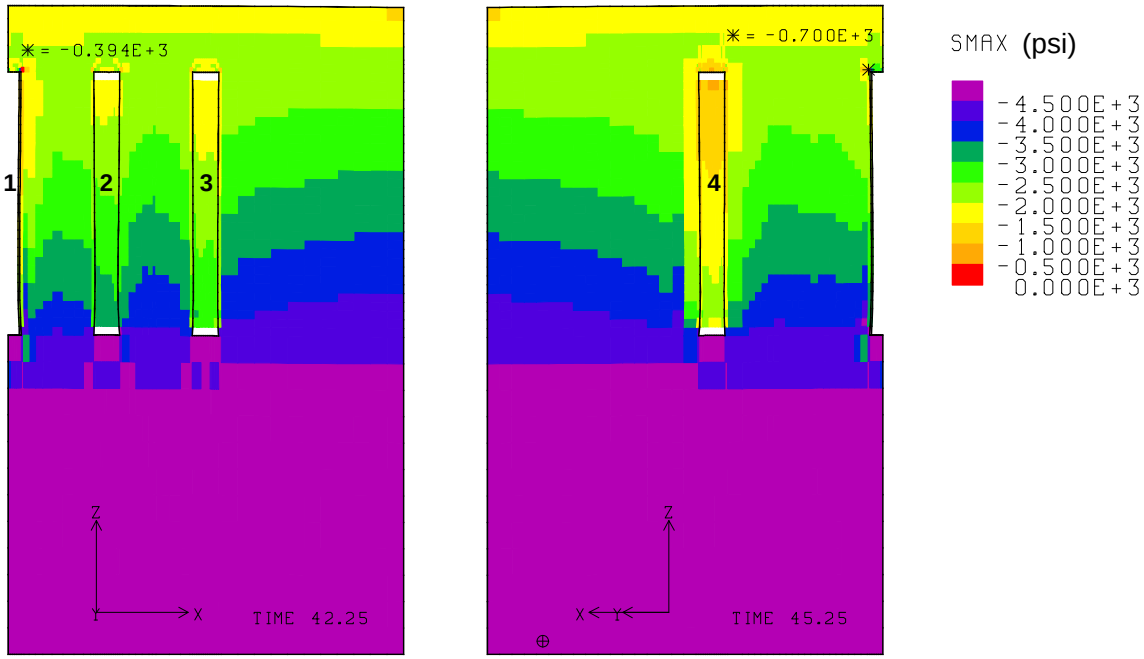

Fig. G-15. 12: Compressive stress contours around the caverns during workover of Cavern 3 and Cavern 4 at 42.25 years and 45.25 years, respectively ($\mathcal{K}_{SR}$=2.0).

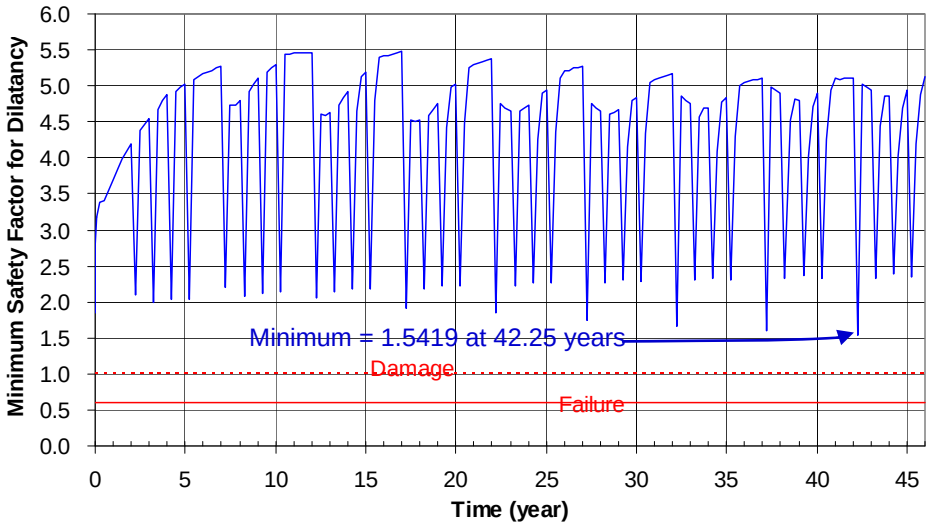

Fig. G-15. 13: Predicted minimum safety factor history against dilatant damage (κ_{SR}=2.0).

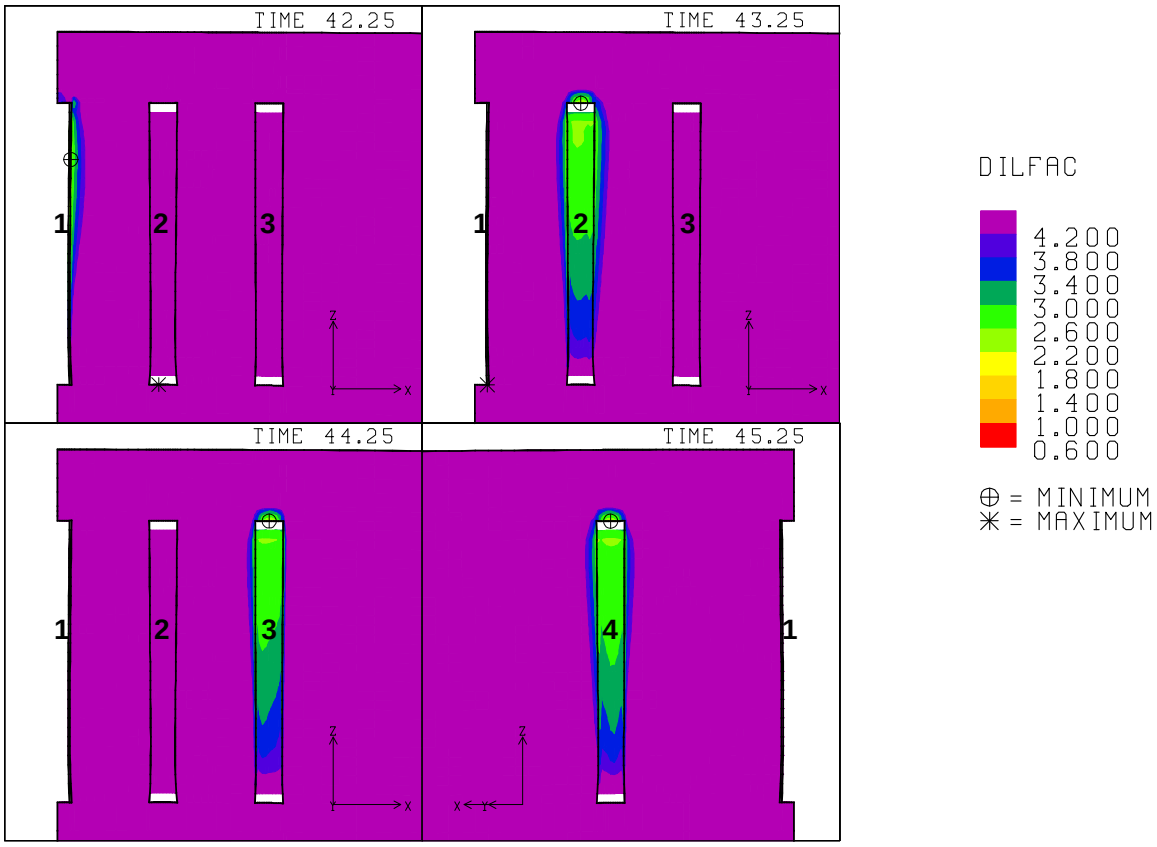

Fig. G-15. 14: Safety factor contours against dilatant damage around the caverns during workover of Caverns 1, 2, 3 and 4 at 42.25 years, 43.25 years, 44.25 years and 45.25 years, respectively (κ_{SR}=2.0).

G-16. Cavern Size, r_C = 200 ft

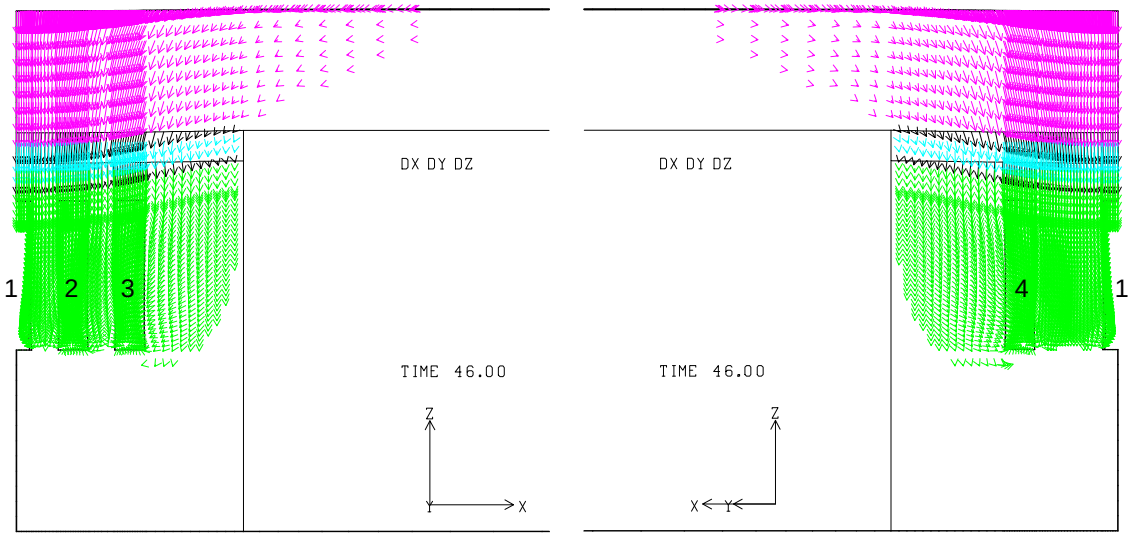

Fig. G-16. 1: Displacement vectors around the caverns at 46 years (r_C=200 ft).

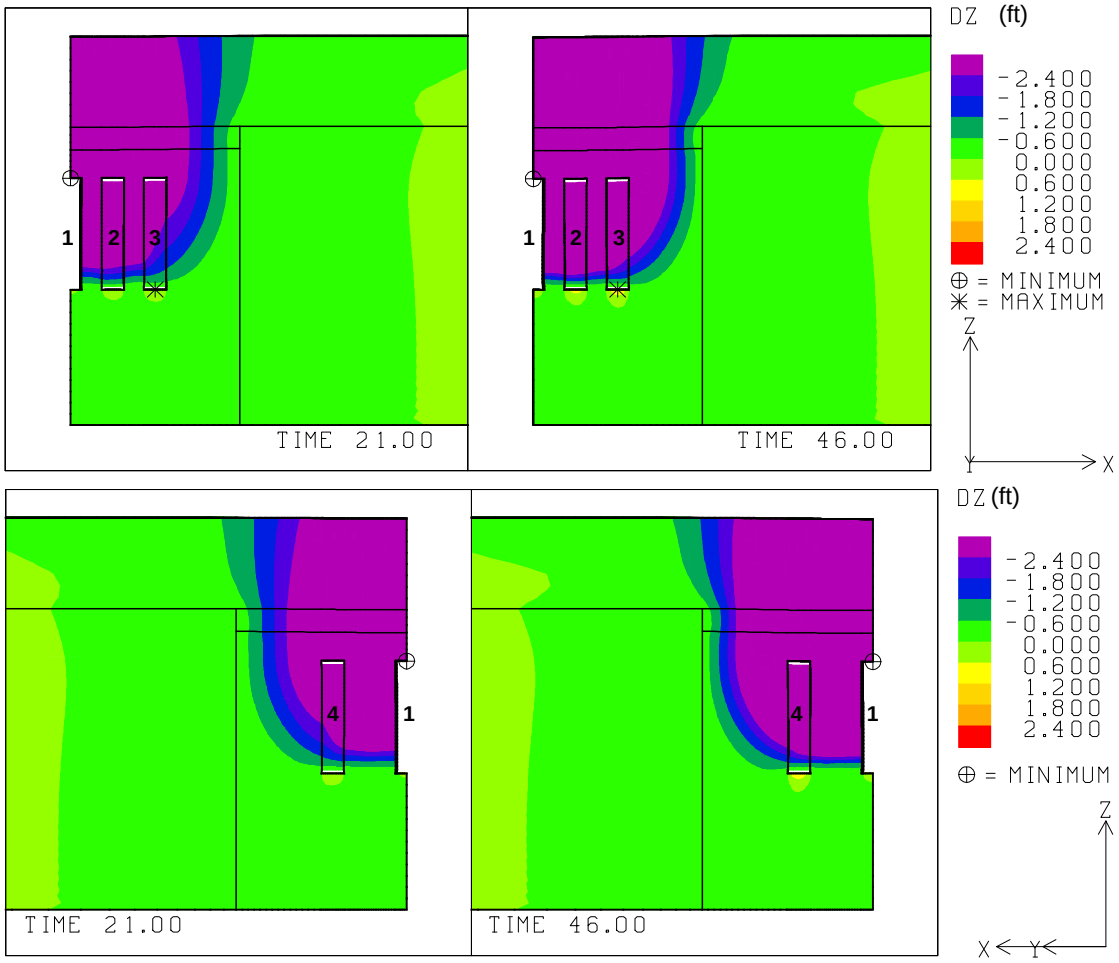

Fig. G-16. 2: Vertical displacement contours around the caverns at 21 and 46 years (r_C=200 ft).

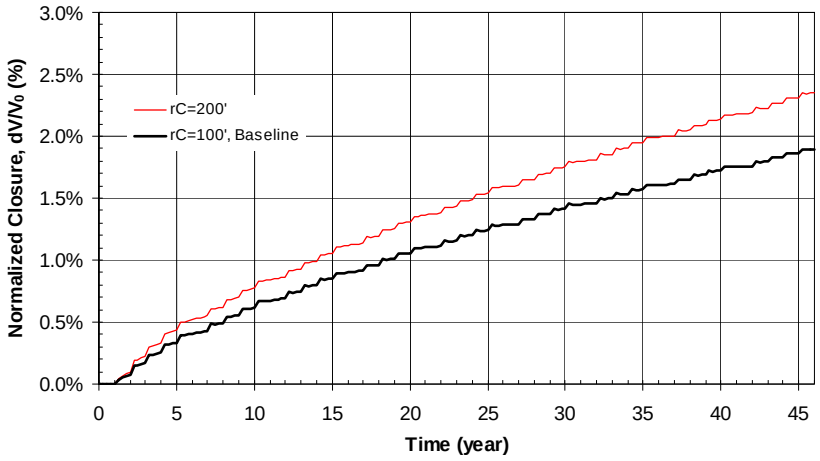

Fig. G-16. 3: Predicted total volumetric closure normalized to initial overall storage volume for the 19 SPR caverns (r_C=200 ft).

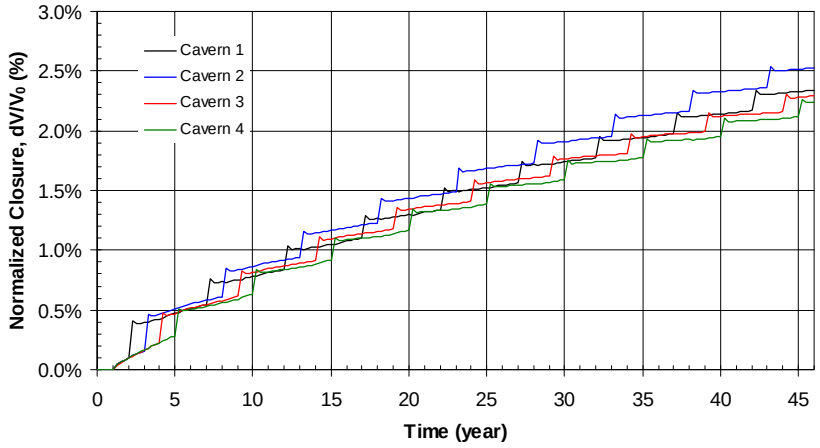

Fig. G-16. 4: Predicted volumetric closure normalized to each initial SPR cavern volume (r_C=200 ft).

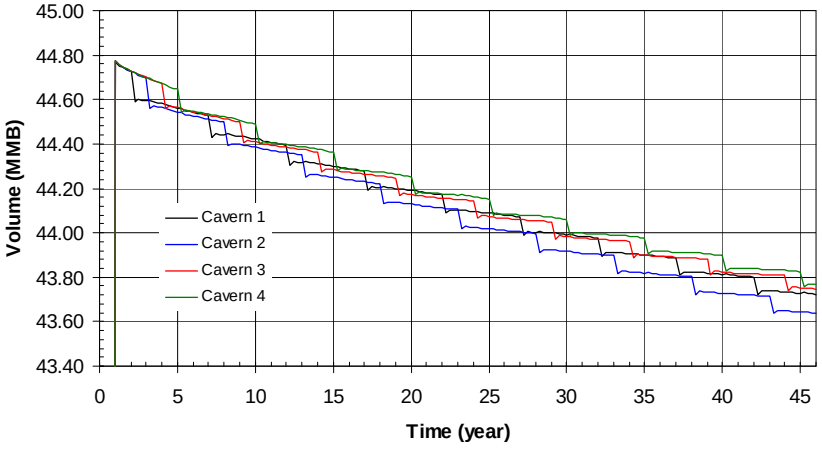

Fig. G-16. 5: Predicted volume change of each SPR cavern due to salt creep closure over time (r_C=200 ft).

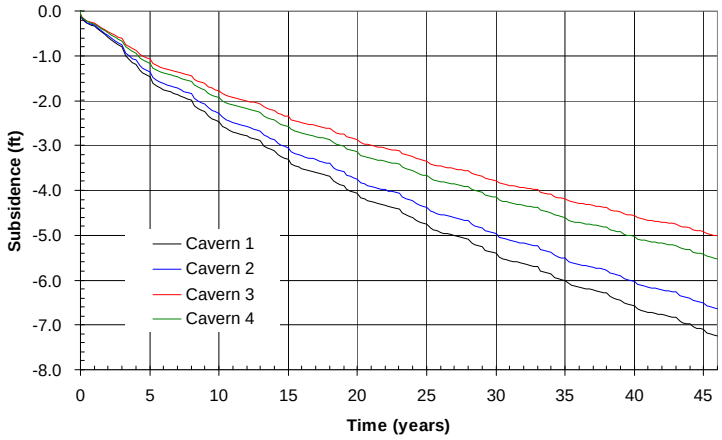

Fig. G-16. 6: Predicted subsidence on the surface above the center of SPR caverns (r_C=200 ft).

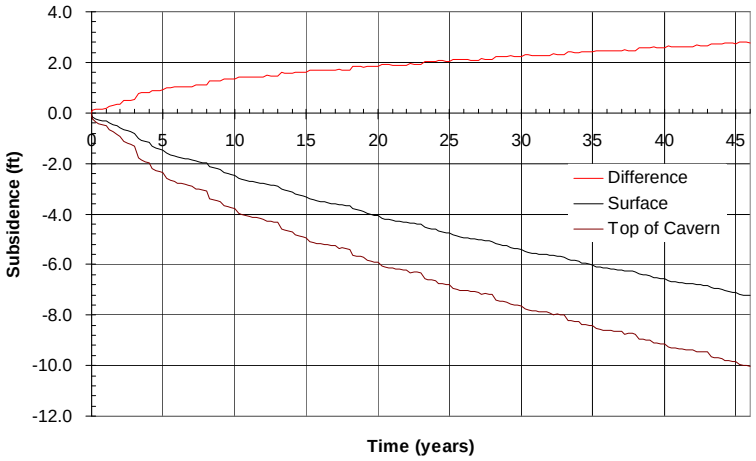

Fig. G-16. 7: Predicted difference between vertical displacement of the top of the central cavern (Cavern 1) and the surface above the cavern as a function of time.

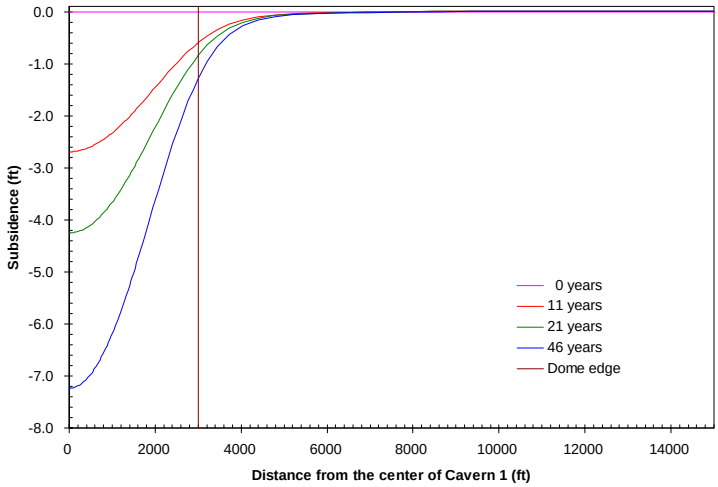

Fig. G-16. 8: Predicted subsidence on the surface from model center to edge with time.

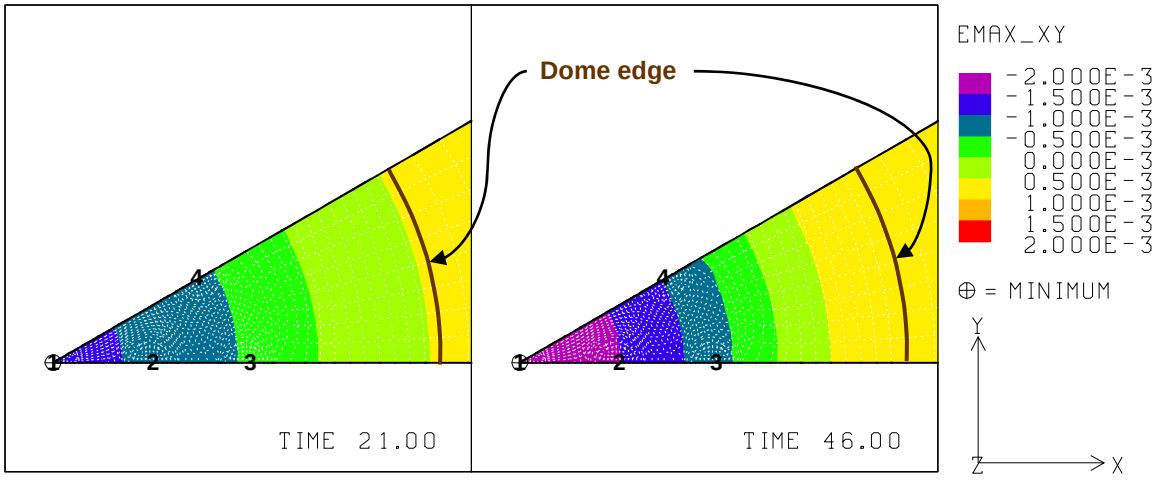

Fig. G-16. 9: Predicted radial surface strains at 21 years and 46 years (r_C=200 ft).

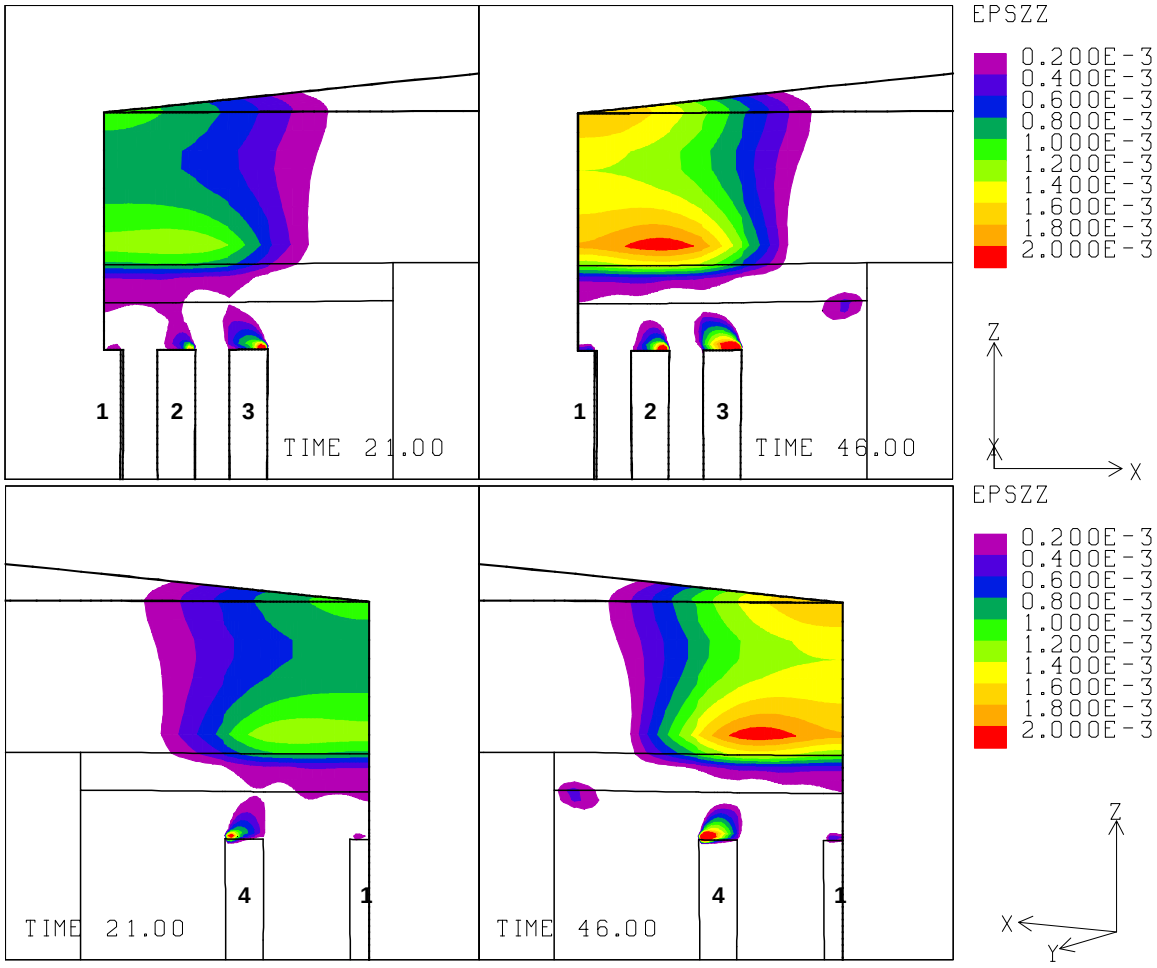

Fig. G-16. 10: Vertical strains around the roof of caverns at 21 years and 46 years (r_C=200 ft).

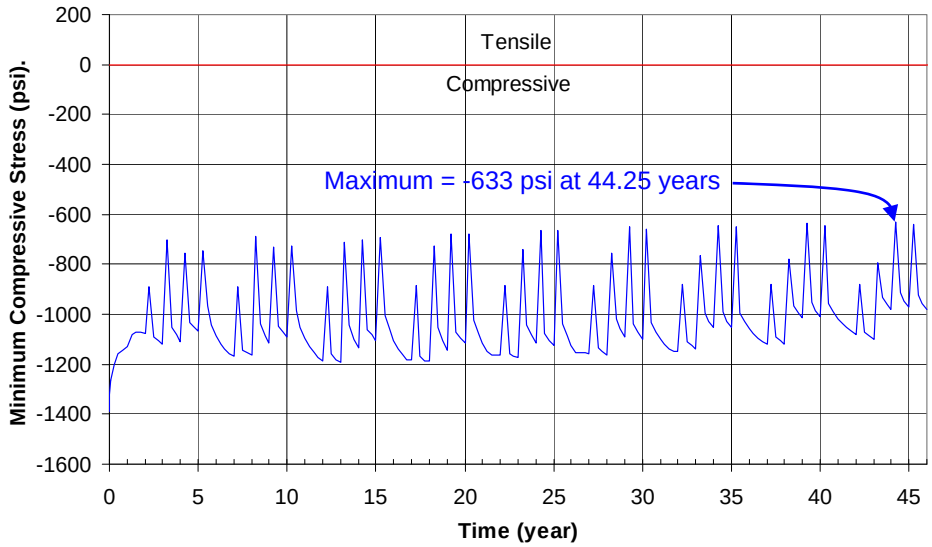

Fig. G-16. 11: Predicted minimum compressive stress history in the salt dome (r_C=200 ft).

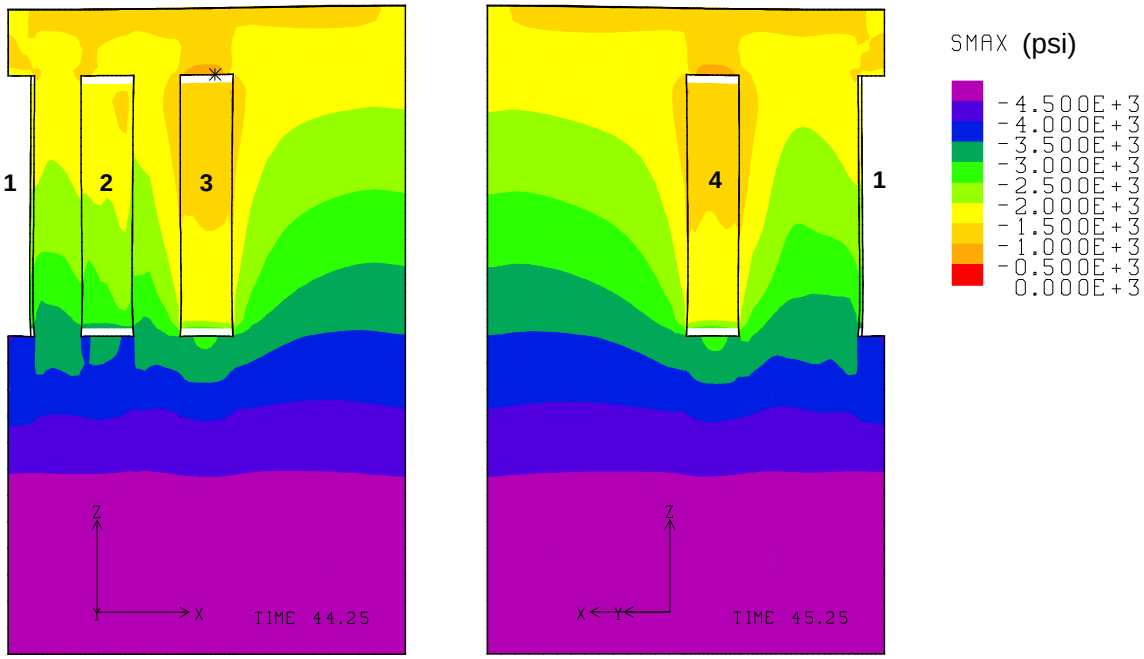

Fig. G-16. 12: Compressive stress contours around the caverns during workover of Cavern 3 and Cavern 4 at 44.25 years and 45.25 years, respectively (r_C=200 ft).

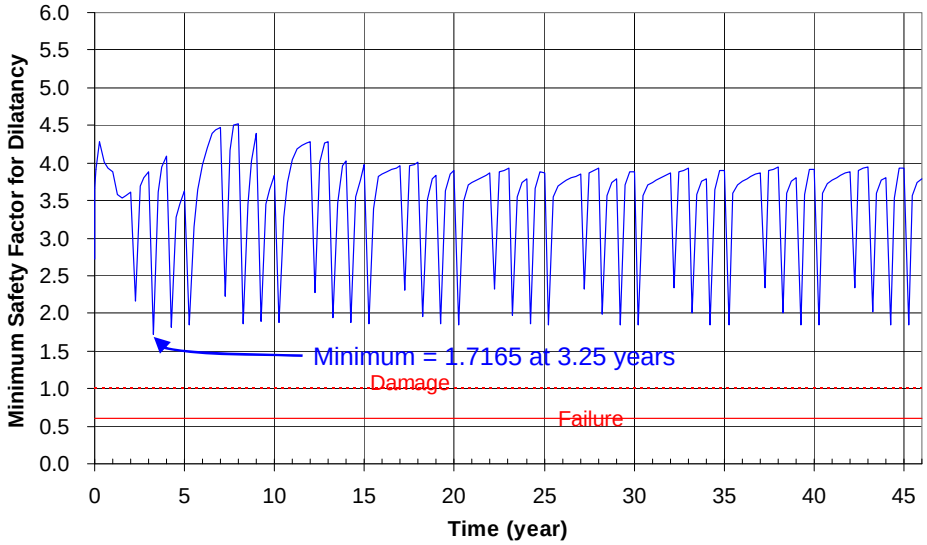

Fig. G-16. 13: Predicted minimum safety factor history against dilatant damage (r_C=200 ft).

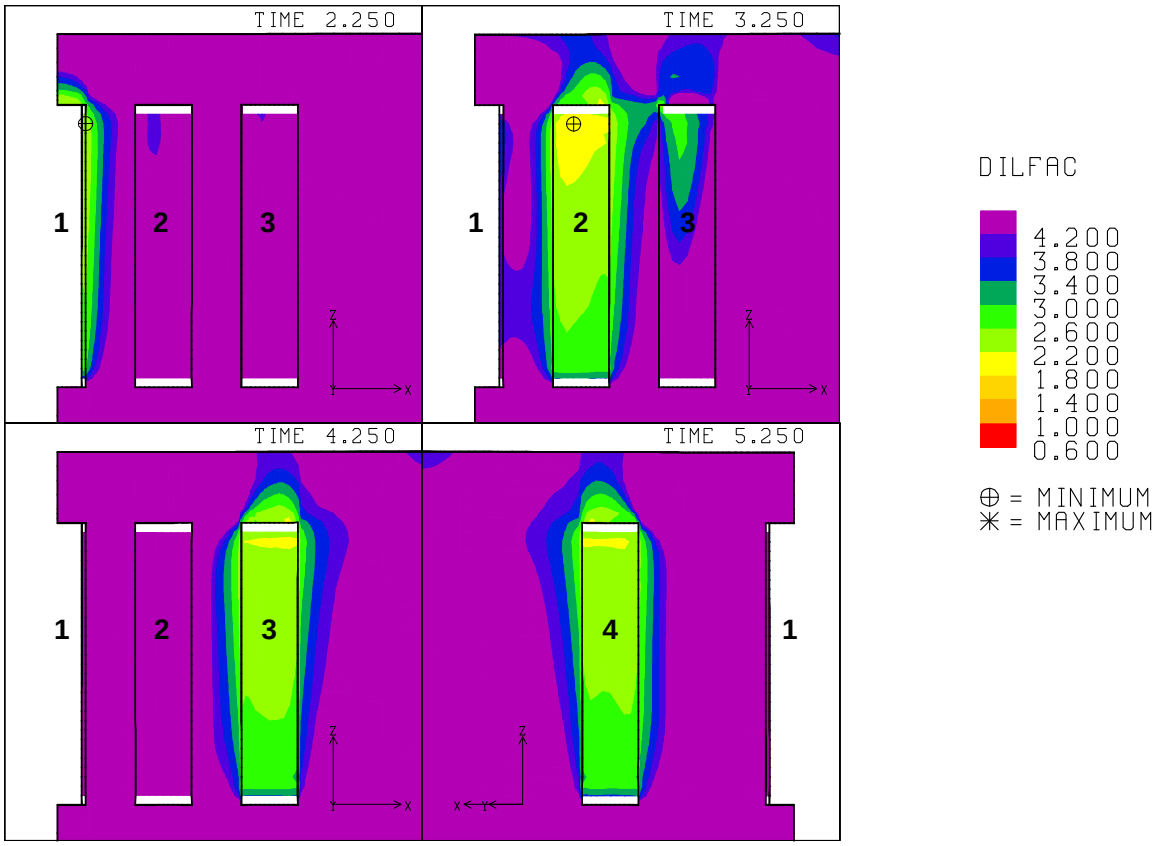

Fig. G-16. 14: Safety factor contours against dilatant damage around the caverns during workover of Caverns 1, 2, 3 and 4 at 2.25 years, 3.25 years, 4.25 years and 5.25 years, respectively (r_C=200 ft).

G-17. Cavern Depth, d_C = 1000 ft, Depth of Salt Dome Top, d_{SD} = 500 ft

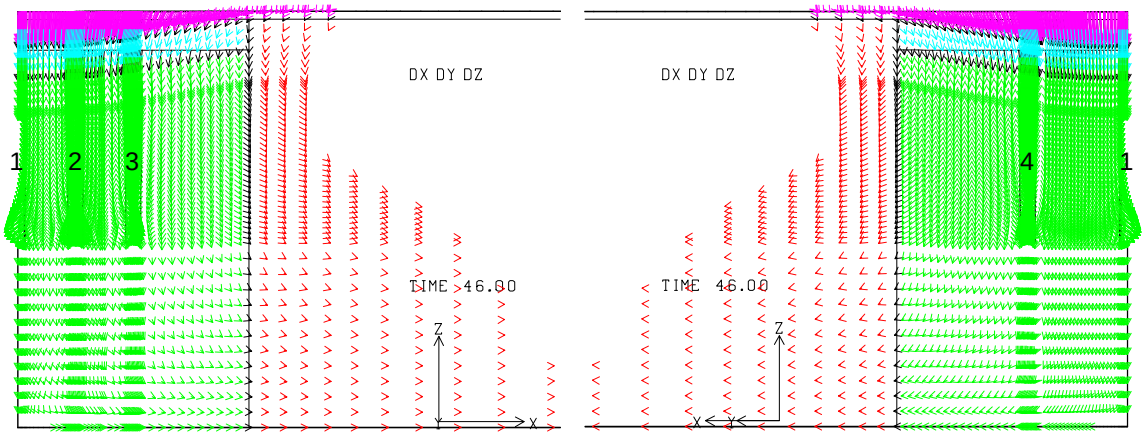

Fig. G-17. 1: Displacement vectors around the caverns at 46 years (d_C=1000 ft, d_{SD}=500 ft).

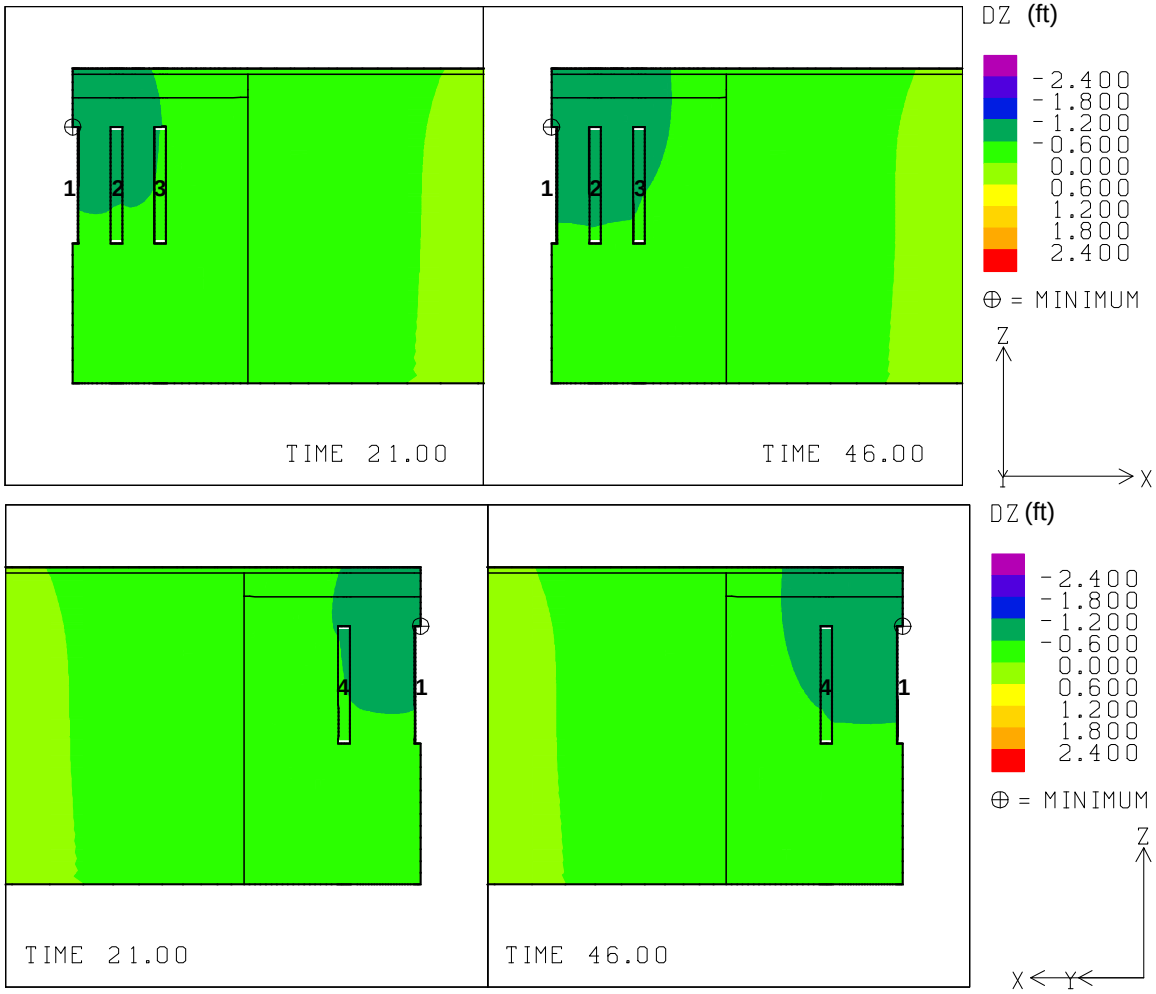

Fig. G-17. 2: Vertical displacement contours around the caverns at 21 and 46 years (d_C=1000 ft, d_{SD}=500 ft).

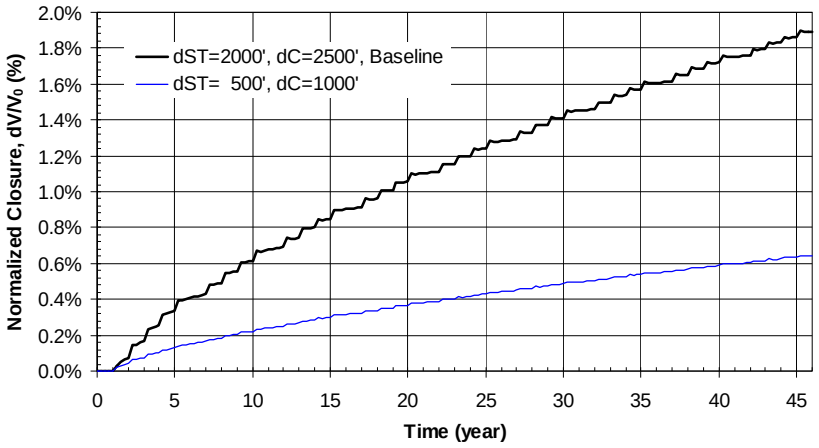

Fig. G-17. 3: Predicted total volumetric closure normalized to initial overall storage volume for the 19 SPR caverns (d_C=1000 ft, d_{SD}=500 ft).

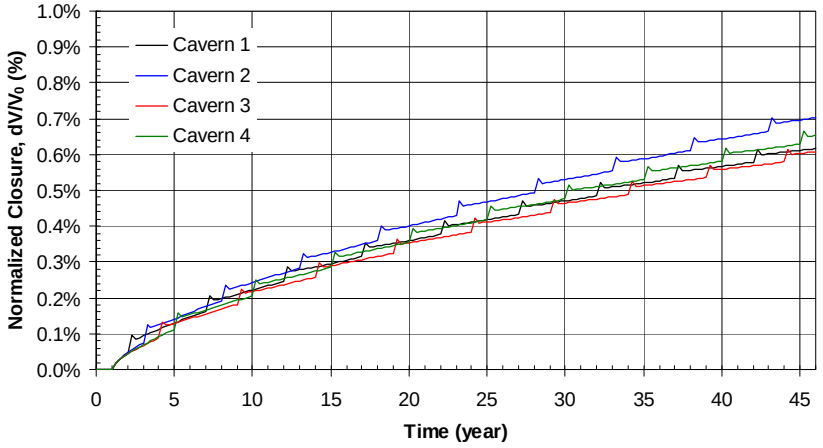

Fig. G-17. 4: Predicted volumetric closure normalized to each initial SPR cavern volume (d_C=1000 ft, d_{SD}=500 ft).

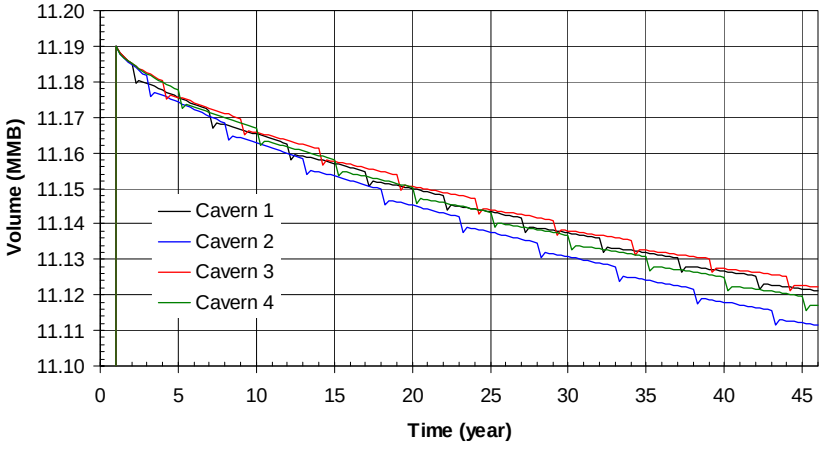

Fig. G-17. 5: Predicted volume change of each SPR cavern due to salt creep closure over time (d_C=1000 ft, d_{SD}=500 ft).

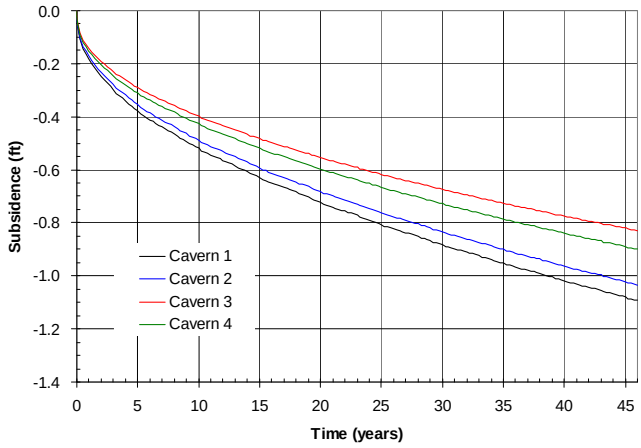

Fig. G-17. 6: Predicted subsidence on the surface above the center of SPR caverns (d_C=1000 ft, d_{SD}=500 ft).

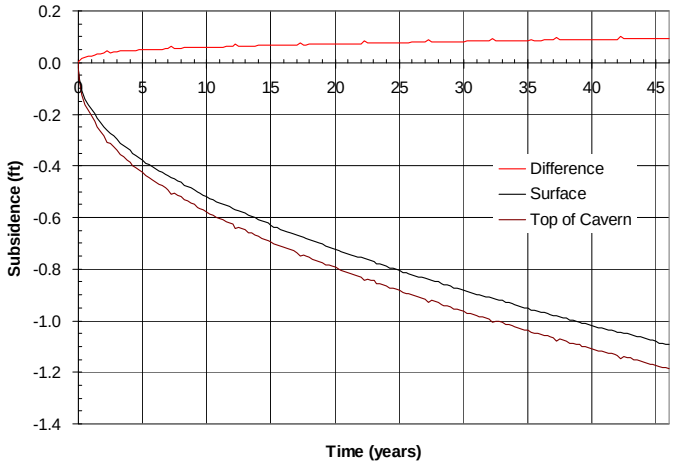

Fig. G-17. 7: Predicted difference between vertical displacement of the top of the central cavern (Cavern 1) and the surface above the cavern as a function of time.

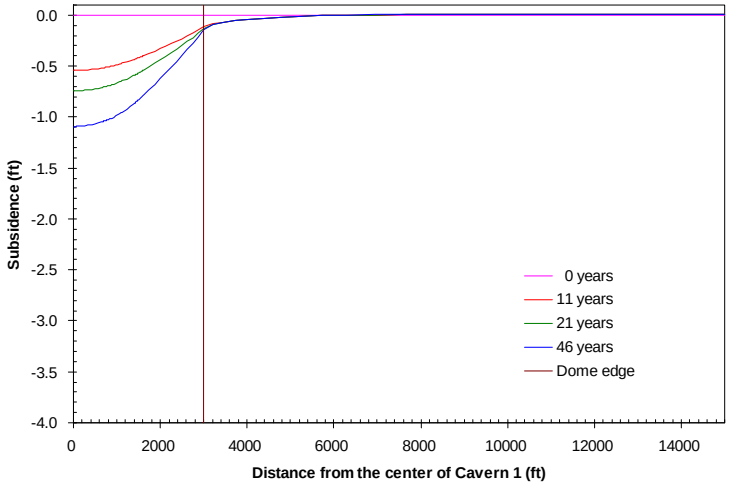

Fig. G-17. 8: Predicted subsidence on the surface from model center to edge with time.

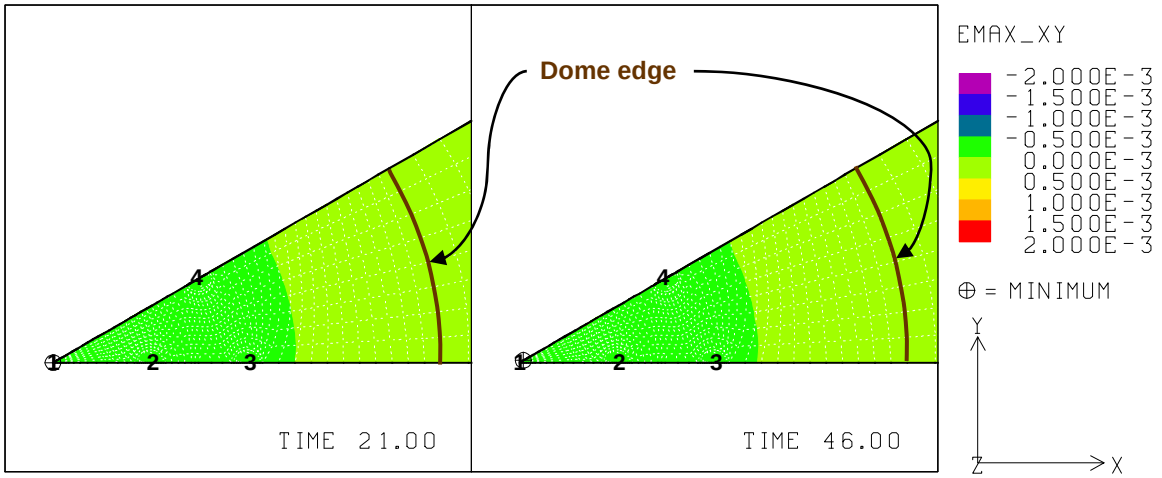

Fig. G-17. 9: Predicted radial surface strains at 21 years and 46 years (d_C=1000 ft, d_{SD}=500 ft).

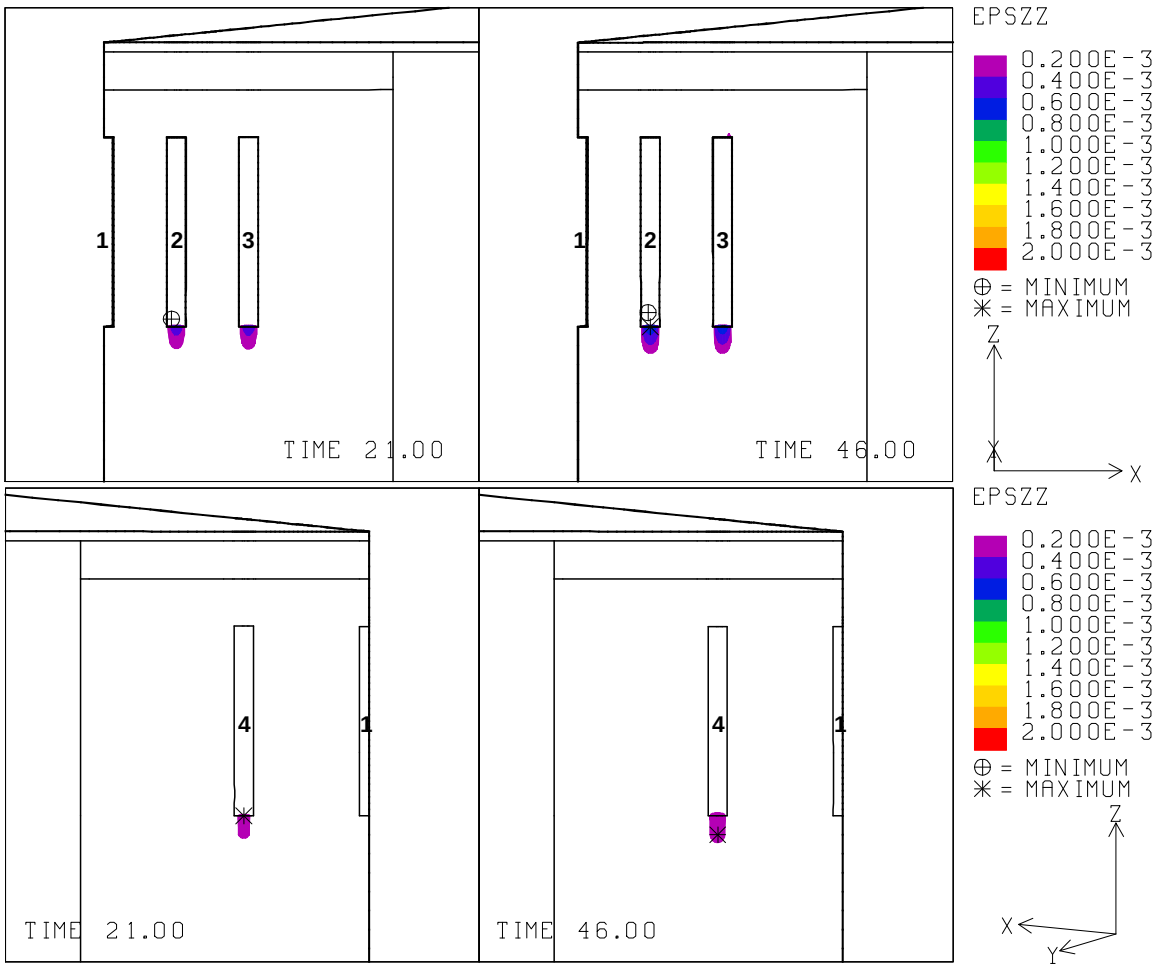

Fig. G-17. 10: Vertical strains around the roof of caverns at 21 years and 46 years (d_C=1000 ft, d_{SD}=500 ft).

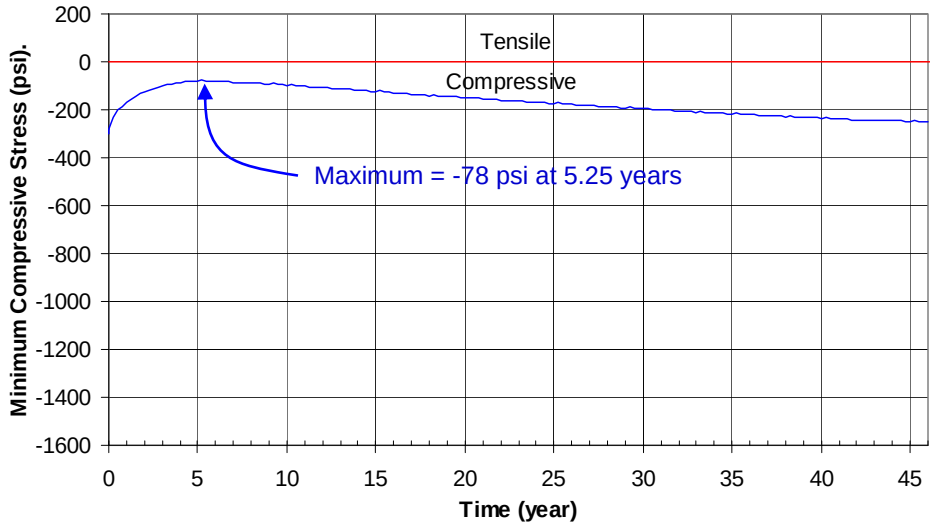

Fig. G-17. 11: Predicted minimum compressive stress history in the salt dome (d_C=1000 ft, d_{SD}=500 ft).

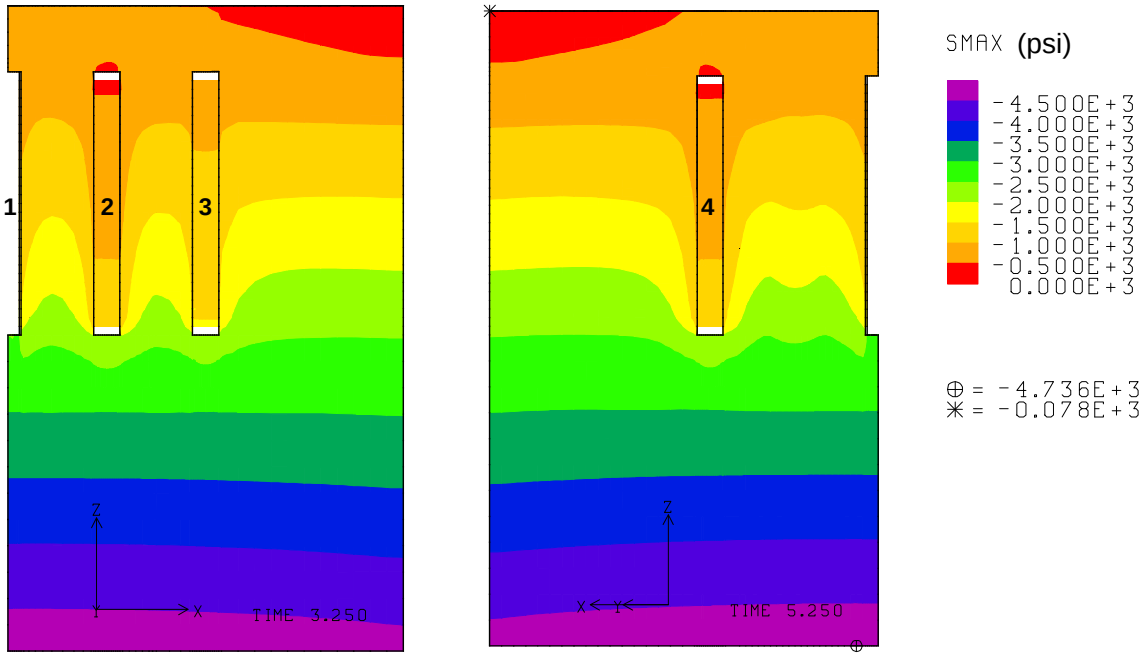

Fig. G-17. 12: Compressive stress contours around the caverns during workover of Cavern 3 and Cavern 4 at 3.25 years and 5.25 years, respectively (d_C=1000 ft, d_{SD}=500 ft).

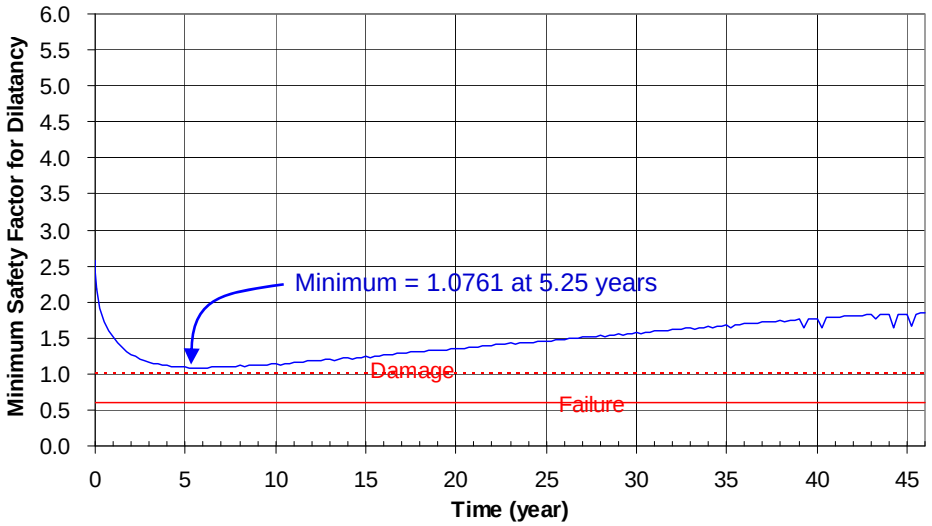

Fig. G-17. 13: Predicted minimum safety factor history against dilatant damage (d_C=1000 ft, d_{SD}=500 ft).

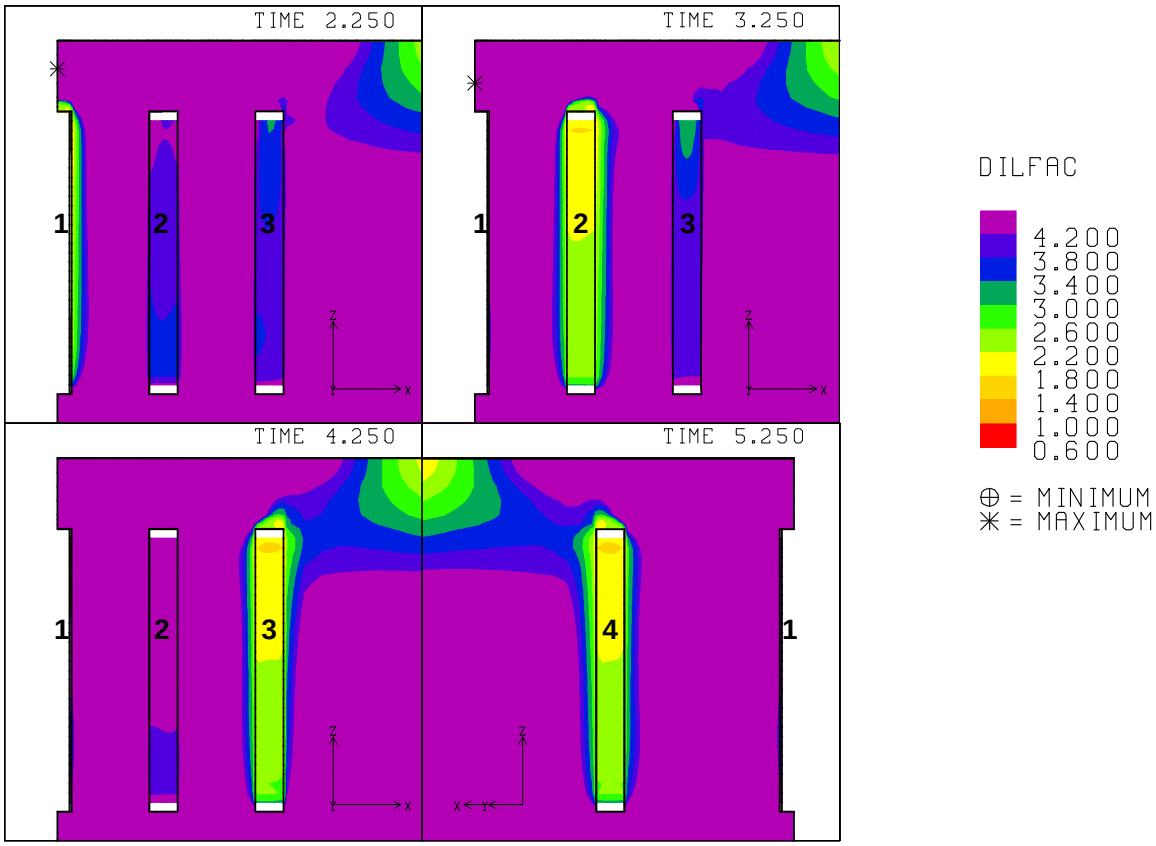

Fig. G-17. 14: Safety factor contours against dilatant damage around the caverns during workover of Caverns 1, 2, 3 and 4 at 2.25 years, 3.25 years, 4.25 years and 5.25 years, respectively (d_C=1000 ft, d_{SD}=500 ft).

G-18. Cavern Depth, d_C = 2100 ft, Depth of Salt Dome Top, d_{SD} = 2000 ft

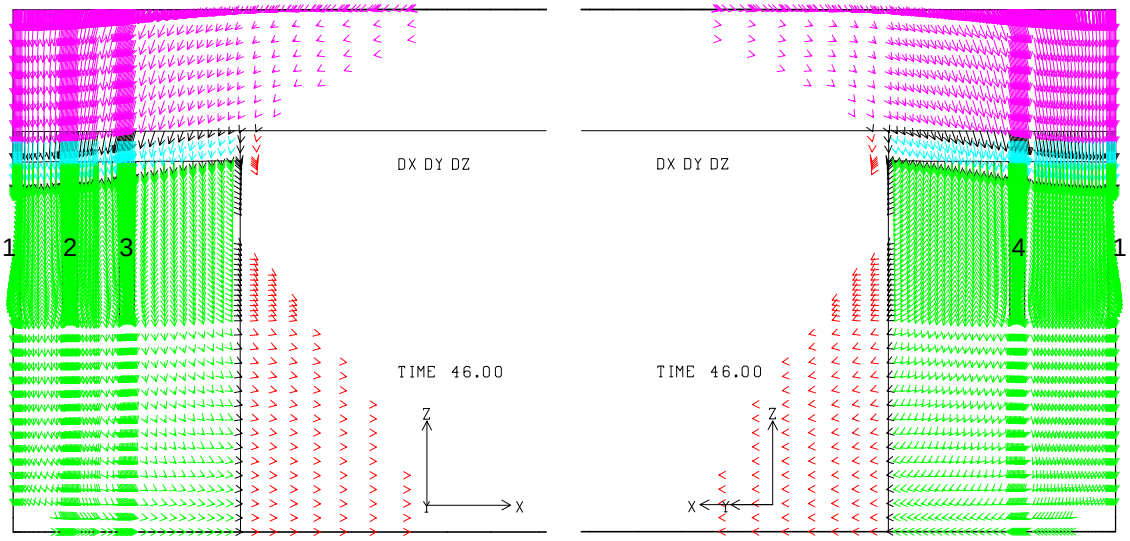

Fig. G-18. 1: Displacement vectors around the caverns at 46 years (d_C=2100 ft, d_{SD}=2000 ft).

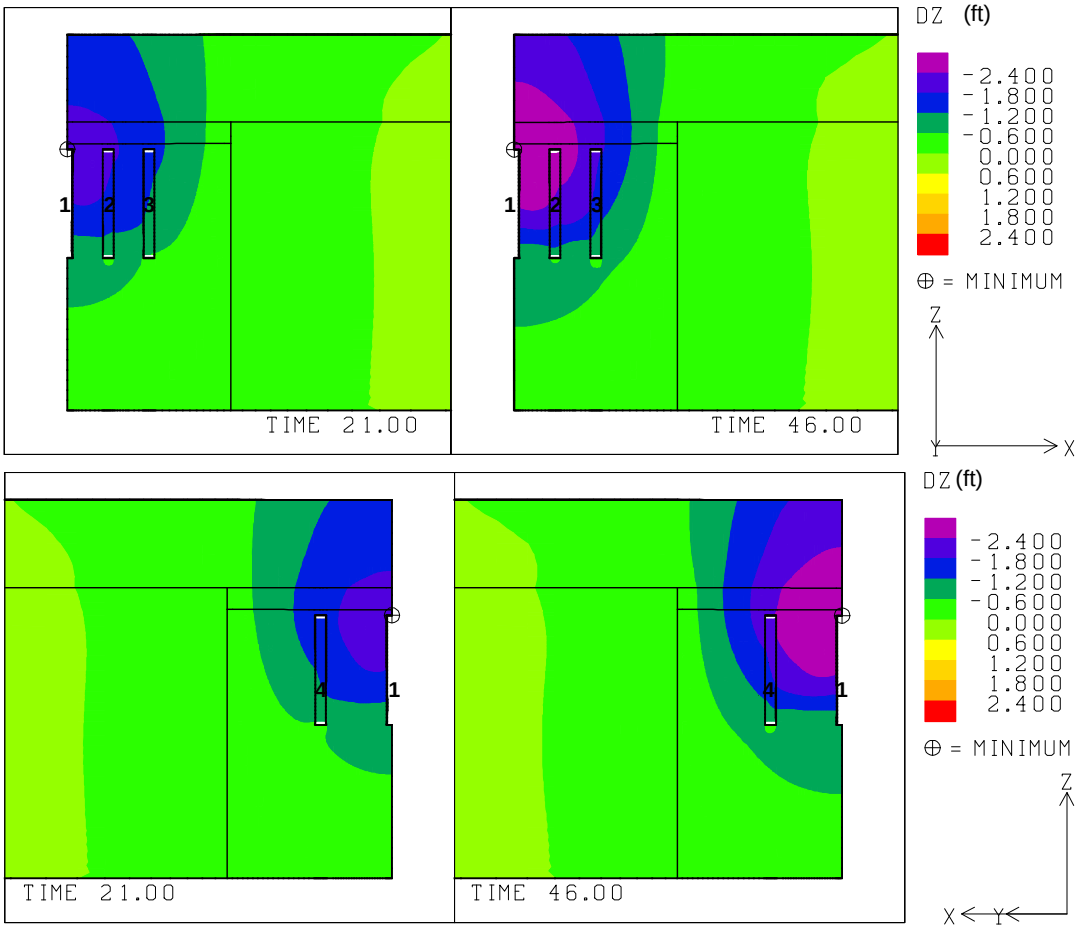

Fig. G-18. 2: Vertical displacement contours around the caverns at 21 and 46 years (d_C=2100 ft, d_{SD}=2000 ft).

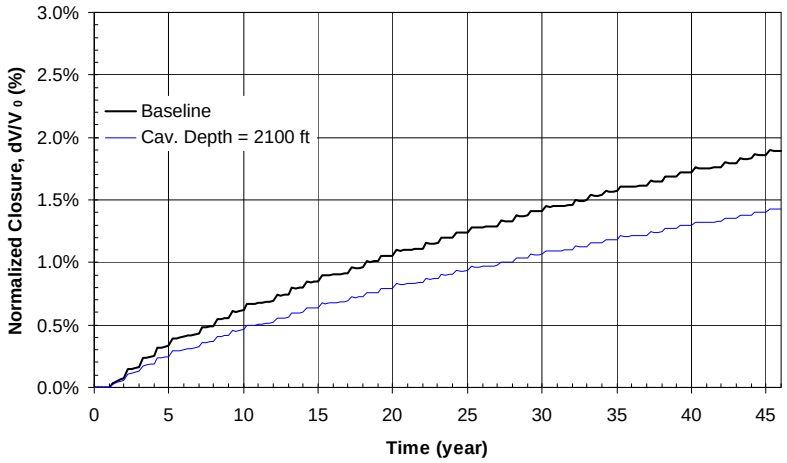

Fig. G-18. 3: Predicted total volumetric closure normalized to initial overall storage volume for the 19 SPR caverns (d_C=2100 ft, d_{SD}=2000 ft).

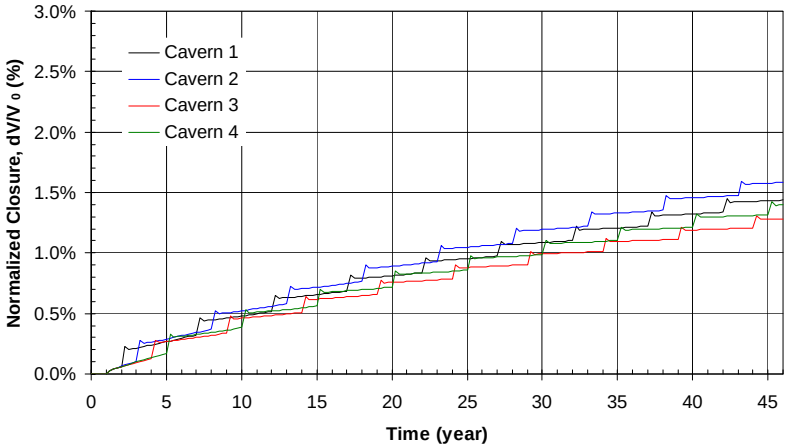

Fig. G-18. 4: Predicted volumetric closure normalized to each initial SPR cavern volume (d_C=2100 ft, d_{SD}=2000 ft).

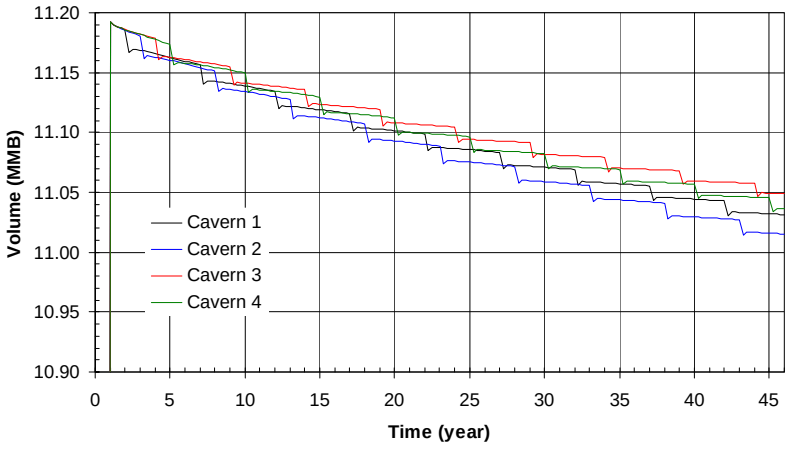

Fig. G-18. 5: Predicted volume change of each SPR cavern due to salt creep closure over time (d_C=2100 ft, d_{SD}=2000 ft).

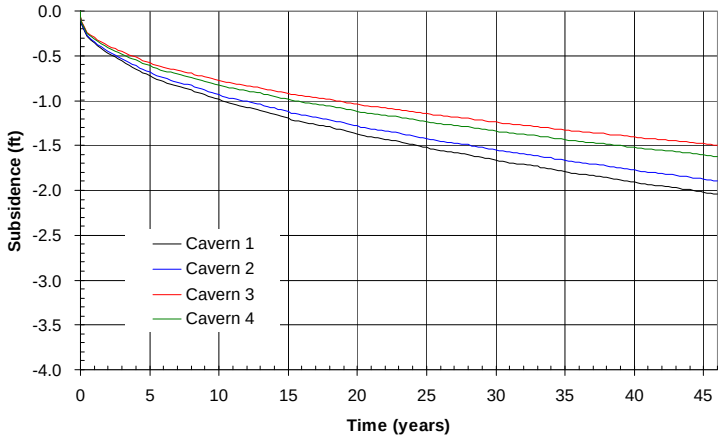

Fig. G-18. 6: Predicted subsidence on the surface above the center of SPR caverns (d_C=2100 ft, d_{SD}=2000 ft).

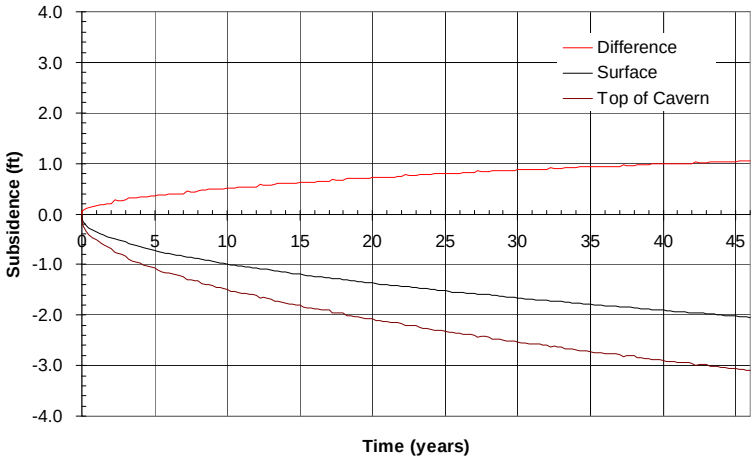

Fig. G-18. 7: Predicted difference between vertical displacement of the top of the central cavern (Cavern 1) and the surface above the cavern as a function of time.

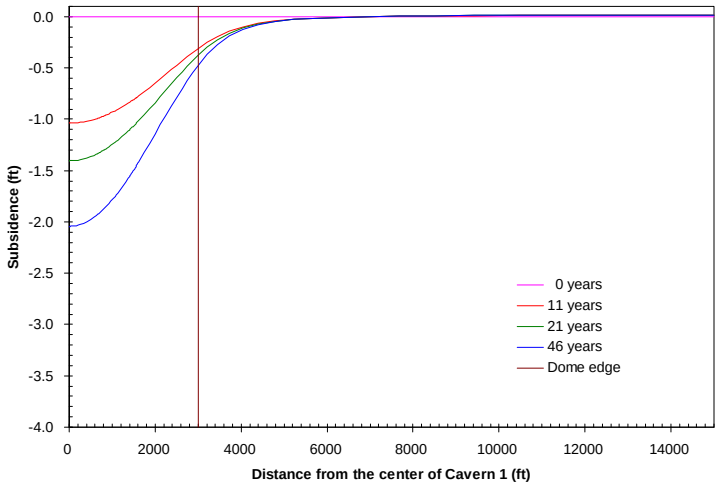

Fig. G-18. 8: Predicted subsidence on the surface from model center to edge with time.

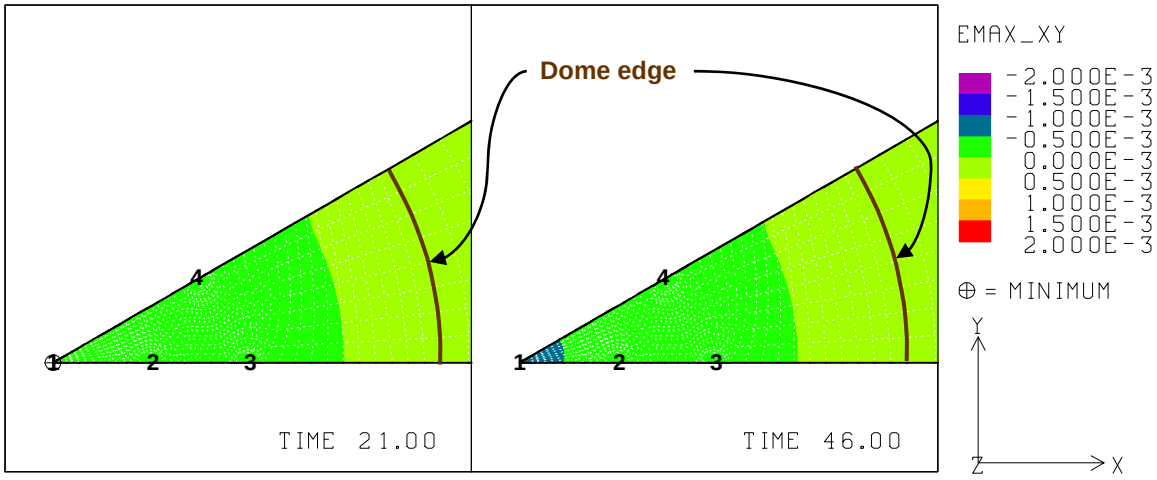

Fig. G-18. 9: Predicted radial surface strains at 21 years and 46 years (d_C=2100 ft, d_{SD}=2000 ft).

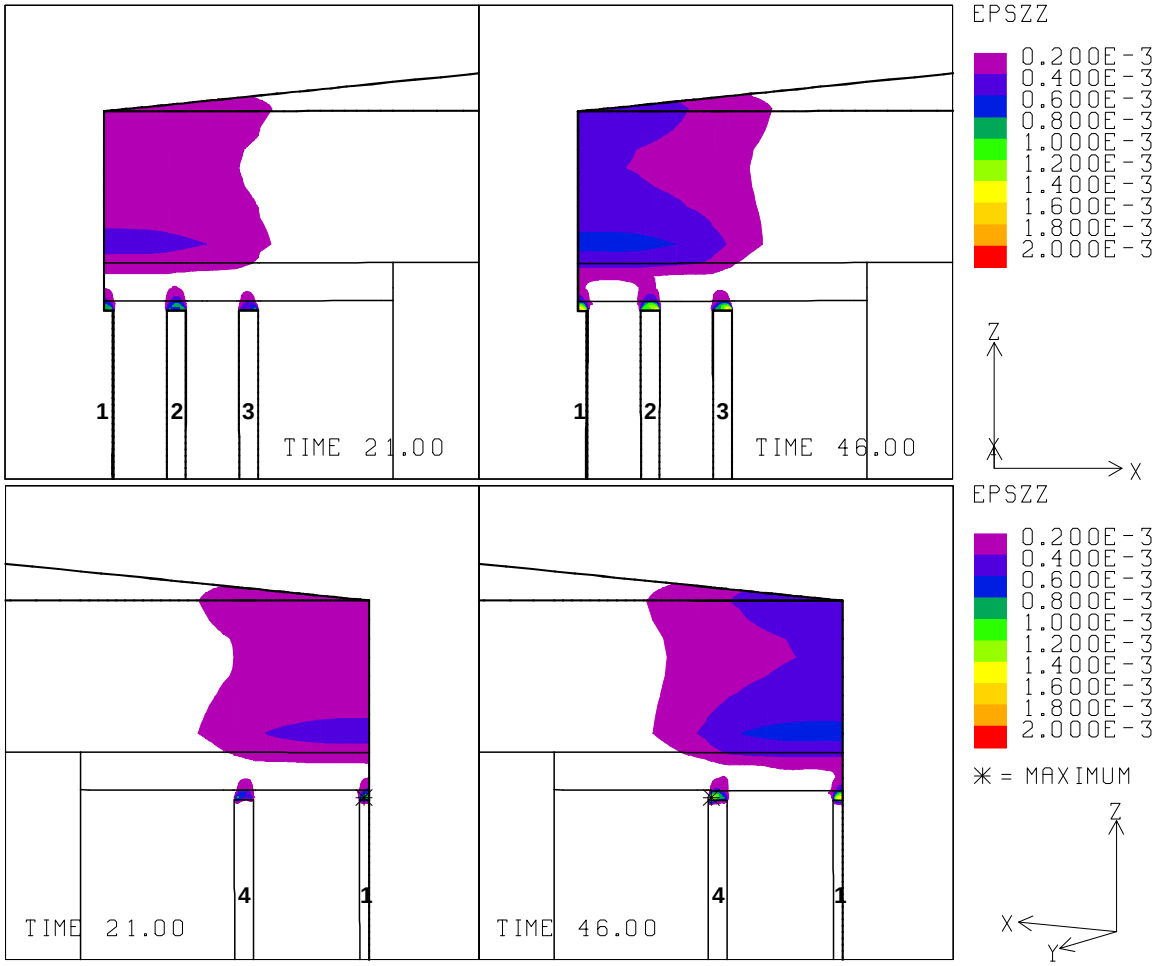

Fig. G-18. 10: Vertical strains around the roof of caverns at 21 years and 46 years (d_C=2100 ft, d_{SD}=2000 ft).

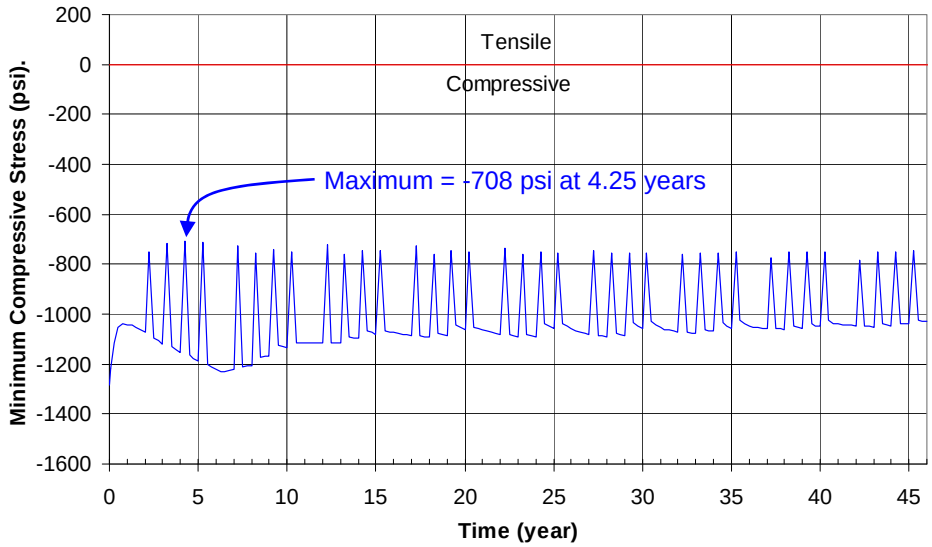

Fig. G-18. 11: Predicted minimum compressive stress history in the salt dome (d_C=2100 ft, d_{SD}=2000 ft).

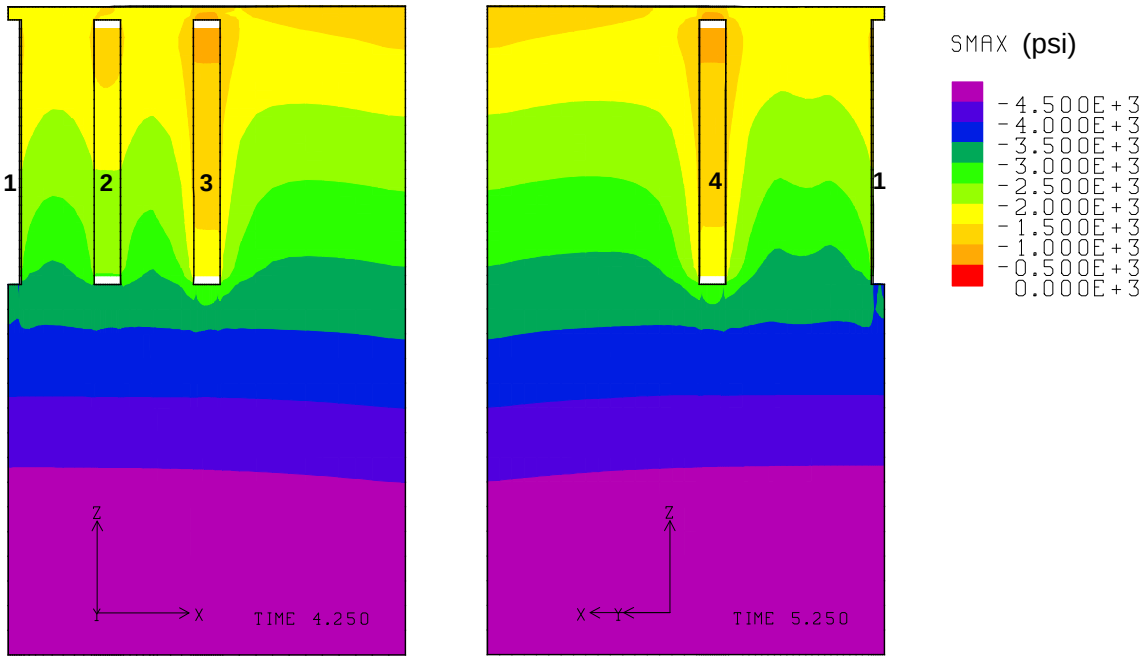

Fig. G-18. 12: Compressive stress contours around the caverns during workover of Cavern 3 and Cavern 4 at 3.25 years and 5.25 years, respectively (d_C=2100 ft, d_{SD}=2000 ft).

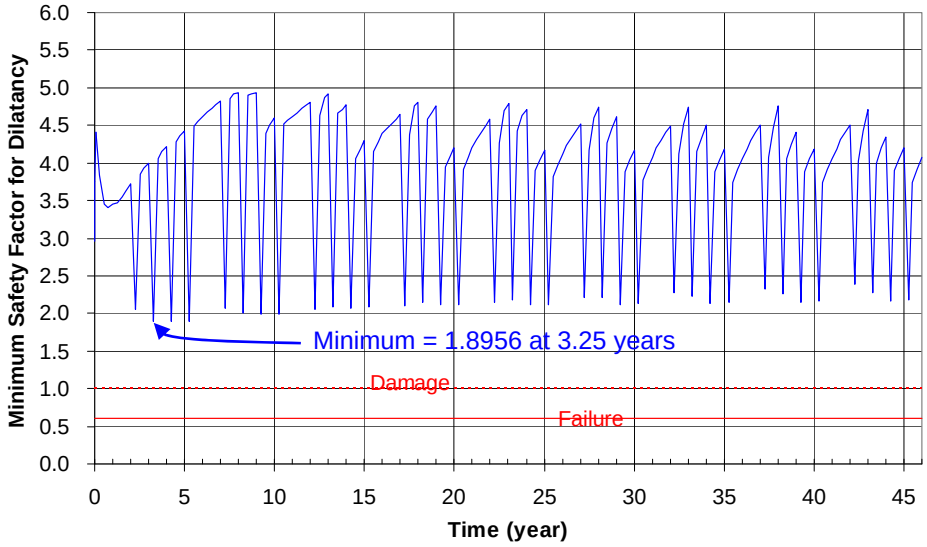

Fig. G-18. 13: Predicted minimum safety factor history against dilatant damage (d_C=2100 ft, d_{SD}=2000 ft).

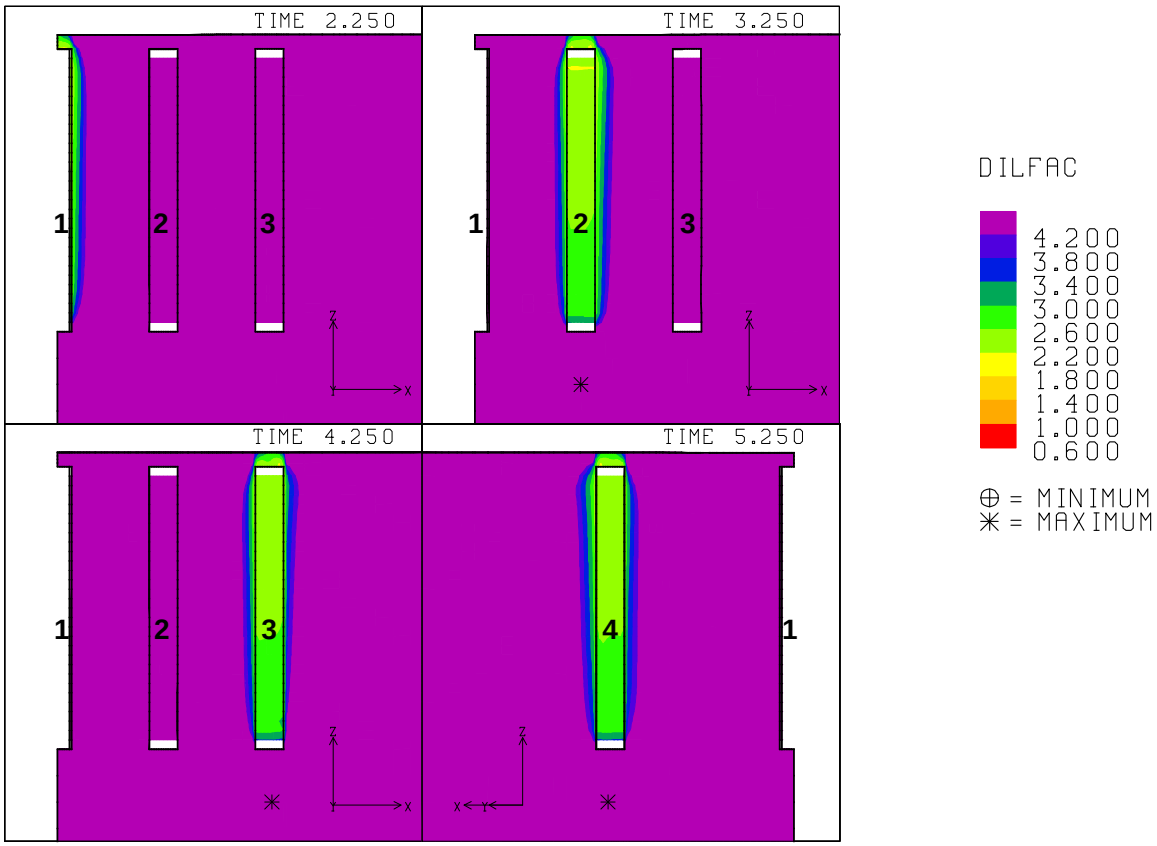

Fig. G-18. 14: Safety factor contours against dilatant damage around the caverns during workover of Caverns 1, 2, 3 and 4 at 2.25 years, 3.25 years, 4.25 years and 5.25 years, respectively (d_C=2100 ft, d_{SD}=2000 ft).

G-19. Cavern Depth, d_C = 4000 ft, Depth of Salt Dome Top, d_{SD} = 2000 ft

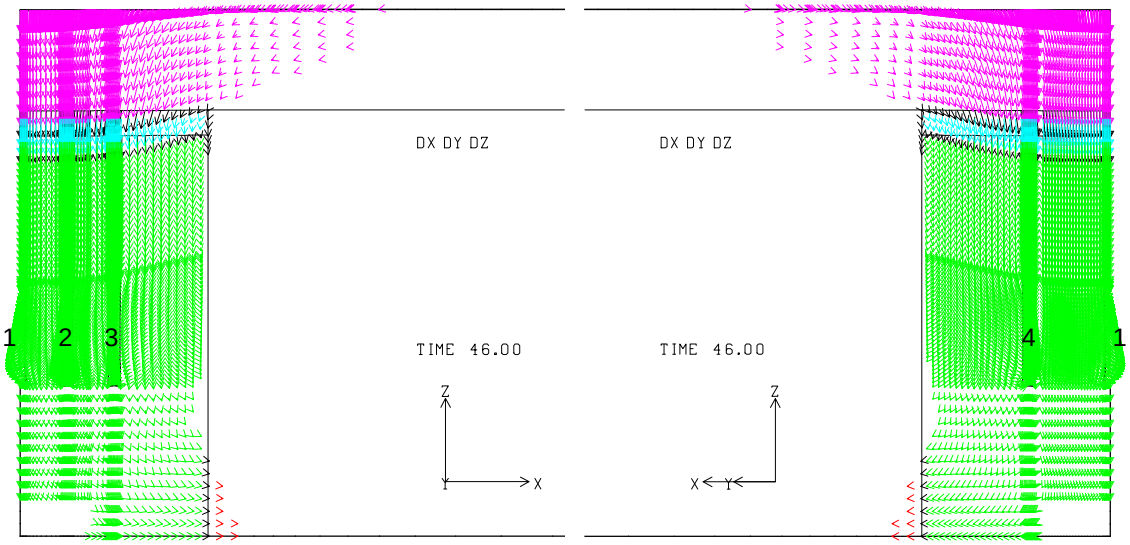

Fig. G-19. 1: Displacement vectors around the caverns at 46 years (d_C=4000 ft, d_{SD}=2000 ft).

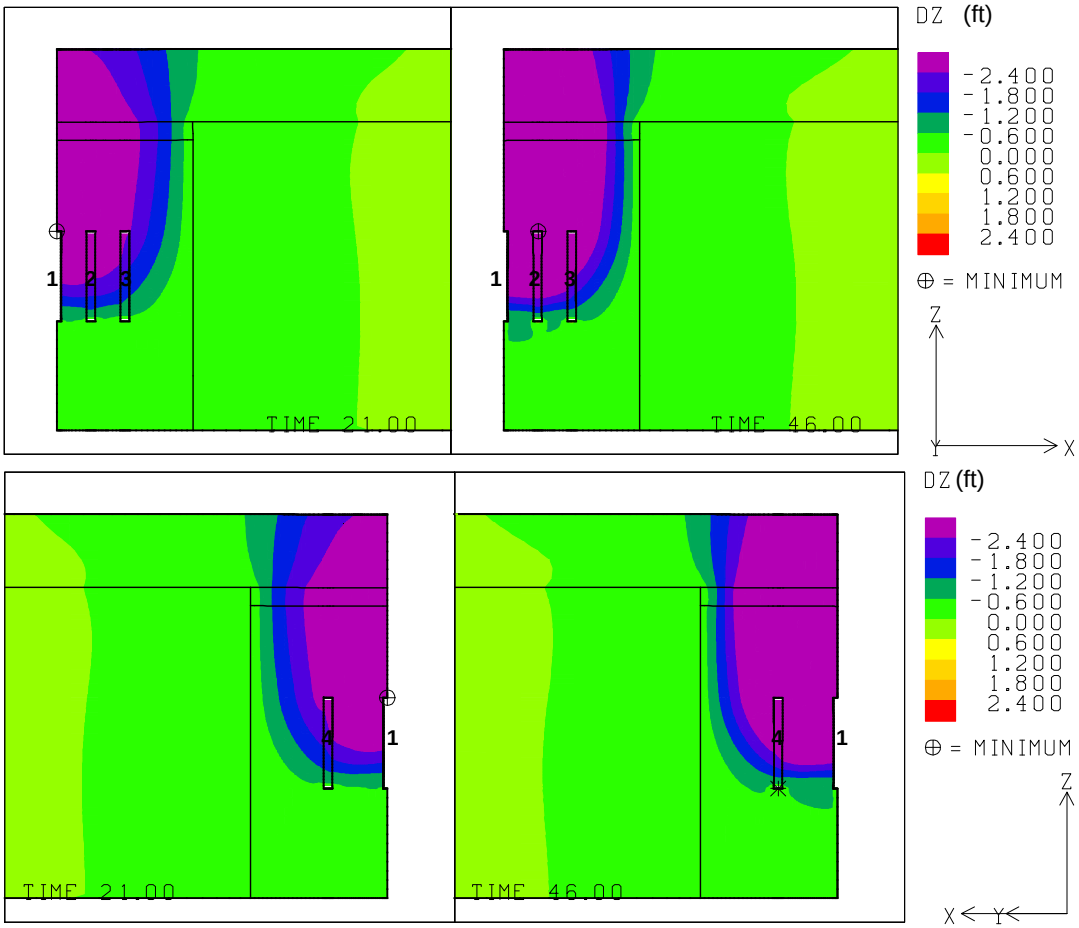

Fig. G-19. 2: Vertical displacement contours around the caverns at 21 and 46 years (d_C=4000 ft, d_{SD}=2000 ft).

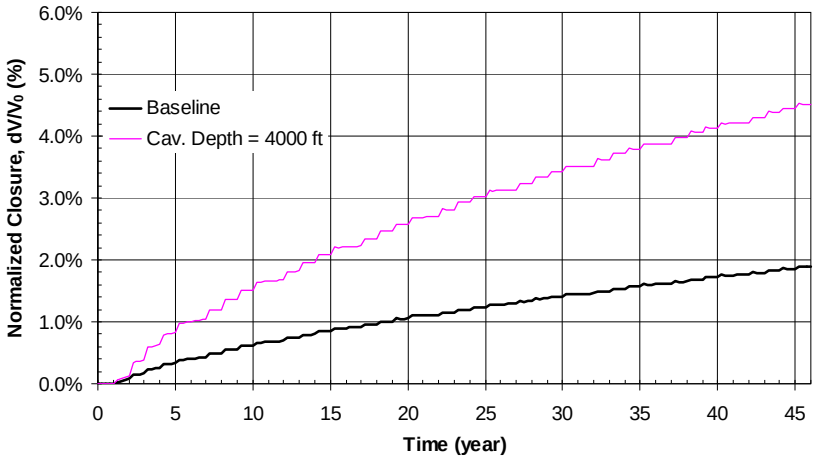

Fig. G-19. 3: Predicted total volumetric closure normalized to initial overall storage volume for the 19 SPR caverns (d_C=4000 ft, d_{SD}=2000 ft).

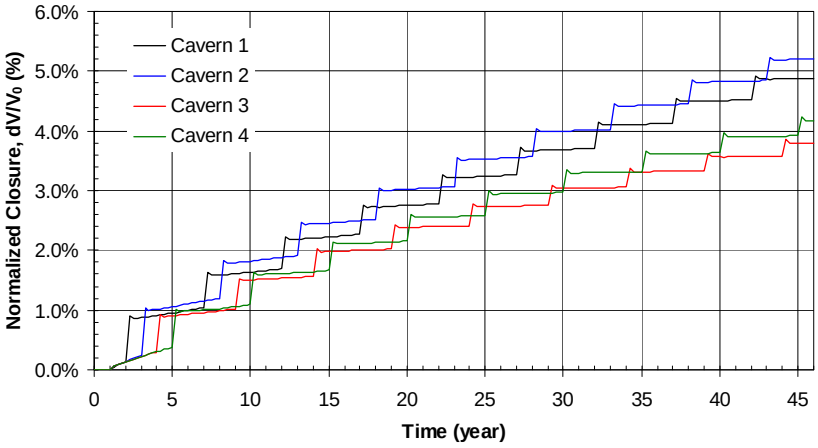

Fig. G-19. 4: Predicted volumetric closure normalized to each initial SPR cavern volume (d_C=4000 ft, d_{SD}=2000 ft).

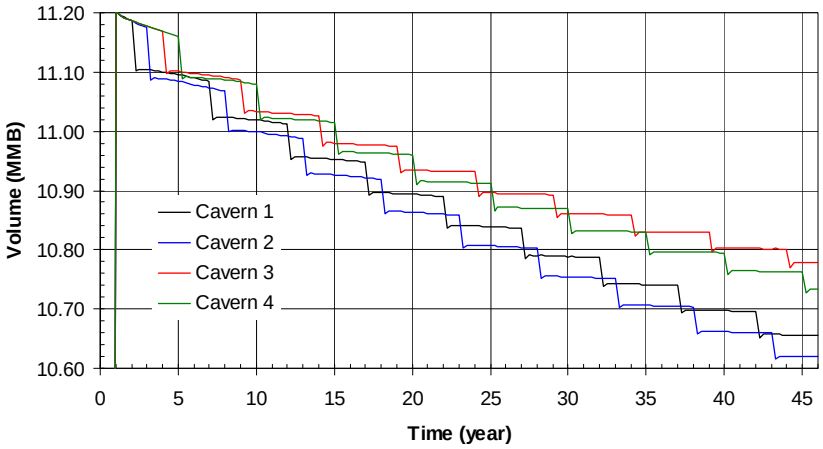

Fig. G-19. 5: Predicted volume change of each SPR cavern due to salt creep closure over time (d_C=4000 ft, d_{SD}=2000 ft).

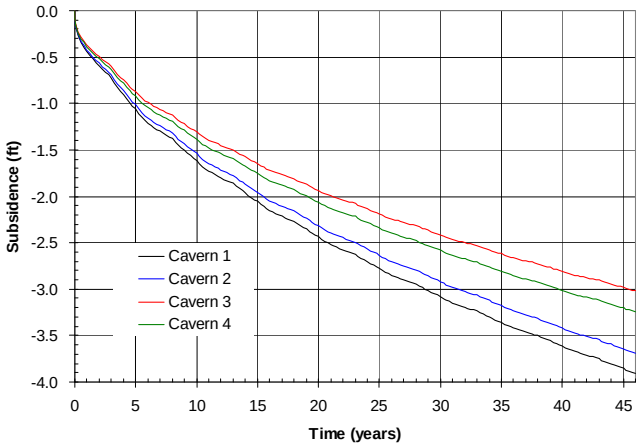

Fig. G-19. 6: Predicted subsidence on the surface above the center of SPR caverns (d_C=4000 ft, d_{SD}=2000 ft).

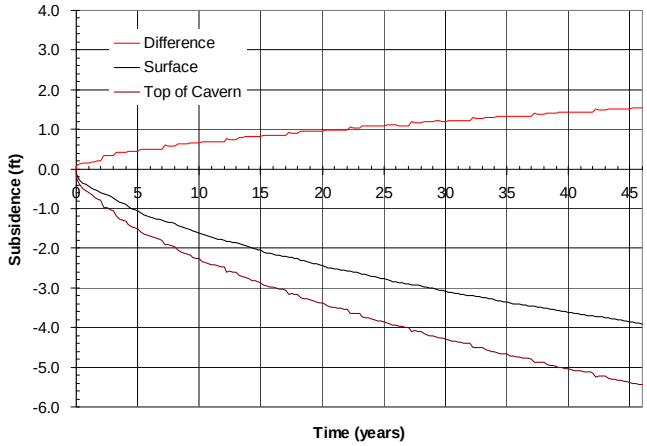

Fig. G-19. 7: Predicted difference between vertical displacement of the top of the central cavern (Cavern 1) and the surface above the cavern as a function of time (d_C=4000 ft, d_{SD}=2000 ft).

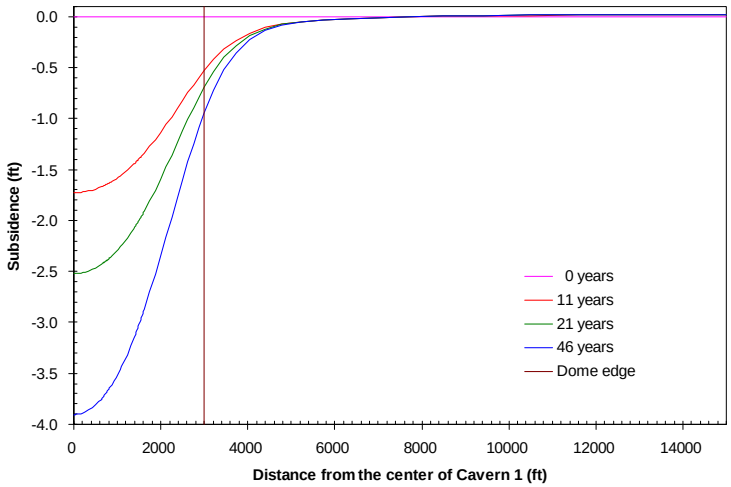

Fig. G-19. 8: Predicted subsidence on the surface from model center to edge with time.

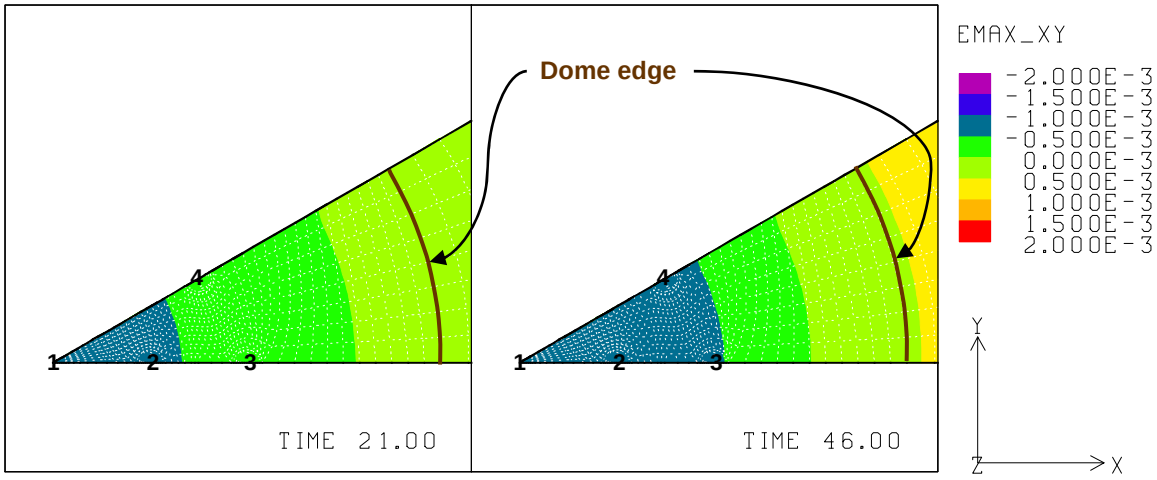

Fig. G-19. 9: Predicted radial surface strains at 21 years and 46 years (d_C=4000 ft, d_{SD}=2000 ft).

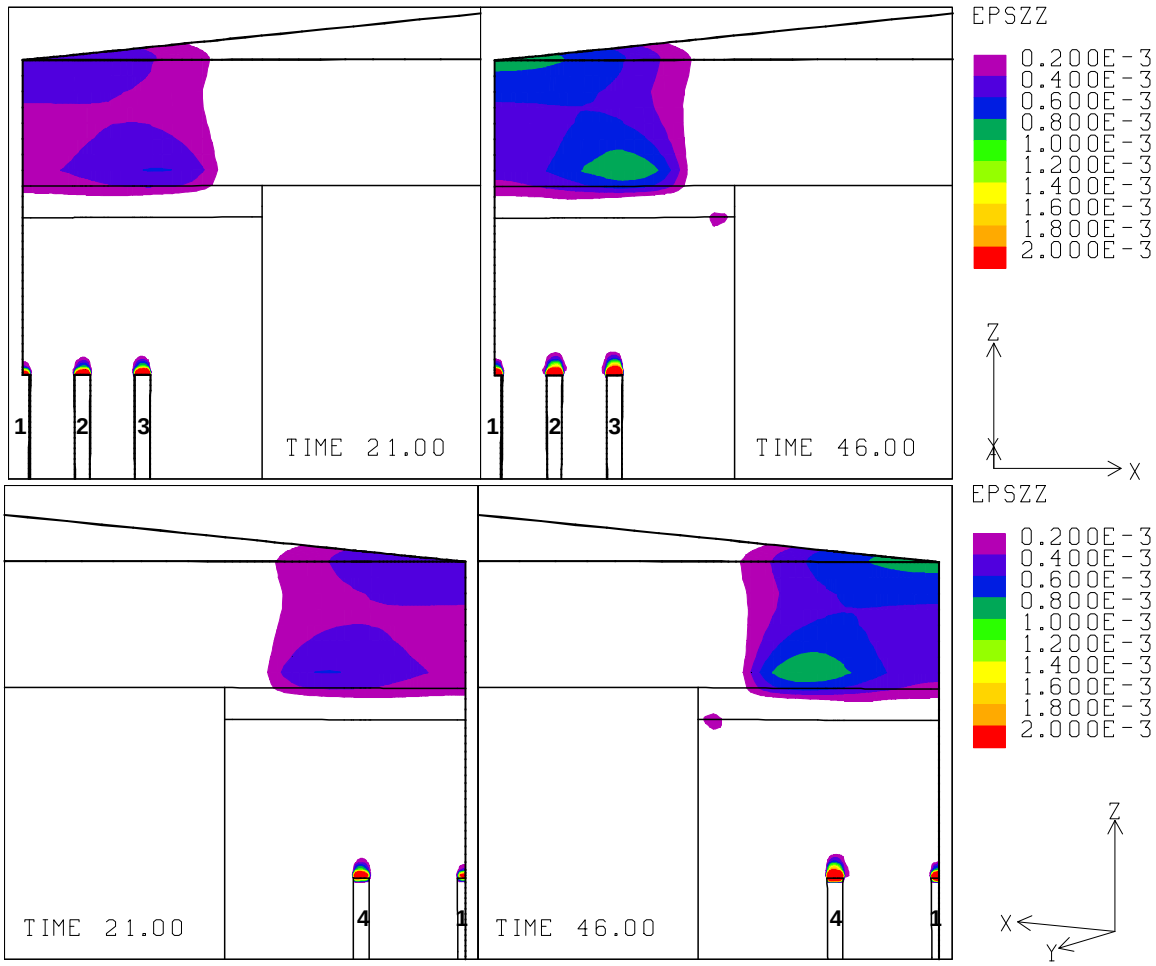

Fig. G-19. 10: Vertical strains around the roof of caverns at 21 years and 46 years (d_C=4000 ft, d_{SD}=2000 ft).

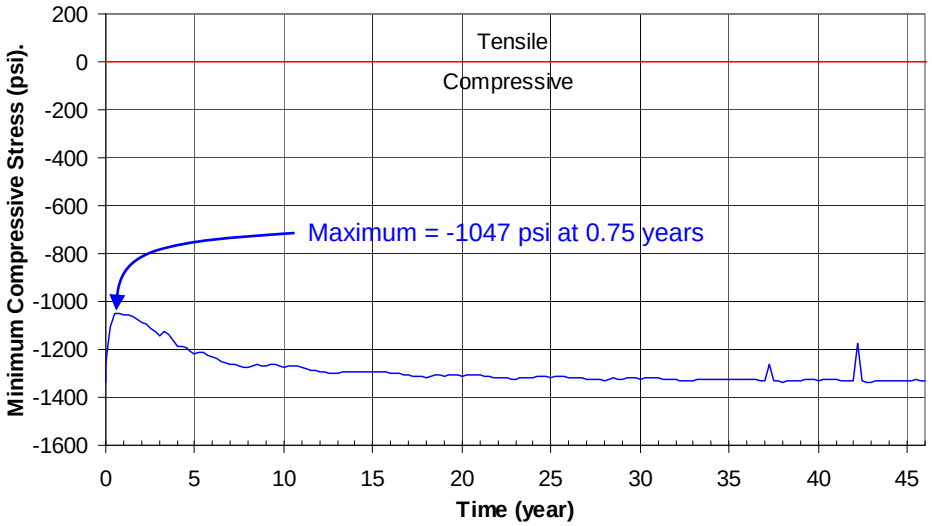

Fig. G-19. 11: Predicted minimum compressive stress history in the salt dome (d_C=4000 ft, d_{SD}=2000 ft).

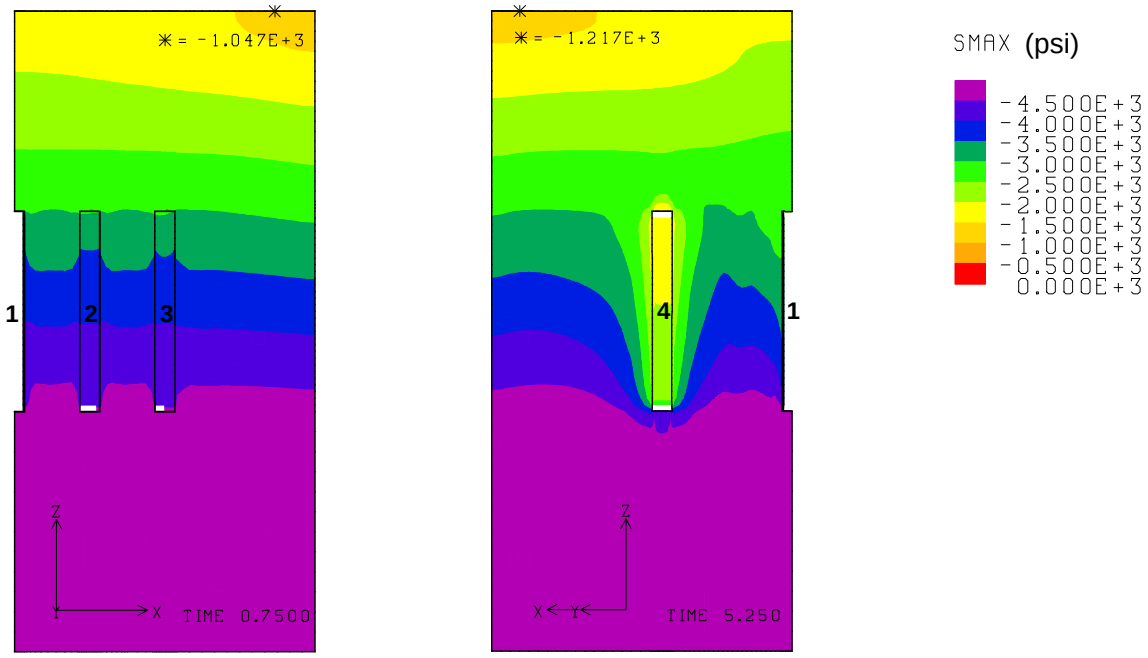

Fig. G-19. 12: Compressive stress contours around the caverns during workover of Cavern 3 and Cavern 4 at 0.75 years and 5.25 years, respectively (d_C=4000 ft, d_{SD}=2000 ft).

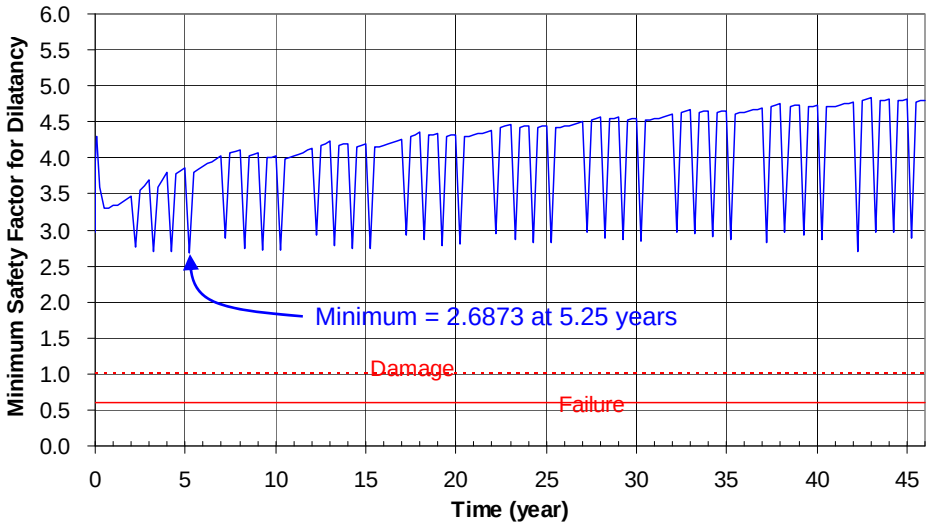

Fig. G-19. 13: Predicted minimum safety factor history against dilatant damage (d_C=4000 ft, d_{SD}=2000 ft).

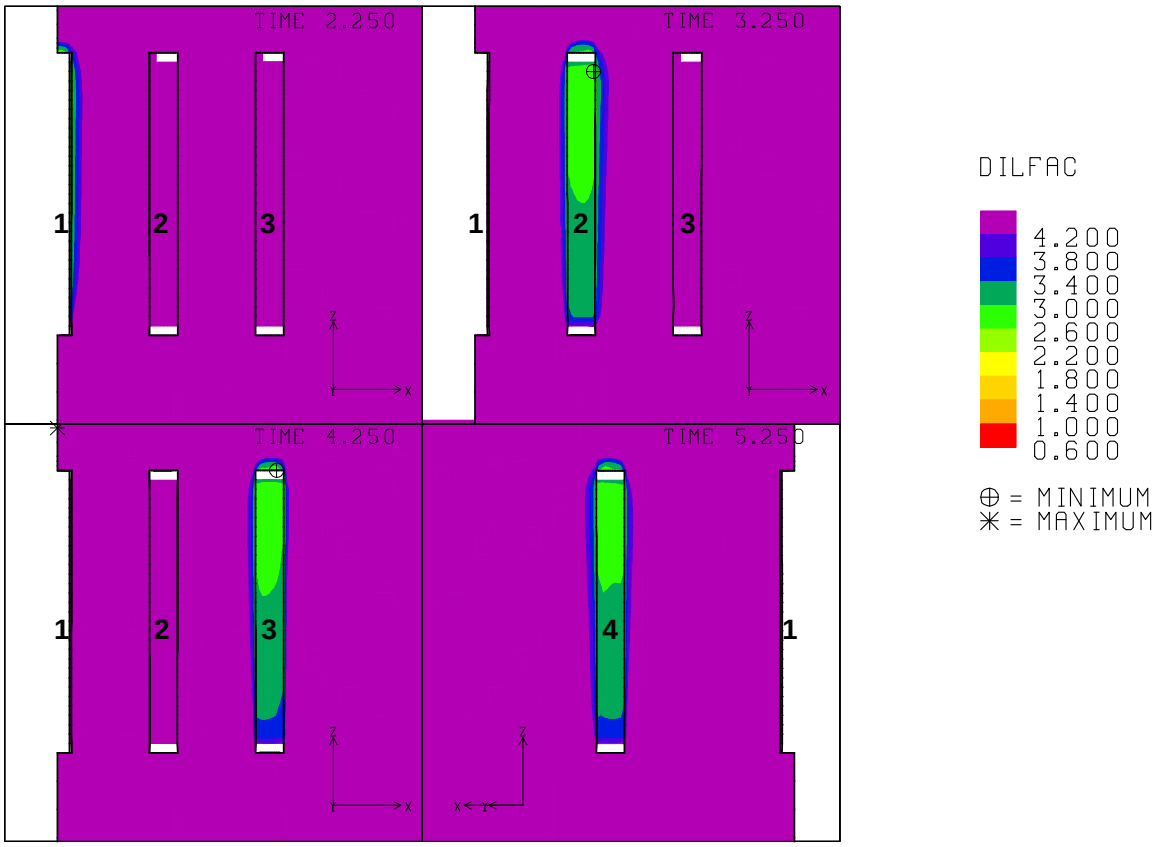

Fig. G-19. 14: Safety factor contours against dilatant damage around the caverns during workover of Caverns 1, 2, 3 and 4 at 2.25 years, 3.25 years, 4.25 years and 5.25 years, respectively (d_C=4000 ft, d_{SD}=2000 ft).

G-20. 31-Cavern Model

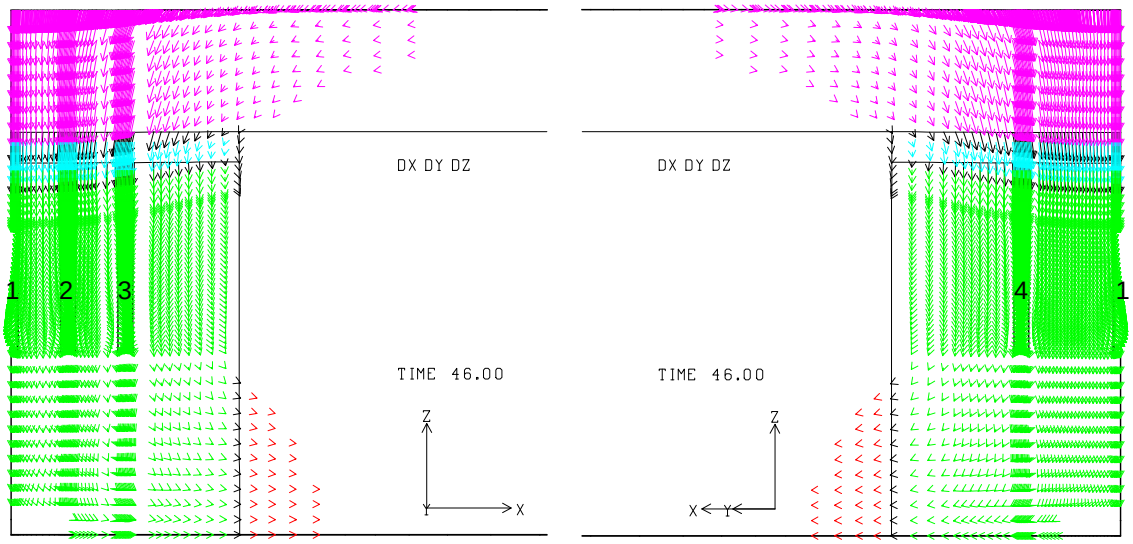

Fig. G-20. 1: Displacement vectors around the caverns at 46 years (31-cavern model).

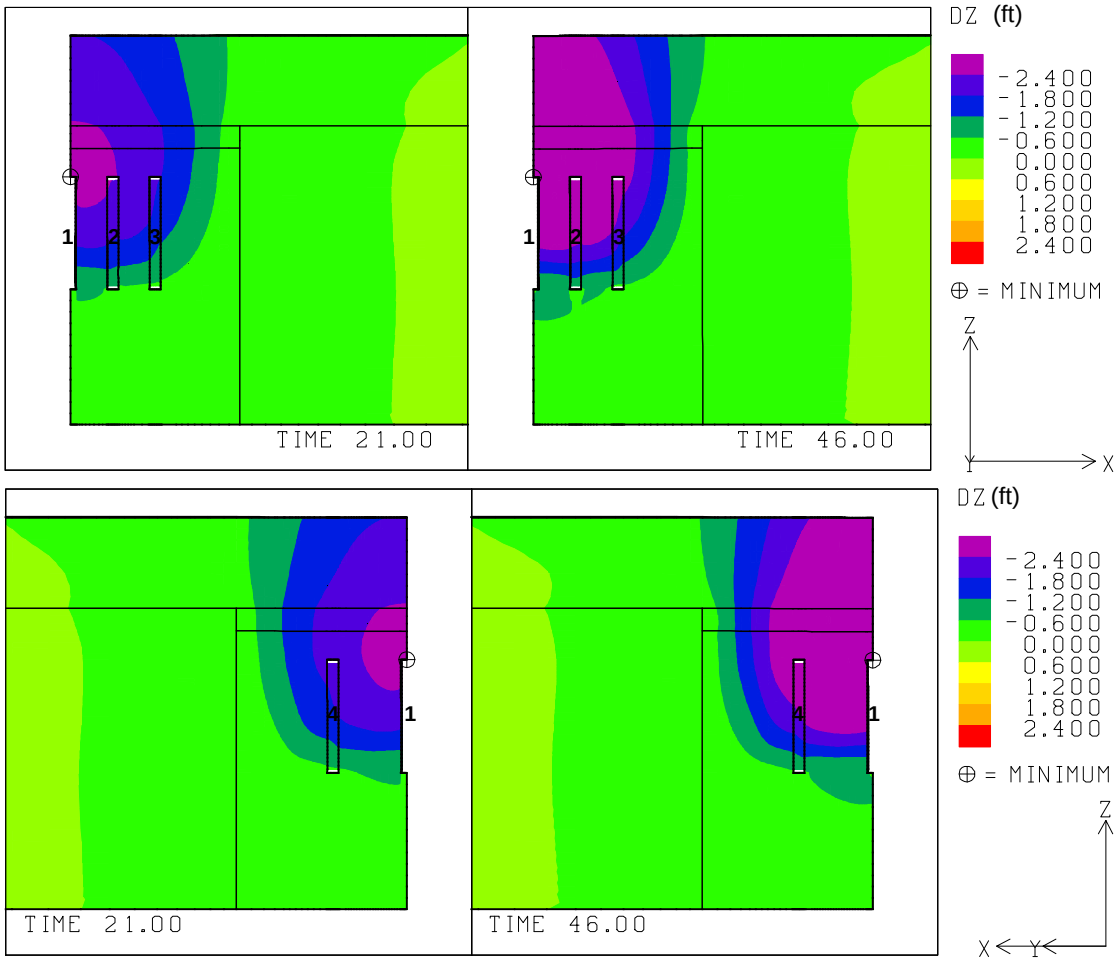

Fig. G-20. 2: Vertical displacement contours around the caverns at 21 and 46 years (31-cavern model).

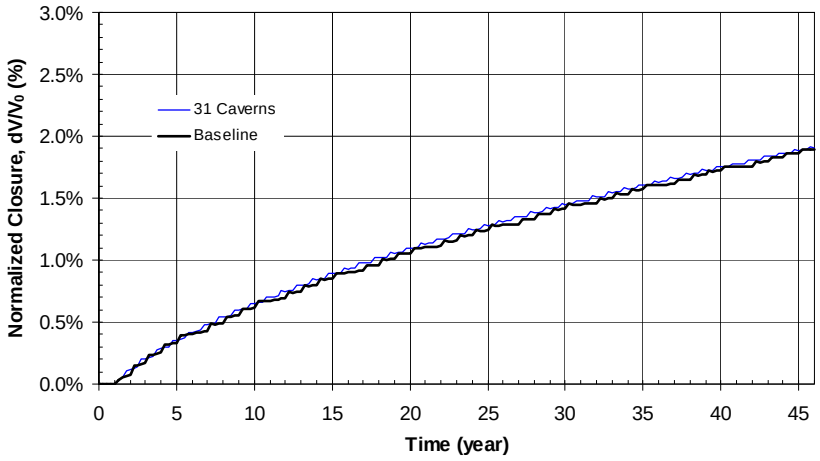

Fig. G-20. 3: Predicted total volumetric closure normalized to initial overall storage volume for the 19 SPR caverns (31-cavern model).

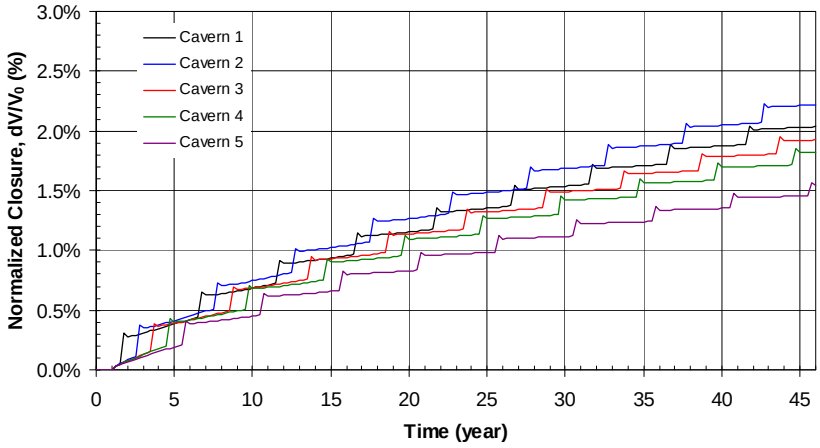

Fig. G-20. 4: Predicted volumetric closure normalized to each initial SPR cavern volume (31-cavern model).

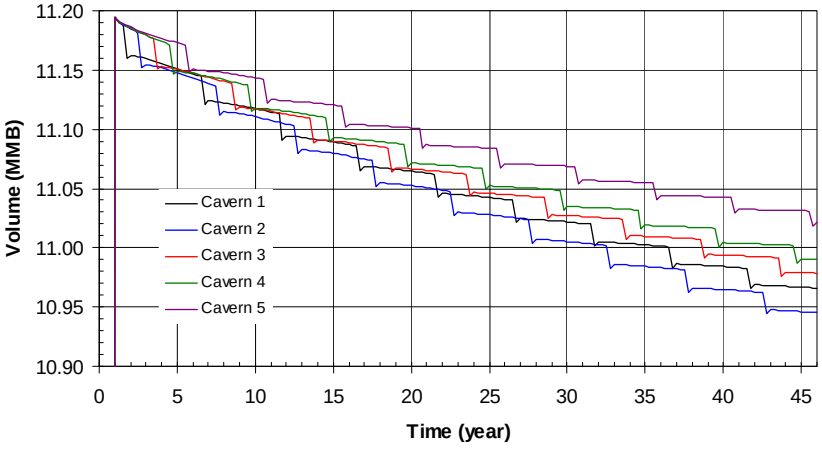

Fig. G-20. 5: Predicted volume change of each SPR cavern due to salt creep closure over time (31-cavern model).

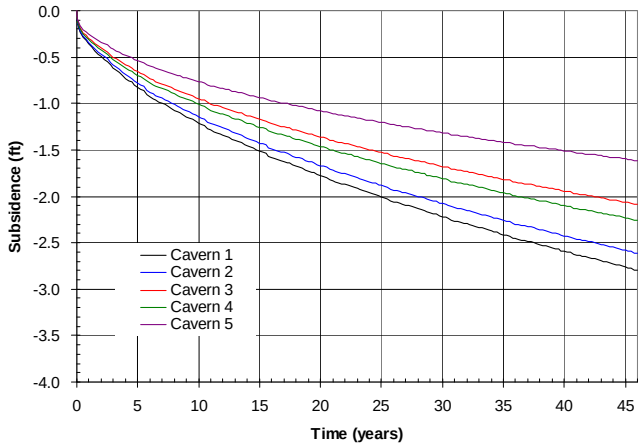

Fig. G-20. 6: Predicted subsidence on the surface above the center of SPR caverns (31-cavern model).

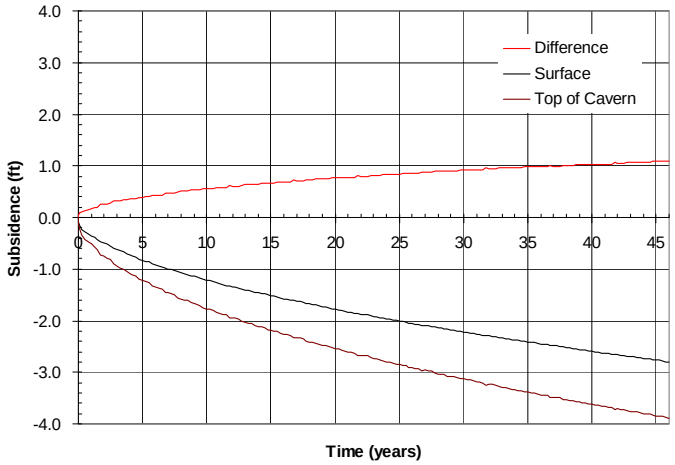

Fig. G-20. 7: Predicted difference between vertical displacement of the top of the central cavern (Cavern 1) and the surface above the cavern as a function of time.

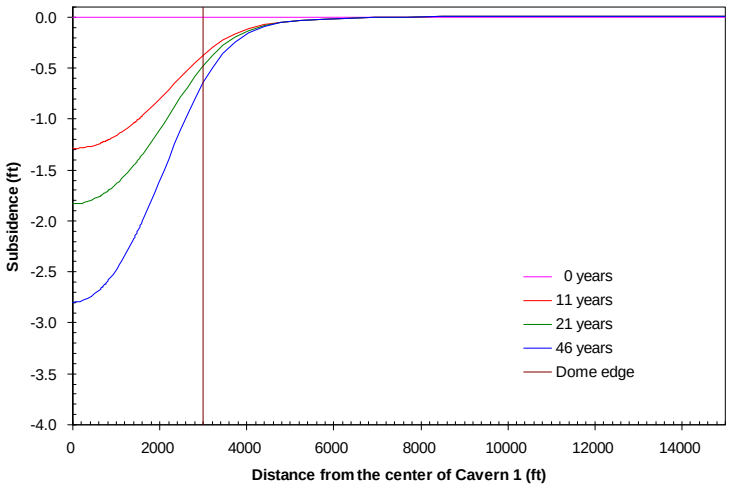

Fig. G-20. 8: Predicted subsidence on the surface from model center to edge with time.

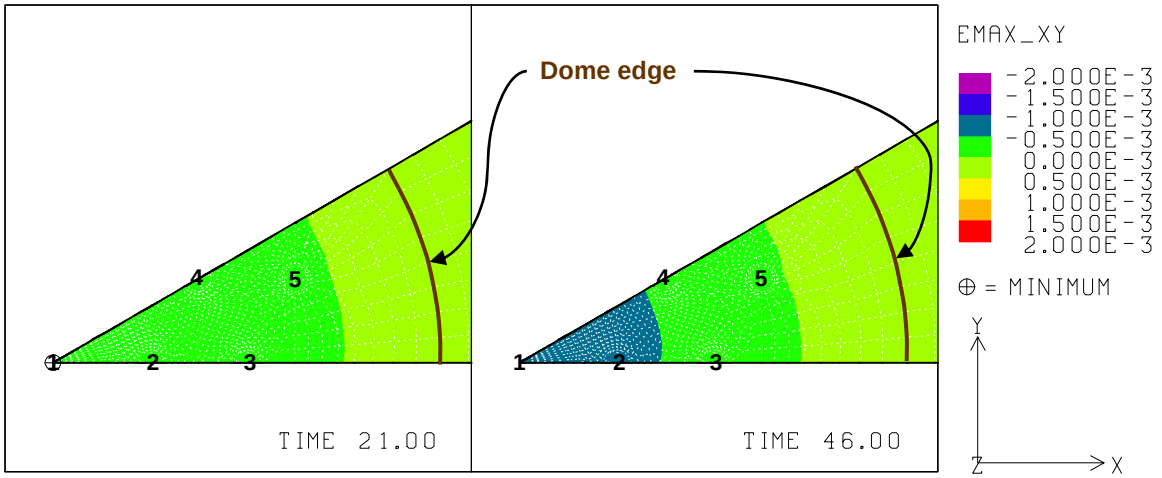

Fig. G-20. 9: Predicted radial surface strains at 21 years and 46 years (31-cavern model).

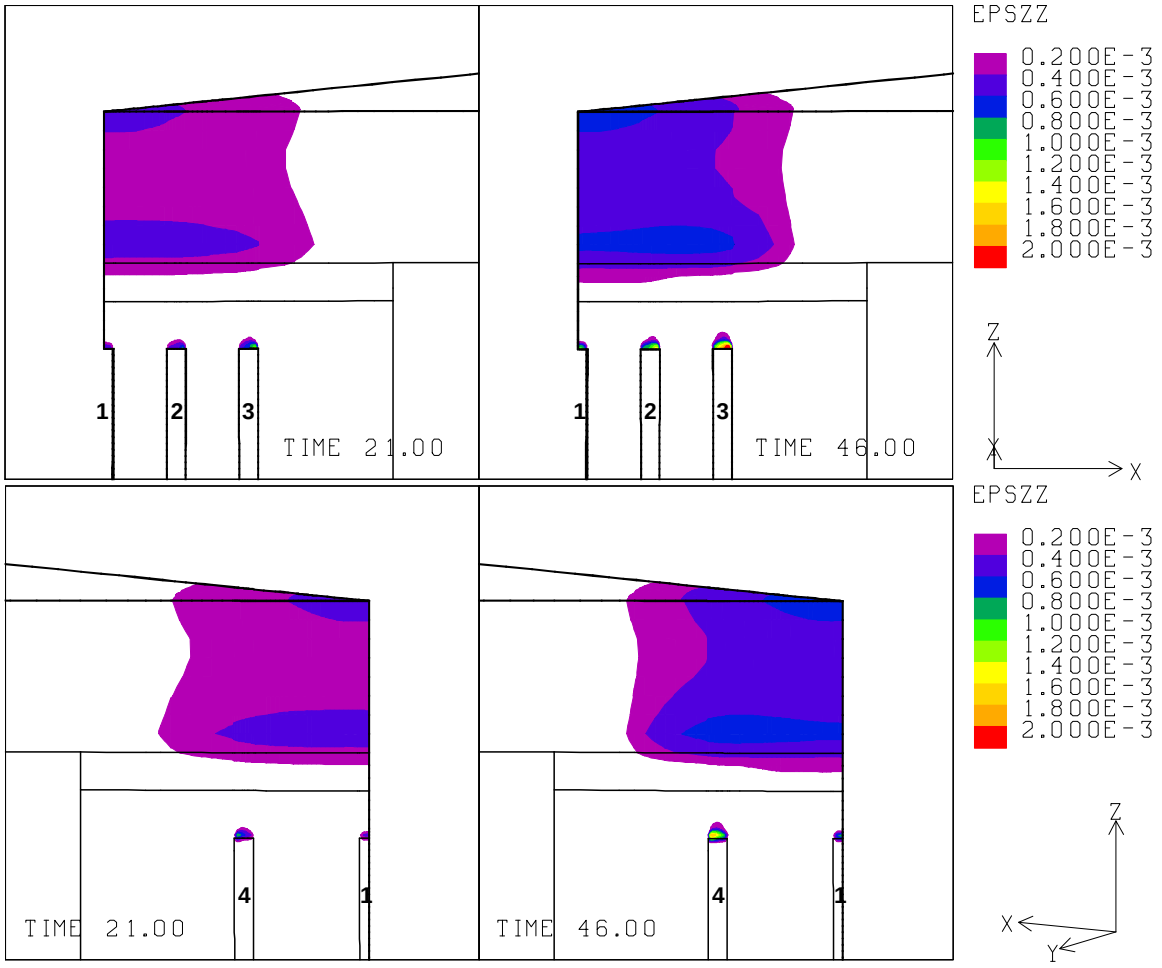

Fig. G-20. 10: Vertical strains around the roof of caverns at 21 years and 46 years (31-cavern model).

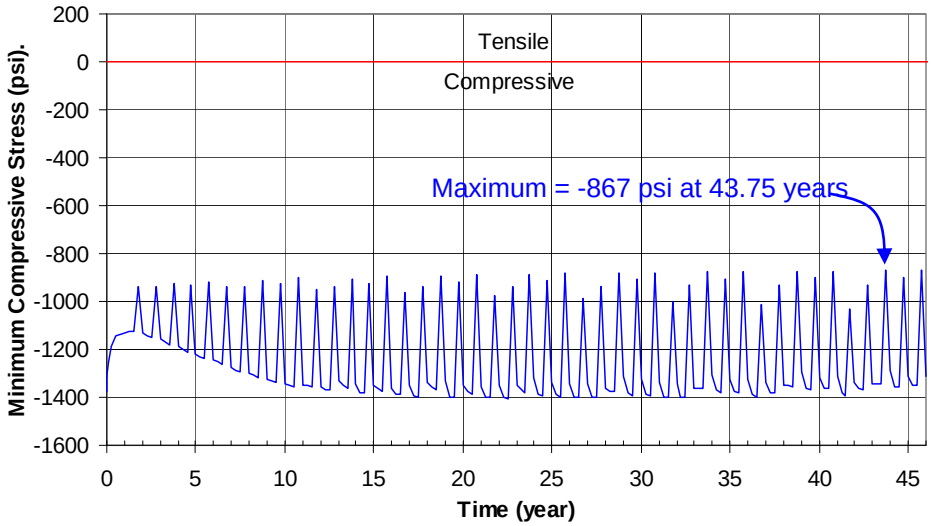

Fig. G-20. 11: Predicted minimum compressive stress history in the salt dome (31-cavern model).

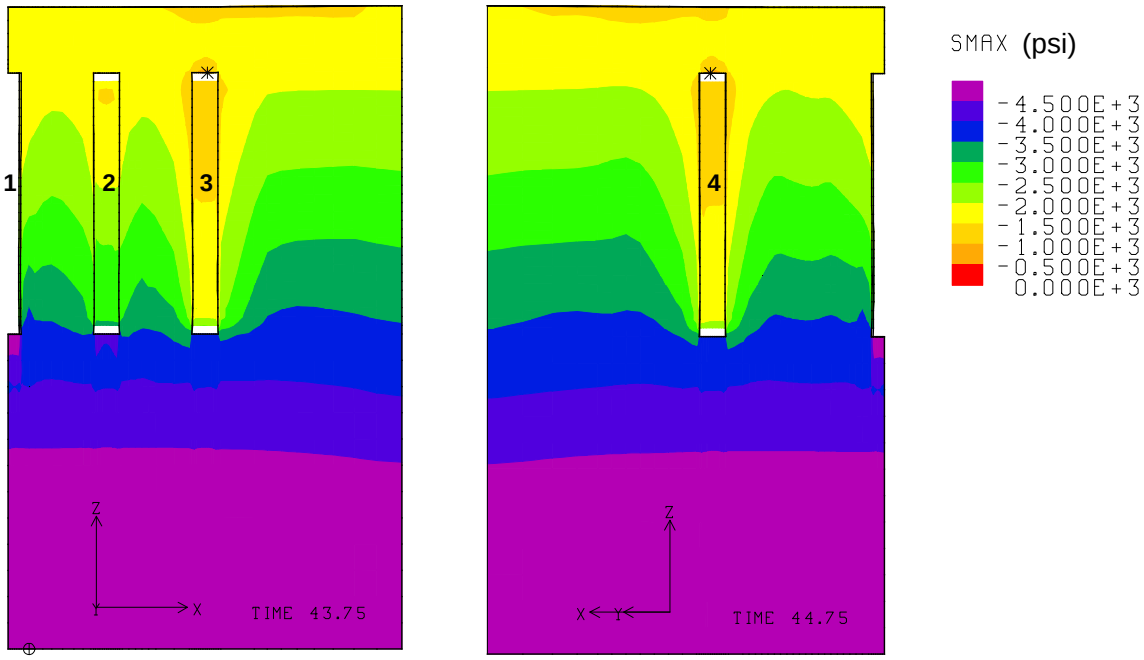

Fig. G-20. 12: Compressive stress contours around the caverns during workover of Cavern 3 and Cavern 4 at 43.75 years and 44.75 years, respectively (31-cavern model).

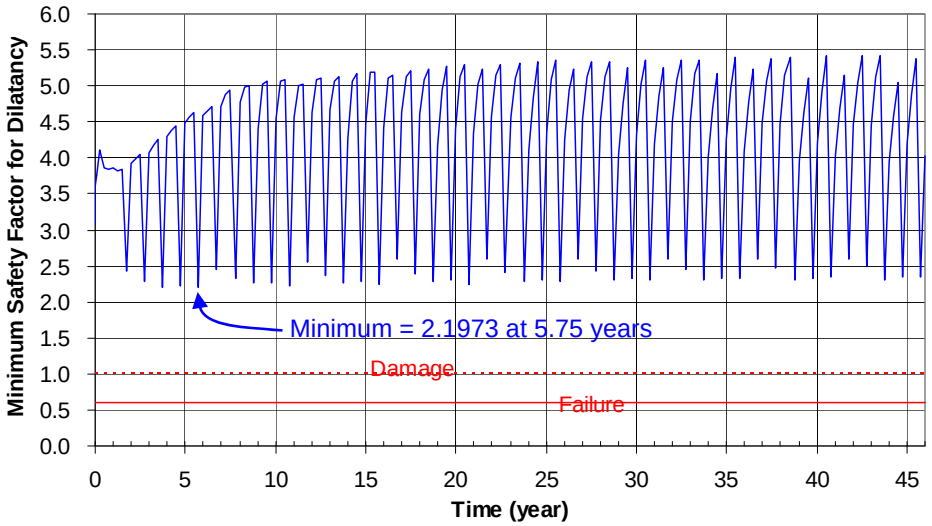

Fig. G-20. 13: Predicted minimum safety factor history against dilatant damage (31-cavern model).

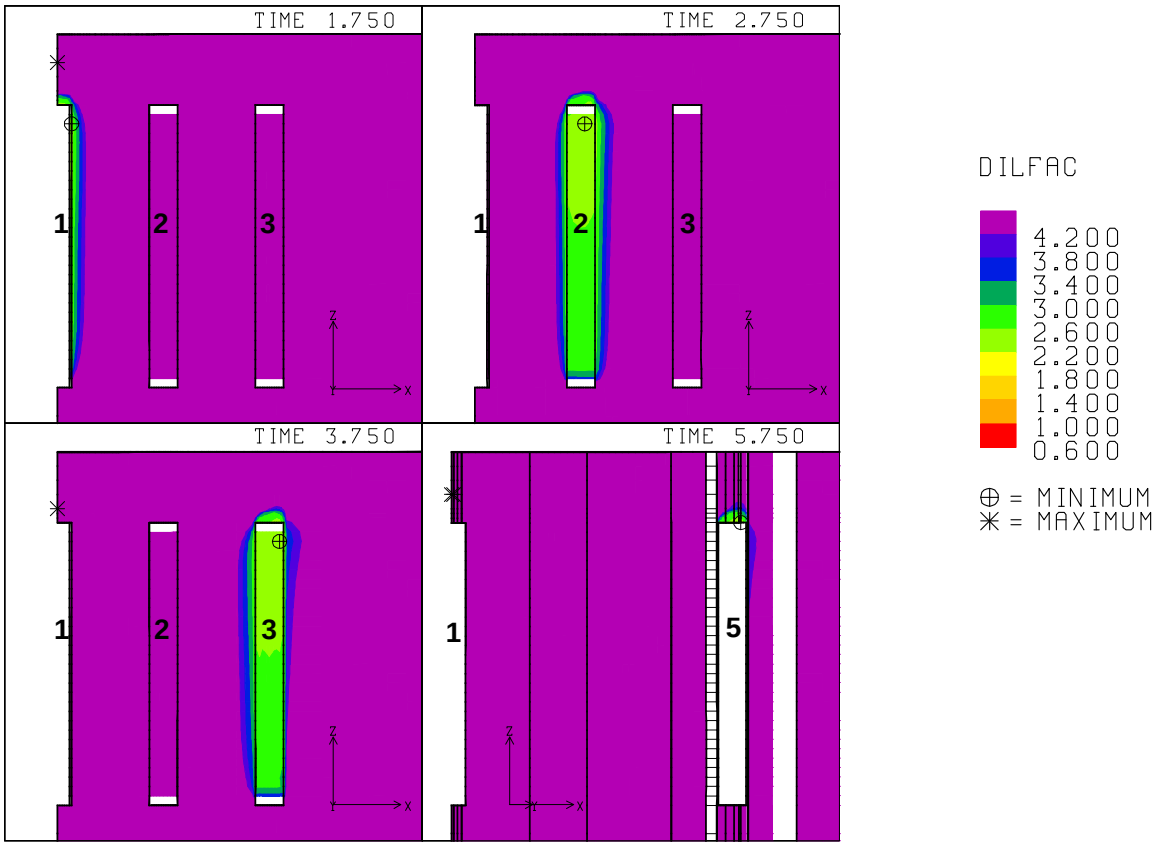

Fig. G-20. 14: Safety factor contours against dilatant damage around the caverns during workover of Caverns 1, 2, 3 and 4 at 1.75 years, 2.75 years, 3.75 years and 4.75 years, respectively (31-cavern model).

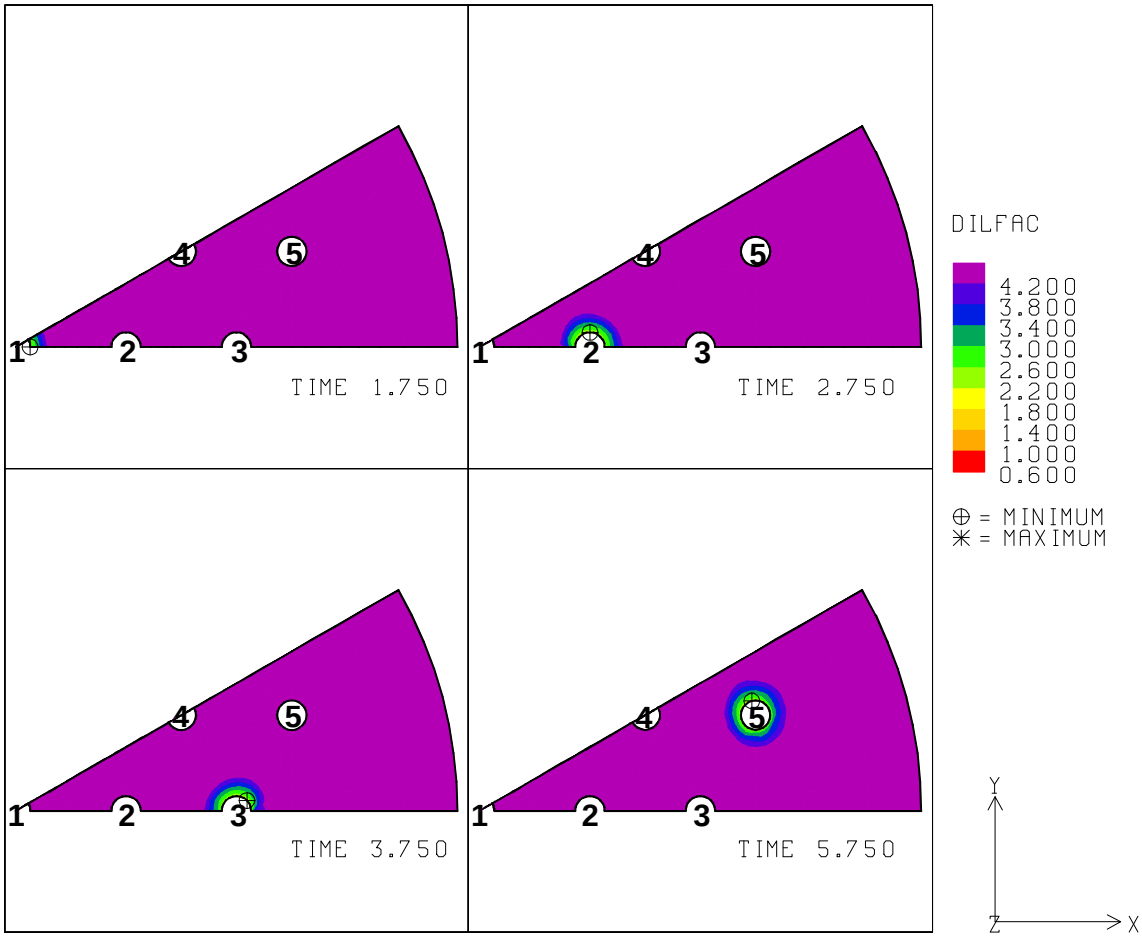

Fig. G-20. 15: Safety factor contours against dilatant damage around the caverns during workover of Caverns 1, 2, 3 and 4 at 1.75 years, 2.75 years, 3.75 years and 4.75 years, respectively (Plan view at the level of minimum safety factor, -2767 ft from the surface) (31-cavern model).

DISTRIBUTION

2 U.S. Department of Energy
Attn: D. Johnson, FE-42
D. Buck, FE-42
Strategic Petroleum Reserve
1000 Independence Avenue SW
Washington, D.C. 20585

1 US Department of Energy
Attn: Deputy Director, RW-2
Office of Civilian Radioactive Waste Mgmt.
Forrestal Building
Washington, DC 20585

Electronic copy only to Wayne Elias at Elias.Wayne@spr.doe.gov for distribution to DOE and DM

1	MS0372	C. M. Stone	1525
1	MS0372	J. G. Arguello Jr.	1525
1	MS0376	J. E. Bean	1524
1	MS0701	F. B. Nimick	6790
1	MS0706	D. J. Borns	6312
5	MS0706	B. L. Ehgartner	6312
1	MS0706	D. L. Lord	6312
1	MS0706	D. E. Munson	6312
1	MS0706	C. A. Rautman	6312
1	MS0706	A. R. Sattler	6312
1	MS0706	Anna C.S. Lord	6312
5	MS0706	S. Wallace	6312 for SPR library
1	MS0735	J. A. Merson	6310
1	MS0735	R. E. Finley	6313
1	MS0751	L. S. Costin	6311
1	MS0751	T. W. Pfeifle	6315
1	MS0751	S. R. Sobolik	6315
1	MS0776	J. S. Stein	6786
1	MS0776	F. D. Hansen	6785
1	MS1104	M. L. Tatro	6200
1	MS1104	R. D. Robinett	6300
1	MS1395	D. S. Kessel	6710
1	MS1395	M. Y. Lee	6711
5	MS1395	B. Y. Park	6711
1	MS1395	C. G. Herrick	6711
1	MS1395	D. J. Clayton	6711
1	MS1395	M.B. Nemer	6711

1	MS1395	C.D. Leigh	6712
1	MS1395	L. H. Brush	6712
1	MS1452	M. K. Knowles	2552
2	MS0899	Technical Library	9536
1	MS0731	823 Library	6850


Sandia National Laboratories